Shape memory alloys for biomedical applications

Related titles:

Dental biomaterials: imaging, testing and modelling
(ISBN 978-1-84569-296-4)
Dental biomaterials: imaging, testing and modelling focuses on the techniques required to undertake research in dental biomaterials. The text forms an instructive and practical review of the scientific methods applied to dental biomaterials, with appropriate case studies. Chapters discuss the practicalities of working on dental biomaterials and methods for characterising dental hand piece performance. Further chapters review optical and electron imaging techniques for biomaterial interfaces. Specific materials, applications and experimental techniques are discussed in addition to chapters reviewing the development and application of computer models to this complex area.

Bioceramics and their clinical applications
(ISBN 978-1-84569-204-9)
Bioceramics and their clinical applications, written by leading academics from around the world, provides an authoritative review of this highly active area of research. Chapters in the first section of the book discuss issues of significance to a range of bioceramics, such as their structure, mechanical properties and biological interactions. The second part reviews the fabrication, microstructure and properties of specific bioceramics and glasses, concentrating on the most promising materials. The final group of chapters reviews the clinical applications of bioceramics.

Surfaces and interfaces for biomaterials
(ISBN 978-1-85573-930-7)
Given such problems as rejection, the interface between an implant and its human host is a critical area in biomaterials. This book presents the current level of understanding on the nature of a biomaterial surface, the adaptive response of the biomatrix to that surface, techniques used to modify biocompatibility, and state-of-the-art characterisation techniques to follow the interfacial events at that surface.

Details of these and other Woodhead Publishing materials books can be obtained by:

- visiting our web site at www.woodheadpublishing.com
- contacting Customer Services (e-mail: sales@woodheadpublishing.com; fax: +44 (0) 1223 893694; tel: +44 (0) 1223 891358 ext. 130; address: Woodhead Publishing Limited, Abington Hall, Granta Park, Great Abington, Cambridge CB21 6AH, England)

If you would like to receive information on forthcoming titles, please send your address details to: Francis Dodds (address, tel. and fax as above; e-mail: francis.dodds@woodheadpublishing.com). Please confirm which subject areas you are interested in.

Shape memory alloys for biomedical applications

Edited by

Takayuki Yoneyama
and Shuichi Miyazaki

CRC Press
Boca Raton Boston New York Washington, DC

WOODHEAD PUBLISHING LIMITED
Cambridge, England

Published by Woodhead Publishing Limited, Abington Hall, Granta Park
Great Abington, Cambridge CB21 6AH, England
www.woodheadpublishing.com

Published in North America by CRC Press LLC, 6000 Broken Sound Parkway, NW,
Suite 300, Boca Raton, FL 33487, USA

First published 2009, Woodhead Publishing Limited and CRC Press LLC

British Library Cataloguing in Publication Data
A catalogue record for this book is available from the British Library.

Library of Congress Cataloging in Publication Data
A catalog record for this book is available from the Library of Congress.

Woodhead Publishing ISBN 978-1-84569-344-2 (book)
Woodhead Publishing ISBN 978-1-84569-524-8 (e-book)
CRC Press ISBN 978-1-4200-7966-1
CRC Press order number WP7966

The publishers' policy is to use permanent paper from mills that operate a sustainable forestry policy, and which has been manufactured from pulp which is processed using acid-free and elemental chlorine-free practices. Furthermore, the publishers ensure that the text paper and cover board used have met acceptable environmental accreditation standards.

Typeset by Ann Buchan (Typesetters), Middlesex
Printed by TJ International Limited, Padstow, Cornwall, England

Contents

Contributor contact details

(* = main contact)

Editors

Professor Takayuki Yoneyama
Department of Dental Materials
Nihon University School of Dentistry
1-8-13 Kanda-Surugadai
Chiyoda-ku
Tokyo 101-8310
Japan

E-mail: yoneyama@dent.nihon-u.ac.jp

Professor Shuichi Miyazaki
Institute of Materials Science
University of Tsukuba
Tsukuba
Ibaraki 305-8573
Japan

E-mail: smamiyazaki@gmail.com

Chapter 1

Professor Shuichi Miyazaki*
Institute of Materials Science
University of Tsukuba
Tsukuba
Ibaraki 305-8573
Japan

E-mail: smamiyazaki@gmail.com

Dr Rohit L. Sachdeva
OraMetrix
2350 Campbell Creek Blvd
#400 Richardson, TX 75082
USA

E-mail: rohitsachdeva@gmail.com

Chapter 2

Associate Professor H. Hosoda* and Assistant Professor T. Inamura
Precision and Intelligence Laboratory
Tokyo Institute of Technology
Tokyo 152-8550
Japan

E-mail: hosoda.h.aa@m.titech.ac.jp
inamura.t.aa@m.titech.ac.jp

Chapter 3

Professor Y. Liu
School of Mechanical Engineering
The University of Western Australia
35 Stirling Highway
Crawley
WA6009
Australia

E-mail: liu@mech.uwa.edu.au

Chapter 4

Associate Professor Hee Young Kim* and Professor Shuichi Miyazaki
Institute of Materials Science
University of Tsukuba
Tsukuba
Ibaraki
305-8573
Japan

E-mail: kimheey@gmail.com
smamiyazaki@gmail.com

Chapter 5

T. Habu
Furukawa Techno Material Co. Ltd
5-1-8 Higashi-Yawata
Hiratsuka-City
Kanagawa Prefecture 254-0016
Japan

E-mail: t_habu@ftm.fitec.co.jp

Chapter 6

Dr Y. Oshida*
Department of Mechanical and Aerospace Engineering
Syracuse University
Syracuse, NY 13244
USA

E-mail: yoshida@syr.edu

Dr Farrokh Farzin-Nia
Director, Technology & Advanced Projects
Ormco Corporation
1332 S. Lone Hill Avenue
Glendora, CA 91740
USA

E-mail: farrokh.farzin-nia@sybrondental.com

Chapter 7

Professor K. Gall
School of Materials Science and Engineering
George Woodruff School of Mechanical Engineering
Georgia Institute of Technology
Atlanta
GA 30332
USA

E-mail: ken.gall@mse.gatech.edu

Chapter 8

Dr M. Maitz
Max Bergmann Center of Biomaterials Dresden
Leibniz Institute of Polymer Research Dresden
Hohe Strasse 6
01069 Dresden
Germany

E-mail: manfred@maitz-online.de

Chapter 9

Dr S. Shabalovskaya*
Ames Laboratory
Ames 50011
Iowa
USA

E-mail: svetinol@yahoo.com
shabalov@ameslab.gov

Professor J. Van Humbeeck
Kasteelpark Arenberg 44
MTM
Katholieke University Leuven
Leuven 3001
Belgium

E-mail: Jan.Vanhumbeeck@mtm.kuleuven.be

Chapter 10

D. Stoeckel,* A. Pelton and T. Duerig
Nitinol Devices & Components
47533 Westinghouse Drive
Fremont
CA 94539
USA

E-mail: dstoecke@ndcus.jnj.com

Chapter 11

Dr F. Farzin-Nia*
Director, Technology & Advanced Projects
Ormco Corporation
1332 S. Lone Hill Avenue
Glendora
CA 91740
USA

E-mail:farrokh.farzin-nia@sybrondental.com

Professor T. Yoneyama
Department of Dental Materials
Nihon University School of Dentistry
1-8-13 Kanda-Surugadai
Chiyoda-ku
Tokyo 101-8310
Japan

E-mail: yoneyama@dent.nihon-u.ac.jp

Chapter 12

Professor T. Yoneyama*
Department of Dental Materials
Nihon University School of Dentistry
1-8-13 Kanda-Surugadai
Chiyoda-ku
Tokyo 101-8310
Japan

E-mail: yoneyama@dent.nihon-u.ac.jp

Dr C. Kobayashi
Pulp Biology and Endodontics
Department of Restorative Sciences
Graduate School
Tokyo Medical and Dental University
1-5-45 Yushima
Bunkyo-ku
Tokyo 113-8549
Japan

E-mail: c.kobayashi.endo@tmd.ac.jp

Chapter 13

L'H. Yahia* and F. Rayes
Innovation and Bioperformance Analysis Laboratory
École Polytechnique de Montréal
Montreal, QC
Canada
H3C 3A7

E-mail: lhocine.yahia@polymtl.ca
fady.rayes@polymtl.ca

A. O. Warrak
Faculty of Veterinary Medicine
University of Montreal, QC
Canada
H3C 3J7

Preface

Metallic biomaterials have been used for many centuries and played an important role in medical treatment. After many metals and alloys had been tried, titanium and its alloys have now become the major metallic materials for surgical implants owing to their superior biocompatibility. Titanium–nickel (Ti–Ni) alloy is one of these titanium alloys and the only biomedically applicable shape memory alloy at present.

Ti–Ni alloy, consisting of titanium and nickel in nearly equal proportions, is a special biomedical titanium alloy that is of interest in two main areas of research. One is related to its unique mechanical properties in the shape memory effect and superelasticity, which have led to medical devices with special functions. The other is the reduced biocompatibility caused by nickel inclusion, although clear Ni-hypersensitivity or toxicity of the Ti–Ni alloy has not been reported. It is therefore essential to understand the properties of this alloy in assessing medical devices using the alloy.

Shape memory alloys for biomedical applications provides a comprehensive review of the properties and applications of shape memory alloys, especially Ti–Ni based alloys. Part I discusses fundamental issues such as mechanical properties, thermodynamics, alternative alloys, fabrication, corrosion in the oral environment, implant failure, surface modification and biocompatibility. Part II covers clinical applications such as self-expanding cardiovascular stents, orthodontic devices, endodontic instruments, orthopaedic and other applications.

Ti–Ni based alloys have been increasingly used in a wide range of biomedical applications, and new methods have been developed for better medical treatment. *Shape memory alloys for biomedical applications* will be an essential resource for materials scientists and engineers working in the medical devices industry and academia as well as senior students in the biomedical courses.

The editors express heartfelt thanks to the distinguished international team of contributors whose scientific efforts unite to form this book. We also express special thanks to the staff at Woodhead Publishing Limited for their assistance.

Takayuki Yoneyama and Shuichi Miyazaki

1

Shape memory effect and superelasticity in Ti–Ni alloys

S. MIYAZAKI
University of Tsukuba, Japan

R. L. SACHDEVA
OraMetrix, USA

Abstract: Shape memory effect and superelastic behavior are discussed. The temperature sensitive nature of deformation behavior of shape memory alloys is summarised. The superelasticity has been extensively applied in many medical devices such as orthodontic arch wires, stents and dental guidewires. The basic characteristics of the superelasticity are described in detail with particular consideration of applications for orthodontics.

Key words: shape memory effect, superelasticity, Ti–Ni alloys, orthodontic arch wires, Ni–Ti, Nitinol.

1.1 Introduction

Shape memory effect (SME) and superelasticity (SE) are associated with the crystallographically reversible nature of the martensitic transformation that appears in shape memory alloys (SMAs). The Ti–Ni alloys have been investigated since the first report on SME in a Ti–Ni alloy in 1963 (Buehler *et al.*, 1993). However, the Ti–Ni alloys had presented many difficult problems associated with puzzling phenomena for about 20 years until 1982 when a basic understanding of the relationship between the microstructure and the corresponding deformation behavior such as SME and SE was achieved (Miyazaki *et al.*, 1982; Miyazaki, 1990). Since then, many basic characteristics of Ti–Ni alloys have been clarified, e.g., the microstructures that cause the rhombohedral phase (R-phase) transformation to appear (Miyazaki and Otsuka, 1984, 1986), the orientation dependence of shape memory and superelastic behavior observed in single crystals (Takei *et al.*, 1993; Miyazaki *et al.*, 1983; Miyazaki *et al.*, 1984; Miyazaki and Wayman, 1988 and Miyazaki *et al.*, 1988), the temperature dependence of deformation and fatigue behavior (Miyazaki *et al.*, 1982; Miyazaki, 1990 and Miyazaki *et al.*, 1986), the shape memory mechanism (Miyazaki *et al.*, 1989).

The Ti–Ni alloys have been successfully applied as biomaterials such as orthodontic arch wires, guide wires and stents in addition to many engineering

applications. The Ti–Ni alloys are also considered as one of the attractive candidates for orthopedic implants.

The great success in using the superelasticity of the Ti–Ni alloy was first achieved in the application to orthodontic therapy. Historically, a number of alloys have been used for orthodontic applications. In the early stage, gold alloys were popularly used for arch wires. Next, stainless steels were introduced and these were widely used in the fabrication of orthodontic appliances. Chrome–cobalt–nickel (Elgiloy) and beta titanium wires have also been used in orthodontic therapy. More recently, work-hardened nickel–titanium (Nitinol) has been introduced to the specialty because of its excellent spring back and low elastic modulus (Andreasen and Hilleman, 1971 and Andreasen and Morrow, 1978).

During orthodontic therapy, the aim is to apply a range of forces to effect appropriate tooth movement in various aspects of the dental arch. Traditionally, this has been made possible by using various wire cross-sections. This strategy is termed 'variable cross-section' orthodontics. However, with the availability of different materials today, orthodontists can vary force range by using materials of different stiffness rather than by changing the cross-section of wire. This particular approach offers the advantage that a low stiffness rectangular cross-section wire is used from the onset of treatment rather than a round cross-section, thus offering greater control in tooth movement. This approach to treatment forms the basis of the 'variable modulus' concept (Burstone, 1981).

More recently superelastic Ti–Ni was introduced to orthodontics (Ohura, 1984; Burstone, 1981; Miura *et al.*, 1986; Sachdeva and Miyazaki, 1988 and Miyazaki *et al.*, 1990). This alloy exhibits unique and ideal mechanical properties for the practice of orthodontic mechanotherapy (Sachdeva and Miyazaki, 1990). The deformation of the superelastic Ti–Ni is associated with the martensitic transformation, which originates in a crystallographically reversible structural change, hence the deformation becomes reversible upon loading and unloading (Miyazaki *et al.*, 1981). The most important characteristic in the superelastic behavior is the generation of a constant force and a large reversible deformation over a long activation span. Besides, the constant force can be adjusted over a wide range by changing manufacturing and metallurgical factors such a thermomechanical treatment, composition, etc. (Miyazaki *et al.*, 1982). The unique properties of superelastic Ti–Ni may be taken avail of in a new orthodontic treatment strategy termed 'variable constant-force' orthodontics (Sachdeva *et al.*, 1989).

The purpose of this chapter is twofold: firstly, to describe the temperature sensitive deformation behavior of Ti–Ni including shape memory effect and superelasticity and, secondly, to review the advantage of using superelasticity in orthodontic treatment.

1.2 Shape memory effect and superelasticity

The deformation behavior of SMAs is strongly temperature sensitive, because the

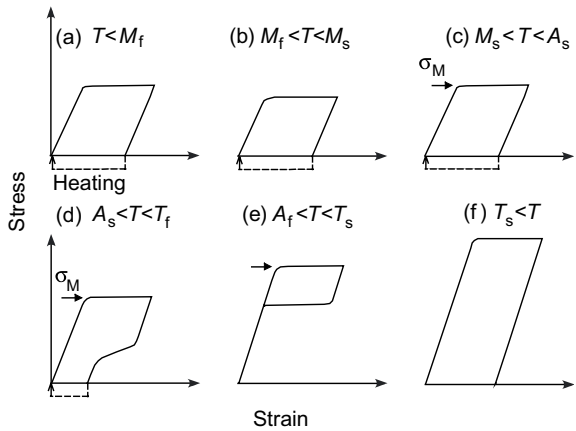

1.1 Schematic stress–strain curves at various temperatures in a Ti–Ni alloy.

deformation is associated with the martensitic transformation: this is different from the plastic deformation by slip that occurs in conventional metals and alloys. Schematic stress–strain curves of a Ti–Ni alloy obtained at various temperatures (T) are shown in Fig. 1.1.

In the temperature range of $T<M_f$ (the martensitic transformation finish temperature), the specimen is fully transformed before applying stress so that the elastic deformation takes place in the martensite phase (the low temperature phase) at first as shown in Fig. 1.1(a), where many martensite variants self-accommodate each other before loading. Upon further loading, twin planes in the martensite phase move to create an apparent plastic deformation. Therefore, the yield stress in Fig. 1.1(a) corresponds to the critical stress for twinning deformation in the martensite phase.

In the temperature range $M_f<T<M_s$ (the martensitic transformation start temperature), the parent and martensite phases coexist so that yielding occurs due to twinning in the martensite phase and/or stress-induced martensitic transformation in the parent phase(the high temperature phase). The stress–strain curves in Fig. 1.1(a) and (b) are essentially the same, except that the yield stress is a little lower in Fig. 1.1(b) than in Fig. 1.1(a).

In the temperature range of $M_s<T<A_s$ (the reverse martensitic transformation start temperature), the parent phase elastically deforms at first and yielding occurs owing to the stress-induced martensitic transformation. Therefore, the yield stress linearly increases with increasing temperature satisfying the Clausius–Clapeyron relationship. The stress-induced martensite phase remains after unloading, because the temperature is below A_s. The shape of the stress–strain curve of Fig. 1.1(c) is similar to those of Fig. 1.1(a) and (b), where the shape of the specimen recovers to the original one by heating above A_f (the reverse martensitic

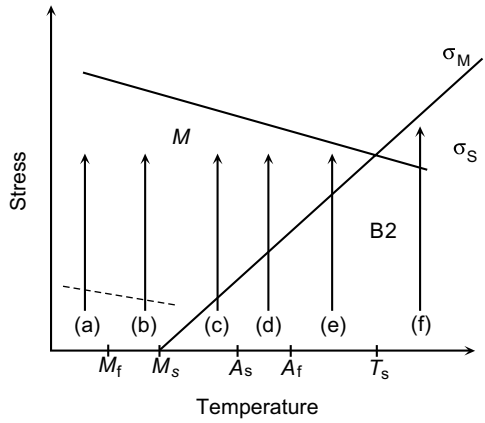

1.2 Critical stresses for inducing the martensitic transformation (σ_M) and for slip deformation (σ_s) shown as a function of test temperature in the sample shown in Fig. 1.1.

transformation finish temperature) as shown by the dashed line revealing the shape memory effect.

In the temperature range $A_s<T<A_f$, the deformation induced by the stress-induced martensitic transformation recovers partially upon unloading as shown in Fig. 1.1(d), resulting in partial superelasticity and partial shape memory effect by subsequent heating.

In the temperature range $A_f<T<T_s$, perfect superelasticity appears as shown in Fig. 1.1(e), where T_s stands for the critical temperature above which the martensitic transformation does not take place and deformation occurs by slip. If T is above T_s, plastic deformation occurs as in conventional metals and alloys as shown in Fig. 1.1(f).

According to Fig. 1.1, the effects of temperature on the critical stress for inducing martensite (σ_M) and on the critical stress for slip (σ_S) are shown by two solid lines in Fig. 1.2. The σ_M line shows a positive temperature dependence, while the σ_S line shows a negative temperature dependence, the two lines intersecting at T_s. The stress for the rearrangement of martensite variants due to the movement of twin planes is shown by a dashed line in the temperature range below M_S. The slope of the dashed line shows a negative temperature dependence as well as the solid line for slip deformation, because both the deformation modes, slip and twinning, are thermal activation processes. Deformation paths corresponding to those shown in Fig. 1.1(a)–(f) are shown in Fig. 1.2.

More detailed information of the temperature sensitive nature of deformation behavior associated with the martensitic transformation are described in Chapter 2. More detailed characteristics of superelasticity will be explained in the following (Miyazaki *et al.*, 1990).

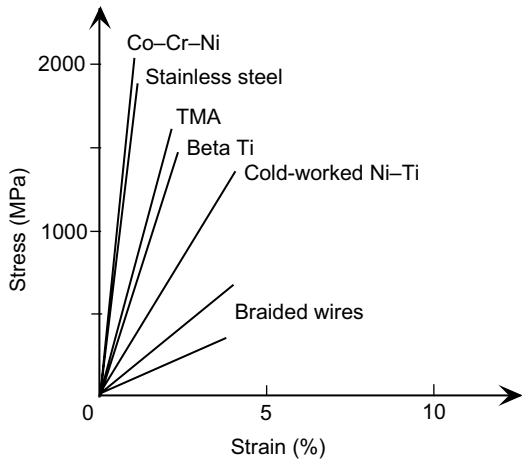

1.3 Stress–strain curves of elastic orthodontic wires.

1.3 Elasticity and superelasticity

The elastic moduli of conventional alloys are compared with each other in the form of stress–strain curves in Fig. 1.3, where the slopes of the curves indicate the elastic moduli of various alloys used in orthodontics.

If a high elastic modulus alloy such as stainless steel is used, an effective strain range (ε_{eff}) corresponding to the optimal force zone is very small as shown in Fig. 1.4. In the optimal force zone, the nature of the applied force is such that it will encourage the optimum biological response, i.e. the bone remodeling response is most efficient. Above the optimal force zone is located the excessive force zone where tissue damage may occur. Forces in this zone can cause a significant amount of tissue damage. Another strain range (ε_0) is also shown in the figure; this corresponds to suboptimal and subthreshold force zones. In this region, the tooth moves less efficiently and may even come to a complete standstill if forces become minimal. The corresponding clinical sitation is shown in Fig. 1.5, where a stainless-steel plain wire is inserted into brackets and the force decreases rapidly as the teeth move. Thus, clinically, there are also four zones of force level corresponding to the force zones shown in Fig. 1.4. The optimal force zone is narrow in Fig. 1.5 because of the high elastic modulus of the stainless steel (Burstone, 1981).

If a low elastic modulus alloy is used, the effective strain range becomes larger as shown in Fig. 1.6, hence clinically the optimal force zone becomes wider as shown in Fig. 1.7. Therefore, a low elastic modulus alloy provides a greater range of activation, and fewer adjustments need to be made to the archwire to move the tooth to its final position. Cold-worked Nitinol and braided wires have been successfully used as such low elastic modulus materials.

The goal of the above approach using low modulus materials is to obtain a zero

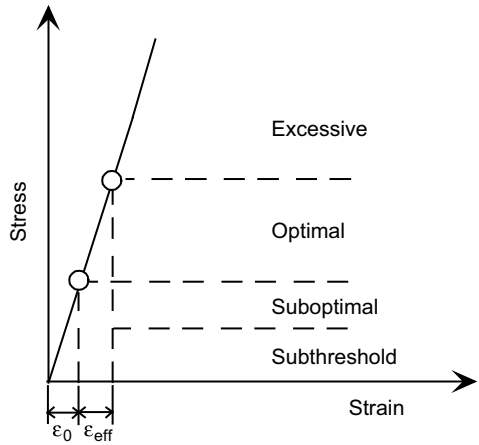

1.4 A schematic stress–strain curve of an elastic orthodontic wire with a high elastic modulus. Effective strain range corresponding to the optimal force zone is small.

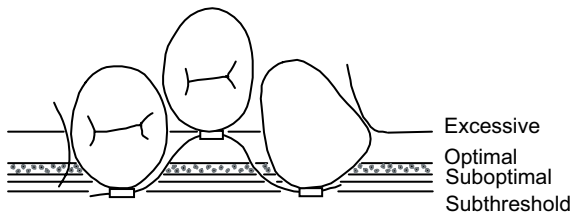

1.5 An elastic orthodontic wire with a high elastic modulus. Optimal force zone is present only over a small range.

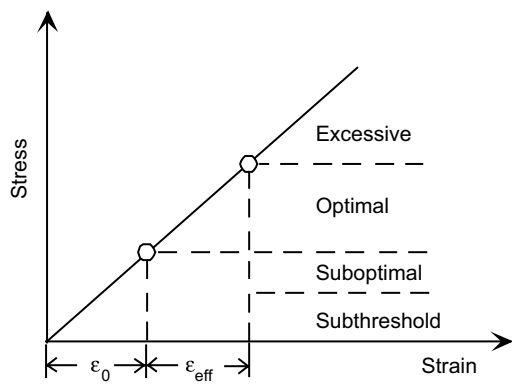

1.6 A schematic stress–strain curve of an elastic orthodontic wire with a low elastic modulus. Effective strain range corresponding to the optimal force zone is larger than in Fig. 1.4.

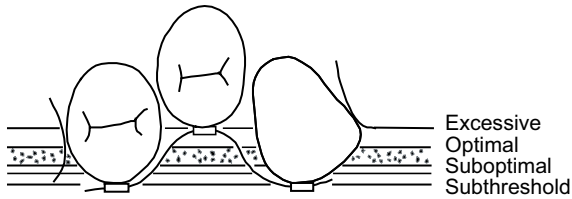

1.7 An elastic orthodontic wire with a low elastic modulus. Optimal force zone is present over a larger range than that of the wire with a high elastic modulus.

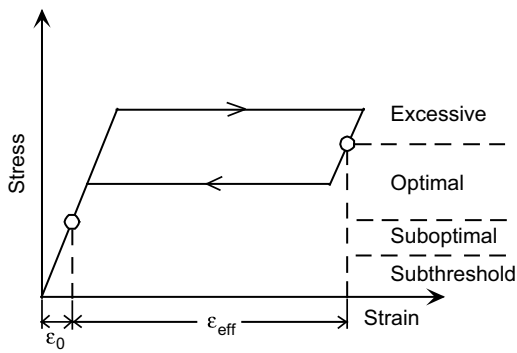

1.8 A schematic stress–strain curve of a superelastic Ti–Ni wire. Effective strain range corresponding to the optimal force zone is larger than that of an elastic wire.

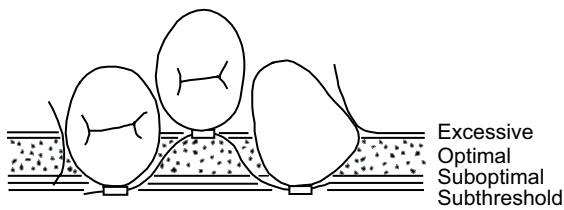

1.9 A superelastic Ti–Ni wire with an optimal force zone presenting over a larger range than that of an elastic wire.

modulus material or a constant-force material, which introduces a few orthodontic treatments named ‘variable constant-force’ orthodontics. Figure 1.8 shows the stress–strain curve of the superelastic wires. It can be seen that the effective strain range corresponding to the optimal force zone is ideally large. The corresponding clinical situation is shown in Fig. 1.9, where the optimal force range during deactivation covers almost the whole range of activation.

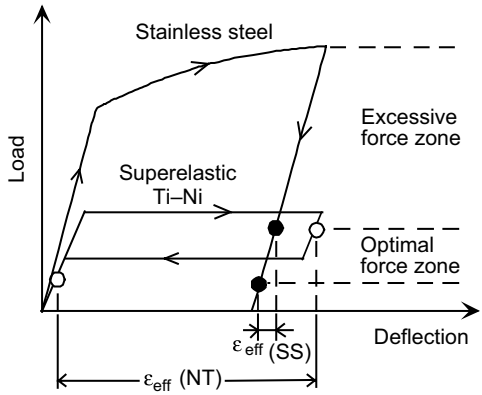

1.10 Schematic load–deflection curves representing the characteristics of stainless steel and superelastic Ti–Ni wires. Effective strain (or deflection) range corresponding to the optimal force zone is larger in the Ti–Ni wire than in the stainless-steel wire.

1.4 Superelasticity in clinical orthodontics

It is apparent that superelasticity presents the orthodontists with better mechanical characteristics when compared with conventional elastic materials. Comparison between the characteristics of a conventional elastic material and a superelastic Ti–Ni alloy is made in Fig. 1.10. However, even for the superelastic wire, there are still some small strain ranges that correspond to the application of excessive and suboptimal/subthreshold forces, which are associated with the initial and final stages of deactivation, respectively. In order to remove these strain ranges, the following two clinical approaches are proposed to orthodontists, based upon the principle of (1) force guided activation and (2) superposition.

Force guided activation involves overactivation of the superelastic orthodontic appliance to expand the optimal force zone by removing the excessive force zone in the initial stage of deactivation. As shown in Fig. 1.11, after conventional activation, the force locates at a closed circle point in the excessive force zone, the corresponding clinical situation being the same as in Fig. 1.9. However, after overactivation the force locates at an open circle point, which is in the optimal force zone. Therefore, the constant force can be applied to the dentition from the initial stage of treatment as shown in Fig. 1.12, in which no excessive force range exists.

The principle of superposition requires the superelastic orthodontic appliance to be overbent to eliminate the suboptimal force and subthreshold force zones during the final stage of deactivation. By overbending the arch wire in the opposite direction to the activation as shown in Fig. 1.13, the malaligned tooth reaches the desired position before the subthreshold force zone is reached. The corresponding stress–strain (or load–deflection) curve is shown in Fig. 1.14, where the starting

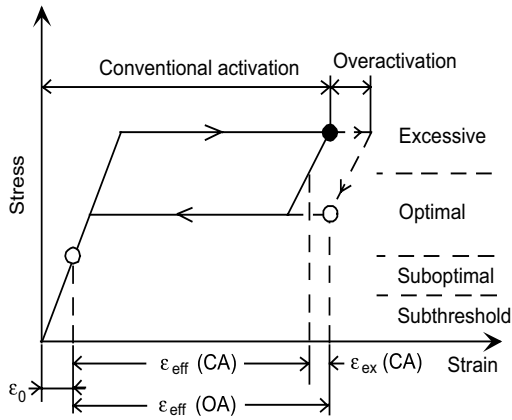

1.11 A schematic stress–strain curve of a superelastic Ti–Ni wire representing the effect of overactivation. Overactivation eliminates the excessive force zone, making the stress constant from the initial stage of deactivation.

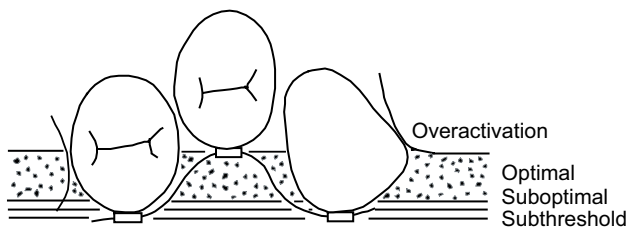

1.12 A superelastic Ti–Ni wire overactivated before it is inserted into brackets. Excessive force zone is eliminated.

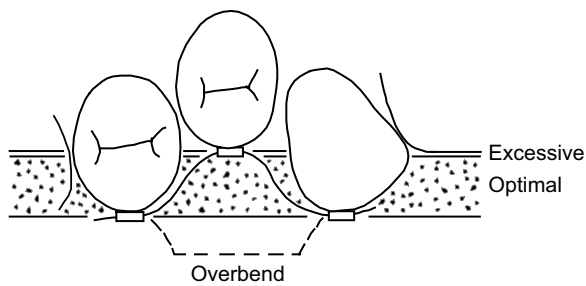

1.13 A superelastic Ti–Ni wire overbent before it is inserted into brackets. Suboptimal and subthreshold force zones are eliminated.

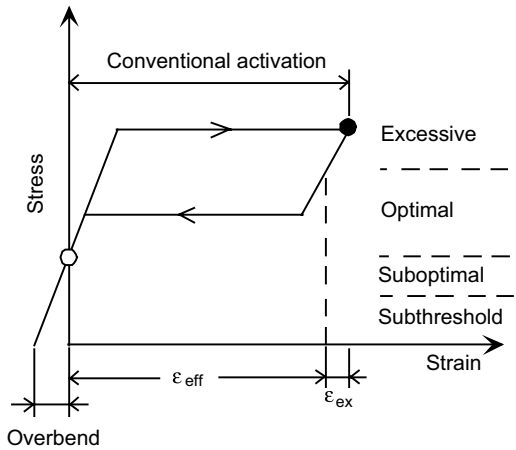

1.14 A schematic stress–strain curve of an overbent superelastic Ti–Ni wire. Effective strain range corresponding to the optimal force zone extends to the final stage of deactivation.

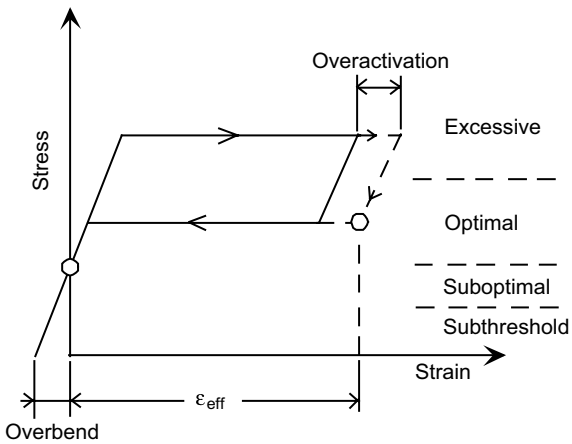

1.15 A schematic stress–strain curve of a superelastic Ti–Ni wire which was overactivated and overbent. Effective strain range corresponding to the optimal force zone extends to the initial and final stages of deactivation.

point of activation is shifted to the minus region of strain (or deflection) and the origin corresponds to the desired position for the tooth.

By applying these two principles (1) force guides activation and (2) superposition in conjunction, the optimal force zone will extend to the initial and final stages of deactivation, the stress–strain curve and clinical situation being shown in Fig. 1.15 and 1.16, respectively.

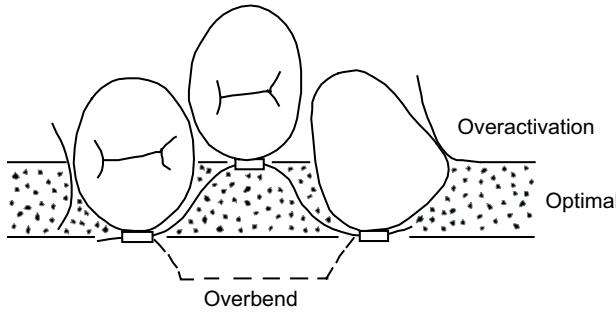

1.16 A superelastic Ti–Ni wire which was overactivated and overbent before being inserted into brackets. Excessive, suboptimal and sub-threshold force zones are eliminated.

1.5 Superelasticity characteristics

As described earlier, superelasticity is characterized by a constant stress (or force) and a large reversible deformation. A schematic stress–strain curve demonstrating ideal superelasticity is shown in Fig. 1.17. Upon activating the superelastic wire, the elastic deformation of the parent phase (austenitic phase) appears, being characterized by a linear relationship between stress and strain and its elastic modulus being defined by the slope (E_P). Upon further activation, the superelastic deformation appears under a constant stress (σ_M).

Since the superelastic deformation is associated with the martensitic transformation, which is a crystal structural change from the parent phase to the martensitic phase, the whole arch wire will be in the martensitic phase at the final stage of the superelastic deformation. Therefore, the elastic deformation of the martensitic phase appears in the initial stage of deactivation, its elastic modulus being defined by the slope (E_M). Upon further deactivation, the superelastic shape recovery occurs under a constant stress (σ_R) so that its elastic modulus or the slope (E_S) is zero. Since the superelastic shape recovery is associated with the reverse transformation from the parent phase to the martensitic phase, the arch wire will be in the parent phase at the final stage of superelastic shape recovery. In the final stage of deactivation, therefore, the shape recovery occurs elastically in the parent phase, the slope being again E_P.

As superelastic deformation is associated with the martensitic transformation instead of with conventional elastic or plastic deformation, this deformation behavior is strongly dependent on deformation temperature. Stress–strain curves of superelastic wire with a diameter of 0.018 inch are shown for various test temperatures in Fig. 1.18. The stresses for the superelastic deformation (σ_M) and superelastic reverse deformation (σ_R) increase with increasing test temperature. These stresses are shown in Fig. 1.19 as a function of temperature. The strong temperature dependence of the stress results in periodic shifts in the load applied

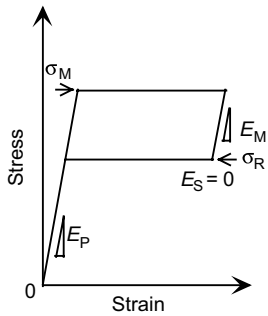

1.17 A schematic stress–strain curve representing superelastic characteristics, i.e. three elastic moduli for three states, i.e. the parent, martensitic and superelastic states, and two critical stresses for activation and deactivation.

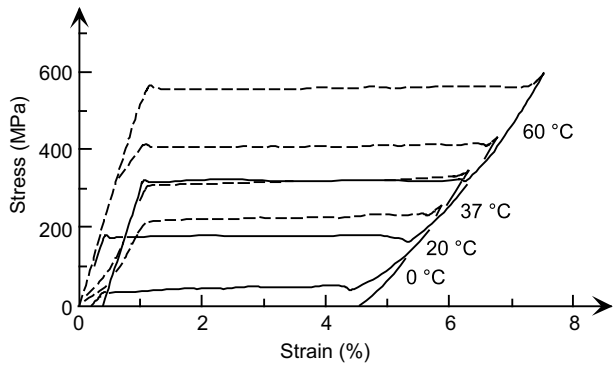

1.18 Stress–strain curves obtained by tensile deforming at various temperatures.

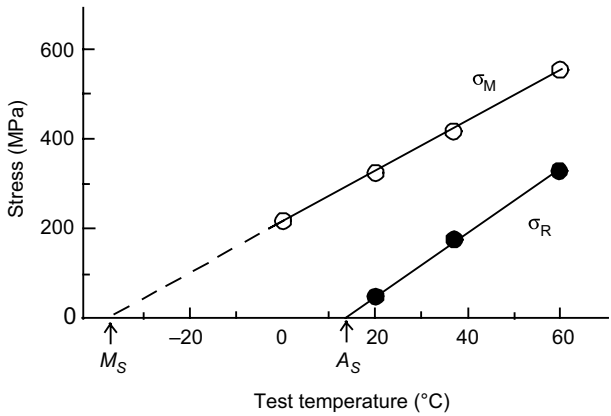

1.19 Temperature dependence of the critical stresses for activation and deactivation.

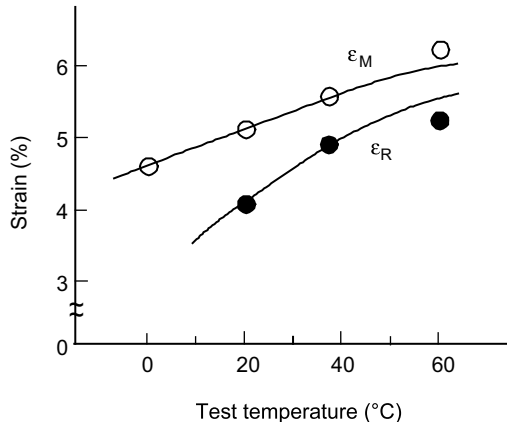

1.20 Temperature dependence of superelastic strains induced during activation and deactivation.

to the dentition as temperature changes in the mouth due to ingestion of various food types. It has been suggested that the thermally induced load-changes may stimulate teeth to move faster.

Extrapolation of these relationships in Fig. 1.19 to zero stress will roughly determine the martensitic transformation and reverse martensitic transformation temperatures, i.e., M_S for the former and A_S for the latter cases, respectively.

We can also see that the superelastic strains both upon activation (ε_M) and deactivation (ε_R) depend on test temperature and they also increase with increasing test temperature as shown in Fig. 1.20, where the strains are shown as functions of temperature, respectively.

1.6 Extrapolation factors affecting superelasticity

In orthodontic therapy, it is very important for orthodontists to be able to use a variety of forces (or stresses) produced by orthodontic appliances. In order to vary the force produced by a superelastic wire at a specific temperature such as the mouth temperature, it is necessary to change the transformation temperatures.

Figure 1.21 shows schematic stress–strain curves of superelastic wires with different transformation temperatures, the deformation temperature (T) being the same. Stresses for superelastic shape recovery in each case are shown in Fig. 1.22(a), (b) and (c) by each linear line as a function of deformation temperature. The reverse martensitic transformation temperature (A_{S1}, A_{S2} or A_{S3}) for each case can be obtained by extrapolating the line to zero stress. It is understood that, at the same deformation temperature (T), the stress increases with decreasing reverse transformation temperature.

There are several manufacturing and metallurgical factors affecting the

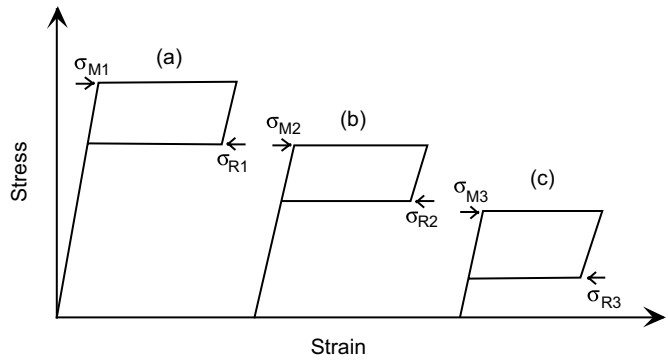

1.21 Schematic stress–strain curves of superelastic Ti–Ni wires with different reverse-transformation temperatures which were deformed at the same temperature.

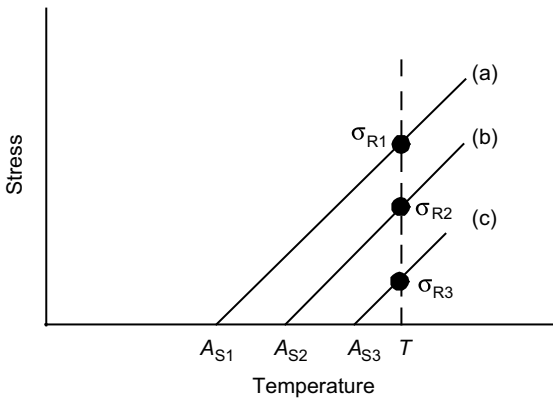

1.22 Temperature dependence of the stress for deactivation in specimens with different reverse-transformation temperatures.

transformation temperatures and superelasticity characteristics, among which Ni-content, annealing temperature, cold working ratio and third element addition are most important (Miyazaki *et al.*, 1982). In the following, the effects of Ni-content and annealing temperature will be described.

Figure 1.23 shows the effect of Ni-content on the superelastic deformation behavior, and the corresponding reverse transformation temperature is also shown in the parenthesis. The specimens were annealed at 400 °C and tensile tested at 37 °C. Both the stresses for superelastic deformation and superelastic reverse deformation increases with increasing Ni-content, since the reverse transformation temperature decreases with increasing Ni-content.

Figure 1.24 shows the effect of annealing temperature on the superelasticity characteristics, i.e., stress–strain curve and the reverse transformation temperature. The composition of the specimens was Ti-50.9at%Ni and these specimens were

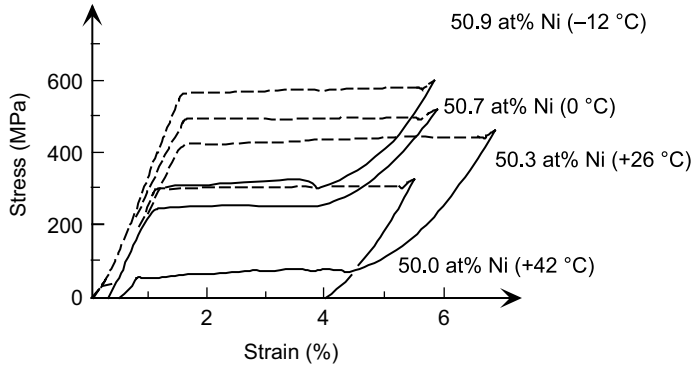

1.23 Stress–strain curves of superelastic Ti–Ni wires with various Ni concentrations which were deformed at 37 °C, annealing temperature being 400 °C. The reverse-transformation temperatures are shown in the parentheses.

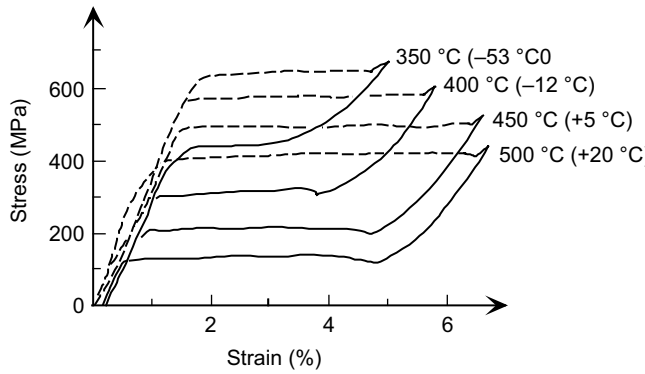

1.24 Effect of annealing temperature on the stress–strain curve of Ti–50.9at%Ni alloy which was deformed at 37 °C. The reverse-transformation temperature is shown in the corresponding parentheses.

tensile tested at 37 °C. Both the stresses for superelastic deformation and superelastic shape recovery increase with decreasing annealing temperature, and the reverse transformation temperature decreases with decreasing annealing temperature.

The effect of annealing temperature is important in orthodontic mechanotherapy and is explained by the following. The fact that the stress for superelastic shape-recovery in wires with the same composition changes depending on annealing temperature means that the force produced in a single orthodontic arch wire can be varied in various segments of the arch wire by annealing the segments at different temperatures (Sachdeva *et al.*, 1990). The stress–strain curves of a superelastic Ti–Ni wire annealed at different temperatures in two segments is shown in Fig. 1.25, where the stress–strain curve exhibits two plateaus, i.e., two superelastic

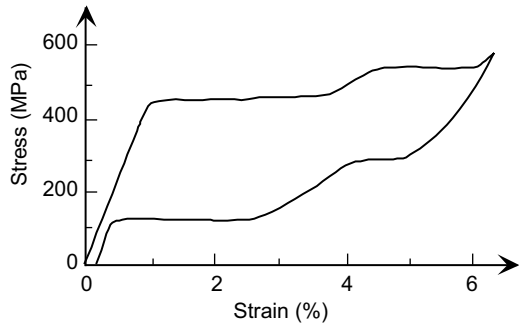

1.25 A stress–strain curve of a superelastic Ti–Ni wire representing two superelastic deformations at different stresses.

deformations at higher and lower stresses in the wire. This orthodontic approach using only a single orthodontic archwire with different forces in its various segments is termed 'single arch-wire, variable constant-force' orthodontics.

1.7 Conclusions

In this chapter, the basic characteristics such as the shape memory effect and superelasticity of shape memory alloys are explained with emphasis on superelastic behavior. The use of the superelastic Ti–Ni alloys offers 'variable constant-force' orthodontics and other medical treatments. The characterization of the superelasticity and the manufacturing and metallurgical factors for developing the superelastic Ti–Ni alloys are reviewed. The superelasticity of Ti–Ni alloys generates a constant force and a large shape recovery over a long activation span. The magnitude of force is temperature sensitive and either increases or decreases in response to thermal changes in the oral and physical environment. Manufacturing and metallurgical factors have a significant effect on the nature of forces generated by the superelastic Ti–Ni alloys, i.e., the constant force increases with increasing Ni-concentration or decreasing annealing temperature. We can expect further improvement for the superelasticity characteristics by adding third and fourth elements, such as a narrow stress hysteresis or flexible and rigid behavior.

1.8 References

Andreasen G F and Hilleman T B (1971), 'An evaluation of 55 cobalt substituted nitinol wire for use in orthodontics', *J. Am. Dent. Assoc.*, **82**, 1373–1375.

Andreasen G F and Morrow R E (1978), 'Laboratory and clinical analysis of nitinol wire', *Am. J. Orthod.*, **73**, 142–151.

Buehler W J, Gilfrich J V and Weiley K C (1963), *J. Appl. Phys.*, **34**, 1463.

Burstone C J (1981), 'Variable-modulus orthodontics', *Am. J. Orthod.*, **80**, 1–16.

Burstone C J, Qin B and Moton J Y (1985), 'Chinese NiTi wire: a new orthodontic alloy', *Am. J. Orthod.*, **87**, 445–452.

Miura F, Mogi M, Ohura Y and Hamanaka H (1986), 'The super-elastic property of the Japanese NiTi alloy wire for use in orthodontics', *Am. J. Orthod. Dentofac. Orthop*., **90**, 1–10.

Miyazaki S, Otsuka K and Suzuki Y (1981), 'Transformation pseudoelasticity and deformation behavior in a Ti-50.6at%Ni alloy', *Scripta Metall.*, **15**, 287–292.

Miyazaki S, Ohmi Y, Otsuka K and Suzuki Y (1982), 'Characteristics of deformation and transformation pseudoelasticity in Ti–Ni alloys', *J. Phys*., **43**, Suppl. 12, C4-255–260.

Miyazaki S, Kimura S, Otsuka K and Suzuki Y (1983), 'Shape memory effect and pseudoelasticity in a Ti–Ni single crystal', *Scripta Metall*., **18**,1057–1062.

Miyazaki S and Otsuka K (1984), 'Mechanical behavior associated with the premartensitic rhombohedral-phase transition in a Ti50–Ni47–Fe3 alloy', *Phil. Mag. A*, **50**, 393–408.

Miyazaki S, Kimura S, Otsuka K and Suzuki Y (1984), 'The habit plane and transformation strains associated with the martensitic transformation in Ti–Ni single crystals', *Scripta Metall.*, **18**, 883–888.

Miyazaki S, Igo Y and Otsuka K (1986), 'Effect of thermal cycling on the transformation temperatures of Ti–Ni alloys', *Acta Metall*., **34**, 2045–2051.

Miyazaki S and Otsuka K (1986), 'Deformation and transformation behavior associated with the R-phase in Ti–Ni alloys', *Metall. Trans. A*, **17**, 53–63.

Miyazaki S and Wayman C M (1988), 'The R-phase transition and associated shape memory mechanism in Ti–Ni single crystals', *Acta Metall*., **36**, 181–192.

Miyazaki S, Kimura S and Otsuka K (1988), 'Shape memory effect and pseudoelasticity associated with the r-phase transition in Ti–50.5at%Ni single crystals', *Phil. Mag. A*., **57**, 467–478.

Miyazaki S, Otsuka K and Wayman C M (1989), 'The shape memory mechanism associated with the martensitic transformation in Ti–Ni alloys', *Acta Metall*., **37**, 1873–1890.

Miyazaki S (1990), 'Thermal and stress cycling effects and fatigue properties in Ti–Ni alloys', *Engineering Aspects of Shape Memory Alloys*, ed. by Duerig T W *et al.*, Butterworth–Heinemann, 394–413.

Miyazaki S, Oshida Y and Sachdeva R (1990), 'Characterization and development of superelastic Ni–Ti alloys for orthodontic applications', Int. Conf. On Medical Application of Shape Memory Alloys, Shanghai, 170–183.

Ohura Y (1984), 'Orthodontic studies on super elastic NiTi wire. 1: Mechanical properties', *J. Jpn. Orthod. Soc*., **43**, 71–80.

Sachdeva R and Miyazaki S (1988), 'Application of shape memory nickel-titanium alloys to orthodontics', *Proc. Int. Mtg. Adv. Mater.*, **9**, 605–610.

Sachdeva R, Fukuyo S, Suzuki K, Oshida Y and Miyazaki S (1990), 'Shape memory NiTi alloys – applications in dentistry', *Proc. Inter. Conf. Martensitic Transformations*, ICOMAT-89, Sydney, 693–698.

Sachdeva R and Miyazaki S (1990), 'Superelastic Ni–Ti alloys in orthodontics', *Engineering Aspects of Shape Memory Alloys*, ed. by Duerig T *et al.*, Butterworth–Heinemann, 452–469.

Takei F, Miura T, Miyazaki S, Kimura S, Otsuka K and Suzuki Y (1983), 'Stress-induced martensitic transformation in a Ti–Ni single crystal', *Scripta Metall*., **17**, 987–992.

2

Mechanical properties of shape memory alloys

H. HOSODA and T. INAMURA
Tokyo Institute of Technology, Japan

Abstract: Mechanical behavior of shape memory alloys and related deformation mechanisms are described: shape memory effect, superelasticity, elastic deformation, reorientation of martensite variants, stress-induced martensite formation and plastic deformation. The importance of strengthening to enhance shape memory effect is explained from the viewpoint of competition of deformation mechanisms. Stress–strain curves, strain–temperature curves, two-way shape memory effect, multistage martensitic transformation and effects of thermomechanical treatment and texture formation on mechanical behavior are also described for the comprehensive understanding of mechanical properties of shape memory and superelastic alloys.

Key words: superelastic alloys, shape memory, Ni–Ti, Ti–Ni, Nitinol, deformation mechanism.

2.1 Introduction

In this chapter, mechanical properties of shape memory alloys (SMAs) are described. SMAs are used in devices such as rice cookers, coffee makers and air conditioners.[1] It is commonly known that, after deformation, the original shape of a SMA can be simply regained by heating using a lighter or hot water. The origin of shape memory effect is a thermoelastic martensitic transformation by changing temperature. As already described in Chapter 1, the deformation behavior of SMAs depends on a complex relationship between the martensitic transformation temperatures, ambient temperature and strength, and it is classified into three: shape memory effect, superelasticity and permanent plastic deformation. When the martensitic transformation temperatures are slightly lower than the applied temperature of SMA, and when the material is sufficiently strong against slip deformation, superelasticity appears. Superelasticity is a large reversible deformation exceeding the usual elastic limit. The origin of the superelasticity is the forward and reverse stress-induced martensitic transformation (SIMT), that is, thermoelastic martensitic transformation by applied stress. Large reversible strain, usually more than a few percent, is generated and the material is shape-recovered by unloading only without the need for heating. In addition, in the superelastic deformation, the stress–strain relationship is nonlinear and does not obey Hooke's law. The apparent Young's modulus during superelastic deformation is nearly

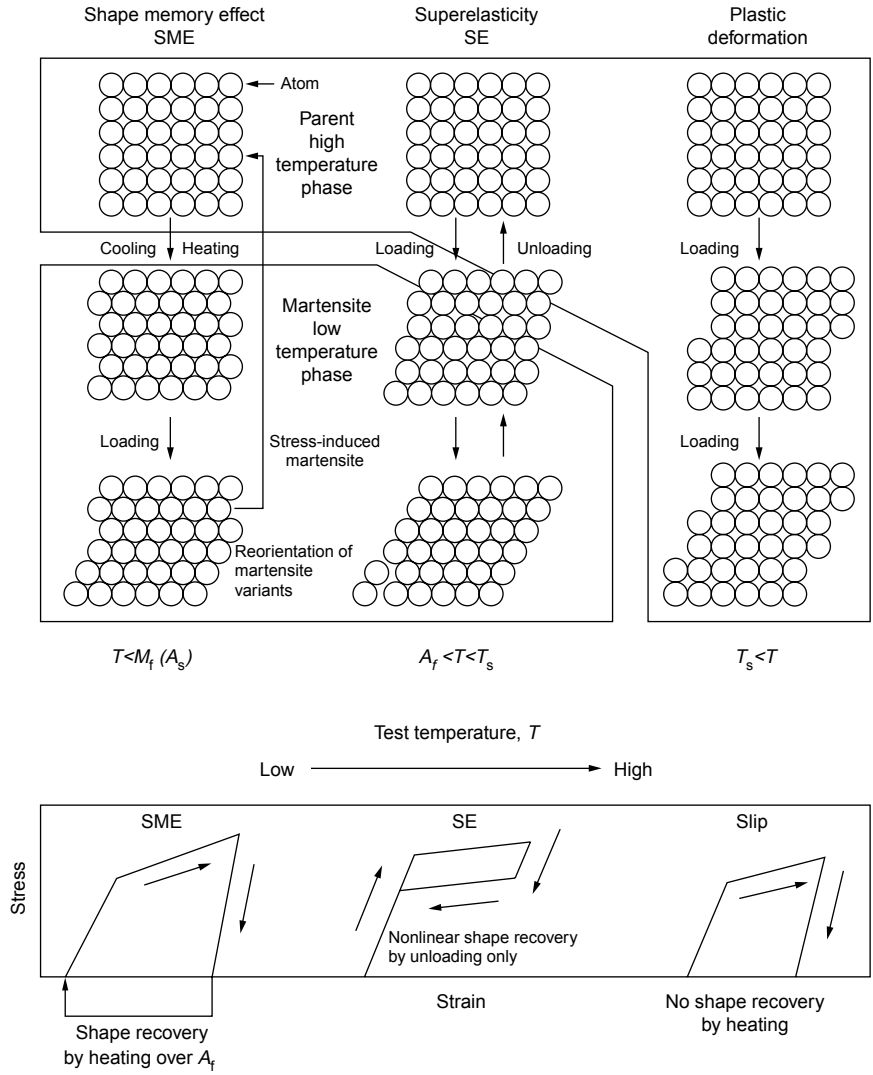

2.1 Schematic illustrations of atomic configurations and stress–strain curves of a shape memory alloy at three typical temperatures (M_f martensitic transformation finish temperature, A_s austenite transformation start temperature, A_f austenite transformation finish temperature, T_s maximum temperature for inducing martensite).

zero. Thus, the superelastic wires are very soft and flexible, and find application as brassière wires, antennas of cellular phones, eyeglass frames, fishing lines and so on. Their usefulness is partially because the retaining force is almost constant regardless of deformation strain. In recent years, superelastic alloys became widely applied in biomedical applications such as orthodontic wires and stents.

However, if the martensitic transformation temperature is much lower than ambient temperature, either the shape memory effect or the superelasticity does not appear. In this case, normal permanent plastic deformation is the result. Thus, the mechanical behavior of SMAs is classified into three types depending on both applied temperature and martensitic transformation temperatures: (1) shape memory effect, (2) superelasticity and (3) permanent plastic (slip) deformation. In order to use SMAs and superelastic alloys effectively, a comprehensive understanding of mechanical properties is quite important in connection with these temperatures. The schematic illustrations of atomic configuration and stress–strain curves of SMAs are shown in Fig. 2.1.

2.2 Stress–strain curves

Figure 2.2(a), a temperature–stress diagram of a SMA, shows four martensitic transformation lines, M_s, M_f, A_s and A_f, and three kinds of stress lines. The critical stress for slip deformation σ_{SLIP}, the stress for starting reorientation of martensite variants σ_s^{RMV}, and the stress for finishing reorientation of martensite variants σ_f^{RMV}. The change in M_s, M_f, A_s and A_f, by applied stress obeys the Clausius–Clapeyron equation. When a material is a parent phase state at a temperature T under stress-free conditions, and the material is transformed into the martensite state by an applied stress σ, the relationship between σ and T can be written as,

$$\begin{aligned} d\sigma/dT &= -\Delta S^{P-M}/\varepsilon^{P-M} \\ &= -\Delta H^{P-M}/T\,\varepsilon^{P-M} \end{aligned} \quad [2.1]$$

where ΔS^{P-M} is the entropy change from the parent to the martensite, ΔH^{P-M} is the enthalpy change from the parent to the martensite, and ε^{P-M} is the strain caused by the transformation. Here, the entropy change ΔS^{P-M} is a constant negative value in this case, and the transformation strain ε^{P-M} is a constant positive value in the material. Then, the value of $-\Delta S^{P-M}/\varepsilon^{P-M}$ is usually a constant positive value.

Based on the temperature–stress diagram in Fig. 2.2(a), the temperature region of SMAs is classified into five: $T<M_f$, $M_f<T<A_s$, $A_s<T<A_f$, $A_f<T<T_s$ and $T_s<T$.

2.2.1 $T<M_f$ (shape memory effect)

The apparent phase is the martensite. As an external stress σ is applied to the material, firstly, elastic deformation occurs. With further increasing σ, the reorientation of martensite variants (RMV) starts when σ reaches σ_s^{RMV}. RMV is a kind of twin deformation, and RMV is continuously taken place with increasing σ. If σ is unloaded, the shape change by the reorientation is kept, and the strain can be recovered to the original shape by heating over A_f. This is the shape memory effect. When σ reaches to σ_f^{RMV}, almost all the material becomes a single variant state. At the single variant state, no further deformation can take place by RMV. This state corresponds to the maximum shape recovery strain. When σ exceeds σ_f^{RMV},

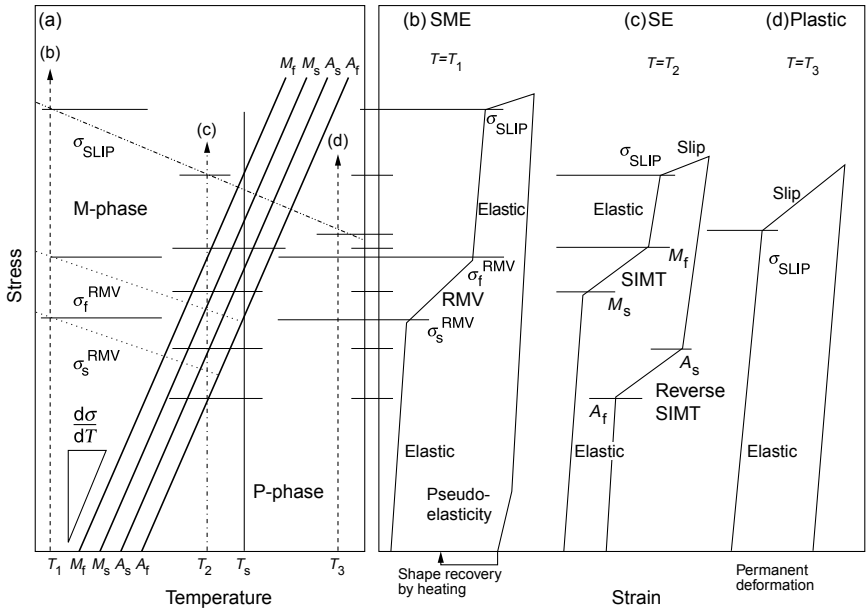

2.2 Schematic temperature–stress diagram showing (a) phase equilibrium in a shape memory alloy, and corresponding stress–strain curves at (b) $T=T_1$ for SME, (c) $T=T_2$ for SE and (d) $T=T_3$ for plastic deformation. The horizontal lines express each stress level.

elastic deformation occurs in the single-variant martensite. When σ reaches to σ_{SLIP}, plastic deformation by dislocation slip occurs. Plastic deformation by dislocation is irreversible, similar to plastic deformation of common metals and alloys. After unloading and heating up to A_f, shape recovery occurs but some amount of residual plastic strain remains. After a severe deformation, a small amount of pseudoelasticity sometimes appears during unloading. The pseudoelasticity is a nonlinear shape recovery caused by a twin deformation of martensite variants due to the formation of an internal stress field made by highdensity dislocations. The corresponding stress–strain curves at $T=T_1$ is shown in Fig. 2.2(b).

2.2.2 $M_f<T<A_s$ (shape memory effect)

In this temperature range, the stable phase is either (or both) the martensite or the parent, and usually both phases appear in a sample. With increasing applied stress, RMV starts at σ_s^{RMV} in the martensite phase of the specimen, and simultaneously, SIMT starts at M_s line in the parent phase region of the specimen. Usually, both RMV and SIMT occur together. When the whole sample becomes the martensite single phase, the martensite is stable and does not transform into the parent phase

even if the applied force is removed. Then, the stress–strain curve of SMAs in this temperature region is similar to that at $T<M_f$ in 2.2.1. Thus, the stress–strain curve in this case is omitted in the figure.

2.2.3 $A_s<T<A_f$ (mixture of shape memory effect and superelasticity)

In this temperature range, the apparent phase is the parent phase when cooling from a solution or ageing treatment temperature down to the ambient temperature. When increasing applied stress, SIMT starts at the M_s line and finishes at the M_f line. Then the whole sample becomes the stress-induced martensite. On the other hand, with decreasing applied stress, the reverse martensitic transformation starts at the A_s line and superelastic shape recovery occurs at the same time. However, the reverse martensitic transformation never finishes because the A_f line at this temperature is lower than zero stress. In other words, the area of the martensite phase formed by the applied stress partially remains in the specimen even after removing the applied stress. This remaining martensite area can be transformed into the parent phase by heating above A_f, in a similar way to that described in Section 2.2.2. This is the shape memory effect. Thus, the sample exhibits both superelastic shape recovery by unloading and shape memory effect by heating. This temperature range is relatively narrow, and the mechanical behavior is not used for practical applications. A stress–strain curve at the temperature range is omitted in Fig. 2.2 for the sake of simplicity.

2.2.4 $A_s<T<T_s$ (superelasticity)

In a similar way to the shape memory effect, elastic deformation occurs firstly by applied stress. When σ reaches the M_s line, SIMT starts and deformation strain appears due to the formation of preferentially oriented martensite variants. By unloading, the shape recovery occurs at the intersection of the A_s line due to the reverse martensitic transformation, and finishes at the intersection of the A_f line. This is superelasticity. The turning points in the stress–strain curve correspond to the forward and reverse martensitic transformation under the applied stresses. If σ exceeds the intersection of the M_f line, almost all the material becomes a single variant state, and elastic deformation followed by plastic deformation of single variant martensite takes place. After plastic deformation has been introduced, shape recovery partially takes place and some amount of residual strain remains. The corresponding stress–strain curves at $T=T_2$ are shown in Fig. 2.2(c).

2.2.5 $T_s<T$ (plastic deformation)

When the temperature is higher than T_s, SIMT cannot take place but plastic deformation occurs by slip. This is because σ does not reach the M_s line before

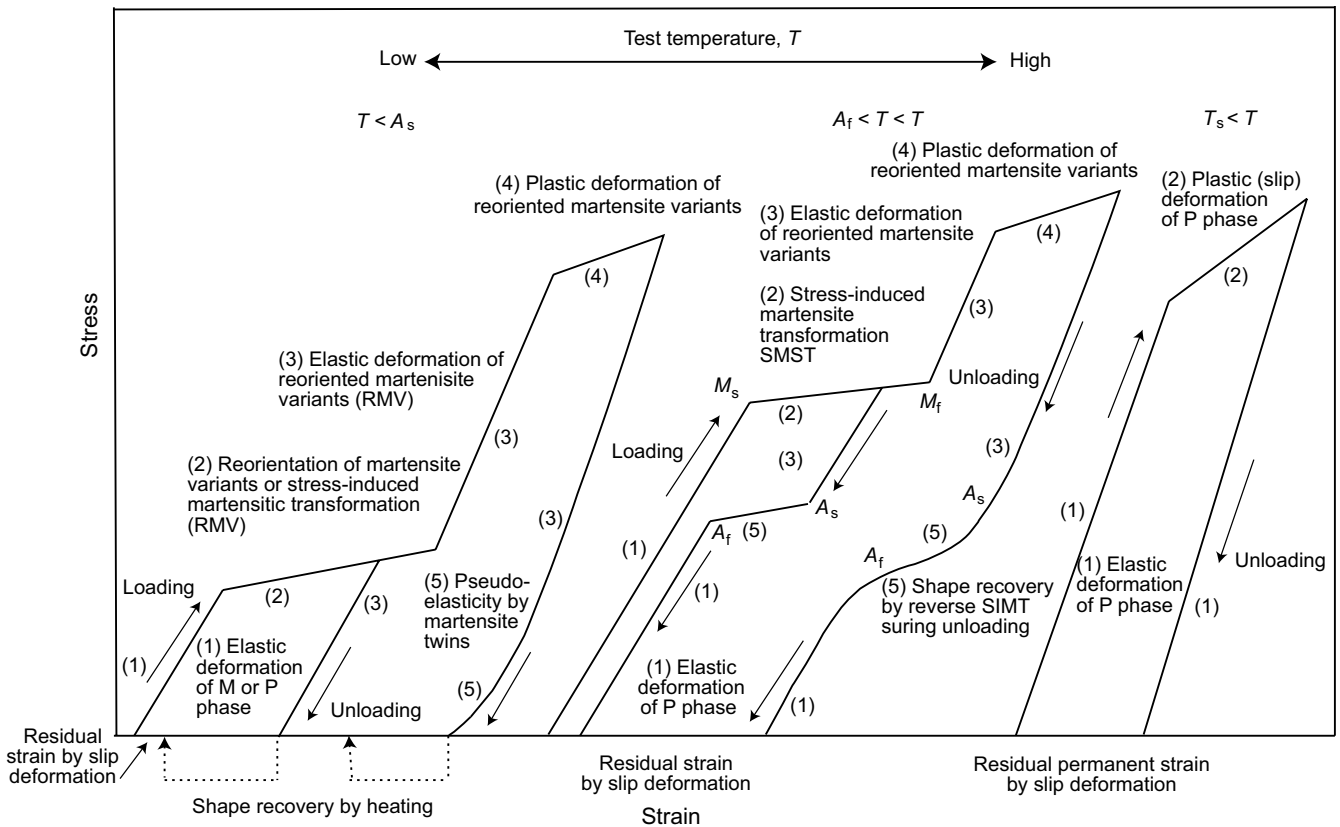

2.3 Stress–strain curves of a shape memory alloy and corresponding deformation mechanisms at three typical temperatures: $T<A_s$, $A_f<T<T_s$ and $T_s<T$.

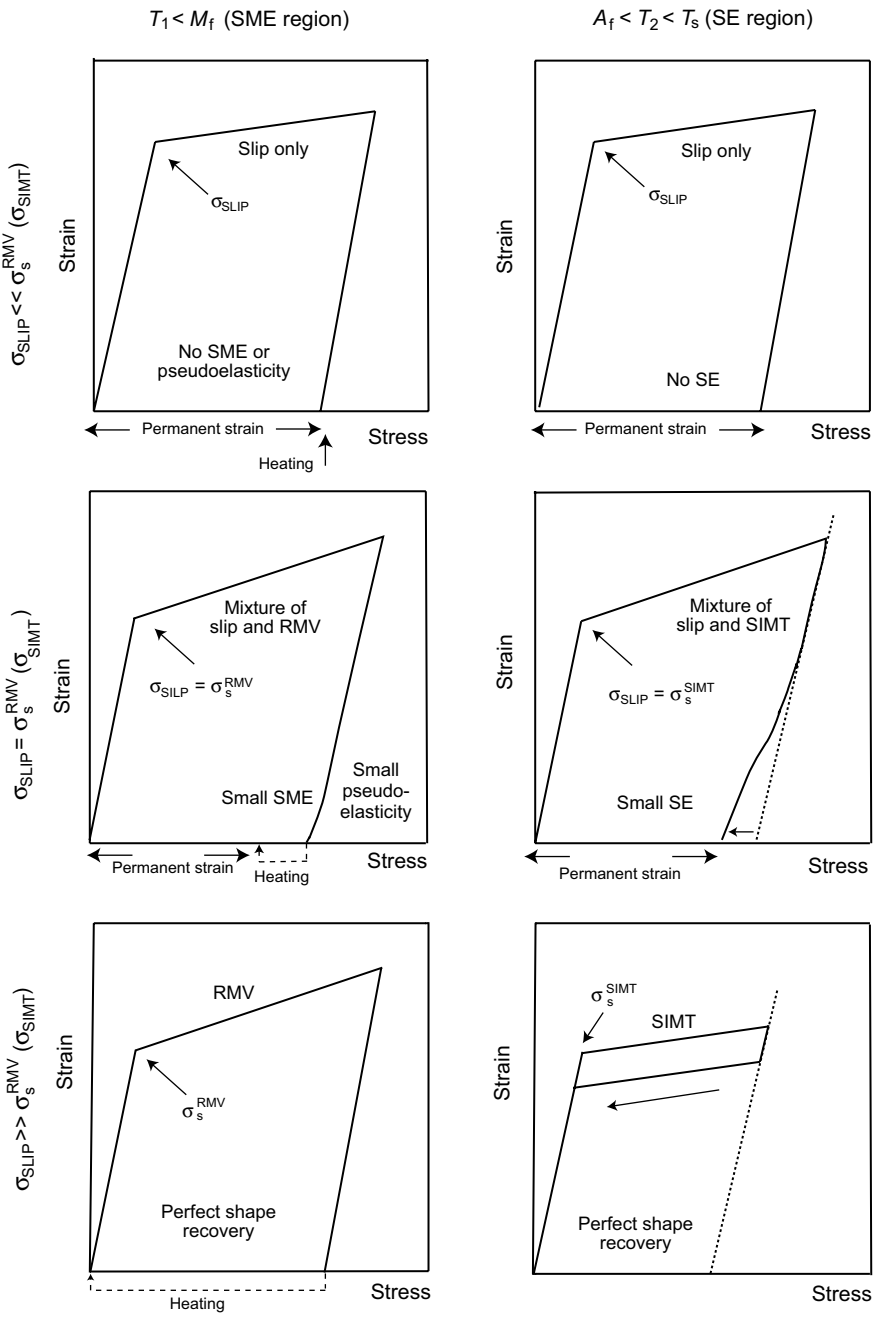

2.4 Stress–strain curves of shape memory alloy depending on the relationships between σ_{SLIP} and $\sigma_s^{RMV}(\sigma_{SIMT})$.

σ_{SLIP}. Thus, neither the shape memory effect nor superelasticity appears. The corresponding stress–strain curve is shown in Fig. 2.2(d). The deformation mechanisms above are summarized in Fig. 2.3.

2.3 Stabilization of shape memory effect and superelasticity

As described above, σ_{SLIP} is one of the important factors that determines the deformation behavior of SMAs, and σ_{SLIP} is not a material constant but a variable factor. Thus, σ_{SLIP} is effective in stabilizing and enhancing the shape memory effect and superelasticity of SMAs without inhibiting the deformation attributed to martensitic transformation. It is easily understood that, if the σ_{SLIP} line drifts upwards (that is, hardening) as shown in Fig. 2.2(a), the temperature range for the appearance of superelasticity simultaneously increases. This is because T_s, which stands for the temperature at the intersection of σ_{SLIP} and A_f lines, moves to the right in Fig. 2.2(a). Conversely, if the σ_{SLIP} line drifts downwards (that is softening), deformation by slip and by reorientation of martensite variants occurs simultaneously and a large amount of unrecoverable strain is introduced. Therefore, the increase in slip deformation leads to the reduction of residual unrecoverable strain. The stress–strain curves of SMAs at T_1 ($T_1<M_f$) and T_2 ($A_f<T_2<T_s$) are shown in Fig. 2.4 where three types of σ_{SLIP} are selected: $\sigma_{SLIP} << \sigma_s^{RMV}(\sigma_{SIMT})$, $\sigma_{SLIP} = \sigma_s^{RMV}(\sigma_{SIMT})$ and $\sigma_{SLIP} >> \sigma_s^{RMV}(\sigma_{SIMT})$. In order to increase σ_{SLIP}, material hardening can be achieved by the following methods:

1 Solid solution hardening
2 Precipitation hardening
3 Work hardening
4 Grain size refinement.

For Ti–Ni alloys, material hardening is achieved industrially by precipitation hardening due to Ti_3Ni_4 formation (especially for superelastic Ti–Ni with a Ni content higher than 50.5 mol%) as well as work hardening by cold working with 20–40% of area reduction for both shape memory and superelastic Ti–Ni.[2] It is noted that, after work hardening is applied, an intermediate-temperature heat treatment at around 600–700 K is carried out for easy movement of martensite variants/stress-induced martensite without decreasing the high dislocation density. Grain size refinement is also effective but it is rarely used in practical applications because of the difficulty of severe cold work in Ti–Ni. Solution hardening by the addition of ternary elements is not used in practice, because martensitic transformation temperatures are changed by the ternary additions, and because there is a relatively low hardening rate amongst these strengthening mechanisms.

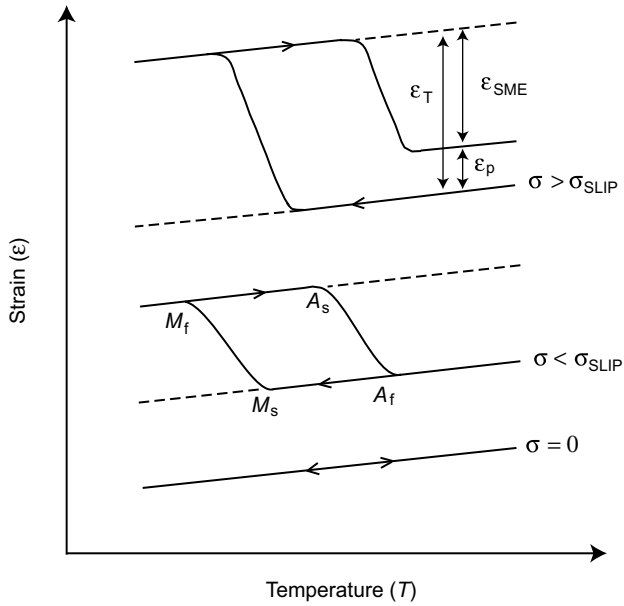

2.5 Strain–temperature curves under constant stresses (σ) of $\sigma = 0$, $\sigma < \sigma_{SLIP}$ and $\sigma > \sigma_{SLIP}$. ε_T, ε_{SME} and ε_p are the applied total strain, shape recovery strain and residual strain, respectively. Volume change of the transformation is neglected here.

2.4 Strain–temperature curves

In order to use the shape memory effect more effectively, the strain–temperature relationship of SMA under an external (bias) constant stress should be well understood. This is because SMAs are often used under cyclic deformation conditions with the bias stresses. Schematic strain–temperature curves are shown in Fig. 2.5, where tensile external stress σ is applied to the SMA: (1) $\sigma = 0$ (stress free), (2) $0 < \sigma < \sigma_{SLIP}$ and (3) $\sigma_{SLIP} < \sigma$. It is seen that, when σ is zero, no shape change except thermal expansion is observed by changing temperature. This is because of the self-accommodation mechanism of martensite variants. When σ is lower than σ_{SLIP}, no deformation except for elastic deformation is introduced at the parent state. In cooling down, tensile deformation strain appears at M_s and the deformation finishes at M_f owing to the formation of preferentially oriented martensite variants against σ. In heating up, shape recovery occurs at A_s and finishes at A_f owing to reverse martensitic transformation. In this case, perfect shape recovery is obtained because no slip deformation by dislocation is introduced. Such shape changes during thermal cycles can be utilized many times without degradation of macroscopic shape recovery. When σ is close to or higher than σ_{SLIP}, plastic deformation is also introduced in the material. In cooling down, shape change

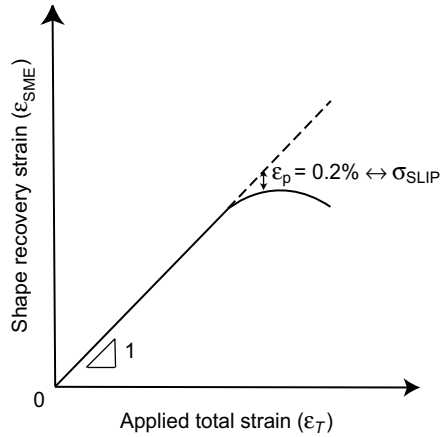

2.6 Relationship between shape recovery strain and applied total strain which are functions of the maximum applied stress. σ_{SLIP} is defined as the stress that introduces ε_p of 0.2%.

appears due to the formation of preferentially oriented martensite variants against σ, in a similar way. After heating up, shape recovery by shape memory effect has taken place, but the shape recovery is not perfect. Residual strain ε_p introduced by slip deformation remains. Thus, σ_{SLIP} is the highest stress in order to give a perfect shape memory effect, and σ_{SLIP} can be evaluated by the strain–temperature curves.

Figure 2.6 shows shape recovery strain ε_{SME} as a function of total applied strain ε_T obtained from strain–temperature curves under constant stresses. When the applied stress is sufficiently lower than σ_{SLIP}, ε_{SME} is equal to ε_T and proportionally increases with ε_T. With increasing ε_T, ε_{SME} reaches a maximum value and permanent unrecoverable strain is introduced; ε_{SME} decreases with further increases in ε_T. The degradation of shape recovery is the result of dislocations, which suppress the martensitic transformation and/or reorientation of martensite variants as obstacles. By using strain–temperature curves, σ_{SLIP} can also be estimated to be the applied stress by which the permanent strain (ε_p in Fig. 2.5) reaches 0.2%, or sometimes 0.5%. In order to prevent degradation of shape memory effect and fatigue failure, the applied (bias) stress should be controlled not to exceed the σ_{SLIP}.

2.5 Thermo-mechanical treatment

Figure 2.7 shows stress–strain curves of Ti–50.5at%Ni reported by Miyazaki and co-workers,[3] where the alloy was homogenized at 1273 K for 1 h and deformed at 77, 283, 296 and 473 K. Clear two-stage yielding phenomena were observed at 77 K and 296 K, due to reorientation of martensite variants. It is generally seen in SMAs that the deformation stress σ_s^{RMV} becomes higher with decreasing test temperature when the test temperature is below M_s: σ^{RMV} is higher at 77 K (around

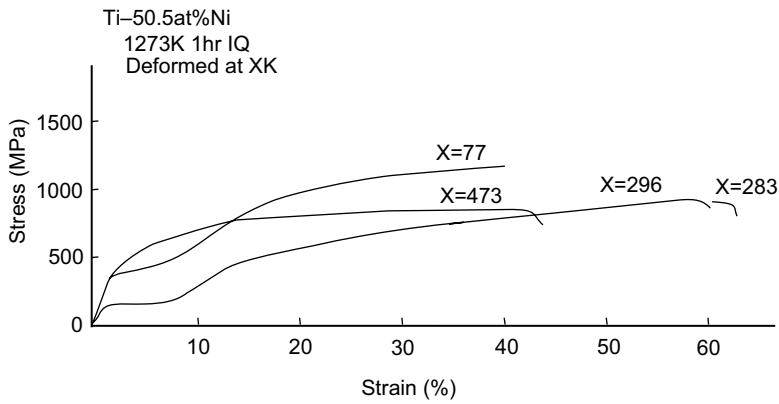

2.7 Stress–strain curves at 77 to 473 K in Ti–50.5at.%Ni samples homogenized at 1273 K for 3.6 ks.[3]

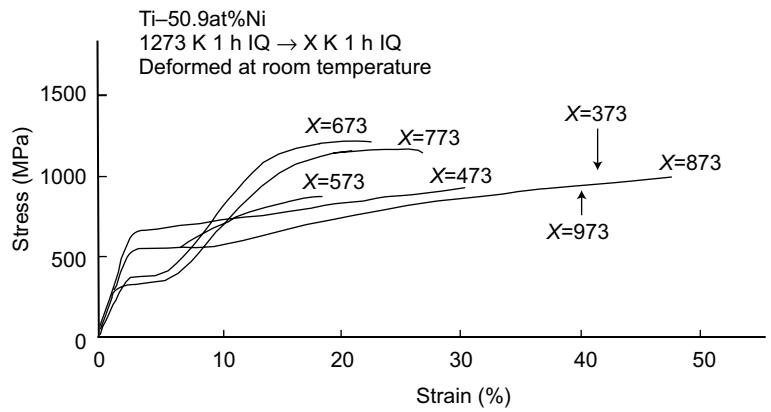

2.8 Stress–strain curves at room temperature in Ti–50.9at.%Ni samples age-treated at 373 to 973 K for 3.6 ks after solution treatment.[3]

150 MPa) than at 296 K (around 400 MPa). The minimization of σ^{RMV} is often seen near M_s. Moreover, the largest tensile elongation, around 60%, was obtained at 283 K. The enhancement of elongation is attributed to the strain generated by reorientation of martensite variants (or stress-induced martensite). However, at 473 K, such a two-stage yielding phenomenon was not seen. This is because the test temperature of 473 K is higher that T_s: the parent phase is always stable regardless of stress and strain. Plastic deformation by slip alone has occurred at this temperature; thus, neither shape memory effect nor superelasticity occurs at 473 K. The highest temperature for shape memory/superelastic deformation is around 370–380 K in Ti–Ni alloys.

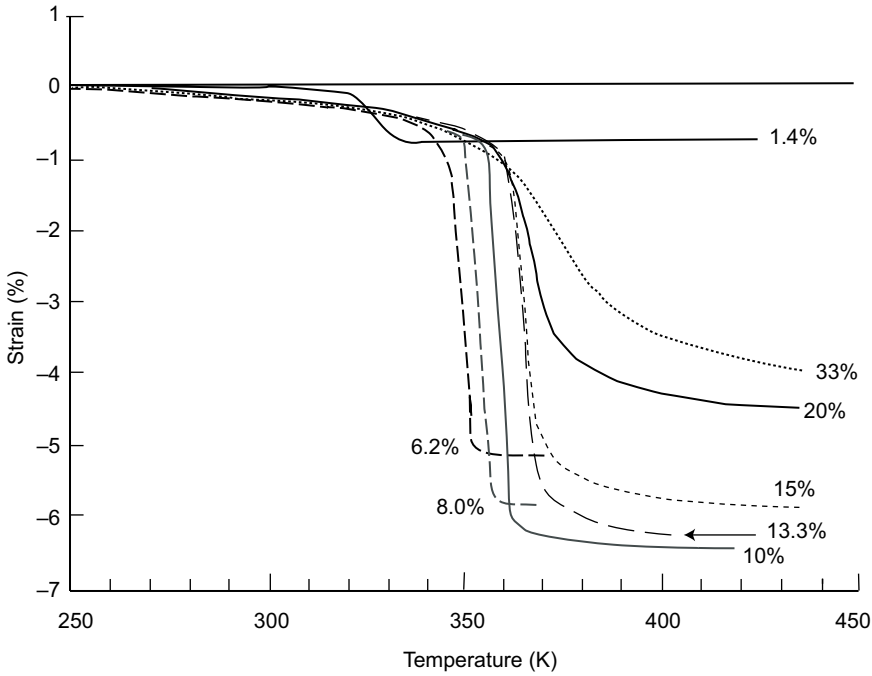

2.9 Effect of pre-deformation on the reverse transformation on the first heating.[4]

Figure 2.8 shows stress–strain curves of Ti–50.9at%Ni at room temperature where the Ti–Ni alloys were homogenized at 1273 K and aged at various temperatures.[3] It is obvious that the shapes of stress–strain curves are different depending on aging temperature even in the same composition. Two-step yielding phenomena as well as high ultimate tensile strength (over 1000 MPa) were clearly seen at the aging temperatures of 673 and 773 K. This is because Ti_3Ni_4 precipitates were formed at the intermediate temperatures around 673–773 K in the Ni-rich Ti–Ni, and the strengthening caused by aging is the precipitation hardening. On the other hand, such a two-step yielding was not seen for the other aging temperatures. Therefore, stabilization of shape memory effect can be achieved by the intermediate aging in this alloy.

Figure 2.9 shows shape recovery phenomena of Ti–Ni drawn in a strain–temperature diagram reported by Liu and co-workers,[4] where Ti–Ni was pre-deformed before testing. Shape recovery takes place at around 320–360 K during heating, and the shape recovery strain depends on the amount of pre-strain. The shape recovery temperature becomes higher with an increasing amount of prestrain as explained in Fig. 2.2(a) due to the development of the internal stress field formed by dislocations, and the number of dislocations increases with increasing pre-strain. The amount of shape recovery strain increases with an

increasing amount of pre-strain, reaches a maximum value around 6.5% by 10% of pre-strain, and decreases with further increases in the amount of pre-strain. The degradation of shape recovery by severe deformation is caused by introducing a large number of dislocations.

After introducing plastic deformation in the martensite state, a two-way shape memory effect (TWSME) often appears. Normal SMA exhibits a one-way shape memory effect, where the deformed material becomes the original shape by heating. In addition to this, in TWSME, a spontaneous shape change occurs from the original (parent phase) shape to the deformed shape (martensite phase) by cooling without applying external stress. In other words, the material with TWSME possesses two different shapes (high-temperature and low-temperature). The stabilization of a specific low-temperature shape is due to the existence of anisotropic internal stress. The anisotropic internal stress is generated in the martensite phase by a unidirectional severe deformation or a heat treatment to form anisotropic (or inhomogeneous) precipitations. In both instances, a preferentially oriented martensite variant instead of self-accommodated martensite variants is stabilized by the anisotropic dislocations and/or precipitates introduced. Thus, even though an external stress is not applied, a spontaneous shape change takes place during cooling due to the formation of preferential martensite variants. The anisotropic precipitates are often formed by a constrained aging in the martensite state. The TWSME is unique and simple, thus, it can be expected to have practical applications. However, TWSME is not used in practice, because the shape recovery force and strain during two-way shape change are relatively small in comparison with the usual one-way shape change and because the appearance of TWSME is often unstable. In addition, similar two-way shape change can be achieved in the usual one-way SMA, where external bias stress by coils and springs is used in the devices. The internal stress in TWSMA acts as the external bias force of one-way SMAs.

2.6 Multistage transformation

Figure 2.10 shows stress–strain curves of a Cu–Al–Ni SMA reported by Otsuka and Shimizu.[5] In this alloy, two-step stress-induced martensitic transformation occurs from γ_1 to β_1 and from β_1 to α_1 at T=223 K ($<M_f$), and from β_1 to β_1' and from β_1' to α_1' at T=354 K ($>A_f$), and reverse martensitic transformation takes place during unloading. The corresponding stress–temperature phase diagram is shown in Fig. 2.11. In such two-step martensitic transformations, two-step superelasticity is often similar to that shown in Fig. 2.9. The superelastic strain is relatively large in comparison with that of one-step transformations. However, such two-step superelasticity is not used in practical applications, partly because of the difficulty of precise control of the martensitic transformation.

For Ti–Ni, such a two-step transformation from martensite (M: B19' phase) phase to R-phase (R: rhombohedral structure) and from R to parent (P: B2 phase)

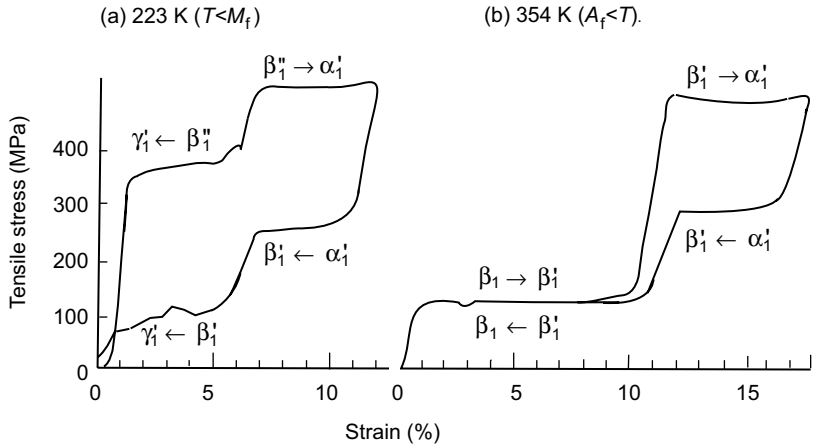

2.10 Two-step superelasticity by the two-step martensitic transformation for (a) $T<M_f$ and (b) $A_f<T$.[4]

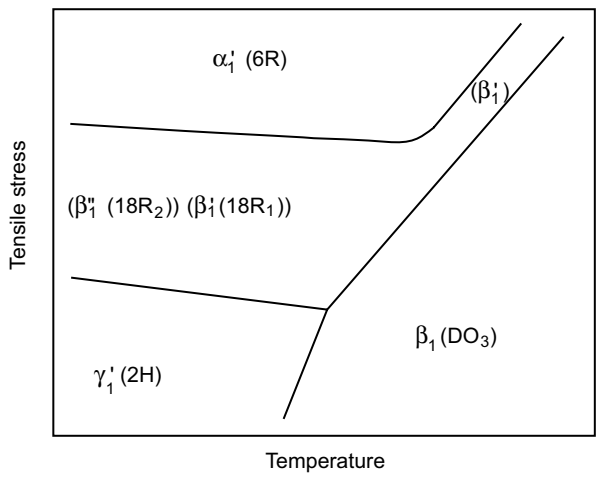

2.11 Stress–temperature diagram for the two-step martensitic transformation in Fig. 2.10.[5]

often appears in Ti–Ni alloys containing some ternary elements such as Fe, or Ti–Ni alloys with plastic deformation. The features of the R-phase transformation are small transformation hysteresis (a few Kelvin), low sensitivity of transformation temperature to change in applied stress (high $d\sigma/dT$ value) and small transformation strain (less than 1%). The stress–strain curves at various temperatures of a Ti–Ni alloy exhibiting multistage transformation between M–R–P are drawn in Fig. 2.12. In a similar way to Fig.2.10, two-step stress–strain curves are obtained when the R-phase appears. However, in many practical applications, only one-step

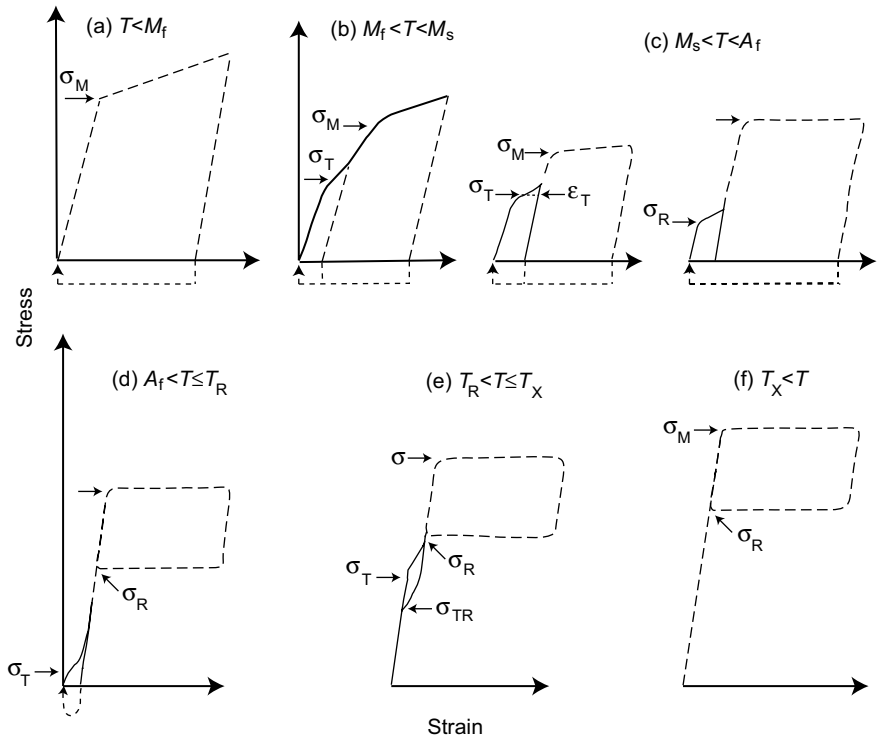

T: Test temperature
M_f: Martensite transformation finish temperature
M_s: Martensite transformation start temperature
A_f: Reverse martenisite transformation finish temperature
T_R: R-phase transformation start temperature
T_X: The maximum temperature to stress-induce R-phase
σ_M: Stress for rearrangement of martensite variants or inducing martensite
σ_T: Stress for rearrangement of R-phase variants or inducing R-phase
σ_R: Stress for reverse martensite transformation
σ_{TR}: Stress for reverse R-phase transformation

2.12 Stress–strain curves at various temperatures in Ti–Ni alloy with R-phase transformation.[5] (T test temperature, M_f martensitic transformation finish temperature, M_s martensitic transformation start temperature, A_f reverse martensitic transformation finish temperature, T_R R-phase transformation start temperature, T_X maximum temperature to stress-induce R-phase, σ_M stress for rearrangement of martensite variants or inducing martensite, σ_T stress for rearrangement of R-phase variants or inducing R-phase, σ_R stress for reverse martensitic transformation, σ_{TR} stress for reverse R-phase transformation)

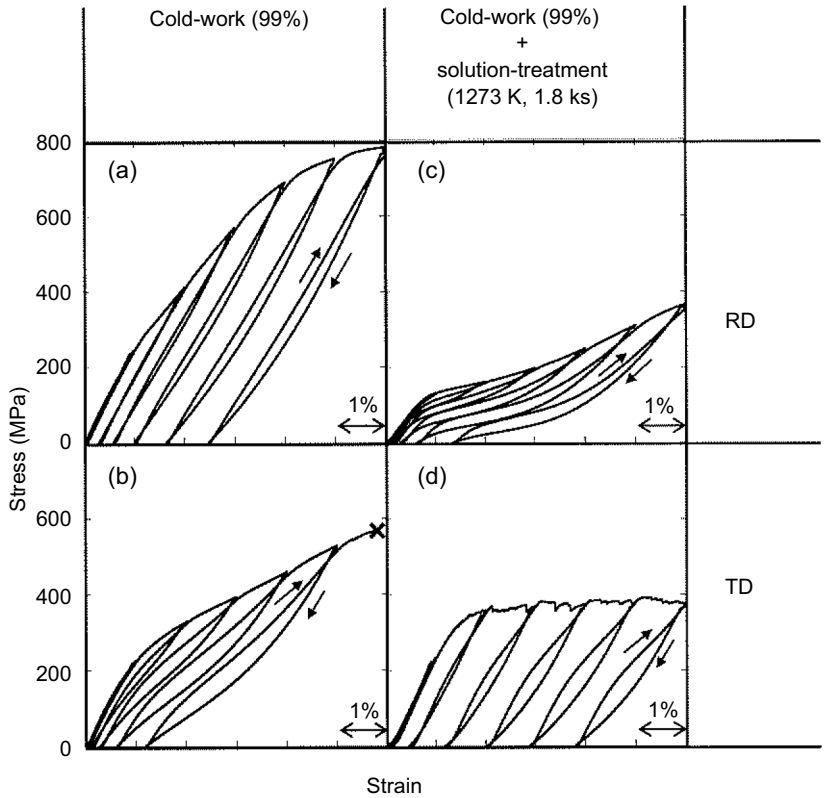

2.13 Stress–strain curves of severely cold-worked Ti–24mol%Nb–3mol%Al superelastic alloy along RD and TD. The left and right columns are for the cold-worked material and cold-worked and solution-treated material.[6]

transformation between R and P is used in this case. In comparison with the M–P transformation, the merits of a single step R–P transformation are higher fatigue resistance owing to small transformation strain, higher response in actuation owing to the small transformation hysteresis, and lower degradation of shape recovery temperatures due to the high $d\sigma/dT$ value, resulting in the long material life. If large actuation stress and strain are not required for the applications, the R-phase transformation is more beneficial.

2.7 Texture effect

Textures are often developed during thermomechanical treatments of alloys and classified into two types: one is the deformation texture caused by a severe deformation process such as cold rolling, and the other is the recrystallization texture caused by a subsequent solution (recrystallization) heat treatment. Figure 2.13

shows cyclic loading–unloading stress–strain curves of cold-rolled [(a) and (b)] and solution-treated [(c) and (d)] Ti–Nb–Al superelastic alloy at room temperature.[6] The Ti–Nb–Al is a Ni-free biomedical SMA that exhibits superior cold workability. The severely cold-rolled Ti–Nb–Al exhibits a strong deformation texture of the $\{100\}_{\beta}<011>_{\beta}$ type developed by cold-rolling with a thickness reduction of ≤99%. The solution-treated Ti–Nb–Al exhibits a recystallization texture of the $\{112\}_{\beta}<110>_{\beta}$ type by a subsequent heat-treatment at 1273 K for 1.8 ks. Figure 2.13 also shows that in (a) and (c) the tensile direction is parallel to the rolling direction (RD), and in (b) and (d) that the tensile direction is parallel to the transverse direction (TD). The origin of the superelasticity in Ti–Nb–Al is a stress-induced martensitic transformation from parent β phase (bcc) to martensite α" phase (C-centered orthorhombic structure). Owing to the strongly developed textures, strong mechanical anisotropy appears. No superelastic deformation is seen in (a) but over 1% superelastic strain is recognized in (b), even though this alloy is severely cold rolled. Moreover, good superelasticity, over 3%, is seen in (c) but little superelasticity appears in (d). Thus, the texture formation should be taken into account for an understanding of the mechanical behavior of the shape memory effect, especially when a severe deformation process is carried out during the thermomechanical treatment.

2.8 Summary

The mechanism of shape memory effect and superelasticity of SMAs and deformation behavior has been explained through stress–strain and strain–temperature relationships. Some actual mechanical behavior was also shown. The deformation behavior is complexly related to the crystallographic relationship between parent and martensite phases, test temperature, martensitic transformation temperatures, microstructures, textures and slip stress. Comprehensive understanding of these mechanisms is very important for the effective utilization of the shape memory effect.

2.9 References

1 *e.g.* http://www.fitec.co.jp/ftm/english/nt-e/appli/index.htm.
2 S. Miyazaki and K. Otsuka, *J. Jpn. Inst. Metals*, **22** (1983) 33.
3 S. Miyazaki, Y. Kohiyama, K. Otsuka and T. W. Duerig, *MatER. Sci. Forum*, **56–58** (1990) 765.
4 Y. Liu, Y. Liu and J. V. Humbeeck, *Acta Mater.*, **47** (1999) 199.
5 K. Otsuka and K. Shimizu, *Int. Met. Rev.*, **31** (1986) 93.
6 H. Hosoda, Y. Fukui, T. Inamura, K. Wakashima and S. Miyazaki, *Ti-2003 Science and Technology*, eds. G. Lütjering and J. Albrecht, Wiley-VCH, (2004) 3385.

3

Thermodynamics of the shape memory effect in Ti–Ni alloys

Y. LIU
The University of Western Australia, Australia

Abstract: The thermodynamic theories of thermoelastic martensitic transformations and their applications to shape memory materials are discussed, with specific reference to Ti–Ni. The equilibrium and phenomenological thermodynamic theories are developed, application of the theories to martensitic transformations in real alloys is clarified and experimental verifications are interpreted in terms of the Lüders-type deformation and the Clausius–Clapeyron relation. A generalisation of the thermodynamic theories is also presented.

Key words: Ti–Ni, Ni–Ti, Nitinol, thermodynamic theory, martensitic transformation, shape memory effect.

3.1 Thermal–mechanical coupling of thermoelastic martensitic transformation

Thermoelastic martensitic transformations are diffusionless first-order crystallographic phase transformations. The crystallographic phase transformation implies a lattice change. The diffusionless nature of the transformation makes the lattice change at the unit cell level accumulated to a global lattice distortion. In this regard, a thermoelastic martensitic transformation is a mechanical process microscopically as well as a phase transformation. Near-equiatomic Ti–Ni alloy is a typical example system that exhibits thermoelastic martensitic transformations.

Figure 3.1 shows some typical thermomechanical behaviour of Ti–Ni. The solid curve in Fig. 3.1(a) depicts the thermal transformation behaviour between a B2 parent phase and a B19' martensite, as detected by differential scanning calorimetry (DSC). The exothermic and endothermic peaks are manifestations of the first order nature of the transformations. The dashed curve is the integration of the DSC curve to show the evolution of the heat effect of the transformation (which may also be viewed as the evolution of the volume fraction of the transformation). Figure 3.1(b) shows the deformation behaviour associated with the B2↔B19' martensitic transformation at a given temperature, commonly known as the 'pseudoelastic behaviour' of shape memory alloys. The behaviour is characterised by an initial elastic deformation followed by a large inelastic deformation over a stress plateau, which is associated with the transformation. The strain magnitude over the stress plateau is intrinsically determined by the transformation lattice distortion and the

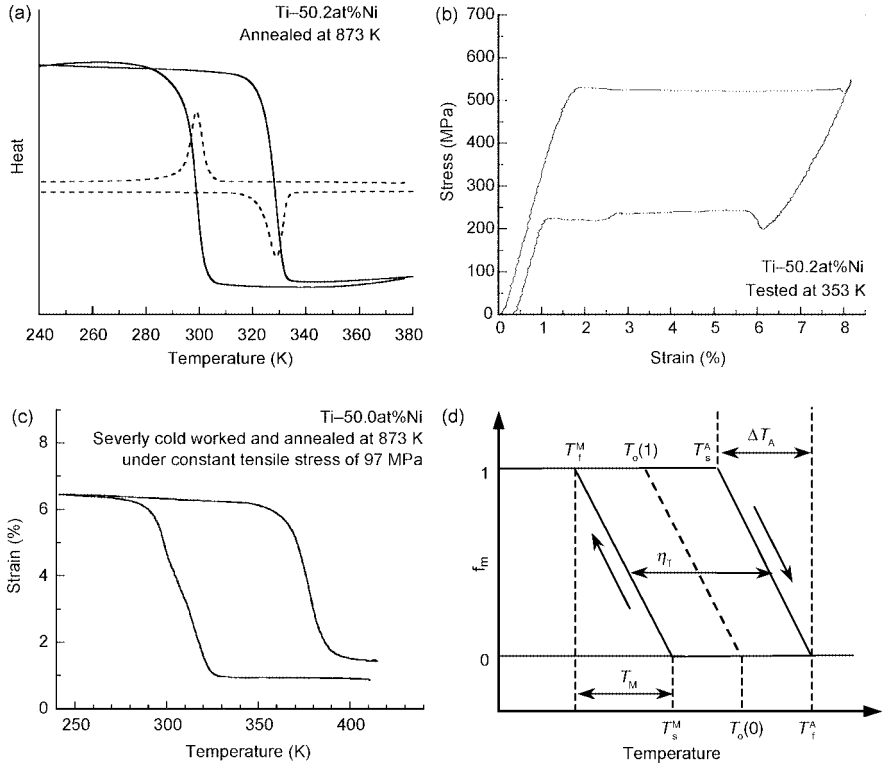

3.1 Thermomechanical behaviour of the thermoelastic B2–B19' martensitic transformation of near-equiatomic Ti–Ni; (a) thermal transformation behaviour, (b) mechanical behaviour, (c) thermomechanical behaviour.

strain position over the stress plateau may also be used as an estimate of the volume fraction of the transformation. Figure 3.1(c) shows the deformation behaviour induced by thermal cycling under a constant tensile stress. Once again, the large strain is associated with the forward and the reverse processes of the B2↔B19' martensitic transformation. These behaviours of the Ti–Ni demonstrate the thermal and mechanical characteristics of the martensitic transformation.

If we rotate the pseudoelastic stress–strain curve shown in Fig. 3.1(b) anticlockwise by 90°, it is easy to see that all these transformation processes exhibit similar hysteresis loops, sometimes referred to as 'hystoelastic' behaviour. For simplicity and clarity of the discussions below (also as adopted in the literature), the hystoelastic behaviour of the transformation is simplified and schematised as shown in Fig. 3.1(d), where the y-axis indicates the volume fraction of the martensite (f_m), as a measure of the extent of the transformation, and the x-axis is the driving force for the transformation, expressed here as temperature. The driving force, as for the forward transformation, may be either decrease of

temperature or increase of stress.

The hystoelastic behaviour may be described by three fundamental parameters: the equilibrium temperature T_o, the transformation temperature interval ΔT (assuming the same quantity for both the forward and the reverse transformations for simplicity), and the transformation hysteresis η_T. The 'thermoelastic' aspect of the transformation is expressed by ΔT, and η_T expresses the hysteretic nature of the transformation. Using these three parameters, the critical temperatures of the transformations, T_s^M, T_f^M, T_s^A and T_f^A (commonly denoted M_s, M_f, A_s and A_f, respectively, in the literature), can be expressed as (assuming equal share of η_T for the forward and the reverse transformations):

$$T_s^M = T_o - \frac{1}{2}\eta_T \qquad [3.1a]$$

$$T_f^M = T_s^M - \Delta T \qquad [3.1b]$$

$$T_s^A = T_o + \frac{1}{2}\eta_T \qquad [3.1c]$$

$$T_s^A = T_f^A - \Delta T \qquad [3.1d]$$

As a phase transformation, it is responsive to temperature variations; as a mechanical process, it is responsive to stress variations. This unique thermal–mechanical combination gives the transformation unique thermodynamic characteristics. To describe these characteristics and to express the laws governing the behaviour of the alloys that exhibit these transformations, fundamental thermodynamic theories of thermoelastic martensitic transformations have been established. The key historical references of the theories in the literature include refs. 1–6. A comprehensive treatment and summary of the theoretical developments is given by Wollants.[1]

Examining past efforts in establishing the thermodynamic theories of thermoelastic martensitic transformations, the development may be viewed in two different approaches: that based on fundamental equilibrium thermodynamic principles and that based on phenomenological considerations. The foundation of the equilibrium thermodynamic theory of martensitic transformations was laid largely by the work of Wollants and colleagues.[2] The framework of the phenomenological theory of thermodynamics of martensitic transformations was established largely by the works of Salzbranner and Cohen[4] and Ortin and Planes.[6]

3.2 Thermoelasticity of martensitic transformations

Martensitic transformation is a popular type of solid-state transformation in many metallic systems. According to their thermodynamic characteristics, or more appropriately, their thermal transformation behaviour, the many martensitic transformations are conventionally classified into two types: thermoelastic martensitic

transformation and non-thermoelastic martensitic transformation. The concept of thermoelastic martensitic transformation was first summarised by Kurdjumov as the following (quoted by Wollants *et al.*[1] from the original report[7]):

> Great elastic energy should arise during the coherent growth of a martensite crystal: at certain conditions this positive part of the free energy change may increase more rapidly during crystal growth than the negative part of the free energy difference between the new and original lattice. Thus the total free energy change may pass through a minimum when the dimensions of the martensite crystal increase. If this happened before disruption of coherence, the growth would stop, and the martensite crystal would be in thermoelastic equilibrium with the original phase. A raising of the temperature would lead to the shrinking of the crystal but lowering of the temperature would lead to its growth.

This explanation describes the experimental observation and suggests a thermodynamic explanation to the phenomenon. It is clear in this statement that transformation hysteresis is not considered. In this regard, the hystoelastic behaviour of martensite shown in Fig. 3.1(d) may be decomposed into two independent components: the reversible aspect and the pure hysteretic aspect of the transformation. Obviously, the concept of thermoelasticity applies only to the reversible aspect, which may be described by two essential characteristics:

1 that the transformation process is thermally reversible on temperature, and
2 that the driving force required for the transformation increases continuously during the process of the transformation.

There have also been attempts in the literature to describe the conditions under which thermoelastic martensitic transformation may happen. Wayman summarised previous observations and proposed the following criteria for martensite thermoelasticity:[8,9]

1 That the interface between the parent phase and the martensite is coherent,
2 That the volume change of the transformation is negligible, and
3 That the thermal hysteresis is small.

Later literature often quotes these conditions as a definition of thermoelasticity of martensitic transformation. This is obviously incorrect. The requirements described above are empirical conditions, or prerequisites, for thermoelasticity of martensite, but do not define the property. Criterion (1) assures the mobility of the transformation interfaces, thus facilitating the reversibility of the transformation. Criterion (2) provides a favourable condition for the interface to be coherent and to help minimise the occurrence of irreversible events, such as defect generation, internal plastic deformation and microcracking, during the process of the transformation. Criterion (3) is merely a consequence, or manifestation of a good thermoelastic transformation, and imposes no requirement for its occurrence.

In principle, a transformation may well have very large thermal hysteresis and yet be perfectly crystallographically and thermally reversible, thus being thermoelastic. This is because there exist many possible reasons for thermal hysteresis, which do not necessarily always lead to internal structural damage that disrupts the crystallographic reversibility of the transformation. Therefore, these conditions cannot be used as criteria to classify thermoelastic and non-thermoelastic martensitic transformations.

The clarification of this fundamental concept is important, as the equilibrium thermodynamic theories are developed specifically with regard to the thermoelastic behaviour of martensitic transformation. In some cases, the behaviour of a particular alloy under a particular condition may not fully comply with the description of thermoelasticity, thus causing errors in the effort to determine its thermodynamic parameters. For example, the pseudoelastic stress–strain curve shown in Fig. 3.1(b) does not satisfy the condition that 'the driving force for the transformation increases continuously during the process of the transformation' whilst being reversible, and attempts to determine the transformation intervals and stored elastic energies would be invalid. In this case, if the deformation process is controlled by stress, the transformation will proceed in a 'burst' manner from onset to completion once the critical stress is reached.

Before we complete the discussion on thermoelasticity, further clarification is needed of the following two points:

1 Thermoelasticity of martensitic transformation is expressed by $T_o = T_o(f_m)$. The physical event underlining this parameter occurs within the local environment of the transformation front, and is irrelevant to the global apparent behaviour of a polycrystalline material. In a practical alloy, many factors may cause apparent transformation intervals and hystereses, such as chemical segregation, spatial variations of internal stress fields and inhomogeneous distribution of precipitates. Under these conditions, the matrix of the alloy may be viewed as a composite of many small domains each being thermodynamically uniform. The martensitic transformation may happen at different temperatures or stresses in different areas within the matrix, giving rise to widened apparent transformation intervals and hystereses.
2 Thermoelasticity of phase transformation refers to the behavioural reversibility of the transformation on temperature scale. Its cause does not have to be a mechanical type of stress. From a thermodynamic viewpoint, any factor that may cause reversible variation of the free energy equilibrium state will cause transformation thermoelasticity. In a general context, incongruent solidification–melting and precipitation–dissolution processes of alloys all belong to this category. Recognition of this generality of transformation thermoelasticity helps recognition of the generality of the thermodynamic theories established for thermoelastic martensite.

3.3 Equilibrium thermodynamic theory of thermoelastic martensitic transformations

From the concept of thermalmechanical coupling of thermoelastic martensitic transformations, it is not difficult to understand the equivalence between temperature and stress as driving forces for the transformation. In fact, this is the central question that the equilibrium thermodynamic theory of thermoelastic martensitic transformations answers.

To explore the relationship between temperature and stress as the driving force for the transformation, Wollants *et al.*[2] examined the energy balance of the system schematically shown in Fig. 3.2. The system is under a uniaxial load F and experiences a deformation from L_o to $(L_o + \Delta L)$ in association with a martensitic transformation. Thus the free energy balance of the system may be expressed as:

$$\Delta G = \Delta H - T\Delta S - F\Delta L \qquad [3.2]$$

The right-hand side of the equation summates all the free energy terms involved in the deformation–transformation process, including the enthalpy energy (ΔH), the temperature–entropy energy ($T\Delta S$), and the mechanical work the environment does to the system ($F\Delta L$). The difference term $\Delta H - T\Delta S$ is a generic free energy quantity for all first-order phase transformations and originates from the structural change of the process. It is commonly referred to as the 'chemical free energy change (ΔG_{chem})'. The term $F\Delta L$ is specific for a stress-induced transformation and is sometimes referred to as the 'non-chemical free energy change ($\Delta G_{non\text{-}chem}$)' (in fact, the term 'non-chemical free energy change' has been used in the literature to refer to all forms of energy contributions other than $\Delta H - T\Delta S$ to the transformation, including non-equilibrium energy contributions, which are invalid in this discussion), or 'mechanical entropy change (ΔH_{mech})'. This mechanical work can also be expressed equivalently as:

$$F\Delta L = V\sigma\varepsilon_t = \frac{1}{\rho}\sigma\varepsilon_t \qquad [3.3]$$

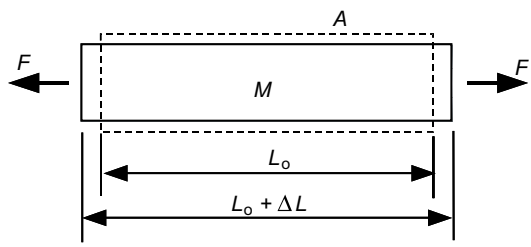

3.2 Schematic of deformation associated with martensitic transformation induced by an applied stress.

where V and ρ are, respectively, the specific volume and density of the material, σ is the applied stress and ε_t is the (actual) strain produced by the transformation.

Therefore, equation 3.2 is more conveniently expressed as:

$$\Delta G = \Delta H - T\Delta S - \frac{1}{\rho}\sigma\varepsilon_t \qquad [3.4]$$

Under the equilibrium condition when $\Delta G = 0$, equation 3.4 becomes:

$$\Delta H - T_o\Delta S\,\frac{1}{\rho}\sigma_o\varepsilon_t = 0 \qquad [3.5]$$

where T_o and σ_o are the equilibrium temperature and equilibrium stress for the transformation, respectively. Differentiating this equation gives:

$$\frac{\mathrm{d}\sigma_o}{\mathrm{d}T_o} = -\frac{\rho\Delta S}{\varepsilon_t} = -\frac{\rho\Delta H}{T_o(0)\varepsilon_t} \qquad [3.6]$$

where

$$\Delta S = \frac{\Delta H}{T_o(0)} \qquad [3.7]$$

Clearly, when ΔS and ΔH are explicitly expressed, respectively, as the 'chemical' entropy and enthalpy changes of the transformation, $T_o(0)$ is the thermodynamic equilibrium temperature between the two phases under no stress. Therefore, it is clear that the right-hand side of the equation contains all material and transformation constants; thus the equation defines a linear relationship between stress and temperature, as shown in Fig. 3.3 (the $\sigma_o(T)$ line).

This is the infamous Clausius–Clapeyron equation for thermoelastic martensitic

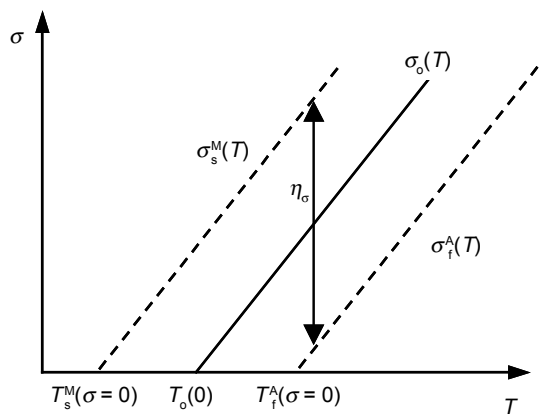

3.3 Effect of stress on the equilibrium temperature of martensitic transformation according to the Clausius–Clapeyron relation.

transformations. This equation expresses the equivalence between stress and temperature as driving forces for the transformation. This relationship has been confirmed experimentally in numerous studies and is widely used in the literature for the analysis of the phenomena of thermoelastic martensitic transformations. However, there have been frequent misinterpretations and misuses of this relationship often leading to inaccurate determination of thermodynamic parameters and miscalculation of property parameters of shape memory alloys. Three common misuses of the relationship are discussed below.

1 Equation 3.6 defines the relationship between the equilibrium temperature and the equilibrium stress of the transformation. It has no implication for the actual temperatures (M_s, A_f) or stresses (σ_s^M, σ_f^A) at which the transformations occur. Following equation 3.1, it is easy to see that:

$$\sigma_s^M = \sigma_o + \frac{1}{2}\eta_\sigma \qquad [3.8a]$$

$$\sigma_f^A = \sigma_o + \frac{1}{2}\eta_\sigma \qquad [3.8b]$$

where σ_s^M is the starting stress for the stress-induced martensitic transformation, σ_f^A is the finishing stress for the reverse transformation and η_σ is the stress hysteresis of the stress-induced transformation, which is dependent on the metallurgical conditions of the material (e.g. grain size, dislocation, precipitates) and the loading conditions (e.g. stress state, strain rate, sample geometry), and is not an intrinsic property of the transformation. It cannot be calculated by thermodynamic principles.

2 Under the assumption that η_σ is not affected by temperature (or stress), σ_s^M and σ_f^A appear as two parallel lines aside $\sigma_o(T)$, as shown in Fig. 3.3. The intersects of these two lines with the x-axis, T_s^M ($\sigma = 0$) and T_f^A ($\sigma = 0$), denote the hypothetical temperatures at which stress-induced martensitic transformation may occur under zero stress and are governed by the magnitude of η_σ, thus cannot be equated to M_s A_f temperatures, which are governed by η_T, of the transformation.

3 It is clear in Fig. 3.2 and equation 3.2 that ΔL is the actual elongation of the sample during the stress-induced martensitic transformation and gives no reference to the crystallographic lattice distortion of the transformation. This implies that the transformation strain, ε_t, in equation (3.6) is the actual strain of a transformation–deformation process instead of a theoretical constant. Many experimental evidences have demonstrated that ε_t varies for NiTi, depending on a number of factors such as material metallurgical conditions,[10] sample geometry, loading conditions,[11,12] transformation cycling[13] and testing temperature.[13] This implies that the value of ε_t for a given alloy system is not unique. Furthermore, under the condition that ε_t varies with temperature ($\varepsilon_t = \varepsilon_t(T)$),

$\frac{d\sigma_o}{dT_o} = -\frac{\rho\Delta H}{T\varepsilon_t(T)}$ no longer defines a linear relationship.[13,14]

In summary, the equilibrium thermodynamic theory of thermoelastic martensitic transformations is based on free energy balance considerations and describes the equivalence between temperature and stress as driving forces for the transformations. It deals only with reversible free energy terms, such as ΔH, ΔS, T_o and σ_o.

3.4 Phenomenological thermodynamic theory of thermoelastic martensitic transformations

The phenomenological thermodynamic theory of thermoelastic martensitic transformations is established on the basis of the observation of the hystoelastic behaviour of thermoelastic martensitic transformations, as shown in Fig. 3.1. The occurrence of a transformation temperature interval indicates a need for a continuous increase in the driving force during the transformation, which, in turn, implies a continuously increasing resistance to the transformation. The reciprocal transformation temperature interval for the reverse transformation implies that this change of transformation resistance is reversible. With specific reference to thermoelastic martensitic transformations, this reversible resistance is ascribed to the storage and release of elastic stress–strain energy during the transformation.[4,5] The occurrence of thermal hysteresis implies irreversible energy losses during the process of the transformation. Consideration of the various contributions to the free energy balance of the transformation leads to the establishment of the following equation:[4,5]

$$\Delta G = \Delta H - T\Delta S + \Delta E_{el} + \Delta E_{ir} \qquad [3.9]$$

In this equation, ΔE_{el} is the elastic strain energy. It is stored into the system during the forward transformation, thus it is a consumption of the transformation driving force (energy) and is considered to increase continuously with increasing volume fraction of martensite. During the reverse transformation, ΔE_{el} is gradually released with the reduction of the volume fraction of martensite and is negative. Its release is an addition to the driving force for the reverse transformation, as given by:

$$\Delta E_{el}^{A\to M} = -\Delta E_{el}^{M\to A} \qquad [3.10]$$

The summation of all irreversible energies involved in the transformation is given by ΔE_{ir}, which, for a given transformation system in a given alloy, is considered to be dependent on the metallurgical conditions of the matrix. It is often assumed to be a constant during the process of a transformation (thus constant transformation hysteresis with respect to martensite volume fraction) and that, unless proven otherwise, it is shared equally between the forward and the reverse processes of the transformation. Therefore, ΔE_{ir} is a net energy consumption of

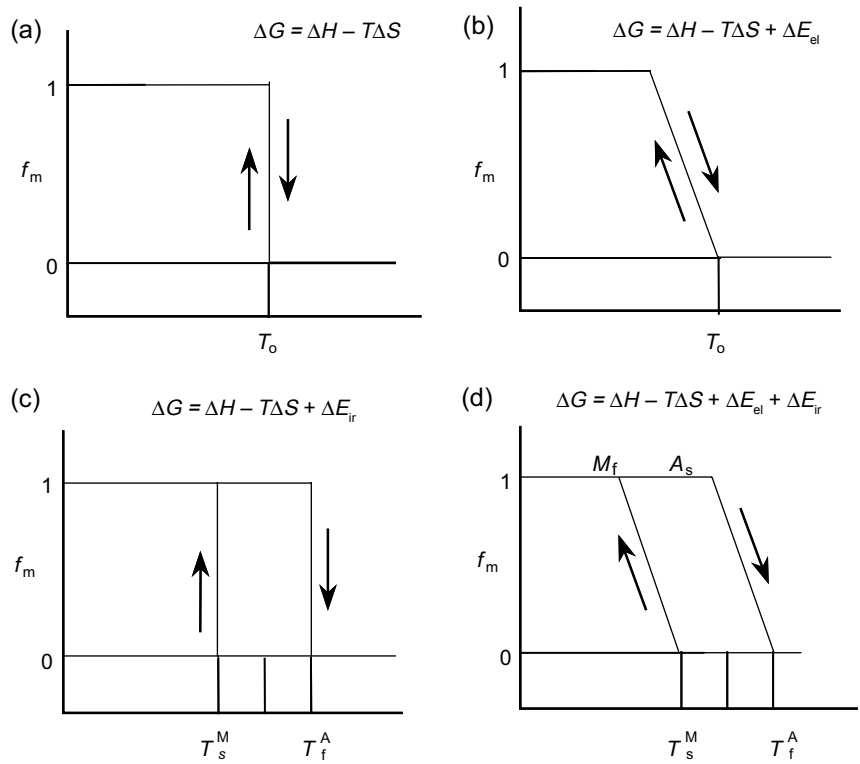

3.4 Schematic illustration of the effects of ΔE_{el} and ΔE_{ir} on the transformation behaviour.

transformation driving force for both the forward and the reverse processes. It is always positive and:

$$\Delta E_{ir}^{A\to M} = \Delta E_{ir}^{M\to A} \qquad [3.11]$$

From these findings, the effects of ΔE_{el} and ΔE_{ir} on the transformation behaviour may be illustrated as shown in Fig. 3.4, where (a) depicts the effect of chemical free energy ($\Delta H - T\Delta S$), (b) depicts the effect of ΔE_{el}, (c) depicts the effect of ΔE_{ir} and (d) depicts the combined effect of ΔE_{el} and ΔE_{ir}. It is obvious that the figure has adopted the following assumptions (for the reason of simplicity):

$$\Delta E_{el}(f_m = 0) = \Delta E_{el}(0) \neq 0 \qquad [3.12]$$

$$\Delta E_{el}(f_m) = \Delta E_{el}(0) + kf_m \qquad [3.13]$$

$$\Delta E_{ir}(f_m) = \Delta E_{ir} \qquad [3.14]$$

where k is a linearity constant.

As apparent from the figure, $\Delta E_{el}(f_m)$ is responsible for the transformation interval and ΔE_{ir} is responsible for the transformation hysteresis. In this context, in

principle, $\Delta E_{el}(f_m)$ and ΔE_{ir} can be experimentally determined by measuring the hysteresis loops of a transformation. However, in application of the theory, much interpretation of equation 3.9 has been intuitive and lacking in rigorous consideration. The following requires clarification.

1 ΔE_{el} is not a state function. For example, compared with $\Delta H = H^M - H^A$, ΔE_{el} cannot be expressed in a similar way, because the system does not have independent states corresponding to E^M or E^A. For a given transformation, $\Delta E_{el}(f_m)$ is dependent on the metallurgical conditions and the martensite variant configurations. To give an example, the value of $\Delta E_{el}(f_m)$ is different for thermally induced self-accommodating martensite and for stress-induced oriented martensite.
2 ΔE_{ir} is not a state function. It is a quantity of a process. Its actual value is dependent on the metallurgical conditions of the matrix and the martensite configuration. For example, the value of ΔE_{ir} is different for a thermally induced transformation and for a stress-induced transformation.
3 Most critically, equation 3.9 does not express the equilibrium condition of the transformation. When the system varies slightly within the vicinity of $\Delta G = 0$, the transformation does not respond spontaneously back and forth in both directions. Owing to the interference of ΔE_{ir}, the transformation occurs at different temperatures for the forward and the reverse processes, as:

$$\text{A}\rightarrow\text{M}: \quad \Delta G^{A\rightarrow M} = \Delta H^{A\rightarrow M} - T\Delta S^{A\rightarrow M} + \Delta E_{el}^{A\rightarrow M} + \Delta E_{ir}^{A\rightarrow M} = 0 \qquad [3.15a]$$

$$\text{M}\rightarrow\text{A}: \quad \Delta G^{M\rightarrow A} = \Delta H^{M\rightarrow A} - T\Delta S^{M\rightarrow A} + \Delta E_{el}^{M\rightarrow A} + \Delta E_{ir}^{M\rightarrow A} = 0 \qquad [3.15b]$$

4 Equations 3.15 describe the balance of specific energies in a local environment at the transformation interface at a given moment during the transformation, instead of the global balance of the cumulated energies over the transformation to that moment. This is to say that the establishment of the equation has nothing to do with what has happened before the moment of concern. This clarification is important to avoid some common misperceptions. For example, it is commonly assumed that the elastic energy of the transformation increases with the increase of the volume fraction of martensite (thus the thermoelasticity). This is obviously a confusion between the specific energy balance over an infinitesimal step of transformation within a local environment and the total cumulated elastic energy stored in the system. The former affects the thermodynamic state of the transformation at the moment of concern whereas the latter does not.

It is seen that consideration of the hystoelastic behaviour of thermoelastic martensitic transformations necessitated the introduction of functional terms ΔE_{el} and ΔE_{ir}. However, the physical meanings of these two terms lack a thorough explanation. Some attempts have been made by Ortin and Planes,[5] Cohen *et al.*[4,15] and Liu and McCormick.[16,17] The understanding of these two terms may be summarised as following.

3.4.1 Elastic energy

In essence, the ΔE_{el} term in equation 3.9 should be the sum of all reversible non-chemical energies. In the specific case of thermoelastic martensitic transformations, the dominant contribution is regarded the elastic strain energy in the matrix caused by the lattice distortion of martensite. Its progressive storing into the matrix during the forward process of the transformation is a continuous consumption of the driving force, whilst its progressive release during the reverse transformation provides extra driving force for the transformation. This description has omitted two important points, as discussed below.

First, taking near-equiatomic Ti–Ni for example, the B2-B19' martensitic transformation in these alloys has up to 10% lattice distortion strain. Most of this lattice distortion is consumed in the self-accommodation of martensite variants and imposes no elastic strain, thus it does not contribute to ΔE_{el}. Only a very small fraction of that lattice distortion is accommodated in the form of elastic strain. In fact, the actual process of elastic energy storage may be envisaged as follows. Owing to lattice distortion, the first martensite crystal imposes an elastic stress field within its vicinity. The intensity of the elastic stress increases rapidly with the growth of the martensite. When this stress reaches the critical level to trigger the formation of a second martensite crystal in an opposite direction, the second crystal forms and the stress field is immediately relaxed. The stress field gradually rebuilds until the next martensite crystal is formed. In this regard, the elastic stress–strain energy does not increase continuously during the process of transformation and the maximum magnitude of the elastic stress (energy) is limited by the critical stress to form another martensite crystal in the matrix.

Secondly, ΔE_{el} in equation 3.9 is the specific energy, or rate of energy generation, at the transformation front, i.e. $\frac{dE_{el}}{df_m}$, instead of global accumulation of elastic energy. The same may be stated in another way: equation 3.9 describes the instantaneous energy balance at a particular moment over an infinitesimal step during the transformation and has nothing to do with the global accumulation of elastic energy. The concept of continuous increase of elastic energy with the growth of martensite described above (in the literature) is correct in a global sense, but is unjustified for the local scene, irrelevant to the local energy balance (equation 3.9) and misleading for the understanding of the thermodynamic behaviour of the transformation. There is no reason to automatically assume that $\frac{dE_{el}}{df_m}$ increases monotonically with the growth of martensite. Therefore, it is not reasonable to attribute the global transformation temperature interval ΔT to ΔE_{el}. In fact, it has been suggested that formation of a new martensite variant relaxes the stress field created by the previous variants, i.e. lowers ΔE_{el}.[18,19]

The above discussion may be schematically illustrated as shown in Fig. 3.5. In the figure, a similar illustration for the situation of ΔE_{ir} is also shown for future use. In the figure, $\Delta E_{el} = \frac{dE_{el}}{df_m}$ is arbitrarily assumed to be a linear function of f_m and $\Delta E_{ir} = \frac{dE_{ir}}{df_m}$ a constant during the process of the transformation. The dashed curves

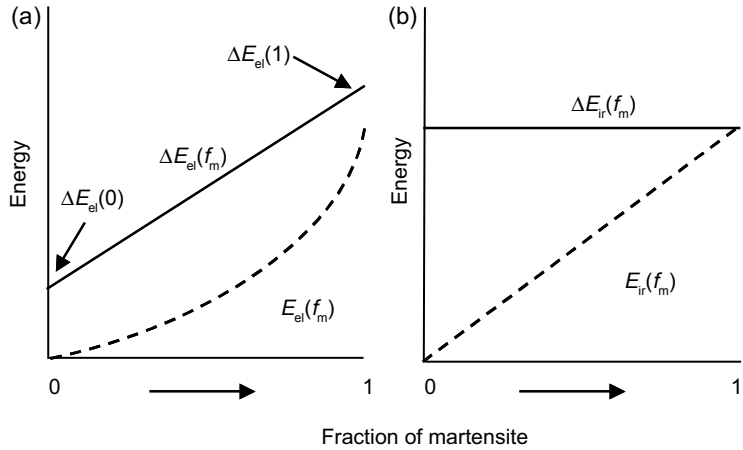

3.5 Schematic illustration of evolution of ΔE_{el} and ΔE_{ir} during transformation.

show the accumulated quantities $E_{el} = \int_0^{f_m} \frac{dE_{el}}{df_m} df_m$ and $E_{ir} = \int_0^{f_m} \frac{dE_{ir}}{df_m} df_m$. With these illustrations, it is clear that $\Delta E_{el}(0)$ shifts the starting temperature of the forward transformation (M_s) and that the variation of ΔE_{el}, i.e. $\Delta E_{el}(1) - \Delta E_{el}(0)$, causes the transformation temperature interval.

3.4.2 Irreversible energies

The process of thermoelastic martensitic transformation is accompanied by many forms of irreversible energy exchanges. Some common irreversible energy losses include the following.

1 Production of structural defects. Martensitic transformations are associated with lattice distortions. Most of the lattice shape change is cancelled in the self-accommodation structure and the rest is accommodated as elastic strain. However, under certain conditions, the local stress may exceed the local strength of the matrix, causing local plastic deformation and creating structural defects. Creation of defects enhances the internal energy of the matrix and is a consumption of the transformation free energy change. This form of energy consumption is irreversible. Experimental evidences have shown thermal cycling through the transformation increases dislocation density in the matrix[20,21] and causes shifts of transformation temperatures.[17,21]
2 Frictional heat. In addition to generating new structural defects, the mechanical movement of the transformation interface also moves and cuts existing dislocations. Such movement generates heat, which causes temperature increase in the sample, which is eventually lost into the environment.[5]
3 Acoustic emission. Martensitic transformations are displacive transformations. Lattice distortions of the transformations create internal stresses. When the

stresses exceed the mechanical resistance of the matrix to the growth of martensite crystals, martensite will grow forward as a mechanical lattice wave, i.e. at the velocity of sound in the matrix and emit acoustic energy to the ambient. Experimental evidences have been reported of the abrupt jerky jumping of transformation interfaces and the emission of acoustic waves.[22]

These irreversible energy losses are all net consumptions of thermodynamic driving forces for the transformation, thus causing thermal hystereses to the transformation. The total of the specific quantity of the irreversible energies, $\Delta E_{ir} = \frac{dE_{ir}}{df_m}$, is effective in determining the transformation temperature and is often assumed to be constant during the process of a transformation. The accumulated irreversible energy, which is irrelevant to the transformation temperature, thus increases during the process of the transformation, as illustrated in Fig. 3.5(b).

It also ought to be clarified that these irreversible events are only irreversible in the thermodynamic energetic context; concurrent with these irreversible energy losses, the martensitic transformation can still be perfectly reversible crystallographically and mechanically.

3.5 Unified thermodynamic expression of thermoelastic martensitic transformations

The two approaches of thermodynamic theories of thermoelastic martensitic transformations have been developed very much along two separate paths, yet both involve the discussion of the effect of stresses, applied or internal. These discussions have not been presented in the same framework so the similarities and dissimilarities of their effects can be put into direct comparison and clarified. The effect of internal stresses on the transformation has often been equated to that of an applied stress in the literature, and this is lack of proper justification, as discussed below. Therefore, it is necessary to merge the two theories in a unified expression of the energy condition of a thermoelastic martensitic transformation, as expressed below:

$$\Delta G = \Delta H - T\Delta S - \frac{1}{\rho}\sigma_{app}\varepsilon_t + \Delta E_{el}\left(f_m\right) + \Delta E_{ir} \qquad [3.16]$$

This equation is a simple combination of equations 3.4 and 3.9. Among the terms, the concepts and effects of ($\Delta H - T\Delta S$) and ΔE_{ir} are simple and clear and those of $\frac{1}{\rho}\sigma_{app}\varepsilon_t$ and $\Delta E_{el}(f_m)$ deserve further examination.

The mechanical energy contribution to the transformation from the applied stress is given by $\Delta E_{mech} = \frac{1}{\rho}\sigma_{app}\varepsilon_t$. It is also referred to in the literature as 'mechanical enthalpy'. The applied stress remains effective during the entire process of a transformation.

In contrast, $\Delta E_{el}(f_m)$ expresses the effect of internal stresses, pre-existing in the

matrix or generated during the transformation, accumulating (e.g. during the forward transformation) or releasing (e.g. during the reverse transformation). This stress varies during the transformation and may be expressed as $\Delta E_{el} = \frac{1}{2\rho}\sigma_{el}\varepsilon_{el}$ where ε_{el} is the elastic strain, limited by the crystal stress for transformation (note: in the local environment at the transformation interface, the stress may be different from the macroscopic stress observed experimentally). It is much smaller compared with the transformation strain (ε_t). A pre-existing internal stress will be relaxed rapidly with the first appearance of martensite locally (assuming the martensite variant grows into the stress field), and further growth of the martensite results in the creation of stresses in the opposite direction. Therefore, pre-existing internal stresses are only effective at the start of the transformation but ineffective in affecting the full process of the transformation. In this regard, attempts to estimate the magnitude of internal stresses based on the shift of transformation temperatures or to attribute the shift of transformation temperature to internal stresses are unjustified and incorrect.

In fact, a large numbers of experimental evidences prove otherwise. Martensitic transformations are suppressed to lower temperature in matrices containing high dislocation densities. Typical conditions include cold working,[23] partial anneal after cold working,[24,25] and thermal transformation cycling.[21] Mechanical cycling via pseudoelasticity is known to cause a decrease of the critical stress for inducing martensitic transformation,[13, 26] which may be regarded as thermodynamically equivalent to the increase in transformation temperature. However, there has not been any direct experimental evidence to demonstrate that transformation temperatures increase as a result of pseudoelastic cycling, thus allowing the verification of the hypothesis of the correlation between internal stresses and transformation temperatures. Another relevant experimental observation is that ageing treatment of Ni-rich Ti–Ni alloys produces coherent Ti_3Ni_4 precipitates,[27–29] which create internal stresses within the matrix. Accompanying the formation of the precipitates, transformation temperatures are found to generally increase. To explain this observation, two possible reasons have been suggested: the decrease of the Ni content of the matrix and the influence of the internal stresses. However, to date, the influence of internal stresses has only been an unproven hypothesis.

3.6 Thermodynamic expression of transformation temperatures

Whereas there has been adequate information regarding the development of the thermodynamic theories of thermoelastic martensitic transformations, discussions of the application of the theories to martensitic transformations in real alloys have been limited. The ground work was laid largely by Ortin and Planes.[5,6] Many of the uses of the reported theories are on an intuitive basis and many are inappropriate, thus requiring further clarification.

3.6.1 Characteristic temperatures of transformation

As discussed above, due to the introduction of the irreversible energy term, equation 3.16 does not express the equilibrium condition of the transformation. In other words, the critical conditions for the forward and the reverse transformation are not equal. Therefore, the critical conditions for the forward and reverse processes must be expressed separately, as:

$$\Delta G^{A\to M} = \Delta H^{A\to M} - T\Delta S^{A\to M} - \frac{1}{\rho}\sigma_{app}\varepsilon_t^{A\to M} + \Delta E_{el}^{A\to M}(f_m) + \Delta E_{ir}^{A\to M}(f_m) \quad [3.17a]$$

$$\Delta G^{M\to A} = \Delta H^{M\to A} - T\Delta S^{M\to A} - \frac{1}{\rho}\sigma_{app}\varepsilon_t^{M\to A} + \Delta E_{el}^{M\to A}(f_m) + \Delta E_{ir}^{M\to A}(f_m) \quad [3.17b]$$

In these equations, S and H are state functions, thus:

$$\Delta H^{A\to M} = -\Delta H^{M\to A} < 0 \quad [3.18]$$

$$\Delta S^{A\to M} = -\Delta S^{M\to A} < 0 \quad [3.19]$$

Under the condition that no plastic deformation is involved in the transformation, strain induced during the forward transformation is fully recovered during the reverse transformation, therefore:

$$\varepsilon_t^{A\to M} = -\varepsilon_t^{M\to A} \quad [3.20]$$

According to the definition, the elastic strain energy stored in the system during the forward transformation is fully released during the reverse transformation, i.e.:

$$\Delta E_{el}^{A\to M}(f_m) = -\Delta E_{el}^{M\to A}(f_m) > 0 \quad [3.21]$$

The irreversible energy is not a state function and its magnitude is determined by the actual transformation path and the metallurgical conditions of the matrix. It is a consumption of the free energy driving force of the transformation. It is often assumed equal between the forward and the reverse transformations, i.e.:

$$\Delta E_{ir}^{A\to M}(f_m) = \Delta E_{ir}^{M\to A}(f_m) > 0 \quad [3.22]$$

Under these conditions, for a thermally induced transformation when $\sigma_{app} = 0$, temperatures of the forward and reverse transformations can be determined from equations 3.17a and 3.17b, respectively, at $\Delta G^{A\to M} = 0$ and $\Delta G^{M\to A} = 0$, as:

$$T^{A\to M}(f_m) = \frac{\Delta H^{A\to M} + \Delta E_{el}^{A\to M}(f_m) + \Delta E_{ir}^{A\to M}(f_m)}{\Delta S^{A\to M}} \quad [3.23]$$

$$T^{M\to A}(f_m) = \frac{\Delta H^{M\to A} + \Delta E_{el}^{M\to A}(f_m) + \Delta E_{ir}^{M\to A}(f_m)}{\Delta S^{M\to A}} \quad [3.24]$$

At $f_m = 0$:

$$T^{A\to M}(0) = M_s = \frac{\Delta H^{A\to M} + \Delta E_{el}^{A\to M}(0) + \Delta E_{ir}^{A\to M}(0)}{\Delta S^{A\to M}} \quad [3.25]$$

$$T^{M\to A}(0) = A_f = \frac{\Delta H^{M\to A} + \Delta E_{el}^{M\to A}(0) + \Delta E_{ir}^{M\to A}(0)}{\Delta S^{M\to A}} \quad [3.26]$$

At $f_m = 1$:

$$T^{A\to M}(1) = M_f = \frac{\Delta H^{A\to M} + \Delta E_{el}^{A\to M}(1) + \Delta E_{ir}^{A\to M}(1)}{\Delta S^{A\to M}} \quad [3.27]$$

$$T^{M\to A}(1) = A_s = \frac{\Delta H^{M\to A} + \Delta E_{el}^{M\to A}(1) + \Delta E_{ir}^{M\to A}(1)}{\Delta S^{M\to A}} \quad [3.28]$$

Equations 3.25–3.28 state that the temperature of the transformation at a particular moment is influenced by the specific elastic and irreversible energies at that moment in addition to the chemical free energy parameters ΔS and ΔH.

3.6.2 Transformation temperature intervals

The temperature interval of the forward transformation can therefore be determined as:

$$\Delta T^{A\to M} = M_s - M_f = \frac{\left[\Delta E_{el}^{A\to M}(0) - \Delta E_{el}^{A\to M}(1)\right] + \left[\Delta E_{ir}^{A\to M}(0) - \Delta E_{ir}^{A\to M}(1)\right]}{\Delta S} \quad [3.29]$$

Similarly for the reverse transformation:

$$\Delta T^{M\to A} = A_f - A_s = \frac{\left[\Delta E_{el}^{M\to A}(0) - \Delta E_{el}^{M\to A}(1)\right] + \left[\Delta E_{ir}^{M\to A}(0) - \Delta E_{ir}^{M\to A}(1)\right]}{\Delta S} \quad [3.30]$$

Equations 3.29–3.30 state that a transformation temperature interval is caused by the differences between the starting value and the finishing value of the specific elastic and the irreversible energies of the transformation. In other words, if the specific elastic energy (similarly the specific irreversible energy) created over an infinitesimal step of the transformation at the beginning and the end are the same, i.e. $\Delta E_{el}(0) = \Delta E_{el}(1)$ and $\Delta E_{ir}(0) = \Delta E_{ir}(1)$, then $\Delta T = 0$, despite that $\Delta E_{el}(f_m) \neq 0$ and $\Delta E_{ir}(f_m) \neq 0$ (and the accumulated energies

$$E_{el}(f_m) = \int_0^{f_m} \frac{dE_{el}}{df_m} df_m \neq 0 \text{ and } E_{ir}(f_m) = \int_0^{f_m} \frac{dE_{ir}}{df_m} df_m \neq 0).$$

Obviously, transformation (stress and temperature) intervals are not determined by the cumulation of elastic energy or the consumption of irreversible energies. On this point there exist many errors in the literature.

3.6.3 Transformation median temperature

The chemical equilibrium temperature between the parent phase and the martensite is determined as:

$$T_0 = \frac{\Delta H}{\Delta S} \qquad [3.31]$$

The median temperature between the forward and the reverse transformation at the start of the transformation ($f_m = 0$) can be determined using equations 3.25 and 3.26 as:

$$T_{1/2} = \frac{1}{2}(A_f - M_s)$$

$$= \frac{1}{2}\left\{\frac{\Delta H^{M\to A} + \Delta E_{el}^{M\to A}(0) + \Delta E_{ir}^{M\to A}(0)}{\Delta S^{M\to A}} - \frac{\Delta H^{A\to M} + \Delta E_{el}^{A\to M}(0) + \Delta E_{ir}^{A\to M}(0)}{\Delta S^{A\to M}}\right\} \qquad [3.32]$$

Accepting conditions defined in equations 3.18, 3.19, 3.21 and 3.22, equation 3.32 reduces to:

$$T_{1/2} = \frac{\Delta H^{A\to M} + \Delta E_{el}^{A\to M}(0)}{\Delta S^{A\to M}} \qquad [3.33]$$

Obviously,

$$T_{1/2} < T_0 \qquad [3.34]$$

Similar conclusions to equation 3.34 have been reached by other workers,[4,30] but for various reasons. One explanation is that the extra demand for nucleation energy lowers $T_{½}$ to below T_0.[4,30] The suggestion of nucleation energy is necessitated by the assumption that the elastic energy at the start of the transformation is zero and this assumption is obviously based on the concept of accumulated stored elastic energy. This is incorrect, as has been discussed above. Furthermore, the demand for nucleation energy will cease once the martensite is nucleated and this will imply a spring back of the driving force (temperature) for the transformation, analogous to the phenomenon of supercooling for nucleation in solidification. Such behaviour is never observed in thermally induced martensitic transformations.

3.6.4 Transformation temperature hysteresis

Transformation temperature hysteresis can be determined using equations 3.23 and 3.24, as:

$$\eta_T = T^{M\to A}(f_m) - T^{M\to A}(f_m)$$

$$= \frac{\Delta H^{M\to A} + \Delta E_{el}^{M\to A}(f_m) + \Delta E_{ir}^{M\to A}(f_m)}{\Delta S^{M\to A}} - \frac{\Delta H^{A\to M} + \Delta E_{el}^{M\to A}(f_m) + \Delta E_{ir}^{A\to M}(f_m)}{\Delta S^{A\to M}}$$

$$= \frac{-2\Delta E_{ir}^{A\to M}(f_m)}{\Delta S^{A\to M}} \qquad [3.35]$$

This relationship is already well recognised. The only precaution for using this equation is that $\Delta E_{ir}(f_m)$ is not a material constant and its value is dependent on the actual path of a transformation.

3.7 Transformation heats

Parallel to the discussions above on transformation temperatures, which are determined by the local free energy balance of the various specific energies at the transformation front, there is another important discussion on the exchange of the absolute amount of energies between the transforming system and the environment. Such discussion is important for both the development of the thermodynamic theories of thermoelastic martensitic transformations and for interpretation of the behaviour of shape memory alloys, for example for the determination of thermodynamic parameters such as enthalpy and entropy changes,[5] the determination and understanding of the linearity constant of the Clausius–Clapeyron relationship,[13,14] and the self-heating effect of stress-induced martensitic transformation in deformation.[31]

It is obvious from equations 3.15 that, due to the participation of non-chemical free energy contributions, the heat effect of the transformation cannot be simply equated to the enthalpy change. For this we need to examine the energy exchange between the transforming system and the environment over an infinitesimal step during the transformation in absolute quantity:

$$dG = dH - TdS + dE_{el}(f_m) + dE_{ir}(f_m) \qquad [3.36]$$

The last term in the equation is the sum of all irreversible energies consumed, including energy stored in the matrix by the generation of defects, frictional heat associated with the moving of internal defects and transformation phase boundaries, and acoustic emissions. From the viewpoint of energy analysis, all these irreversible energies may be separated in two groups, irreversible heat ($E_{ir,q}$) and irreversible work other than heat ($E_{ir,w}$), i.e.

$$dE_{ir}(f_m) = dE_{ir,q}(f_m) + dE_{ir,w}(f_m) \qquad [3.37]$$

When a transformation proceeds under 'quasi-equilibrium' conditions at $dG^{A\to M} = 0$ or $dG^{M\to A} = 0$ (note: this is not a thermodynamic equilibrium condition because they define two different conditions), we have:

$$dH - TdS + dE_{el}(f_m) + dE_{ir,q}(f_m) + dE_{ir,w}(f_m) = 0 \quad [3.38]$$

In this equation both $T\mathrm{d}S$ and $E_{\mathrm{ir,q}}(f_{\mathrm{m}})$ are heat terms, thus:

$$dq = TdS - dE_{ir,q}(f_m) = dH + dE_{el}(f_m) + dE_{ir,w}(f_m) \quad [3.39]$$

Therefore, the total heat accumulated during the process of the transformation from $0 \rightarrow f_{\mathrm{m}}$ may be computed as (for per unit mass of sample):

$$\begin{aligned} Q(f_m) &= \int_0^{f_m} dq = \int_0^{f_m} [dH + dE_{el}(f_m) + dE_{ir,w}(f_m)] \\ &= \int_o^{f_m} \Delta H df_m + \int_o^{f_m} \Delta E_{el}(f_m) df_m + \int_o^{f_m} \Delta E_{ir,w}(f_m) df_m \\ &= \Delta H f_m + E_{el}(f_m) + E_{ir,w}(f_m) \end{aligned} \quad [3.40]$$

where $E_{\mathrm{el}}(f_{\mathrm{m}})$ and $E_{\mathrm{ir,w}}(f_{\mathrm{m}})$ are the accumulated elastic strain energy and the non-heat irreversible work of the transformation over the process of $0 \rightarrow f_{\mathrm{m}}$, therefore:

$$E_{el}(0) = 0 \quad [3.41]$$

$$E_{ir}(0) = 0 \quad [3.42]$$

For a complete transformation, $f_{\mathrm{m}} = 1$, thus;

$$Q = \Delta H + E_{el}(1) + E_{ir,w}(1) \quad [3.43]$$

It is seen that the heat effect of a martensitic transformation is the sum of the three energies, instead of the pure enthalpy change. For the forward and the reverse processes, the heat effects are:

$$\mathrm{A}\rightarrow\mathrm{M}: \quad Q^{A\rightarrow M} = \Delta H^{A\rightarrow M} + E_{el}^{A\rightarrow M}(1) + E_{ir,w}^{A\rightarrow M}(1) \quad [3.44a]$$

$$\mathrm{M}\rightarrow\mathrm{A}: \quad Q^{M\rightarrow A} = \Delta H^{M\rightarrow A} + E_{el}^{M\rightarrow A}(1) + E_{ir,w}^{M\rightarrow A}(1) \quad [3.45b]$$

where $Q^{\mathrm{A}\rightarrow\mathrm{M}}$ is an exothermic heat and $Q^{\mathrm{M}\rightarrow\mathrm{A}}$ is an endothermic heat, i.e.

$$Q^{\mathrm{A}\rightarrow\mathrm{M}} < 0 \quad [3.46a]$$

$$Q^{\mathrm{M}\rightarrow\mathrm{A}} > 0 \quad [3.46b]$$

and (the equality between $E_{ir,w}^{A\rightarrow M}$ and $E_{ir,w}^{M\rightarrow A}$ is an assumption of convenience)

$$E_{el}^{A\rightarrow M}(1) = -E_{el}^{M\rightarrow A}(1) > 0 \quad [3.47]$$

$$E_{ir,w}^{A\rightarrow M}(1) = E_{ir,w}^{M\rightarrow A}(1) > 0 \quad [3.48]$$

Re-presenting equation 3.18 here for convenience:

$$\Delta H^{A\to M} = -\Delta H^{M\to A} < 0 \quad [3.49]$$

We may express the heat loss over a complete transformation cycle, as:

$$\Delta Q = Q^{A\to M} + Q^{M\to A} = 2E_{ir,w} \quad [3.50]$$

The sum of the heats of the forward and the reverse transformations defines:

$$Q^{M\to A} - Q^{A\to M} = 2\Delta H^{M\to A} + 2E_{el}^{A\to M} \quad [3.51]$$

or

$$E_{el} = \Delta H - \frac{1}{2}(Q^{M\to A} - Q^{A\to M}) \quad [3.51b]$$

In equations 3.50 and 3.51, all the terms on the right-hand side are positive values. Equation 3.50 states that the heat loss over a complete transformation cycle, as determined by calorimetry measurement, equals the non-heat component of the irreversible energy consumed during the full process of the transformation cycle (instead of the total irreversible energy). Equation 3.51b states that the total elastic strain energy stored in the matrix may be estimated by the difference between the enthalpy change and the average of the absolute values of the heat effects of the forward and the reverse transformations.

3.8 Experimental verifications and interpretations

3.8.1 Lüders-type deformation and transformation interval

It is commonly observed experimentally that stress-induced martensitic transformations in near-equiatomic NiTi in tension proceed over a stress plateau, which is often accompanied by an apparent 'upper-lower yielding' phenomenon at the start of both the forward and the reverse transformation processes.[32–35] Figure 3.6 shows a collection of pseudoelastic stress–strain curves of a Ti–50.2at%Ni alloy wire deformed in tension at different temperatures.[13] Such behaviour has been referred to as a Lüders-type deformation, in reference to its behavioural similarity to the Lüders deformation of mild steels. Whilst there has been much debate regarding the mechanisms of such phenomena,[36–38] the interest here is on the thermodynamic state of the sample during the process of deformation over the stress plateau. It has been well established that deformation of the sample over the stress plateau is localised, with two distinctive regions of deformation, as schematically illustrated in the inset in Fig. 3.6. The strain in region A corresponds to that at the beginning of the stress plateau (e.g. 1.7% in the case shown in the figure) and the strain in region B corresponds to that at the end of the stress plateau (e.g. 8.1% in the case shown in the figure). Continuation of the global deformation over the stress plateau occurs by the expansion of the 'Lüders bands' of stress-induced martensite in region B at the expense of region A along the length of the sample, whilst the strains within the two regions remain unchanged all the way to the end of the stress

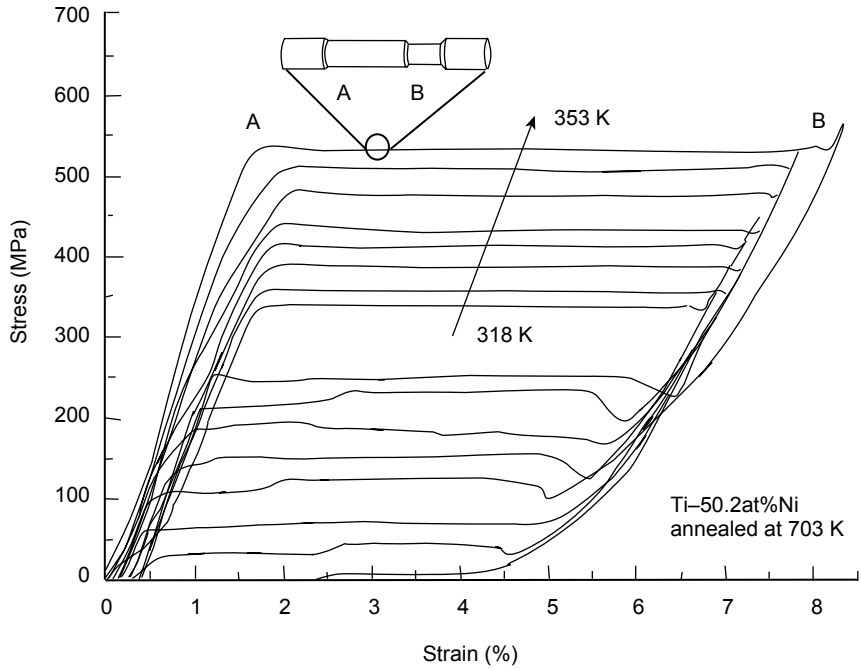

3.6 Effect of temperature on pseudoelastic behaviour of Ti–50.2at%Ni wire in tension.[13] (Reproduced with permission from American Institute of Physics.)

plateau. Such behaviour has the following important implications for our thermodynamic discussion:

1 The stress-induced transformation proceeds at a single value of stress. This stress is characteristic of both the beginning and the end of the stress-induced transformation process. It is unjustified to correlate the intercept temperature of the dependence of this stress to temperature (see section 8.2 for more details) to zero stress to either M_s or M_f, as commonly perceived.
2 The continuation of the deformation over the stress plateau is not a continuous evolution of the thermodynamic equilibrium condition during the transformation for the thermoelasticity described in section 3.2. Instead, each small step of deformation over the stress plateau is a complete journey of the process of transformation and the continuation of deformation over the stress plateau is a continuous repetition of the same process under the same set of conditions.
3 The occurrence of the Lüders-type deformation conveniently makes it possible to determine the actual strain that occurs across the transformation interface between the austenite and the martensite during the stress-induced transformation. It equals exactly the strain span of the stress plateau. This parameter is important in determining the constant of the Clausius–Clapeyron relation, as expressed in equation 3.6.

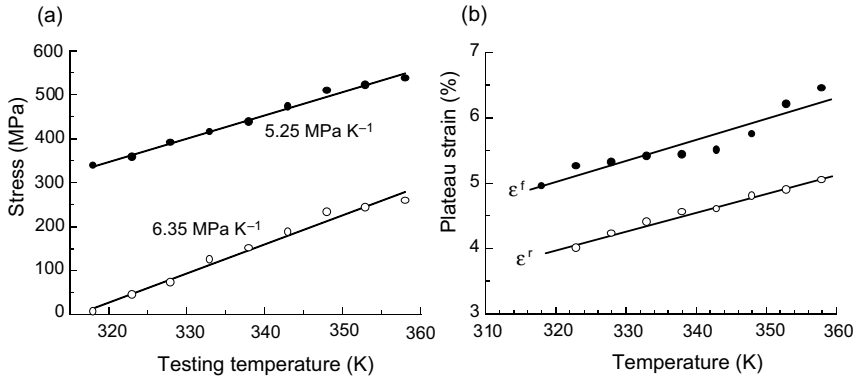

3.7 Temperature dependences of (a) critical stresses and (b) plateau strains for stress-induced B2→B19' martensitic transformation in Ti–50.2at.%Ni.[13] (Reproduced with permission from American Institute of Physics.)

3.8.2 Clausius–Clapeyron relation

Transformation strain dependence of the Clausius–Clapeyron relation

The Clausius–Clapeyron relation between stress and temperature for martensitic transformations, as expressed in equation 3.6, has been widely observed experimentally under various conditions for various shape memory alloys. It is seen in Fig. 3.6 that both the forward and the reverse processes of the stress-induced transformation may proceed over a stress plateau in a Lüders-type manner. Figure 3.7(a) shows the dependence of the plateau stress on temperature, demonstrating the linear relationships described by the Clausius–Clapeyron relation expressed in equation 3.6. The slopes of the linear relationships for the forward and the reverse transformations are determined to 5.25 and 6.35 MPa K^{-1}, respectively. It is seen in equation 3.6 that the actual value of $\frac{d\sigma}{dT}$ is proportional to $\frac{1}{\varepsilon_t}$, where ε_t is the actual strain at the transformation interface. Referring to the discussion above, it is known that the stress plateau length is exactly the strain across the transformation interface in the case of Lüders-type deformation, and it is obvious in Fig. 3.6 that the plateau strain for the forward transformation is larger than that of the reverse transformation. The difference in the $\frac{d\sigma}{dT}$ value for the forward and the reverse transformations is obviously caused by the difference in the stress plateau strain between the two processes.

In addition, it is also obvious from Fig. 3.6 that the plateau strain varies with varying temperature. The variation of the stress plateau strains for the forward (ε_{pl}^{f}) and the reverse (ε_{pl}^{r}) transformations are shown in Fig. 3.7b. It is seen that both ε_{pl}^{f} and ε_{pl}^{r} increase with increasing temperature. According to equation 3.6, this implies a decrease of $\frac{d\sigma}{dT}$ with increasing temperature, deviating the $\sigma - T$ dependence

from linearity to a parabolic relationship. However, such prediction is obviously not observed, at least to the accuracy of the measurement.

Transformation dependence of Clausius–Clapeyron relation

It is known that near-equiatomic Ti–Ni alloys exhibit three separate martensitic transformations among three phases: the B2 parent phase, a trigonal R phase and a monoclinic B19' martensite.[39–41] All transformations among these three phases, including B2↔B19', B2↔R and R↔B19', can be induced by external stresses. The three transformations have different values of transformation entropy change and transformation strain, thus exhibit different stress–temperature dependences. Figure 3.8(a) shows the measurements of the critical stress and temperatures for B2→R, R→B19' and B19'→B2 transformations for a Ti–50.2at%Ni alloy.[42] The Clausius–Clapeyron slopes for the transformations are determined to be [42,43]

$$\left.\frac{d\sigma}{dT}\right|_{B2\to B19'} = 6.4\,MPa/K,\quad \left.\frac{d\sigma}{dT}\right|_{R\to B19'} = 5.6\,MPa/K \text{ and}$$

$$\left.\frac{d\sigma}{dT}\right|_{B2\to R} = 15.6\,MPa/K.$$

Figure 3.8(b) shows schematically a more comprehensive presentation of the conditions.[44]

The $\frac{d\sigma}{dT}$ values reported in the literature for stress-induced martensitic transformation for near-equiatomic Ti–Ni typically are 5~7 MPa. On one hand, it is seen in the discussion in section 3.8.4 and equation 3.6 that $\frac{d\sigma}{dT}$ varies with ε_t, which is affected by a range of factors such as the geometry of the sample, the loading mode (being tension or compression),[11,12,45,46] the metallurgical conditions of the material and the testing temperature.[10,13] Therefore, $\frac{d\sigma}{dT}$ is not a material constant. On the other hand, these values fall well within the limits for $\left.\frac{d\sigma}{dT}\right|_{B2\to B19'}$ and $\left.\frac{d\sigma}{dT}\right|_{R\to B19'}$. A mixed mode of deformation via stress-induced B2↔B19' and R↔B19' transformation may result in $\frac{d\sigma}{dT}$ value being within the limits for the two pure transformations. Such a deformation mode is common for age-hardened Ni-rich Ti–Ni alloys and cold-worked and partially annealed near-equiatomic Ti–Ni.

3.8.3 Transformation sequence

It is known that near-equiatomic NiTi exhibit three common transformation sequences, as shown in Fig. 3.9.[47] Transformation sequence (a) is a single step B2↔B19' transformation. Transformation sequence (b) is B2→R→B19' on cooling and B19'→B2 on heating. The R→B2 transformation may be observed by heating immediately after the completion of the B2→R transformation, as shown in the small curve for a partial transformation cycle. Transformation sequence (c)

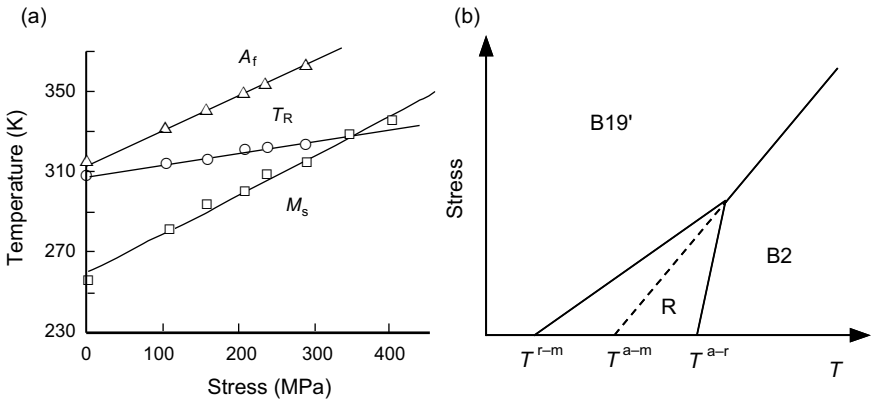

3.8 Stress–temperature dependences of stress-induced transformations in Ti–50.2at%Ni; (a) experimental measurement,[42] (b) schematic expression (reproduced with permission from Elsevier).

is the reversible process of B2↔R↔B19'. The B2↔R transformation is characteristic of a small hysteresis of 3~5 K, whereas the B2↔B19' transformation is characteristic of a larger hysteresis of typically ~30 K.

The interesting point is the appearance of the R phase in-between the B2 and the B19' martensite upon cooling and the disappearance of the R phase transformation on heating. This phenomenon has been explained in terms of the effect of irreversible energies,[48] as shown in Fig. 3.10(a).[47] In the figure, because of the influence of irreversible energies, the forward and the reverse processes of the B2–B19' martensitic transformation occurs at two different temperatures T^{a-m} and T^{m-a}, respectively, away from the thermodynamic equilibrium temperature (T_o). Such common knowledge is expressed in this figure by splitting the free energy state of the B19' martensite into two lines, denoted G^{M-} for the cooling transformation and G^{M+} for the heating transformation. The separation distance between the two lines reflects the magnitude of the irreversible energy. Detailed discussion of this method has been presented by Liu.[47,48] Given the fact that the thermal hysteresis of the B2–R phase transformation is much smaller than that of the B2–B19' transformation, the split of the free energy line for the R phase is much narrower. In this expression, at high temperature, the system is in B2 austenite state. Upon cooling to T^{a-r} where $G_{ch}^{A} = G_{ch}^{R-}$, austenite transforms to the R phase. Further cooling to T^{r-m} where $G_{ch}^{R-} = G_{ch}^{M-}$, the R phase transforms to the martensite. The B2→B19' transformation, which is to occur at T^{a-m}, is thermodynamically prohibited. For heating from the martensite state, the system free energy state is expressed by G_{ch}^{M+}, owing to the hysteresis of the B2–B19' transformation. Upon heating, the martensite reverts back to austenite directly at T^{m-a}. The B19'→R transformation, which occurs at T^{m-r}, is thermodynamically prohibited. The reverse R→B2 transformation is observed by heating from between T^{a-r} and T^{r-m}.

Figure 3.10(b) depicts the situation for the transformation sequence of

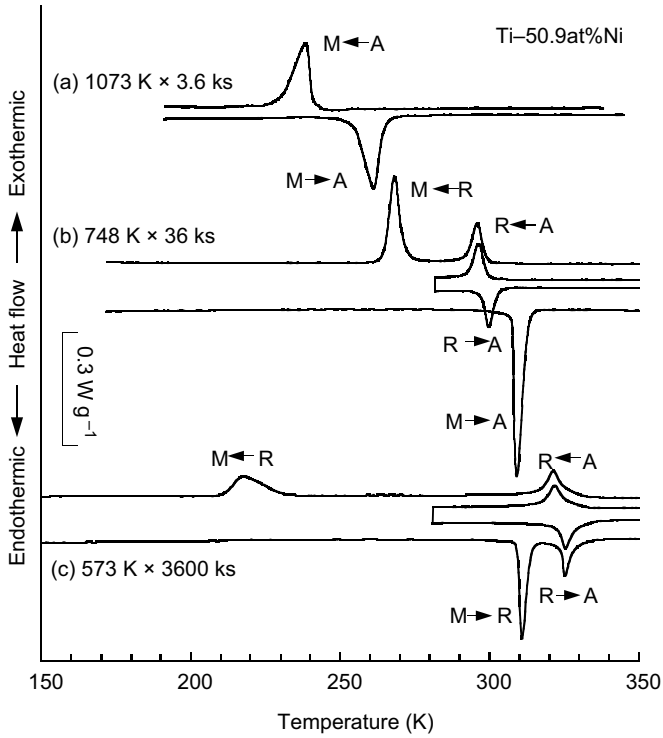

3.9 Common transformation sequences of near-equiatomic Ti–Ni.[48] (Reproduced with permission from Taylor & Francis.)

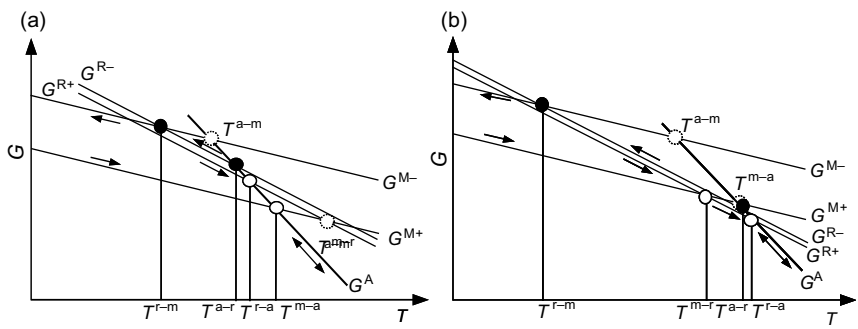

3.10 Thermodynamic expressions of the transformation sequences: (a) B2→R→B19' on cooling and B19'→B2 on heating; (b) B2↔R↔B19'.[48] (Reproduced with permission from Taylor & Francis.)

B2↔R↔B19' shown in curve (c) in Fig. 3.9. Referring to both Fig. 3.10(a) and (b), the following conclusions may be drawn:

1 The B19'→R transformation is omitted in transformation sequence (b) shown in Fig. 3.9 because the large thermal hysteresis of the B2↔B19' transformation.
2 The common notion of M_s temperature for the 'martensitic' transformation in the literature is inappropriate when the B2–R transformation occurs on cooling. T^{a-m} and T^{r-m} are clearly two different temperatures for two different phase transformations.
3 The thermal hysteresis of R↔B19' transformation ($T^{m-r} - T^{r-m}$) is greater than the thermal hysteresis of B2↔B19' transformation ($T^{m-a} - T^{a-m}$). This is intrinsically determined by the fact that $S^M > S^R$. The commonly observed temperature difference between T^{r-m} and T^{m-a} is not a valid thermal hysteresis for thermodynamic discussion.
4 The separation between the two cooling transformations B2→R and R→B19' is always greater than the separation between the two heating transformations B19'→R and R→B2.

3.8.4 Thermal–mechanical inequality

The Clausius–Clapeyron relation expressed in equation 3.6 describes the equivalence between stress and temperature in inducing a martensitic transformation. With this understanding, attempts have been made in the literature to correlate transformation parameters determined from thermally induced transformations to those from mechanically induced transformations. A typical example is between the M_s temperature and the critical stress for stress-induced transformation.

However, as discussed in section 3.6, actual temperatures and stresses at which a transformation may occur are dependent on the elastic strain energy and irreversible energy, and neither of the elastic strain energy and irreversible energy are materials constants. The elastic energy is dependent on the configuration of the martensite variants and the irreversible energy is dependent on the actual path of the transformation. The martensite variant configuration and the actual path of the transformation are different between thermally induced and stress-induced transformations. Therefore, such correlation is inappropriate. In fact, there has been adequate experimental evidence showing the inequality between thermally induced and mechanically induced martensitic transformations. A typical example is the mechanically induced martensite stabilisation, [44,49,50] as shown in Fig. 3.11.[50] Sample (a) is in the as-annealed state. Sample (b) has been deformed via martensite reorientation to 6.1% shear strain prior to the DSC measurement. The curve labelled 'first heating' depicts the reverse transformation of the stress-induced martensite, whereas the complete thermal transformation cycles labelled 'second

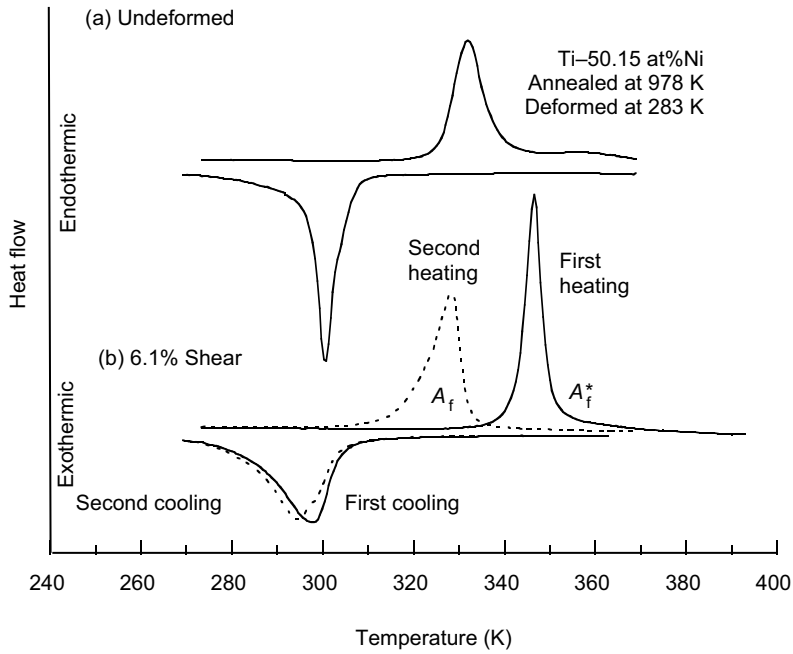

3.11 Mechanically induced martensite stabilisation, demonstrating the difference between mechanically induced and thermally induced martensite.[51] (Reproduced with permission from Elsevier.)

heating' and 'second cooling' was measured after the first reversion. It is obvious that the reverse transformation of the stress-induced, oriented B19' martensite occurs at a higher temperature than the thermally formed, self-accommodating martensite.

One immediate conclusion for this observation is that the shape memory effect, or the shape recovery, does not happen at A_f but at A_f^*.[44] It has commonly been claimed in the literature that complete pseudoelasticity occurs at $T > A_f$, and this is obviously an unconsidered claim.

There exist a range of other phenomena of inequality between thermally induced and mechanically induced martensitic transformations. For example, the B2↔B19' transformation in fully annealed equiatomic NiTi has a typical thermal hysteresis of ~30 K[25] whereas the pseudoelastic stress hysteresis of partially annealed equiatomic Ti–Ni may be >300 MPa,[10] much greater than that estimated using the Clausius–Clapeyron relation of ~7 MPa/K. Such discrepancies imply that it is inappropriate to design of shape memory apparatuses, which almost exclusively involve deformation and shape recovery, using transformation parameters determined from thermally induced transformation. Great caution and proper verifications are needed to make use of experimental data in design.

3.9 Generalisation of thermodynamic theories of thermoelastic martensitic transformations

The free energy balance of the transformation expressed in equation 3.2 considers only the effect of force-displacement energy in addition to the chemical free energies. In fact, many other forms of energy contributions may also influence the transformation free energy balance. Wollants *et al.*[1] generalised the concept and suggested that based on the first law of thermodynamics:

$$\mathrm{d}U = \delta Q + \delta W \qquad [3.52]$$

where δW represents all the non-heat work of the system, the free energy of the system may be most generally expressed as:

$$G = U - \sum X_i Y_i \qquad [3.53]$$

where $\sum X_i Y_i$ expresses the sum of all energy contributions except the internal energy, including temperature–entropy energy, pressure–volume energy, force–displacement energy, magnetic field–magnetisation energy, etc. Correspondingly, under the condition of constant temperature, pressure, force, magnetic field, etc., the free energy change of a first-order phase transformation may be expressed as:

$$\Delta G = \Delta U - \sum Y_i \Delta X_i = \Delta U - T\Delta S + P\Delta V - F\Delta L - H\Delta M - \ldots \qquad [3.54]$$

This equation is the general form of equation 3.2. At the moment of transformation equilibrium when $\Delta G = 0$, differentiating equation 3.54 against each pair combination of individual external parameters defines various Clausius–Clapeyron type relations, including:

$$\left.\frac{\partial P}{\partial T}\right|_{H,F} = \frac{\Delta S}{\Delta V} \qquad [3.55a]$$

$$\left.\frac{\partial F}{\partial T}\right|_{H,P} = -\frac{\Delta S}{\Delta L} \qquad [3.55b]$$

$$\left.\frac{\partial H}{\partial T}\right|_{F,P} = -\frac{\Delta S}{\Delta M} \qquad [3.55c]$$

$$\left.\frac{\partial H}{\partial F}\right|_{T,P} = -\frac{\Delta L}{\Delta M} \qquad [3.55d]$$

$$\left.\frac{\partial H}{\partial P}\right|_{T,F} = \frac{\Delta V}{\Delta M} \qquad [3.55e]$$

The essence of equations 3.55 may be described as the following:

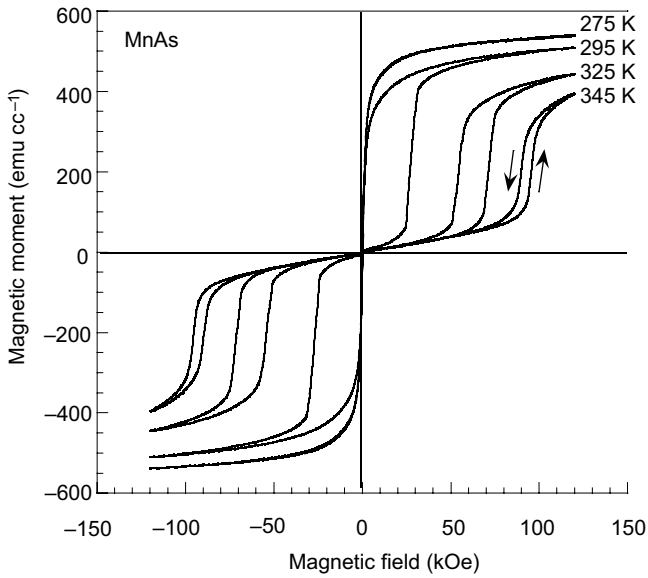

3.12 Temperature-dependence of magnetic field induced martensitic transformation in MnAs.

1 If the transformation involves volume change, its temperature is affected by hydrostatic pressure;[51,52]
2 If the transformation involves linear dimensional change, its temperature is affected by force;[2,13,43]
3 If the transformation involves magnetisation change, its temperature is affected by magnetic field;[53,54]
4 If the transformation involves magnetisation change and linear dimensional change, the critical stress for inducing the transformation is affected by magnetic field.

More mathematical forms may be derived from equation 3.54, but they are of less relevance to practical engineering shape memory alloys, at least for those known today. Equation 3.55a is, in effect, the original form of the Clausius–Clapeyron equation. Equation 3.55b is in effect the same as equation 3.6. Equations 3.55c–e express the relationships between magnetic field and temperature, magnetic field and mechanical load and pressure, respectively. Some of these relationships have been experimental verified, for example the experimental observation shown in Fig. 3.12. Figure 3.12 shows the magnetisation behaviour of MnAs, which experiences a paramagnetic–ferromagnetic martensitic transformation between an orthorhombic MnP-type parent phase and a hexagonal NiAs-type martensite. The higher magnetisation state represents the martensite phase and the lower magnetisation state represents the parent phase. The magnetisation transformation process

exhibits typical hysteresis loops. It is seen that a higher magnetic field is required to induce the ferromagnetic martensite when the temperature is increased, and the dependence of the critical field on temperature has been shown to be linear.[53] Similar phenomena are also observed in other alloy systems, such as FeRh,[54,55] GdSiGe[56,57] and the Heusler NiCoMnSn.[58]

3.10 Summary

The fundamental thermodynamic principles of thermoelastic martensitic transformations have been well understood and documented. Formulation of thermodynamic expressions of the transformation processes has been established. However, the application of the theories to practical shape memory alloys as reported in the literature contains many misperceptions and incorrect concepts.

The thermodynamic theories developed provide useful tools for the interpretation of experimental observations and understanding of the behaviour of shape memory alloys. On the other hand, the theories lack the capability to accurately determine or extract materials parameters so to be used as mathematical tools in the design of shape memory apparatuses.

3.11 References

1 P. Wollants, J. R. Roos, L. Delaey, *Prog. Mater. Sci*. **37** (1993) 227–288.
2 P. Wollants, M. De Bonte, J. R. Roos, *Z. Metallkd*. **70** (1979) 113.
3 P. Wollants, J. R. Roos, L. Delaey, *Scripta Metall.* **14** (1980) 1217–1223.
4 R. J. Salzbrenner, M. Cohen, *Acta Metall*. **27** (1979) 739–748.
5 J. Ortin, A. Planes, *Acta Metall.* **36** (1988) 1873–1889.
6 J. Ortin, A. Planes, *Acta Metall.* **37** (1989) 1433–1441.
7 G. V. Kurdjumov, *J. Metals* **11** (1959) 449.
8 C. M. Wayman, *Mater. Sci. Forum* 56–58 (1990) 1–32.
9 C. M. Wayman, in: *Int. Conf. Solid–Solid Phase Transformations,* ASM–AIME, Pittsburg, USA, 1982, p. 1119.
10 G. S. Tan, T. Suseno, Y. Liu, *Mater. Sci. Forum* 394–395 (2002) 249–252.
11 Y. Liu, Z. Xie, J. V. Humbeeck, L. Delaey, *Acta Mater*. **46** (1998) 4325–4338.
12 L. Orgeas, D. Favier, *J. Phys. IV* **5** (1995) 605–610.
13 Y. Liu, H. Yang, *Smart Mater. Struct.* **16** (2007) 22–27.
14 Y. Liu, H. Yang, *Mater. Sci. Eng. A* **260** (1999) 240–245.
15 G. B. Olson, M. Cohen, *Scripta Metall*. **9** (1975) 1247.
16 Y. Liu, P. G. McCormick, *Acta Metall. Mater.* **42** (1994) 2401–2406.
17 P. G. McCormick, Y. Liu, *Acta Metall. Mater.* **42** (1994) 2407–2413.
18 S. Zhang, P. G. McCormick, *Acta Mater.* **48** (2000) 3081–3089.
19 S. Zhang, P. G. McCormick, *Acta Mater*. **48** (2000) 3091–3101.
20 J. Perkins, R. O. Sponholz, *Metall. Trans*. **15A** (1984) 313.
21 S. Miyazaki, Y. Igo, K. Otsuka, *Acta Metall.* **34** (1986) 2045–2051.
22 A. Rotini, A. Biscarini, R. Campanella, B. Coluzzi, G. Mazzolai, F. M. Mazzolai, *Scripta Mater*. **44** (2001) 719–724.
23 H. C. Lin, S. K. Wu, T. S. Chou, H. P. Kao, *Acta Metall. Mater.* **39** (1991) 2069–2080.

24 Y. Liu, P. G. McCormick, *ISIJ Int.* **29** (1989) 417–422.
25 T. Todoroki, H. Tamura, *Trans. JIM* **28** (1987) 83.
26 S. Miyazaki, T. Imai, Y. Igo, K. Otsuka, *Metall. Trans. A* **17A** (1986) 115–120.
27 M. Nishida, C. M. Wayman, T. Honma, *Metall. Trans. A* **17A** (1986) 1505–1515.
28 J. Khalil-Allafi, G. E. Antonin Dlouhy, *Acta Mater*. **50** (2002) 4255–4274.
29 L. Bataillard, J.-E. Bidaux, R. Gotthardt, *Phil. Mag. A* **78** (1998) 327–344.
30 H. C. Tong, C. M. Wayman, *Acta Metall*. **22** (1974) 887–896.
31 P. G. McCormick, Y. Liu, S. Miyazaki, *Mater. Sci. Eng. A* **167** (1993) 51–56.
32 Y. Liu, Y. Liu, J. V. Humbeeck, *Scripta Mater*. **39** (1998) 1047–1055.
33 J. A. Shaw, S. Kyriakides, *Int. J. Plasticity* **13** (1997) 837–871.
34 S. Miyazaki, T. Imai, K. Otsuka, Y. Suzuki, *Scripta Metall*. **15** (1981) 853–856.
35 H. B. Sun, F. Yoshida, M. Ohmori, X. Ma, *Mater. Lett*. **57** (2003) 4535–4539.
36 P. Sittner, Y. Liu, V. Novak, *J. Mech. Phys. Solids* **53** (2005) 1719–1746.
37 J. A. Shaw, S. Kyriakides, *Acta Mater*. **45** (1997) 683–700.
38 Y. Liu, *Mater. Sci. Eng. A Lett*. **271** (1999) 506–508.
39 K. Otsuka, X. Ren, *Prog. Mater. Sci*. **50** (2005) 511–678.
40 K. Otsuka, T. Sawamura, K. Shimizu, *Phys. Status Solidi (a)* **5** (1971) 457.
41 R. F. Hehemann, G. D. Sandrock, *Scripta Metall*. **5** (1971) 801.
42 G. B. Stachowiak, P. G. McCormick, *Scripta Metall*. **21** (1987) 403–406.
43 G. B. Stachowiak, P. G. McCormick, *Acta Metall*. **36** (1988) 291–297.
44 Y. Liu, S. P. Galvin, *Acta Mater*. **45** (1997) 4431–4439.
45 K. Gall, H. Sehitoglu, *Int. J. Plasticity* **15** (1999) 69–92.
46 K. Gall, H. Sehitoglu, Y. I. Chumlyakov, I. V. Kireeva, *Acta Mater*. **47** (1999) 1203–1217.
47 Y. Liu, J. I. Kim, S. Miyazaki, *Phil. Mag. A* **84** (2004) 2083–2102.
48 Y. Liu, P. G. McCormick, *Mater. Trans., JIM* **37** (1996) 4691–4696.
49 Y. Liu, D. Favier, *Acta Mater*. **48** (2000) 3489–3499.
50 Y. Liu, *Mater. Sci. Eng. A* 273–275 (1999) 668–672.
51 T. Kakeshita, T. Saburi, K. Shimizu, *Mater. Sci. Eng. A* 273–275 (1999) 21–39.
52 T. Goto, M. I. Bartashevich, K. Kondo, K. Terao, H. Yamada, H. Ido, *J. Alloys Compounds* **325** (2001) 18–23.
53 R. W. D. Blois, D. S. Rodbell, *J. Appl. Phys*. **34** (1963) 1101–1103.
54 M. R. Ibarra, A. Aigarabel, C. Marquina, Y. Otani, S. Yuasa, I. Miyajima, *J. Magnetism Magnetic Mater*. 140–144 (1995) 231–232.
55 M. R. Ibarra, A. Aigarabel, *Phys. Rev. B* **50** (1994) 4196–4199.
56 L. Morellon, P. A. Algarabel, C. Magen, M. R. Ibarra, *J. Magnetism Magnetic Mater*. **237** (2001) 119–123.
57 L. Morellon, P. A. Algarabel, M. R. Ibarra, J. Blasco, B. Garcia-Landa, Z. Arnold, F. Albertini, *Phys. Rev. B* **58** (1998) R14 721–724.
58 R. Kainuma, Y. Imano, W. Ito, H. Morito, Y. Sutou, K. Oikawa, A. Fujita, K. Ishida, S. Okamoto, O. Kitakami, T. Kanomata, *Appl. Phys. Lett*. **88** (2006) 192513.

4

Alternative shape memory alloys

H. Y. KIM and S. MIYAZAKI
University of Tsukuba, Japan

Abstract: Concerns about the release of Ni ion during long-term use in human body have stimulated the development of Ni-free shape memory and superelastic alloys, although Ti–Ni alloys are considered to be safe to the human body. In this chapter, the basic characteristics of Ti-based alloys are reviewed, including the martensitic transformation and shape memory properties that make these alloys promising materials for biomedical shape memory and superelastic alloys.

Key words: titanium alloys, alloy design, heat treatment, microstructure, texture, Ni–Ti, Ti–Ni, Nitinol.

4.1 Introduction

Recently, the use of Ti–Ni shape memory alloys in the field of biomaterial and medical devices has shown a remarkable increase. For example, superelastic Ti–Ni alloys have been successfully applied as orthodontic arch wires, guide wires and stents. These alloys have been also considered as attractive candidates for orthopedic implants since the effective modulus is extremely low when considering their superelastic effect. However, it has been pointed out that pure Ni is a toxic element and causes Ni-hypersensitivity. Although the Ti–Ni alloys are considered to be safe to the human body, the risk of Ni-hypersensitivity has restricted the use of Ti–Ni alloys as implant materials, mostly due to psychological reasons since Ti–Ni alloys contain about 50 at.% Ni.

Concerns about the release of Ni ion during long-term use in human body have stimulated the development of Ni-free shape memory and superelastic alloys. Besides Ti–Ni alloys, Cu-based shape memory alloys such as Cu–Zn–Al and Cu–Al–Ni have been intensively investigated due to their low cost of alloying elements and good properties. However, it is doubtful whether Cu-based shape memory alloys can be used as an alternative to Ti–Ni alloys in terms of biocompatibility, since none of Cu, Al or Ni is particularly biocompatible. On the other hand, extensive research has shown that β-type Ti-based alloys consisting of only biocompatible or less toxic elements are promising materials for biomedical shape memory and superelastic alloys. To date, many Ti-based shape memory and superelastic alloys have been developed, e.g. Ti–Nb–Sn (Takahashi *et al.*, 2002), Ti–Nb–Al (Fukui *et al.*, 2004), Ti–Nb–Ta (Kim H Y *et al.*, 2006a, 2006e), Ti–Nb–

Zr (Kim J I *et al.*, 2005b, 2006), Ti–Nb–O (Kim J I *et al.*, 2005a), Ti–Nb–Pt (Kim H Y *et al.*, 2007), Ti–Mo–Ga (Kim H Y *et al.*, 2004a), Ti–Mo–Sn (Maeshima and Nishida, 2004a) and Ti–(8–10)Mo–4Nb–2V–3Al (mass%) (Zhou *et al.*, 2004). It has been confirmed that shape memory and superelastic properties of Ti-based alloys can be considerably improved by thermomechanical treatment (Kim H Y *et al.*, 2004b, 2006b, 2006c).

The aim of this chapter is to provide up-to-date information regarding β-type Ti-based shape memory alloys. The effect of composition on shape memory effect and superelasticity of Ti–Nb based alloy is addressed in Sections 4.2 and 4.3. The effect of heat treatment condition and texture on shape memory properties of Ti–Nb based alloy is included in Sections 4.4 and 4.5. Sections 4.6 and 4.7 cover the basic characteristics of Ti–Mo and Ti–V based shape memory alloys.

4.2 Shape memory effect and superelasticity in Ti–Nb based alloys

Shape memory effect and superelasticity have been confirmed in many Ti–Nb based alloys, e.g. Ti–Nb (Kim H Y *et al.*, 2004b, 2006b), Ti–Nb–Sn (Takahashi *et al.*, 2002), Ti–Nb–Al (Fukui *et al.*, 2004), Ti–Nb–Ta (Kim H Y *et al.*, 2006a, 2006e), Ti–Nb–Zr (Kim J I *et al.*, 2005a, 2006), Ti–Nb–Pd (Ping *et al.*, 2005) and Ti–Nb–Pt (Kim H Y *et al.*, 2007) since the first report on shape memory effect (SME) in a Ti–35wt%Nb (Ti-21.7at%Nb) alloy (Baker, 1971).

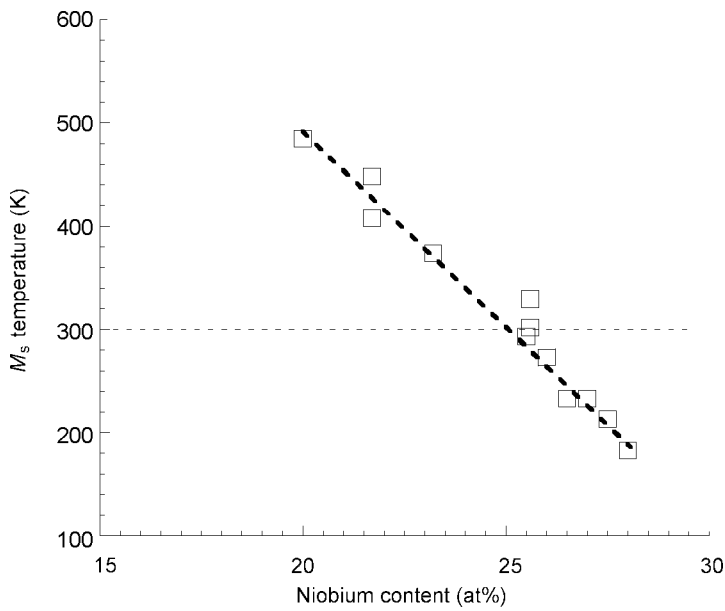

4.1 Niobium content dependence of *Ms* for Ti–Nb binary alloys.

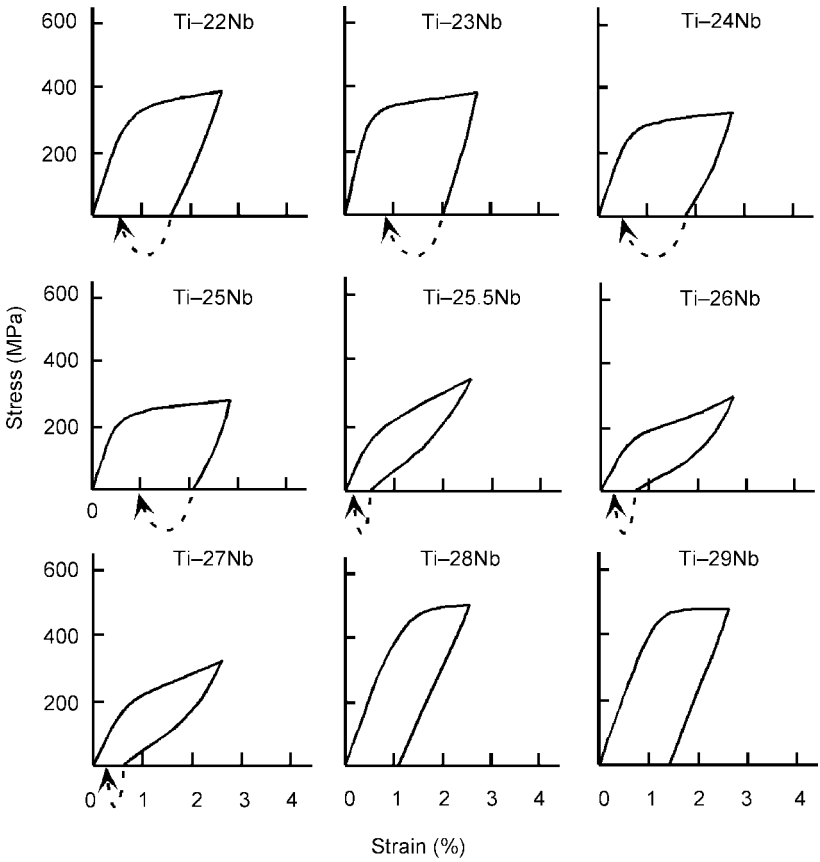

4.2 Stress–strain curves for Ti–(22–29)at.%Nb binary alloys.

Figure 4.1 shows the Nb content dependence of the martensitic transformation start temperature *Ms* for Ti–Nb binary alloys (Kim H Y *et al.*, 2006b). It is seen that *Ms* decreases by 40 K with 1 at.% increase of Nb content for Ti–(20–28)Nb alloys. *Ms* becomes lower than room temperature when the Nb content increases more than 25.5 at.%. Ti–(25.5–27)at.%Nb alloys exhibit superelasticity at room temperature while shape memory effect is observed in Ti–(22–25)at.%Nb alloys. Figure 4.2 shows the series of stress–strain curves for Ti–(22–29)at.%Nb alloys subjected to the solution treatment after cold rolling with the reduction of 95% in thickness (Kim H Y *et al.*, 2004b). The maximum recovered strain of 3% was obtained at about 5% tensile strain in solution treated Ti–(25–27)at.%Nb alloys. The small recovery strain is due to a small intrinsic transformation strain and a low critical stress for slip deformation. Figure 4.3 shows the Nb content dependence of transformation strains for three representative orientations: [011]β, [001]β and $[\bar{1}11]\beta$. It has been reported that a strong deformation texture of {100}<110> is developed in severely cold-rolled β-Ti alloys. A strong recrystallization texture of

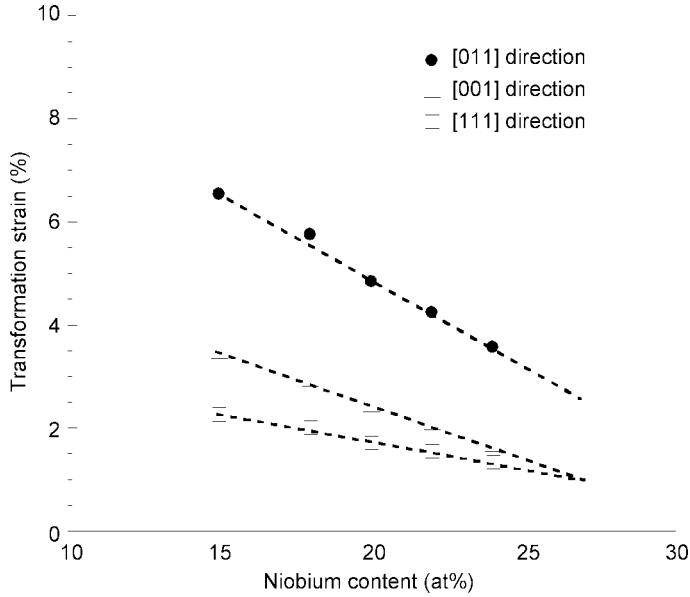

4.3 Niobium content dependence of the transformation strain for Ti–Nb binary alloys.

{112}<110> is developed by solution treatment, indicating that the maximum transformation strain can be obtained along the rolling direction for both deformation and recrystallization textures. It is noted that the transformation strain along the [011]β direction, $\varepsilon_M^{[011]}$, of the Ti–27at.%Nb alloy which shows superelastic behavior at room temperature is only 2.5%. This value is much smaller than that for the B2-B19′ transformation in Ti–Ni alloys. This intrinsic small transformation strain is one of drawbacks of Ti–Nb superelastic alloys.

Additions of all alloying elements, which have been reported up to now, decrease *Ms* of Ti–Nb binary alloys. It has been reported that *Ms* decreases by about 30 K or 35 K with 1 at.% increase of Ta or Zr content in the Ti–22at.%Nb alloy, respectively (Miyazaki *et al.*, 2006). The transformation temperatures *Ms* and *Af* decrease by 150 K with increasing Sn content from 4 to 5 at.% in Ti–16Nb–Sn alloys (Takahashi *et al.*, 2002). It is noted that Zr and Sn considerably lower *Ms*, although they have been considered as neutral elements for α/β transformation temperature. Noble alloying elements also decrease transformation temperature: *Ms* decreases by about 160 K with an increase of 1 at.% Pt (Kim H Y *et al.*, 2007). It is also noted that an addition of Al decreases *Ms* with a slope of 40 K/at.%Al even though Al is considered to be an α-stabilizer (Fukui *et al.*, 2004; Inamura *et al.*, 2007b). Other α-stabilizers such as Ga, Ge and O also decrease transformation temperature of Ti–Nb based alloys (Kim J I *et al.*, 2005b; Inamura *et al.*, 2005a).

It has been reported that the addition of ternary alloying elements such as Zr, Pt, Sn and Al is effective for improving shape memory effect and superelasticity of

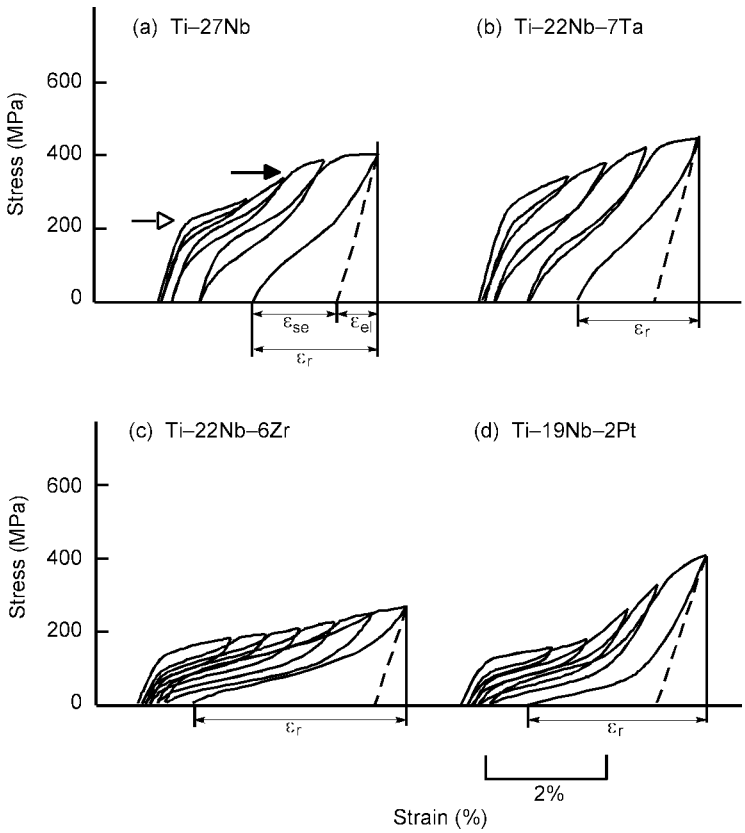

4.4 Stress–strain curves obtained by strain increment cyclic loading and unloading tensile tests in (a) Ti–27Nb, (b) Ti–22Nb–7Ta, (c) Ti–22Nb–6Zr and (d) Ti–19Nb–2Pt.

Ti–Nb alloys. Figure 4.4 shows stress–strain curves of Ti–27at.%Nb and Ti–Nb based ternary alloys exhibit superelasticity at room temperature. The recovery strain ε_r consists of a superelastic component ε_{se} and an elastic component ε_{el}. It is seen that the Ti–22Nb–7Ta (at.%) alloy exhibits superelastic behavior similar to the Ti–27at.%Nb alloy. The maximum recovery strain ε_r of 1.9% was obtained in the Ti–22Nb–7Ta (at.%) alloy. On the other hand, the Ti–22Nb–6Zr (at.%) and Ti–19Nb–2Pt (at.%) alloys exhibit good superelasticity with a larger recovery strain. The maximum ε_r of 3.5 and 3.0% was obtained in the Ti–22Nb–6Zr (at.%) and Ti–19Nb–2Pt (at.%) alloys, respectively. It is supposed that a larger recovery strain of the Ti–22Nb–6Zr (at.%) and Ti–19Nb–2Pt (at.%) alloys is due to a large transformation strain. Figure 4.5(a) shows the effect of Ta or Zr addition on the transformation strain $\varepsilon_M^{[011]}$. The transformation strain decreases by 0.13 or 0.28% with 1 at.% increase of Zr or Ta content, respectively. It is noted that the transformation strain $\varepsilon_M^{[011]}$ decreases by 0.34% with 1 at.% increase of Nb content

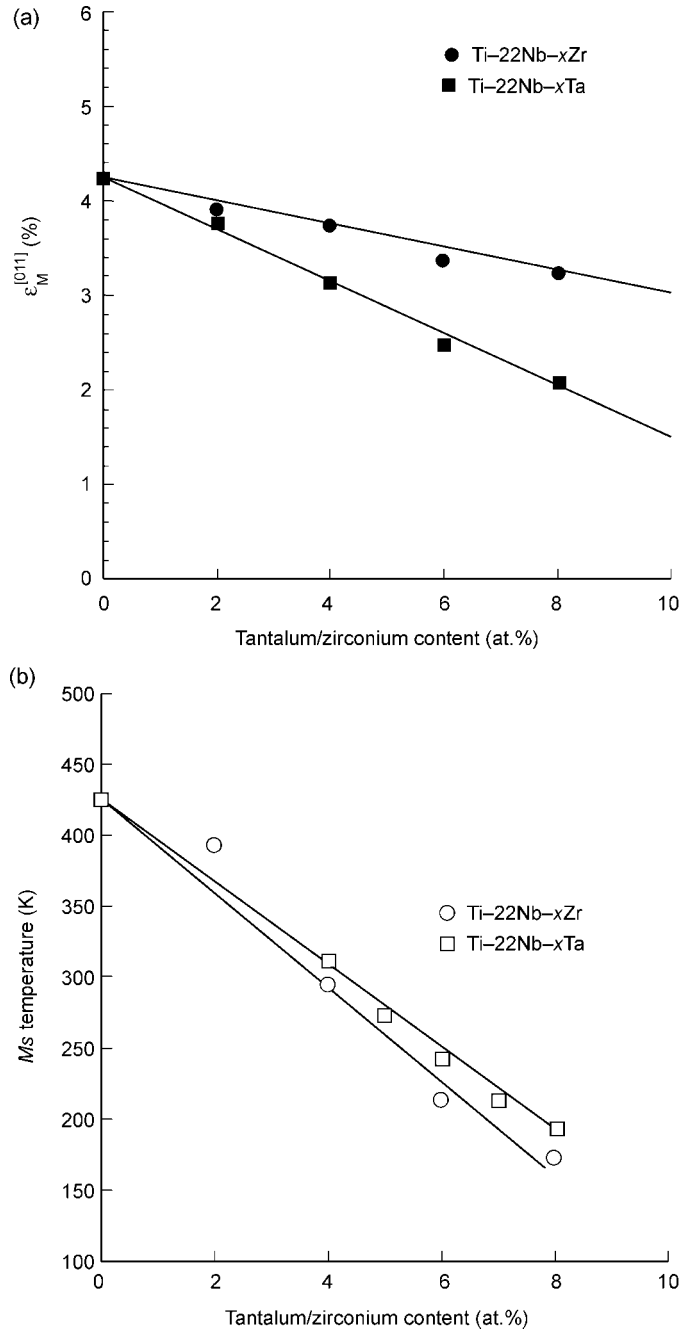

4.5 Effect of tantalum and zirconium addition on (a) transformation strain along the [011]β direction and (b) *Ms* in the Ti–22Nb–*x*Ta and Ti–22Nb–*x*Zr.

as shown in Fig. 4.3. When comparing different composition alloys which reveal similar *Ms*, for example, Ti–27at.%Nb, Ti–22Nb–6Zr (at.%) and Ti–22Nb–7Ta (at.%) alloys, it is clear that the addition of Zr is most effective in increasing the transformation strain. This indicates that the addition of Zr as a substitute of Nb is effective in increasing the transformation strain while keeping *Ms* similar. Many Ti–Nb–Zr ternary alloys such as Ti–22Nb–6Zr (at.%), Ti–18Nb–12Zr (at.%), Ti–16Nb–16Zr (at.%) and Ti–14Nb–18Zr (at.%) alloys exhibit stable superelasticity at room temperature. The superelastic recovery strain increased with increasing Zr content when comparing different composition alloys which reveal similar transformation temperatures. The superelastic recovery strain of 6.4% was obtained in the Ti–14Nb–18Zr (at.%) alloy.

It has been reported that the addition of Pt as a substitute for Nb is also effective to increase the transformation strain of Ti–Nb based superelastic alloys, because Pt is four times more effective for decreasing *Ms* than Nb, while Pt is only three times more effective for decreasing transformation strain than Nb (Kim H Y *et al.*, 2007).

Nitta *et al.* (2001) reported that shape memory effect and superelasticity are observed in Ti–Nb–Sn alloys. The maximum recovered strain is evaluated to be about 3.5% in Ti–18Nb–4Sn (at.%). They claimed that larger superelastic strain is obtained at high Sn content due to solid solution hardening effect of Sn. It has been also reported that Sn addition lowers the elastic modulus of Ti–Nb alloys, resulting in enhancement of superelasticity. The lattice deformation strains decrease with increasing Sn content.

An addition of Al is also effective in enhancing shape memory effect and superelasticity of Ti–Nb alloys. Recently, many aspects of Ti–Nb–Al alloys, e.g. crystallography, textures and mechanical properties, have been investigated (Fukui *et al.*, 2004; Inamura *et al.*, 2004, 2007a, 2007b). For Ti–*x*Nb–3Al alloys, superelastic behavior is obtained when the Nb content is 24at.% at room temperature, since the transformation temperatures decrease with increasing Al content. The maximum recovery strain of over 4% is observed along the rolling direction in Ti–24Nb–3Al (at.%).

4.3 Effect of interstitial alloying elements on shape memory properties of Ti-based shape memory alloys

The low critical stress for slip is one of major drawbacks of Ti–Nb alloys. However, substitutional alloying elements such as Zr, Ta, Al, Pt and Sn exhibited little effect on critical stress for slip deformation. Addition of interstitial elements is effective in increasing the critical stress for slip deformation and improving superelastic properties. The effect of interstitial alloying elements such as O, N and B on the superelastic properties of Ti–Nb based alloys has been investigated (Kim J I *et al.*, 2005a, Tahara *et al.*, 2007). For example, stress–strain curves for the Ti–22Nb–(0–2.0)O (at.%) alloys are shown in Fig. 4.6. A black-headed arrow

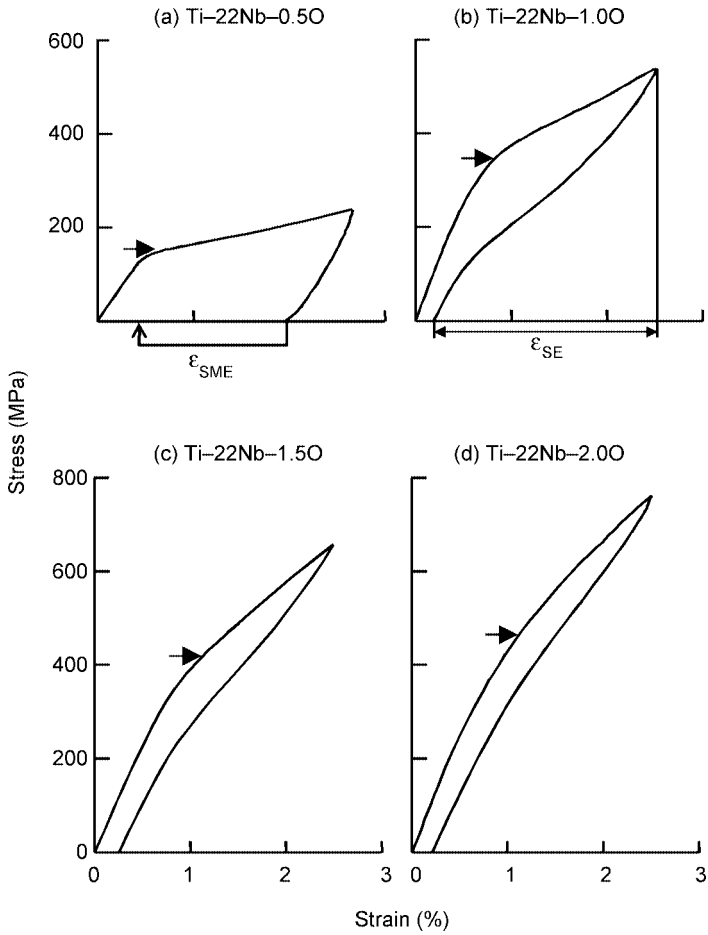

4.6 Stress–strain curves for Ti–22Nb–(0.5–2.0)O (at.%) alloys.

indicates the apparent yield stress which is defined by the 0.2% offset yield stress. The shape memory effect is observed in the Ti–22Nb–0.5O (at.%) alloy while superelastic behavior is seen in the Ti–22Nb–(1.0–2.0)O (at.%) alloys, confirming that oxygen decreases transformation temperatures. Not only the stress for inducing martensite but also the critical stress for slip increases with increasing oxygen content. The critical stress for slip increases up to 890 MPa in a Ti–22Nb–1.5O (at.%) alloy (Kim J I *et al.*, 2005a). It is also interesting to note that the Ti–22Nb–2.0O (at.%) alloy shows non-linear elastic behavior with a large recovery strain. The maximum total recovery strain decreases from 4% in the Ti–22Nb–0.5O (at.%) alloy to 3% in the Ti–22Nb–1.5O (at.%) alloy. Figure 4.7 shows the stress–strain curves of Ti–22Nb–1O (at.%), Ti–22Nb–1N (at.%) and Ti–20Nb–4Zr–2Ta–0.6N (at.%) alloys obtained by a strain increment tensile test at room temperature. It is seen that all the specimens exhibit superelasticity at room

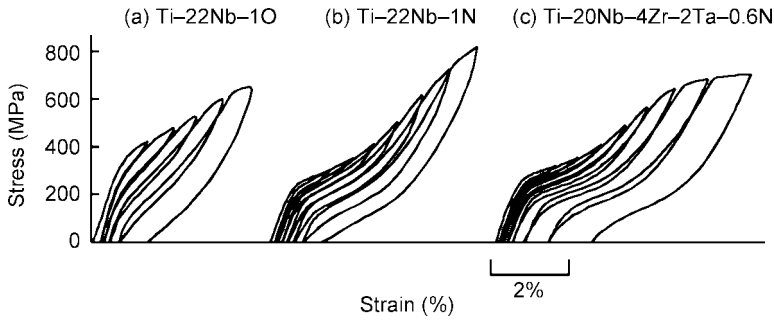

4.7 Stress–strain curves obtained by strain increment cyclic loading and unloading tensile tests in (a) Ti–22Nb–1O, (b) Ti–22Nb–1N and (c) Ti–20Nb–4Zr–2Ta–0.6N.

temperature. The Ti–22at.%Nb alloy exhibits shape memory effect at room temperature and the *Ms* of the Ti–22at.%Nb alloy is about 430 K, indicating that O and N reduce the transformation temperature remarkably. The transformation temperature decreased by about 200 K with 1 at.% increase of O or N content in Ti–Nb alloys. Figure 4.7 also shows that both O and N significantly increased the critical stress for slip, which is the stress for the second stage yielding, when compared with the result of Ti–27at.%Nb as shown in Fig. 4.4(a). It is supposed that the increase of the critical stress for slip by the addition of O or N is due to the solution hardening effect because no precipitates were observed in the solution treated specimens. On the other hand, the addition of B exhibited little effect on superelastic properties due to its limited solubility in β Ti–Nb alloys. The addition of O or N was also effective in suppressing the formation of ω phase. The maximum recovery strain of 2.7 and 3.9% were obtained in the Ti–22Nb–1O (at.%) and Ti–22Nb–1N (at.%) alloys, respectively. It is noted that the Ti–22Nb–1N (at.%) alloy exhibits a higher critical stress for slip and lower stress for inducing martensitic transformation than the Ti–22Nb–1O (at.%) alloy, resulting in more stable superelasticity with a larger recovery strain. The Ti–20Nb–4Zr–2Ta–0.6N (at.%) alloy reveals almost perfect superelasticity when an applied strain is less than 3.5% as shown in Fig. 4.7(c). The large superelastic recovery strain of 4.0% and high critical stress for slip of 660 MPa were obtained in the Ti–20Nb–4Zr–2Ta–0.6N (at.%) alloy, which is due to the combined effects of Zr and N. As a result, it is suggested that Ti–Nb–Zr based alloys with a small amount of interstitial elements such as O and N can be good candidates for biomedical superelastic alloys.

4.4 Effect of heat treatment condition on shape memory properties of Ti-based shape memory alloys

Superelastic properties of the Ti–Nb based alloys can be improved by thermomechanical treatment. Annealing at a temperature below the recrystallization

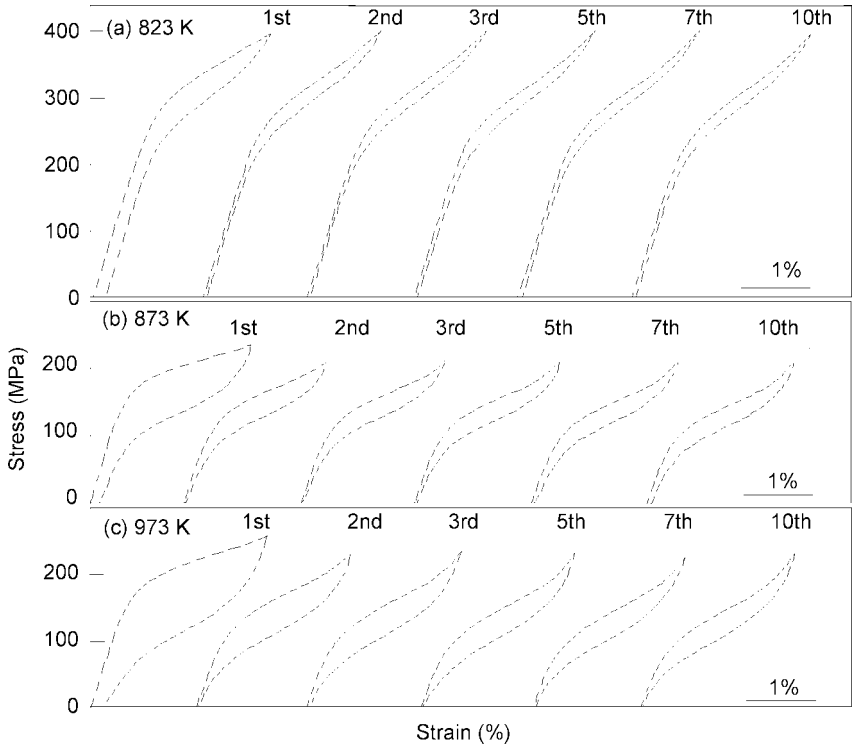

4.8 Stress–strain curves obtained by repeated loading to the maximum strain of 2.5% followed by unloading at room temperature in the Ti–22Nb–6Zr annealed at (a) 823 K, (b) 873 K and (c) 973 K.

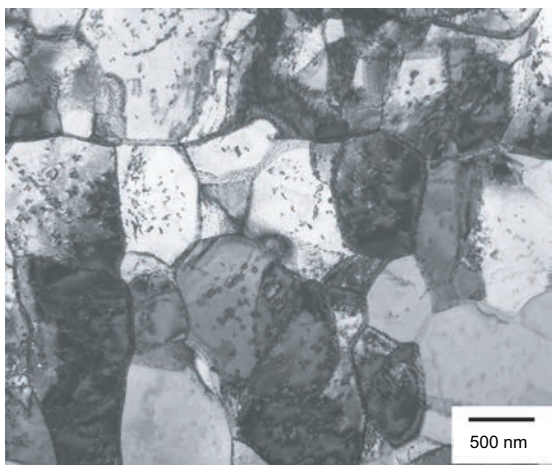

4.9 A bright field TEM micrograph of Ti–22Nb–6Zr annealed at 823 K after 95% cold rolling.

temperature after severe cold working improves the superelastic properties. Figure 4.8 shows the stress–strain curves of the Ti–22Nb–6Zr (at.%) alloy annealed at different temperature (Kim J I *et al.*, 2006). It is seen that the specimen annealed at 823 K exhibits better superelastic behavior with a high stress for inducing martensitic transformation and a narrow stress hysteresis. This is because of the presence of fine α precipitates and fine subgrain structure for the specimen annealed at 823 K as shown in Fig. 4.9. It is noted that annealing at a temperature below 773 K causes a loss of ductility.

Aging at a temperature between 473 and 673 K is also effective to increase the critical stress for slip and stabilize superelasticity. The increase of the critical stress for slip is due to fine and dense ω precipitates. It is generally acknowledged that the ω phase formed by aging, this being called the thermal ω phase, causes deleterious effects on mechanical properties of Ti-based alloys. However, it has been confirmed that fine ω precipitates (10–50 nm particle size) is effective to improve superelasticity without a severe loss of ductility (Kim H Y *et al.*, 2006b). It has been well known that the ω phase is Ti-rich (Williams 1973, Williams *et al.*, 1971). This implies that the increase in the amount of ω phase increases the Nb content of the matrix, resulting in a decrease of the martensitic transformation temperature. The dispersed ω particles mechanically suppress the martensitic transformation, also causing the transformation temperature to decrease. Furthermore, low-temperature annealing followed by aging exhibits excellent superelasticity due to the combined effect of work hardening and age hardening. Perfect shape recovery was obtained within 3.0% in the Ti–26at.%Nb alloy annealed at 873 K for 0.6 ks followed by aging treatment at 573 K for 3.6 ks.

4.5 Effect of textures on shape memory properties of Ti-based shape memory alloys

Typically the β-type Ti alloys exhibit excellent cold workability. The texture developed during the cold working and subsquent heat treatment affects the shape memory and superelastic behavior. In particular, the transformation strain and Young's modulus are strongly dependent on the crystallographic orientation. The effect of textures on shape memory properties was reported for several alloys (Kim H Y *et al*., 2006). Figure 4.10(a) shows the φ_2=45° section of crystallite orientation distribution function (ODF) obtained from the Ti–22Nb–6Ta (at.%) alloy cold-rolled with a reduction of 99% in thickness. The ODF indicates that a strong {001}<110> texture was formed by cold rolling. The same {001}<110> deformation texture was also reported in the cold rolled Ti–24Nb–3Ga (at.%), Ti–24Nb–3Ge (at.%), and Ti–24Nb–3Al (at.%) alloys (Inamura *et al.*, 2004, 2005a). The deformation texture is intensified by annealing at intermediate temperature as shown in Fig. 4.10(b). This indicates that recrystallization did not occur by annealing at 873 K for 0.6 ks but the deformation texture was intensified by recovery. The texture changes from the {001}<110> texture to the {112}<110> texture with increasing

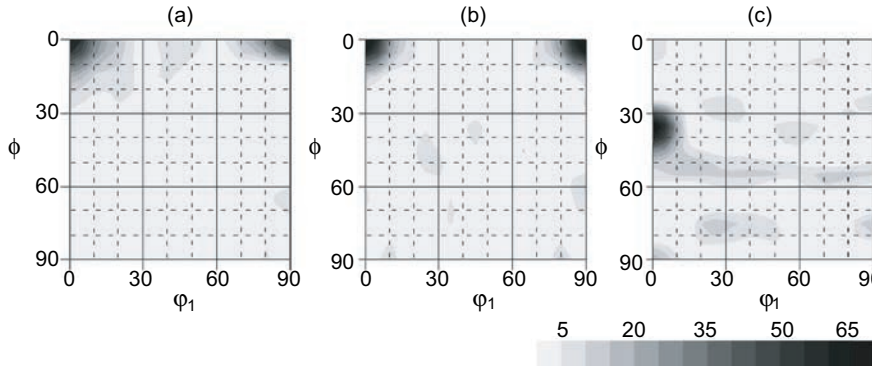

4.10 Sections (φ_2 = 45°) of the ODFs for the cold rolled specimen with a reduction of 99% and subsequently heat treated specimens; (a) an as-rolled specimen, (b) a specimen heat-treated at 873 K for 0.6 ks after the cold rolling and (c) a specimen heat treated at 1173 K for 1.8 ks after the cold rolling.

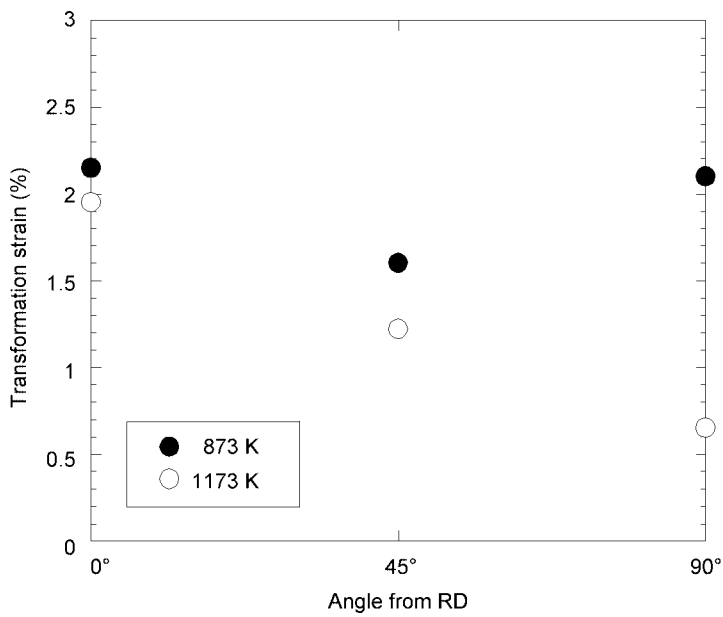

4.11 The orientation dependence of transformation strain obtained by tensile tests for the specimens heat treated at 873 K and 1173 K.

annealing temperature which is due to recrystallization as shown in Fig. 4.10(c). It is important to note that the rolling direction is parallel to <110> crystal directions in both textures.

Figure 4.11 shows the orientation dependence of transformation strain obtained by tensile tests for the specimens heat treated at 873 and 1173 K (Kim H Y *et al.*, 2006e). The transformation strain was obtained by subtracting the elastic strain from the recovery strain. For the specimen heat treated at 873 K, the transformation strain exhibits the minimum when the transverse direction is 45° from the RD and the transformation strains along the RD and TD exhibit larger values. The {001}<110> texture in the specimen heat treated at 873 K implies that the directions 0°, 45° and 90° from the RD in the rolling plane exhibit high axis densities of [110], [010] and [110], respectively. The transformation strain decreases with changing direction from [011] towards the directions of [001] and [111], respectively. Thus, it can be seen that the transformation strains along the RD and TD exhibit similar values and the transformation is smallest along 45° from the RD.

On the other hand, the transformation strain tends to decrease monotonously from the RD to TD for the specimen heat treated at 1173 K. The specimen heat treated at 1173 K exhibits the {112}<110> recrystallization texture, indicating that the 0°, 45° and 90° from the RD reveal high axis densities of [110], [012] and [111], respectively. Thus, the orientation dependence of transformation strain in the specimen heat treated at 1173 K is also reasonably explained by the texture. It is also noted that transformation strains of the rolling direction are similar in both specimens because the crystal direction along the RD is same as <110> in both textures.

It is interesting to note that superelastic strain does not show strong anisotropy in the specimens exhibiting the {001}<110> texture although the transformation strain exhibits a minimum along the 45° from the RD as mentioned above. The superelastic strain consists of transformation strain and elastic components. Young's modulus of this alloy is lowest along the <100>, indicating that the elastic strain exhibits the largest value along the 45° from the RD (Kim H Y *et al.*, 2006e, Inamura *et al.*, 2005b). As a result, the relatively isotropic superelastic strain in the specimen exhibiting the {001}<110> texture is due to the fact that the large elastic strain along the 45° from the RD compensates for the small transformation strain. This indicates that the isotropic superelasticity can be obtained by texture control. Similar orientation dependence of superelastic properties was also confirmed in the Ti–24Nb–3Al (at.%) alloy (Inamura *et al.*, 2006).

4.6 Ti–Mo based shape memory alloys

Shape memory effect and superelasticity have also been observed in Ti–Mo based alloys, e.g. Ti–Mo–Al (Sasano and Suzuki, 1985), Ti–Mo–Sn (Maeshima and Nishida, 2004a; Maeshima *et al.*, 2006), Ti–Mo–Ga (Kim H Y *et al.*, 2004a), Ti–

(8–10)Mo–3Al–2V–4Nb (wt%) (Zhou *et al.*, 2004), and β-CEZ [Ti–4Mo–5Al–2Sn–4Zr–2Cr–1Fe (wt.%)] alloys (Grosdidier and Philippe, 2000), with recoverable strains in the range 2.0–4.0%. Sasano and Suzuki (1985) reported that Ti–(12–14)Mo–3Al (wt.%) alloys exhibit shape memory effect with recovery strain about 3%. They also investigated the effect of Mo content on the transformation temperature: *Af* decreases by about 75 K with an increase of 1 wt.% Mo. Ti–14Mo–3Al (wt.%) and Ti–14Mo–5Al (wt.%) alloys exhibits superelasticity at 150 K. However, it is noted that these alloys do not exhibit superelasticity at room temperature. Superelastic behavior was reported in β-CEZ alloy which was initially developed for turbine disk applications. The maximum recovered strain of 2.0% was obtained after an initial strain of about 3%. It has been confirmed that superelasticity in the β-CEZ alloy is a result of the stress-induced α" and its reverse transformation (Grosdidier and Philippe, 2000).

Lei *et al.* (1997) have investigated the effect of alloying elements on superelastic properties of Ti–Mo–Al alloys in order to develop Ni-free orthodontic wires. Maximum recovered strain of 3.5% was obtained at about 6% tensile strain in solution treated Ti–11Mo–3Al–2V–4Nb (wt.%) alloy. It is noted that aging of the Ti–11Mo–3Al–2V–4Nb (wt.%) alloy at temperatures of 473 to 673 K decreased the superelastic recovery strain because of the formation of a thermal ω phase. Zhou *et al.* (2004) reported that the effect of Mo content on the superelastic properties of Ti–*x*Mo–3Al–2V–4Nb (wt.%) alloys. They claimed that superelastic behavior is observed in the compositions between 7.5 and 9.5 wt.% Mo equivalent (Mo_{eq}) and the best superelastic properties is obtained when Mo_{eq} is about 9.0 wt.%, where: Mo_{eq} = 1.00Mo + 0.28Nb + 0.22Ta + 0.67V +1.60Cr +2.90Fe – 1.00Al.

Recently, shape memory effect and superelasticity have been reported in Ti–Mo–Ga alloys with recovery strain of about 4% (Kim H Y *et al.*, 2004a). For example, Ti–6Mo–3Ga (at.%) and Ti–7Mo–4Ga (at.%) alloys exhibit shape memory effect and superelasticity at room temperature, respectively. The Ti–Mo–Ga alloys are very susceptible to ω phase embrittlement. A premature failure occurred in the Ti–Mo–Ga alloys subjected to annealing or aging at intermediate temperatures 573 to 773 K. A short time annealing for 120 s at 1073 K was effective to improve shape memory and superelastic properties. It has been also reported that the addition of Nb was effective to suppress the ω phase (Kim H Y *et al.*, 2006d).

More recently, Maeshima and Nishida (2004a, 2004b) have systematically investigated the shape memory effect of Ti–Mo–(Ag, Sn, Sc) alloys. Shape memory effect with a recovery strain of about 3–5% was obtained in Ti–6Mo–5Sc (at.%), Ti–5Mo–(2–5)Ag (at.%) and Ti–5Mo–(1–3)Sn (at.%) alloys. These alloys do not exibit superelastic behavior at room temperature. Superelasticity with a recovery strain of 3% was observed in solution-treated Ti–5Mo–5Sn alloy. A short time aging at 873 K was effective to improve superelasticity. The maximum recovery strain of 3.5% was obtained by aging at 873 K for 300 s after solution treatment (Maeshima *et al.*, 2006). They also reported that an addition of Sc is

effective to the grain refinement of Ti–Mo and Ti–Mo–Sn alloys due to the grain boundary pinning effect of scandium oxide (Maeshima and Nishida, 2004b).

4.7 Ti–V based shape memory alloys

Shape memory effect in Ti–10V–2Fe–3Al has been reported in the early 1980s by Duerig *et al.* (1982). They reported that a perfect shape recovery is obtained up to tensile strain of 3%. The Ti–10V–2Fe–3Al alloy did not exhibit superelasticity at room temperature because *As* of the alloy is 439 K. They confirmed the stress induced β to α" transformation and its reverse transformation by heating. One-way shape memory effect has been also reported in Ti–V–Al ternary alloys by Lei *et al.* (1992): a maximum shape recovery of 3.8% was observed by deforming room temperature followed by heating. They also reported that V decreases the reverse transformation temperatures with a slope of 46 K/wt.% V. Recently, Furuhara *et al.* (2006) have investigated the effect of N addition on superelastic properties of the Ti–10V–2Fe–3Al alloy. The addition of 0.1–0.2 wt.% N decreased transformation temperatures and superelastic behavior was observed at room temperature. The maximum recovery strain of about 2% was observed in 0.2 wt.% N added Ti–10V–2Fe–3Al alloy. The addition of N increased the amount of elastic strain due to the increase of the stress for inducing martensitic transformation. They also mentioned that decreasing cooling rate after solution treatment is effective in improving superelastic properties.

4.8 Conclusions

The basic characteristics such as the martensitic transformation and shape memory properties of Ti-based alloys have been reviewed. In many Ti-based alloys, shape memory effect and superelasticity have been confirmed. Although the superelastic recovery strain is still small compared with Ti–Ni superelastic alloys, Ti-based superelastic alloys are considered as promising candidates for biomedical materials by combining with other attractive properties such as excellent cold workability, good biocompatibility and low Young's modulus. It is expected that superelastic properties can be further improved by alloy design and thermomechanical treatment. The development of the Ti-based alloys will further accelerate the medical applications of SMAs in the near future.

4.9 References

Baker C (1971), 'The shape-memory effect in a titanium–35 wt.% niobium alloy', *J Metal Sci*, **5**, 92–100.

Duerig T W, Albrecht J, Richter D and Fischer P (1982), 'Formation and reversion of stress induced martensite in Ti–10V–2Fe–3Al', *Acta Metall*, **30**(12), 2161–2172.

Fukui Y, Inamura T, Hosoda H, Wakashima K and Miyazaki S (2004), 'Mechanical properties of a Ti–Nb–Al shape memory alloy', *Mater Trans*, **45**(4), 1077–1082.

Furuhara T, Annaka S, Tomio Y and Maki T (2006), 'Superelasticity in Ti–10V–2Fe–3Al alloys with nitrogen addition', *Mater Sci Eng A*, 438–440, 825–829, doi: 10.1016/j.msea.2006.02.084.

Grosdidier T and Philippe M J (2000), 'Deformation induced martensite and superelasticity in a beta-metastable titanium alloy', *Mater Sci Eng A*, **291**(1–2), 218–213.

Inamura T, Fukui Y, Hosoda H, Wakashima K and Miyazaki S (2004), 'Relationship between texture and macroscopic transformation strain in severely cold-rolled Ti–Nb–Al superelastic alloy', *Mater Trans*, **45**(4), 1083–1089.

Inamura T, Fukui Y, Hosoda H, Wakashima K and Miyazaki S (2005a), 'Mechanical properties of Ti–Nb biomedical shape memory alloys containing Ge or Ga', *Mater Sci Eng C*, **25**(3), 426–432, doi: 10.1016/j.msec.2005.01.025.

Inamura T, Hosoda H, Wakashima K and Miyazaki S (2005b), 'Anisotropy and temperature dependence of Young's modulus in textured TiNbAl biomedical shape memory alloy', *Mater Trans*, **46**(7), 1597–1603.

Inamura T, Kinoshita Y, Kim J I, Kim H Y, Hosoda H, Wakashima K, Miyazaki S (2006), 'Effect of {001}<110 > texture on superelastic strain of Ti–Nb–Al biomedical shape memory alloys', *Mater Sci Eng A*, **438–440**, 865–869, doi: 10.1016/j.msea.2006.02.092.

Inamura T, Hosoda H, Wakashima K, Kim J I, Kim H Y and Miyazaki S (2007a), 'Damping capacity of Ti–Nb–Al shape memory beta-titanium alloy with {001}(beta)<110>(beta) texture', *Mater Trans*, **48**(3), 395–399, doi: 10.2320/matertrans.48.395.

Inamura T, Kim J I, Kim H Y, Hosoda H, Wakashima K and Miyazaki S (2007), 'Composition dependent crystallography of alpha"-martensite in Ti–Nb-based beta-titanium alloy', *Phil Mag*, **87**(23), 3325–3350, doi: 10.1080/14786430601003874.

Kim H Y, Ohmatsu Y, Kim J I, Hosoda H and Miyazaki S (2004a), 'Mechanical properties and shape memory behavior of Ti–Mo–Ga alloys', *Mater Trans*, **45**(4), 1090–1095.

Kim H Y, Satoru H, Kim J I, Hosoda H and Miyazaki S (2004b), 'Mechanical properties and shape memory behavior of Ti–Nb alloys', *Mater Trans*, **45**(7), 2443–2448.

Kim H Y, Ohmatsu Y, Kim J I, Inamura T, Hosoda H and Miyazaki S (2006d), 'Effect of Nb addition on shape memory behavior of Ti–Mo–Ga alloys', *Mater Trans*, **47**(3), 518–522.

Kim H Y, Kim J I, Inamura T, Hosoda H and Miyazaki S (2006c), 'Effect of thermomechanical treatment on mechanical properties and shape memory behavior of Ti–(26–28)at.%Nb alloys'. *Mater Sci Eng A*, **438–440**, 839–843, doi: 10.1016/j.msea.2006.02.136.

Kim H Y, Hashimoto S, Kim J I, Inamura T, Hosoda H and Miyazaki S (2006a), 'Effect of Ta addition on shape memory behavior of Ti–22Nb alloy', *Mater Sci Eng A*, **417**(1–2), 120–128, doi: 10.1016/j.msea.2005.10.065.

Kim H Y, Sasaki T, Okutsu K, Kim J I, Inamura T, Hosoda H and Miyazaki S (2006e), 'Texture and shape memory behavior of Ti–22Nb–6Ta alloy', *Acta Mater*, **54**(2), 423–433, doi: 10.1016/j.actamat.2005.09.014.

Kim H Y, Ikehara Y, Kim J I, Hosoda H and Miyazaki S (2006b), 'Martensitic transformation, shape memory effect and superelasticity of Ti–Nb binary alloys', *Acta Mater*, **54**(9), 2419–2429, doi: 10.1016/j.actamat.2006.01.019.

Kim H Y, Oshika N, Kim J I, Inamura T, Hosoda H and Miyazaki S (2007), 'Martensitic transformation and superelasticity of Ti–Nb–Pt alloys', *Mater Trans*, **48**(3), 400–406, doi: 10.2320/matertrans.48.400.

Kim J I, Kim H Y, Inamura T, Hosoda H and Miyazaki S (2005b), 'Shape memory characteristics of Ti–22Nb–(2–8)Zr(at.%) biomedical alloys', *Mater Sci Eng A*, **403**(1–2), 334–339, doi: 10.1016/j.msea.2005.05.050.

Kim J I, Kim H Y, Hosoda H and Miyazaki S (2005a), 'Shape memory behavior of Ti–22Nb–(0.5–2.0)O(at%) biomedical alloys', *Mater Trans*, **46**(4), 852–857.

Kim J I, Kim H Y, Inamura T, Hosoda H and Miyazaki S (2006), 'Effect of annealing temperature on microstructure and shape memory characteristics of Ti–22Nb–6Zr(at%) biomedical alloy', *Mater Trans*, **47**(3), 505–512.

Lei C Y, Pak J S L, Inoue H R P and Wayman C M (1992), 'Shape memory behavior of Ti–V–Al alloys' *Proceedings of the International Conference on Martensitic Transformations*, Monterey, California, USA, Monterey Institute for Advanced Studies, 539–544.

Lei C Y, Wu M H, Schetky L M and Burstone C J (1997), 'Development of pseudoelastic beta titanium orthodontic wires', *Proc. Inter. Conf. Displ. Phase Transformations and Their Applications in Material Science*, Warrendale Pennsylvania, USA, TMS, 413–418.

Maeshima T and Nishida M (2004a), 'Shape memory and mechanical properties of biomedical Ti–Sc–Mo alloys', *Mater Trans*, **45**(4), 1101–1105.

Maeshima T and Nishida M (2004b), 'Shape memory properties of biomedical Ti–Mo–Ag and Ti–Mo–Sn alloys', *Mater Trans*, **45**(4), 1096–1100.

Maeshima T, Ushimaru S, Yamauchi K and Nishida M (2006), 'Effects of Sn content and aging conditions on superelasticity in biomedical Ti–Mo–Sn alloys', *Mater Trans*, **47**(3), 513–517.

Miyazaki S, Kim H Y and Hosoda H (2006), 'Development and characterization of Ni-free Ti-base shape memory and superelastic alloys', *Mater Sci Eng A*, **438–440**, 18–24, doi: 10.1016/j.msea.2006.02.054.

Nitta K, Watanabe S, Masahashi N, Hosoda H and Hanada S (2001), 'Ni-free Ti–Nb–Sn shape memory alloys', Structural Biomaterials for 21st Century, Warrendale, Pennsylvania, USA, TMS, 25–34.

Ping D H and Mitarai Y and Yin F X (2005), 'Microstructure and shape memory behavior of a Ti–30Nb–3Pd alloy', *Scripta Mater*, **52**(12), 1287–1291, doi: 10.1016/j.scriptamat.2005.02.029.

Sasano H and Suzuki T (1985), 'Shape memory effect in Ti–Mo–Al alloys', *Proceedings of the 5th International Conference on Titanium*, Frankfurt, Germany, Deutsche Gesellschaft fur Metallkunde, 1667–1674.

Tahara M, Kim H Y, Inamura T, Hosoda H and Miyazaki S (2007), 'Effect of N addition on mechanical properties of Ti–20Nb–4Zr–2Ta (at%) biomedical superelastic alloy', *Proc. 11th World Conference on Titanium*, Kyoto, Japan, The JIM, 1453–1454.

Takahashi E, Sakurai T, Watanabe S, Masahashi N and Hanada S (2002), 'Effect of heat treatment and Sn content on superelasticity in biocompatible TiNbSn alloys', *Mater Trans*, **43**(12), 2978–2983.

Williams J C, Hickman B S, Leslie D H (1971), 'The effect of ternary additions on the decomposition of metastable beta-phase titanium alloys', *Metall. Trans. B*, **2**(2), 477–484.

Williams J C (1973), 'Critical review kinetics and phase transformation', Titanium Science and Technology, *Proceedings of Second International Conference on Titanium*, New York, USA, Plenum Press, 1433–1494.

Zhou T, Aindow M, Alpay S P, Blackburn M J and Wu M H (2004), 'Pseudo-elastic deformation behavior in a Ti/Mo-based alloy', *Scripta Mater*, **50**(3), 343–348, doi: 10.1016/j.scriptamat.2003.10.012,

5

Fabrication of shape memory alloy parts

T. HABU
Furukawa Techno Material Co. Ltd, Japan

Abstract: The fundamental fabrication processes and problems in making Ti–Ni alloys such as melting, hot working, cold working, annealing and heat treatment, are described.

Key words: shape memory alloy, Ti–Ni alloy fabrication, Ni–Ti, superelastic, transformer temperature, workability, Nitinol.

5.1 General processing techniques for Ti–Ni alloys

5.1.1 Raw materials

Titanium is extracted from titanium ore using the Kroll Process (magnesium reduction) and emerges as sponge titanium. The titanium used to make Ti–Ni alloys is either sponge titanium itself, or ingots that are made by re-melting sponge titanium. The nickel used in Ti–Ni alloys is extracted electrolytically from nickel chloride solution by electrowinning. Impurities can significantly affect the properties of Ti–Ni alloys, so purity control of the raw materials is very important. The manufacturing process fro Ti–Ni alloys is shown in Fig. 5.1.

5.1.2 Alloy design

The ratio of titanium to nickel in the Ni–Ti alloy has a significant influence on transformation temperature. Figure 5.2 shows the change in transformation temperature according to nickel composition.[1] A 0.1% change in nickel composition results in a 10° C change in the transformation temperature. In commercial production, analysis for chemical composition is often done in situ or on a button sample. However, in the case of Ti–Ni alloys, it is difficult to evaluate whether the composition is correct or not by analyzing chemical composition, because melting and casting of Ni–Ti alloy is performed under vacuum, and also because a small change in nickel and titanium content causes a large change in transformation temperature. For these reasons, Ti–Ni alloy composition is commonly evaluated using differential scanning calorimetry (DSC).

To measure the nickel and titanium content using DSC, it is important that the sample has been annealed in a vacuum or inactive gas (specified by the heat

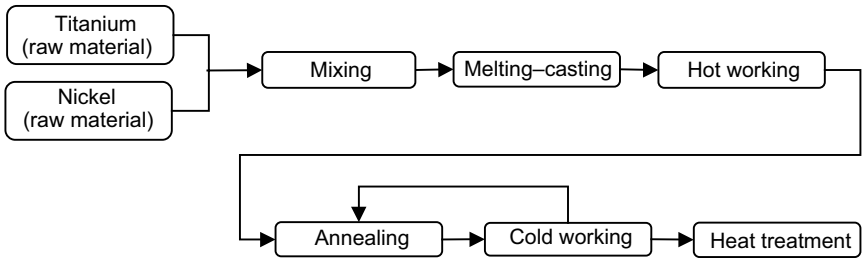

5.1 Fabrication process of Ti–Ni shape memory alloy.

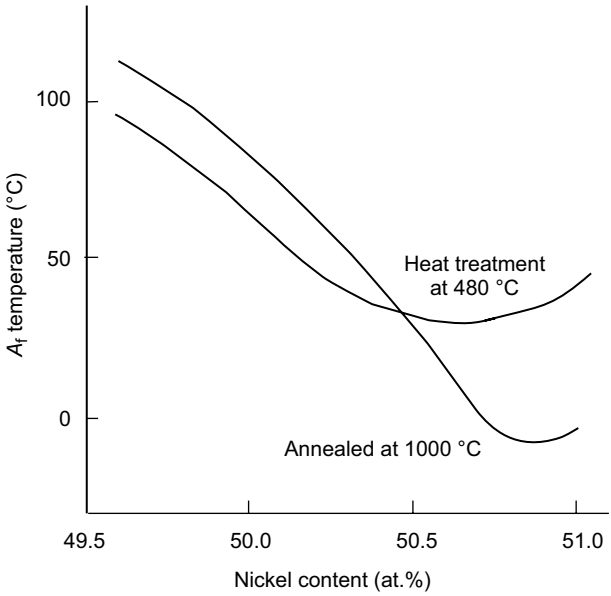

5.2 Relation between nickel content and A_f temperature.

treatment method defined by ASTM, JIS, etc.), and has been protected from processing distortion or oxidization. Figure 5.3 shows a typical DSC curve for a shape memory alloy.[2] DSC measures endothermic and exothermic reactions at phase changes.

In order to control the transformation temperature and mechanical properties of a Ti–Ni alloy, it is common to add a third element. The element added most commonly is copper, because it can be in a solid solution with Ti–Ni alloy at a Cu content of 30% or more. Ni–Ti–Cu alloy is used as an actuator, which utilizes the shape memory characteristic. Other elements such as Fe, Cr, Co and Pd, can also be added to Ti–Ni alloys and almost all the additions lower the transformation temperature (Fig. 5.4) or improve formability.[3] However, additional elements are not permitted in Ti–Ni alloys used for medical devices, under specification ASTM F2063-05.

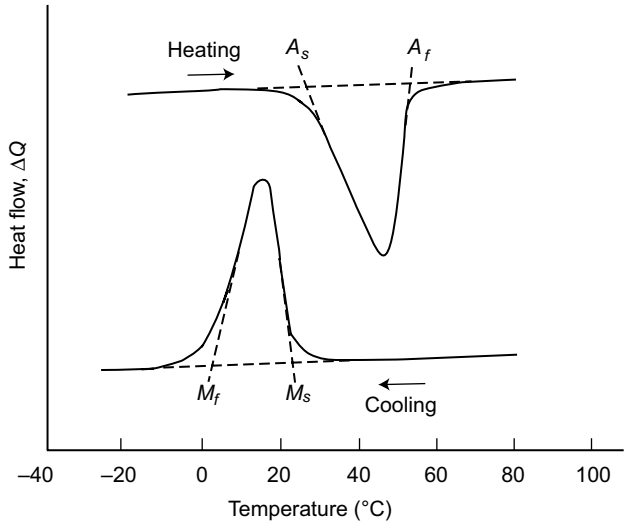

5.3 Typical DSC curve of shape memory alloy.

5.1.3 Melting and casting

Since the variation in transformation temperature for Ti–Ni alloys is as result of various factors, such as composition and presence of impurities, especially carbon and oxygen, it is very important to control casting conditions and maintain high vacuum levels. Molten titanium is so reactive in oxygen that Ti–Ni alloys must be melted in high vacuum or an inert gas atmosphere. It is also necessary to prevent a reaction with the crucible. Industrial casting for Ti–Ni alloys is usually carried out using vacuum induction melting (vacuum high frequency dissolution furnace, VIM), or vacuum arc remelting (consumable electrode type vacuum arc casting, VAR), or a combination of both.

VIM (Fig 5.5) is most commonly used to melt Ti–Ni alloys.[4] The main advantage of VIM is the homogeneity of chemical composition throughout the ingot, because the alternating current inducted has a mixing effect on the molten alloy. The recommended material for the crucible is carbon (graphite) or calcia (CaO). Carbon crucibles are cheap and durable, and, under good melting conditions, oxygen contamination is negligible and the carbon content can be kept to less than 0.05%. Calcia does not react with the molten Ti–Ni alloy, so pure molten alloy can be obtained. However, calcia is brittle under physical and thermal shock, so it is more difficult to store. It is also more expensive and absorbs moisture, making it problematic for industrial use.

Since VAR does not require a crucible, this method avoids the problem of contamination from the crucible, and it can be used to manufacture larger sizes of ingot than VIM. In VAR, a discharge arc is generated between an electrode and the

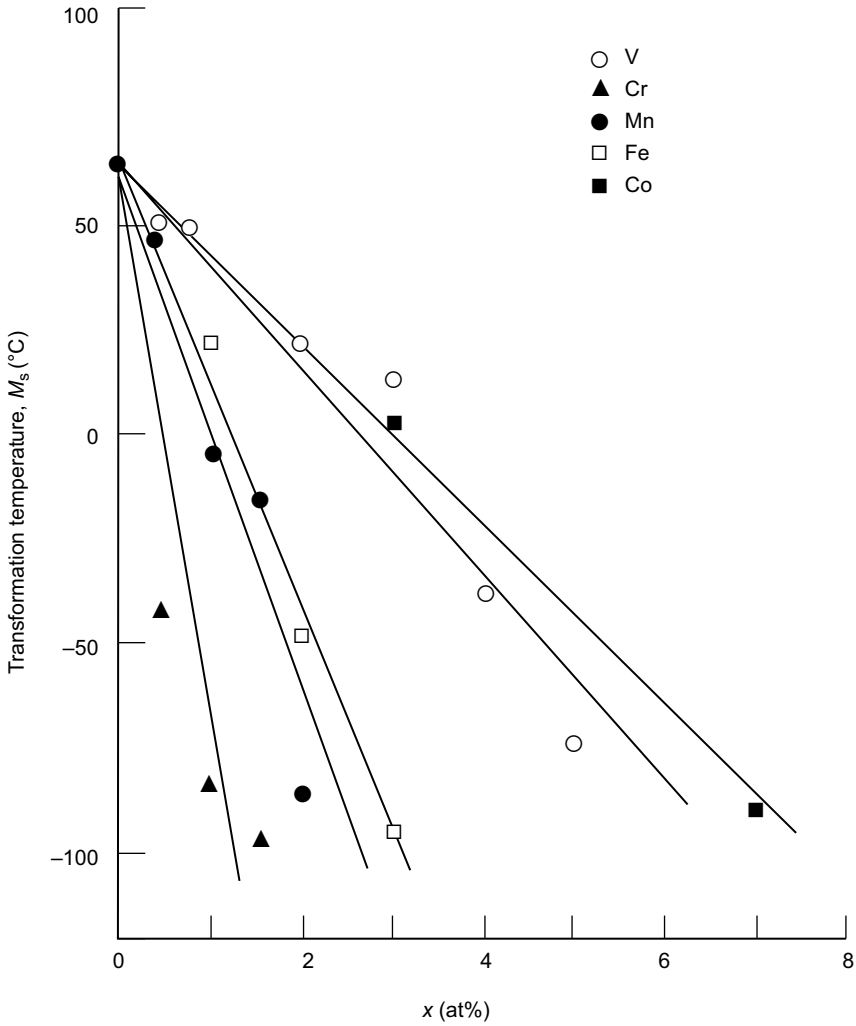

5.4 Effect of third element upon M_s.

mold bottom, or between an electrode and an ingot, and the electrode melts and drops into a water-cooled copper mold, so ingots are obtained one by one (Fig. 5.6).[5] However, the melting process of VAR is extremely complicated, i.e. only a part of the Ni–Ti electrode melts and then solidifies immediately, so totally homogenous ingots cannot be obtained. In order to improve homogeneity, it is necessary to remelt several times.

It is possible to get homogeneous and large-scale ingots by using both methods together.

The electron-beam melting method is not suitable for Ti–Ni alloys because melting is only partial, but it may be used with the raw materials.

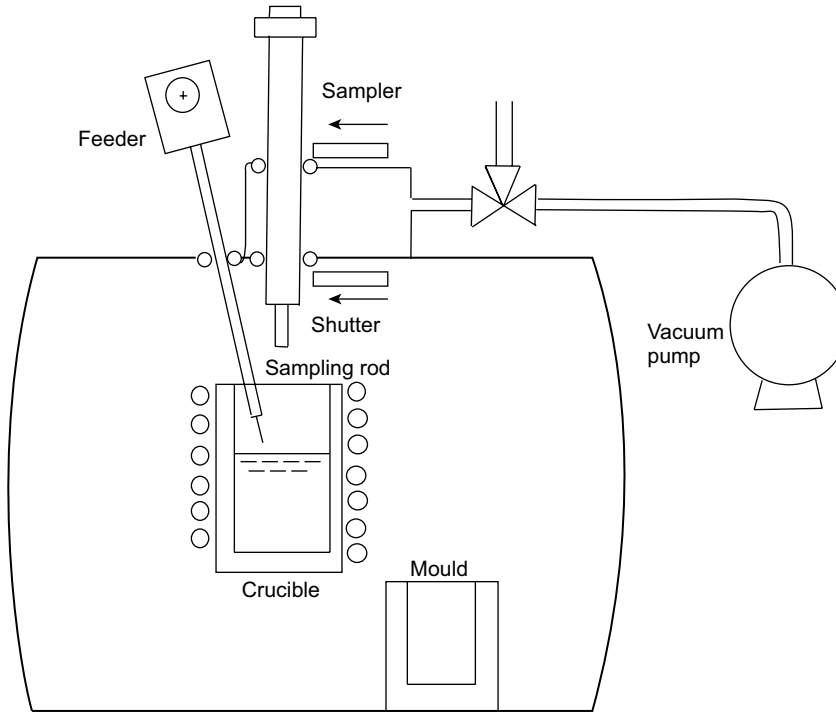

5.5 Model of VIM.

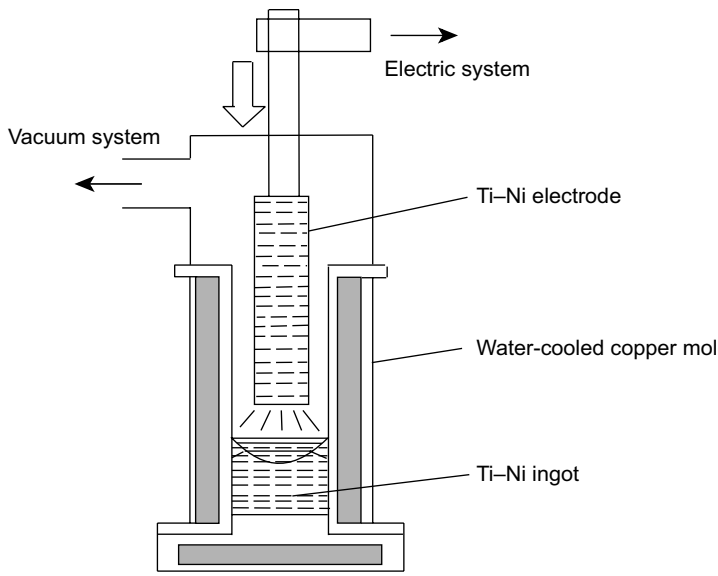

5.6 Model of VAR.

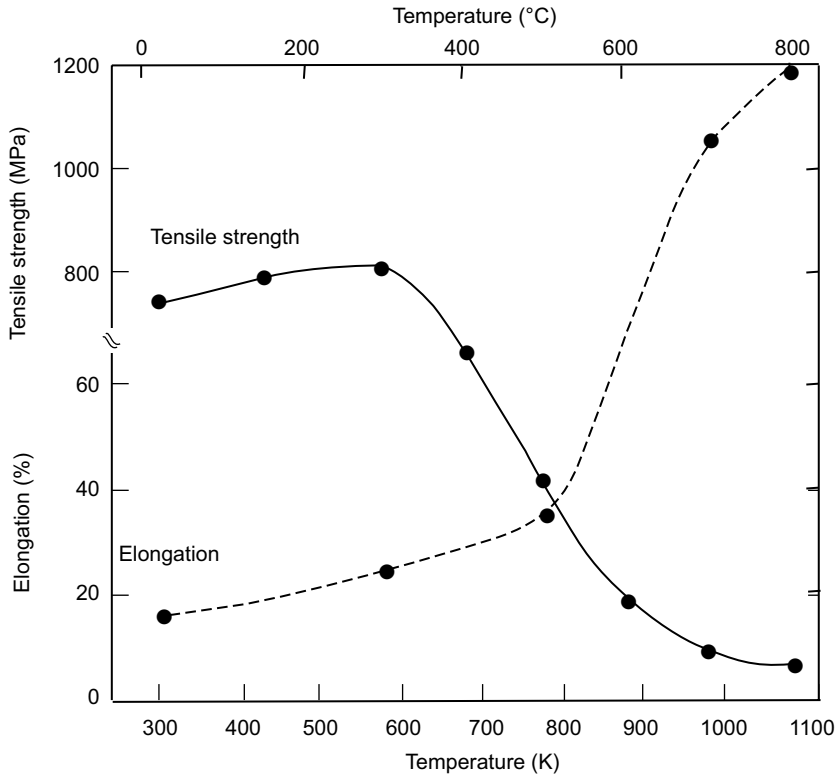

5.7 Tensile strength and elongation of 50.0at.% Ti–Ni alloy at high temperature.

5.1.4 Hot working

Cold workability of Ti–Ni alloy is low, so hot working is usually employed for large deformations. Casting creates a heterogeneous composition in the same way as in general metals. Hot work, such as hot rolling and hot forging, causes dynamic recrystallization. The strength of Ti–Ni alloy begins dropping at temperatures above 700K (Fig. 5.7), so workability in hot temperatures is much better than at cold temperatures.[6] It is common to perform hot work at temperatures above 900 K.

5.1.5 Cold working

Since the Ti–Ni alloy is an intermetallic compound, cold workability is not good and there are many problems with using this method of fabrication. In cold working, it is necessary to keep the cold work rate at around 40% and then soften by annealing. Figure 5.8 shows the work hardening curve. Because the work hardening rate of Ti–Ni is high, this makes the decrease in workability worse.

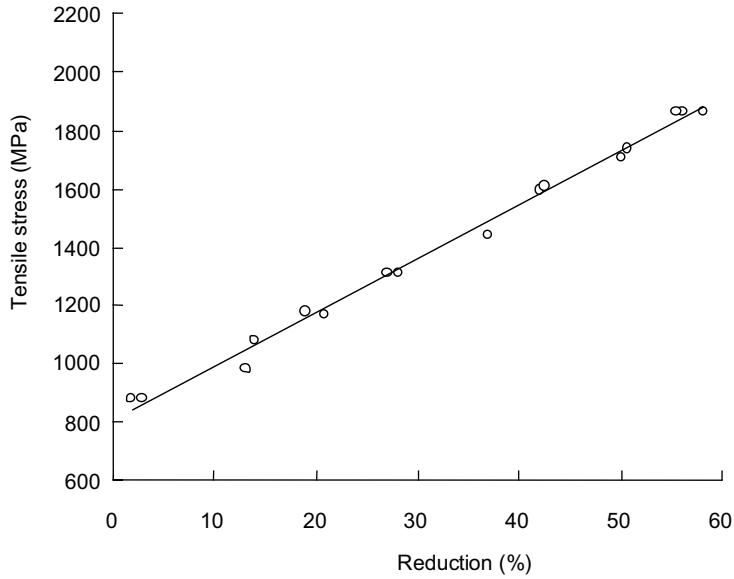

5.8 Work hardening ratio (Ti–50.8Ni).

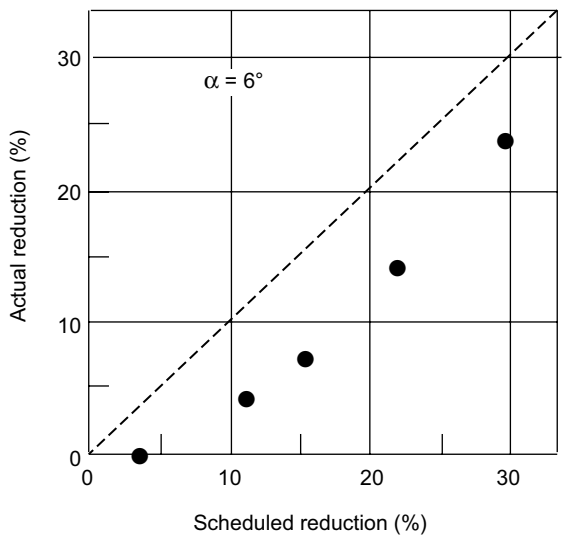

5.9 Relationships between actual reduction and scheduled reduction.

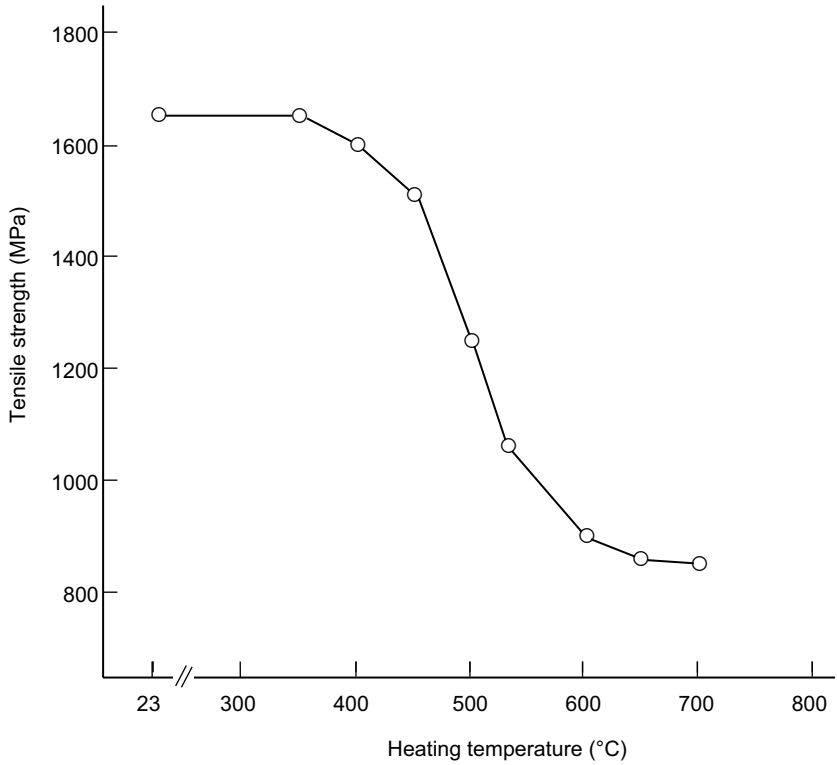

5.10 Softening curve of Ti–51at.% Ni–Ti.

The shape-memory and superelastic characteristics of the alloy also produce difficulties, since even if the material is deformed, it will revert to its original shape. Figure 5.9 shows the relationship of actual diameter to required diameter under cold drawing.[7] The ratio to return depends on various drawing conditions, such as lubrication, dice angle α, and surface conditions. The tendency of the shape memory effect to make the metal recover its original dimensions causes problems in controlling the diameter of wire, ability to grind and cut, and the shape change at annealing. Drawing can also lead to defects such as draw lines and scratches resulting from internal stresses during the process.

5.1.6 Annealing

After cold working, annealing is carried out to remove the stress cold work causes. Figure 5.10 shows the softening curve.[8] Annealing is usually carried out in an air atmosphere, but to avoid oxidation, it is necessary to anneal Ti–Ni alloys in a vacuum or an inert gas atmosphere, such as Ar or N_2. Hydrogen cannot be used because it causes embrittlement. Cooling can be done with water or air, although

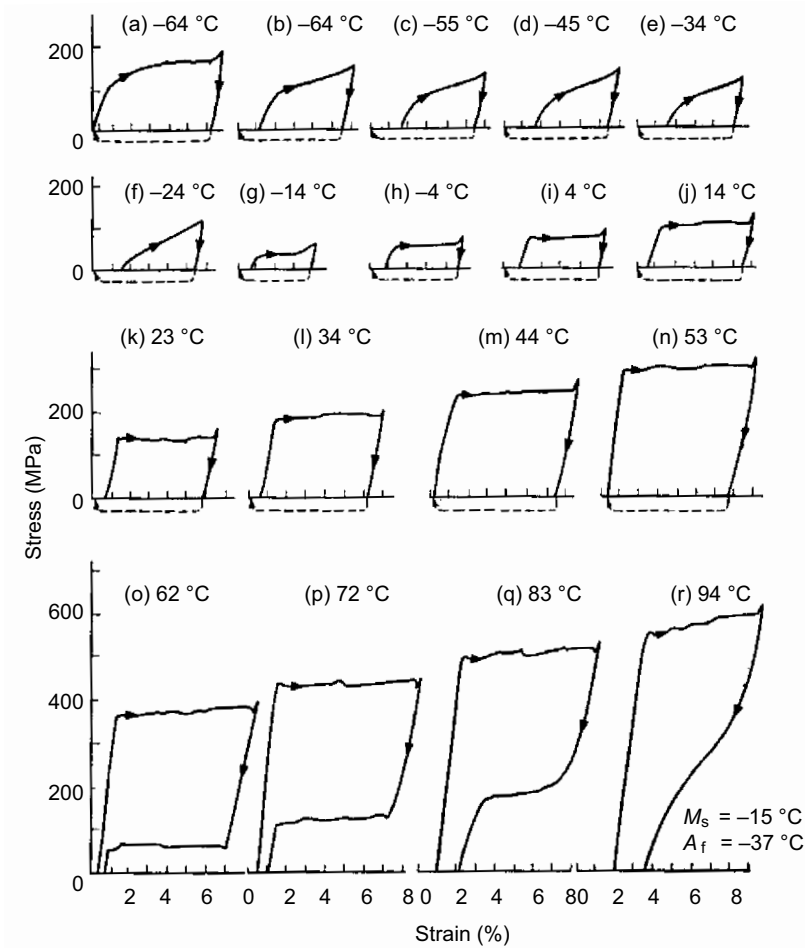

5.11 Stress–strain curves for Ti–49.8at.%Ni alloy with 500 °C heat treatment.

air-cooling is preferable. Cooling has to be managed slowly and carefully so that the mesophase occurs.

5.1.7 Heat treatment

Three types of heat treatment are used to create the shape memory or superelasticity effect in Ti–Ni alloys, medium, low and aging.

Medium heat treatment restricts the Ti–Ni alloy to the required shape after cold work, and involves heating the alloy at temperatures of 573–823 K for a duration from several minutes up to several hours. This heat-treatment method is used for many shape memory and superelastic products. Figure 5.11 shows the stress–strain curve for a Ti–Ni alloy under medium heat treatment at 500 °C.[9]

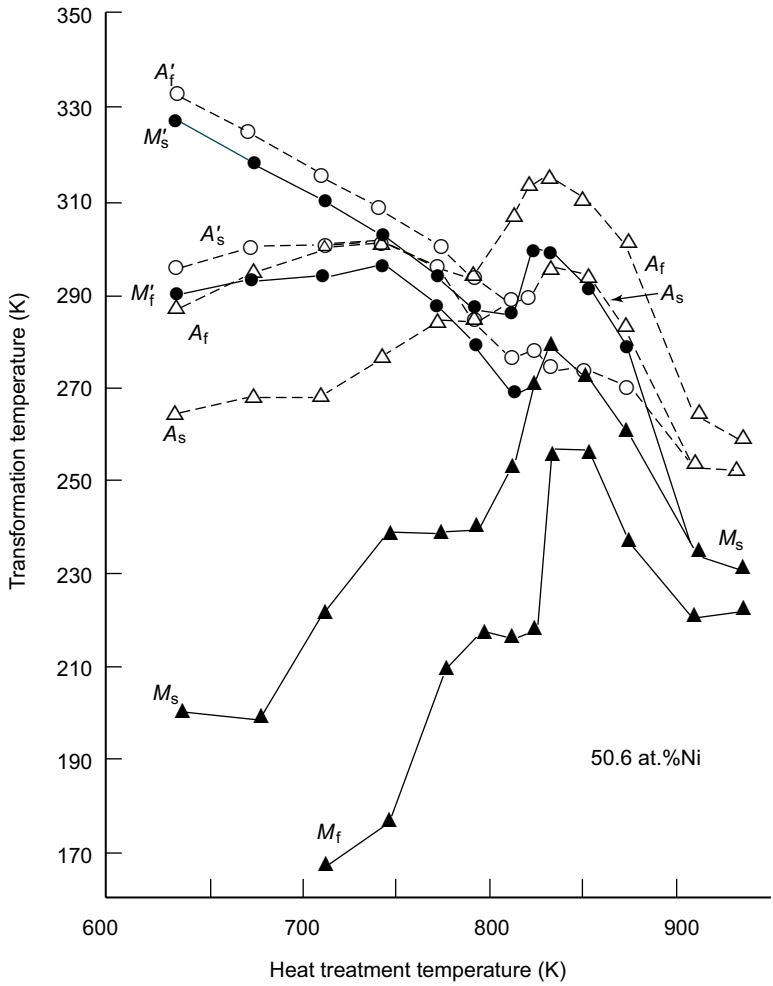

5.12 Relation between heat-treatment temperature and the transformation temperatures of Ti–50.6at.%Ni alloy.

Low heat treatment is carried out after annealing and forming into the required shape, and takes place at 200–300 °C. This method is widely used for making eyeglass frames, and to mold an alloy after complete annealing.

Aging heat treatment involves dissolving at 800 to 1000 °C and quenching immediately with cold water. This method can only be used for alloys with a high Ni content, i.e. more than 50.5% nickel. Subsequent prescription processing at around 400 °C for several hours can create superelasticity, however, this method is not used in industry. As Ti–Ni alloys return to their original shape after heat-treatment, it is necessary to restrict the shape during heat treatment with a jig.

Heat-treatment temperatures and the metamorphic temperature change are

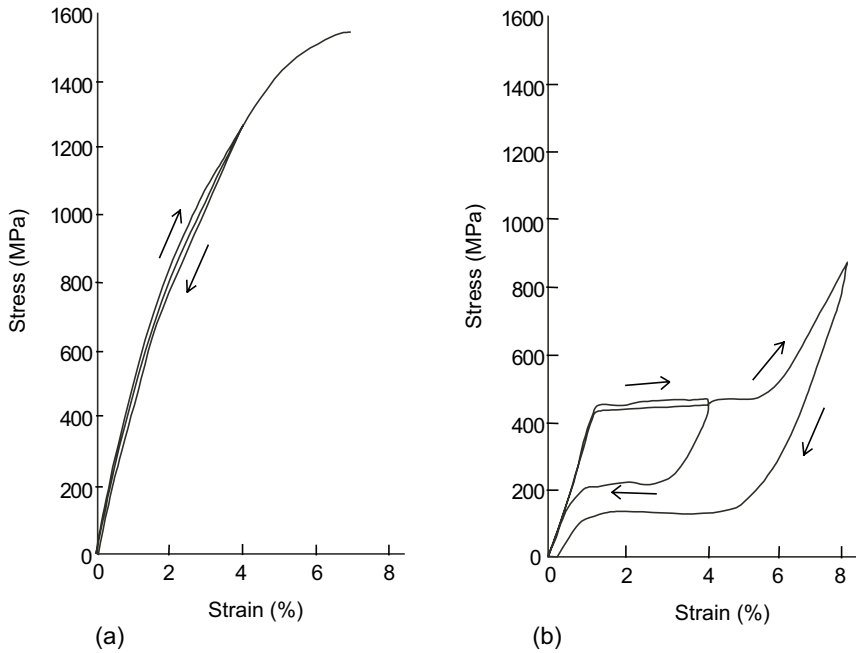

5.13 Property of guide wire (a) FHP type, (b) superelastic type.

shown in Fig. 5.12. The behavior differs, depending on alloy composition and addition of other elements.[10]

Guide wires that use superelasticity characteristics show a breaking point, as shown in Fig. 5.13b, and have a superelasticity stage. A new type of guide wire called FHP-NT (Fig. 5.13a) does not have this characteristic. It has higher pushability, stiffness and straightness than normal superelastic guide wires.

5.2 Other machining methods for Ti–Ni alloys

5.2.1 Fabrication of Ti–Ni tubes

Ti–Ni tubes are becoming more widely used in many medical devices (Fig. 5.14). Outer diameters from 0.1mm to 20mm are available (Fig. 5.15). In making tubes from other materials, it is very common to make a loop using sheet forming. Welding difficulties make it impossible to use such a process for Ti–Ni alloys. Ti–Ni alloy tubes can be made using the seamless tube manufacturing process, which is widely used and consists of making a rod, making a hole in the rod using a gun drill and then reducing the outer diameter. Another method is to make a hollow tube from an ingot by hot extruding. Tubes have several important dimensions that must be controlled, including outer diameter, wall thickness and inner diameter, and this control is particularly critical in medical devices such as stents (Fig. 5.16).

5.14 Ti–Ni tubing.

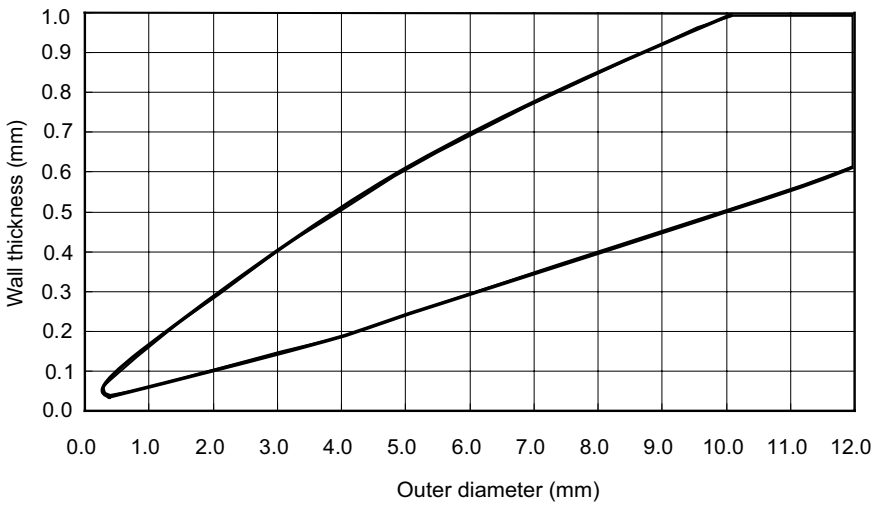

5.15 Product range of Ti–Ni tubing.

5.2.2 Fabrication of Ti–Ni sheets

Ti–Ni alloys can be formed into sheets. Sheets of around 200 mm in width and 50 μm thick have been manufactured industrially, but production difficulties make them expensive.

5.2.3 Fabrication of Ti–Ni tape

It is possible to make a tape with a rectangular or square cross-section. These types of tape are used in orthodontics wire and brassière core wire. Rectangular and

5.16 Stent from Ti–Ni tubing (courtesy of Biotronik GmbH & Co.).

square cross-sections are more suitable than round cross-sections from the point of view of directionality and bindingness. Ti–Ni alloy tape is commonly manufactured by rolling from wire into tape.

5.2.4 Welding

Ti–Ni alloys can theoretically be welded.[11] However, the welding must be carried out in an inert gas atmosphere to prevent oxidation, which would otherwise weaken the weld. Welding can lead to inclusions, and the influence of heat must also be considered. Welding Ti–Ni alloys with other materials is commonly used in the production of guide wires.

5.2.5 Machineability

It is difficult to cut Ti–Ni alloys because, as intermetallic compounds, they are very hard. Another significant problem is the shape recovery property itself. This recovery property can damage and shorten the lifespan of cutting tools, so cutting conditions must be optimized in order to machine Ti–Ni alloys.

5.2.6 Surface

Ti–Ni alloys generate an oxidation film at annealing, which can depend on the lubrication used. Ti–Ni alloys exhibit various oxidation colors similar to those of

Ti-based alloys, so it is possible to use blue or gold oxidation films as the final product color. The oxidation film can be removed easily with nitric or other acids, but care should be taken over hydrogen content, because hydrogen can be absorbed by the Ti–Ni alloy and cause embrittlement.

5.3 Required properties of Ti–Ni alloys used in medical devices

5.3.1 ASTM F 2063-05

The specifications of Ti–Ni alloys used for medical devices are controlled under ASTM F 2063-05, which prescribes chemical ingredients, mechanical characteristics, superelastic characteristics, metamorphic temperature, inclusions and grain size.

5.3.2 New fabrication methods for medical devices

The field of medical devices is growing rapidly, and new applications using Ti–Ni alloys are being developed as part of this growth. Along with the conventional manufacturing methods discussed above, new manufacturing methods are becoming necessary, such as laser cutting, electrolytic machining, coating, plating and sterilization. These methods require a greater understanding of Ti–Ni alloys, including structural control, Ni solvency control, transformation temperatures, superelastic stress control and durability.

5.4 Prospects

The difficulties in controlling composition, transformation temperature, workability and shape recovery make the production of Ti–Ni alloys expensive, thus restricting their use as an industrial product. Recent applications in the medical devices field, however, have made it increasingly important to meet stringent size and properties tolerances. The disadvantage for Ti–Ni alloys as a commercial material lies in the fact that they have only been available for about 40 years. The future will no doubt bring improvements in manufacturing methods and therefore extend the use of Ti–Ni alloys.

5.5 References

1 Y. Suzuki, Jitsuyo Keijyo-Kioku Gokin (in Japanese), *Kogyo Chosa-kai*, 25, 1987.
2 Y. Suzuki, Jitsuyo Keijyo-Kioku Gokin (in Japanese), *Kogyo Chosa-kai*, 29, 1987.
3 T. Honma *et al.*, Proc.4th Intern. Conf. on Ti, Kyoto, 1455, May 1980.
4 Y. Suzuki, Proc. MRS Int. Mtg. on Advanced Materials, **9**, 557, 1989.

5 M. Aiba *et al.*, *Materia Japan*, **31**(6), 541,1992.
6 Y. Suzuki, Jitsuyo Keijyo-Kioku Gokin (in Japanese), *Kogyo Chosa-kai*, 135, 1987.
7 K. Yoshida, *J. JSTP*, **31**(355), 1990–8.
8 S. Miyazaki, K. Shiroyama *et al.*, Keijyo-kioku-goukin no tokusei to ouyoutennkai (in Japanese), CMC, 135, 2001.
9 S. Miyazaki, K.Otsuka and Y. Suzuki, *Scripta Metall*., **15**, 287,1981.
10 T. Todoroki *et al.*, Trans. Japan Inst. Metals, **28**(2), 83–94, 1987
11 A. Hirose, *Metal (Japan)*, 61–68, Aug 1989.

6

Response of Ti–Ni alloys for dental biomaterials to conditions in the mouth

Y. OSHIDA
Syracuse University and Indiana University, USA
F. FARZIN-NIA
Ormco Corporation, USA

Abstract: The longevity and functionality of biomaterials such as Ti–Ni are governed by their surface reactions in *in vivo* environments. These reactions at interfaces include chemical, electrochemical, physical, mechanical (particularly, biotribological) and thermal reactions, and any combinations of these. In this chapter, discoloration, corrosion in various media (containing fluoride, chlorine, saliva, and body fluid), microbiology-induced corrosion, and oxidation and stability of oxide films are overviewed. Furthermore, compatibility-related problems (such as metals in release and dissolution reactions) as well as toxicity, allergic reaction, cytotoxicity, and biocompatibility are also discussed.

Key words: corrosion, metal release, dissolution, oxidation, oxide structures, biomaterial compatibility, microbiology-induced corrosion, Ti–Ni, Ni–Ti, nitinol.

6.1 Introduction

The biolongevity and biofunctionality of materials are governed by their surface reactions in *in vivo* environments. The intraoral environment is a hostile corrosive environment to Ti–Ni materials and mechanical actions inside the mouth produce significant stress on the materials. The oral cavity is continuously filled with saliva, an aerated aqueous solution of chloride with varying amounts of Na, K, Ca, PO_4, CO_2, sulfur compounds and mucin. The pH value is normally 6.5 to 7.5 but under plaque deposits it may be as low as 2.0. Temperatures can vary ±36.5 °C and a variety of food and drink concentrations (with pH values of 2.0 to 14.0) stay inside the mouth for short periods of time. Loads can go up to 1000 N (normally 200 N as a masticatory force) and sometimes it can be in an impact manner. Trapped food debris may decompose and release sulfur compounds, causing discoloration of natural teeth and restorative materials. Under these chemical and mechanochemical intraoral environments, materials in service in the mouth are expected to last for relatively long periods of time.[1] Such surface reactions can also influence physical,

tribological, and biological processes. In Ti-based alloys, including CpTi (commercially pure titanium), Ti–6Al–4V, and Ti–Ni, the aforementioned surface reactions are controlled by the stability of oxide(s) or oxide films formed on substrate layers of titanium. In this chapter these crucial aspects will be discussed and the work of a significant number of researchers in the field will be reviewed.

6.2 Discoloration

Teeth that have been exposed to a long-term coffee and/or cigarette usage are normally stained. Viral bleaching of such teeth reflects patients' increasing desire to achieve an optimal esthetic appearance.[2,3] Currently, mouth-rinses, toothpaste, dental prophylactic agents containing fluoride, and bleaching treatment agents are popular for esthetic purposes and prevention of plaque and cavity formation. Normal orthodontic patients are referred to general dentists for fluoride treatments once every six months during the course of orthodontic mechanotherapy. Among various bleaching treatments for whitening stained teeth, an overnight (normally for 8 h each day for two consecutive weeks) bleaching agents containing 10% carbamide peroxide are popular.[4] Some patients undergoing the nightguard bleaching (e.g., for 8-h treatment) are likely to have restorations containing metals (i.e., amalgam, crowns made of gold or porcelain fused to a base metal, fixed or removable prosthodontic bridge or partial denture frameworks made of base alloys, and/or titanium implant fixtures). The corrosive effect of these agents (normally containing fluoride and hydrogen peroxide) on dental metallic materials has not been documented well, although it was reported to decrease the corrosion resistance of titanium in solutions containing fluoride.[5,6,7,8]

The evaluation of discoloration caused by fluoride treatment agents (2.0% NaF with pH 7.0, 0.4% SnF_2 with pH 7.0, and 1.23% acidulated phosphate fluoride (APF) with pH 3.5) and bleaching agents (10% carbamide peroxide) were conducted on CpTi (grade 2), Ti–Ni, Ti–6Al–4V, 17–4 PH stainless steel, 70Ni–15Cr–5Mo, type IV gold alloy (70Au–10Ag–15Cu), and Disperalloy amalgam.[9] The degree of discoloration on these treated alloys was examined by a colorimeter and the naked eye. After the baseline measurements of L^*, a^* and b^*, comparisons were made with the Commission Internationale d'Eclairage (CIE–L^*a^*b) color system, and the value of ΔE^* was calculated by $[(L_i - L_f)^2 + (a_i - a_f)^2 + (b_i - b_f)^2]^{1/2}$, where subscripts 'i' and 'f' indicate the initial value and final value, respectively. It was found that (i) all tested metallic materials exhibit discoloration to various degrees, ranging from 10 to 18 in ΔE^*, (ii) the tooth brushing between each treatment for both fluoride and bleaching treatments led to a remarkable reduction in the degree of discoloration (i.e., ΔE^* reduced to 2 to 8) of all tested materials, and (iii) although it is indicated to use beaching agent to natural tooth, it is clearly contraindicated for metallic restorations.[9,10]

6.3 Corrosion of Ti–Ni alloys in various media

Internal fluids have chloride ion concentrations about seven times higher than that of oral fluids. A diet rich in sodium chloride, added to large volumes of acidulated beverages (phosphoric acid), provides a continuous source of corrosive agents despite the relatively short exposure. In addition, it has been calculated that an average urban mouth-breather inhales about a cubic meter of air every two hours, with a potential intake of between 0.11 and 2.3 mg of sulfur dioxide.[11] Both sulfur dioxide and hydrogen sulfide have been found to accelerate the tarnishing and corrosion of metal implants.

Besides chlorine ion levels and pH of intraoral fluids, there is one more important factor involved in corrosion evaluation. It is an intraoral electrochemical potential. Electrochemical corrosion studies are normally performed by means of potentiostatic or potentiodynamic measurements. Interpretation of the electrochemical corrosion data requires knowledge of expected intraoral potentials. Nilner *et al.*[12] reported that the intraoral potential ranged from –431 to –127 mV, which was measured on 407 amalgam restorations in the mouths of 28 patients. Corso *et al.*[13] reported that the intraoral potential ranged from –300 to +300 mV. Reclaru *et al.*[14] reported a range from 0 to +300 mV. Ewers *et al.*[15] reported that it ranged from –380 and +50 mV. Hence, the range of overlapping data is a very narrow window of a potential zone of 0 to +50 mV.

In addition to the above listed intraoral chemistry and electrochemistry, it is important to know how to simulate the intraoral environments when the *in vitro* chemical or electrochemical corrosion test is prepared and conducted. Most of the corrosion studies were carried out using physiological isotonic electrolyte solutions such as 0.9% saline,[16,17,18] Ringer's,[19,20] Tyrode's,[21] Hank's[22] solutions, lactic acid to simulate the accumulated plaque,[23,24] and artificial saliva[25,26] or simulated body fluid (SBF), as seen later.

There are numerous studies on corrosion behavior of Ti–Ni materials. One reason for this is the fact that almost half of the atomic percentage weight of this alloy is Ni, which is considered as one of the three heavy toxic elements frequently used in biocompatible alloys. The other two elements are Cr and V. Therefore, the safety and biocompatibility should be examined thoroughly. Over the last decade, because of their unique SME (shape memory effect) and SE (superelasticity) characteristics, Ti–Ni alloys have been increasingly considered for use in external and internal biomedical devices, e.g., orthodontic wires, endodontic files, blade-type dental implants, self-expanding cardiovascular and urological stents, bone fracture fixation plates and nails, etc. For applications in the human body, the corrosion resistance of Ti–Ni becomes extremely important, as the amount and toxicity of corrosion products control the alloy biocompatibility.

6.4 Corrosion behavior of Ti–Ni alloys in fluoride-containing solution

The corrosion resistances of Ti–Ni, Ti–Ni–Co and Ti–6Al–4V were compared with that of CpTi in Fusayama Meyer artificial saliva with different pH and fluoride contents, using electrochemical polarization resistance measuring methods. It was reported that the corrosion resistance of (i) Ti–6Al–4V alloy is as good as that of CpTi in Fusayama Meyer saliva and acid salivary solution, except Ti–Ni and Ti–Ni–Co alloys, (ii) a remarkable localized corrosion phenomenon of Ti–Ni, Ti–Ni–Co, and Ti–6Al–4V alloys in fluoride and acid–fluoride salivary solutions, and (iii) the fluoride ions could cause the breakdown of the protective passivation layer that normally exists on the titanium and its alloys, leading to pit corrosion.[25]

The electrochemical studies on TMA, Ti–Nb, Ti–Ni and Ti–Ni–Cu showed that the alloys could be divided into two groups; in one groups were the Ti–Ni alloys, which were subjected to strong corrosion in the presence of monofluorophosphate, whereas in the other group were Ti–Nb, which was the most resistant to corrosion, and TMA, which was corroded strongly by the stannous fluoride.[26] Yoon *et al.*[27] tested CpTi, Ti–6Al–4V, and Ti–Ni in 2% NaF electrolyte containing 1~20 ppm fluorine ion. It was reported that CpTi and Ti–6Al–4V showed similar current density, whereas Ti–Ni had a higher current density (meaning a lower resistance to corrosion) than the other two alloys.

When albumin was mixed with fluoride-containing corrosion media, the corrosion behavior was noticed to change remarkably. Takemoto *et al.*[7] investigated the corrosion behavior and surface characterization of passive films on titanium immersed in a solution containing 2.0 g ℓ^{-1} fluoride and albumin (either 0.1 or 1.0 g ℓ^{-1}). It was found that (i) fluorine was detected on the titanium surface immersed in the solution containing fluoride, and dissolution of the titanium was confirmed, (ii) the titanium immersed in a solution containing both fluoride and albumin had an albumin film regardless of the albumin concentration level, and (iii) in addition, the amount of dissolved titanium from the titanium immersed in the solution was less than when the solution contained no albumin.[7] It was, therefore, suggested that the formation of adsorbed albumin films on the passive film acted not only to protect the titanium from attack by the fluoride but also to suppress dissolution of the titanium–fluoride compounds. Although this study was done for CpTi, the materials should include Ti–Ni as well as Ti–6Al–4V since the main oxide formed on these Ti-based alloys is TiO_2, which is the same as the oxide formed on the CpTi surface.

The effect of fluoride prophylactic agents on the mechanical properties of Ti–Ni and Ti–Ni–Cu orthodontic archwires was investigated in an acidulated fluoride agent, a neutral fluoride agent, or distilled water (control) for 1.5 h at 37 °C.[28] After immersion, the loading and unloading elastic modulus and yield strength of the wires were measured with a 3-point bend test in a water bath at 37 °C as given in the ANS/ADA Specification No. 32 for Orthodontic Wires. It was noted that (i)

unloading mechanical properties of Ti–Ni orthodontic wires were significantly decreased after exposure to both fluoride agents; however, (ii) Ti–Ni–Cu wire mechanical properties were not significantly affected by either fluoride agent suggesting that using topical fluoride agents with Ti–Ni wire could decrease the functional unloading mechanical properties of the wire and contribute to prolonged orthodontic treatment.

6.5 Corrosion behavior of Ti–Ni alloys in solution containing chloride ion

Localized corrosion behavior of some Ti–Ni shape memory alloys in chloride environments has been studied by Rondelli *et al.*[29] It was reported that (i) potentiodynamic tests pointed out a fairly good localized corrosion resistance similar to that of Ti–6Al–4V alloy in the potential range of practical interest whereas (ii) potentiostatic scratch tests as given in the ASTM F746 standard test method revealed poor localized corrosion resistance of Ti–Ni and Ti–Ni–Fe alloys.

The corrosion behaviors of CpTi, Ti–6Al–4V, and Ti–Ni were studied in a buffered saline solution using anodic polarization and EIS techniques.[30] Pitting potential as low as +250 mV (vs. SCE) was recorded for Ti–45Ni. The initiated pits continued to propagate at potentials as low as –150 mV (vs. SCE). It was possible to increase the pitting potential of Ti–45Ni to values greater than +800 mV using a H_2O_2 surface treatment procedure; however, due to unstable passivation, this surface modification process had no beneficial effect on the rate of pit repassivation. It was reported that the surface oxide layer consists of a porous outer layer and an inner barrier layer. The nature of this porous layer was found to depend on the nature of the electrolyte material and the presence of phosphate anions in the saline-buffered solution. Much higher porous layer resistances were recorded for CpTi and also for Ti–6Al–4V in the absence of the phosphate anions.[30]

Three Ti-based alloys (50.7Ni–49.4Ti, 51.4Ni–48.4Ti–0.19Cr, and 45.1Ni–49.6Ti–0.29Cr–4.97Cu) were electrochemically evaluated in 0.9% NaCl and 1% lactic acid solutions. It was concluded that small amounts of Cr and Cu changed the superelastic characteristics, but did not change the corrosion resistance of the Ti–Ni alloy.[31] Using the ASTM F746 'scratch' test, in 40 °C 0.9% NaCl solution,[32] 50Ni–50Ti, 44Ni–51Ti–5Cu, and 88Ti–6.5Mo–3.5Zr–2Sn[33] were examined through electrochemical tests. It was concluded that (i) both Ti–Ni and Ti–Ni–Cu wires exhibit low corrosion potential (50 ~ 150 mV vs. SCE), indicating an inferiority to that of Ti–Mo alloy (which agreed with results[34]), and (ii) Ti–Mo proved to be immune to localized corrosion attacks up to 800 mV.[33]

The corrosion behaviors of a Ti–Ni alloy orthodontic wire and a polished plate with the same composition in 0.9% NaCl and 1% lactic acid solutions were examined using an electrochemical technique, an analysis of released ions, and a surface analysis by X-ray photoelectron spectroscopy (XPS).[35] The effect of

polishing the wire on corrosion was also examined. The XPS analysis demonstrated the presence of a thick oxide film mainly composed of TiO_2, with trace amounts of nickel hydroxide, which had formed on the wire surface during the heat treatment and subsequent pickling processes. It was mentioned that the oxide layer contributed to the higher resistance of the as-received wire to both general and localized corrosion in 0.9% NaCl solution, compared with that of the polished plate and the polished wire. It was also reported that the thick oxide layer, however, was not stable and did not protect the orthodontic wire from corrosion in 0.1% lactic acid solution.[35]

The corrosion behavior of Ti–Ni alloy has been examined in physiological Ringer's solution by means of electrochemical techniques (open-circuit potential measurement, potentiodynamic and potentiostatic polarizations) and capacitance measurements. The results indicate that the passive film is stable at open-circuit condition, but many of the anodic current transients are observed at potentiodynamic and potentiostatic polarizations.[36]

Kuphasuk *et al.*[37] tested and compared CpTi (grade II), Ti–5Al–2.5Fe, Ti–4.5Al–3V–2Mo–2Fe, Ti–5Al–3Mo–4Zr, Ti–6Al–4V, and Ti–Ni for their corrosion resistances and passivation capabilities in Ringer's solution at 37 °C. It was found that (i) all samples showed good resistance to electrochemical corrosion over the potential relevant to intraoral conditions, (ii) CpTi and Ti–5Al–2.5Fe showed significantly different corrosion properties from Ti–6Al–4V and Ti–Ni; the former pair exhibited the lowest corrosion rate; the latter pair exhibited the highest corrosion rate, (iii) but Ti–Ni alloys revealed transpassive (in other words, breakdown of stable passivation) behavior at the potential between 0.5 and 0.75 V (vs. SCE: saturated calomel electrode as a standard electrode, having 0.2444 V vs. hydrogen electrode) accompanied with pitting corrosion, and (iv) all samples tested were covered mainly with the rutile type of TiO_2, which was identified by electron transmission diffraction.

6.6 Corrosion behavior of Ti–Ni alloys in artificial saliva

The synergistic effect of pH, temperature, and Cl^- concentration on the electrochemical behavior of Ti–Ni shape memory alloy in artificial saliva was studied. The results showed that the pitting potential for Ti–Ni in artificial saliva decreased at low and high pH; at 25 °C the pitting potential was the lowest compared to those at 10 °C, 37 °C and 50 °C; when the Cl^- concentration was not less than 0.05 mol ℓ^{-1} the pitting potential decreased with the increase of Cl^- concentration. The free corrosion potential of austenitic TiNi was lower than that of a mixture of austenite and martensite.[38]

As Ti–Ni alloys are, on some occasions, utilized under stressing conditions, the corrosion resistance of stressed Ti–Ni and stainless-steel wires was studied using cyclic potentiodynamic and potentiostatic tests in acid artificial saliva at 37 °C.[39]

The cyclic potentiodynamic test results showed that the pH had a significant influence on the corrosion parameters of the stressed Ti–Ni and stainless steels. The pitting potential, protection potential, and passive range of stressed Ti–Ni and stainless-steel wires decreased on decreasing pH, whereas the passive current density increased on decreasing pH. The load had no significant influence on the above corrosion parameters. For all pH and load conditions it was reported that stainless-steel wire showed a higher pitting potential and wider passive range than Ti–Ni wire, whereas Ti–Ni wire had a lower passive current density than stainless steel, suggesting that Ti–Ni can be passivated more easily than stainless steel.

Similar studies, which were performed using a cyclic potentiodynamic test in artificial saliva with various acidities, were done by Huang[40] on as-received commercial Ti–Ni orthodontic archwires from various manufacturers . The results showed that the surface structure of the passive film on the tested Ti–Ni wires were identical, containing mainly TiO_2, with small amounts of NiO. The corrosion tests showed that both the wire manufacturer and solution pH had a statistically significant influence on the corrosion potential, corrosion rate, passive current, passivation breakdown potential, and crevice-corrosion susceptibility. It was observed that various orthodontic wire manufacturers use their own proprietary techniques for wire drawing into the final specified dimensions resulting in various surface cleanness as well as roughness.[41]

6.7 Corrosion behavior of Ti–Ni alloys in simulated body fluid

The corrosion performance of Ti–Ni alloys in human body simulating fluids were evaluated in comparison with other implant materials (Ti–6Al–4V, 302 and 316L stainless steels).[33] As for the passivity current in potentiostatic condition, taken as an index of ion release, the values are about three times higher for Ti–Ni than for Ti–6Al–4V and stainless steels. Regarding the localized corrosion, while plain potentiodynamic scans of the Ti–Ni alloy show good resistance to pitting attack similar to Ti–6Al–4V, tests in which the passive film is abruptly damaged indicate that the characteristics of the passive film formed on the Ti–Ni alloy (whose strength can be related to the alloy's biocompatibility) are not as good as those on Ti–6Al–4V, but are similar or inferior to those of stainless steels. Therefore, it is suggested that the self-healing (i.e. re-passivation) capability of Ti–Ni is inferior to that of Ti–6Al–4V.

The breakdown potentials for passivation (or transpassivation potential) were measured for unpolished and mechanically polished Ti–Ni wires in simulated body fluids. It was reported that (i) significantly higher passivation breakdown potentials (which indicate a higher stability of passive film formed on Ti–Ni surface) were observed for cross-section wire samples, and (ii) some wires were tested in human blood and the passivation breakdown values were higher than that measured in Ringer and 0.9% NaCl solutions. It was also reported that the

oxide film formed on Ti–Ni was predominantly made up of TiO_2, with a very thin layer of NiO at the outer surface.[42] Carroll *et al.*[43] conducted the galvanic corrosion tests on Ti–Ni wires that were coupled with gold, elgiloy/phynox, and stainless steel. Ti–Ni was found to be anodic in all combinations. In tests in which Ti–Ni-gold couples were immersed in 0.9% NaCl for periods of up to 12 months only very small amounts of nickel (in the parts per billion range) were detected, indicating that TiO_2 with trace amounts of NiO protects the substrate material as well.[43]

Although the above-mentioned electrolytes simulate body fluids by reproducing the concentrations of various salts, the *in vivo* corrosion measurements have indicated lower corrosion rates than those predicted from these *in vitro* experiments. The actual *in vivo* environment is made up of salts and proteins.[44] Clark *et al.*[45] found that pure metals that form stable passive layers, such as Ti and Al, were unaffected by the presence of proteins; however, the corrosion rate of other transition metals with variable valences was increased, suggesting that this could be due to the ability of these metals to form stable complexes with the proteins. Speck *et al.*[46] looked at the effect of the amino acids cysteine and tryptophan on titanium alloys. They found that the pitting potential of Ti–Ni was adversely affected by cysteine, but Ti–6Al–4V was not affected by either amino acid.

6.8 Effects of alloying elements in Ti–Ni alloys on corrosion behavior

The effect of alloying elements (Cr and Cu) in Ti–Ni alloy has been investigated[47] using potentiodynamic polarization measurements in 0.9% NaCl and 1% acetic acid solution and an analysis of released metals by atomic absorption spectrophotometry (AAS). It was found that addition of 0.19 at.% Cr had little effect on the structure of the oxide films and the corrosion resistance of the Ti–Ni alloys. For Ti–Ni–5Cu–0.3Cr alloy, the metallic Cu was enriched at the alloy/oxide film interface, resulting in increased susceptibility to pitting corrosion above +1000 mV. However, the passive current density and the amount of released Ni were not significantly increased by the addition of Cu. Small amounts of Cr are effective in lowering the transformation temperature and in improving rigidity, while the addition of Cu is also effective in reducing stress-hysteresis and in improving the stability of the superelastic against cyclic loading. Therefore, it was shown that small amounts of Cr and Cu added to change the superelastic characteristics do not change the corrosion resistance of the Ti–Ni alloy freely immersed in simulated physiological environments.[31]

An electrochemical study aimed at the evaluation of corrosion parameters using potentiodynamic and potentiostatic techniques (scratch and modified ASTM F746) was conducted in 0.9% NaCl on wires from equiatomic Ti–Ni and ternary $Ni_{44}Ti_{51}Cu_5$ superelastic alloys with $Ti_{90}Mo_{10}$ as a reference material.[33] The results,

using potentiostatic tests, indicated that both Ti–Ni and Ti–Ni–Cu wires exhibit low corrosion potential (about 50~150 mV vs SCE) inferior to that of TiMo alloy, which was immune to localized corrosion attacks up to 800 mV.

6.9 Effect of surface modification on corrosion resistance

The effect on corrosion resistance and surface characteristics of electropolishing, heat treatment, and nitric acid passivation of Ti–Ni stents was investigated.[47] It was shown that all of these surface treatments improve the corrosion resistance of the alloy. This improvement is attributed to the plastically deformed native oxide layer removal and replacement by a newly grown, more uniform one.

Ti–Ni (55.6 wt% of Ni) was coated by use of the powder immersion reaction assisted nitrization (TiN), followed by annealing at 900 and 1000 °C.[48] Samples were corrosion-tested in a solution (9.00 g ℓ^{-1} NaCl, 0.20 g ℓ^{-1} $NaHCO_3$, 0.25 g ℓ^{-1} $CaCl_2 6H_2O$, 0.4 g ℓ^{-1} KCl) at 37 °C. It was concluded that (i) the modified Ti–Ni surface consisted of a thin outer layer of gold-colored titanium nitride (TiN), with a thicker Ti_2N layer underneath, (ii) untreated Ti–Ni was found to be susceptible to pitting corrosion, but (iii) the nitriding treatment improved the corrosion resistance of Ti–Ni.[48]

Hence, from the above, the good corrosion resistance of Ti–Ni may result from the formation of stable, continuous, highly adherent and protective oxide films on its surface. In fact, due to the high chemical activity of the Ti surface, a damaged oxide film can generally heal itself if at least some trace of oxygen or water (moisture) is present in the environment.[49,50] In addition, calcium-phosphate surface films can be naturally formed on Ti alloys in a biological environment,[51,52] which can act as a further barrier against ion diffusion from the subsurface alloy. Indeed, any surface treatments of Ti–Ni devices have a critical influence on biocompatibility. Two methods have been considered for improving the corrosion resistance and performance of an additional surface barrier layer against ion diffusion, such as TiN, TiC and TiB_2. One method involves implantation of diffusion species,[53~55] the other relies on increasing the thickness of the oxide layer by anodizing, thermal oxidation, or implantation with oxygen.[33,56]

Ti–Ni was treated by carbon plasma immersion ion implantation and deposition (PIII&D). Corrosion tests in simulated body fluid tests indicate that either an ion-mixed amorphous carbon coating fabricated by PIII&D or direct carbon PIII can drastically improve the corrosion resistance and block the diffusion out of Ni from the materials. It was also reported that tribological tests show that the treated surfaces are mechanically superior and cytotoxicity tests reveal that both sets of plasma-treated samples favor adhesion and proliferation of osteoblasts.[57]

6.10 Release of metal ions and dissolution of Ti–Ni alloys

There are essential elements (sometimes called bioelements) that the human body requires to maintain homeostasis; such bioelements include Ni, which is contained in human tissue at ~0.1 ppm.[58,59] The potential for higher nickel concentration release from Ti–Ni material may generate harmful allergic, toxic or carcinogenic reactions.[60,61] The atomic bonding forces between Ni and Ti in intermetallic Ti–Ni are considerably higher than in a Ti alloy with a small amount of Ni,[62] and will not produce the same reactions as pure metals. Thus, it is important to recognize the synergistic effect of alloying elements when evaluating the biocompatibility for any alloy.[58]

Metal ion release is strongly related to stability of the passive film. If the film suffer from pitting corrosion, the metal ion release takes place from the substrate surface. The formation of pits is related to the equilibrium potentials of (passive) film formation given as a function of the activities of the components of the film substance. The solubility of the product, with respect to the ions in the electrolyte, depends on the electrode potential, since oxidation states of the metal in the film and in the electrolyte are often different. Heusler[63] discussed the kinetics of uniform film formation and dissolution with respect to (1) equilibrium of all components across both interfaces, (2) partial equilibrium of one component at the outer film/electrolyte interface, and (3) irreversible ion transfer reactions at the outer interface. Examples are oxide films on iron (i.e. F_2O_3 and/or F_3O_4), titanium (TiO_2) and aluminum (Al_2O_3). It was mentioned that the processes during the incubation time (which should include chlorine ion adhesion and absorption) of pitting corrosion corresponded to non-uniform dissolution and formation of the passivating film.[63]

Since nickel release during the bio-degradation of Ti–Ni is an important concern for its use as an implant or other prostheses, several studies[64–70] have been undertaken to measure this value. The common finding among these studies is that nickel element released from Ti–Ni alloy was at a noticeable level for a brief period of time, but the release amount decreased rapidly after 24 to 48 h in Hank's solution.

Huang *et al.*[71] evaluated four commercially available orthodontic superelastic Ti–Ni wires in modified Fusayama artificial saliva. The value of pH was adjusted to 2.5, 3.75, 5.0 and 6.25 by addition of either lactic acid or sodium hydroxide. Tests were conducted at 37 °C for 1 to 28 days. It was concluded that (i) the released amount of metal ions increased with immersion period, (ii) the amount of metal ions released in solutions of pH>3.75 was much less than that at pH 2.5, (iii) pre-existing surface defects in Ti–Ni wire might be the preferred sites for corrosion, while Ti–Ni wire, with a rougher surface, did not exhibit a higher ion release, and (iv) the average amount of Ni ions released per day from the tested Ti–Ni wires was well below the critical concentration necessary to introduce allergy (600 ~ 2500 μg)[72] and under daily dietary intake level (300 ~ 500 μg).[73]

Wever *et al.*[74] studied the nickel element release in Hank's solution. For clinical implantation purposes in shape memory metals, the nearly equiatomic Ti–Ni alloy is generally used. The corrosion properties and surface characteristics of this alloy were investigated and compared with two reference controls (316L stainless steel and Ti–6Al–4V). The anodic polarization curves, performed in Hank's solution at 37 °C, demonstrated a passive behavior for the Ti–Ni alloy. A more pronounced difference between the corrosion and breakdown potential, i.e. a better resistance to chemical breakdown of passivity was found for the Ti–Ni alloy compared with 316L stainless steel. The passive film on the Ti–Ni consists of mainly TiO_2-based oxide with minimal amounts of nickel in the outermost surface layers. After immersion in Hank's solution, the growth of a calcium–phosphate layer was observed. The passive diffusion of Ni from the Ti–Ni alloy measured by AAS, reduced significantly in time from an initial release rate of 14.5×10^{-7} µg cm^{-2} s^{-1} to a nickel release that could not be detected after 10 days. It is suggested that the good corrosion properties of Ti–Ni alloy and the related promising biological response, as reported in literature, may be ascribed mainly to the presence of a TiO_2-based surface layer and its specific properties, including the formation of a calcium phosphate later after exposure to a bioenvironment.

Kimura *et al.*[75] coated Ti–Ni implants with oxide film to suppress dissolution of Ni, and estimated the corrosion resistance in 1% NaCl solution by means of anodic polarization measurement. It was found that (i) by coating, dissolution at low potential was suppressed and the dissolute current density decreased, (ii) a further decrease in current density, which results from stabilization of the passive state on the surface, was observed by the repeated polarization, and (iii) the oxide film showed close adhesion with the matrix, and did not form cracks or peel off by plastic deformation associated with the shape memory effect.

To control the effects of Ni allergy from Ti–Ni alloy implants, hydroxyapatite [$Ca_{10}(PO_4)_6(OH)_2$; HA], alumina (Al_2O_3), or titanium (Ti) was coated onto Ti–Ni alloy plates to form 1-µm thick films using radio frequency magnetron sputtering.[78] After the plates had been immersed in physiological saline for periods of one, four, or eight weeks, the concentration of Ni ions released in each solution was detected using microwave induced plasma mass spectrometry. After eight weeks, it was found that the concentration of Ni ions released from the non-coated, the Ti-coated, the HA-coated, and the alumina-coated plates were 238, 19.7, 183, and 106 ppb, respectively. The non-coated, the HA-coated, the alumina-coated, and the Ti-coated plates were implanted into the femurs of a dog for four weeks for histological observation. In the case of the non-coated plates, connective tissue more than 300 µm thick was observed, whereas for the coated plates the thickness of the connective tissue was around 100 µm.[76]

6.11 Allergic reaction, toxicity, and biocompatibility of Ti–Ni alloys

6.11.1 Allergic reaction

Allergy symptoms are the result of too much immunity. The immune system produces antibodies to fight infections. Acquired Immune Deficiency Syndrome (AIDS) is a result of too little immunity. Metal sensitivity is thought to be a very important factor in the overall biocompatibility of implants. Although titanium has not been found to show sensitivity, other materials such as nickel from stainless steel, other high nickel alloys (for example, Ti–Ni alloy), and cobalt from cobalt-based alloys have been shown to be sensitizers in skin dermatitis and might, therefore, show an allergic response upon implantation.[77] Allergic contact dermatitis to metals is a common skin disease in many countries of the world. Ni allergy is most frequent, and the prevalence is reported to be 10% in females and 1% in men.[78] The incidence of Ni allergy has increased especially in the young female generation, where the cause is probably due to the increased habit of ear piercing in females in recent years.[79,80]

Nickel is one of the most common causes of allergic contact dermatitis and produces more allergic reactions than all other metals combined. Currently, several brands of orthodontic wires are made of Ti–Ni alloy and potentially have a high enough nickel content to provoke manifestations of allergic reactions in the oral cavity. Although no cytotoxic effect caused by Ti–Ni alloy has been reported,[68] information concerning the biological side effects of Ni is available in literature.[60,81–83] Nickel is capable of eliciting toxic and allergic responses.[81] Nickel can produce more allergic reactions than all other metal elements.[82] Another study was conducted on Ni hypersensitivity in adolescents in relation to sex, onset, duration and type of orthodontic treatment, and the age at which ears were pierced. The subjects were 700 Finnish adolescents, from 14 to 18 years of age, of which 476 (68%) had a history of orthodontic treatment with metallic appliances. The study consisted of patch-testing for a Ni allergy and a patient history obtained by a questionnaire and from patient records. The frequency of Ni sensitization in the whole group was 19%. Nickel allergy was significantly more often found in girls (30%) than in boys (3%) and in subjects with pierced ears (31%) than in those with no piercing of ears (2%). Orthodontic treatment did not seem to affect the prevalence of Ni sensitization. None of the girls who were treated with fixed orthodontic appliances before ear piercing showed hypersensitivity to Ni, whereas 35% of the girls who had experienced ear piercing before the onset of orthodontic treatment were sensitized to Ni. The results suggest that orthodontic treatment does not seem to increase the risk for Ni hypersensitivity. Rather, the data suggests that treatment with Ni-containing metallic orthodontic appliances before sensitization to Ni (ear piercing) may have reduced the frequency of Ni hypersensitivity.[82] In the *in vivo* study, Ti–Ni alloys show cytotoxic reactions.[86] Cases also show the

conversion of Ni-nonsensitive subjects into Ni-sensitive subjects following the use of Ti–Ni wires.[60] A study was done (1) to determine if standard orthodontic therapy can sensitize patients to Ni, and (2) to assess gingival response to nickel-containing orthodontic appliances in patients who are nickel sensitive before treatment. Nickel sensitivity patch tests were conducted to confirm hypersensitivity to Ni. The tests involved 29 patients, ranging in age from 12 to 48 years (18 female and 11 males). Five of the patients had a positive Ni patch test, a rate of 18.5%. It was concluded that there may be a risk of sensitizing patients to Ni with long-term exposure to nickel-containing appliances as occurs in routine orthodontic therapy.[60]

Nickel is a strong biological sensitizer and consequently may induce a delayed hypersensitivity reaction (type IV immune response). Because Ni is a component of the majority of the orthodontic alloys, the objectives of this cross-sectional study were to determine the prevalence of nickel hypersensitivity reaction before, during, and after orthodontic therapy with conventional stainless-steel brackets and wires; to evidence the induction of this reaction by the orthodontic appliances; and to characterize the Ni hypersensitive persons. Nickel patch tests and a questionnaire were used to evaluate the hypersensitivity to Ni. The total sample consisted of 170 patients, 105 females and 65 males, from the orthodontic department at Bauru Dental School, University of São Paulo. It was suggested that orthodontic therapy with conventional stainless-steel appliances does not initiate or aggravate a Ni hypersensitivity reaction.[84]

6.11.2 Cytocompatibility and cytotoxicity

Cytotoxicity of Ni ions on fibroblasts was examined by cell count and neutral red assay. It was found that (i) Ni ions had dose-dependent cytotoxicity and (ii) the dissolution of Ni ions from Ni-containing metallic restorations must be lower than these concentration levels to avoid severe damage of body tissues.[85]

A study was done to characterize qualitatively and quantitatively the substances released from orthodontic brackets and Ti–Ni wires and to assess comparatively the cytotoxicity of the ions released from these orthodontic alloys.[86] Two full sets of stainless-steel brackets and Ti–Ni wires were immersed in 0.9% saline solution for a month. Human periodontal ligament fibroblasts and gingival fibroblasts were exposed to various concentrations of the two immersion media; nickel chloride was used as a positive control for comparison purposes. It was reported that there was no ionic release for the Ti–Ni alloy aging solution, whereas measurable Ni and traces of Cr were found in the stainless-steel bracket-aging medium. Concentrations of the nickel chloride solution greater then 2 mM were found to reduce by more than 50% the viability and DNA synthesis of fibroblasts; however, neither orthodontic materials-derived media had any effect on the survival and DNA synthesis of either cell.

Porous Ti–Ni alloys represent new biomaterials for long-term implantation.

Their porosity properties might confer them the capacity to trigger fluid capillarity and tissue ingrowth, as well as good tissue-implant apposition and fixation. Porous Ti–Ni was therefore extracted in a saline semi-physiological solution and materials were evaluated for potential cytotoxicity and genotoxicity reactions. From the results, it was concluded that porous Ti–Ni can be considered completely cytocompatible and genocompatible, and therefore represents a good candidate for long-term implantation.[87]

By the prolonged use of Ti–Ni material in a human body, deterioration of the corrosion resistance of the materials becomes a critical issue because of the increasing possibility of deleterious ions released from the substrate to living tissues. It was proven that certain surface modifications, such as nitrogen, acetylene, and oxygen plasma immersion ion implantation (PIII or PI^3) can improve the corrosion resistance and mechanical properties of the materials. With this modification it was reported that (i) the release of Ni is drastically reduced as compared with the untreated control, and (ii) the *in vitro* tests show that the plasma-treated surfaces are well tolerated by osteoblasts.[88,89]

6.11.3 Biocompatibility

Numerous studies have examined the biocompatibility of Ti–Ni *in vitro* and *in vivo*, with differing results. Biocompatibility of a material may be simply defined as its ability to be well accepted by the body. Since every (foreign) material will generate a 'foreign body reaction' when implanted in the 'host' vital soft/hard tissue, the degree of biocompatibility is related to the extent of this reaction. In order to study this phenomenon, *in vitro* testing with cell cultures allows isolation of the reaction from each cell and physiological media, whereas, *in vivo* testing provides a more complete response involving the biological environment and immune system. Both types of tests have been undertaken to better understand the biological response to Ti–Ni.

Biological compatibility (or, in short, biocompatibility) is the ability of a material to perform with an appropriate host response in a specific application. There are three definitions of biocompatibility: (1) the ability of a material to perform with an appropriate host response in a specific application, (2) the quality of not having toxic or injurious effects on biological systems, and (3) comparison of the tissue response produced through the close association of the implanted candidate material to its implant site within the host animal to that tissue response recognized and established as suitable with control materials.[88]

Filip *et al.*[89] characterized the surface and the bulk structure of Ti–Ni implants by scanning electron microscopy (SEM), transmission electron microscopy (TEM), X-ray photoemission spectroscopy (XPS), and scanning Auger electron microprobe analysis (AES). Ti–Ni implants were compared with otherwise identically prepared non-implanted specimens, sputter-cleaned, and reoxidized samples. Non-implanted and implanted samples had essentially the same surface topogra-

phy and microstructure. Ti, O, and C were the dominant elements detected on the surface. Trace amounts (~1 at%) of Ni and Ca, N, Si, B, and S were also detected. Ti was present as TiO_2 on the surface, while Ni was present in metallic form. A significant difference in Ni peak intensity was observed when retrieved or non-implanted control samples (very low Ni content) were compared with sputter-cleaned and reoxidized samples (well-detected Ni). It is mentioned that (i) the method of passivation is crucial for Ni loosening, and (ii) no major changes occurred in the Ti–Ni sample bulk structure or in the surface oxide during the implantation periods investigated.[93]

The biocompatibility of Ti–Ni derives from the formation of an oxide layer (TiO_2) on the substrate surface. This is similar to the TiO_2 on CpTi (commercially pure titanium), which enhances its biocompatibility as an implant material.[94] The passivation layer can range in thickness from 2 nm to ~1 μm.[47,90,91] Resistance of this layer to damage correlates with the corrosion resistance and, hence, biocompatibility of the implants. Overall thickness of the passivation layer is less germane to biocompatibility than its uniformity.[89] Because the oxide layer is a brittle ceramic, the superelasticity of the Ti–Ni substrate can induce stresses in the passivation layer as the implant deforms, causing cracking and resulting in a pitting attack of the Ti–Ni substrate.[92] Obtaining the integrity of the passivation layer is paramount with nitinol to prevent the potential release of metallic Ni into the body. It has been established that Ni *in vivo* is highly toxic, producing severe inflammatory responses, along with being a potential carcinogen.[93]

The Ni in Ti–Ni is chemically joined to the Ti by a strong intermetallic bond, so the risk of reaction, even in patients with Ni-sensitivity, is extremely low.[94,95] The surface-preparation techniques have been shown to have a significant effect on the biocompatibility of the alloy.[96] Ion release measurements on Ti–Ni alloy have shown that the initial rate of Ni ion release is high, but falls rapidly within 2 days, which is similar to that of Ni released from 316L stainless steel,[68,74] although 316L stainless steel contains only 8 wt%. Armitage *et al.*[97] prepared Ti–Ni which was mechanically polished, followed by buff-polishing with the diamond paste, in order to study the influences of surface modifications on the biocompatibility. For another modification, surfaces were shot-peened with 160 μm spherical glass media, and electropolished in 30% HNO_3 in CH_3OH. It was reported that (i) cytotoxicity and cytocompatibility studies with both fibroblast and endothelial cells showed no differences in the biocompatibility of any of the Ti–Ni surfaces, (ii) the cytotoxicity and cytocompatibility of all surfaces were favorable compared with the untreated controls, (iii) the hemolysis caused by a range of Ti–Ni surfaces was no different from that caused by polished 316L stainless steel or polished titanium surfaces (iv) heat treatment (by in-air oxidation at 400 °C for 30 min or 600 °C for 30 min) of Ti–Ni was found to significantly reduce thrombogenicity to the level of the control, (v) the XPS results showed a significant decrease in the concentration of surface Ni with heat treatment and changes in the surface Ni itself from a metallic to an oxide state, and (vi) surface contact angle of both pre-oxidized surfaces showed much lower

(36.3° and 13.5° for 400 and 600 °C oxidation, respectively) than polished surfaces (64.6° for buff-polished and 42.5° for electro-polished),[97] indicating that pre-oxidation makes the Ti surface more active.

A number of ternary Ti–Ni–X alloys have been introduced with the aim of improving the fatigue properties and to decreasing the thermal hysteresis range; well-known ternary alloying elements are Cu and Fe.[98~100] In particular, Cu has been shown to dissolve in the B2 (austenitic) phase in concentrations up to 30 at.% However, Ti–Ni–Cu solid solutions containing more than 10 at.% are characterized by poor formability, so that alloys of technical interest usually contain Cu in the range from 5 to 10 at.%. Ti–Ni (57.6 wt% Ni, 42.4 wt% Ti) and Ti–Ni–Cu (50.7 w/o Ni, 42.4 wt% Ti, 6.9 wt% Cu) were evaluated by the Tada method.[101] It was concluded that (i) a significant difference in the *in vivo* biocompatibility between the binary and ternary alloy was shown and (ii) the presence of the binary alloy led to few morphological changes and a slight reduction of dehydrogenase activity of epithelial cell cultures, whereas the effect of the ternary alloy appears to be more pronounced, obviously due to the releasing of copper ions.[101]

The genotoxicity level of Ti–Ni was compared with that of its pure constituents, pure Ni and pure Ti powders, and also to 316L stainless steel as a clinical reference material. In order to do so, a dynamic *in vitro* semiphysiological extraction was performed with all metals using agitation and ISO requirements. Peripheral blood lymphocytes were then cultured in the presence of all material extracts, and their comparative genotoxicity levels were assessed using electron microscopy-*in situ* end-labeling coupled to immuno gold staining. Cellular chromatin exposition to pure Ni and 316L stainless steel demonstrated a significantly stronger gold binding than exposition to Ti–Ni, pure Ti, or the untreated control. In parallel, graphite furnace AAS was also performed on all extraction media. The release of Ni atoms took the following decreasing distribution for the various resulting semiphysiological solutions: pure Ni, 316L stainless steel, Ti–Ni, Ti, and controls. Ti elements were detected after elution of pure titanium only. Both pure titanium and Ti–Ni specimens obtained a relative *in vitro* biocompatibility. Therefore, this quantitative *in vitro* study provides optimistic results for the eventual use of Ti–Ni alloys as surgical implant materials.[102]

Cutright *et al.*[103] have studied the tissue response to subcutaneous implantation of Ti–Ni wire sutures in rats for a period of 9 weeks. The inflammatory response was minimal starting 3 days after implantation, and the healing process initiated after 1–2 weeks consisted of a fibrous capsule formation around the implant. This reaction was similar to the one generated by similar stainless-steel wires. In addition, Castleman *et al.*[104] evaluated the biocompatibility of chemically passivated Ti–Ni by inserting plates into beagle femurs for periods ranging from 3 to 17 months. The histological analysis of muscular tissue surrounding the implantation site showed no significant difference between Ti–Ni and Cr–Co plates. Neutron activation analyses near the Ti–Ni implants have indicated that there was no significant presence of metallic Ni in the muscle.

Putters *et al.*,[105] using the inhibition of mitosis in human fibroblasts cultured on nitinol, titanium and Ni substrates, stated that the results indicated that nitinol is similar to titanium in its biocompatibility. Sarkar *et al.*,[106] showed that Ti–Ni had an earlier breakdown of its passive oxide layer than other implant materials such as CpTi, stainless steel and Cr–Co alloys when subjected to potentiodynamic cyclic polarization tests in a sodium chloride solution. It should be noted that these studies focused on the surfaces of solid Ti–Ni, thus, it may be expected that porous Ti–Ni may have diminished corrosion resistance by the fact of its greater surface area in contact with bodily fluids.

There are works on porous-structured Ti–Ni materials. Disks consisting of macroporous Ti–Ni alloy are used as implants in clinical surgery for fixation of spinal dysfunctions. Prymak *et al.*[107] preformed the biocompatibility studies by co-incubation of porous Ti–Ni samples with isolated peripheral blood leukocyte fractions (polymorphonuclear neutrophil granulocytes, PMN; peripheral blood mononuclear leukocytes, PBMC) in comparison with control cultures without Ti–Ni samples. The cell adherence to the Ti–Ni surface was analyzed by fluorescence microscopy and SEM. The activation of adherent leukocytes was analyzed by measurement of the released cytokines using enzyme-linked immunosorbent assay. It was found that (i) the cytokine response of PMN (analyzed by the release of IL–1ra and IL–8) was not significantly different between cell cultures with or without Ti–Ni, (ii) there was a significant increase in the release of IL–1ra, IL–6, and IL–8 from PBMC in the presence of Ti–Ni samples, but (iii) in contrast, the release of TNF–α by PBMC was not significantly elevated in the presence of Ti–Ni, and IL–2 was released from PBMC only in the range of the lower detection limit in all cell cultures.[107] These results indicate good biocompatibility acceptance of porous Ti–Ni and are very promising towards eventual Ti–Ni medical device approbation.[108]

There are two additional important concerns regarding the corrosion behavior of Ti materials. In the following two subsections we will discuss the galvanic corrosion and microbiology-induced corrosion.

6.12 Galvanic corrosion of Ti–Ni alloys

There are two types of galvanic cell: the first type is the micro-cells (or local cells) and the second type is the macro-cells. For micro-cells, within a single piece of metal or alloy there exist different regions of varying composition and hence different electrode potentials. This is true for different phases in heterogeneous alloys.[109] The positive way of applying these phenomena is by etching the polished surface of metal to reveal the microstructures for metallographic observations. A severely deformed portion within one piece of a material can serve as an anodic site.[110] For example, a portion of a fully annealed nail was bent, and the whole nail immersed into a NaCl aqueous solution. After several hours it was easily noticed that the localized plastic-deformed portion gets rusted. For macro-cells, which take

place at the contact point of two dissimilar metals or alloys with different electrode potentials, the so-called galvanic corrosion is probably the best known of all the corrosion types.[110] Titanium is the metal choice for implant material due to excellent tissue compatibility; however, superstructures of such Ti implants are usually made of different alloys. This polymetallism leads to detectable (in macro-level) galvanic corrosion.

The intensity of the galvanism phenomenon is due to a number of factors such as the electrode potential, the extent of the polarization, the surface area ratio between anodic site and cathodic site, the distance between the electrodes, the surface state of the electrodes, the conductivity of the electrolyte, and the passage of a galvanic current on the electrolytic diffusion, stirring, aeration or deareation, temperature, pH and the composition of the electrolytic milieu, coupling manner, and an accompanying crevice corrosion. When two solid bodies are in contact, it is fair to speculate that there could be marginal gaps between them because they are not subject to any bonding method like diffusion bonding or fusion welding. Therefore, when the galvanic corrosion behavior is studied in a dissimilar material couple, the crevice corrosion is another important localized corrosion measurement accompanied with galvanic corrosion.[23,111~114]

Among these numerous influencing factors, the surface area ratio between anodic surface and cathodic surface appears to be the most important factor to be considered. If the ratio of surface A_C/A_A (cathode area/anode area) is large, the increased corrosion caused by coupling can be considerable. Conductivity of the electrolyte and geometry of the system may be difficult to determine. The effective cathode area is only that section of the cathode where the resistance between anode and cathode is not a controlling factor.[115]

6.13 Microbiology-induced corrosion (MIC) of Ti–Ni alloys

Microbiology-induced corrosion (MIC) is defined as the deterioration and degradation of metallic structures and devices by corrosion processes that occur directly or indirectly as a result of the activity of living microorganisms, which either produce aggressive metabolites, or are able to participate directly in the electrochemical reactions occurring on the metal surface. Corrosion has long been thought to occur by one of three means: oxidation, dissolution, or electrochemical interaction. To this list the newly discovered microbiological corrosion must be added.[116,117] Oxidation is somewhat beneficial in the case of stainless steel (mainly the Cr element) and Ti because they create a non-porous layer of passive oxide film that protects the substrate surface from further oxidation: Cr_2O_3 or $(Fe,Ni)O(Fe,Cr)_2O_3$ for stainless steel and TiO_2 for titanium materials. However, dissolution and electrochemical reactions are responsible for most of the detrimental corrosion. MIC has received increased attention by corrosion scientists and engineers in recent years. MIC is caused by the presence of microorganisms on a

metal surface, which leads to changes in the rates, and sometimes also the types of the electrochemical reactions that are involved in the corrosion processes. It is, therefore, not surprising that many attempts have been made to use electrochemical techniques (corrosion potential, the redox potential, the polarization resistance, the electrochemical impedance, electrochemical noise, and polarization curves including pitting) to study the details of MIC and determine its mechanism. Applications range from studies of the corrosion of steel pipes in the presence of sulfate-reducing bacteria to investigating the formation of biofilms and calcareous deposits on stainless steel in seawater, to the destruction of concrete pipes in sewers by microorganisms producing very low pH solutions, and to dental prostheses exposed to various types of bacteria intraorally.[118,119]

Study of MIC is a typical interdisciplinary subject that requires at least some understanding in the fields of chemistry, electrochemistry, metallurgy, microbiology, and biochemistry. In many cases, microbial corrosion is closely associated with biofouling phenomena, which are caused by the activity of organisms that produce deposits of gelatinous slime, or biogenically induced corrosion debris in aqueous systems. Familiar examples of this problem are the growth of algae in cooling towers, and barnacles, mussels and seaweed on marine structures. These growths either produce aggressive metabolites or create micro-habitats suitable for the proliferation of other bacterial species, e.g. anaerobic conditions favoring the well-known sulfate-reducing bacteria. In addition, the presence of growths or deposits on a metal surface encourage the formation of differential aeration or concentration cells between the deposit and the surrounding environment, which might stimulate existing corrosion processes.[116] It is probable, however, that microbiological corrosion rarely occurs as an isolated phenomenon, but is coupled with some type of electrcochemical corrosion. For example, corrosion induced by sulfate-reducing bacteria usually is complicated by the chemical action of sulfides. Corrosion by an aerobic organism, by definition, always occurs in the presence of oxygen. To further compound the problem, microbiocidal chemicals may also have some conventional properties, such as corrosion inhibitors (e.g. film-forming). The materials on which a biofilm is developed have higher, or nobler, E_{CORR} (potential at corrosion current) values than those obtained in the absence of biofilms.[120]

Microbes seem to accelerate the corrosion process. They locate susceptible areas, fix anodic sites, and produce or accumulate chemical species that promote corrosion. The microscopic heterogeneity of many materials – whether created intentionally or as an artifact – is quite clear on the scale of microbes, and is an important and overlooked factor in microbiologically influenced corrosion. Weld regions are particularly attractive to microbes in many of the systems,[121] since the weld line normally exhibits slight differences in chemical compositions as well as microstructures, resulting in a possibility for galvanic corrosion occurrence. Microbes are extremely tenacious. They can exist over a wide range of temperatures and chemical conditions, they are prolific, and they can exist in large colonies. They form synergistic communities with other microbes or higher life

forms and accomplish remarkably complex chemical reactions in consort. Microbes can metabolize metals directly and they require many of the chemical species produced by the physical chemistry of corrosion processes for their metabolisms. Microbes can also act to depolarize anodic or cathodic reactions and, in addition to catalyzing existing corrosion mechanisms, many microbes produce organic or mineral acids as metabolic products.[121] Accordingly, it is difficult to specify just what the important variables are when corrosion is influenced by microorganisms. In addition to the variables most important for the type of corrosion under consideration, variables such as dissolved oxygen, pH, temperature, and nutrients, which affect the life cycle of the bacteria, become important for both corrosion testing and corrosion mechanism. The critical situation involved in MIC is limited to the interfacial thin layer (usually with thickness in the 10 to 500 μm range) between the biofilm and metallic surface, since the chemistry of the electrolyte solution at the metal surface is ever-changing. Therefore, the bulk electrolyte properties may have little relevance to the corrosion as influenced by organisms within the film. The organism right at the metal surface influences corrosion activity, and those organisms multiply so rapidly on the surface that a low density of organisms in the bulk quickly becomes irrelevant.[122]

Bacteria must adhere, spread, and proliferate on metallic surfaces in order to cause corrosive reactions. The process of bacterial adhesion is mediated by both an initial physiochemical interaction phase (i.e. electrostatic forces and hydrophobicity) and specific mechanisms (i.e. adhesion–receptor interactions, which allows bacteria to bind selectively to the surface), followed by a subsequent molecular and cellular interaction phase, which is normally followed by a plaque formation in dentistry.[123] The molecular and cellular interaction are complicated processes affected by many factors, including the characteristics of the bacteria themselves, the target material surface, and environmental factors such as the presence of serum proteins or bacterial substances. Microbial adhesion to surfaces is a common phenomenon. Many bacteria demonstrate a preference for the surface regions of solids, teeth, plant fibers, roots, etc. where nutrients may be concentrated by the adsorption of dissolved organic material. Since microorganisms act as colloidal particles, their interaction with solid surfaces can be anticipated, based on colloidal theory. However, microorganisms are more complex than typical colloids as they are capable of independent locomotion, growth in different shapes, and the production of extracellular polymeric materials that aid in anchoring the microbe to the surface.[123]

Adhesion is a situation where bacteria adhere firmly to a surface by complete physiochemical interactions between them, including an initial phase of reversible physical contact, and a time-dependent phase of irreversible chemical and cellular adherence.[124] Bacteria and other microorganisms have a natural tendency to adhere to surfaces as a survival mechanism. This can occur in many environments including the living host, industrial systems and natural waters. The general outcome of bacterial colonization of surfaces is the formation of an adherent layer (biofilm) composed of bacteria embedded in an organic matrix.[125] The starvation

and growth phase influence bacterial cell surface hydrophobicity. Both the number and kind of microorganisms that colonize metal surfaces depend on the type of metal and the presence of an imposed electrical potential. No significant differences in attachment and growth of a pure culture were observed when metal surfaces were dipped in an exogenous energy source. The chemical composition of naturally occurring organic films adsorbed on metal surfaces was shown to be independent of surface composition and polarization.[126]

Chang *et al.*[127] investigated electrochemical behaviors of CpTi, Ti–6Al–4V, Ti–Ni, Co–Cr–Mo, 316L stainless steel, 17–4 PH stainless steel, and Ni–Cr in (1) sterilized Ringer's solution, (2) *Streptococcus mutans* mixed with sterilized Ringer's solution, (3) sterilized tryptic soy broth, and (4) byproduct of *S. mutans* mixed with sterilized tryptic soy broth. It was concluded that (i) of the four electrolytes, the byproduct mixed with sterilized trypic soy broth was the most corrosive media, leading to an increase in I_{CORR} and reduction in E_{CORR}, (ii) CpTi, Co–Cr–Mo and stainless steel increased their I_{CORR} significantly, but Ti–6Al–4V and Ti–Ni did not show a significant increase in I_{CORR}.[127]

Koh *et al.*[112] studied the effect of surface area ratios on bacterial galvanic corrosion of commercially pure Ti coupled with other dental alloys. CpTi was coupled with a more noble metal (type IV dental gold alloy) and a less noble metal (Ni–Cr alloy) with various surface area ratios (ranging from 4:0 to 0:4 – in other words, 4:0 ratio indicates that entire surface area of a noble metal was masked, while 0:4 ratio indicates that only CpTi surface was masked, and area ratios between 4:0 and 0:4 indicate that both surfaces were partially masked to produce different surface areas). Galvanic couples were then electrochemically tested in bacterial culture media and culture media containing bacteria byproducts. It was found that I_{CORR} (and hence, corrosion rate) profiles as a function of surface area ratio showed a straight-line trend (meaning surface area ratio independence) for Ti/Au couples, whereas the representative curve for the Ti/Ni–Cr alloy was bowl-shaped. The latter curve indicates further higher corrosion rates at both ends (larger area of either CpTi or Ni–Cr), meaning that lowest corrosion rate was exhibited at the bottom of bowl (at equal surface area ratio),[112] supporting results obtained by Al–Ali *et al.*[23] and Garcia.[111]

6.14 Formation of titanium oxides

The ASTM F86[128] standard recommends an appropriate chemical treatment of metallic implants to ensure a passive surface condition; such recommended treatment for stainless steel includes a nitric acid chemical passivation or electropolishing to modify the surface oxide characteristics and increase their corrosion resistance, thus improving their biocompatibility. Ti–Ni is a passive alloy like CpTi and stainless steel and a stable surface oxide protects the substrate material from general corrosion.

As mentioned in the introduction, the surface oxide film or layer is the extreme

outer layer on the titanium materials and such an extreme surface consists mainly of titanium oxide. Accordingly, the longevity and safety as well as biological reactions are all strongly related to the characteristics and crystal structures of formed oxides.

Titanium is a highly reactive metal and will react within microseconds to form an oxide layer when exposed to the atmosphere.[129] Although the standard electrode potential was reported to range from –1.2 to –2.0 volts for the $Ti \leftrightarrow Ti^{+3}$ electrode reaction,[130,131] owing to strong chemical affinity to oxygen, it easily produces a compact oxide film, ensuring high corrosion resistance of the metal. This oxide, which is primarily TiO_2, forms readily because it has one of the highest heats of reaction known (ΔH = –915 k mol^{-}) (for 298.16 ~ 2000 °K).[132,133] It is also quite impenetrable by oxygen (since the atomic diameter of Ti is 0.29 nm, the primary protecting layer is only about 5 to 20 atoms thick).[134] The oxide layer formed adheres strongly to the titanium substrate surface. The average single-bond strength of the TiO_2 to Ti substrate was reported to be about 300 kcal mol^{-} while it is 180 kcal mol^{-} for Cr_2O_3/Cr, 320 kcal mol^{-} for Al_2O_3/Al and 420 kcal mol^{-} for both Ta_2O_5/Ta and Nb_2O_5/Nb.[135] Adhesion and adhesive strength of Ti oxide to substrates are controlled by oxidation temperature and thickness of the oxide layer as well as the significant influence of nitrogen on oxidation in air. In addition, adhesion is greater for oxidation in air than in pure oxygen,[136] suggesting that the influence of nitrogen on the oxidation process is significant.

Several studies have demonstrated that passivated Ti–Ni surface layers consist predominantly of a titanium oxide layer (TiO_2),[40,42,47,74,137~140] similar to that found on Ti alloys.[141] This is in agreement with theoretical thermodynamics which specifies that the free energy of formation of TiO_2 is favored over the other Ni or other titanium oxides.[138]

In addition to these oxidation conditions, it is well known that several parameters can modify the accommodation of the stresses developed during the oxidation of a metal and consequently play an important role in maintaining the protective properties of oxide layers. The results show that the adhesion of the oxide layers to the metal substrate decreases as the layer thickness increases. It is shown that the adhesion of the oxide layers decreases when the oxidation temperature increases, despite the increase in oxide plasticity.[142] Adhesive strength between Ti substrate and TiO_2 is also related to the thermal mismatching when the Ti/TiO_2 couple was subjected to the elevated temperatures. Although TiO_2 does not exhibit any phase transformation up to its melting point (i.e. 1885 °C), its substrate Ti metal has an allotropic phase transformation at 885 °C (below which it is hexagonal closed-packed (HCP) crystalline structure and above which it becomes body-centered cubic (BCC) crystalline structure). Accordingly, when Ti substrate is exposed beyond this phase transformation temperature, the bond strength between Ti and TiO_2 will be weakened due to the significant differences in coefficients of thermal expansion, particularly during the cooling stage passing through the 885 °C transus temperature.

The performance of titanium and its alloys in surgical implant applications can be evaluated with respect to their biocompatibility and capability to withstand the corrosive species involved in fluids within the human body.[143] This may be considered as an electrolyte in an electrochemical reaction. It is well documented that the excellent corrosion resistance of titanium materials is because of the formation of a dense, protective, and strongly-adhered film, which is called a passive film. Such a surface situation is referred to as passivity, or a passivation state. The exact composition and structure of the passive film covering titanium and its alloys is controversial. This is the case not only for the 'natural' air oxide, but also for films formed during exposure to various solutions, as well as for those formed anodically. The 'natural' oxide film on titanium ranges in thickness from 2 to 7 nm, depending on such parameters as the composition of the metal and surrounding medium, the maximum temperature reached during the working of the metal and the surface finish.

Passivity is a property of a metal commonly defined in two ways. One of these is based on a change in the electrochemical behavior of the metal, and the other on its corrosion behavior.[144] Passivity is an unusual phenomenon observed during the corrosion of certain metals, indicating a loss of chemical or electrochemical reactivity under certain environmental conditions.[145] Such passivity appears on certain so-called passivating metals, many of which are 'transition metals', characterized by an unfilled d group of electrons in an inner electron shell. Passivating metals are, for example, Fe (covered with Fe_2O_3 and/or Fe_3O_4), Cr (with Cr_2O_3), Zr (with ZrO_2), and Ti (with TiO_2).[139,140,145] This type of passivity is ascribed to an invisibly thin but dense and semiconducting oxide film on the metal substrate surface, displacing the electrode potential of the metal strongly in the positive (or more noble) direction (for example, Ti passive film exhibits its stable passivity up to 1.5 ~ 2.0 volts). Hence, comparing the electrode potential (–1.2 ~ –1.5V) to this stable passivity potential, surface nobility was remarkably improved.

Using the electron diffraction techniques transmission electron diffraction (TED) method on stripped films, and the reflection electron diffraction (RED) method on bulk specimens with formed oxide film) and other surface microanalytical techniques, composition and structure of the oxide film that forms on titanium under various conditions were investigated. The findings are summarized as follows.

6.15 Air-formed titanium oxides

When fresh titanium is exposed to the atmosphere by such cutting acts as lathing, milling, or sawing, an oxide layer begins to form within nanoseconds.[134] After only 1 s, a surface oxide layer (2 to 7 nm thick) will be formed. Air oxidation at room temperature produced titanium monoxide (TiO) with small quantities of titanium oxide, Ti_3O_5. Titanium has proved to be a highly successful material for implants inserted into human bone. Under certain conditions, titanium will establish and maintain a direct contact with the bone tissue in a process called osseointegration.

The mechanisms underlying this behavior are not yet understood. However, it is clear that the properties of the implant surface are of vital importance for a successful osseointegration. The properties of titanium implant surfaces are determined by the thin (20–70 Å) oxide film that covers the metal. Thus, the biocompatibility of titanium implants is associated with the surface TiO_2 and not with the bulk titanium metal.[129,139,140,146,147] The surface oxide is also formed during the implant preparation procedures. During the machining of the implants, pure Ti metal is exposed to air and is rapidly oxidized. In the following cleaning and autoclaving procedures, oxide film is then modified and grows. In order to obtain an oxide film that is reproducible with respect to the chemical composition, structure and thickness, it is important that the different steps of the implant preparation are performed under carefully controlled conditions. Even small changes in the preparation procedures might lead to considerable changes of the implant surface.[148]

As mentioned previously, because the surface air-formed oxide is nearly impenetrable, once this thin passivating film has formed, oxygen is prevented from reaching the metal beneath and further oxide layer thickening is quickly halted because the oxide film is dense and semi-conductive (not like an electron-conductive metal substrate). The compositional structure and exact thickness of the passivating oxide layer are dependent on many factors associated with its formation. These include such factors as type of machining, surface roughness, coolants used during machining, and sterilization procedures. The biocompatibility of devices reported by different investigatorsvaries to a significant degree.[134]

It is well recognized that the excellent tissue-bone compatibility of Ti is mainly due to the properties of its stable surface oxide layer. Biocompatibility of implant materials relies on the chemical and electrochemical stability of this surface oxide layer, which interfaces with the soft and hard tissue and bone structure. Oxide layers formed on Ti change from lower to higher oxides as oxidation progresses and temperature increases. The following phases form in air: $Ti + O \rightarrow Ti(O) \rightarrow Ti_6O \rightarrow Ti_3O \rightarrow Ti_2O \rightarrow TiO \rightarrow Ti_2O_3 \rightarrow Ti_3O_5 \rightarrow TiO_2$. Among these oxides of different stoichiometry (e.g. TiO, Ti_2O_3, TiO_2), TiO_2 is the most common and stable thermodynamically. TiO_2 can have three different crystal structures – rutile, anatase, and brookite – but also can be amorphous. TiO_2 is very resistant to chemical attack, which makes Ti one of the most corrosion resistant metals.

Another physical property that is unique to TiO_2 is its high dielectric constant, which ranges from 14 to 110 (in 10^6 cycles; dielectric strength: 350 V mm^{-1}, volume resistivity: 10^{14}–10^{16} ohm cm) depending on crystal structure.[149] This high dielectric constant would result in considerably stronger van der Waals' bonds on TiO_2 than on other oxides. TiO_2, like many other transition metal oxides, is catalytically active for a number of inorganic and organic chemical reactions, which also may influence the interface chemistry.

The surface and the 'bulk' structure of Ti–Ni implants were characterized using SEM, TEM, XPS, and AES. Ti–Ni implants were compared with otherwise

identically prepared non-implanted specimens, and sputter-cleaned and reoxidized samples. Non-implanted and implanted samples had essentially the same surface topography and microstructure. Ti, O, and C were the dominant elements detected on the surface. Trace amounts (~1 at%) of Ni and Ca, N, Si, B, and S were also detected. Ti was present as TiO_2 on the surface, while Ni was present in metallic form. A significant difference in Ni peak intensity was observed when retrieved or non-implanted control samples (very low Ni content) were compared with sputter-cleaned and reoxidized samples (readily-detected Ni content). It is evident that the method of passivation is crucial for Ni loosening. No major changes occurred in the Ti–Ni samples bulk structure or in the surface oxide during the implantation periods investigated.[89]

6.16 Passivation of Ti–Ni alloys

Passive films can be formed by either chemically or electrochemically (or anodic) treating Ti surfaces. Fraker *et al.*[150] found using TEM, that more rigid oxidizing conditions produce higher oxides of Ti alloy (thin films) in saline water (3.5% NaCl), at 100 to 200 °C. The oxides ranged from Ti_2O to TiO_2 (anatase), with the higher oxides corresponding to the higher temperatures. Concerning oxide films formed anodically on Ti, most investigators agree that the film consists of TiO_2. All three crystalline forms of TiO_2 have been reported, as will be discussed later. It has also been reported that the anodic film has either an excess of oxygen or a deficiency. The controversy is widened by reports that the film is hydrated or contains mixed oxides. In addition to variations in O stoichiometry, the films may contain various amounts of elements other than Ti and O, or incorporate such additional element(s) into TiO_2 structure. Thus, it is most probable that the anodic film is not necessarily stoichiometric TiO_2, and that the films studied by different authors had different compositions due to differences in the conditions of oxidation.[150]

More recently, Trépanier *et al.*[151] performed an *in vivo* study on passivated Ti–Ni stents. Implantation of the material in rabbit paravertebral muscles and the study of the inflammatory reaction for periods ranging from 3 to 12 weeks demonstrated good biological responses to Ti–Ni. Analysis of the fibrous capsule surrounding Ti–Ni stents revealed a decrease in thickness with time. A comparative 26-week follow-up study was conducted on rats to assess the effect of different materials on soft tissues.[152] In this study, short-time biocompatibility of polished Ti–Ni was similar to polished Ti–6Al–4V and electropolished stainless steel when in contact with muscle and perineutral tissue. These results indicate promising soft tissue biocompatibility of Ti–Ni material.

When Ti alloys (Ti–6Al–7Nb and Ti–6Al–4V) were chemically treated, surface oxide films appear to be more complicated. Sittig *et al.*[153] treated these alloys along with CpTi in nitric acid – hydrogen fluoride and identified formed oxides. Three types of oxides (TiO_2, Ti_2O_3, and TiO) were identified on the CpTi substrate, and

it was found that the dissolution rate depends on grain orientations. On the other hand, for Ti–6Al–7Nb and Ti–6Al–4V alloys, Al_2O_3, Nb_2O_5 or V–oxides such as V_2O_5, were formed in addition to TiO_2 oxide and it was found that the selective α-phase dissolution and enrichment of the β-phase appears to occur.[153]

Studies on the nature and properties of thin films formed by the electrolytic oxidation on titanium, which, in turn, determine the behavior of the electrode in the open circuit, indicate the duplex nature of these films.[154] In both the acid and alkaline media, the outer layer of the anodic oxide film was found to be more susceptible to dissolution than the inner layer, thereby indicating a more defective structure of the outer layer. The surface reactivity was found to be higher in oxygen-saturated versus nitrogen-saturated solutions. Galvanostatic anodization of titanium has been studied in N_2-deaerated, 1N solution of NaOH, Na_2SO_4, H_2SO_4, HCl, $HClO_4$, HNO_3, and H_2PO_4 at 25 °C at current densities ranging from 4 to 50 × 10^{-6}A cm^{-2}. From formation rate values, the following arrangement of passivation was obtained: (from the highest rate to the lowest rate) NaOH > Na_2SO_4 > $HClO_4$ > NHO_3 > HCl > H_3PO_4 > H_2SO_4.[154]

Metikoš-Huković *et al.*[155] employed structurally sensitive *in situ* methods, such as photopolarization and impedance, to examine the passivation process and the properties of the protective oxide layers on Ti. The thickness of anodic oxidation and the non-stoichiometry of the surface oxide were correlated. It was mentioned that the composition of the anodic film on T changes with the relative potential from lower to higher oxidation stages according to the equation: TiH_2 + TiO → $nTi_2O_3{\cdot}nTiO_2$ → Ti_5O_9 or Ti_6O_{11} → Ti_3O_5 → TiO_2. The characteristic behavior of titanium can easily be seen at higher anodic potential (approximately +1.5 V vs. SCE in 5M H_2SO_4) when the electrode is covered with a nearly stoichiometric TiO_2 layer. The semiconducting properties of TiO_2 were investigated using an anodic film stabilized at + 2V (vs. SCE with 0.2444 V vs. NHE), and it was found that TiO_2, like the lower titanium oxides, is an n-type (metal-excess) semiconductor under anodic polarization.[155]

Re-passivation capability[156] associated with Ti substrate can be considered as another reason for the high corrosion resistance and biocompatibility of Ti materials.

The re-passivation capability can be evaluated by the physical scratch damage on the sample surface, while being immersed in a certain corrosion media, and by studying the polarization behavior by the method of ASTM F746.[32]

A recent *in vitro* study revealed no significant differences between cell growth behavior near the surfaces of different implant materials (mechanically polished CpTi and Ti–Ni, electropolished 316L stainless steel). Passivated Ti–Ni showed no cytotoxic, allergic or genotoxic activity based on cytotoxicity tests, a guinea-pig sensitization test and genotoxicity testing, respectively.[157] In a different study that addressed only the genocompatibility of the material, TiNi exhibited a good biocompatibility behavior similar to CpTi and 316L stainless steel on cellular chromatin.[158]

Rondelli *et al.*[159] carried out potentiodynamic polarization scans, potentiostatic scratch tests, and modified ASTM F746 tests in simulated body fluids on commercial orthodontic wires made of different classes of materials and on CpTi as a reference. The stability of passivating films, evaluated by electrochemical techniques that abruptly damage it, i.e. potentiostatic scratch tests, increased in the following order: Ti–Ni < stainless steel < Cr–Co alloy < CpTi. Because satisfactory biocompatibility of implants relies on the presence of a stable and efficient self-healing passive film, this ranking should be considered in view of *in vivo* applications. Moreover, scratch tests show that it is not possible to enhance the performance of Ti–Ni samples by modifying surface-passive film by dipping it in an HF/HNO_3 mixture. Finally, straining of Ti–Ni wires under superelastic conditions and the consequent presence of stress-induced martensite does not substantially modify their localized corrosion resistance.

Cissé *et al.*[160] investigated the surface treatment effect on corrosion behavior of Ti–Ni alloy. The near-equiatomic superelastic Ti–Ni (Ni 55.8 wt%) alloy was used. The surface of heat-treated samples were modified by mechanical polishing (MP), electropolishing (EP), and electropolishing followed by chemical passivation (CP). Heat-treated samples with straw-colored oxide finishes (SCO) and blue-colored oxide finishes (BO) were also prepared. It was shown that surface roughness increased in the order of CP < EP < SCO < BO < MP. The Ni releases within the five groups of Ti–Ni samples, as determined by AAS, reduced in time over the measured period. The level of Ni ions released over a 25-day immersion period was highest in the SCO sample (0.002 μg/day). This Ni level is negligible compared with the daily intake of Ni in an ordinary diet. The surface oxide thickness increased in the order CP < EP < MP < BO < SCO. On the other hand, for the electrodes treated under the same conditions, the mean breakdown potential value decreased in the order BO > MP > CP > EP > SCO, while the corrosion current density and rate increased in the order CP < SCO < EP < BO < MP.

The effect of surface roughness on the relative corrosion rates of wires of four alloys (stainless steel, Ti–Ni, Co–Cr alloy, and beta Ti) was investigated.[161] Batches of wire were divided into two groups: one group for polishing to provide a uniform surface finish, and the second group for as-received. The samples of as-received wires showed variations in surface finish, with beta Ti having the roughest appearance and Co–Cr the smoothest. Ti–Ni and stainless-steel surfaces were similar. Mechanical polishing provided a more uniform finish, but significantly reduced the diameter of the wires. The relative corrosion rates (expressed in terms of corrosion current density) in a 0.9% NaCl solution were estimated using polarization resistance. Ti–Ni wires exhibited the greatest corrosion current density in the as-received group. Mechanical polishing significantly reduced the corrosion rate of Ti–Ni, such that comparison between the four alloys in the polished state revealed no significance in their relative corrosion rate/corrosion current density.[161]

Passive films formed on pure Ti and crystalline and amorphous Ti–Ni alloys

containing from 30 to 60 at.% Ti in a sulfuric acid solution were studied by XPS and photoelectrochemical methods. The photocurrent increased with applied anodic potential. The band-gap energies in the surface films were in the range of 3.2–3.4 eV which decreased with increasing applied potential. In the surface film, Ti ions were enriched. The Ti in the film consisted of Ti^{4+}, Ti^{3+} and Ti^{2+} ions. The ratios between them on a specimen were independent of the applied potential, although the thickness of the surface film itself increased with the increasing potential. The surface films on pure Ti and Ti–Ni alloys contained OH-type oxygen.[162]

6.17 Oxidation at elevated temperatures

Above 100 °C, the surface is a lower oxide type, such as TiO. At elevated temperatures (above 200 °C); complex oxides are formed, such as Al_2TiO_5 on Ti–6Al–4V and $NiTiO_3$ on TiNi, in addition to rutile-type TiO_2.[139,140] Oxidation in air at 875 to 1050 °C produced a flaky scale of TiO, Ti_2O_3, and rutile (TiO_2). It was reported that the high oxide TiO_2 appears on the surface of titanium in the presence of the most rigid conditions of oxidation; in less rigid conditions a lower oxide ($3Ti_2O_3 \cdot 4TiO_2$) forms, while, in still weaker oxidizing conditions, the formation of even lower oxides (for example, TiO) are possible.[136]

The characteristics of high-temperature oxidation of Ti are the main obstacle to strong Ti–ceramic bonding.[163] A thin oxide layer (approximately 32 nm) with good adherence to the substrate was formed when CpTi was oxidized at 750 °C in 0.1 atm, and a thick layer (approximately 1 μm) with poor adherence was formed when oxidized at 1000 °C.[164] In another study,[165] the thickness of TiO_2 on the CpTi surface increased with an increase in oxidation temperatures. Ti surface hardness also increases substantially after oxidation at and above 900 °C.[165] Therefore, the substrate is now in the BCC structure range. Lower Ti-ceramic bond strength was attributed to a thick TiO_2 zone on the metal surface when Ti was oxidized at higher temperatures.[166] Enhanced bond strength between Ti and ceramic was reported when porcelain was fired on cast Ti in a reduced argon atmosphere.[167]

Modifying Ti surfaces to control high temperature oxidation has been examined. Published studies show that Ti surface nitridation[168] or a thin Cr coating[169] is an effective method in limiting Ti oxidation at high temperatures. Improved Ti–ceramic bonding was found when a thin layer of Si_3N_4 was deposited on Ti surface.[170]

Mechanically polished Ti–Ni alloy (50 at.% Ni) was subjected to heat treatment in air in the temperature range 300–800 °C and characterized by SEM, x-ray diffraction (XRD), XPS and Raman spectrometry. Thermogravimetry measurements were carried out to investigate the kinetics of oxidation. The results of thermodynamic calculations were compared with the experimental observations. It was found that Ti–Ni alloy exhibits different oxidation behaviors at temperatures below and above 500 °C. A Ni-free zone was found in the oxide layer for oxidation

temperatures of 500 and 600 °C. The oxidation at 500 °C produces a smooth protective Ni-free oxide layer with a relatively small amount of Ni species at the air/oxide interface, which is in favor of good biocompatibility of Ti–Ni implants. The oxidation mechanism for the Ti–Ni shape memory alloy is given by Firstov *et al.*[171]

The corrosion of pure Ni and of binary Ti–Ni alloys containing 5, 10, and 15 wt% Ti, respectively, in molten $(0.62Li,0.38K)_2CO_3$ at 650 °C under air has been studied. The corrosion of the single-phase Ni–5Ti alloy was slower than that of pure Ni, forming an external scale composed of NiO and TiO_2. The two-phase Ni–10Ti and Ni–15Ti alloys underwent much faster corrosion than pure Ni, producing an external scale containing NiO and TiO_2, and a thick internal oxidation zone of titanium mainly involving the intermetallic compound $TiNi_3$ in the original alloys. The rates of growth of the external scales for the Ti–Ni alloys were reduced with the increase of their titanium content, while the internal oxidation was significantly enhanced. The corrosion mechanism of the alloys is also discussed.[172]

Intravascular stents are being designed, which utilize the shape memory properties of Ti–Ni alloy. Despite the clinical advantages afforded by these stents, their application has been limited by concerns about the large Ni ion content of the alloy. In this study, the surface chemistry of Ti–Ni alloy was modified by mechanical polishing and oxidizing heat treatments and subsequently characterized using XPS. The effect of these surfaces on monolayer formation and the barrier integrity of human umbilical vein endothelial cells (HUVEC) was then assessed by confocal imaging of the adherent's junctional molecule VE-cadherin, perijunctional actin and permeability to 42 kDa dextrans. Dichlorofluorescein assays were used to measure oxidative stress in the cells. XPS analysis of Ti–Ni revealed its surface to be dominated by TiO_2. However, where oxidation had occurred after mechanical polishing or post-polishing heat treatments at 300 and 400 °C in air, a significant amount of metallic Ni or nickel oxide species (10.5 and 18.5 at.%) remained on the surface. Exposure of HUVECs to these surfaces resulted in increased oxidative stress within the cells, loss of VE-cadherin and F-actin and significantly increased paracellular permeability. These pathological phenomena were not found in cells grown on Ti–Ni, which had undergone heat treatment at 600 °C. At this temperature, thickening of the TiO_2 layer had occurred due to diffusion of Ti ions from the bulk of the alloy, displacing Ni ions to sub-surface areas. This resulted in a significant reduction in Ni ions detectable on the sample surface (4.8 at.%). This study proposes that the integrity of human endothelial monolayers on Ti–Ni is dependent upon the surface chemistry of the alloy and that this can be manipulated, using simple oxidizing heat treatments.[173]

During implantation, titanium releases corrosion products into the surrounding tissue and fluids even though it is covered by a thermodynamically stable oxide film.[174~176] An increase in oxide thickness, as well as incorporation of elements from the extracellular fluid (P, Ca, and S) into the oxide, has been observed as a function of implantation time.[177] Moreover, changes in the oxide stoichiometry,

composition, and thickness have been associated with the release of Ti corrosion products *in vitro*.[178] Properties of the oxide, such as stoichiometry, defect density, crystal structure and orientation, surface defects, and impurities were suggested as factors determining biological performance.[147,148,179]

6.18 Crystal structures of titanium oxides

It should be clear that the proven high biocompatibility of titanium as implant material is connected with the properties of its surface oxide. In air or water, Ti quickly forms an oxide thickness of 2 to 7 nm at room temperature. TiO_2 possesses three crystalline structures: anatase, rutile, and brookite. Anatase-type TiO_2 is a tetragonal crystalline system with $a_o = 3.78$ Å and $c_o = 9.50$ Å; the rutile-type TiO_2 is also a tetragonal structure, but the lattice constants are quite different from those of anatase-type (i.e. $a_o = 4.58$ Å and $c_o = 2.98$ Å). The third type is brookite-type, and has an orthorhombic crystalline structure with $a_o = 9.17$ Å, $b_o = 5.43$ Å, and $c_o = 5.13$ Å .[180] Among these oxides, rutile is known to be the most stable phase.[181]

Identification of crystalline structures of formed oxides can be achieved in several ways. Thin-film XRD (TFXRD) or XRD if the oxide film is reasonably thick enough, so that diffracted intensities can be obtained, which are high enough to be identified, and differentiated from each other and background noise. The alternative way will be diffraction using accelerated electrons. If an appropriate sample holding device can be manufactured and installed inside the transmission electron microscope, then the oxidized sample with surface oxide can be tilted almost parallel to the accelerated electron beam, resulting in a half ring of RED (reflection electron diffraction),[182~184] from which one can identify the crystalline structure(s) of the oxide(s). Another way for crystalline identification of formed oxides is based on stripping (or isolating) formed oxide from the substrate by chemically etching the back-side (the interface side of formed oxide and substrate) to be isolated from the metallic substrate. Normally for stainless steel, 10% bromine in anhydrous methanol solution is used,[184,185] and for Ti materials, a mixture of HNO_3 and HF is used[37] or 10% bromine in ethyl acetate.[181] The stripped thin oxide film is carried on a copper mesh and transmission electron diffraction (TED) can be performed.[37,186]

Information on titanium oxides of anatase-type, rutile-type, brookite-type, or a mixture of these, appears to be scattered. It is useful here to review and summarize these data to determine some common findings. The plasma-assisted chemical vapor deposition process appears to form anatase type oxide.[187,188] By dry oxidation, the oxides are identified as rutile type oxide, oxidized at 300 °C for 0.5 h,[139,140] 400 °C × 0.75 h,[189] 500 °C × 3 h,[189] 750 °C,[190] and 875 –1050 °C.[149]

On the other hand, crystalline structures of oxides formed through wet oxidation are varied. Only the rutile type of TiO_2 was identified by boiling in 5 wt% H_2SO_4 or 10 wt% HCl,[186] anodizing with 0.5M H_2SO_4 at 5–10 V,[191] boiling in 10% H_2SO_4,[134] boiling in 10% HCl,[192] and treating with 0.5–1M HCl.[193] A mixture of

rutile and anatase type oxide was found when CpTi was treated in $HF/HNO_3/H_2O$, followed by heating in 5M NaOH at 75 °C,[186] followed by air-oxidation at 600 °C × 1 h,[186], or boiling in 0.1 wt% H_2SO_4.[187] On the other hand, mainly anatase, with a small fraction of rutile type mixture, was identified by anodizing in 40% H_2SO_4 at 8 V,[153] and boiling in 10% CrO_3 or 65% HNO_3 for 3 h.[153] When CpTi was treated in alkaline or mildly acid solution, formed oxides were identified to be solely anatase type. This can be formed by treating CpTi in an electrolyte containing $Ca(H_2PO_4)_2$, $Ca(COCH_3)_2$ and Na(EDTA) (pH 14),[188] 1–10% H_2O_2, followed by air oxidation at 500 °C × 3 h,[190] anodizing in HNO_3 solution,[192] 0.1M Na_2CO_3 or 0.01M HCl,[193] anodizing in 0.1M H_2SO_4 at 12.5 mA/cm^2 [194], anodizing in 0.1M H_2SO_4at 5V [195], or anodizing in 1M H_2SO_4 at 155V [196]. It was also reported that, when CpTi was boiled in 0.2 wt.% HCl for 24 h, a mixture of anatase and brookite was formed[197].

In summary, rutile type oxides are favored when the CpTi surface is exposed to iair oxidation at elevated temperature. Processes involved in plasma spraying or vapor deposition produce CpTi surfaces coated with anatase type oxide. In wet oxidation (by either simply boiling or electrochemically anodizing), if the electrolyte (or solution) is a strong acid, the rutile type oxide is favorable, whereas if the treating solution is mild or alkaline, anatase becomes dominant, with a small fraction of rutile type.[198]

The surface electronic states on Ti–Ni ($Ti_{1-x}Ni_x$) electodes, which have five types of intermetallic compounds (Ti, Ti_2Ni, TiNi, $TiNi_3$, Ni) and three types of oxides (TiO_2, $NiTiO_3$, NiO), were investigated by cyclic voltammetry for various nickel mole fractions. An oxidation current peak attributed to the oxidation of the surface states appeared at 0.53 V vs. SCE in the cyclic voltammogram.[199]

6.19 Characterization of oxides

To understand the complex interfacial phenomena between Ti and a biological system, Hanawa[200] prepared CpTi, Ti–6Al–4V, Ti–Ni, 316L stainless steel, Co–30Cr–5Ni, Ni–20Cr, Au–9Cu–6Ag, Ag–20Pd–15Cu–12Au, which were polished and immersed in Hank's electrolyte (pH 7.4) at 37 °C for 1 h, 1 day, and 30 days. Such sample surfaces were microanalyzed. It was found that (i) calcium phosphate layers are formed on the passive films of Ti and its alloys, stainless steel, Co–Cr and Ni–Cr alloy, in a neutral electrolyte solution. The calcium phosphate formed on Ti, more so than that formed on the other alloys, is similar to apatite. In all these materials, the formation of calcium phosphates is related to the biocompatibility of the material, while the passive oxide films are related to the corrosion resistance.[200]

Oshida *et al.* investigated the surface physics of oxides formed on various biomaterials, including Ti materials.[139,140] Interfaces between biomaterials, tissue, and body fluids such as blood, play a key role in determining the nature of the interaction between biomaterials and the living organism. The wettability of these biomaterials in relation to their microenvironment is an important factor to

consider when characterizing surface behavior. The measure of the contact angle between a fluid and material surface can be used to define wettability for that particular microenvironment. In this study, pure Ti, Ti–6Al–4V alloy, austenitic and martensitic Ti–Ni alloys, pure Ni, AISI Type 316L stainless steel, Co–Cr alloy, and α-alumina were investigated. All metallic materials were mechanically polished and oxidized at 300 °C for 30 min in pure oxygen. Oxide films formed on the surfaces of these materials were examined under the electron microscope and their crystalline structures were identified by the electron diffraction method. The initial contact angle (θ_o) and its changes ($\delta\theta/\delta t$) as a function of time in 1% NaCl solution drop were measured. The results of this study indicated that (i) Ti and its alloys were covered with mainly TiO_2 (tetragonal structure), (ii) NiO (cubic structure) was found on pure Ni, (iii) the spinel -ype oxide (cubic structure) was formed on both 316L stainless steel and Co–Cr alloy, (iv) TiO_2 (except for oxides formed on Ti–6Al–4V alloy) showed a rapid spreading characteristic in 1% NaCl solution; while (v) a relatively slow spreading behavior was observed on the cubic structure oxides.[139]

The effects of surface roughness on wettability were further investigated.[140] In addition, the spontaneous half-cell potential of all tested biomaterials was measured to correlate the wettability phenomenon to initial surface chemistry. Pure Ti and its alloys, including Ti–6AI–4V and Ti–Ni alloys, AISI Type 316L stainless, Co–Cr alloy, and pure Ni, were mechanically polished, shot-peened and pre-oxidized at 300 °C for 30 min in pure oxygen. It was found that (i) shot-peening homogenized the surface conditions in terms of initial contact angles, (ii) TiO_2 shows a higher spreading coefficient, while cubic structure oxides show a lower value, and (iii) the spreading coefficient was correlated to the magnitude of the spontaneous half-cell potential.[140]

6.20 Oxide growth, stability and breakdown

The oxide layer forms spontaneously in air, and normally has a thickness of between 2 and 7 nm, as mentioned previously. During machining, the relatively high surface temperature can produce a much thicker oxide layer.[201] There is much evidence suggesting that this layer grows steadily *in vivo*. The stoichiometry of the oxide is similar to titanium oxide (TiO_2) at the surface, and changes to a mixture of oxides at the metal/oxide interface.[129,202] TiO_2 is an n-type (metal-excess or donor type) semi-conductor, while TiO and Ti_2O_3 are listed as amphoteric conductors.[203] The surface is also known to have at least two types of hydroxyl groups attached to it.[204] TiO_2 is non-conducting, but electrons can tunnel through the layer. Thin oxide layers can allow the passage of electrons, leading to conformational changes and denaturing of proteins.[205]

For implants located in cortical bone, the thickness of the interfacial oxide layer remains unaffected, while it increases by a factor of 3–4 on samples located in bone marrow.[177] In general, when foreign agents, such as implant-material surface

particles, are exposed to host tissue, circulating neutrophils and/or monocytes are recruited from the intravascular compartment to the location of the exposure.[206] Following recognition, the particles are encapsulated – literally engulfed by the phagocyte – and lysosomal granules, along with the particles, from a complex unit, the phagolysosome. Simultaneously, in the cytoplasmic vacuoles, enzyme releases occurs and, as a result, degrading of several components takes place. Upon recognition, neutrophils and monocytes experience a 'respiratory burst' and during the period, almost 20-fold oxygen consumption by the cells is observed.[207] There is convincing evidence that the consequent increase in oxygen secretion by these cells is mainly the result of this initial respiratory activity.[208] In addition, polymorphonuclear cells have been found to secrete superoxide anion (O_2^-) and hydrogen peroxide (H_2O_2) upon activation induced by several stimuli, including immunoglobulins and opsonized bacteria, among others.[209]

O'Brien *et al.*[210] passivated Ti–Ni wires and vascular stent components in 10% nitric acid solution, and evaluated electrochemical corrosion behaviors. It was reported that (i) potentiodynamic polarization tests demonstrated a significant increase in breakdown potential for passivated samples (600–700 V vs. SCE), compared with heat-treated surfaces (250–300 V vs. SCE), (ii) surface analysis indicated that the passivation reduces Ni and NiO content in the oxide and increases TiO_2 content, (iii) long-term immersion tests demonstrated that Ni release from the surface of the material decreases with time and the quantity of Ni released is lower for passivated samples, and (iv) the improved corrosion resistance is maintained after prolonged immersion at 37 V in 0.9% NaCl solution.[210]

6.21 Reaction with hydrogen peroxide

The insertion of an implant is inevitably associated with an inflammatory response due to the surgical trauma. Whether this reaction will subside or persist may very well be dependent on the material selected, as well as the site of implantation and the loads put on it.[211] It is most probable that the interaction between material and inflammatory cells, either directly or via mediators of cell activation and migration such as complement factors,[212] is of main importance for the biocompatibility of an implanted material. Further, experimental studies suggest that oxygen free radicals generated in large amounts during the respiratory burst by inflammatory cells are important for the tissue damage and persistence of the inflammatory reaction.[213] Further, it has been observed that an oxide-like layer grows on Ti as well as on stainless-steel implants *in vivo* during the implantation.[177,214] Model experiments have indicated that hydrogen peroxide in buffered saline solution in the millimolar concentration range produces an oxide-like layer on titanium surfaces *in vitro*, [215] and at higher H_2O_2 concentrations, several oxidation intermediates are distinguished in the Ti–H_2O_2 system. It is well known that H_2O_2 is one of the strongest oxidizing agents. These observations lead one to believe that *in vivo* the interaction of H_2O_2 and oxygen with Ti would be the cause of the oxide growth observed.[209] It

is well known that Ti^{4+} ions will not produce hydroxyl radicals from H_2O_2; however, in the presence of the superoxide radical (O_2^-), both H_2O_2 and OH· may be produced through the action of superoxide dismutase and a cyclic Fenton reaction.[216–219] Such a superoxide radical (O_2^-) generated during the metabolic activation is (in the body) enzymatically dismuted by H_2O_2 through the reaction: $O_2^- + O_2^- + 2H^+ \rightarrow H_2O_2 + O_2$. Superoxide or H_2O_2 alone is not potent enough in degrading adducts and, therefore, several possible mechanisms, starting from the reaction above have been suggested.[219] As a removal mechanism of bacteria inside the body, neutrophil activates such superoxidants of the cells to generate hydrochlorous acid, which possesses the strongest antibacterial agent among various chlorine compounds. The most interesting is the Fenton type of reaction: $M^{n+} + H_2O_2 \rightarrow M^{(n+1)+} + OH\cdot + OH^-$, where the potent hydroxyl radical, OH· is formed. In the presence of O_2^-, the oxidized metal ion, $M^{(n+1)+}$ is reduced again (to M^{n+}), and a cyclic continuous production of OH· would occur.[219] Hence, hydroxyl radicals formed from H_2O_2 during the inflammatory response are potent agents for cellular deterioration. The behavior of implanted material in terms of its ability to sustain or stop free radical formation may be therefore very important. *In vitro* studies of Ti, which is known to be biocompatible and osseointegrates into human bone, were carried out. The production of free radicals from H_2O_2 at Ti and TiO_2 surfaces was measured by spin trapping techniques. It was found that there is no sustained hydroxyl radical production at a titanium (oxide) surface, due to the quenching of the Fenton reaction through both trapping and oxidation of superoxide radicals in a TiO·OH adduct. Janzén *et al.* concluded that the degree of surface-induced hydroxyl radical formation from H_2O_2 through the Fenton reaction may be of importance for the behavior of implanted materials.[220]

Tengvall *et al.*[221] investigated the role of Ti and TiO_2, as well as other metals, in the inflammatory response through the Fenton reaction. The TiO·OH matrix formed traps the superoxide radical so that no, or very small amounts of, free hydroxyl radicals are produced. Ellipsometry and spin trapping with spectrophotometry and electron spin resonance were used to study the interaction between Ti and H_2O_2. Spectrophotometric results indicated that Ti, Zr, Au and Al are low free OH-radical producers. It was suggested that a hydrated TiO·OH matrix, after the inflammatory reaction, responded to good ion-exchange properties, and extracellular components may interact with the Ti^{4+}–H_2O_2 compound before matrix formation. The TiOOH matrix is formed when the H_2O_2 coordinated to the Ti^{4+}–H_2O_2 complex is decomposed to water and oxygen.[221]

It has been reported that (i) Ti implants inserted in the human body for many years have shown high oxidation rates at the areas relatively adjacent to the Ti implant, and (ii) the implants have shown a dark pigmentation due to the interaction with H_2O_2.[222] It is well known that H_2O_2 is a strong oxidant that will increase the redox potential of the system. Gas evolution was observed on the Ti surface in the presence of H_2O_2 in the PBS (phosphate-buffered saline) solution. This is due to the decomposition of H_2O_2 into water and molecular oxygen according to:

$2H_2O_2 \rightarrow H_2O + O_2$, which is catalyzed by the presence of TiO_2 on the surface due to the combined effect of the electron-donating and electron-accepting properties of TiO_2 occurring simultaneously,[221] and the formation of some Ti-complex, which can lead to a higher electrode potential.[223] Pan *et al.*[224] performed electrochemical measurements, XPS, and scanning tunneling microscopy analyses to study the effect of H_2O_2 on the passivity of CpTi (grade II) in a phosphate-buffered saline (PBS) solution. The results indicate that the passive film formed in the PBS solution – with and without addition of H_2O_2 – may be described with a two-layer structure model. The inner layer has a structure close to TiO_2, whereas the outer layer consists of hydroxylated compounds. The introduction of H_2O_2 in the PBS solution broadens the hydroxylate-rich region, probably due to the formation of a Ti^{4+}–H_2O_2 complex. Furthermore, the presence of H_2O_2 results in enhanced dissolution of Ti and a rougher surface on a microscopic scale. It was also observed that H_2O_2 addition furthermore seems to facilitate the incorporation of phosphate ions into the thicker porous layer.[224]

The influence of H_2O_2 generated by an inflammatory response has also been suggested as an explanation for the high rate of Ti oxidation/corrosion in *vivo*.[221~225] The incorporation of mineral ions into the oxide film is believed to be important for the osseointegration behavior, which can lead to direct bone–Ti contact and strong bonding that in turn can contribute to the load-bearing capacity of Ti implants.[226] To analyze the response of Ti to representative surgical wound environments, Bearinger *et al.*[227] examined CpTi and Ti–6Al–4V, which were exposed to PBS with 30 mM H_2O_2 addition. The study was characterized by simultaneous electrochemical atomic force microscopy and step-polarization impedance spectroscopy. It was found that (i) surfaces were covered with protective oxide domes that indicated topography changes with potential and time of immersion, and (ii) less oxide dome coarsening was noted on surfaces treated with PBS containing H_2O_2 than on surfaces exposed to pure PBS. In both types of solutions, oxide (early) resistances of CpTi samples were higher than Ti–6Al–4V oxide resistances, but CpTi oxide resistance was lower in the H_2O_2 solution compared with pure PBS. Differences in electrical properties between CpTi and Ti–6Al–4V surfaces suggest that CpTi, but not Ti–6Al–4V, has catalytic activity on H_2O_2, and that the catalytic activity of CpTi oxide affects its ability to grow TiO_2.[227]

6.22 Reaction of titanium with hydrogen

It is generally agreed that the solubility of hydrogen in α-phase Ti and Ti alloys is quite low, namely of the order of 20–2000 ppm at room temperature.[228] However, severe problems can arise when Ti-based alloys pick up large amounts of hydrogen, especially at elevated temperatures.[229–233] The strong stabilizing effect of hydrogen on the β-phase field results in a decrease of the (HCP crystalline structure) → β (BCC crystalline structure) transformation temperature from 885 °C to a eutectoid temperature of 300 °C.[229] Hydrogen absorption from the

surrounding environment leads to degradation of the mechanical properties of the material.[234] This phenomenon has been referred to as hydrogen embrittlement over the past years. Hydrogen absorption often becomes a problem for high-strength steels even in air,[235] and it also occurs for Ti in methanol solutions containing hydrochloric acid.[237–240] Hydrogen damage of Ti and Ti-based alloys is manifested as a loss of ductility (embrittlement) and/or reduction in the stress-intensity threshold for crack propagation.[228] CpTi is very resistant to hydrogen embrittlement, but it becomes susceptible to hydrogen embrittlement under an existence of notch, at low temperature, high strain rates, or large grain sizes.[241] Eventually, all of these thermal and mechanical situations make the material more brittle in nature. For α and near α Ti material, it is believed that such hydrogen embrittlement occurs due to precipitation of brittle hydride phases.[242] For $\alpha+\beta$ phase alloys, when a significant amount of β phase is present, hydrogen can be preferentially transported with the β lattice, and will react with α phase at α/β boundaries. Under this condition, degradation will generally become severe.[243] For β alloys, hydrogen embrittlement was observed to occur in the Ti–Mo–Nb–Al,[244] Ti–V–Cr–Al–Sn,[245] and Ti–V–Fe–Al alloys,[246] due to δ-hydride phase formation, which is brittle at low temperatures.[228]

There are some processes by which hydrogen could develop, and possibly be absorbed, under passive conditions: direct absorption of hydrogen produced by water hydrolysis, and absorption of atomic hydrogen produced by the corrosion processes to give an oxide. Under anodic conditions, when passive corrosion prevails, the corrosion potential for passive Ti must rise at a value at which water reduction can cause Ti to oxidize, $Ti + 2H_2O \rightarrow TiO_2 + 2H_2$. Since titanium hydrides are thermodynamically stable at these potentials, the passive film can only be considered as a transport barrier, and not an absolute barrier. The rate of hydrogen absorption will be controlled by the rate of corrosion reaction, which dictates the rate of production of absorbable hydrogen. Since TiO_2 is extremely insoluble, the corrosion reaction will be effectively limited to an oxide film growth reaction.[247] Titanium corrosion processes are often accompanied with hydrogen production, introducing the possibility of the absorption of hydrogen into the material. Crevice corrosion, once initiated, is supported by both the reduction of oxygen on passive surfaces external to the crevice and the reduction of protons ($Ti + 4H^+ \rightarrow Ti^{4+} + 2H_2$) inside the crevice, leading to the absorption of atomic hydrogen in sufficient quantities to produce extensive hydride formation. For passive non-creviced or inert-crevice conditions, corrosion could be sustained by reaction with water under neutral conditions ($Ti + 2H_2O \rightarrow TiO_2 + 2H_2$), and should proceed at an extremely slow rate. In the first step to possible failure by hydrogen-induced cracking, the hydrogen generated must pass through the TiO_2 film before absorption into the underlying Ti alloy. For absorption to proceed, redox transformation ($Ti^{4+} \rightarrow Ti^{3+}$) in the oxide film is necessary. This requires significant cathodic polarization of the metal, generally achievable by galvanic coupling to active materials (such as carbon steel), or application of cathodic protection potential.[248]

Superelastic Ti–Ni wire is widely used in orthodontic clinics, but delayed fracture in the oral cavity has been observed. Because hydrogen embrittlement is known to cause damage to Ti alloy systems, Yokoyama *et al.*[249] treated orthodontic wires cathodically in 0.9% NaCl solution for charging hydrogen, followed by conducting tensile tests and fractographic observations. It was reported that (i) the strength of the Co–Cr alloy and stainless steel used in orthodontic mechanotreatment was not affected by the hydrogen charging; however, Ti–Ni wire showed significant decreases in its strength, and (ii) the fractured surface of the alloy with severe hydrogen charging exhibited dimple patterns similar to those in the alloys from patients. In view of the galvanic current in the mouth, the fracture of the Ti–Ni alloy might be attributed to the degradation of the mechanical properties due to hydrogen absorption.[248] Hydrogen-induced embrittlement of Ti–Ni was also found when it was tested in acidic solutions and fluoride-containing solutions such as APF.[250,251] However, it was suggested that the work-hardening Ti–Ni alloy was less sensitive to hydrogen embrittlement compared with Ti–Ni superelastic alloy.[247]

The reaction of Ti with hydrogen is not necessarily a useless phenomenon. The formation of titanium hydrides can provide an engineering advantage. It is well known that Ti is one of the most promising materials for hydrogen storage due to a stable formation of non-stoichiometric titanium hydrides (δ, ε, or γ type) over the composition range from $TiH_{1.53}$ to $TiH_{1.99}$.[236]

6.23 References

1 Brockhurst P J, 'Dental Materials: New Territories for Materials Science'. Metals Forum. *Australian Inst Metals*, 1980 **3** 200–210.
2 Attin T, 'The security and use of carbamide peroxide gels in bleaching therapy', *Dtsch Zahnärztl Z*, 1998 **53** 11–16.
3 Rosentritt M, Lang R, Plein T, Behr M, Handel G, 'Discoloration of restorative materials after bleaching application', *Quintessence Int*, 2005 **36** 33–39.
4 Goldstein G R, Kiremidjian-Schuhmacher L. Bleaching, 'Is it safe and effective?', *J Prosthet Dent*, 1993 **69** 325–328.
5 Wilhelmsen W, Grande A P, 'The influence of hydrofluoric acid and fluoride ion on the corrosion and passive behavior of titanium', *Electrochim Acta*,1987 **32** 1469–1472.
6 Nakagawa M, Matsuya S, Udoh K, 'Effect of fluoride and dissolved oxygen concentration on the corrosion behavior of pure titanium and titanium alloys', *Dent Mater J,* 2002 **21** 83–92.
7 Takemoto S, Hatori M, Yoshinari M, Kawada E, Oda Y, 33'Corrosion behavior and surface characterization of titanium in solution containing fluoride and albumin', *Biomaterials*, 20053 **26** 829–837.
8 Dahl J E, Pallesen U, 'Tooth bleaching – a critical review of the biological aspects', *Crit Rev Oral Biol Med*, 2003 **14** 292–304.
9 Oshida Y, Sellers C B, Mirza K, Farzin-Nia F, 'Corrosion of dental materials by dental treatment agents', *Mater Sci Eng*, 2005 **C25** 343–348.
10 Oshida Y, Mirza K, Sellers C B, Panyayong W, Farzin-Nia F, 'Effects of dental treatment agents on discoloration/corrosion behavior of metallic dental materials' In: *Medical*

device materials. Shrivastava S, editor. Materials Park OH: ASM International. 2004, pp. 467–470
11 Barton K, *Protection against atmospheric corrosion*, New York: J.Wiley & Sons. 1973, p. 202.
12 Nilner K, Holland R I, 'Electrochemical potentials of amalgam restorations *in vivo*', *Scand J Dent Res*, 1985 **93** 357–359.
13 Corso P P, German R M, Simmons H D, 'Corrosion evaluation of gold-based dental alloys'. *J Dent Res*, 1985 **64** 854–859.
14 Reclaru L, Meyer J M, 'Zonal coulometric analysis of the corrosion resistance of dental alloys', *J. Dent Res*, 1995 **23** 301–311.
15 Ewers G J, Thornber M R, 'The effect of a simulated environment on dental alloys', *J Dent Res*, 1983 **62** 330 (Abstract No. 330).
16 Brown S A, Simpson J P, 'Crevice and fretting corrosion of stainless-steel plates and screws', *J Biomed Mater Res*, 1981 **15** 867–878.
17 Man H C, Gabe D R, 'A study of pitting potentials for some austenitic stainless steels using a potentiodynamic technique', *Corr Sci*, 1981 **21** 713–721.
18 Oshida Y, Sachdeva R, Miyazaki S, 'Microanalytical characterization and surface modification of NiTi orthodontic arch wires'. *J Biomed Mater Eng*, 1992 **2** 51–69.
19 Cahoon J R, Bandyopadhya R, Tennese L, 'The concept of protection potential applied to the corrosion of metallic orthopedic implants', *J Biomed Mater Res*, 1975 **9** 259–264.
20 Sutow E J, Pollack S R, Korostoff A, 'An *in vitro* investigation of the anodic polarization and capacitance behavior of 316L stainless steel', *J Biomed Mater Res*, 1976 **10** 671–693.
21 Syrett B C, Wing S S, 'An electrochemical investigation of fretting corrosion of surgical implant materials', *Corrosion*, 1978 **34** 379–386.
22 Hoar T P, Mears D C, 'Corrosion-resistant alloys in chloride solutions: materials for surgical Implants', *Proc Royal Soc*, 1966 **294A** 486–510.
23 Al-Ali S, Oshida Y, Andres C J, Barco M T, Brown D T, Hovijitra S, Ito M, Nagasawa S, Yoshida T, 'Effects of coupling methods on galvanic corrosion behavior of commercially pure titanium with dental precious alloys', *J Biomed Mater Eng*, 2005 **15** 307–316.
24 Dunigan-Miller J, *Electrochemical corrosion behavior of commercially pure titanium materials fabricated by different methods in three electrolytes*, Indiana University Master Thesis. 2004.
25 Schiff N, Grosgogeat B, Lissac M, Dalard F, 'Influence of fluoride content and pH on the corrosion resistance of titanium and its alloys', *Biomaterials*, 2002 **23** 1995–2002.
26 Schiff N, Grosgogeat B, Lissac M, Dalard F, 'Influence of fluoridated mouthwashes on corrosion resistance of orthodontics wires', *Biomaterials*, 2004 **25** 4535–4542.
27 Yoon S J, Kim C W, Lim B S, 'Electrochemical corrosion of dental titanium in fluoride ion', *J Dent Res*, 1997 **76** 81 (Abstract No. 538).
28 Waler M P, White R J, Kula K S, 'Effect of fluoride prophylactic agents on the mechanical properties of nickel–titanium-based orthodontic wires', *Amer J Orthodont Dentfac Orthop*, 2005 **127** 662–669.
29 Rondelli G, Vicentini B, Cigada A, 'The corrosion behaviour of nickel titanium shape memory alloys', *Corrosion Science*, 1990 **30** 805–812.
30 Aziz-Kerrzo M, Conroy K G, Fenelon A M, Farrell A T, Breslin C B, 'Electro-chemical studies on the stability and corrosion resistance of titanium-based implant materials', *Biomaterials*, 2001 **22** 1531–1539.
31 Iijima M, Endo K, Ohno H, Mizoguchi I, 'Effect of Cr and Cu addition on corrosion behavior of Ni–Ti alloys', *Dent Mater J*, 1998 **17** 31–40.
32 ASTM F 746-87 Standard Test method for pitting or crevice corrosion of metallic

surgical implant materials. In: *Annual book of ASTM standards*, Vol. 13.01. Philadelphia, PA: American Society for Testing and Materials 1996, pp. 80–85.
33 Rondelli G, Vicentini B, 'Effect of copper on the localized corrosion resistance of Ni–Ti shape memory alloy', *Biomaterials*, 2002 **23** 639–644.
34 Rondelli G, 'Corrosion resistance tests on NiTi shape memory alloy', *Biomaterials*, 1996 **17** 2003–2008.
35 Iijima M, Endo K, Ohno H, Yonekura Y, Mizoguchi I, 'Corrosion behavior and surface structure of orthodontic Ni–Ti alloy wires', *Dent Mater J*, 2001 **20** 103–113.
36 Sun E X, Fine S, Nowak W B, 'Electrochemical behavior of nitinol alloy in Ringer's solution' *Journal of Materials Science: Materials in Medicine*, 2002 **13** 959–964.
37 Kuphasuk C, Oshida Y, Andres C J, Hivijitra S T, Barco M T, Brown D T, 'Electrochemical corrosion of titanium and titanium-based alloys', *J Prosthet Dent*, 2001 **85** 195–202.
38 Wang J, Li N, Han E-H, Ke W, 'Effect of pH, temperature and Cl^- concentration on electrochemical behavior of NiTi shape memory alloy in artificial saliva' *Journal of Materials Science: Materials in Medicine*, 2006 **17** 885–890.
39 Huang H-H, 'Corrosion resistance of stressed NiTi and stainless-steel orthodontic wires in acid artificial saliva', *J Biomed Mater Res*, 2003 **66** 829–839.
40 Huang H-H, 'Surface characterizations and corrosion resistance of nickel–titanium orthodontic archwires in artificial saliva of various degrees of acidity', *J Biomed Mater Res*, 2005 **74A** 629–639.
41 Oshida Y, Farzin-Nia F, unpublished data, 2007.
42 Steinemann S, 'Corrosion of surgical implants – in vivo and in vitro tests', In: *Evaluation of biomaterials.* Winters GD, Leray JL, deGroot K, editors. Chishester: John Wiley. 1980, pp.1–34.
43 Carrol W M, Kelly M J, 'Corrosion behavior of nitinol wires in body fluid environments', *J Biomed Mater Res*, 2003 **67A** 1123–1130.
44 Revie R W, Greene N D, 'Comparison of the in vivo and in vitro corrosion of 18–8 stainless steel and titanium', *J Biomed Mater Res*, 1969 **3** 465–470.
45 Clark G C F, Williams D F, 'The effect of proteins on metallic corrosion', *J Biomed Mater Res*, 1982 **16** 125–134.
46 Speck K M, Fraker A C, 'Anodic polarization behavior of Ti–Ni and Ti–6Al–4V in simulated physiological solutions', *J Dent Res*, 1980 **59** 1590–1595.
47 Trépanier C, Tabrizian M, Yahia L'H, Bilodeau L, Piron D L, 'Effect of modification of oxide layer on NiTi stent corrosion resistance', *Journal of Biomedical Materials Research; Applied Biomaterials*, 1998 **43** 433–440.
48 Starosvetsky D, Gotman I, 'Corrosion behavior of titanium nitride coated Ni–Ti shape memory surgical alloy', *Biomaterials*, 2001 **22** 1853–1859.
49 Tan L, Dodd R A, Crone W C, 'Corrosion and wear-corrosion behavior of NiTi modified by plasma source ion implantation', *Biomaterials*, 2003 **24** 3931–3939.
50 Stone P, Bennett R A, Bowker M, 'Reactive re-oxidation of reduced TiO_2(110) surfaces demonstrated by high temperature STM movies', *New J Phys*, 1999 **1** 1–12.
51 Hanawa T, Ota M, 'Calcium phosphate naturally formed on titanium in electrolyte solution', *Biomaterials*, 1991 **12** 767–776.
52 Demri B, Hage-Ali M, Moritz M, Muster D, 'Surface characterization of C/Ti 6Al 4V coating treated with ion beam', *Biomaterials*, 1997 **18** 305–310.
53 Green S M, Grant D M, Wood J V, Johanson A, Johnson E, Sarholt-Kristensen L, 'Effect of N^+ implantation on the shape memory behavior and corrosion resistance of an equiatomic NiTi alloy', *J Mater Sci Lett*, 1993 **12** 618–619.
54 Chen J. Conrad J R, Dodd R A, 'Methane plasma source ion implantation (PSII) for

improvement of tribological and corrosion properties', *J Mater Process Tech*, 1995 **49** 115–124.
55 Riviere J P, 'Formation of hard coatings for tribological and corrosion protection by dynamic ion mixing', *Surf Coat Tech*, 1998 **108** 276–283.
56 Mandl S, Krause D, Thorwarth G, Sader R, Zeilhofer F, Horch H H, Rauschenbach B, 'Plasma immersion ion implantation treatment of medical implants', *Surf Coat Tech*, 2001 **142** 1046–1050.
57 Poona R W Y, Yeungb K W K, Liua X Y, Chua P K, Chunga C Y, Lub W W, Cheungb K M C, Chanc D, 'Carbon plasma immersion ion implantation of nickel–titanium shape memory alloys', *Biomaterials*, 2005 **26** 2265–2272.
58 Trépanier C, Venugopalan R, Pelton A R, 'Corrosion resistance and biocompatibility of passivated NiTi', in L'H Yahia, *Shape memory implants*, Springer, New York, 2000, 35–45.
59 K.Fuwa, '*Living body and heavy metals'*, Kodansha-Scientific, Tokyo, 1980, 33–56.
60 Bass J K, Fine H, Cisneros G J, 'Nickel hypersensitivity in the orthodontics patent', *Am J Orthod Dentofacial Orthop*, 1993 **103** 280–285.
61 Takamura K, Hayashi K, Ishinishi N, Sugioka Y, 'Evaluation of carcinogenicity and cronic toxicity associated with orthopedic implants in mice', *J Biomed Mater Res*, 1994 **28** 583–589.
62 Hultgren R, Desai P D, Hawkins T, Gleiser M, Kelley K K, 'Selected value of the thermodynamic properties of binary alloys', *American Society for Metals*, Metals Park OH, 1973, 1244–1246.
63 Heusler K E, 'The influence of electrolyte composition on the formation and dissolution of passivating films', *Corr Sci* 1989 **29** 131–147.
64 Park H Y, Shearer T R, '*In vitro* release of nickel and chromium from simulated orthodontic appliances', *Am J Orthod*, 1983 **84** 156–159.
65 Kerosuo H, Moe G, Kleven E, 'In vitro release of nickel and chromium from different types of simulated orthodontic appliances', *Angle Orthod*, 1995 **65** 111–116.
66 Barrett R D, Bishara S E, Quinn J K, 'Biodegradation of orthodontic appliances. Part I. Biodegradation of nickel and chromium *in vitro*', *Am J Orthod Dentofacial Orthop*, 1993 **103** 8–14.
67 Bishara S E, Barrett R D, Selim M I, 'Biodegradation of orthodontic appliances. Part II. Changes in the blood level of nickel', *Am J Orthod Dentofacial Orthop*, 1993 **103** 115–119.
68 Ryhanen J, Niemi E, Serlo W, Niemela E, Sandvik P, Pernu H, Salo T, 'Biocompatibility of nickel–titanium shape memory metal and its corrosion behavior in human cell cultures' , *J Biomed Mater Res*, 1997 **35** 451–457.
69 Jia W, Beatty M W, Reinhardt R A, Petro T M, Cohen D M, Maze C R, Strom E A, Hoffman M, 'Nickel release from prthodontic arch wires and cellular immune response to various nickel concentrations', *J Biomed Mater Res*, 1999 **48** 488–495.
70 Endo K, Ohno H, 'Corrosion behavior of NiTi alloys in a physiological saline solution', in L'H Yahia ed., *Shape memory implants*, Springer, New York, 2000, 177–193.
71 Huang H-H, Chiu Y-H, Lee T-H, Wu S-C, Yang H-W, Su K-H, Hsu C-C, 'Ion release from NiTi orthodontic wires in artificial saliva with various acidities', *Biomaterials*, 2003 **24** 3585–3592.
72 Kaaber K, Veien N K, Tjell J C, 'Low nickel diet in the treatment of patients with chronic nickel dermatitis', *Br J Dermatol*, 1978 **98** 197–201.
73 Schroeder H A, Balassa J J, Tipton I H, 'Abnormal trace metals in man-nickel. *J Chronic Dis*, 1962 **15** 51–62.

74 Wever D J, Veldhuizen A G, deVries J, Busscher H J, Uges D R A, van Horn J R, 'Electrochemical and surface characterization of a nickel–titanium alloy' *Biomaterials*, 1998 **19** 761–769.
75 Kimura H, Sohmura T, 'Improvement in corrosion resistance of Ti–Ni shape memory alloy by oxide film coating', *Jpn J Dent Mater*, 1988 **7** 106–110.
76 Ozeki K, Yuhta T, Aoki H, Fukui Y, 'Inhibition of Ni release from NiTi alloy by hydroxyapatite, alumina, and titanium sputtered coatings' *Bio-Medical Mater Eng*, 2003 **13** 271–279.
77 Wood J F L, 'Patient sensitivity to alloy used in partial denture' , *Br Dent J*, 1974 **136** 423–424.
78 Menne T, Christophersen J, Green A, 'Epidemiology of nickel dermatitis', In: *Nickel and the skin: immunology and toxicology*. Maibach HI, Menne T editor. Boca Raton, FL, CRC Press 1989, pp. 109–116.
79 Romaguera C, Grimalt F, Vilaplana J, 'Contact dermatitis from nickel: an investigation of its source', *Contact Dermatitis*, 1988 **19** 52–57.
80 Meijer C, Bredberg M, Fisher T, Widstrom L, 'Ear piercing and nickel and cobalt sensitization, in 520 young Swedish men doing compulsory military service', *Contact Dermatitis*, 1995 **32** 147–179.
81 McKay G C, Macnair R, MacDonald C, Grant M H, 'Interactions of orthopaedic metals with an immortalized rat osteoblast cell line', *Biomaterials*, 1996 **17** 1339–1344.
82 Kerosuo H, Kullaa A. Kerosuo E, Kanerva L, Hensten-Petterson A, 'Nickel allergy in adolescents in relation to orthodontic treatment and piercing of ears', *Am J Orthod Dentofac Orthop*, 1996 **109** 148–154.
83 Berger-Gorbet M, Broxup B, Rivard C, Yahia L'H, 'Biocompatibility testing of NiTi screw using immuno histochemistry on sections containing metallic implants', *J Biomed Mater Res*, 1996 **32** 243–248.
84 Janson G R, Dainesi E A, Consolaro A, Woodside D G, deFreitas H R, 'Nickel hypersensitivity reaction before, during, and after orthodontic therapy', *Amer J Orthod Dentofac Orthop*, 1998 **113** 655–660.
85 Taira M, Toguchi M S, Hamada Y, Takahashi J, Itou R, Toyosawa S, Ijyuin N, Okazaki M, 'Studies on cytotoxic effect of nickel ions on three cultured fibroblasts' *J Mater Sci: Mater Med*, 2001 **12** 373–376.
86 Eliades H, Pratsinis H, Kletsas D, Eliades G, Makou M, 'Characterization and cytotoxicity of ion released from stainless steel and nickel–titanium orthodontic alloys*' Amer J Orthodont Dentfac Orthop*, 2004 **125** 24–29.
87 Assad M, Chernyshov A, Leroux M A, Rivard C-H, 'A new porous titanium–nickel alloy: Part 1. Cytotoxicity and genotoxicity evaluation', *Bio-Medical Mater Eng*, 2002 **12** 225–237.
88 Yeung K W K, Poon J W Y, Lie X Y, Ho J P Y, Chung C Y, Chu P K, Lu W W, Chan D, Cheung K M C, 'Investigation of nickel suppression and cytocompatibility of surface-treated nickel–titanium shape memory alloys by using plasma immersion ion implantation', *J Biomed Mater Res*, 2005 **72A** 238–245.
89 Filip P, Lausmaa J, Musialek J, Mazanec K, 'Structure and surface of NiTi human implants', *Biomaterials*, 2001 **22** 2131–2138.
90 Endo K, 'Chemical modification of metallic implant surfaces with biofunctional proteins (Part 1) molecular structure and biological activity of a modified NiTi alloy surface' *J Biomed Mater Res*, 1995 **14** 185–198.
91 Endo K, 'Chemical modification of metallic implant surfaces with biofunctional proteins (Part 2) corrosion resistance of a chemically modified NiTi alloy' *J Biomed Mater Res*, 1995 **14** 199–210.

92 Villermaux F, Tabrizian M, Yahia L'H, Czeremuszkin G, Piron D L, 'Corrosion resistance improvement of NiTi osteosynthesis stapes by plasma polymerized tetrafluroethylene coating', *Biomed Mater Eng*, 1996 **6** 241–254.
93 Ayers R A, Bateman T A, Simke S J, 'Porous NiTi as a materials for bone engineering' in L'H Yahia ed., *Shape Memory Implants*, Springer, New York, 2000, 73–88.
94 Oshida Y, Miyazaki S., 'Corrosion and biocompatibility of shape memory alloys', *Corr Eng*, 1991 **40** 1009–1025.
95 Castleman L S, Motzkin S M, 'Biocompatibility of nitinol'. In: *Biocompatibility of clinical implant materials*. Williams D F, editor. CRC Press. 1981, pp. 129–154.
96 Assad M, Lomardi S, Bernèche S, DesRosiers E A, Yahia L'H, Rivard C H, 'Cytotoxicity testing of the nickel titanium shape memory alloy', *Ann Chir,* 1994 **48** 731–736.
97 Armitage D A, Parker T L, Grant D M, 'Biocompatibility and hemocompatibility of surface-mosdified NiTi alloys', *J Biomed Mater Res*, 2003 **66A** 129–137.
98 Maurer A M, Merritt K, Brown S A, 'Cellular uptake of titanium and vanadium from addition of salts or fretting corrosion in vitro', *J Biomed Mater Res*, 1994 **28** 241–246.
99 Yang R S, Tsai K S, Liu S H, 'Titanium implants enhance pulmonary nitric oxide production and lung injury in rats exposed to endotoxin', *J Biomed Mater Res*, 2004 **69A** 561–566.
100 Tada H, Shibo O, Kuroshima K, Koyama M, Tsukamoto K, 'An improved colorimetric assay for interleukin-2', *Immunol Methods,* 1986 **93** 157–165.
101 Es-Souni M, Es-Souni M, Brandies H F, 'On the transformation behavior, mechanical properties and biocompatibility of two NiTi-based shape memory alloys: $NiTi_{42}$ and $NiTi_{42}Cu_7$', *Biomaterials*, 2001 **22** 2153–2161.
102 Assad M, Lemieux N, Rivard C H, Yahia L'H, 'Comparative *in vitro* biocompatibility of nickel–titanium, pure nickel, pure titanium, and stainless steel: genotoxicity and atomic absorption evaluation', *Bio-Medical Mater Eng*, 1999 **9** 1–12.
103 Curtright D E, Bashker S N, Perez B, Johnson R M, Cowan Jr G C M, 'Tissue reaction to nitinol wire alloy', *Oral Surg Oral Med Oral Pathol Oral Radiol Endodontics*, 1973 **35** 578–584.
104 Castleman L S, Motzkin S M, Alicandri S M, Bonawit V L, 'Biocompatibility of nitinol alloy as an implant material', *J Biomed Mater Res*, 1976 **10** 695–731.
105 Putters J L M, Kaulesar Sukul D M K S, deZeeuw G R, Bijima A, Besselink P A, 'Comparative cell culture effects of shape memory metal (Nitinol), nickel and titanium: a biocompatibility estimation', *Eur Surg Res*, 1992 **24** 378–382.
106 Sarkar N K, Redmond W, Schwaniger B, Goldberg A J, 'The chloride behaviour of four orthodontic wires' *J Oral Rehabil*, 1983 **10** 121–128.
107 Prymak O, Bogdanski D, Köller M, Esenwein SA, Muhr G, Beckmann F, Donath T, Assad M, Epple M, 'Morphological characterization and in vitro biocompatibility of a porous nickel–titanium alloy', *Biomaterials*, 2005 **26** 5801–5807.
108 Rhalmi S, Odin M, Assad M, Tabrizian M, Rivard C H, Yahia L'H, 'Hard, soft tissue and *in vitro* cell response to porous nickel–titanium: a biocompatibility evaluation' *Bio-Medical Mater Eng*, 1999 **9** 151–162.
109 Wranglén G. *An Introduction to corrosion and protection of metals*. New York: Chapman and Hill. 1985, pp. 85–87.
110 Van Black L H. *Elements of materials science and engineering*. Reading MA: Addison-Wesley Pub. 1989, pp. 509–511.
111 Garcia I, *Galvanic corrosion of dental implant materials*. Indiana University Master Degree Thesis. 2000.

112 Koh Il-W, *Effects of bacteria-induced corrosion on galvanic couples of commercially pure titanium with other dental alloys*. Indiana University Master Degree Thesis. 2003.
113 Fontana M G, Greene N D, *Corrosion engineering*. New York: McGraw-Hill Book Co. 1967, pp. 20–25 and pp. 330–338.
114 Tomashov N D, *Theory of corrosion and protection of metals*. New York: MacMillan Co. 1966, pp. 212–218.
115 Uhlig H H, Revie R W, *Corrosion and corrosion control*. New York: John Wiley & Sons. 1985, pp. 101–105.
116 Tiller A K, 'Aspects of microbial corrosion'. In: *Corrosion processes*. Parkins, RN, editor. London: Applied Science Pub. 1982, pp. 115–119.
117 Matasa C G, 'Stainless steels and direct-bonding brackets, III: Microbiological properties. *Inf Orthod Kierferorthop*, 1993 **25** 269–271.
118 Mansfeld F, Little B J, 'A technical review of electrochemically techniques applied to microbiologically influenced corrosion', *Corr Sci*, 1991 **32** 247–272.
119 Dexter S C, Duquette D J, Siebert O W, Videla H A, 'Use and limitations of electrochemical techniques for investigation microbiological corrosion', *Corrosion*, 1991 **47** 308–318.
120 Pope D H, Stoecker J G, 'Microbiologically influenced corrosion. *Proc. Industries Corrosion NACE*. 1986, p. 235.
121 Walsh D, Pope D, Danford M, Huff T, 'The effect of microstructure on microbiologically influenced corrosion', *JOM*, 1993 **45** 22–30.
122 Dexter S C, 'Microbiological effects'. In: R.Baboian ed. *Corrosion tests and standards: application and interpretation*. ASTM Manual Series MNL 20. 1995, pp. 419–429.
123 Gibbons R J, Cohen L, Hay D I, 'Strains of *Streptococcus mutans* and *Streptococcus sobrinus* attach to different pellicle receptors', *Infect Immun*, 1986 **52** 555–561.
124 An Y H, Friedman R J, 'Concise review of mechanisms of bacterial adhesion to biomaterial surfaces', *J Biomed Mater Res*, 1998 **43** 338–348.
125 Tsibouklis J, Stone M, Thorpe A A, Graham P, Peters V, Heerlien R, Smith J R, Green K L, Nevell T G, 'Preventing bacterial adhesion onto surfaces: the low-surface-energy approach', *Biomaterials*, 1999 **20** 1229–1235.
126 Little B J, Wagner P, 'Factors influencing the adhesion of microorganism to surfaces', *J Adhesion*, 1986 **20** 187–210.
127 Chang J-C, Oshida Y, Gregory R L, Andres C J, Barco T M, Brown D T, 'Electrochemical study on microbiology-related corrosion of metallic dental materials', *J Biomed Mater Eng*, 2003 **13** 281–295.
128 American Society for Testing and Materials, 'ASTM F86 Standard practice for surface preparation and making of metallic surgical implants', ASTM, Philadelphia PA, 1995, 6–8.
129 Kasemo B, 'Biocompatibility of titanium implants: surface science aspects', *J Pros Dent*, 1983 **49** 832–837.
130 Tomashov N D, *Theory of corrosion and protection of metals: The science of corrosion*. New York: The MacMillan Co., 1966, p. 144.
131 *CRC handbook of chemistry and physics*. The 47th edition. Cleveland: The Chemical Rubber Co., 1966, p. D–54.
132 *CRC handbook of chemistry and physics*. The 47th edition. Cleveland: The Chemical Rubber Co., 1966, p. D-27.
133 West J M, *Basic corrosion and oxidation*, 2nd ed. London: John Wiley and Sons. 1986, pp. 27–30.

134 Lautenschlager E P, Monaghan P, 'Titanium and titanium alloys as dental materials', *Int Dent J*, 1993 **43** 245–253.
135 *Oxidation of metals and alloys*. Ohio: American Society for Metals, 1971, p. 46.
136 Coddet C, Chaze A M, Beranger G, 'Measurements of the adhesion of thermal oxide films: application to the oxidation of titanium', *J Mater Sci*, 1987 **22** 2969–2974.
137 Trigwell S, Selvaduray G, 'Effects of surface finish on the corrosion of NiTi alloy for biomedical applications', in A. R. Pleton *et al.* (ed) *Shape memory and superelastic technologies*, Pacific Grove, San Francisco CA, 1997, 383–388.
138 Chan C M, Trigwell S, Duerig T, 'Oxidation of a NiTi alloy', *Surface Interface Anal*, 1990 **15** 349–354.
139 Oshida Y, Sachdeva R, Miyazaki S, 'Changes in contact angles as a function of time on some pre-oxidized biomaterials', *J Mater Sci: Mater Med*, 1992 **3** 306–312.
140 Oshida Y, Sachdeva R, Miyazaki S, Daly J, 'Effects of shot peening on surfaces contact angles of biomaterials', *J Mater Sci: Mater Med*, 1993 **4** 443–447.
141 Lausmaa J, Mattsson L, Rolander U, Kasemo B, 'Chemical composition and morphology of titanium surface oxides', *Materials Research Society Symposium Proceeding* Vol. 55, Materials Research Society, Pittsburgh PA, 1986, 351–359.
142 *Oxidation of Metals and Alloys*. Ohio: American Society for Metals, 1971, pp. 142–143.
143 Solar R J, 'Corrosion resistance of titanium surgical implant alloys: a review'. In: *Corrosion and degradation of implant materials*, ASTM STP 684. Syrett BD, editor. Philadelphia: American Society for Testing and Materials, 1979, pp. 259–273.
144 Uhlig H H, '*The corrosion handbook'*. New York: John Wiley & Sons, 1966, p. 20.
145 Fontana M G, Greene N D, *Corrosion engineering*. New York: McGraw-Hill Book, 1967, pp.319–321.
146 Wranglén G, *An introduction to corrosion and protection of metals*. London: Chapman and Hall, 1985, pp. 65–66.
147 Albrektsson T, Brånemark P I, Hansson H A, Kasemo B, Larsson K, Lundstroem I, McQueen D H, Skalak R, 'The interface zone of inorganic implants in vivo: titanium implants in bone', *Ann Biomed Eng*, 1983 **11** 1–27.
148 Lausmaa J, Kasemo B, Hansson S, 'Accelerated oxide growth on titanium implants during autoclaving caused by fluorine contamination', *Biomaterials*, 1985 **6** 23–27.
149 *CRC handbook of chemistry and physics*. The 47th edition. Cleveland: The Chemical Rubber Co., 1966, p. E–58.
150 Fraker A C, Ruff A W, 'Corrosion of titanium alloys in physiological solutions. In: *Titanium science and technology*, Vol. 4. New York: Plenum Press, 1973, pp. 2447–2457.
151 Trépenier C, Leung T K, Tabrizian M, Yahia L'H, Bienvenu J-G, Tanguay J-F, Piron D L, Bilodeau L, 'Preliminary investigation of the effects of surface treatments on the biological response to shape memory NiTi stents', *J Biomed Mater Res* 1999 **48** 165–171.
152 Ryhänen J, Kallioinen M, Tuukkanen J, Junila J, Niemela E, Sandvik P, Serlo W, '*In vivo* biocompatibility evaluation of nickel–titanium shape memory metal alloy: muscle and perineural tissue responses and encapsule membrane thickness', *J Biomed Mater Res*, 1998 **41** 481–488.
153 Sittig C, Textor M, Spencer N D, Wieland M, Vallotton P-H, 'Surface characterization of implant materials c.p. Ti, Ti–6Al–7Nb and Ti–6Al–4V with different pretreatments', *J Mater Sci: Mater Med*, 1999 **10** 35–46.
154 Mazhar A A, Heakal F.El-T, Gad-Allah A G, 'Anodic behavior of titanium in aqueous Media', *Corrosion*, 1988 **44** 705–710.

155 Metikoš-Hukoviæ M, Ceraj-Ceriæ M, 'Anodic oxidation of titanium: mechanism of non-stoichiometric oxide formation', *Surf Technol*, 1985 **24** 273–283.
156 Hanawa T, Asami K, Asaoka K, 'Repassivation of titanium and surface oxide film regenerated in stimulated bioliquid', *J Biomed Mater Res*, 1998 **40** 530–538.
157 Wever D J, Veldhuizen A G, Sanders M M, Schakenraas J M, van Horn J R, 'Cytpotoxic, allergic and genotoxic activity of a nickel–titanium alloy', *Biomaterials*, 1997 **18** 1115–1120.
158 Assad M, Yahia L'H, Rivard C H, Lemieux N, 'In vitro biocompatibility assessment of a nickel–titanium alloy using electron microscopy *in situ* end labeling (EM-ISEL)', *J Biomed Mater Res*, 1998 **44** 154–161.
159 Rondelli G, Vicentini B, 'Evaluation of electrochemical tests of the passive film stability of equiatomic Ni–Ti alloy also in presence of stress-induced martensite', *J Biomed Mater Res*, 1999 **51** 47–54.
160 Cissé O, Savadogo O, Wu M, Yahia L'H, 'Effect of surface treatment of NiTi alloy on its corrosion behavior in Hank's solution', *J Biomed Mater Res*, 2001 **61** 339–345.
161 Hunt N P, Cunningham S J, Golden C G, Sheriff M, 'An investigation into the effects of polishing on surface hardness and corrosion of orthodontic archwires', *Angle Orthodont* 1999 **69** 433–439.
162 Asami K, Chen S-C, Habazaki H, Hashimoto K, 'The surface characterization of titanium and titanium–nickel alloys in sulfuric acid', *Corrosion Sci*, 1993 **35** 43–49.
163 Hruska A R, Borelli P, 'Quality criteria for pure titanium casting, laboratory soldering, intraoral welding, and a device to aid in making uncontaminated castings', *J Prosthet Dent*, 1999 **66** 561–565.
164 Adachi M, Mackert J R Jr, Parry E E, Fairhurst C W, 'Oxide adherence and porcelain bonding to titanium and Ti–6Al–4V alloy', *J Dent Res*, 1990 **69** 1230–1235.
165 Kimura H, Horng C J, Okazaki M, Takahashi J, 'Oxidation effects on porcelain–titanium interface reactions and bond strength', *Dent Mater J*, 1990 **9** 91–99.
166 Hautaniemi JA, Herø H. Porcelain bonding on Ti: its dependence on surface roughness, firing and vacuum level. *Surf Interface Anal* 1993 **20** 421–436.
167 Atsü S, Berksun B, 'Bond strength of three porcelain to two forms of titanium using two firing atmospheres', *J Prosthet Dent*, 2000 **84** 567–574.
168 Oshida Y, Hashem A, 'Titanium–porcelain system. Part I: Oxidation kinetics of nitrided pure titanium, simulated to porcelain firing process', *J Biomed Mater Eng*, 1993 **3** 185–198.
169 Wang R R, Fung K K, 'Oxidation behavior of surface-modified titanium for titanium–ceramic restorations', *J Prosthet Dent*, 1997 **77** 423–434.
170 Wang R R, Welsch G, Monteiro O, 'Silicon nitride coating on titanium to enable titanium–ceramic bonding', *J Biomed Mater Res*, 1999 **46** 262–270.
171 Firstov G S, Vitchev R G, Kunmar H, Blanpain B, van Humbeeck J, 'Surface oxidation of NiTi shape memory alloy', *Biomaterials*, 2002 **23** 4863–4871.
172 Zeng C L, We W T, 'Corrosion of Ni–Ti alloys in the molten $(Li,K)_2CO_3$ eutectic mixture', *Corr Sci*, 2002 **44** 1–12.
173 Plant S D, Grant D M, Leach L, 'Behaviour of human endothelial cells on surface modified NiTi alloy', *Biomaterials*, 2005 **26** 5359–5367.
174 Meachim G, Williams D F, 'Changes in nonosseous tissue adjacent to titanium implants', *J Biomed Mater Res*, 1973 **7** 555–572.
175 Ferguson A B, Akahoshi Y, Laing P G, Hodge E S, 'Characteristics of trace ions released from embedded metal implants in the rabbit', *J Bone Joint Surg*, 1962 **44–A** 323–336.

176 Ducheyne P, Williams G, Martens M, Helsen J, 'In vivo metal-ion release from porous titanium–silver material', *J Biomed Mater Res*, 1984 **18** 293–308.
177 Sundgren J-E, Bodö P, Lundström I, 'Auger electron spectroscopic studies of the interface between human tissue and implants of titanium and stainless steel', *J Colloid Interf Sci*, 1986 **110** 9–20.
178 Ducheyne P, Healy K E, 'Surface spectroscopy of calcium phosphate ceramic and titanium implant materials'. In: *Surface characterization of biomaterials*. Ratner B D, editor. Amsterdam: Elsevier Science, 1988, pp. 175–192.
179 Albreksson T, Hansson H A, 'An ultrastructural characterization of the interface between bone and sputtered titanium or stainless-steel surfaces', *Biomaterials*, 1986 **7** 201–205.
180 Wyckoff R W G. *The Structure of Crystals*. New York: Chemical Catalog Co., 1931, p. 134, p. 239.
181 Tang H, Prasad K, Sanjinès R, Schmid P E, Lévy F, 'Electrical and optical properties of TiO_2 anatase thin films', *J Appl Phys*, 1994 **75** 2042–2047.
182 Douglass D L, van Landuyt J, 'The structure and morphology of oxide films during the initial stages of titanium oxidation', *Acta Met*, 1966 **14** 491–503.
183 Nakayama T, Oshida Y, 'Effects of surface working on the structure of oxide films by wet oxidation in austenitic stainless steels', *Trans Jpn Inst Metals*, 1971 **12** 214–217.
184 Mahla E M, Nielsen N A, 'A study of films isolated from passive stainless steels', *Trans Electrochem Soc*, 1948 **81** 913–916.
185 Nakayama T, Oshida Y, 'Identification of the initial oxide films on 18-8 stainless steel in high temperature water', *Corrosion*, 1968 **24** 336–337.
186 Lim Y J, Oshida Y, Andres C J, Barco M T, 'Surface characterization of variously treated titanium materials', *Int J Oral Maxillofac Implants*, 2002 **16** 333–342.
187 Gluszek J, Masalski J, Furman P, Nitsch K, 'Structural and electrcochemical examinations of PACVD TiO_2 films in Ringer solution', *Biomaterials*, 1997 **18** 789–794.
188 Liu X, Ding C, 'Plasma sprayed wollastonite/TiO_2 composite coatings on titanium alloys', *Biomaterials*, 2002 **23** 4065–4077.
189 Browne M, Gregson P J, 'Surface modification of titanium alloy implants', *Biomaterials* 1994 **15** 894–898.
190 Takemoto S, Yamamoto T, Tsuru K, Hayakawa S, Osaka A, Takashima S, 'Platelet adhesion on titanium oxide gels: effect of surface oxidation', *Biomaterials*, 2004 **25** 3845–3892.
191 Allen K W, Alsalim H S, 'Titanium and alloy surfaces for adhesive bonding', *J. Adhesion*, 1974 **6** 229–237.
192 Felske A, Plieth W J, 'Raman spectroscopy of titanium dioxide layers', *Electrochim Acta* 1989 **34** 75–77.
193 Matthews A, 'The crystallization of anatase and rutile from amorphous titanium dioxide under hydrothermal conditions', *Amer Min*, 1976 **61** 419–424.
194 Yahalom J, Zahavi J, 'Electrolytic breakdown crystallization of anodic oxide films on Al, Ta and Ti', *Electrochem Acta*, 1970 **15** 1429–1435.
195 Ohtsuka T, 'Structure of anodic oxide films on titanium', *Surf Sci*, 1998 **12** 799–804.
196 Liang B, Fujibayashi S, Neo M, Tamura J, Kim H-M, Uchida M, Kikubo T, Nakamura T, 'Histological and mechanical investigation of the bone-bonding ability of anodically oxidized titanium in rabbits', *Biomaterials*, 2003 **24** 4959–4966.
197 Koizumi T, Nakayama T, 'Structure of oxide films formed on Ti in boiling dilute H_2SO_4 and HCl', *Corros Sci*, 1968 **8** 195–199.

198 Oshida Y, *Bioscience and bioengineering of titanium materials*, Elsevier, UK, 2006, pp. 81–103.
199 Kodama A, Ikeda H, Nakase C, Masuda T, Kitahara K, Arai A, Onuma Y, Tanaka K, Hayashi K, Yamashita J, Aikawa Y, 'Electrochemical characterization of electronic states at NiTi alloy/aqueous solution interface', *J Corros Sci Eng*, 2005 **7** 23–31.
200 Hanawa T, 'Titanium and its oxide film: A substrate for formation of apatite'. In: *The bone–biomaterial interface*. Davies J E, editor Toronto: Univ. of Toronto Press, 1991, pp. 49–61.
201 Sutherland D S, Forshaw P D, Allen G C, Brown I T, Williams K R, 'Surface analysis of titanium implants', *Biomaterials*, 1993 **14** 893–899.
202 Lausmaa G J, Kasemo B, 'Surface spectroscopic characterization of titanium implant materials', *Appl Surf Sci*, 1990 **44** 133–146.
203 Kubaschewski O, Hopkins B E, *Oxidation of metals and alloys*. London: Butterworths, 1962, p. 24.
204 Healy K E, Ducheyne P, 'The mechanisms of passive dissolution of titanium in a model physiological environment', *J Biomed Mater Res*, 1992 **26** 319–338.
205 Tummler H, Thull R, *Model of the metal/tissue connection of implants made of titanium or tantalum. Biological and biochemical performance of biomaterials'*. The Netherlands: Elsevier, 1986, pp. 403–408.
206 Eliades T, 'Passive film growth on titanium alloys: physiochemical and biologic considerations', *Int J Oral Maxillofac Implant*, 1997 **12** 621–627.
207 Drath D B, Karnovsky M L, 'Superoxide production by phagocytic leukocytes', *J Exp Med*, 1975 **144** 257–261.
208 Root B K, Metcalf J A, 'H_2O_2 release from human granulocytes during phagocytosis: Relationship to superoxide anion formation and cellular catabolism of H_2O_2. Studies with normal and cytochalasin B-treated cells', *J Clin Invest*, 1977 **60** 1266–1279.
209 DeChatelet L R, 'Oxide bactericidal mechanisms of PMN', *J Infect Dis*, 1975 **131** 295–303.
210 O'Brien B, Carroll W M, Kelly M J, 'Passivation of nitinol wire for vascular implants – a demonstration of the benefits', *Biomaterials*, 2002 **23** 1739–1748.
211 Tengvall P, Elwing H, Sjöqvist L, Lundström I, 'Interaction between hydrogen peroxide and titanium: a possible role in the biocompatibility of titanium', *Biomaterials*, 1989 **10** 118–120.
212 Jacob H S, Craddock P R, Hammerschmidt D E, Moldow C F, 'Induced granulocyte aggregation – unsuspected mechanism of disease', *New Engl J Med*, 1980 **302** 789–794.
213 Del Masestro R F, 'An approach to free radicals in medicine and biology', *Acta Physiol Scand*, (Suppl) 1980 **492** 153–168.
214 Sundgren J-E, Bodö P, Lundström I, Berggren A, Hellem S, 'Auger electron spectroscopy studies of stainless-steel implants', *J Biomed Mater Res*, 1985 **19** 663–671.
215 Tengvall P, Bjursten L M, Elwing H, Lunström I, 'Free radicals oxidation of metal implants and biocompatibility', 2nd Int Conf Biointeractions '87. London 1987.
216 Jaeger C D, Bard A J, 'Spin-trapping and electron spin resonance detection of radical intermediates in the photodecompositions of water at TiO_2 particulate systems', *J Phys Chem*, 1979 **83** 3146–3151.
217 Barb W G, Baxendale J H, George P, Hargrave K R, 'Reactions of ferrous and ferric ions with hydrogen peroxide', *Trans Faraday Soc*, 1951 **47** 462–500.
218 Bielski B H J, 'Fast kinetic studies of dioxygen-derived species and their metal-complexes', *Phil Trans Roy Soc Lond B*, 1985 **311** 473–482.

219 Armstrong D, *Free Radicals in Molecular Biology, Aging and Disease*. New York: Raven Press. 1984.
220 Janzén E G, Wang Y Y, Shetty R W, 'Spin-trapping with α-(4-pyridyl-1-oxide)-N-tert-butylnitrone in aqueous solutions: a unique electron spin resonance spectrum for the hydroxyl radical adduct', *J Am Chem Soc*, 1978 **100** 2923–2925.
221 Tengvall P, Lundström I, Sjöqvist L, Elwing H, Bjursten L M, 'Titanium–hydrogen peroxide interaction: model studies of the influence of the inflammatory response on titanium implants', *Biomaterials*, 1989 **10** 166–175.
222 Pan J, Thierry D, Leygraf C, 'Electrochemical and XPS studies of titanium for biomaterial applications with respect to the effect of hydrogen peroxide', *J Biomed Mater Res*, 1994 **28** 113–122.
223 Bianchi G, Malaguzzi S, 'Cathodic reduction of oxygen and hydrogen peroxide on titanium'. *Proc. 1st Intl Congr Metallic Corrosion*, London, April 10–15, 1961, pp. 78–83.
224 Pan J, Thierry D, Leygraf C, 'Hydrogen peroxide toward enhanced oxide growth on titanium in PBS solution: Blue coloration and clinical relevance', *J Biomed Mater Res*, 1996 **30** 393–402.
225 Pan J, Liao H, Leygraf C, Thierry D, Li J , 'Variation of oxide films on titanium induced by osteoblast-like cell culture and the influence of an H_2O_2 pretreatment', *J Biomed Mater Res*, 1998 **40** 244–256.
226 Albrektsson T, 'The response of bone to titanium implants'. CRC *Crit Rev Bicompatibility.* 1984, **1** 53–84.
227 Bearinger J P, Orme C A, Gilbert J L, 'Effect of hydrogen peroxide on titanium surfaces: *In situ* imaging and step-polarization impedance spectroscopy of commercially pure titanium and titanium, 6-aluminum, 4-vanadium', *J Biomed Mater Res*, 2003 **67A** 702–712.
228 Moodey N R, Costa J E, 'Microstructure/property relationship in titanium alloys and titanium aluminides'. Kim Y W, Boyer R R, editors. Warrendale PA: TMS, 1991, pp. 587–604.
229 Tal-Gutelmacher E, Eliezer D, 'The hydrogen embrittlement of titanium-based alloys', *J Metals*, 2005 **57** 46–49.
230 Williams D N, Jaffee R I, 'Relationships between impact and low-strain-rate hydrogen embrittlement of titanium alloys', *J Less-Common Metals*, 1960 **2** 42–48.
231 Hardie D, Quyang S, 'Effect of hydrogen and strain rate upon the ductility of mill-annealed Ti6Al4V', *Corros Sci*, 1999 **41** 155–177.
232 Soloviоff G, Eliezer D, Desch P B, Schwarz R B, 'Hydrogen-induced cracking in an Al–Al_3Ti–Al_4C_3 alloy', *Scripta Metall Mater*, 1995 **33** 1315–1320.
233 Froes F H, Eliezer D, Nelson H G, 'Hydrogen effects in materials'. Thompson A W, Moody N R, editors. Warrendale PA: TMS, 1994, pp. 719–733.
234 Ogawa T, Yokoyama K, Asaoka K, Sakai J, 'Hydrogen absorption behavior of beta titanium alloy in acid fluoride solutions', *Biomaterials*, 2004 **25** 2419–2425.
235 Hirth J P, 'Effects of hydrogen on the properties of iron and steel', *Metall Trans A*, 1980 **11A** 861–890.
236 Yokoyama K, Kaneko K, Ogwa T, Moriyama K, Asaoka K, Sakai J, 'Hydrogen embrittlement of work-hardened Ni–Ti alloy in fluoride solutions', *Biomaterials*, 2005 **26** 101–108.
237 Paton N E, Williams L C, 'Effect of hydrogen on titanium and its alloys'. In: *Hydrogen in metals*. American Society for Metals, 1974, pp. 409–432.
238 Ebtehaj K, Hardie D, Parkins R N, 'The stress corrosion and pre-exposure embrittlement of titanium in methanolic solutions of hydrochloric acid', *Corros Sci*, 1985 **25** 415–429.

239 Hollis A C, Scully J C, 'The stress corrosion cracking and hydrogen embrittlement of titanium in methanol–hydrochloric acid solutions', *Corros Sci*, 1993 **34** 821–835.
240 Nakahigashi J, Tsuru K, Yoshimura H, 'Application of hydrogen-treated titanium alloy to dental prosthesis. – Experimental manufacture of crown by superplastic forming', *J Jpn Soc Dental Mater Devices*, 2005 **24** 291–295.
241 Gerard D A, Koss D A, 'The combined effect of stress state and grain size on hydrogen embrittlement of titanium', *Scripta Met Mater*, 1985 **19** 1521–1524.
242 Shih D S, Robertson I M, Birnbaum H K, 'Hydrogen embrittlement of α titanium: *In situ* TEM studies', *Acta Metall*, 1988 **36** 111–124.
243 Nelson H G, 'Hydrogen embrittlement of α titanium: *In situ* tem studies', *Met Trans*, 1973 **4** 364–367.
244 Young G A, Scully J R, 'Effects of hydrogen on the mechanical properties of a Ti–Mo–Nb–Al alloy', *Scripta Met Mater*, 1993 **28** 507–512.
245 Kolman D G, Scully J R, 'Effects of the environment on the initiation of crack growth', West Conshohocken PA: ASTM, 1997, pp. 61–73.
246 Costa J E, Williams J C, Thompson A W, 'The effect of hydrogen on mechanical properties in Ti–10V–2Fe–3Al', *Met Trans*, 1987 **A18** 1421–1430.
247 Hua F, Mon K, Pasupathi P, Gordon G, Scoesmith D, 'Modeling the hydrogen-induced cracking of titanium alloys in nuclear waste repository environments', *J Metals*, 2005 **57** 20–26.
248 Murai T, Ishikawa M, Miwa C, 'The absorption of hydrogen into titanium under cathodic polarization', *Corros Eng*, 1977 **26** 177–183.
249 Yokoyama K. Hamada K, Moriyama K, Asaoka K, 'Degradation and fracture of Ni–Ti superelastic wire in an oral cavity', *Biomaterials*, 2001 **22** 2257–2262.
250 Yokoyama K, Kaneko K, Moriyama K, Asaoka K, Sakai J, Nagumo M, 'Delayed fracture of Ni–Ti superelastic alloys in acidic and neutral fluoride solutions', *J Biomed Mater Res*, 2004 **69A** 105–113.
251 Yokoyama K, Kaneko K, Moriyama K, Asaoka K, Sakai J, Nagumo M, 'Hydrogen embrittlement of Ni–Ti superelastic alloy in fluoride solution', *J Biomed Mater Res*, 2003 **65A** 182–187.

7

Understanding, predicting and preventing failure of Ti–Ni shape memory alloys used in medical implants

K. GALL
Georgia Institute of Technology, USA

Abstract: In this chapter, the focus is on the mechanical fatigue of shape memory alloys intended for use in biomedical applications. Emphasis is placed on understanding the current state of knowledge regarding processing–structure–property relationships under cyclic loading. In addition, the major factors to consider when designing a Ti–Ni device for resistance to mechanical fatigue are discussed.

Key words: metal fatigue, stress/strain shape memory alloys, crack growth, microstructure, Ti–Ni, Ni–Ti, Nitinol.

7.1 Introduction

Shape memory alloys and traditional metallic materials used in biomedical implants are invariably subjected to mechanical loading during and after implantation. Responses of individual materials to mechanical loading can differ substantially depending on the application environment and mechanical properties of the material. In particular, the presence of the martensitic phase transformation in shape memory alloys can positively or negatively impact the mechanical 'life' of a shape memory alloy device relative to stainless-steel or titanium implants. For example, under strain-controlled low-cycle fatigue conditions, Ti–Ni shape memory alloys will easily outperform either titanium or stainless steel for equivalent applied strain levels. However, in stress-controlled high-cycle fatigue conditions, the fatigue life of Ti–Ni shape memory alloys can be less than that of traditional metallic implant materials, a factor that must be considered in low stress, high-cycle fatigue. In order to avoid mechanical failure of shape memory alloy implants it is of utmost importance to understand the mechanisms that control failure and quantitatively link failure modes to mechanical driving forces.

The overarching goal of this chapter is to provide a foundation to fundamentally understand, predict, and avoid the failure of shape memory alloys as biomedical implants. Although deformation, fracture, and fatigue studies have been performed on nearly all shape memory alloy compositions, this chapter will focus exclusively on research efforts in Ti–Ni (Nitinol) shape memory alloys, which

have the only proven history of use in biomedical applications and hold significant promise for future applications. In this chapter, we begin by reviewing *mechanically driven* failure modes in Ti–Ni shape memory alloys in section 7.2. Other chapters in this book deal with chemical and/or biological failure mechanisms. Following the overview, section 7.3 covers the plastic deformation and fracture of Ti–Ni with emphasis on understanding and avoiding monotonic failure and fast fracture. Subsequently, the cyclic loading and mechanical fatigue of Ti–Ni is discussed in section 7.4. After covering the overall driving forces and analysis tools for monotonic and cyclic failure, sections 7.5 and 7.6 focus on the inherent resistance of Ti–Ni to failure and how to tailor relevant material properties through processing and manufacturing. Finally, sections 7.7 and 7.8 give predictions of future trends and provide a summary of where to obtain more information on the mechanical failure of Ti–Ni shape memory alloys.

7.2 Overview of Ti–Ni mechanical failure modes

From a fundamental perspective, the failure 'modes' and driving forces for mechanical failure in Ti–Ni shape memory alloys are the same as in traditional metallic implant materials. These general failure modes can be divided into monotonic or cyclic failures. Monotonic failures are those driven by damage from a single, mechanical loading cycle, irrespective of prior loading history. Cyclic failures are those driven by multiple loading cycles resulting in damage accumulation as a function of cycling, and ultimately failure. Monotonic failure is typically the largest concern when initially implanting a shape memory alloy, for example, when a stent is self-expanding into a torturous artery, or a Ti–Ni bone staple is being pre-bent. In some instances, such as peripheral stenting, overload failure is a possibility *in vivo* since significant loads can be transmitted to the device from outside the body. Similarly, kink-resistant Ti–Ni guidewires, which are often used once and discarded, have potential for overload failure through local plasticity if the bend radius exceeds a critical value.

In addition to the possibility of monotonic failure, fatigue failure is a significant concern in nearly all Ti–Ni implants, a fact that is clear in recent cardiovascular stent data.[1–3] Depending on the intended use of the Nitinol implant,[4–9] the device and material may be required to withstand millions (typical for orthopedic implants) to hundreds of millions of cycles (typical for cardiovascular implants) in order to be considered safe and effective for regulatory clearance or approval. Fatigue failures in metals are typically separated into low-cycle and high-cycle regimes due to the fundamental difference in deformation mechanisms and analysis tools when the materials are repeatedly deformed at stresses above the yield stress (low-cycle fatigue) or below the yield stress (high-cycle fatigue).

The response of Ti–Ni to fatigue loading is similar to traditional materials below its critical transformation or initial 'yield' stress (high-cycle regime), although notable differences exist as will be presented herein. In the low-cycle regime, Ti–

Ni alloys demonstrate superior lives to traditional metallic materials, although they ultimately experience the same fate with cycling. Fatigue failure occurs through the progression of damage, specifically the nucleation and propagation of fatigue cracks that ultimately lead to fast fracture. As a consequence, fatigue of Ti–Ni can be analysed by either considering all of the stages in a lumped model (stress/strain life approaches) or individual stages in a more conservative approach (fracture mechanics-based approach); results of both approaches are reported in this chapter.

Depending on the operating conditions, other mechanical failure modes, such as fretting, wear, or combinations of wear and fatigue, can limit the life of a Ti–Ni implant. However, much less research has been performed on non-fatigue failure modes, since the operating conditions of current Ti–Ni biomedical implants do not subject the material to conditions of wear and fretting. However, it should be mentioned that researchers have measured the wear response of Ti–Ni, with positive results, and it may be a factor to consider in future device design. It is the responsibility of the product designer to ensure they have considered all relevant failure modes when assessing the safety and efficacy of a Ti–Ni medical device for implantation. Finally, aspects such as surface treatment, corrosion resistance, and biocompatibility have been extensively studied in Ti–Ni shape memory alloys, and the reader is recommended to refer to articles within this book or in published articles[10–29] for further understanding on these topics. During the design of a Nitinol device it is important to concurrently consider the effect of surface treatment on the biocompatibility and fatigue and fracture behaviour of the material, especially resistance to high-cycle fatigue, which depends strongly on surface quality.

7.3 Inelastic deformation and fracture

7.3.1 Stress–strain response

Before examining the fatigue and fracture of Ti–Ni shape memory alloys, it is essential to fully understand the stress–strain response of the material until failure. The key results of a recent review[30] of the tensile response of Ti–Ni shape memory alloys will be discussed here. Figure 7.1 presents a schematic of the tensile stress–strain response of a Ti–Ni shape memory alloy until fracture.[30] As shown in Fig. 7.1, the stress–strain response of Ti–Ni typically exhibits four distinguishable stages.[31,32] Stage I is typically attributed to elastic loading of either the austenite or martensite phase, depending on the testing temperature. Stage II is driven by inelastic deformation usually attributed to either martensite reorientation or a stress-induced austenite to martensite transformation, depending on the initial structure of the material. Stage III is often accredited to pure elastic deformation of martensite. Stage IV is usually attributed to plastic deformation of the martensite phase. Although the aforementioned Stage I–IV descriptions are convenient, and are often assumed in device design methodologies, they are oversimplifications of the complex tensile behavior of Ti–Ni shape memory alloys.[30] Moreover, it is well

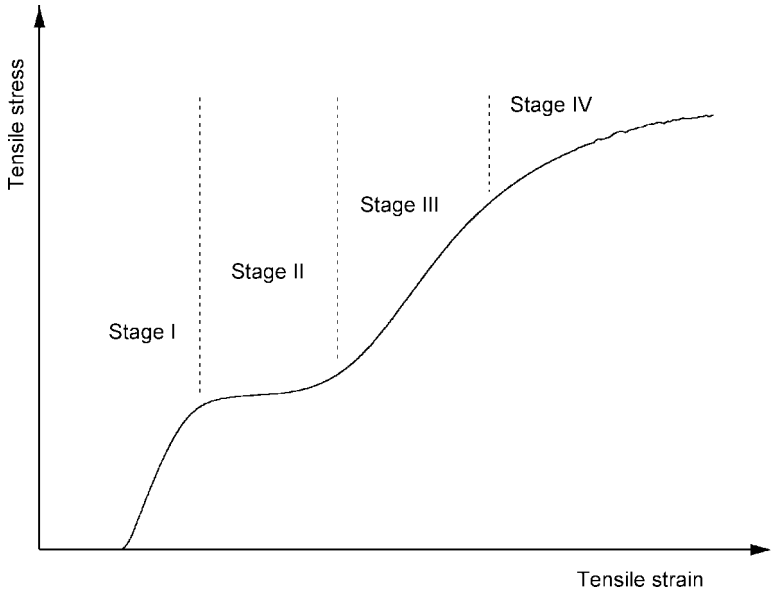

7.1 Schematic of the tensile stress–strain response of a Ti–Ni shape memory alloy up to fracture of the material. Adapted from Gall *et al.*[30]

known that the compressive response of Nitinol differs considerably from the tensile response, showing considerable differences in the magnitude of stress and strain in all four stages shown in Fig. 7.1. The asymmetry in tension and compression can be an important factor to consider in device design because it can influence the distribution of stresses, causing unexpected elevations in local compressive or tensile stress relative to predictions from symmetric stress analysis tools.

In some situations, it is appropriate to assume the behaviors outlined above for the four stages of deformation. However, such assumptions can sometimes lead to errors, especially when predicting the life and failure resistance of a Ti–Ni component using quantitative modeling. In reality, the four stages contain major components of the deformation mechanisms outlined above, but each stage typically contains contributions from multiple deformation mechanisms.[30] For example, stage III deformation is commonly assumed to be pure elastic deformation of the martensite, and that the slope of this curve is used as the martensite modulus. The slope of the tensile stress–strain response in Stage III is usually of the order of 20–40 GPa, a value often quoted in Ti–Ni handbooks or literature. Using various approaches, materials researchers have demonstrated that Stage III does not correspond to pure elastic deformation under tension and that the martensite modulus is several times greater than 40 GPa.[32–34] Indeed, very recent studies have shown that the end of the Stage II stress plateau does not mark the end of inelasticity, but rather the end of strain localization, with inelastic behavior

continuing well into stage III .[31,35–38] It is important to point out that many Ti–Ni-based biomedical devices are designed to utilize Stage II and/or III deformation in their storage and deployment. Another problem can be the austenite modulus, which is typically used as the slope of the Stage I stress–strain curve. Values for this modulus also vary considerably in the literature, and extreme caution should be used when employing a 'textbook' or 'handbook' value for the austenite modulus, as this modulus can vary with heat treatment or temperature due to non-elastic contributions to total strain at very low stress levels.[30] It is recommended that designers have the stress–strain curve of their exact material in hand before designing or using 'standard' material properties, especially in fatigue analysis where elastic modulus may be used to transcend between stress and strain values in life prediction. A more thorough review of the various stages and deformation mechanisms is provided by Gall *et al.*[30]

The tensile properties of Ti–Ni alloys are very important in the screening of Ti–Ni alloys for preliminary assessment of fatigue and fracture resistance. The Standard Test Method for Tension Testing of Nickel–Titanium Superelastic Materials[39] bases its characterization on the schematic in Fig. 7.1 with an intermittent unload at 6% strain before loading the sample to failure. Properties such as the upper and lower plateau strengths, the residual elongation, tensile strength, and uniform elongation can be calculated from the measured curves and then used for the purposes of quality control screening or predictive correlation to other failure properties. The monotonic mechanical properties of Ti–Ni vary considerably with heat treatment, composition, percent working, and product form (tube, wire, rod). Representative examples of properties for biomedical grade cold drawn Ti–Ni wire are tensile strengths of 900 to 1500 MPa and respective elongations 20 to 10% in a peak aged, pseudoelastic condition. Annealed product forms have lower tensile strengths in the range of 700 MPa and elongations in the 30% range. Target property values can vary considerably depending on the design requirements of the device, and product form required to meet geometrical and manufacturing specifications.

7.3.2 Fast fracture

Fast fracture occurs when a crack-like flaw, caused by, for example, manufacturing, prior overload, or fatigue crack growth, becomes unstable under applied load and causes mechanical failure of the material. The resistance to fast fracture in a material can be measured by fracture toughness, an important mechanical property that indicates a material's sensitivity to cracking and can be used to quantitatively predict a material's combined tolerance for crack size and applied loading. The fracture toughness of Ti–Ni materials in thin-walled tubular form has been recently measured to be in the range of 10 to 30 MPa $m^{½}$, depending on the crack size and orientation.[40] The steady state fracture toughness of the tubes was measured to be approximately 34 MPa $m^{½}$. It should be noted that these values do not represent the

typically measured 'plane strain fracture toughness', but they are the most reliable fracture toughness measurements on Ti–Ni in the literature. The fracture toughness of Ti–Ni is only slightly below other high-strength biomedical materials such as solution treated and aged Ti–6Al–4V alloys, which would have a typical strength of around 1200 MPa and a fracture toughness of around 40 MPa $m^{1/2}$. Considering their intermetallic B2 structure, Ti–Ni shape memory alloys have exceptional fracture toughness. Other B2 intermetallics, such as Al–Ni superalloys, have fracture toughness in the 4 to 8 MPa $m^{1/2}$ range.[41]

The resistance to fast fracture in Ti–Ni shape memory alloys is influenced by various factors, especially the stress-induced martensitic phase transformation, which provides a dissipative mechanism at ambient testing temperatures. Several researchers[42–44] have examined the effect of microstructure on the fracture of Ti–Ni shape memory alloys. Research on Ti–Ni single crystals[42] demonstrated that crystallographic orientation has a profound influence on the fracture behavior of Ti–Ni, with soft orientations such as [111] demonstrating considerable fracture resistance compared with hard orientations such as [100]. The single crystal results[42] are consistent with recent measurements,[40] revealing that specimen orientation in a textured polycrystalline tube has an influence on the initiation fracture toughness of Ti–Ni. Other work has used *in-situ* microscopy and modeling to examine and understand notch effects and microstructural fracture paths in Ti–Ni shape memory alloys.[43,44] This work supported the importance of the stress-induced martensitic transformation in providing the resistance to fast fracture of Ti–Ni, although considerable work is still needed to fully understand the effect of the phase transformation on fast fracture. Avoiding fast fracture is a matter of keeping the combinations of crack-like flaws (from manufacturing or due to fatigue crack growth) below a critical size governed by the fracture mechanics relationship and the measured fracture toughness of Nitinol. Even in the absence of 'pre-existing' flaws, it is advised to keep local maximum applied strains in Nitinol below 6–7% (near the end of the Stage II plateau) in safety critical applications where local fracture would result in sudden catastrophic failure of the device or drive rapid fatigue failure of the device. At local strains above 6–7%, stresses rise rapidly and local monotonic damage nucleates and grows, leading up to ultimate failure of the material.

7.4 Fatigue failure and life analysis

The mechanical fatigue of traditional metals is separated into low-cycle, high-stress fatigue and high-cycle, low-stress fatigue. The transition between the two regimes is often marked by the occurrence of sample yielding, when the maximum applied stress during cycling exceeds the yield stress of the material. The lifetime of samples cycled in the low- and high-cycle regimes typically differs by orders of magnitude and the fatigue mechanisms are considerably different in the two regimes. Ti–Ni shape memory alloys require a similar distinction between low-

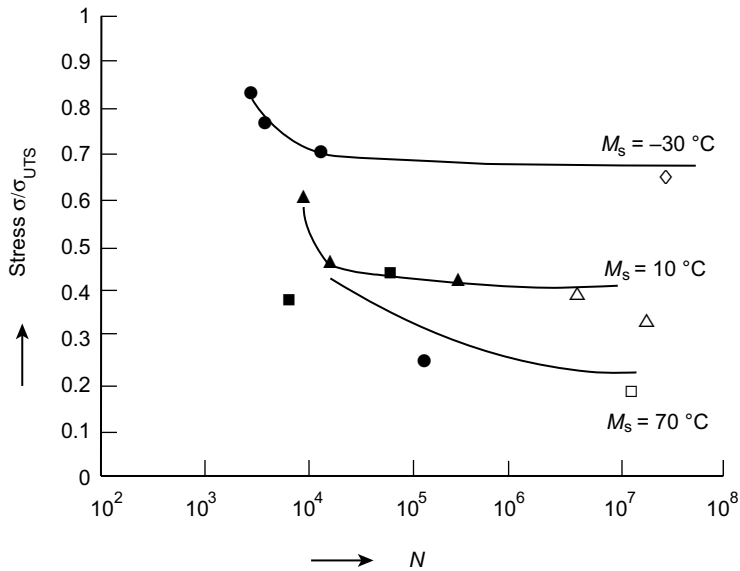

7.2 First comprehensive stress-life data published on Ti–Ni shape memory alloys. Adapted from Melton and Mercier.[45]

and high-cycle fatigue, especially in light of the widespread existence of the phase transformation at or above a critical stress level.

Melton and Mercier published the first comprehensive set of Ti–Ni fatigue data in 1979.[45] Their stress-life curves in this early work are reproduced in Fig. 7.2 for three Ti–Ni materials: (1) *M*s = –30 °C, σ_{UTS} = 600 MPa, (2) *M*s = 10 °C, σ_{UTS} = 700 MPa, (3) *M*s = 70 °C, σ_{UTS} = 700 MPa. The properties of the Ti–Ni alloys span pseudoelasiticy (*M*s = –30 °C) and shape memory (*M*s = 70 °C). The transition from low-cycle to high-cycle fatigue is evident in Fig. 7.2. Focusing on the pseudoelastic material, the stress-life curve experiences a sharp upturn between 10^3 and 10^4 cycles, corresponding to about 0.75 σ_{UTS} or 450 MPa, close to the critical transformation stress of the alloy. The 10^7 cycle endurance limit of the pseudoelastic alloy was quoted to be 400 MPa,[45] below the critical transformation stress. This early work was groundbreaking in studying the fatigue of Ti–Ni shape memory alloys, as it considered various materials, low-cycle fatigue, high-cycle fatigue, and also fatigue crack growth. One of the important findings of the work was that relative to ultimate tensile strength (which only varied a small amount between the various alloys) the pseudoelastic alloy had considerably better resistance to high-cycle fatigue relative to the shape memory materials. The primary drawback of this early work was the low strength of the Ti–Ni alloys, a σ_{UTS} of 600 MPa is considered very low compared with biomedical grade Ti–Ni, which has tensile strengths in the range of 1000 MPa.

Before examining more current fatigue studies on Ti–Ni, we will further discuss the low- and high-cycle distinction in Ti–Ni fatigue. Eggeler and Wagner[46,47]

introduced the terms 'structural fatigue' and 'functional fatigue' for the cyclic loading and degradation of Ti–Ni shape memory alloys. These terms are useful because they distinguish how fatigue mechanisms or parameters may differ depending on the targeted application. Structural fatigue implies the effect of cyclic loading on the 'load bearing life' of the Ti–Ni component when it is in use. Structural fatigue is similar to classical metal fatigue in the sense that fatigue life (number of cycles to failure) is the most important failure parameter and components would be often designed to have an 'infinite life' by assuring cyclic stresses/strain were kept below an endurance limit or other loading threshold. Functional fatigue implies degradation of recovery or 'functional' properties of Ti–Ni with cycling. For example, a Ti–Ni shape memory alloy that is repeatedly cycled through a strain recovery cycle will typically recover less total strain each cycle, and this degradation of recoverable strain would be considered functional fatigue. Although not always the case, structural fatigue is typically synonymous with high-cycle fatigue and functional fatigue is often synonymous with low-cycle fatigue, since in Ti–Ni, both low-cycle fatigue and functional fatigue require cycling through the phase transformation. It is important to note that many applications, such as a Ti–Ni cardiovascular stents, can experience both structural fatigue (the device must resist repeated contractions due to artery pulsation) and functional fatigue (the device may be required to experience multiple full deployments without accumulation of permanent strain during proof testing).

7.4.1 Low-cycle fatigue (functional fatigue)

Cycling Ti–Ni shape memory alloys repeatedly through their transformation results in relatively small numbers of cycles to failure in bulk samples. As such, low-cycle fatigue studies in Ti–Ni typically focus on changes in the functional properties of the alloy.[48–68] The observed behavior of Ti–Ni subjected to low-cycle fatigue loading is summarized in Fig. 7.3, although exceptions exist. During pure mechanical cycling of a pseudoelastic response, the critical transformation stress level, $\sigma_{critical}$, decreases, the transformation stress–strain slope increases, dissipated hysteresis energy, ΔW, decreases, and residual strains accumulate.[48] On the other hand, thermomechanical fatigue conditions exist during use of the pure shape memory effect. During thermomechanical cycling, an applied stress causes the accumulation of transformation strain along the direction of the applied stress.[55–58] This concept is demonstrated in Fig. 7.2 where the strain under the imposed stress is greater for cycle N versus cycle 1. Accumulation of plastic strain during thermomechanical cycling can also cause the shift of the zero strain level to a finite value, analogous to the pure mechanical response.

The responses in Fig. 7.3 are generalized, and researchers have discovered many external factors that influence the evolution in functional properties with cycling. The work of Lim and McDowell considered multiaxial loading states on pseudoelastic Ti–Ni[52,59] and demonstrated considerable path dependence on

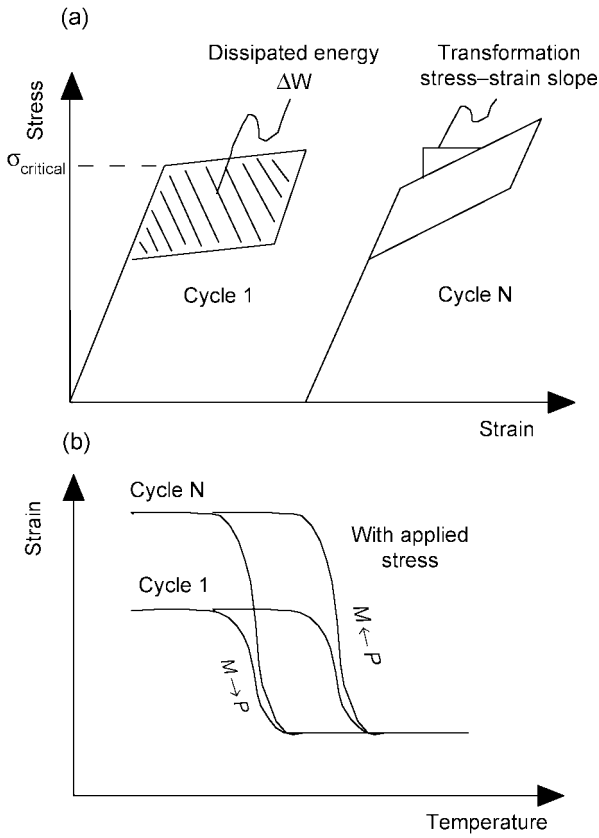

7.3 Schematic of (a) mechanical and (b) thermomechanical cyclic deformation of Ti–Ni shape memory alloys in the low-cycle, high-stress regime.

property evolution. Under tension–tension pseudoelastic loading researchers have shown that the generation and character of Luders band transformation fronts can change with cyclic loading.[63] Latent heating due to repeated transformation cycles at relatively high rate can also play a critical role in the evolution of properties, as higher temperatures can lead to increases in transformation stress levels and early fatigue failure. It is recommended that researchers conduct low-cycle functional fatigue tests representative of their application in the event that the materials will be subjected to repeated transformation cycles. Quantification of the evolution of functional properties will provide designers with the information necessary to account for changes in, for example, recoverable strain (accumulation of permanent device deformation) and changes in the critical transformation stress level (loss of actuation force) with cycling.

Along this vein, considerable research has been performed on the rotating

bending fatigue of Ti–Ni wires driven by dental drill applications.[69–75] The objective of the majority of these studies is to understand how the life of the rotating drill depends on various factors such as rotation speed, environment, temperature, and material properties. Although cycled in the low-cycle regime, the 'functional' properties of the drill are typically not studied, since loss of function is typically not imparted until complete fracture. Early work[71–73] demonstrated that atmosphere had a negligible effect on fatigue life (water versus air) and increased temperature (either applied or through latent heating) decreased fatigue life. It is important to note that this early work also determined that fatigue life was only shorter in air when latent heating was not kept under control. More recent work[75] has studied a broader range of strain ranges, confirmed validity of a Coffin–Manson approach to strain life, and also demonstrated the importance of the volume of material exposed to cyclic conditions, in line with fatigue philosophies on classical materials. The adherence to a Coffin–Manson relation renders strain life modeling a useful predictive tool for the life of Ti–Ni implants subjected to low-cycle fatigue conditions.

7.4.2 High-cycle fatigue (structural fatigue)

The commercialization of Nitinol cardiovascular stents has driven recent work on the high-cycle fatigue of Ti–Ni. While early work was restricted to rotating bending tests on Ti–Ni wires, recent studies have considered miniature specimens laser cut from thin-walled Ti–Ni tubes to mimic stent production processes and realistic material volumes.[76,77] The most common approach to quantifying and predicting the high-cycle fatigue resistance of Ti–Ni is the strain-life approach. Figure 7.4 provides a compilation of strain-life fatigue data from various researchers in academia and industry.[45,76–77] For reference, the average strain-life curve for various high-strength Ti alloys is also included in Fig. 7.4.[78] Of course, the strain life of specific titanium alloys will vary from this average depending on processing, surface finish, and material structure.

In the low-cycle regime ($N_f < 10^4$), Fig. 7.4 highlights the superior fatigue resistance of Ti–Ni compared with a conventional metal (Ti) as discussed in the previous section of this chapter. The representative Ti–Ni data from the literature lies above the average line for Ti alloys with some of the materials demonstrating a low-cycle fatigue life almost two orders of magnitude greater than the Ti average at an equivalent applied strain level. In the high-cycle fatigue regime, the Ti–Ni data is scattered and essentially similar to Ti on a strain-life basis. Since the modulus of Ti is higher than that of Ti–Ni, the 'endurance limit' or stress at 10^6 cycles to failure would be higher in Ti compared with Ti–Ni for an equivalent strain amplitude. Some of the Ti–Ni strain-life fatigue data shows long life for strain amplitudes aproaching 1% for small wires[45] and miniature laser cut samples.[77] Based on the amount of high-cycle fatigue data on Ti–Ni (Fig. 7.4), more work is needed to understand the fatigue resistance of Ti–Ni as a function of material structure and surface finish.

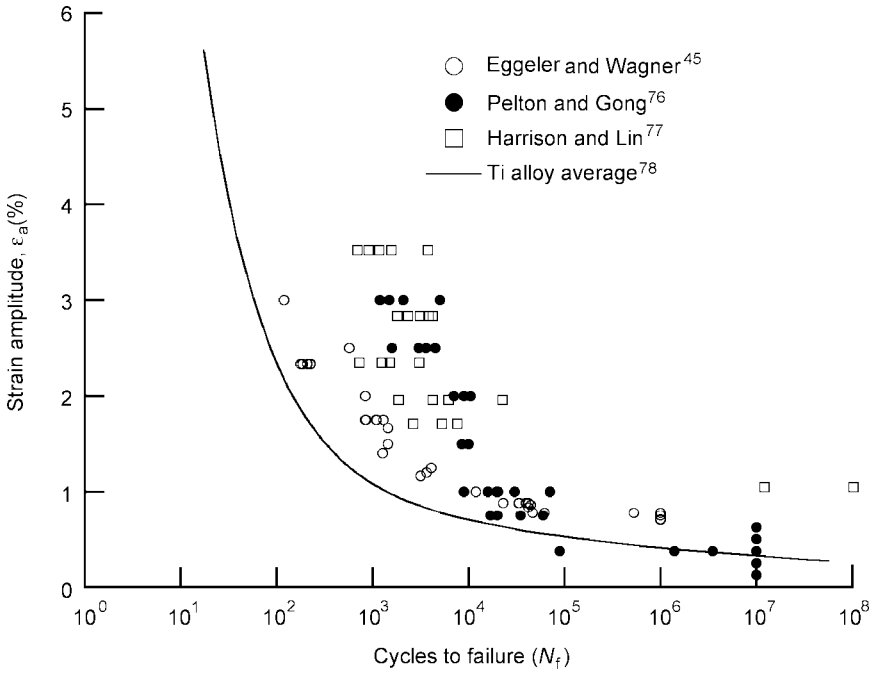

7.4 Compilation of representative strain-life fatigue data from the literature.

The data in Fig. 7.4 demonstrate that Ti–Ni provides a clear advantage over Ti alloys in terms of strain capacity, hence 'device flexibility', for large applied strains and cycle numbers below 10^4. However, caution should be exercised when comparing the strain capacity and fatigue life of Ti–Ni and Ti (or any conventional alloy for that matter) in the high-cycle regime (greater than 10^5 cycles). The data in Fig. 7.4 does not conclusively demonstrate that Ti–Ni will provide a long-term life advantage over Ti alloys at equivalent local strain levels (comparison based on stress level would be different based on the distinct modulus of the two materials). The relative benefit of Ti–Ni over Ti in the high-cycle regime will be very dependent on the specific structure and properties of the two materials, and exhaustive testing would be needed to ultimately compare the life of the two materials for their intended application. At present, Ti–Ni biomedical devices, such as stents, are designed such that high-frequency, low-amplitude strains are kept locally well below 1% (typically below 0.5%) to assure device life in the range of hundreds of millions of cycles. This 'safe' cyclic strain amplitude for avoiding high-cycle fatigue of Ti–Ni will probably vary according to device function and material structure.

The aforementioned results pertain to a standard loading ratio, R, of $R = \sigma_{min}/\sigma_{max} = -1$. An interesting phenomenon in Ti–Ni occurs as the R ratio is increased,

mirroring an increase in the applied mean strain or stress. Traditional metals demonstrate a decrease in fatigue life at equivalent strain amplitude with increasing mean stress, a phenomenon accounted for in fatigue life prediction through a Goodman diagram. On the other hand, several researchers have demonstrated that Ti–Ni alloys demonstrate increasing fatigue life for equivalent strain amplitude and increasing mean strain.[61,62,76] The origin of the 'anomalous' mean strain effect in Ti–Ni is still a topic of debate. However, it is clear that the relative fatigue resistance of the martensite and austenite phases plays a role in the mean strain effect, since the relative fraction of the two phases changes with increasing mean strain. Further work is needed to fully quantify and understand the effect of mean strains and stresses on the high-cycle fatigue of Ti–Ni.

7.4.3 Fatigue crack growth and fracture mechanics based approach

Fatigue failures in the aerospace industry spawned an alternative approach to understanding and predicting fatigue denoted by the fracture-mechanics based approach (also referred to as the damage tolerant approach). Essentially, the damage tolerant approach uses (1) a distinct set of material properties (fatigue crack growth data and fracture toughness), (2) information on an initial 'flaw' or 'crack' size, and (3) fracture mechanics solutions linking applied stress, component geometry, and crack size to provide a conservative prediction of fatigue life. Predictions from the fracture mechanics based approach are conservative since they do not traditionally consider the fraction of fatigue life spent nucleating fatigue cracks, although nucleation life can be captured with appropriate modifications.[82] In addition, information on fatigue crack growth thresholds can be used to gain first-order estimates of the endurance limit of a material if one assumes that small cracks behave similarly to large cracks. In reality, small cracks tend to grow faster than large cracks at equivalent applied stress intensity ranges, thus approximations of endurance limits based on fatigue crack growth thresholds tend not to be conservative.

The fracture mechanic-based approach has been traditionally used in structures when coupled with a capacity for crack detection and component removal. However, Ritchie and co-workers have studied and discussed the applicability of a fracture mechanics approach to biomedical implants,[83] in particular Ti–Ni.[40,79,80] The advantages include a conservative tool for life prediction that has the capacity to quantitatively link manufacturing and surface quality (through assumed initial flaw size) to final component life. Early work on fatigue crack growth studied the effect of temperature (hence material phase) on fatigue crack growth rates and thresholds.[80] It was discovered that fatigue crack growth resistance was highest in the pure martensite phase (tested at low temperature) and relatively lower in the austenite phase (tested at high temperature) for the same alloy.[80] More recent fatigue crack growth work has focused on the effects of environment, specimen

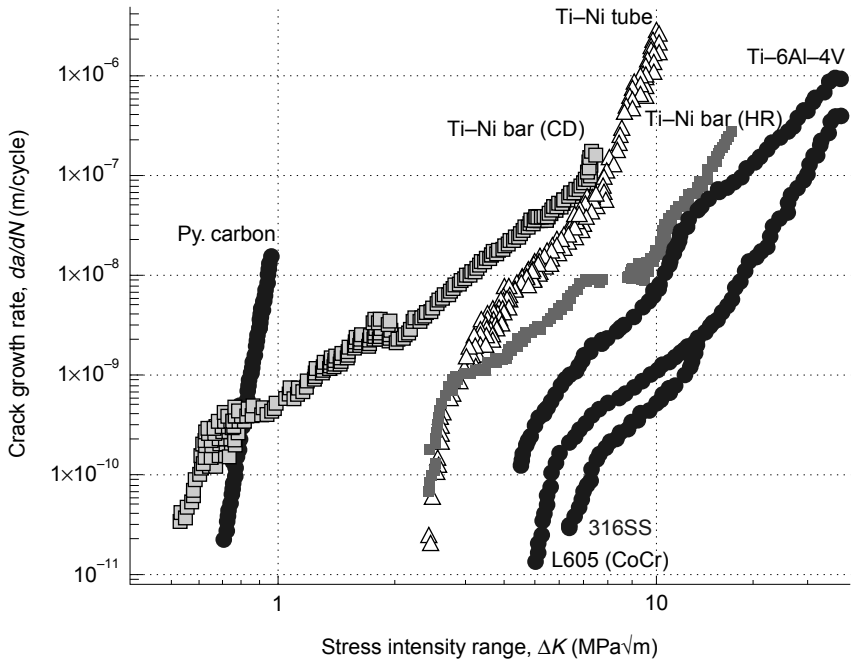

7.5 Comparison of fatigue crack growth data on various Ti–Ni product forms and other biomedical materials. Adapted from Gall *et al.*[84]

orientation, load ratio, and testing frequency on fatigue crack growth behavior.[40] Owing to the strong texture in Ti–Ni, specimen orientation was found to influence fatigue crack growth resistance.[40] In addition, increased load ratio resulted in increased crack growth rates and decreased fatigue crack growth thresholds. Finally, environment (air versus Hanks' balanced saline solution) and cycling rate (1 versus 50 Hz) were found to have a negligible effect on fatigue crack growth rates or thresholds.[40] This finding is of utmost important in terms of justifying accelerated testing of Ti–Ni components at frequencies well above physiological cycling rates.

Very recent work has examined fatigue crack growth in Ti–Ni barstock as a function of heat treatment and processing route (hot rolled versus hot rolled and cold drawn) and compared it with prior work on Ti–Ni tubes and other biomedical materials.[84] Figure 7.5 is a summary of fatigue crack growth results on Ti–Ni tubes (stents) and Ti–Ni barstock (hot rolled versus cold drawn). The hot rolled bar and cold drawn Ti–Ni tube had similar fatigue crack growth curves at low cyclic amplitudes, with the hot rolled bar demonstrating increased crack growth resistance at larger crack tip driving forces (higher delta K). The cold drawn (25 mm) barstock demonstrated extremely low fatigue crack growth threshold and relatively poor resistance to fatigue crack growth, an effect attributed to residual stresses in the large diameter bar.[84] The data in Fig. 7.5 also draws comparison with

other common biomedical grade alloys such as 316 stainless, Ti–6Al–4V, and CoCr, all of which have a long history of use in biomedical applications. In general, Ti–Ni alloys demonstrate lower resistance to fatigue crack growth compared with the traditional biomedical alloys. The difference in fatigue crack growth resistance implies that for equivalent flaw size, Ti–Ni devices would have to be designed to experience lower stresses to achieve infinite life, consistent with the lower 'endurance limit' of Ti–Ni compared with Ti discussed previously.

7.5 Influence of processing and material structure on material failure

A tremendous amount of work has been performed on the relationship between material structure and the monotonic mechanical properties of Ti–Ni. It would be impossible to review this immense body of literature in a single book chapter and the other chapters in this book provide sufficient introduction to the metallurgy and monotonic mechanical properties of Ti–Ni shape memory alloys. The general approach to strengthening Ti–Ni is very much different from traditional metallic alloys. The only subtle, but important, difference is that heat treatments and deformation processing conditions that alter material strength can also alter transformation properties and it is critical to understand the variation in both properties before a material can qualify as a biomedical device. The ASTM standard tensile test for Ti–Ni[39] is aimed at understanding both variation in transformation properties and ultimate strength properties, thus is an ideal tool for studying the effects of material processing on monotonic mechanical properties.

The key to developing Ti–Ni such that it undergoes the transformation with minimal risk of inelastic (non-recoverable) strain or fracture is by promoting the martensitic transformation at sufficiently low stresses and mitigating dislocation motion through matrix strengthening. Nitinol alloys are typically strengthened by three different approaches (1) grain size strengthening, (2) precipitation hardening, or (3) strain hardening. In fact, in the early years, many researchers believed that as-cast Ti–Ni did not demonstrate shape memory properties due to insufficient material strength. However, if one uses precipitation hardening to strengthen cast Ti–Ni, it demonstrates excellent shape recovery properties even with mm sized grains.[85] Wire and thin-walled tube Nitinol alloys used in medical devices are traditionally strengthened by all three mechanisms above. The grain size strengthening and strain hardening comes from the 20–50% reductions experienced by the material during the wire or tube forming operation. The precipitation hardening component is driven by the precipitation of Ti_3Ni_4 particles in Ni-rich commercial alloys (often Ti–50.8at%Ni materials). Although classical work on strengthening of Ti–Ni has focused on wire and tube, recent work has considered processing-structure relationships in Ti–Ni barstock[86] that has both medical and civil engineering applications.[87,88]

The effect of material structure on the fatigue of Ti–Ni has received consider-

ably less attention than the monotonic properties. Very early work demonstrated a strong influence of Ti–Ni microstructure on fatigue properties.[45,48] It was demonstrated that precipitation hardening and deformation processing could lead to improvements in the functional fatigue properties of Ti–Ni during pseudoelastic cycling.[48] Subsequent researchers verified preliminary findings and also sought to tailor thermomechanical treatments to optimize the fatigue resistance of various Ti–Ni alloys.[46,67,68,89–94] Although it is well accepted that thermomechanical treatments can be used to improve the fatigue resistance of Ti–Ni alloys, there is not a universal understanding of how these treatments apply across all product forms (e.g. Ti–Ni wire, tube, and bar stock). In particular, recent work[84] has demonstrated that selecting heat treatments for Ti–Ni bars based on prior knowledge of Ti–Ni wire, or selected monotonic mechanical properties, can lead to non-optimized fatigue resistance. Future work is expected in relating the complex structure and transformation behavior of Ti–Ni to both low-cycle and high-cycle fatigue properties across multiple product forms and material structures. Without such knowledge, it is important for designers to either (1) obtain fatigue properties on their specific Nitinol material as a function of heat treatment and surface condition or (2) compare fatigue data at the selected heat treatment to existing data in the literature to assure adequate fatigue resistance. It is not advised to use 'textbook' properties for fatigue life predictions of new Ti–Ni devices due to the relative uncertainty in such properties across material composition, heat treatment, deformation processing, manufacturing, and surface treatment.

7.6 Influence of manufacturing and surface finish on material failure

The surface treatment of Nitinol has been extensively studied in regard to the material's corrosion resistance and biocompatibility.[10–29] With the exception of a few studies on endodontic instruments, minimal published work exists on the effect of surface finish on the high-cycle fatigue of Ti–Ni alloys. Much of the work performed in this area has been done in industry with optimized treatments becoming unpublished trade secrets, especially in cardiovascular stenting. Similarly to conventional metals, surface finish can be a significant factor in the resistance of Ti–Ni to high-cycle fatigue. Rough, defected surfaces provide sources for rapid fatigue crack nucleation and significantly decreased high-cycle fatigue life. Provided the material contains an inclusion or porosity distribution under the maximum surface flaw size, fatigue cracks will almost always nucleate at Nitinol surfaces. Given a sufficiently polished surface finish, fatigue cracks will start at large near surface inclusions, similarly to conventional metals.

Given the absence of quantitative data on the effects of manufacturing and surface finish on the fatigue resistance of Nitinol, the reader is advised to use the surface treatment approaches[10–29] coupled with conventional wisdom regarding the effect of surface finish on metal fatigue abundant in the scientific literature. To

manage fatigue crack nucleation, surfaces must have, for example, low roughness, controlled residual stresses, and a uniform, stable oxide layer. The latter point is especially important in Nitinol since the oxide must be thin enough to remain stable under large strain deformation but thick enough to protect the Ti–Ni from corrosion. A thick, non-uniform oxide can potentially create sites for fatigue crack nucleation and lower fatigue life, especially if the oxide fractures in high strain loading during device preloading, packaging, or deployment.

One distinct advantage of the fracture mechanics-based approach, which employs fatigue crack growth data and an initial flaw size, is that it can quantitatively (conservatively) link expected fatigue life to the worse case scenario surface flaw size by assuming a crack-like surface flaw.[40,79,80] The fracture mechanics methodology thus enables assessment of the extent to which it is necessary to refine surface finish and avoid imperfections to maintain superior fatigue resistance. Of course, if inclusions exist in the Nitinol, it is necessary to consider these imperfections as crack-like flaws in case they are large enough to be a life-limiting imperfection rather than a surface flaw.

7.7 Summary and future trends

Researchers have been studying the deformation, fatigue, and fracture of Ti–Ni shape memory alloys for nearly four decades. Until the past decade, prior work focused mostly on the monotonic deformation of Ti–Ni shape memory alloys. The recent surge of innovative biomedical applications around the world, coupled with strict requirements for proving safety and efficacy of medical devices, has resulted in a push to practically and fundamentally understand the fatigue and fracture of Ti–Ni.

The deformation of Ti–Ni is highly non-linear, dependent on temperature, and difficult to implement in constitutive model-based design tools such as the finite element method. However, it is essential to emphasize the importance of using advanced design tools in Nitinol biomedical device design. Failure to do so can lead to inaccurate stress and strain prediction, local damage, and ultimately device failure *in vivo*. From a monotonic deformation standpoint, it is important to maximize the martensite yield strength (transition to Stage IV deformation) and keep local strains below approximately 6–7% to avoid monotonic overload. At present, materials scientists and design engineers have a reasonable understanding of how to optimize the monotonic mechanical properties of Nitinol through processing and also how to tailor the geometry of a biomedical device to avoid monotonic failure.

The fracture, and particularly the fatigue, of Nitinol are relatively less understood, even though fatigue is the life-limiting behavior of Nitinol medical devices, and approval or clearance of medical devices depends on adequate fatigue resistance. The low-cycle fatigue of Ti–Ni can be predicted using a Coffin–Manson law, and the number of cycles to failure is typically larger than other biomedical metals

deformed at equivalent applied strain amplitudes in the low-cycle regime. In the high-cycle regime, the fatigue resistance of current Ti–Ni materials is basically similar to Ti alloys based on a strain life approach. The last point is important because it implies that Nitinol's inherent 'flex' and 'transformation-induced compliance' can only be used in the low-cycle regime (up to 10s of thousands of cycles). Exceptions to this paradigm may exist in newer Nitinol materials or in very small Nitinol elements (like thin films) where the transformation may be employed well past 10 000 cycles and provide long life. Given the higher modulus of Ti versus Ti–Ni, and the comparable strain life curves in the high cycle regime, the 'endurance limit' of Ti–Ni can be lower relative to Ti, a factor that should be considered in biomedical device design. Depending on processing method and material structure, the fatigue-crack growth resistance of Nitinol spans extremely poor to strong. At present, Ti–Ni biomedical devices are not designed using fatigue crack growth data in a damage tolerant framework, although this conservative design approach is highly recommended for fatigue failure critical applications.

It is the opinion of the present author that future research on Nitinol should focus on better understanding the link between fatigue and fracture properties and material structure driven by processing conditions. Except for the recent work of Ritchie and Robertson,[40] at present there is a large disconnect between practical fatigue studies on Nitinol thin-walled tubes used for cardiovascular stent applications and fundamental fatigue studies on Ti–Ni bars or wires. The gap is driven by (1) the difficulty of fatigue testing of thin-walled tubes and (2) difficulty in assessing the microstructure of thin-walled tubes. Researchers doing basic science find it more convenient to perform work on Nitinol bars or wires, and researchers doing applied work on thin-walled stent tubes are uncertain of how existing basic work extends to tubes because of expected differences in texture, grain size, dislocation density, precipitate structure, and surface finish. Bridging this gap depends on careful structural *and* fatigue characterization of various Nitinol product forms, and uncovering of the fundamental microstructural factors providing fatigue failure resistance. Such research should provide fundamental information that can be used to improve the fatigue resistance of current Nitinol materials and also motivate the development of new, fatigue-resistant, Ti–Ni alloys.

7.8 Sources of further information and advice

The information in this chapter aims to provide a general overview of the mechanical deformation, fatigue, and fracture of Ti–Ni shape memory alloys intended for use in biomedical applications. The reader is encouraged to dig deeper into the papers referenced herein for further information on specific topics, as it is impossible to cover the depth provided in such papers in this overview. In addition, in the past few decades there have been numerous conferences focused on the basic science and technology of martensitic transformations and shape memory alloys. The reader will find an exhaustive body of work on Ti–Ni shape memory alloys in

the proceedings of these conferences, sometimes published as journal special issues. The International Conference on Martensitic Transformations (ICOMAT) is the largest and considered the top venue for fundamental work on martensitic transformations. Papers from ICOMAT are typically published as a proceedings set in *Journal De Physique IV*. The European Symposium on Martensitic Transformations and shape memory (ESOMAT) is another excellent conference with a recent focus on shape memory alloys. Proceedings from ESOMAT vary, but recent proceedings include a special issue in *Materials Science and Engineering A*, 2004, volume 378, issues 1–2, an excellent resource on the state of the art in shape memory alloys. The conference most relevant to this chapter, especially fatigue resistance, is the Shape Memory and Superelastic Technologies (SMST) conference, which has recently joined with ASM International. Proceedings from SMST contain a wealth of information on Ti–Ni shape memory alloys, emphasizing practical applications and fundamental research primarily related to biomedical applications. The SMST conference is targeted towards researchers from industry who use Ti–Ni shape memory alloys, however, it also has sufficient scientific focus in some areas to appeal to academic researchers.

7.9 References

1 Riepe G, Heintz C, Kaiser E, Chakfe N, Morlock M, Delling M, Imig H. What can we learn from explanted endovascular devices? *Eur. J. Vasc. Endovasc. Surg.* 2002; **24**(2): 117–122.

2 Jacobs T S, Won J, Gravereaux E C, Faries P L, Morrissey N, Teodorescu V J, Hollier H L, Marin M L. Mechanical failure of prosthetic human implants: A 10-year experience with aortic stent graft devices. *J. Vasc. Surg.* 2003; **37**(1): 16–26.

3 Allie D E, Hebert C J, Walker C M. NitiNOL stent fracture in the SFA. *Endovasc. Today*. 2004; July/August: 22–34.

4 Shabalovskaya S A. On the nature of the biocompatibility and on medical applications of NiTi shape memory and superelastic alloys. *Bio-Med. Mat. Eng*. 1996; **6**: 267–289.

5 Brailovski V, Trochu F. Review of shape memory alloys medical applications in Russia. *Bio-Med. Mat. Eng*. 1996; **6**: 291–298.

6 Dai K R, Chu Y Y. Studies and applications of NiTi shape memory alloys in the medical field in China. *Bio-Med. Mat. Eng*. 1996; **6**: 233–240.

7 Duerig T W, Pelton A R, Stockel D. The utility of superelasticity in medicine. *Bio-Med. Mat. Eng*. 1996; **6**: 255–266.

8 Morgan N B. Medical shape memory alloy applications – the market and its products. *Mat. Sci. and Eng. A*. 2004; **378**: 16–23

9 El Feninat F, Laroche G, Fiset M, Mantovani D. Shape memory materials for biomedical applications. *Adv. Eng. Mater*. 2002; **4**: 91–104.

10 Thierry B, Tabrizian M, Trepanier C, Savadogo O, Yahia L H. Effect of surface treatment and sterilization processes on the corrosion behavior of NiTi shape memory alloy. *J. Biomed. Mater. Res*. 2000; **51**(4): 685–693.

11 Shih C C, Lin S J, Chung K H, Chen Y L, Su Y Y. Increased corrosion resistance of stent materials by converting current surface film of polycrystalline oxide into amorphous oxide. *J. Biomed. Mater. Res*. 2000; **52**(2): 323–332.

12 Shih C C, Lin S J, Chen Y L, Su Y Y, Lai S T, Wu G J, Kwok C F, Chung K H. The cytotoxicity of corrosion products of nitinol stent wire on cultured smooth muscle cells. *J. Biomed. Mater. Res*. 2000; **52**(2): 395–403.
13 Cisse O, Savadogo O, Wu M, Yahia L. Effect of surface treatment of NiTi alloy on its corrosion behavior in Hanks' solution. *J. Biomed. Mater. Res*. 2002; **61**(3): 339–345.
14 Carroll W M, Kelly M J. Corrosion behavior of nitinol wires in body fluid environments. *J. Biomed. Mater. Res. Part A* 2003; **67A**(4): 1123–1130.
15 Shabalovskaya S, Rondelli G, Anderegg J, Xiong J P, Wu M. Comparative corrosion performance of black oxide, sandblasted, and fine-drawn nitinol wires in potentiodynamic and potentiostatic tests: Effects of chemical etching and electropolishing. *J. Biomed. Mater. Res. Part B – Applied Biomaterials* 2004; **69B**(2): 223–231.
16 Ryhanen J, Niemi E, Serlo W, Niemela E, Sandvik P, Pernu H, Salo T. Biocompatibility of nickel–titanium shape memory metal and its corrosion behavior in human cell cultures. *J. Biomed. Mater. Res*. 1997; 35(4): 451–457.
17 Assad M, Yahia LH, Rivard CH, Lemieux N. *In vitro* biocompatibility assessment of a nickel–titanium alloy using electron microscopy *in situ* end-labeling. *J. Biomed. Mater. Res.* 1998; **41**(1): 154–161.
18 Ryhanen J, Kallioinen M, Tuukkanen J, Junila J, Niemela E, Sandvik P, Serlo W. *In vivo* biocompatibility evaluation of nickel–titanium shape memory metal alloy: Muscle and perineural tissue responses and encapsule membrane thickness. *J. Biomed. Mater. Res.* 1998; 41(3): 481–488.
19 Trepanier C, Leung T K, Tabrizian M, Yahia L, Bienvenu J G, Tanguay J F, Piron D L, Bilodeau L. Preliminary investigation of the effects of surface treatments on biological response to shape memory NiTi stents. *J. Biomed. Mater. Res*. 1999; **48**(2): 165–171.
20 Wataha J C, Lockwood P E, Marek M, Ghazi M. Ability of Ni-containing biomedical alloys to activate monocytes and endothelial cells *in vitro*. *J. Biomed. Mater. Res.* 1999; **45**(3): 251–257.
21 Shih C C, Shih C M, Chen Y L, Su Y Y, Shih J S, Kwok C F, Lin S J. Growth inhibition of cultured smooth muscle cells by corrosion products of 316 L stainless-steel wire. *J. Biomed. Mater. Res*. 2001; **57**(2): 200–207.
22 Armitage D A, Parker T L, Grant D M. Biocompatibility and hemocompatibility of surface-modified NiTi alloys. *J. Biomed. Mater. Res. Part A* 2003; **66A**(1): 129–137.
23 Simske S J, Sachdeva R. Cranial bone apposition and ingrowth in a porous nickel–titanium implant. *J. Biomed. Mater. Res*. 1995; **29**(4): 527–533.
24 BergerGorbet M, Broxup B, Rivard C, Yahia L H. Biocompatibility testing of NiTi screws using immunohistochemistry on sections containing metallic implants. *J. Biomed. Mater. Res*. 1996; **32**(2): 243–248.
25 Ayers R A, Simske S J, Bateman T A, Petkus A, Sachdeva R L C, Gyunter V E. Effect of nitinol implant porosity on cranial bone ingrowth and apposition after 6 weeks. *J. Biomed. Mater. Res*. 1999; **45**(1): 42–47.
26 Assad M, Jarzem P, Leroux M A, Coillard C, Chernyshov A V, Charette S, Rivard C H. Porous titanium–nickel for intervertebral fusion in a sheep model: Part 1. Histomorphometric and radiological analysis. *J. Biomed. Mater. Res. Part B – Applied Biomaterial*s 2003; **64B**(2): 107–120.
27 Assad M, Chernyshov A V, Jarzem P, Leroux M A, Coillard C, Charette S, Rivard C H. Porous titanium–nickel for intervertebral fusion in a sheep model: Part 2. Surface analysis and nickel release assessment. J. *Biomed. Mater. Res. Part B – Applied Biomaterials* 2003; **64B**(2): 121–129.

28 Ryhanen J, Kallioinen M, Serlo W, Peramaki P, Junila J, Sandvik P, Niemela E, Tuukkanen J. Bone healing and mineralization, implant corrosion, and trace metals after nickel–titanium shape memory metal intramedullary fixation. *J. Biomed. Mater. Res*. 1999; **4447**(4): 472–480.
29 Jia W Y, Beatty M W, Reinhardt R A, Petro T M, Cohen D M, Maze C R, Strom E A, Hoffman M. Nickel release from orthodontic arch wires and cellular immune response to various nickel concentrations. *J. Biomed. Mater. Res.* 1999; **48**(4): 488–495.
30 Gall K, Tyber J, Brice V, Frick C P, Maier H J, Morgan N. Tensile deformation of NiTi wires. *J. Biomed. Mater. Res.* 2005; **75A**: 810–823.
31 Tan G, Liu Y. Comparative study of deformation-induced martensite stabilisation via martensite reorientation and stress-induced martensitic transformation in NiTi. *Intermet*. 2004; **12**: 373–381.
32 Liu Y, Xiang H. Apparent modulus of elasticity of near-equiatomic NiTi. *J. Alloys Comp*. 1998; **270**: 154–159.
33 Melton K N, Mercier O. Deformation behavior of NiTi-based alloys. *Met. Trans. A* 1978; **9A**: 1487–1488.
34 Frick, C P, Ortega, A M, Tyber, J, Gall, K, Maier H J. Multi-scale structure and properties of cast and deformation processed polycrystalline NiTi shape memory alloys. *Met. Mater. Trans*. 2004; **35A**: 2013–2025.
35 Brinson L C, Schmidt I, Lammering R. Stress-induced transformation behavior of a polycrystalline NiTi shape memory alloy: micro and macromechanical investigations via in situ optical microscopy. *J. Mech. Phys. Solids* 2004; **52**: 1549–1571.
36 Sittner P, Novak V. Experiment feedbacks in micromechanics modeling of thermomechanical behaviors of SMA polycrystals. *Scr. Mater*. 2004; **51**(4): 321–326.
37 Vaidyanathan R, Bourke M A M, Dunand D C. Texture, strain, and phase-fraction measurements during mechanical cycling in superelastic NiTi. *Met. Mater. Trans.* 2001; **32**: 777–786.
38 Khalil-Allafi J, Hasse B, Klonne M, Wagner M, Pirling T, Predki W, Schmahl W W. In-situ diffraction investigation of superelastic NiTi shape memory alloys under mechanical stress with neutrons and with synchrotron radiation. *Mater. Wissen. Werk*. 2004; **35**: 280–283.
39 ASTM F2516-06. The Standard Test Method for Tension Testing of Nickel–Titanium Superelastic Materials. ASTM International.
40 Robertson, S W, Ritchie R O. *In vitro* fatigue-crack growth and fracture toughness behavior of thin-walled superelastic Nitinol tube for endovascular stents: A basis for defining the effect of crack-like defects. *Biomaterials* 2007; **28**(4): 700–709.
41 Miracle D B. The physical and mechanical properties of NiAl. *Acta Metall. Mater.* 1993; **41**(3), 649–684.
42 Gall K, Yang N, Sehitoglu H, Chumlyakov Y I. Fracture of precipitated NiTi shape memory alloys. *Int. J. Fract.* 2001; **109**(2), 189–207.
43 Wang G Z. Effects of notch geometry on stress–strain distribution, martensite transformation and fracture behavior in shape memory alloy NiTi. *Mat Sci. Eng A*. 2006; **434**(1–2), 269–279.
44 Chen J H, Sun W, Wang G Z. Investigation on the fracture behavior of shape memory alloy NiTi. *Met. Mater. Trans*. 2006; **36A**, 941–955.
45 Melton K N, Mercier O. Fatigue of thermoelastic martensites. *Acta Metall*. 1979; **27**, 137–144.
46 Eggeler G, Hornbogen E, Yawny A, Heckmann A, Wagner M. Structural and functional fatigue of NiTi shape memory alloys. *Mat. Sci. Eng. A* 2004; **378**(1–2): 24–33.

47 Wagner M, Sawaguchi T S, Kaustrater G, Hoffken D, Eggeler G. Structural fatigue of pseudoelastic NiTi shape memory wires. *Mat. Sci. Eng. A* 2004; **378**(1–2): 105–109.
48 Miyazaki S, Imai T, Igo Y, Otsuka K. Effect of cyclic deformation on the pseudoelasticity characteristics of Ti–Ni alloys. *Metall. Trans. A*, 1986; **17**: 115–120.
49 Li D Y, Wu X F, Ko T. The effect of stress on soft modes for the phase transformation in a Ti–Ni alloy. II. Effects of ageing and thermal cycling on the phase transformation. *Phil. Mag A*, 1991; **63**: 603–616.
50 McCormick P G, Liu Y. Thermodynamic analysis of the martensitic transformation in NiTi – II. Effect of transformation cycling. *Acta Metall. Mater.* 1994; **42**: 2407–2413.
51 Jordan L, Masse M, Collier J- Y, Bouquet G. Effects of thermal and thermomechanical cycling on the phase transformations in NiTi and Ni–Ti–Co shape memory alloys. *J. Alloys Comp.* 1994; **211**: 204–207.
52 Lim T J, McDowell D L. Path dependence of shape memory alloys during cyclic loading. *J. Int. Mat. Sys. Struc.* 1995; **6**: 817–830.
53 Strnadel B, Ohashi S, Ohtsuka H, Ishihara T, Miyazaki S. Cyclic stress–strain Ccharacteristics of Ti–Ni and Ti–Ni–Cu shape memory alloys. *Mat. Sci. Eng. A* 1995; **202**: 148–156.
54 Xie Z, Liu Y, Van Humbeeck J. Microstructure of NiTi shape memory alloy due to tension–compression cyclic deformation. *Acta Mater.* 1998; **46** 1989–2000.
55 Bo Z H, Lagoudas D C. Thermomechanical modeling of polycrystalline SMAs under cyclic loading, Part I: theoretical derivations. *Int. J. Eng. Sci.* 1999; **37**: 1089–1140.
56 Lagoudas D C, Bo Z H. Thermomechanical modeling of poly-crystalline SMAs under cyclic loading, Part II: material characterization and experimental results for a stable transformation cycle. *Int. J. Eng. Sci.* 1999; **37**: 1141–1173.
57 Bo Z H, Lagoudas D C. Thermomechanical modeling of polycrystalline SMAs under cyclic loading, Part III: evolution of plastic strains and two-way shape memory effect. *Int. J. Eng. Sci.* 1999; **37**: 1175–1203.
58 Bo Z H, Lagoudas D C. Thermomechanical modeling of polycrystalline SMAs under cyclic loading, Part IV: modeling of minor hysteresis loops. *Int. J. Eng. Sci.* 1999; **37**: 1205–1249.
59 Lim T J, McDowell D L. Mechanical behavior of an Ni–Ti shape memory alloy under axial-torsional proportional and nonproportional loading. *J. Eng. Mat. Tech.* 1999; **121**: 9–18.
60 Liu Y, Houver I, Xiang H, Bataillard L, Miyazaki S. Strain dependence of pseudoelastic hysteresis of NiTi. *Met. Mater. Trans A* 1999; **30**: 1275–1282.
61 Tabanli R M, Simha N K, Berg B T. Mean strain effects on the fatigue properties of superelastic NiTi. *Metall. Mater. Trans*. 2001; **2**(7): 1866–1869.
62 Tabanli R M, Simha N K, Berg B T. Mean stress effects on fatigue of NiTi. *Mat Sci Eng A* 1999; **275**: 644–648.
63 Iadicola M A, Shaw J A. The effect of uniaxial cyclic deformation on the evolution of phase transformation fronts in pseudoelastic NiTi wire. *J. Int. Mater. Sys. Struc*. 2002; **13**: 143–155.
64 Frick C P, Ortega A M, Tyber J, Gall K, Maier H J. Multi-scale structure and properties of cast and deformation processed polycrystalline NiTi shape memory alloys. *Met. Mater. Trans*. 2004; **35A**: 2013–2025.
65 Gall K, Sehitoglu H, Chumlyakov Y I, Kireeva I. Pseudoelastic cyclic stress–strain response of over-aged single crystal Ti–50.8at%Ni. *Scr. Mater.* 1999; **40**: 7–12.
66 Sehitoglu H, Anderson R, Karaman I, Gall K, Chumlyakov Y. Cyclic deformation behavior of single crystal NiTi. *Mater. Sci. Eng. A* 2001; **314**(1–2): 67–74.

67 Gall K, Maier H J. Cyclic deformation mechanisms in precipitated NiTi shape memory alloys. *Acta Mater.* 2002; **50**(18): 4643–4657.
68 Hurley J, Ortega A M, Lechnaik J, Gall K, Maier H J. Structural evolution during the cycling of NiTi shape memory alloys. *Zeitschr. Metallk.*, 2003; **94**: 547–552.
69 Pompa G, Gambarini G, Pongione G, Floridi G, Di Carlo F, De Luca M, Quaranta M. Cyclic fatigue testing of new and used NiTi rotary instruments. *J. Dental Res*. 2000; **79**: 440–440.
70 Kuhn G, Jordan L. Fatigue and mechanical properties of nickel–titanium endodontic instruments. *J. Endod.* 2002; **28**(10): 716–720.
71 Tobushi H, Hachisuka T, Hashimoto T, Yamada S. Cyclic deformation and fatigue of a TiNi shape memory alloy wire subjected to rotating bending. *J. Eng. Mater. Technol. Trans. ASME* 1998; **120**: 64 –70.
72 Tobushi H, Hachisuka T, Yamada S, Lin P H. Rotating-bending fatigue of a TiNi shape-memory alloy wire. *Mech Mater* 1997; **26**: 35–42.
73 Tobushi H, Nakahara T, Shimeno Y, Hashimoto T. Low-cycle fatigue of TiNi shape memory alloy and formulation of fatigue life. *J. Eng. Mater. Technol.* 2000; **122**: 186–191.
74 Miyazaki S, Mizukoshi K, Ueki T, Sakuma T, Liu Y. Fatigue life of Ti–50 at Ni and Ti–40Ni–10Cu (at%) shape memory alloy wires. *Mater. Sci. Eng. A* 1999; **273–275A**: 658 –663.
75 Young JM, Van Vliet KJ. Predicting in vivo failure of pseudoelastic NiTi devices under low cycle, high amplitude fatigue. J. Biomed. Mater. Res. 2005 72B (1): 17–26.
76 Pelton A R, Gong X-Y, Duerig, T W. Fatigue testing of diamond shape specimens. In *Proceedings of SMST-2003*. (Eds: Pelton A R, Duerig T W), SMST Society, Pacific Grove, CA, 2004; 293–302.
77 Harrison W J, Lin Z C. The Study of Nitinol bending fatigue, In *Proceedings of SMST-2000*. (Eds: Pelton A R, Duerig T W), SMST Society, Pacific Grove, CA, 2001; 391–396.
78 Meggiolaro M A, Castro J T P. Statistical Eevaluation of fatigue crack initiation predictions. *Int. J. Fatigue* 2004; **26**: 463–476.
79 McKelvey A L, Ritchie R O. Fatigue-crack propagation in Nitinol, a shape-memory and superelastic endovascular stent material. *J. Biomed. Mater. Res*. 1999; **47**(3): 301–308
80 McKelvey, A L, Ritchie R O. Fatigue-crack growth behavior in the superelastic and shape-memory alloy Nitinol. *Metall. Mater. Trans. A* (*Phys. Metall. Mater. Sci.*) 2001; **32A**(3A): 731–743.
81 Stankiewicz J, Robertson S, Ritchie R . On the fatigue-crack growth properties of thin-walled superelastic austenitic Nitinol tube for endovascular stents. *J. Biomed. Mater. Res. A* 2007; **80A**: doi: 10.1002/jbm.a.31100.
82 McDowell D L, Gall K, Horstemeyer M F, Fan J. Microstructure-based fatigue modeling of cast A356-T6 alloy. *Eng. Fract. Mech.* 2003; **70**(1): 49–80.
83 Marrey R V, Burgermeister R, Grishaber R B, Ritchie R O. Fatigue and life prediction for cobalt–chromium stents: a fracture mechanics analysis. *Biomaterials* 2006; **27**: 1988–2000.
84 Gall K., Tyber J., Wilkesanders G., Robertson S., Ritchie R O, Maier H J. Effect of microstructure on the fatigue of NiTi shape memory alloys. *Mater. Sci. Eng. A* 2008; **486**: 389–403.
85 Ortega A M, Frick C P, Gall K, Tyber J, Maier H J. Cast NiTi shape memory alloys. *Adv. Eng. Mater.* 2005; **7**(6): 492–507.
86 Frick C P, Gall K, Ortega A M, Tyber J, Maier H J, Maksoud A El M, Liu Y. Thermal processing of polycrystalline NiTi shape memory alloys. *Mater. Sci. Eng. A* 2005; **405**: 34–49.

87 McCormick J, Tyber J, DesRoches R, Gall K, Maier H J. Structural engineering with NiTi. Part II: Mechanical and scaling. *J. Eng. Mech.* 2007; **133**(9): 1019–1029.
88 Tyber J, McCormick J, Gall K, DesRoches R, Maier H J, Maksoud A E A. Structural engineering with NiTi. Part I: Basic materials characterization. *J. Eng. Mech.* 2007; **133**(9): 1009–1019.
89 Hornbogen E. Thermo-mechanical fatigue of shape memory alloys. *J. Mater. Sci.* 2004; **39**(2): 385–399.
90 Hornbogen E, Heckmann A. Improved fatigue resistance of pseudo-elastic NiTi alloys by thermo-mechanical treatment. *Mater. Wiss. Werk.* 2003; **34**(5): 464–468.
91 Heckmann A, Hornbogen E. Effects of thermomechanical pre-treatments on pseudo-elastic fatigue of a NiTi alloy. *Mater. Sci. Forum* 2001; **394–3**: 325–328.
92 Brailovski V, Terriault P, Prokoshkin S. Influence of the post-deformation annealing heat treatment on the low-cycle fatigue of NiTi shape memory alloys. *J. Mater. Eng. Perform*. 2002; 1**1**(6): 614–621.
93 Holtz R L, Sadananda K, Imam M A. Fatigue thresholds of Ni–Ti alloy near the shape memory transition temperature. *Int. J. Fatigue* 1999; **21**: S137–S145.
94 Liu, Y, Xie Z, Van Humbeeck J. Cyclic deformation of NiTi shape memory alloys. *Mater. Sci. Eng. A* 1999; **273–275**: 673–678.

8

Surface modification of Ti–Ni alloys for biomedical applications

M. F. MAITZ
Leibniz Institute of Polymer Research Dresden, Germany

Abstract: The naturally grown titanium oxide film on biomedical devices made of the memory shape alloy Ti–Ni frequently is not sufficient to prevent corrosion and hazardous nickel release. Surface treatment techniques, including mechanical abrasive techniques, polishing, electropolishing, oxidation and nitriding are discussed in this chapter. They are applied to adjust surface properties for specific medical applications, to decrease the nickel concentration in the surface layer and to reduce the amount of nickel released. Superposed coatings act as additional sealing layers. The sterilization used as a final treatment of a medical device has a further effect on the surface concentration of nickel and the amount of nickel released.

Key words: surface modification, medical device sterilization, corrosion, nickel release, Ti–Ni, Ni–Ti, Nitinol, titanium oxide coating.

8.1 Introduction

Among the shape memory materials based on copper, iron, nickel or titanium,[1] only the equi-atomic Ti–Ni alloy has been used, mainly under the trade name Nitinol, in biomedical applications such as orthodontic wires in dentistry, as endoluminal stents in cardiology, radiology, urology and gasteroenterology, as tissue connectors, as spring rods for scoliosis correction and many more.[2]

Ti–Ni is a safe material for biomedical implants and is also approved by the FDA for long-term applications. The biocompatibility of the alloy in many clinical studies has been excellent; however, there have been also conflicting results. The high content of Ni in the alloy still raises concerns about the safety of the alloy, as Ni ions may elicit allergic and toxic reactions. Pit-like corrosion defects and release of Ni ions from Ti–Ni are clinically evident.[3–5] Serum nickel concentrations after implantation of Ti–Ni devices rise up to 4–6 ng mL^{-1} and normalize within 2–3 months.[3,4] *In vivo* Ni concentrations in the tissue around Ti–Ni devices are reported to be approximately 0.2 µg g^{-1} in animal studies;[4] inhibition of cell growth by Ni ions has been found *in vitro* for concentrations in a range of 10 µg g^{-1}.[6–8]

It is frequently reported that Ti–Ni alloys naturally express a titanium oxide surface with no or only very low Ni concentration;[9,10] however, this property is not very consistent and apparently depends on the purity and manufacturing condi-

tions of the material.[11] Further, the titanium oxide provides high corrosion protection in static investigation.[12] Yet, as a matter of principle, the memory shape alloys find application in mechanically demanding situations. While the metal can follow this, the titanium oxide protective layer as a ceramic is more brittle, expressing defects, which allow corrosion and the release of Ni ions.[13]

Surface modification of Ti–Ni therefore frequently follows special demands concerning an enhanced passivating and corrosion protective layer to prevent Ni release. In addition, general surface treatments like polishing, sand blasting or coatings for specific biological properties are requested, with the intention of transferring approved surface properties from other devices to the shape memory material. Also these techniques need special consideration, as the superelastic material shows specific behaviour for some treatments. In addition, various coatings are applied as a sealing layer to prevent Ni release or to exhibit specific properties for the desired application.

8.2 Surface finishing

Wires and tubings of Ti–Ni typically are cold drawn and plates and strips are rolled. Generally, the surface is smooth when inspected at low magnification. Further device formation methods include general machining techniques like milling, cutting and drilling. Vascular stents are typically laser cut from tubings. Pointing by centerless grinding may be necessary for guide wires. After the formation of these crude biomedical devices, surface finishing is usually necessary to remove burrs from cutting and to adjust the surface roughness. A modification of the surface chemistry and gain of special properties is not intended by this treatment, but such changes inevitably occur.

8.2.1 Blasting techniques

Slurry basting is a method for degreasing and for removing the drawing texture from the inner diameter of tubings or for deburring vascular stents after the laser cutting process.[14] A dispersion of abrasive media, such as silica, alumina, carborundum, carbides or diamond is circulated through the tube and forms a smooth finish. The method is highly abrasive and causes a measurable loss of material. In contrast to the mainly tangential flow at slurry blasting, microblasting uses mainly orthogonal impinging particles. The method is an attenuated modification of sand blasting with fine abrasive media and lower flow rates. It is mainly applied to remove oxides and produces a matt-finished, finely textured surface. The rough surface after sand blasting is frequently preferred for improved osseointegration of dental or orthopaedic implants. The mechanical abrasive techniques are followed by cleaning procedures in ultrasound, typically with water and/or organic solvents to remove abrasive particles, organic contamination and debris. The surface quickly oxidizes in air, forming an oxide layer 2–3 nm thick.[15]

It was found that blasting techniques frequently remove the natural, pre-passivated oxide film only incompletely. Shabalovskaya *et al*. found that at least one flake of thick oxide layer remained per centimetre of sand blasted wire.[16] Particles of the abrasive media remain impinged in the surface and cannot be removed by ultrasound cleaning. Lubricants are captured within cracks or beneath the loosened oxide flakes. Such impurities of the surface lead to enhanced corrosion of the material with pitting and release of toxic Ni ions. Moreover, the corrosion and passivation behaviour is highly unpredictable and irregular.[16,17]

8.2.2 Polishing and electropolishing

For most biomedical applications, highly polished surfaces are required. Various mechanical, chemical, electrochemical and plasma treatments are applied.[15] Mechanical, metallurgical polishing is preferentially applied on flat surfaces using abrasive papers and dispersions with silicon carbide or alumina particles down to 0.3 μm. Mirror finishing of the surface is achieved by this method with a roughness R_a below 10 nm.[15] Due to the complex geometry of biomedical devices, they are generally electropolished. Electrolyte solutions for Ti–Ni electropolishing are mainly based on hypochloride with methanol or acetic acid.[16–18] The result is highly influenced by the exact description of the electrolyte and electropolishing conditions like temperature and voltage.[19] These parameters are generally non-disclosed properties of the medical device companies. The reported roughness for electropolished Ti–Ni is 100 nm.[15] Chemical etching in HF–NHO_3 solution or etching in Ar plasma both lead to roughness of 200 nm.[15]

Decrease of surface roughness is the predominant intention of the polishing techniques. However, they also significantly influence the surface chemistry and corrosion properties. Metallurgical polishing as an abrasive technique has similar effects to the blasting techniques. A 2–3 nm oxide film forms by oxidation in air. For the purely abrasive technique, the equi-atomic Ti/Ni ratio of the bulk is maintained also in the oxide layer. The oxidation of Ti is thermodynamically much more favoured than the oxidation of Ni; this leads to a preferential oxidation of Ti, whereas Ni stays in the metallic form.[10] In the oxide film, therefore titanium mainly is found as TiO_2 with minor amount of sub-stoichiometric Ti_2O_3, whereas nickel is present in the oxide layer as elemental Ni and sub-stoichiometric NiO or Ni_2O_3.[10,15] The method leads to plastic deformation and amorphization of the surface; grain boundaries, which generally are most susceptible for corrosion, are not visible.[20] However, due to the high amount of metallic nickel, the surface shows highest susceptibility to corrosion with the most active corrosion potential and highest corrosion currents of all surface treatments. In consequence also, the release of Ni ions into solution is high.[21] In practice, this method usually is followed by a passivation step to prevent this oxidation.

Plasma etching with argon plasma also acts as an abrasive method. Depending on plasma parameters there can be preferential sputtering of one element; the Ti/

Ni ratio on the surface can range from 0.8 to 4.3, i.e. shifts in both directions are possible.[10,15] However, the Ni concentration still remains high compared with other surface treatment techniques. Ni remains in elemental or only sub-stoichiometric oxidized form, where it can easily be dissolved into body solutions.

Chemical etching and electropolishing significantly shift the surface element concentration to Ti with reported Ti/Ni ratios of 4.3 and 5.6, respectively.[15] Nickel is selectively depleted from a 3–15 nm[15,21] surface layer, where the remaining Ti oxidizes to a protective layer. The higher smoothness, better depletion of Ni and thus better corrosion resistance[22] make electropolishing the preferential surface treatment. However, after chemical etching, a chemical passivation step can enhance the corrosion resistance.[21] It has been shown that the smooth electropolished surface also improves the mechanical properties of Ti–Ni upon tensile stress.[23]

8.3 Surface passivation

The high amount of Ni in Ti–Ni and its possible release by corrosion is the main concern with the medical application of the alloy. Corrosion of devices of Ti–Ni in medical application is clinically described and enhanced Ni concentrations in blood and tissue after implantation have been described *in vivo*.[3–5] The essential trace element Ni is known to induce contact allergy, which has a high prevalence of 10–30% in the female population.[24,25] Ni ions interact with cellular proteins and inhibit their activity, leading to cell death and inflammation *in vivo* and *in vitro* at concentrations of 10–50 $\mu g\, g^{-1}$, whereas nickel concentrations below 10 $\mu g^{-1} g$ were reported without histological effect.[8] Carcinogenic effects of long-term occupational exposure to Ni have been described epidemiologically and confirmed by experimental studies.[26,27] Surface passivation of Ti–Ni in order to prevent corrosion and nickel release therefore is a predominant requirement for all types of surface treatment of Ti–Ni. It is a subsequent step to most polishing techniques.

8.3.1 Oxidation

An oxide layer on Ti–Ni exhibits various principles to reduce corrosion and Ni release. Titanium oxide is resistant to degradation and dissolution in the aggressive body environment, forming a chemically protective coating. Oxidation of Ti in the layer is thermodynamically favoured over the oxidation of Ni as indicated by free binding energies in Table 8.1. Thus, the presence of Ti keeps the Ni mainly in the metallic Ni^0 state.[10,28,29] At elevated temperature, the preferential oxidation of titanium causes a migration of nickel from the surface oxide layer into deeper zones. This forms an especially Ni-depleted titanium oxide surface layer covering a Ni-enriched zone.[29] Titanium oxide as a ceramic, however, does not show the superelastic properties of the bulk Ti–Ni. The elastic modulus of the TiO_x film is in the range of 48–68 GPa,[30] whereas the value for martensitic Ti–Ni is ~30 GPa.[31,32]

Table 8.1 Free energy of formation for metal oxides relevant in Ti–Ni[10]

Oxide	ΔG (at 25 °C) (kJ mol^{-1})
NiO	–212
TiO	–495
TiO_2	–890

This difference in elastic properties between bulk and coating causes a risk of crack formation and delamination, which may induce local element formation and enhanced corrosion.[13,16] Crystal structure and purity of the coating also vary with the techniques of oxidation, leading to different corrosion resistance. Amorphous coatings are more corrosion resistant than crystalline coatings.[9] High uniformity of the oxide film leads to better corrosion resistance than improved composition or thickness of the film.[33] This shows that methods and parameters of surface oxidation can lead to different surface properties and performances of the material.

Thermic oxidation

The shape setting process of Ti–Ni usually is performed in air at 500 °C for ~15 min and results in a blue surface colour. This treatment, if performed under non-optimized conditions can lead to an enrichment of Ni on the surface.[11,34] Conditions of thermic oxidation protocols therefore have to be selected carefully in order to obtain a Ni-depleted, corrosion-resistant surface.

Metallurgically polished Ti–Ni was heat treated at atmospheric conditions for 30 min at 300 to 600 °C, resulting in a temperature-dependent decrease of the surface Ni concentration.[35] At lower temperatures Ni oxidizes in the surface, but is still present in the oxide layer, whereas surface Ni depletion occurs at 600 °C.[36] Oxidation at ambient conditions leads to predominantly anatase TiO_2, whereas at 350 to 450 °C oxidation an orthorhombic rutile crystal structure is formed together with NiO and intermetallic phases beneath the metal oxide phase. At 600 °C, mainly tetragonal rutile TiO_2 is formed. The thickness of the oxide layer ranges from 14 to 40 nm for the naturally grown oxide film from the oxidation at 600 °C.[30]

Modifications of the thermic oxidation at air have been developed to produce a more homogeneous and pure stoichiometric TiO_2 layer without Ni oxidation. Thermal treatment at a reduced pressure of 3×10^{-2} mbar, 400 °C leads to slower and more homogeneous oxidation and more complete Ni depletion than oxidation in air. Subsequent treatment in boiling water very efficiently leaches out remaining Ni ions, leading to further Ni depletion down to <2 at.% in a layer of typically 5–10 nm, but values up to 90 nm have been reported.[11,37] Clinical steam sterilization at 121 °C also causes a minor decrease of the nickel surface concentration to 5%, but also the formation of nickel hydroxides.[32]

The heat treatment may be applied to the surface only, without affecting the bulk. Suggested methods are laser melting in air or Ar atmosphere or electron beam treatment.[38–41] The decrease of surface Ni concentration is below 2% in a TiO_2 layer of 75 nm. This is similar to a treatment of the whole device. Slow melting in Ar caused the best Ni depletion.[38] The Ni concentration may be further decreased by additional boiling in water. An advantage of this technique is the more homogeneous and amorphous surface. However, a relatively thick surface layer of 100 μm is treated, which may become harder, resulting in a change of mechanical properties. The techniques obviously have economic disadvantages as they are line-of-sight scanning techniques.

Chemical oxidation

Various wet chemical treatments have been applied to passivate the Ti–Ni surface. Electropolishing and chemical etching, which utilize the preferential dissolution of Ni from the Ti–Ni surface to form a Ni-depleted layer has been described above. However, in these cases, additional passivation techniques are usually applied to enhance the corrosion resistance.

Oxidation in 10 or 100 mmol L^{-1} H_2O_2 for up to 74 h has been used for chemical etching and passivation of titanium.[42,43] An amorphous, porous gel layer of TiO_2 is formed on the surface. Subsequent tempering leads to the formation of anatase or rutile TiO_2 for treatment at 300 °C or 800 °C, respectively and mixed phases in between. The method has been transferred to Ti–Ni, but leads to high surface Ni concentrations of almost 30% in a postulated $TiNi_4O_3$ oxide. The high Ni concentration in this surface exhibited toxic effects *in vitro*.[44] A combination of peroxide treatment with alkaline etching of Ti–Ni for enhanced calcium phosphate precipitation has been proposed.[45,46] H_2O_2 surface treatment of Ti–Ni, however, remains interesting: the surface is bioactive, as it stimulates the precipitation of hydroxyapatite from a simulated body fluid with saturated calcium phosphate concentration.[42]

The standard for chemical passivation of Ti–Ni is by dipping in 10% nitric acid (HNO_3) at room temperature according to ASTM-F86.[47] The treatment modifies only about 3 nm of the outmost surface layer,[33,48] but an amorphous state has been reported at a depth >50 nm,[19] forming a uniform highly corrosion-resistant TiO_2 layer.

Physical (plasma-phase) oxidation

Surface passivation of Ti–Ni with O^{2-} ion implantation from a physical plasma has been performed experimentally and suggested for commercial application.[49–53] Figure 8.1 shows examples of element profiles of O^{2-} ion implanted Ti–Ni. The method is better controlled than the wet chemical techniques, as the implantation depth can be adjusted by the energy typically to 20–40 nm and ion doses are applied in the range of 10^{17} to 10^{18} cm^{-2}. Ion implantation principally leads to

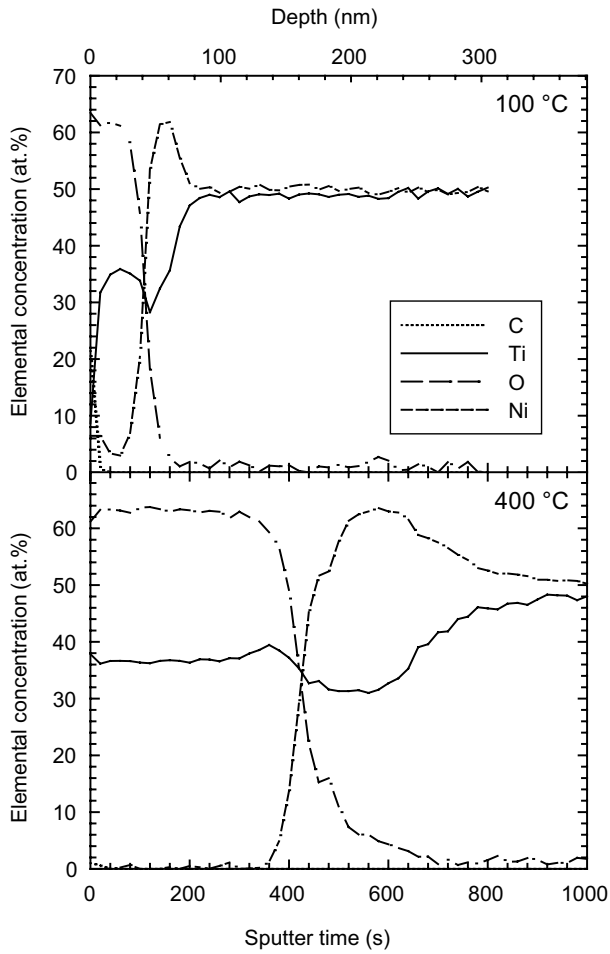

8.1 Element profiles of oxygen ion implanted NiTi (10^{17} cm^{-2}) with ion implantation performed at ≤100 °C and 400 °C as determined by Auger electron spectroscopy. Argon sputter times are given as depth information; the metric depth information is estimated and assumes a constant sputter coefficient in all layers and between samples.

amorphization of the surface, and re-crystallization can partly be controlled by tempering. Diffusion of O^{2-} into the bulk occurs for annealing at 400–600 °C, and a deeper oxygen profile is formed, as presented in Fig. 8.1. Following the O^{2-} profile, the oxidation state of Ti also decreases from Ti^{4+} at the surface to Ti^{3+} and Ti^{2+} in the deeper oxide layers. The O profile was found to be deeper after annealing at higher temperature (600 °C), but the amount of Ti^{4+} is decreased in that case.[53] Annealing at 600 °C after O^{2-} ion implantation caused best corrosion resistance with regards to corrosion and breakthrough potential.[53] The Ni

concentration in the oxide layer is decreased to the detection limit with an increased concentration in the sublayer, indicating diffusion processes of the metals during the implantation. The surfaces show improved corrosion resistance. Although there is a gradual transition between bulk and oxide layer without a sharp interface, the thick layer of the harder ceramic phase raises concerns about the stability at major deformation.[19] By implantation of Ta with co-implantation of O^{2-}, an improved repassivating ability and resistance against pitting has been found,[54] so that corrosion resistance may be maintained also for defects in the coating.

8.3.2 Nitriding

Nitriding of metals is an approved method to increase the surface hardness against scratches and wear. It is frequently applied for biomedical devices of Ti alloys. Various techniques have been established technically, which are also applied to Ti–Ni. They include plasma nitriding, gas nitriding, nitrogen ion implantation, or powder immersion reaction assisted coating (PIRAC).[55–59] Besides the improved hardness, the nitrided Ti–Ni surface has a decreased friction coefficient and improved corrosion resistance. Also this treatment causes Ni depletion of the surface and forms a Ni-enriched subsurface. Depending on the parameters, the surface can be more crystalline or amorphous. Good biocompatibility and hemocompatibility of the surface has been demonstrated *in vitro* and *in vivo*, but surface nitriding of Ti–Ni has not found clinical application yet. The high elastic modulus of the surface layer can cause problems with crack formation and increased corrosion under dynamic loading.[13] Experimental studies, comparing the different methods of Ti–Ni nitriding do not exist yet.

8.4 Coatings

Coatings form a layer on top of the outer surface of Ti–Ni. This is in contrast to the above-described methods, which transform the Ti–Ni surface. The coating as a separate layer can provide more versatile surface modifications than other surface treatments. The intention therefore is to provide functionalities for specific applications, like integration in bone, hemocompatibility or low friction of guide wires. Polymer coatings may be applied for sealing and additional corrosion protection. The interface with the substrate for coatings is sharper than for the surface modifications. Coatings on the elastic substrate therefore are more prone to delaminate than other surface modifications.

8.4.1 Inorganic coatings

Titanium oxide and titanium nitride

Frequently, it is intended to enhance the corrosion protection of an otherwise

produced titanium oxide film on Ti–Ni by higher film thickness. For this, Ti, titanium oxide and titanium nitride films are deposited on the Ti–Ni surface. Energetic processes like chemical vapour deposition, ion beam assisted deposition (IBAD), or plasma immersion ion implantation are restricted to visible surfaces of a device and have restrictions at intersections and inner pores of a porous material. They can build up connective layers and graded interfaces, which promise stable adherence.[60]

Sol–gel deposition of titanium oxides from nano-sized particle dispersions already has wide technical application.[61] The method has the advantage that porous materials can also be coated homogeneously. It has been applied on Ti–Ni for evaluation purposes, forming a compact 200 nm coating, which exhibited corrosion resistance and hemocompatibility.[62] For the preparation of the film, tetrabutyltitanate $[Ti(C_4H_9)_4]$ in ethyl alcohol is used as TiO_2 precursor. A nanocolloid dispersion (sol) is obtained by hydrolytic polycondensation, oxidation and polymerization. The deposition is performed as dip coating with a typical withdrawal speed of 0.3–0.5 mm s^{-1} at room temperature, followed by a sintering step at 500–600 °C and ultrasonic cleaning in ethanol and acetone.[61,63,64] Repeated deposition and sintering steps are applied to obtain the required thickness.[65,66] Sol–gel coatings primarily are amorphous; however, depending on the sintering temperature, crystallization occurs. For heat treatment at 400–500 °C mainly anatase is found, whereas rutile TiO_2 is predominant for heat treatment above 800 °C and mixed phases exist at temperatures in between.[64] The mean surface roughness R_a is 4 nm.[64]

Sol–gel TiO_2 films tend to be rich in TiOH groups. These groups are bioactive in the sense that they precipitate calcium phosphate in the form of hydroxyapatite from simulated body fluids. The bioactivity was found to be best for the 500 °C tempering step.[67]

A drawback of sol gel coating is the sharp interface between the substrate and the coating, which tends to delaminate. During the tempering process, a titanium oxide interface forms, which reduces the adhesion strength of the ceramic coating.[68] In a detailed study, it was found that sol–gel coatings especially on mirror polished and electropolished surfaces tend to delaminate, whereas especially etching in 60 °C 10 mol L^{-1} NaOH or nitriding improves the adhesion. The temperature of the heat treatment had only a minor effect on the adhesion strength of the coating.[67] It is concluded that the TiOH groups, which are formed during the NaOH etching process, support the chemical bonding of the sol–gel layer on the surface; nitriding of Ti–Ni prevents excessive oxidation during the tempering step with its detrimental effects.

Calcium phosphate coatings

Calcium phosphate coatings, mainly in form of hydroxyapatite, are frequently applied on orthopaedic or dental implants of titanium alloys. Hydroxyapatite as the mineral phase of bone is osteoconductive, i.e. it supports the continuous growth of

Table 8.2 Ion concentration in simulated body fluid used for calcium phosphate precipitation and in human blood plasma.[69] *Ionized calcium only

Ion	Simulated body fluid (mmol L^{-1})	Human blood plasma (mmol L^{-1})
Na^+	142.0	135–144
K^+	5.0	3.6–4.8
Mg^{2+}	1.5	0.73–1.06
Ca^{2+}	2.5	1.12–1.37*
Cl^-	148.8	97–108
HCO_3^-	4.2	21–26
HPO_4^{3-}	1.0	0.84–1.45
SO_4^{2-}	0.5	

bone. Clinically, it accelerates the integration of an implant in bone. Coating methods range from plasma spray, sputtering, ion beam assisted deposition, electrodeposition, sol–gel dip coating to deposition from saturated solutions. When applied on Ti–Ni, the hard character of the coating on the superelastic material may lead to cracking of the coating.[32]

The approach mainly followed for coating of hydroxyapatite on Ti–Ni is a biomimetic deposition from simulated body fluids with saturated or supersaturated calcium phosphate concentration (Table 8.2).[32,45,46,69] The calcium phosphate obtained from simulated body fluid is a small crystalline or mainly amorphous carbonated hydroxyapatite, which resembles the apatite in bone. The process is adjusted from the method for hydroxyapatite precipitation on titanium originally described by Kim and Kokubo.[69] A bioactive surface is required, which provides nucleation points for the hydroxyapatite precipitation. Many metal hydroxides, among them TiOH, are capable of accumulating Ca and phosphate ions and precipitate hydroxyapatite.[70] On Ti–Ni they are obtained by a combined alkaline and H_2O_2 treatment[45,46] or by the sol–gel dip-coating TiO_2 film.[67] In both types of surface treatment, the hydroxyl groups are stable at ~500 °C tempering, and treatment at this temperature provides the most bioactive surface. Heat treatment as for surface passivation also activates the Ti–Ni surface without other activating steps; the anatase phase of titanium oxide, which is formed at 600 °C tempering, was found to be most effective for the precipitation of calcium phosphate.[71]

The direct application of the device with the activated surface eliminates the need for a brittle hydroxyapatite coating. There are concerns that the bioactivity may interfere with the repassivation of surface defects.[32,72]

Inorganic carbon coatings

Besides oxygen and nitrogen, Ti also has high affinity to carbon. Energetic ion implantation of C and the formation of Ti–C phases therefore also reduces the surface Ni concentration and shifts Ni to deeper layers. The release of Ni to the medium of a C-implanted Ti–Ni is reduced to 3.4% compared with an untreated

control.[73] Electrochemical corrosion current at breakdown of the passivation film decreases by at least one order of magnitude.[74] If the temperature during the implantation and deposition process does not exceed 150 °C, the coating is flexible enough to maintain the barrier properties of the modified surface under deformation of the device.[73]

Low-temperature isotropic pyrolytic carbon (LTIC) generally is too brittle to be a coating on the superelastic Ti–Ni. Thin diamond C films deposited by plasma immersion ion implantation and deposition from ethylene plasma make use of the reactivity of Ti with C, forming a graded and reactive interlayer.[73,75,76] Coatings of C are known as diamond-like C (DLC) and are of special interest due to their bioinertness, low friction and high abrasion resistance in combination with good biocompatibility. They have clinical application as a thromboresistant coating on stainless-steel stents, and are suggested also as a barrier against Ni release.[77–79] Control of the sp^2/sp^3 ratio or ion doping of DLC with N or P has been suggested to enhance the hemocompatibility.[80–83] The influence of the structural properties of the inorganic C coatings on blood compatibility is, however, uncertain. An enhanced ratio of graphitic sp^2 to diamond-like sp^3 bondings was reported to enhance hemocompatibility. Among sp^2 bondings, a lower ratio of the Raman D-band (ringlike structures) to G-band (–C=C– chains) appeared preferable for hemocompatibility.[80] Otherwise, a normally formed sp^2 layer also on top of pure sp^3 mainly annihilates these differences.[84,85]

8.4.2 Polymer coatings

Polymer coatings tend to be thicker than inorganic coatings. In general, their elastic modulus is better adjusted to the properties of the superelastic metal and they can better follow the deformation without cracking or delamination. Extensive cleaning of the surface with water and organic solvents in a water bath and frequently also in Ar plasma is required to reach a sufficient adhesion strength of the polymer on the metal substrate.

Polymers as coatings can provide a wide range of specific surface properties to a biomedical device. A basic application is sealing the surface to prevent corrosion and the release of metal ions. Orthopaedic clamps of Ti–Ni have been coated with plasma polymerized polytetrafluorethylene (PTFE) for this. Apparently also repassivation of damaged films was improved by this treatment.[86] PTFE is known for its low friction coefficient, therefore it finds application as coating on guidewires.

Similar or even better corrosion resistance than for PPTFE has been observed for plasma polymerization of hexamethyldisilazane (HMDSN) on a Ti–Ni surface. This coating could withstand 2% strain deformation before failure.[87] Yet the higher elasticity of PTFE and the wide application of that polymer in medicine render PTFE the more attractive polymer coating.

Polymers of other classes have also been applied as coatings on Ti–Ni. The medical-grade polyurethane ChronoFlex™AR (Cardiotech International) is a

solution-based elastomeric polycarbonate polyurethane for dipping application. Application on vascular stents at 25–30 μm thickness has been applied to decrease the corrosion from 275 to <13 μm/year. The corrosion resistance was maintained at surface expansion up to 225%.[88–90] Crosslinked polyurethaneurea films with Ta particles as radiopaque filler were synthesized directly on Ti–Ni stents. Firm adhesion of the film on the surface was achieved by N^- ion implantation and sputter cleaning of the metal followed by 2,4 toluenediisocyanate pretreatment, which provides covalent bondings to the polymer and therefore improved adhesion of the coating.[91,92] The siloxane-based polyurethane copolymer Elast-Eon™ has FDA approval for medical application and was used for dip-coating of stents. The study did not provide corrosion data, but showed highly improved hemocompatibility concerning coagulation and inflammation.[48]

Polymer coatings are frequently applied to fulfil specific tasks besides corrosion resistance. In order to attain even better hemocompatibility characteristics, the polymers are designed to support the adhesion and proliferation of endothelial cells on the surface. Plasma treatment of polymer coatings has been applied to improve adhesion of endothelial cells. Because of reorientation in the polymer, effects of this treatment usually are time limited. There are also concerns that the formation of free radicals and dangling bondings in the polymer by the energetic treatment could accelerate the ageing and deteriorate the mechanical stability. Yet for ChronoFlex™AR it has been shown that the mechanical properties are maintained after He plasma treatment.[89]

Tetraethyleneglycol dimethyl ether (tetraglyme) has been plasma polymerized on Ti–Ni. It forms a very hydrophilic surface, which prevents protein adsorption, blood platelet adhesion and reduces the blood coagulation potential of the surface.[93,94] Corrosion protection and prevention of nickel release would not be expected from this coating.

A variety of porous polymers have been applied on Ti–Ni stents in the sense of a stent graft. These include polyethylene terephthalate (Dacron)[95] or mechanically stretched, expanded polytetrafluoroethylene (ePTFE)[96] Although they are described as coatings, the unprotected Ti–Ni surface in these cases is in contact with body fluids. Dedicated ways of Ti–Ni surface passivation therefore are necessary to prevent Ni release.

8.4.3 Bioactive coatings

Bioactive coatings exhibit specific biological properties, targeting selected biomolecules. Calcium phosphate coatings on orthopaedic and dental implants, stimulating the integration in bone by their osteoconductive properties, have been discussed above.

For vascular stent application, coatings usually are much more target-designed than for application as orthopaedic implants. The prepared coatings show anticoagulant properties and antiproliferative properties against blood vessel wall

proliferation and restenosis. These treatments are not specific for Ti–Ni, but they are a linear transfer from coating of other substrates, which are reviewed elsewhere.[97] The main concept is that bioactive substances, drugs, are provided locally at a pharmaceutically effective concentration, whereas the dose on the whole body is negligible and systemic side effects should not occur.

These coatings mainly have a polymer as carrier. The polymer either provides the chemical functionalities for immobilization of the bioactive substances, or the drugs are immobilized in the matrix of the polymer. From there, they are slowly released by diffusion or during biodegradation of the polymer. Because of consumption or degradation, the coatings exhibit their activity only for a limited time. After that time the bare metal surface or a non-functionalized polymer of the device is exposed.

Heparin as a physiological anticoagulant has been suggested for immobilization on Ti–Ni stents.[48,98] Various technologies for adsorptive deposition or covalent immobilization of heparin to amine groups of a polymer have been developed.[99] Heparin exhibits its activity by binding and activating antithrombin III (AT III), therefore the control of heparin immobilization frequently is by its AT III binding capacity. AT III binding of 6–12 pmol cm^{-2} was found to provide good anticoagulation;[100] however, the molecule undergoes too rapid degradation for long-term coagulation protection.

Implantation of a vascular stent is associated with mechanical irritation and damage of the vessel wall. The biological reaction is proliferation of vascular smooth muscle cells and restenosis. Drug-eluting stents, releasing antiproliferative drugs paclitaxel (Taxol), sirolimus or everolimus significantly decrease the restenosis. The drugs are incorporated in a polymer matrix of poly(styrene-β-isobutylene-β-styrene) (SIBS) (Taxus, Boston Scientific SCIMED) or in a combination of polyethylene-co-vinyl acetate (PEVA) and poly (n-butyl methacrylate) (PBMA) (Cypher, Cordis), where the drug constitutes 30–35% of the mixture.[101–103] Because of high blood coagulation on these polymers, release systems with degradable polymers of polylactic acid are under development;[104–106] use of the biodegradable polysaccharide chitosan is more of an experimental approach.[98] The coronary drug-eluting stents on the market are made of stainless steel, but the concept of drug release is applied also on Ti–Ni stents for the carotis or the superficial femoral artery.[103,107]

8.5 Sterilization

Sterilization is generally not considered to be surface modification of a device, as it is supposed not to influence the physical or chemical properties of a surface. However, it is obligatory to decontaminate a biomedical device before its clinical application. The most frequently applied autoclaving at 120 °C in saturated water vapour resembles the boiling, used for leaching surface Ni. Autoclaving of freshly polished Ti–Ni also could reduce the surface Ni concentration and enhance the Ti/Ni

ratio; for a typical 20–30 min clinical autoclavation, the ratio increased to 1.7.[44] Autoclavation (132 °C, 4 min), dry heat (132 °C, 60 min), ethylene oxide (54 °C, 130 min), peracetic acid, hydrogen peroxide plasma and peracetic acid plasma as clinically established sterilization methods were applied.[20,108] Ethylene oxide or hydrogen peroxide plasma did not influence the corrosion properties. Dry heat or autoclavation, however, can increase the surface roughness, cause cracking of the surface, decrease the breakdown potential and lead to localized corrosion. The sterilization methods applying elevated temperature also tended to increase the Ni concentration in the surface layer of an electropolished Ti–Ni specimen, whereas with plasma treatment there had been less influence. Discoloration with steam sterilization or ethylene oxide sterilization were found and were related to an increase of the oxide layer or surface contamination left on the surface after evaporation of the water. Sterilization by ionizing radiation, gamma or electron beam, has not been analyzed; however, the effect on surface properties should be less.

8.6 Summary

Ti–Ni is the only shape memory metal with standard application in medicine, therefore development in surface modification is mainly limited to this alloy. The high amount of the allergenic and toxic element Ni in the almost equi-atomic Ti–Ni alloy and its potential release to the body are at the centre of attention when considering the surface treatment as part of general manufacturing. The alloy forms a Ni-depleted titanium oxide surface layer on top, which prevents Ni release. The thickness, homogeneity and diffusion properties of this coating can be influenced by surface treatments. Figure 8.2 summarizes electrochemical corrosion data of various surface treatments of Ti–Ni compiled from the literature. Mechanical abrasive treatments, such as blasting or metallurgical polishing, remove the natural surface oxide layer. Repassivation only leads to a thin film with insufficient corrosion protection. Chemical etching and electropolishing form a Ni-poor surface layer, which acts as a barrier against Ni release. Further passivation by leaching in boiling water, heat treatment, chemical passivation, energetic oxidation or nitriding processes can enhance the barrier function and add additional mechanical properties to the surface. The main influences of these surface treatments are summarized in Table 8.3.

Coatings as an additional layer deposited on Ti–Ni are designed to enhance the pre-existent surface passivation layer by deposition of additional titanium oxide or nitride. Plasma-based and sol–gel methods are discussed in this context. Coating technologies otherwise are applied with little substrate dependence. Hydroxyapatite coatings, inorganic C, polymers and drug release systems on Ti–Ni mainly are a direct transfer of technologies approved in other systems.

Sterilization as the final step of biomedical device formation is also considered to be a form of surface modification, because the conditions applied there can have significant influence on the corrosion and nickel release of the device.

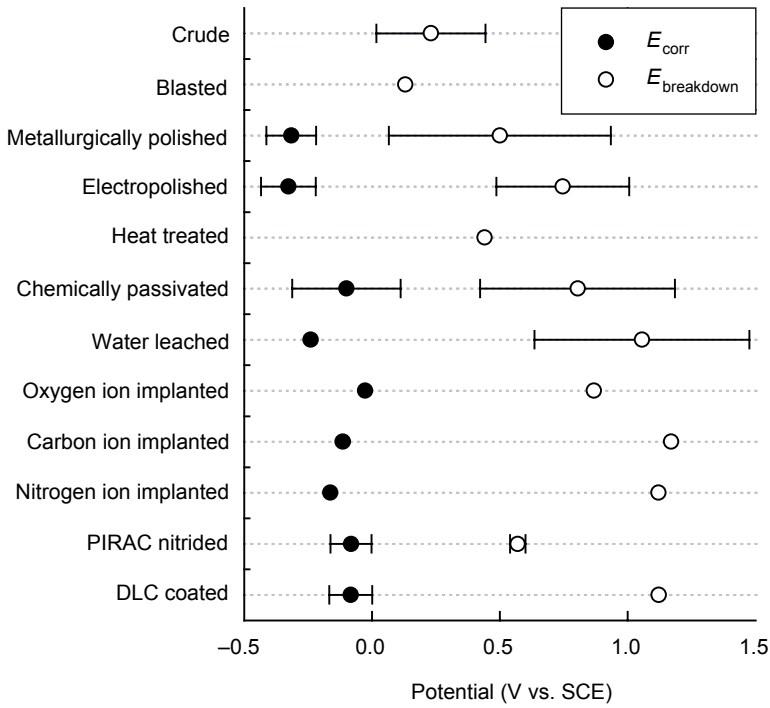

8.2 Corrosion potential E_{corr} and breakdown (pitting) potential $E_{breakdown}$ of various surface treatments of Ti–Ni; data compiled from the literature. Different surface treatment parameters within one type of treatment are ignored and influences of medium, temperature or initial potential on the corrosion measurement are not considered.

Table 8.3 Summary of the surface effects induced by the various surface treatments

Modification	Roughness R_a (nm)	Oxide thickness (nm)	Surface Ti/Ni ratio
Blasting	Variable	2–3[15]	1–2[11]
Mechanically polished	<10[15]	20[21]	1–2[11]
Electropolished	100[15]	3–13[15,21]	5–6[15]
Chemically etched	200[15]	6.5[21]	2–4.5[11,15]
Heat oxidized	100[37]	14–40[30]	14[37]
Water boiled	—		4–40[11,37]
Plasma oxidized	—	50–150	~50

8.7 References

1 Anson T, 'Shape memory alloys – medical applications' *Mater World*, 1999 **7**(12), 745–7.

2 Duerig T, Pelton A, Stöckel D, 'An overview of nitinol medical applications' *Mater Sci Eng A*, 1999 **273–275**, 149–60.

3 Ries M W, Kampmann C, Rupprecht H-J, Hintereder G, Hafner G, Meyer J, 'Nickel release after implantation of the Amplatzer occluder' *Am Heart J*, 2003 **145**, 737–41.

4 Assad M, Chernyshov A V, Jarzem P, Leroux M A, Coillard C, Charette S, Rivard C H, 'Porous titanium–nickel for intervertebral fusion in a sheep model: Part 2. Surface analysis and nickel release assessment' *J Biomed Mater Res*, 2003 **64B**(2), 121–9.

5 Heintz C, Riepe G, Birken L, Kaiser E, Chakfe N, Morlock M, Delling G, Imig H, 'Corroded nitinol wires in explanted aortic endografts: an important mechanism of failure?' *J Endovasc Ther*, 2001 **8**(3), 248–53.

6 Shih C-C, Lin S-J, Chen Y-L, Su Y-Y, Lai S-T, Wu G J, Kwok C-F, Chung K-H, 'The cytotoxicity of corrosion products of nitinol stent wire on cultured smooth muscle cells' *J Biomed Mater Res*, 2000 **52**(2), 395–403.

7 Shih C C, Shih C M, Chen Y L, Su Y Y, Shih J S, Kwok C F, Lin S J, 'Growth inhibition of cultured smooth muscle cells by corrosion products of 316 L stainless-steel wire' *J Biomed Mater Res*, 2001 **57**(2), 200–7.

8 Wataha J C, O'Dell N L, Singh B B, Ghazi M, Whitford G M, Lockwood P E, 'Relating nickel-induced tissue inflammation to nickel release in vivo' *J Biomed Mater Res*, 2001 **58**(5), 537–44.

9 Shih C-C, Lin S-J, Chung K-H, Chen Y-L, Su Y-Y, 'Increased corrosion resistance of stent materials by converting current surface film of polycrystalline oxide into amorphous oxide' *J Biomed Mater Res*, 2000 **52**(2), 323–32.

10 Chan C-M, Trigwell S, Duerig T, 'Oxidation of an NiTi alloy' *Surf Interface Anal*, 1990 **15**(6), 349–54.

11 Shabalovskaya S A, Anderegg J, Laab F, Thiel P A, Rondelli G, 'Surface conditions of Nitinol wires, tubing, and as-cast alloys. The effect of chemical etching, aging in boiling water, and heat treatment' *J Biomed Mater Res B Appl Biomater*, 2003 **65**(1), 193–203.

12 Wever D J, Veldhuizen A G, Sanders M M, Schakenraad J M, van Horn J R, 'Cytotoxic, allergic and genotoxic activity of a nickel–titanium alloy' *Biomaterials*, 1997 **18**(16), 1115–20.

13 Peitsch T, Klocke A, Kahl-Nieke B, Prymak O, Epple M, 'The release of nickel from orthodontic NiTi wires is increased by dynamic mechanical loading but not constrained by surface nitridation' *J Biomed Mater Res A*, 2007 **82A**(3), 731–9.

14 Klein E J, 'Apparatus and method for polishing lumenal prostheses' Localmed Inc. (Palo Alto CA), 1998, **US 556341**.

15 Trigwell S, Hayden R D, Nelson K F, Selvaduray G, 'Effects of surface treatment on the surface chemistry of NiTi alloy for biomedical applications' *Surf Interface Anal*, 1998 **26**(7), 483–9.

16 Shabalovskaya S, Rondelli G, Anderegg J, Xiong J P, Wu M, 'Comparative corrosion performance of black oxide, sandblasted, and fine-drawn nitinol wires in potentiodynamic and potentiostatic tests: Effects of chemical etching and electropolishing' *J Biomed Mater Res*, 2004 **69B**(2), 223–31.

17 Es-Souni M, Es-Souni M, Fischer-Brandies H, 'On the properties of two binary NiTi shape memory alloys. Effects of surface finish on the corrosion behaviour and in vitro biocompatibility' *Biomaterials*, 2002 **23**(14), 2887–94.

18 Zhao H, van Humbeeck J, de Scheerder I, 'Surface conditioning of nickel–titanium alloy stents for improving biocompatibility' *Surf Eng*, 2001 **17**(6), 451–8.
19 Shabalovskaya S A, 'Surface, corrosion and biocompatibility aspects of Nitinol as an implant material' *Biomed Mater Eng*, 2002 **12**(1), 69–109.
20 Thierry B, Tabrizian M, Savadogo O, Yahia L, 'Effects of sterilization processes on NiTi alloy: surface characterization' *J Biomed Mater Res*, 2000 **49**(1), 88–98.
21 Cissé O, Savadogo O, Wu M, Yahia L H, 'Effect of surface treatment of NiTi alloy on its corrosion behaviour in Hanks' solution' *J Biomed Mater Res*, 2002 **61**(3), 339–45.
22 Bruce G P, 'Susceptibility of nitinol to localized corrosion' *J Biomed Mater Res A*, 2006 **77A**(1), 185–91.
23 Miao W D, Mi X J, Zhu M, Guo J F, Kou Y M, 'Effect of surface preparation on mechanical properties of a NiTi alloy' *Mater Sci Forum*, 2002 **394–395**, 173–6.
24 Schubert H, Berova N, Hegyi E, Jirasek L, Kohanka V, Korossy S, Michailov P, Nebenführer L, Prater, 'Epidemiology of nickel allergy' *Contact Derm*, 1987 **16**, 122–8.
25 Dalmau L B, 'Immunological mechanism of delayed hypersensitivity to nickel compounds' *Quintessence Int*, 1984 **15**, 559–61.
26 Costa M, 'Molecular mechanisms of nickel carcinogenesis' *Annu Rev Pharmacol Toxicol*, 1991 **31**, 321–37.
27 Lu H, Shi X, Costa M, Huang C, 'Carcinogenic effect of nickel compounds' *Mol Cell Biochem*, 2005 **279**(1), 45–67.
28 Clarke B, Carroll W, Rochev Y, Hynes M, Bradley D, Plumley D, 'Influence of nitinol wire surface treatment on oxide thickness and composition and its subsequent effect on corrosion resistance and nickel ion release' *J Biomed Mater Res A*, 2006 **79A**(1), 61–70.
29 Espinós J P, Fernández A, González-Elipe A R, 'Oxidation and diffusion processes in nickel–titanium oxide systems' *Surf Sci*, 1993 **295**(3), 402–10.
30 Danilov A, Tuukkanen T, Tuukkanen J, Jämsä T, 'Biocompatibility-related surface characteristics of oxidized NiTi' *J Biomed Mater Res A*, 2007 **82A**(4), 810–19.
31 Mercier O, Melton K N, Gremaud G, Hägi J, 'Single-crystal elastic constants of the equiatomic NiTi alloy near the martensitic transformation' *J Appl Phys*, 1980 **51**(3), 1833–4.
32 Shabalovskaya S A, 'Physicochemical and biological aspects of Nitinol as a biomaterial' *Int Mater Rev*, 2001 **46**(5), 233–50.
33 Trépanier C, Tabrizian M, Yahia L H, Bilodeau L, Piron D L, 'Effect of modification of oxide layer on NiTi stent corrosion resistance' *J Biomed Mater Res*, 1998 **43**(4), 433–40.
34 Shabalovskaya S, Rondelli G, Anderegg J, Simpson B, Budko S, 'Effect of chemical etching and aging in boiling water on the corrosion resistance of Nitinol wires with black oxide resulting from manufacturing process' *J Biomed Mater Res B Appl Biomater*, 2003 **66**(1), 331–40.
35 Plant S D, Grant D M, Leach L, 'Behaviour of human endothelial cells on surface modified NiTi alloy' *Biomaterials*, 2005 **26**(26), 5359–67.
36 Plant S, Leach L, Grant D M, 'Behaviour of endothelial cells on surface modified NiTi'. In: *7th World Biomaterials Congress*. 2004. Sydney, Australia.
37 Michiardi A, Aparicio C, Planell J A, Gil F J, 'New oxidation treatment of NiTi shape memory alloys to obtain Ni-free surfaces and to improve biocompatibility' *J Biomed Mater Res B Appl Biomater*, 2006 **77B**(2), 249–56.
38 Cui Z D, Man H C, Yang X J, 'The corrosion and nickel release behavior of laser surface-melted NiTi shape memory alloy in Hanks' solution' *Surf Coat Technol*, 2005 **192**(2–3), 347–53.

39 Villermaux F, Tabrizian M, Yahia L H, Meunier M, Piron D L, 'Excimer laser treatment of NiTi shape memory alloy biomaterials' *Appl Surf Sci*, 1997 **109–110**, 62–66.

40 Meisner L L, Lotkov A I, Psachje S G, Barmina E G, Rotshtein V P, Karlik K V, Markov A B, 'Effect of the pulsed electron beam melting on a chemical composition and surface layer microstructure of the TiNi alloy'. In: *7th International Conference on Modification of Materials with Particle Beams and Plasma Flows*. 2004. Tomsk, Russia.

41 Meisner L L, Lotkov A I, Sivokha V P, Rotshtein V P, Barmina E G, Girjakova Y L, 'Structural-phase condition, unelastic and plastic behavior and nanohardness of the TiNi surface layers modified by an ion- and electron irradiation' *Mater Sci Eng A*, 2006 **438–440**, 558–62.

42 Wälivaara B, Lundström I, Tengvall P, 'An in-vitro study of H_2O_2-treated titanium surfaces in contact with blood plasma and a simulated body fluid' *Clin Mater*, 1993 **12**(3), 141–8.

43 Wälivaara B, Aronsson B-O, Rodahl M, Lausmaa J, Tengvall P, 'Titanium with different oxides: in vitro studies of protein adsorption and contact activation' *Biomaterials*, 1994 **15**(10), 827–34.

44 Shabalovskaya S A, Anderegg J W, 'Surface spectroscopic characterization of TiNi nearly equiatomic shape memory alloys for implants' *J Vac Sci Technol A*, 1995 **13**(5), 2624–32.

45 Choi J, Bogdanski D, Köller M, Esenwein S A, Müller D, Muhr G, Epple M, 'Calcium phosphate coating of nickel–titanium shape-memory alloys. Coating procedure and adherence of leukocytes and platelets' *Biomaterials*, 2003 **24**, 3689–96.

46 Bogdanski D, Esenwein S A, Prymak O, Epple M, Muhr G, Köller M, 'Inhibition of PMN apoptosis after adherence to dip-coated calcium phosphate surfaces on a NiTi shape memory alloy' *Biomaterials*, 2004 **25**(19), 4627–32.

47 ASTM International, 'ASTM F86-04 Standard practice for surface preparation and marking of metallic surgical implants', *Annual book of ASTM standards*, ASTM, Philadelphia, 1996.

48 Tepe G, Schmehl J, Wendel H P, Schaffner S, Heller S, Gianotti M, Claussen C D, Duda S H, 'Reduced thrombogenicity of nitinol stents – in vitro evaluation of different surface modifications and coatings' *Biomaterials*, 2006 **27**(4), 643–50.

49 Mändl S, Sader R, Thorwarth G, Krause D, Zeilhofer H-F, Horch H H, Rauschenbach B, 'Investigation on plasma immersion ion implantation treated medical implants' *Biomol Eng*, 2002 **19**(2–6), 129–32.

50 Poon R W Y, Liu X Y, Chung J C Y, Yeung K W K, Lu W W, Cheung K M C, Chu P K, 'Corrosion resistance of NiTi after nitrogen, oxygen, and hydrogen plasma immersion ion implantation'. In: *6th World Biomaterials Congress*. 2004. Sydney, Australia.

51 Maitz M F, Shevchenko N, 'Plasma immersion ion implanted nitinol surface with depressed nickel concentration for implants in blood' *J Biomed Mater Res A*, 2005 **76A**(2), 356–65.

52 Yankov R A, Shevchenko N, Rogozin A, Maitz M F, Richter E, Möller W, Donchev A, Schütze M, 'Reactive plasma immersion ion implantation for surface passivation' *Surf Coat Technol*, 2007 **201**, 6752–8.

53 Poon R W Y, Ho J P Y, Liu X, Chung C Y, Chu P K, Yeung K W K, Lu W W, Cheung K M C, 'Anti-corrosion performance of oxidized and oxygen plasma-implanted NiTi alloys' *Mater Sci Eng A*, 2005 **390**(1–2), 444–51.

54 Cheng Y, Wei C, Gan K Y, Zhao L C, 'Surface modification of TiNi alloy through tantalum immersion ion implantation' *Surf Coat Technol*, 2004 **176**(2), 261–5.

55 Starosvetsky D, Gotman I, 'TiN coating improves the corrosion behavior of superelastic NiTi surgical alloy' *Surf Coat Technol*, 2001 **148**, 268–76.
56 Shenhar A, Gotman I, Radin S, Ducheyne P, Gutmanas E Y, 'Titanium nitride coatings on surgical titanium alloys produced by a powder immersion reaction assisted coating method: residual stresses and fretting behavior' *Surf Coat Technol*, 2000 **126**, 210–8.
57 Endo K, Sachdeva R, Araki Y, Ohno H, 'Effects of titanium nitride coatings on surface and corrosion characteristics of Ni–Ti alloy' *Dent Mater J*, 1994 **13**(2), 228–39.
58 Liu X M, Wu S L, Chan Y L, Chu P K, Chung C Y, Chu C L, Yeung K W K, Lu W W, Cheung K M C, Luk K D K, 'Surface characteristics, biocompatibility, and mechanical properties of nickel–titanium plasma-implanted with nitrogen at different implantation voltages' *J Biomed Mater Res A*, 2007 **82A**(2), 469–78.
59 Shevchenko N, Pham M-T, Maitz M F, 'Studies of surface modified NiTi alloy' *Appl Surf Sci*, 2004 **235**(1–2), 126–31.
60 Cheng Y, Zheng Y F, 'Effect of N_2/Ar gas flow ratio on the deposition of TiN/Ti coatings on NiTi shape memory alloy by PIIID' *Mater Lett*, 2006 **60**(17–18), 2243–47.
61 Samuneva B, Kozhukharov V, Trapalis C, Kranold R, 'Sol–gel processing of titanium-containing thin coatings. Part I. Preparation and structure' *J Mater Sci*, 1993 **28**(9), 2353–60.
62 Liu J-X, Yang D-Z, Shi F, Cai Y-J, 'Sol–gel deposited TiO_2 film on NiTi surgical alloy for biocompatibility improvement' *Thin Solid Films*, 2003 **429**(1–2), 225–30.
63 Dislich H, Hussmann E, 'Amorphous and crystalline dip coatings obtained from organometallic solutions: Procedures, chemical processes and products' *Thin Solid Films*, 1981 **77**(1–3), 129–40.
64 Polonchuk L, Elbel J, Eckert L, Blum J, Wintermantel E, Eppenberger H M, 'Titanium dioxide ceramics control the differentiated phenotype of cardiac muscle cells in culture' *Biomaterials*, 2000 **21**(6), 539–50.
65 Peltola T, Patsi M, Rahiala H, Kangasniemi I, Yli-Urpo A, 'Calcium phosphate induction by sol–gel-derived titania coatings on titanium substrates in vitro' *J Biomed Mater Res*, 1998 **41**(3), 504–10.
66 Liu X, Chu P K, Ding C, 'Surface modification of titanium, titanium alloys, and related materials for biomedical applications' *Mater Sci Eng R*, 2004 **47**(3–4), 49–121.
67 Pätsi M E, Hautaniemi J A, Rahiala H M, Peltola T O, Kangasniemi I M O, 'Bonding strengths of titania sol–gel derived coatings on titanium' *J Sol-Gel Sci Technol*, 1998 **11**(1), 55–66.
68 Hautaniemi J A, Juhanoja J T, Herø H, 'Porcelain bonding on Ti: Its dependence on surface roughness, firing time and vacuum level' *Surf Interface Anal*, 1993 **20**(5), 421–26.
69 Kim H M, Miyaji F, Kokubo T, Nakamura T, 'Preparation of bioactive Ti and its alloys via simple chemical surface treatment' *J Biomed Mater Res*, 1996 **32**(3), 409–17.
70 Li P, Ohtsuki C, Kokubo T, Nakanishi K, Soga N, de Groot K, 'The role of hydrated silica, titania, and alumina in inducing apatite on implants' *J Biomed Mater Res*, 1994 **28**(1), 7–15.
71 Gu Y W, Tay B Y, Lim C S, Yong M S, 'Biomimetic deposition of apatite coating on surface-modified NiTi alloy' *Biomaterials*, 2005 **26**(34), 6916–23.
72 Wever D J, Veldhuizen A G, de Vries J, Busscher H J, Uges D R, van Horn J R, 'Electrochemical and surface characterization of a nickel–titanium alloy' *Biomaterials*, 1998 **19**(7–9), 761–9.
73 Chu P K, 'Enhancement of surface properties of biomaterials using plasma-based technologies' *Surf Coat Technol*, 2007 **201**(19–20), 8076–82.

74 Sui J H, Cai W, 'Effect of diamond-like carbon (DLC) on the properties of the NiTi alloys' *Diam Rel Mater*, 2006 **15**(10), 1720–26.
75 Chu P K, 'Plasma surface treatment of artificial orthopedic and cardiovascular biomaterials' *Surf Coat Techn*, 2007 **201**(9–11), 5601–6.
76 Poon R W Y, Yeung K W K, Liu X Y, Chu P K, Chung C Y, Lu W W, Cheung K M C, Chan D, 'Carbon plasma immersion ion implantation of nickel–titanium shape memory alloys' *Biomaterials*, 2005 **26**(15), 2265–72.
77 Barragan P, Herbst F, Kalachev A, Nader W F, Roquebert P O, Silvestri M, Siméoni J B, 'The BioDiamond and BioDiamond F stents'. In: Serruys P W, Kutryk M J B (eds), *Handbook of coronary stents*, 3 edn., Dunitz, London, 2000, pp. 29–39
78 Colombo A, Stankovic G, Moses J W, 'Selection of coronary stents' *J Am Coll Cardiol*, 2002 **40**(6), 1021–33.
79 Antoniucci D, Bartorelli A, Valenti R, Montorsi P, Santoro G M, Fabbiocchi F, Bolognese L, Loaldi A, Trapani M, Trabattoni D, Moschi G, Galli S, 'Clinical and angiographic outcome after coronary arterial stenting with the carbostent' *Am J Cardiol*, 2000 **85**(7), 821–5.
80 Chen J Y, Wang L P, Fu K Y, Huang N, Leng Y, Leng Y X, Yang P, Wang J, Wan G J, Sun H, Tian X B, Chu P K, 'Blood compatibility and sp^3/sp^2 contents of diamond-like carbon (DLC) synthesized by plasma immersion ion implantation–deposition' *Surf Coat Technol*, 2002 **156**(1–3), 289–94.
81 Kwok S C H, Yang P, Wang J, Liu X, Chu P K, 'Hemocompatibility of nitrogen-doped, hydrogen-free diamond-like carbon prepared by nitrogen plasma immersion ion implantation–deposition' *J Biomed Mater Res*, 2004 **70A**(1), 107–14.
82 Yang P, Huang N, Leng Y X, Yao Z Q, Zhou H F, Maitz M, Leng Y, Chu P K, 'Wettability and biocompatibility of nitrogen-doped hydrogenated amorphous carbon films: Effect of nitrogen' *Nucl Instrum Methods Phys Res B*, 2006 **242**, 22–5.
83 Okpalugo T I T, Murphy H, Ogwu A A, Abbas G, Ray S C, Maguire P D, McLaughlin J, McCullough R W, 'Human microvascular endothelial cellular interaction with atomic N-doped DLC compared with Si-doped DLC thin films' *J Biomed Mater Res B Appl Biomater*, 2006 **78B**(2), 222–9.
84 Davis C A, Amaratunga G A J, Knowles K M, 'Growth mechanism and cross-sectional structure of tetrahedral amorphous carbon thin films' *Phys Rev Lett*, 1998 **80**(15), 3280.
85 Vinnichenko M, Gago R, Huang N, Leng Y X, Sun H, Kreissig U, Kulish M P, Maitz M F, 'Spectroscopic ellipsometry investigation of amorphous carbon films with different sp3 content: relation with protein adsorption' *Thin Solid Films*, 2004 **455–456C**, 530–4.
86 Villermaux F, Tabrizian M, Yahia L, Czeremuszkin G, Piron D L, 'Corrosion resistance improvement of NiTi osteosynthesis staples by plasma polymerized tetrafluoroethylene coating' *Biomed Mater Eng*, 1996 **6**(4), 241–54.
87 Yang M-R, Wu S K, 'DC plasma-polymerized hexamethyldisilazane coatings of an equiatomic TiNi shape memory alloy' *Surf Coat Technol*, 2000 **127**(2–3), 273–80.
88 Clerc C O, Miller K M, 'Method of manufacturing a covered stent', 2005, **US20050255230**.
89 Trigwell S, De S, Sharma R, Mazumder M K, Mehta J L, 'Structural evaluation of radially expandable cardiovascular stents encased in a polyurethane film' *J Biomed Mater Res B Appl Biomater*, 2006 **76B**(2), 241–50.
90 Mazumder M M, De S, Trigwell S, Ali N, Mazumder M K, Mehta J L, 'Corrosion resistance of polyurethane-coated nitinol cardiovascular stents' *J Biomater Sci Polym Ed*, 2003 **14**(12), 1351–62.
91 Kondyurin A, Romanova V, Begishev V, Kondyurina I, Guenzel R, Maitz M F,

'Crosslinked polyurethane coating on vascular stents for enhanced X-ray contrast' *J Bioact Compat Polym*, 2005 **20**(1), 77–93.

92 Kondyurin A, Klyachkin Y, 'Vibrational spectra of some diisocyanates in the liquid state or on EPDM-40 rubber surface' *J Appl Polym Sci*, 1994 **54**(10), 1385–93.

93 Yang J, Wang J, Tong S, 'Surface properties of bio-implant Nitinol modified by ECR cold plasma' *Mater Sci Technol*, 2004 **20**(11), 1427–30.

94 Cao L, Chang M, Lee C-Y, Castner D G, Sukavaneshvar S, Ratner B D, Horbett T A, 'Plasma-deposited tetraglyme surfaces greatly reduce total blood protein adsorption, contact activation, platelet adhesion, platelet procoagulant activity, and *in vitro* thrombus deposition' *J Biomed Mater Res A*, 2007 **81A**(4), 827–37.

95 Schellhammer F, Walter M, Berlis A, Bloss H G, Wellens E, Schumacher M, 'Polyethylene terephthalate and polyurethane coatings for endovascular stents: preliminary results in canine experimental arteriovenous fistulas' *Radiology*, 1999 **211**(1), 169–75.

96 Cejna M, Virmani R, Jones R, Bergmeister H, Losert U, Xu Z, Yang P, Schoder M, Lammer J, 'Biocompatibility and performance of the Wallstent and several covered stents in a sheep iliac artery model' *J Vasc Interv Radiol*, 2001 **12**(3), 351–8.

97 Werner C, Maitz M F, Sperling C, 'Current strategies towards hemocompatible coatings' *J Mater Chem*, 2007 **17**, 3376–84.

98 Thierry B, Merhi Y, Silver J, Tabrizian M, 'Biodegradable membrane-covered stent from chitosan-based polymers' *J Biomed Mater Res A*, 2005 **75A**(3), 556–66.

99 Kidane A G, Salacinski H, Tiwari A, Bruckdorfer K R, Seifalian A M, 'Anticoagulant and antiplatelet agents: their clinical and device application(s) together with usages to engineer surfaces' *Biomacromolecules*, 2004 **5**(3), 798–813.

100 Andersson J, Sanchez J, Ekdahl K N, Elgue G, Nilsson B, Larsson R, 'Optimal heparin surface concentration and antithrombin binding capacity as evaluated with human non-anticoagulated blood in vitro' *J Biomed Mater Res A*, 2003 **67**(2), 458–66.

101 Acharya G, Park K, 'Mechanisms of controlled drug release from drug-eluting stents' *Adv Drug Deliv Rev*, 2006 **58**(3), 387–401.

102 Ranade S V, Miller K M, Richard R E, Chan A K, Allen M J, Helmus M N, 'Physical characterization of controlled release of paclitaxel from the TAXUS™ Express²™ drug-eluting stent' *J Biomed Mater Res*, 2004 **71A**(4), 625–34.

103 Duda S H, Pusich B, Richter G, Landwehr P, Oliva V L, Tielbeek A, Wiesinger B, Hak J B, Tielemans H, Ziemer G, Cristea E, Lansky A, Bérégi J P, 'Sirolimus-eluting stents for the treatment of obstructive superficial femoral artery disease: six-month results' *Circulation*, 2002 **106**(12), 1505–9.

104 Sousa J E, Serruys P W, Costa M A, 'New frontiers in cardiology: drug-eluting stents: Part I' *Circulation*, 2003 **107**(17), 2274–9.

105 Sousa J E, Serruys P W, Costa M A, 'New frontiers in cardiology: drug-eluting stents: Part II' *Circulation*, 2003 **107**(18), 2383–9.

106 Shulze J E, Betts R E, Savage D R, 'Drug-delivery endovascular stent and method for treating restenosis' Ltd S B, 2004, **US20040030380**.

107 Tepe G, Muschick P, Laule M, Reddig F, Claussen C D, Dinkelborg L M, Tielemans H, Wehrmann M, Duda S H, 'Prevention of carotid artery restenosis after sirolimus-coated stent implantation in pigs' *Stroke*, 2006 **37**(2), 492–4.

108 Thierry B, Tabrizian M, Trepanier C, Savadogo O, Yahia L, 'Effect of surface treatment and sterilization processes on the corrosion behavior of NiTi shape memory alloy' *J Biomed Mater Res*, 2000 **51**(4), 685–93.

9

Biocompatibility of Nitinol for biomedical applications

S. SHABALOVSKAYA
Ames Laboratory, USA

J. VAN HUMBEECK
Katholieke University Leuven, Belgium

Abstract: Recent studies on the biocompatibility of dense and porous Nitinol (Ti–Ni) *in vitro* and *in vivo* are reviewed and the biological status of this biomaterial is evaluated. The evolution of our knowledge and understanding of the biological aspects is emphasized and both Nitinol's strong attributes and its deficits are pointed out. Nickel release and cell responses are analysed, and the mechanisms of Ni accumulation in the surface sublayers along with its low-temperature diffusion to the interfaces are addressed. Plasma protein adsorption and platelet adhesion pertinent to Nitinol thrombogenicity are analysed and the comparative biocompatibility of modified Nitinol surfaces is discussed. An analysis of performances of self-expanding implant devices is presented and the problem with Nitinol debris is addressed. This chapter will be of interest for both academic and industrial use.

Key words: Nitinol, Ti–Ni alloys, biocompatibility, nickel release, superelastic stents, bone implant, Ni–Ti.

9.1 Introduction

Nitinol, a group of nearly equiatomic, Ti–Ni alloys is widely recognized and accepted for medical use. Nitinol's shape memory, superelasticity, and high-wear resistance have allowed novel instrumentation and implants to be designed in surgery fields ranging from orthopaedics to vascular interventions. The excellent malleability and ductility of Nitinol allow it to be manufactured in the form of wires, ribbons, tubes, sheets, or bars, thereby providing a wide spectrum of opportunities for medical applications. For example, the biomaterial has been shown to be suitable not only for minimally invasive procedures, which are often performed in out-patient clinics, but also on patients whose health and age status will not allow for major 'open' surgeries. Additionally, Nitinol is known to be appropriate for treatment of younger populations, especially children with congenital defects. Although Nitinol has been in use for more than 40 years, important features continue to be discovered as scientists try to grasp its complexity.

The following chapter provides an overview of the literature on Nitinol biocompatibility *in vitro* and *in vivo*. Our primary goal is to present a comprehensive picture of the current biological status of this biomaterial – emphasizing the evolution of our knowledge and understanding of biological aspects, while pointing out Nitinol's strong attributes as well as its deficits. This chapter, while grounded in biocompatibility, not only explores the central issue of Ni release and cell responses, but also addresses the mechanisms of Ni accumulation in surface sublayers along with its diffusion to the interfaces, particularly at low temperatures. We will analyze *in vitro* plasma protein adsorption and platelet adhesion pertinent to Nitinol thrombogenicity and touch on the biocompatibility of modified Nitinol surfaces in order to understand whether there is any improvement in the biological responses. From analysis of the literature, we will demonstrate the progress achieved in the biological performances of self-expanding implant devices, pinpoint problems that are still looking for solutions, analyze the implant/living tissues interfaces for porous and nonporous materials, and discuss potential problems with Nitinol debris. The systematic presentation of material in this chapter should be of interest to both researchers and students of biomaterial science as well as to the developers of material and implant devices

9.2 Biomechanical compatibility

Biocompatibility is defined as the ability of a material to perform with an appropriate host response in a specific application (Williams, 1987). An important aspect of the biocompatibility of implant devices is their ability to perform desirable functions in close contact with body tissues. For a long time, knowledge of the regularities in the physico-mechanical behaviour of living tissues did not significantly influence the selection or design of metallic materials for implantation. The major criteria for traditional medical alloys were high strength and corrosion resistance. The higher the elastic modulus of an implant material, however, the higher the stress level exerted onto a bone. Thus, good mechanical compatibility required carefully matching an implant's elastic modulus to that of the elastic modulus of a specific bone. The elastic modulus of cortical bone is 15–30 GPa, while that of cancellous bone is 0.1–1.5 GPa (Cooke, 1996). Nitinol has a low elastic modulus that, in the presence of porous material, can be reduced to even lower values (0.1–1.5 GPa), thereby making it a suitable match for either bone type (Assad, 2003a).

Another approach to the design of biomaterials, which is based on a concept of biomechanical compatibility, is rooted in the knowledge of the mechanical behaviour of body tissues (Fung, 1991, Gunther, 2000). A functional (i.e., smart) implant material should be similar in its mechanical behaviour to that of living tissue. Living tissues are complex structures, which are known to exhibit both viscous and elastic characteristics. When body tissues are strained and the strain remains constant, the corresponding stresses decrease with time; this phenomenon is called

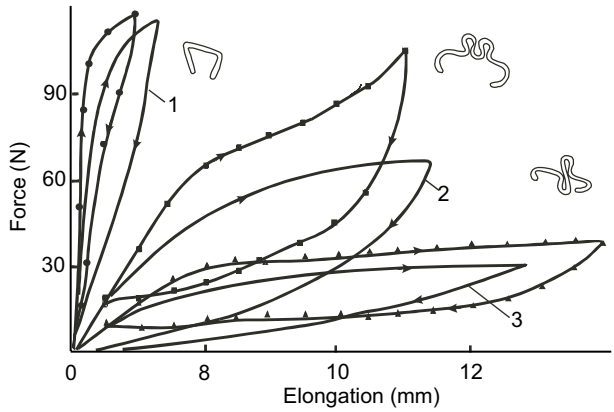

9.1 The mechanical behaviour of living tissues. Smooth curves: 1 cortical bone, 2 interspinal ligament, 3 fibrous tissue. The curves with the experimental points correspond to various superelastic Ti–Ni constructs (reproduced with the permission from the authors, Itin 2006).

stress relaxation. If a body is stressed, however, and the stress is kept constant, the body continues to deform to relieve the stress; this phenomenon is called creep. If body tissues are subjected to cyclic loading, the stress–strain relationship in the loading process is different from that in the unloading stage; this is called hysteresis. Relaxation, creep, and hysteresis, known collectively as viscoelasticity, are found in many body tissues (Fung, 1991, Saraf, 2006). Thus, biomechanical compatibility is achieved when an implant is elastic; has a stress–strain diagram close to that of a corresponding living tissue; and exhibits a similar magnitude of hysteresis in the loading/unloading cycle (Fig. 9.1).

9.3 Comparative metal toxicity

An appropriate response to a biomaterial is one that is non-toxic, non-allergenic, and non-carcinogenic. Toxicity is generally manifested by the release, through dissolution, of chemical constituents from the material. In the case of Nitinol, which is composed of approximately 56% Ni by weight, a potential release of Ni (acknowledged as a rather notorious metallic element, although essential to the human body) presents a major problem. Implants of pure Ni are known to be toxic and produce severe inflammatory reactions (Uo, 1999, Wataha, 2001). Ni dermatitis involving specific skin cells has been reported among industrial workers as well as in the general population. It is worth noting, however, that Co – one of the major constituents of Co-base medical alloys and of stainless steel (SS) – has a similar ability to cause contact dermatitis (Lacy, 1996). There are also reports indicating that allergic reactions can be triggered due to internal or oral exposure to Ni- or Co-containing implants, including the use of orthodontic brackets when

Ni sensitivity of the skin seems not to be involved (Lacy, 1996, Al-Waheidi, 1995). Analysis of comparative metal toxicity indicates that a toxic Ni effect on osteoblast and fibroblast cells is either similar to, or less than, that of the major components of stainless steel: Fe, Co, and Cr (Okazaki, 1998). Although both Ni and Ti are on the list of known carcinogens, which also includes Co, Cr, and Fe (Sunderman, 1984, Michel, 1987), neither mutagenic or carcinogenic effects have been reported so far for Ti–Ni. The importance of Ni to everyday life is also well documented (Shabalovskaya, 1996). The Ni-containing proteins (nickeloplasmin) were isolated from human and rabbit serum (Sunderman, 1984). Human blood serum typically contains 1–6 $\mu g\, L^{-1}$ of Ni based on different estimates (Assad, 2003b).

Titanium, on the other hand, has a good reputation as an implant material. The naturally formed surface oxide film, titanium dioxide or titania (TiO_2) is inert in the human body, prevents metal release from implants, and inhibits electron exchange on the implant–tissue interface. Once dissolved, however, Ti can induce the release of potentially osteolytic cytokins that are involved in implant loosening (Wang, 1996). The histology of tissue reactions has also been interpreted against pure Ti implants (Riede, 1974). Depending on the surface finish, Ti specimens could induce significant suppression of rat lymphocytes (Shabalovskaya, 1996) and stimulate fibroblast proliferation (Ryhänen, 1997). Porous Ti provided a lower ingrowth of bone tissue into the body of implants and lower bone apposition (Itin, 1996) compared with Ti–Ni (Versaigne, 1998). Implants made of pure Ti and its alloys are not suitable for *in vivo* bearing applications because of their low wear resistance. Additionally, Ti is not on the list of elements essential to the human body.

The biological response to biomaterial is controlled largely by surface chemistry. Nitinol biocompatibility, however, relies not only on the protective layer of TiO_2 spontaneously formed on the material surface. The intermetallic nature Ti–Ni existing in a very low concentration window implies stronger interatomic bond compared with the alloys with wide concentration windows or unlimited solubility of alloy components like Cu–Zn, for instance. Appropriately passivated Nitinol surfaces have excellent corrosion resistance and very low, if any, Ni release (Shabalovskaya, 2004a, 2008a). The situation with Ni release from Nitinol, however, is not trivial. For this reason, its surface tendencies should be carefully studied to ensure safe long-term use in the human body.

9.4 Patterns of nickel release from Nitinol

Ni release is a central issue in Nitinol biocompatibility. Our understanding of the patterns of Ni release from Nitinol evolved significantly. Observations on Ti–Ni alloys prepared in laboratories (Ryhänen, 1997, Wever, 1998, Michiardi, 2006a) showed that Ni release from Nitinol might be higher than from SS during the first days of exposure to biological solutions, even though it dropped to almost undetectable levels after 10–14 days (Fig. 9.2, curve 1). Studies of Ni release from

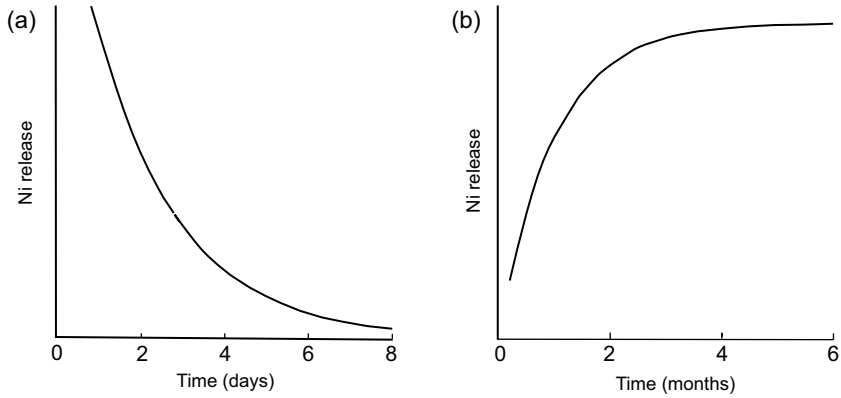

9.2 Schematic presentation of Ni release from (a) Ti–Ni alloys with none or low processing degrees and (b) from commercial materials.

commercial material, however, pointed at different patterns (curve 2), where an increase was noted at the beginning of exposure and its stabilization was observed only after a few months (Cisse, 2002, Kobayashi, 2005, Sui, 2006, Clarke, 2006). The amount of released Ni differed significantly (Clarke, 2006), pointing at the effects of processing, which is in agreement with variable Ni surface concentrations reported for Nitinol wires (0.4–15 at.%) (Shabalovskaya, 2003a). High-temperature treatments, which promote the formation of a thicker external TiO_2 layer, result in Ni accumulation in the internal surface layers. These buried layers can be easily activated due to surface damage.

Another avenue leading to accumulation of Ni in the surface can be surface treatment itself. Some of the techniques used for Ti–Ni coatings employ pre-treatment protocols, which aim at producing a thick TiO_2 layer similar to that grown on pure Ti. Thus, in the case of the deep immersion calcium phosphate (CaP) coating technique, involves soaking or boiling Nitinol in 30% hydrogen peroxide (H_2O_2), followed by a subsequent soaking for many hours in solutions of potassium hydroxide (KOH) or calcium hydroxide [$Ca(OH)_2$], at temperatures varying from 60 to 160 °C (Choi, 2003). These pre-treatments are then followed by further soaking in oversaturated phosphate solutions at the same temperatures. As Bogdanski (2005) showed, the resulting Ti–Ni surfaces caused high and lasting Ni release, exceeding by two to three orders of magnitude the Ni release from non-treated material (Fig. 9.3).

The Ni concentrations induced by these surfaces (5000–9000 ng mL^{-1}) fell in the range of lethal, as defined for endothelial cells by Wataha *et al.* (2004). Chemical analysis of Nitinol surfaces pre-treated according to the protocol already mentioned revealed two surface sublayers (Shabalovskaya, 2008a): (1) an external flake-like layer less than 1 μm in thickness enriched on Ti ($C_{35}Ti_{20}Ni_{12}O_{33}$), and (2) an internal smoother and denser sublayer highly enriched on Ni ($C_8Ti_{11}Ni_{58}O_{22}$). Strong Ti reactivity and the correct stoichiometry of dioxide ($Ti_{11}O_{22}$) imply that Ni

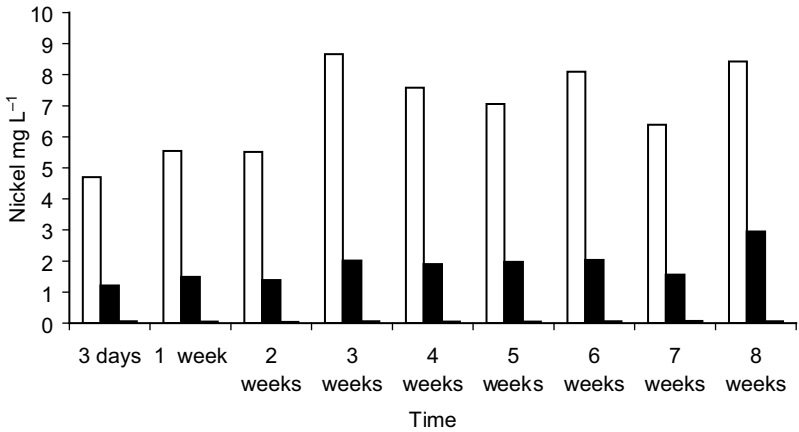

9.3 Ni release into PBS at pH 7.4 measured after exposure to Ti–Ni samples. From left to right: pre-treated for CaP deposition using etching in alkaline solution described in the text; finally CaP coated; as-received states. The lowest Ni release was detected for as-received samples, it dramatically increased after surface pre-treatment and reduced after CaP coating deposition (reprinted from the study of Bogdanski (2005) with the permission from the author).

is in an elemental state. This Ni can easily diffuse to the surface through the external porous Ti-enriched layer, as well as through the porous CaP layer that is deposited on top, and thus be released into biological environments.

In order to avoid undesirable effects from surface pre-treatments, the Ti–Ni surface should either be initially depleted of Ni, or oxidation itself must not be as aggressive, thereby allowing the simultaneous release of free Ni atoms as well as the gradual oxidation of Ti, rather than the simultaneous oxidation of both Ti and Ni. The temperatures in the 60–160 °C interval that are employed in various pre-treatment protocols for pure Ti are not high enough to expect significant atomic diffusion through vacancies. However, Ni atoms are liberated from the Ni–Ti interatomic bonds already at room temperature because a thin Ti-based oxide is formed spontaneously on Ti–Ni surface. These Ni atoms are lattice defect, interstitial atoms in the structure of the Ti-surface oxides. Besides, due to the shortage of O atoms, surface oxides are customarily non-stoichiometric. The sites of the missing O atoms present structural O vacancies. These O vacancies can be used by Ni atoms to migrate through the titanium oxides; thus, Ni diffusion can occur effectively already at low temperatures. Furthermore, the smaller size of Ni atoms (as compared with Ti and O atoms) also helps Ni diffusion through an interstitial path.

Metal release depends not only on the state of the surface, but also on the corrosive media, which the material is exposed. Thus, it has been shown that the amount of Ni released from Ti–Ni was three-fold higher in plasma compared with

that detected in phosphate-buffered saline (PBS) (Bogdanski, 2005), while in fibroblast culture medium Ni release was higher than in osteoblast culture medium (Ryhänen, 1997). Another factor to consider is the type of mechanical loading for Nitinol. For instance, the dynamic loading of orthodontic superelastic wire with a force similar to physiological situations caused a 40-fold increase in Ni release as compared with unloaded wires both in pure water and in saline solutions (Peitsch, 2007). Ni release should also increase owing to deterioration of the corrosion resistance of modified surfaces under strain as observed by Heßing *et al*. (2007). For the reasons mentioned above, an elimination of Ni release achieved upon coating or surface modifications in a strain-free Nitinol state, cannot be automatically expected in a strained state.

9.5 Response of cells to Ni release

It is inevitable that implant surfaces in the body degrade over time and that is why it is important to know the biological effects of various non-toxic Ni concentrations induced by the material. Table 9.1 summarizes the results from an analysis of the effects of various Ni concentrations on different animal and human cells; the corresponding results for SS corrosion products (Morais, 1998) are presented for comparison. Ni concentrations in the 0–11 $\mu g\,L^{-1}$ range induced anywhere from 0 to 25–30% either stimulation or suppression, depending on the type of cells involved [e.g., peripheral blood mononuclear cells (PBMCs), smooth muscle cells (SMCs), or human vascular endothelial cells (HMVECs)]. It follows from the findings of Ryhänen *et al.* (1997) that fibroblast and osteoblast proliferation were almost similar for the Ti, Ti–Ni, SS, and control (no metal) groups when Ni content in the media dropped from an initial level of 130 to 5 $\mu g\,L^{-1}$ on the 10th day of exposure of cells to metals.

A toxic effect of the Ni concentration (0–11 $\mu g\,L^{-1}$) on HMVEC is illustrated in Fig. 9.4 (Shabalovskaya, 2004a). The corresponding Ti and Ni surface concentrations together with the Ni release induced into the medium for HMVEC are presented in Table 9.2. One can see that the Ni surface concentrations in the range of 0–6.7% caused no or ~30% cell suppression with maximal suppression induced by chemically etched (CE) and mechanically polished (MP) samples.

It has been reported that the response of SMCs is dose- and time-sensitive and concentration of Ni of 150 $\mu g\,L^{-1}$ suppressed SMC proliferation by 70% (Shih, 2000). A severe suppression of PBMC proliferation (97%) – consistent with the death of almost all cells – was observed in a 1080–4700 $\mu g\,L^{-1}$ interval of Ni concentrations. As shown in Table 9.1, a concentration of SS corrosion products of a similar order of magnitude (~8800 $\mu g\,L^{-1}$) induced the equivalent suppression. Although Table 9.1 focuses on the chemical toxicity of Ni, it should be stressed that differences in factors such as surface morphology, texture, stress, and roughness also contributed to the biological effects listed above (Ponsonnet, 2003). As stated earlier in this chapter, the Ni concentration in human blood serum is 1–6 $\mu g\,L^{-1}$

Table 9.1 The responses of cells to various concentrations of nickel released from Ti–Ni and to the corrosion products from stainless steel (SS)

SS corrosion products ($\mu g\ L^{-1}$)	Rat bone marrow (1)	Ni released from NiTi ($\mu g\ L^{-1}$)	Fibro/ osteo-blast (2)	PBMC (3)	SMC rat (4)	EC human (3)	Cytokine secretion (5)
8.8×10^1	N*	0–11		~25% St* Human	N–25% Sp*	N–30% Sp	
		5–130	N				
8.8×10^2	Impaired	150			70% Sp		
		400		~25% St Rat			
		460–1000					30% Secretion IL 1b TNF-α
		1080		40–97% Sp Human			
		4700		97% Sp Rat			
8.8×10^3	Death	7.2×10^3					30% Monocyte St
		20×10^3					ICAM Expression HMVEC

*N – normal response, St – stimulation, Sp – suppression. The numbers indicate references: 1 – (Morais 1998), 2 – (Ryhänen 1997), 3 – (Shabalovskaya 2004a), 4 – (Shih 2000), 5 – (Wataha 1999).

Table 9.2 Ni and Ti concentrations (at. %) on the surfaces of Nitinol and pure Ni and Ti samples obtained using XPS analysis for a 20° surface sensitive electron escape angle; Ni concentrations (ng/mL/cm^2) in biological medium for HMVEC found after exposure to corresponding metal samples with various surface treatments

Sample	Surface treatment								
	Mp 600	Mp	Ep2	Ep1	Ce	CeWb	MpHt 600	CeWbHt	Pure metal
Ti (at.%)	5.7	10.3	13	15	15	16.1	18.9	21.6	1
Ni (at.%)	1.4	3.0	5.0	2.5	6.7	2.2	8.2	0.9	14.6
Ni release ($ng\ mL^{-1}\ cm^{-2}$)	6(1)*	–	7(1)	6(3)	11(3)	0(0)	–	1(1)	1080 (20)

*numbers in brackets are mean standard deviations (±).

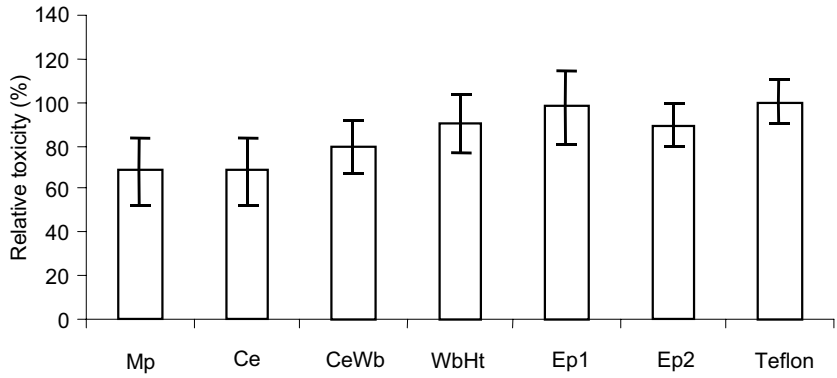

9.4 Cytotoxicity of Nitinol surfaces to human microvascular endothelial cells (HMVEC) based on mitochondrial succinic dehydrogenase (SDH) activity. SDH activity was expressed as a percentage of Teflon (negative control). Surface designations: Mp mechanically polished 600 grit-finish; Ce etched in $1HF+4HNO_3$ aqueous solution; CeWb additionally boiled in distilled water for 30 min; CeWbHt additional heat treatment at 520 °C for 15 min, mimicking shape setting procedure; Ep1 and Ep2 electropolished in austenite phase at room temperature and in martensite at T~ –45 °C, respectively. There is only a mild toxic effect observed for Mp (600 grit finish) and Ce samples (Shabalovskaya 2008a).

(Assad, 2003b), while in HMVECs it is 61 $\mu g\,L^{-1}$ (Shabalovskaya, 2004a). Based on these results, it can be concluded that Ni release less than 11 $\mu g\,L^{-1}$ may be considered non-toxic, or only moderately toxic, to human cells.

Successful attachment and proliferation of ECs and SMCs, which have been observed on thin Nitinol films even in the absence of plasma proteins (Menchaka, 2004), is also an indication of very low toxicity of the material. An interesting observation from this latter study was that HMVECs proliferated significantly faster than SMCs, which is beneficial as faster proliferation of ECs promotes endothelialization, but they migrated slower than SMCs. It was also noted that crystalline surfaces of thin films somehow promoted SMC migration, when compared with surfaces in the amorphous state.

The effect of heat treatments on the response of HMVECs has also been evaluated (Plant, 2005). It has been shown that mechanically polished and heat-treated (MpHt) surfaces increased endothelial permeability, resulting in reduced inertness of the epithelium. Oxidative stress levels of ECs varied, with the least damage (170%) caused by MpHt samples (600 °C) and the most damage (270%) caused by Mp samples, when compared with control gelatine (100%).

It is worth mentioning the effect of pure Ni samples. A significant variability in the response of human lymphocytes (i.e., PBMCs activated by concanavalin A), to toxic Ni concentrations of 1080 $\mu g\,L^{-1}$ was observed (Shabalovskaya, 2004a). Although Ni concentrations in the 0–11 $\mu g\,L^{-1}$ interval induced by various bare

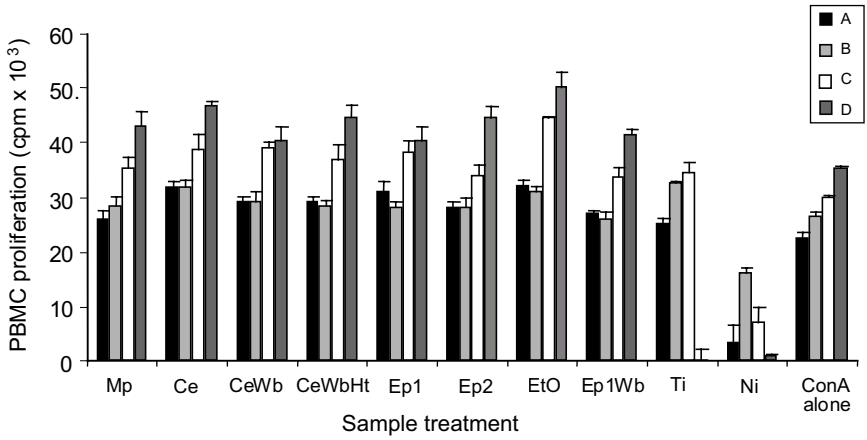

9.5 Proliferation of peripheral blood mononuclear cells (PBMC) activated by Concanavalin A and exposed for 72 h to Ti–Ni samples with various surface treatments, to pure Ti and pure Ni samples as compared with cells with no metal 'ConA alone'. Proliferation is expressed in counts per minute (Cpm). Sample designations are the same as in Fig. 9.4. 'EtO' corresponds to CeWb samples sterilized in ethylene oxide, Ep1Wb refers to Ep1 samples boiled in water for 30 min (Shabalovskaya 2004a).

Nitinol surfaces caused ~25% stimulation of PBMC, the Ni release from pure Ni samples significantly suppressed cell proliferation (Fig. 9.5). The level of suppression of cell proliferation varied among four donors within a 40–97% interval. This variability may be linked to the history of Ni exposure as well as to the donors' health states. For example, one human subject – whose lymphocytes proliferated quite successfully (with only 40% suppression) under conditions when the lymphocytes of other donors did not survive – rejected a dental bridge made of a Rexillium alloy containing 62% Ni. This bridge had been installed next to another metal filling, which caused galvanic corrosion and the sensation of current flow in the mouth. The exposure to this Ni-rich alloy induced inflammation of frenum tissue in the mouth, an approximately 7 mm lump in the breast glandular tissue, and pain and discomfort in the upper right abdominal area. After the bridge was removed, all symptoms gradually cleared and the lump dissolved. It is important to note that this subject did not have Ni skin sensitivity, but suffered chronic eczematous dermatitis that was activated with exposure to chemicals or stress. According to a study of Koster *et al.* (2000), eczematous skin conditions not only can provoke an allergic reaction to metals released from implants, but also may enhance the chances of stent restenosis. The same mechanism was perhaps involved in response to the Rexillium dental bridge; thus, excessive proliferation of lymphocyte under toxic conditions may be interpreted as a sign of an allergic reaction.

Ni release from porous Nitinol and its accumulation in the remote organs was

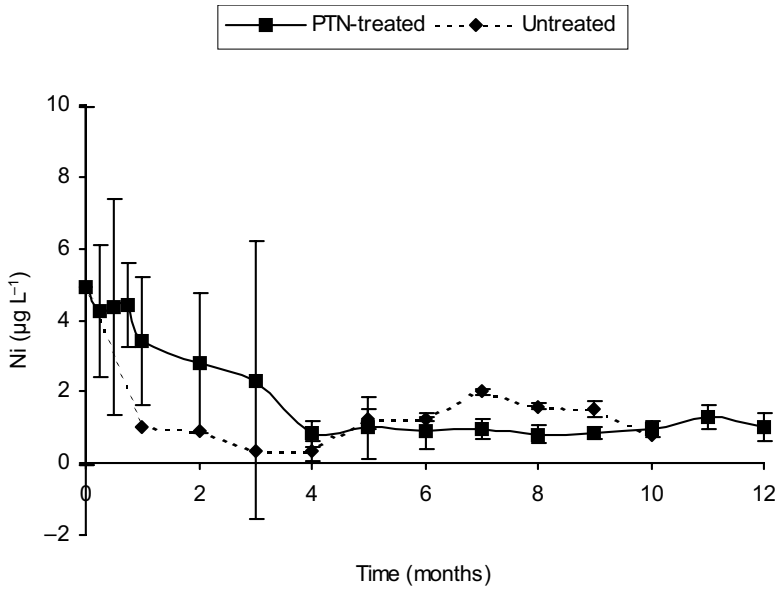

9.6 Nickel content in blood of sheep as a function of post-surgery recovery time after implantation of porous Nitinol (adapted from Assad *et al.* 2003b, Fig. 5; an original was generously provided by Biorthex Inc).

evaluated in an implantation study with sheep (Assad, 2003b). Following surgery, no significant increase in the blood Ni content was detected, when compared with the pre-operative level of 4.9 $\mu g\,L^{-1}$ (Fig. 9.6). Moreover, regardless of the postsurgical recovery time, Ni levels in the implant-adjacent tissues (muscle, nerves, spinal cord) of the remote and detoxification organs were similar for animals, with and without Nitinol implants (Fig. 9.7). These findings are in agreement with earlier implantation studies on dense material of Castleman (1976) and Ryhänan (1999), as well as with the low Ni release observed during a 12-month follow-up period reported for Amplatzer occluders (Ries, 2003). The low Ni release from Ti–Ni *in vivo* is in agreement with low corrosion rates, which dropped from 0.001 to 0.0001 mm/year during one year of implantation, thereby suggesting surface passivation in the body (Lu, 1990).

Finally, it is also appropriate to mention here the results of a comparative implantation study performed on rats (Gunther, 2000), which aimed at evaluating the carcinogenic potential of Ti–Ni alloy doped with a small amount of molybdenum (<1%). According to that study, a group of rats carrying Ti–Ni implants outperformed groups with pure Ni and pure Ti implants. The Ti–Ni group had a longer period preceding detection of the first lump (394 days for Ti–Ni vs. 119 days for Ni, 364 days for Ti, and 365 days for the intact group). Furthermore, by the end of 30 months of implantation, the only surviving rats were in the intact (15%) and the Ti–Ni (6%) groups. These results may be interpreted in favour of an

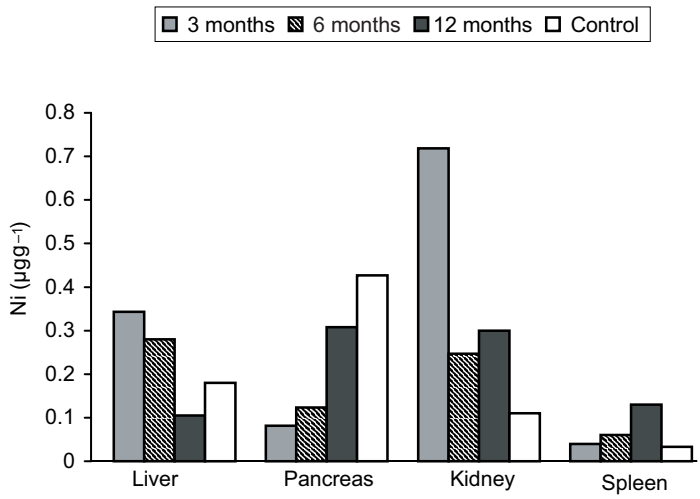

9.7 Nickel content in remote detoxification organs of sheep over 12-month post-surgery recovery time after implantation of porous Nitinol (adapted from Assad *et al.* 2003b, Fig. 4; an original was generously provided by Biorthex Inc).

immuno-stimulatory effect caused by Ti–Ni based alloy in rats. This, and a 25% stimulation of lymphocytes, when activated by Concanavalin A at sub-toxic Ni concentrations, may be considered as an enhanced response of immune system cells to biologically significant concentrations of Ni released from Nitinol.

9.6 Thrombogenic potential, platelet adhesion, and protein adsorption

Controversies exist in the literature regarding the thrombogenic potential of bare Nitinol surfaces. One group of researchers provided data from an *ex vivo* study indicating that Nitinol was significantly less thrombogenic than SS (Thierry, 2002), while another group found that SS has the lowest thrombogenicity among metals and alloys (Palmaz, 2002). These controversies may be related to differences in Nitinol surface chemistry that result from various surface treatment protocols, as will be shown in this section.

In a study on serum protein adsorption (Shabalovskaya, 2008a), fibrinogen adsorption to Nitinol surfaces varied over a wide range (130–300 ng cm^{-2}) (Fig. 9.8) suggesting that Nitinol may have variable thrombogenic potential. Albumin adsorption also varied significantly among studied surfaces but was always lower than that of fibrinogen. This observation is in agreement with the results reported for pure Ti (Cai, 2006). Interestingly, surfaces Ep in different electrolytes differed by as much as twice in albumin adsorption, which also suggests a possibility for the manipulation of Nitinol thrombogenicity. No obvious correlations between protein

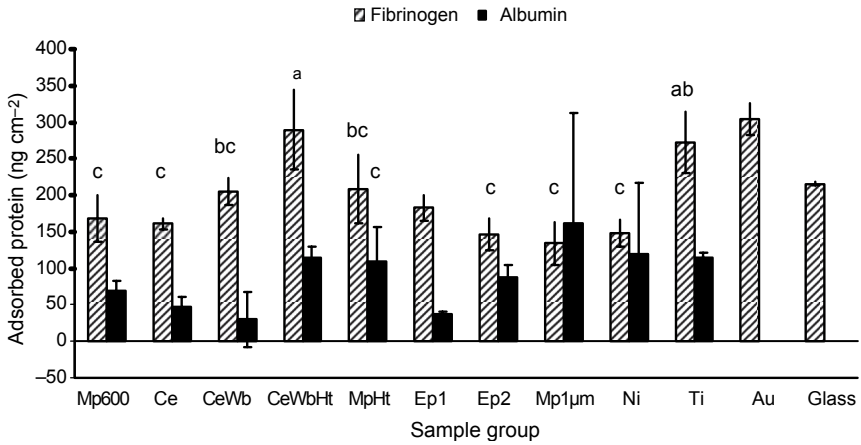

9.8 Fibrinogen and albumin adsorption to various Ti–Ni surfaces, to pure nickel and titanium, and positive controls gold and glass. The results of statistical analysis indicate that only two distinct sample groups 'a' and 'c' may be selected with $p<0.05$. The samples from the 'ab' and 'bc' groups may be equally assigned to any of those sub-groups (Shabalovskaya 2008a).

adsorption and surface roughness or oxide thickness were revealed. From the analysis of the nano-features of Nitinol surface topography it followed, however, that the increase of fibrinogen adsorption in a Ce, CeWb, CeWbHt sample sequence correlated with the increase in surface area available for protein adsorption (Shabalovskaya, 2008b). Thus, while the size of the crystals increased from 2 to 20–30 nm, fibrinogen adsorption increased from 160 to almost 300 ng cm^{-2}. A link between fibrinogen adsorption and Ti surface concentration was also evident (Fig. 9.9). Ti–Ni surfaces with the maximal Ti content of approximately 22 at.% adsorbed the highest fibrinogen amount, equal to that of pure Ti.

Further investigation into chemical and electrochemical surface properties (Shabalovskaya, 2008a) suggested that the amount of adsorbed fibrinogen is correlated with open circuit potentials (OCPs), and thus also with surface charge (Schmutz, 2005). Thus, as the negative charge on Nitinol surface increases (i.e., more negative OCP), fibrinogen adsorption decreases proportionally (Fig. 9.9) reflecting also the negative charge of fibrinogen molecules.

In the study of protein adsorption to Ti–Ni alloys, Michiardi *et al.* (2006b), deduced a direct proportionality of albumin adsorption to the polar component of surface energy and a inverse proportionality to the Ni concentration in the bulk of the alloys. However, this latter varied only within 1 at.% among the studied three alloys of nearly equiatomic compositions (49.5–50.5 at.%), and it is not clear for the moment how this very small difference in Ni concentration could affect Ni surface content and albumin adsorption. It was previously hypothesized that the presence of Ni on surface may encourage adsorption of albumin to Ti–Ni

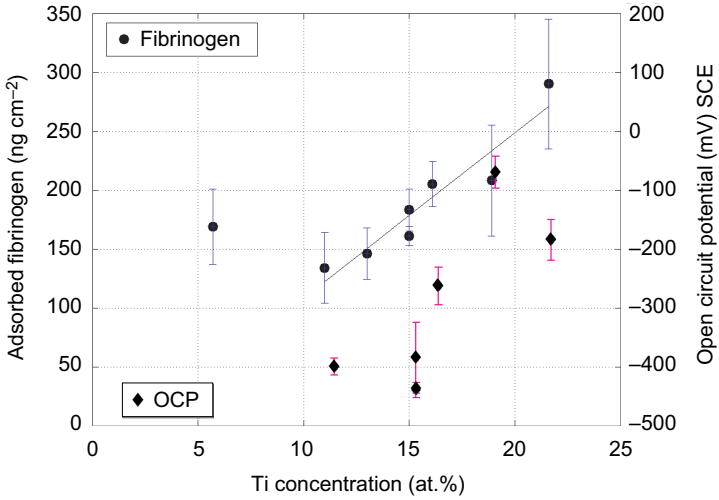

9.9 Fibrinogen adsorption to various bare Ti–Ni surfaces plotted versus Ti surface concentration, as presented in Table 9.2. With the exception of highly defective surfaces (Mp600 grit-finish), fibrinogen amounts found on Ti–Ni are in direct proportion to the Ti concentrations. A correlation between adsorbed fibrinogen and open circuit potential (OCP) indicates that gradual alteration in surface charge governs fibrinogen adsorption (Shabalovskaya 2008a).

(Shabalovskaya, 2002, 2004a), as albumin is known for its affinity to Ni (Lucassen, 1997). The results on albumin adsorption to Nitinol wires with the variable Ni surface concentrations (Clarke, 2007) seem to support this hypothesis. It is worthwhile also to note that Ni samples were the only one amongst those studied that induced albumin adsorption similar to that of fibrinogen, as can be seen in Fig. 9.8.

In a study on Ti–Ni hemocompatibility, Mp and Ep surfaces revealed a two-fold higher percentage of spread platelets than MpHt samples heated at 400 °C (Fig. 9.10) (Armitage, 2003). The platelet spreading was completely eliminated after the Ht at 600 °C. The reduced platelet activation upon Ht was attributed by Armitage *et al.* (2003) to a lower Ni release due to the binding of elemental Ni into compounds such as $Ni(OH)_2$. This assumption, nevertheless, needs to be proven through estimation of actual Ni release. Moreover, it is not entirely clear at the moment whether a complete absence of fully spread platelets is an advantage or disadvantage of Ht surfaces, as the importance of a monolayer of fully spread platelets for clinical compatibility of a biomaterial has been shown (Goodman, 1999).

In agreement with (Armitage, 2003), platelet spreading and aggregation on Nitinol varied depending on surface treatments (Shabalovskaya, 2004a, 2008). Thus, the only platelets that were detected on MpHt Nitinol samples were in the

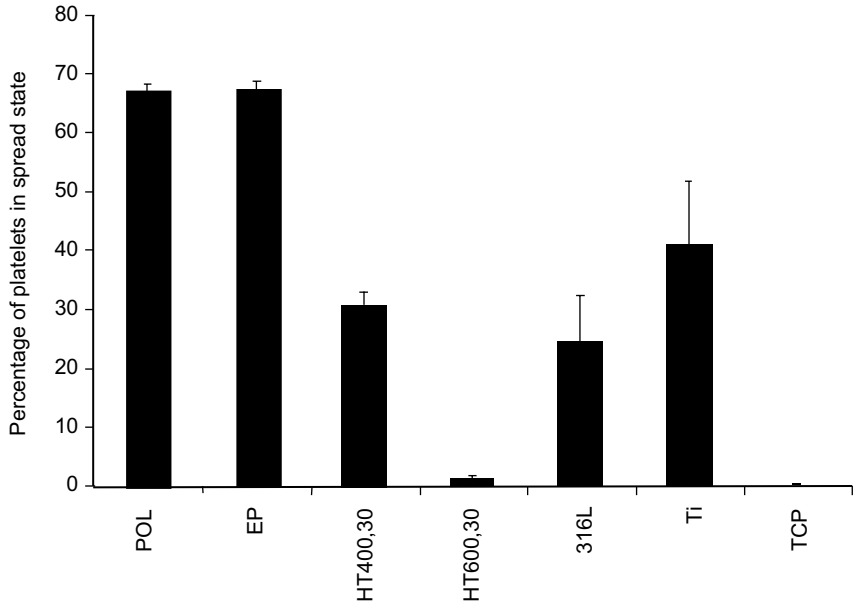

9.10 Percentage of platelets in spread state on various Ti–Ni surfaces. POL polished (finish 1 μm), EP electropolished, HT400,30 and HT600,30 heat treated for 30 min at 400° C and 600 °C, respectively, 316L stainless steel, pure Ti and TCP tissue culture plastic control (Armitage 2003, reprinted with the permission of John Wiley & Sons, Inc, © Wiley Periodicals, Inc).

fully spread state (Fig. 9.11f). In all other cases, fully spread platelets also form a base layer (Fig. 9.11), but they coexist with non-activated round platelets in the case of Ce samples (a); with activated platelets in a spread dendritic state for CeWb (c,d) as well as EP samples (g,h); and with platelets that aggregated in thrombi after heat treatment in CeWbHt state (e). It can be seen that similar HT applied to the different original surfaces caused a dramatic difference in platelet behaviour: platelets aggregation and thrombi-like formations in the case of CeWbHt samples (e) and no secondary platelets were detected on MpHt samples (f). Platelet aggregations were also obvious on the Mp finish surfaces (b). A gradual increase in platelets activation observed in the row of the samples Ce, CeWb, CeWb with a similar original surface topography (Ce) could be due to increased fibrinogen adsorption because of the developing nano-crystallinity of Nitinol surfaces upon Ht (Shabalovskaya, 2008b). The activated platelet released cytokines that activated other platelets, which were not in a direct contact with the surface and caused cell aggregation in thrombi. Higher thrombogenicity of certain Nitinol surfaces may be considered as their advantage in the orthopaedic and osseogenic implants applications because of the important role activated platelets play in early wound healing events recruiting other cells into healing compartment through the variety

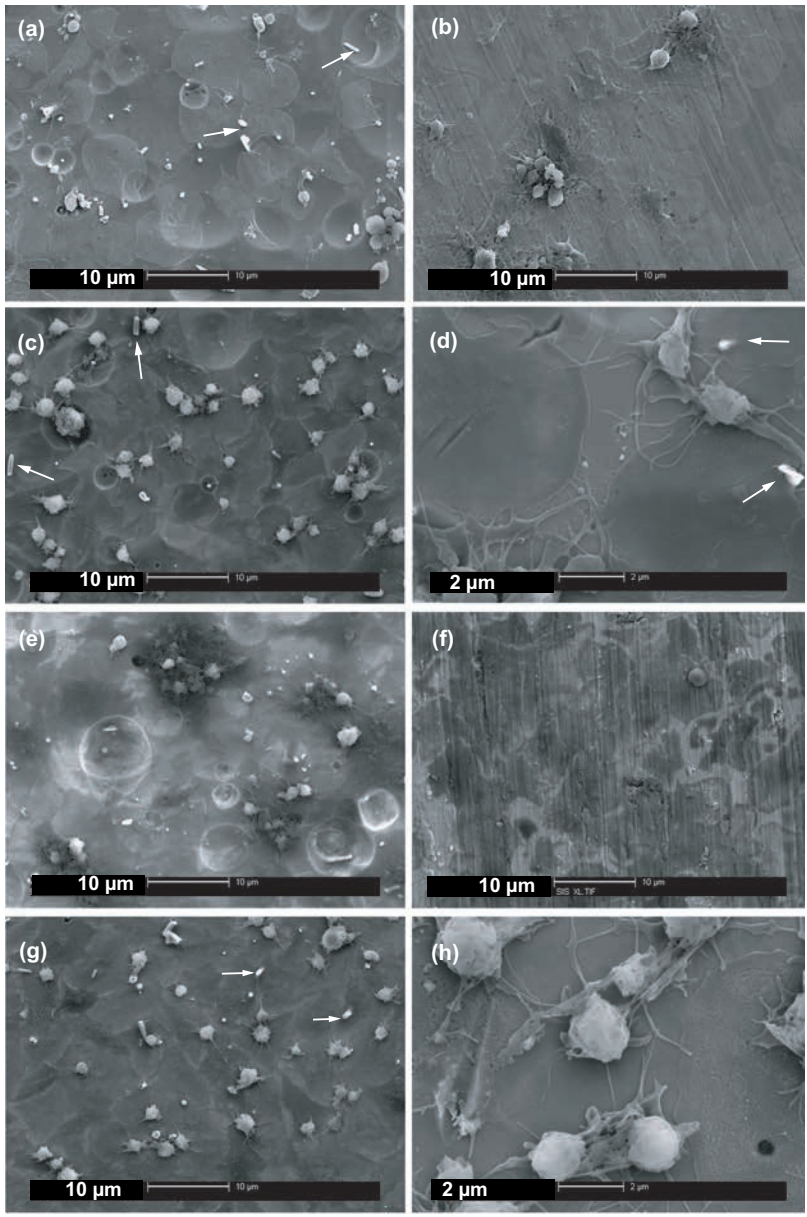

9.11 SEM images of human platelets adhered to Ti–Ni surfaces (Shabalovskaya 2008a) : (a) Ce, (c) and (d) CeWb, (e) CeWbHt, (b) Mp600, (f) MpHt, (g) and (h) – electropolished in austenite state at room temperature, Ep1. Sample designation is the same as in Fig. 9.4. As shown, human platelets can form a monolayer of fully spread cells on Ti–Ni surfaces that is considered to be important for clinical biocompatibility of implants (Goodman 1999).

of platelet-derived cytokines and intacellular signalling (Park, 2001). The Ni content in the above-mentioned sequence of the surfaces (Ce, CeWb, CeWbHt) decreased from approximately 7 to 2.2 at 0.9 at.%, also pointing at a possible link between higher Ni surface concentration and lower surface thrombogenicity.

The *in vitro* studies analysed above suggest that Nitinol thrombogenicity may be manipulated within a wide range depending on the needs for implantation in the body. Additionally, the results of recent animal and clinical studies show that the biological performances of various bare Nitinol implant devices were similar or better than that of SS (Sigler, 2000, Janke, 2002, Sabeti, 2004). It is important to note that while stent applications rely on the non-thrombogenicity of Nitinol, its use for occlusion devices requires, in fact, enhanced thrombogenicity (Sigler, 2005), which is achieved currently through the use of polyester textile fabric incorporated into implant devices. It is possible that the selection of an appropriate surface treatment for Nitinol could eliminate the use of fabric associated with chronic inflammation (Sigler, 2000) and also simplify implant design.

9.7 Biological responses to modified Nitinol surfaces

Efforts are continuing toward the development of new coatings and surface modifications for Nitinol, which aim at improving corrosion performance and decreasing Ni release. A critical analysis of studies published on this topic as well as a discussion of biological responses to modified surfaces can be found elsewhere (Shabalovskaya, 2008b). Because studies on plasma ion immersion implanted (PIII) Nitinol surfaces are more numerous and their results seem not to be in agreement, we will mention them here.

It has been demonstrated that, although the total fibrinogen adsorption to DLC – and oxygen PII – implanted samples was slightly reduced, an undesirable denaturated portion of fibrinogen increased significantly when compared with the untreated state (Maitz, 2006). Surprisingly, the increase in the amount of denaturated fibrinogen did not affect platelet adhesion. Platelet spreading was reduced on DLC-coated surfaces compared with Mp controls (Cheng, 2006). The activity of alkaline phosphate (a marker enzyme of mature bone forming cells) measured after 7 days exposure did not reveal statistically significant differences between implanted and non-implanted samples (Shevchenko, 2004). An evaluation of the death of bovine marrow cells based on lactate dehydrogenase (LDH) release performed by the same group also showed that there was no statistically significant variation among PIII, non-implanted Ti–Ni, SS (positive control), and pure Ni (negative control) samples; the fact that this test did not distinguish between negative and positive controls, however, is of some concern. It should also be admitted that non-implanted Ti–Ni samples for biological studies by Shevchenko *et al.* (2004) were subjected to a complex protocol (Ar ion sputtered, sterilized in steam, pickled in 0.1M HCl and soaked in phosphate-buffered saline) with no justifications or evaluation of resulting surface chemistry that is critical for the biological performances.

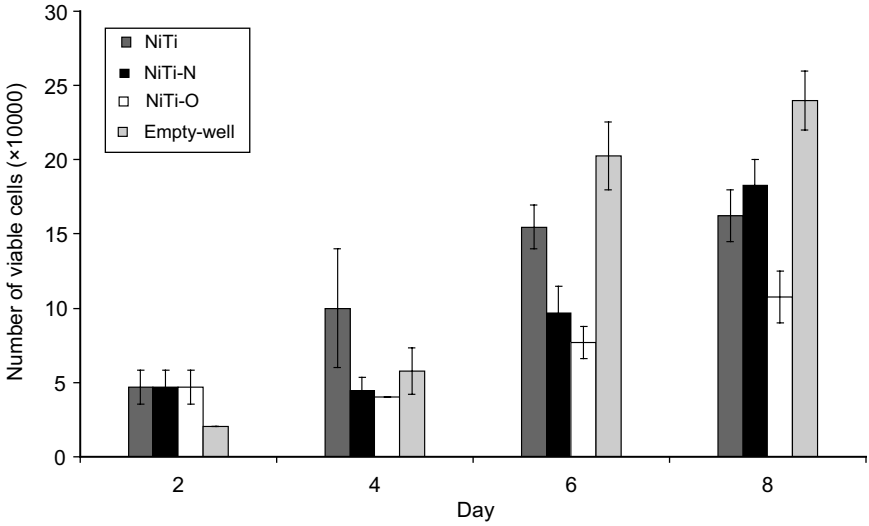

9.12 Osteoblast proliferation detected after 2, 4, 6 and 8 days of exposure to Ti–Ni samples (controls: polished to 'shiny', N and O implanted) and 'empty wells' cells with no samples (Yeung 2005), (courtesy of K. Cheung).

The cytocompatibility of PII implanted surfaces was also analysed in a study on osteoblasts. The results (Yeung, 2005) displayed in Fig. 9.12 indicate that, by the eighth day, the number of viable osteoblasts exposed to oxygen-implanted samples was reduced by 57% as compared with the negative control, while samples implanted with N and C suppressed osteoblast proliferation by approximately 20–25%. In contrast, direct acetylene (C_2H_2) plasma deposition (Poon, 2005) caused approximately 25–45% osteoblast stimulation, which indicates that the response may not be neutral. Slightly better growth of human gingival fibroblasts was detected on a 1 μm thick DLC coating as compared with control-untreated orthodontic arch wires (Ohgoe, 2006).

The results of bio-active surface studies of Ti–Ni should also be mentioned. Thus, in summary, a comparative thrombogenicity study of coated Ti–Ni stents by Tepe *et al.* (2006), concluded: 'Heparin coating and passivation in HNO_3 did not cause significant effect compared to mechanically polished control stents; mild reduction in thrombogenicity was observed with electropolished, sandblasted and ceramic coated stents; certain beneficial effect in the case of polyurethane polymer; and for clinical use, Nitinol stents should be at least electropolished.' In another study of bio-active surfaces (Kong, 2002), uncoated Ti–Ni performed better than coated. It showed higher EC coverage compared to r-hirudin and heparin coated. The heparin-coated surface was unable to sustain EC adhesion even after 48 h of incubation though heparin immobilization is considered as highly desirable for improved thrombogenicity.

9.8 *In vivo* responses

A number of *in vivo* Nitinol studies have been conducted worldwide. With rare exceptions (Berger-Gorbet, 1996, Takeshita, 1997), these studies have acknowledged the superior biocompatibility of Nitinol in accord with the first study by Castleman (1976), which established that cells and living tissues readily adapt to Nitinol surfaces. We will discuss only some of the more recent representative and systematic studies on implantation in orthopaedics and vascular surgery. For example, Ryhänen (1999) undertook a systematic implantation study in which cellular, tissues, and bone responses combined with Ni release, were evaluated. It was concluded that inflammatory responses and mean encapsule membrane thickness were similar for Nitinol, SS alloy, and Ti6Al4V alloy after 26 weeks of implantation. Necrosis, granulomas, or dystrophic tissue calcification were not observed. The immune cell reaction to Nitinol remained almost neutral, while the response of neural and perineural tissues was non-toxic and non-irritating; muscular response was also non-toxic.

Balakrishnan *et al.* (2005) observed that little or no inflammation or fibrosis was detected when Nitinol was placed in contact with the bladder; in fact, Nitinol appeared more inert to mucosa than SS, which showed affinity.

9.8.1 Implant–bone interface

An evaluation of the interface between implant and living tissue showed that cells adhere to Nitinol through a thin interfacial layer of organic amorphous material (Ryhänen, 1999), and there is always a close contact with fibrous capsule layers or single cells. New bone formation started two weeks earlier in Ti alloy; by eight weeks, however, Ti–Ni and SS had greater cortical bone width and, at 12 weeks, no differences were seen. Slower initial osteogenesis could be related to higher Ni release during the first days after implantation. Berger-Gorbet (1996) also reported slow bone remodelling, very little contact between bone and Ti–Ni, and diminished activity of osteoblasts to osteonectin. Abnormalities in bone formation within a few months after implantation of commercial Nitinol screws might be caused by lasting Ni release, as seen in the analysis presented in Section 9.4.

9.8.2 Biocompatibility of porous Nitinol

Porous superelastic Nitinol, as originally developed and extensively studied in Russia (Gunther, 1995, Itin, 1996), is equally suitable for orthopaedics, spine implants, soft tissue reconstructive and maxillofacial surgeries, as well as for dental implantology (Gunther, 1995, Shabalovskaya, 2002). The superelasticity of this biomaterial offers the possibility for certain *in situ* recovery of the implant shape after an injury to the implants, or to the surrounding hard tissues. For long-term replacement of bone defects, Nitinol offers the advantage of interfacial

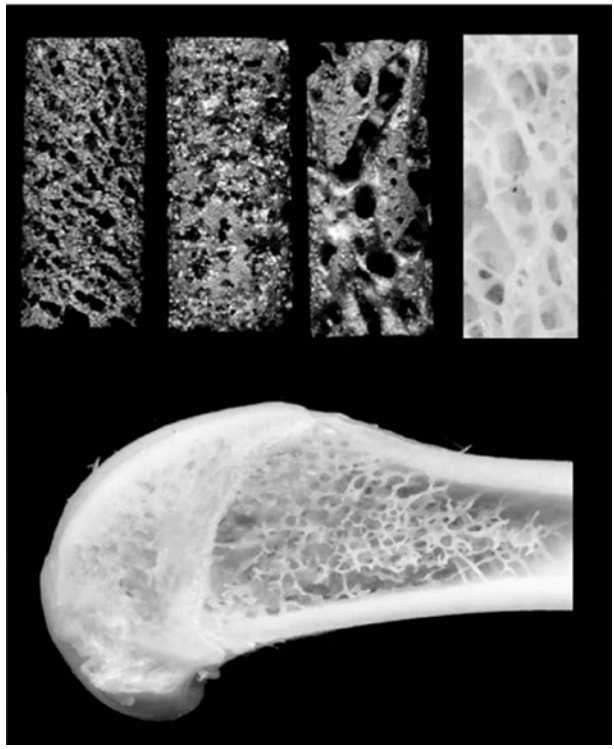

9.13 Nitinol implants with variable porosity (66.1, 59.2, and 46.6%, top left to right, respectively), a sample of human trabecular bone from the femoral neck (upper right), and a cross section of an implantation site at a distal rat femur (bottom). Reproduced by the permission of the authors) (Kujala, 2003).

porosity as well as a permanent structural framework. Figure 9.13 shows Nitinol of different porosity, along with a sample of human trabecular bone from the femoral neck and a cross-section of an implantation site in a distal rat femur (Kujala, 2003). Owing to the permeable porous structure of Nitinol, living tissues grow directly into the body of implant, thereby transforming it into a new composite material. It has been shown that, after three months in the body, a newly formed implant–bone composite acquired properties superior to both the original alloy and the bone as seen in Fig. 9.14 (Itin, 1996). An evaluation of explants indicated that bone tissue penetrated in all the labyrinth of porous material, providing excellent attachment and biological functioning.

Various researchers have reported varying times necessary for the growth of bone tissues into the body of porous Nitinol (Sysolyatin, 1994, Simske, 1995, Yahia, 2000, Assad, 2003a). New bone in the body of porous Nitinol is detected as early as three weeks after implantation, but the percentage of new bone varied from one to 15% from sample to sample (Yahia, 2000). The performance of

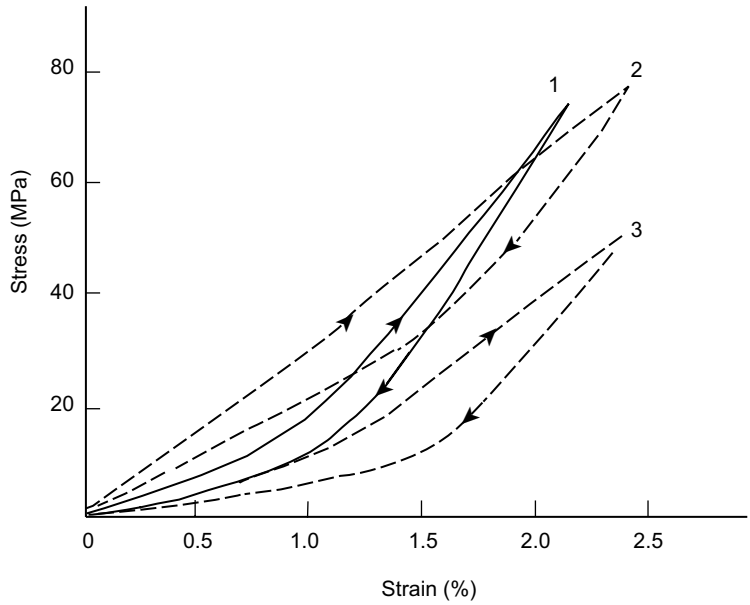

9.14 Stress versus strain diagram in compression mode for original porous Nitinol implant (2) and after tissue in-growth upon implantation in rabbit for one (3) and three months (1) (reproduced with the permission of the author Itin *et al.*, 2006).

Nitinol was always found to be superior to porous Ti or Ti6Al4V alloy, as illustrated in Fig. 9.15 (Assad, 2003a). Although, after three months of implantation, the level of osseointegration was similar for both materials, after 12 months, Nitinol outperformed the Ti6Al4V alloy (Fig. 9.15a). As far as apposition is concerned, it was significantly higher for Nitinol (Fig. 9.15b) regardless of the implantation time; total bone apposition was maximal (51%) for the material with approximately 66% porosity (Fig. 9.13, upper left corner). By comparison with other materials, an average osseointegration value for Nitinol (65% porosity) is about 38% after one year in the body, while the apposition range for implants with porous coatings is 5–40%; for hydroxyapatite of 30% porosity, it is 25% (Ayers, 1999).

Evaluation of inflammatory responses showed that cytokine release from polymorphonuclear neutrophile granulocytes, PMN (IL-1ra and IL-8) was not significantly different between cell cultures, with or without porous Nitinol. However, in the case of PBMCs, there was a significant increase in the release of IL ra, IL-6, and IL-8 in the presence of porous material, although the release of TNF-α was not significantly affected (Prymak, 2005).

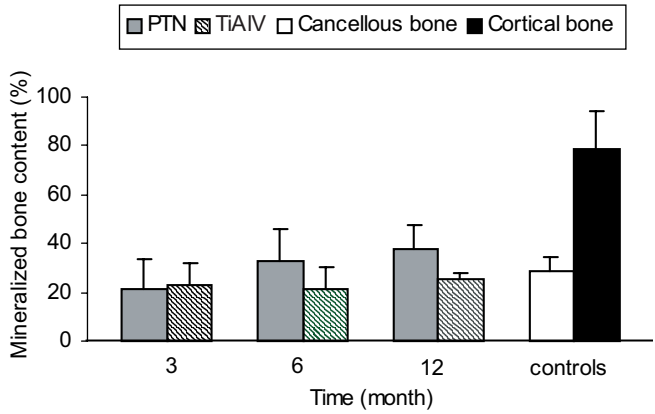

9.15a Osteointegration over 12-month postsurgery recovery time in sheep model (three and six, and twelve months) together with controls for cancellous and cortical bones. There was no significant difference in osteointegration between porous Ti–Ni (PTN) and TiAlV alloys (reprinted from Assad, 2003a, originals generously provided by Biorthex Inc).

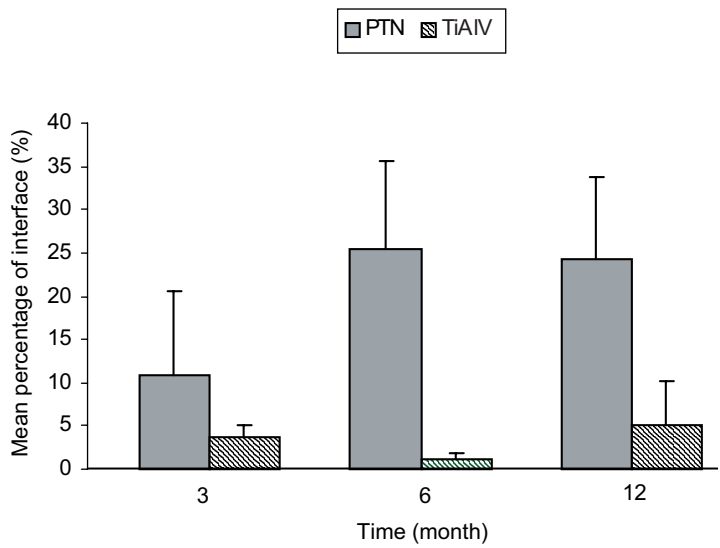

9.15b Bone apposition over twelve-month postsurgery recovery time for PTN-porous Ti–Ni (PTN) and TiAlV alloy in sheep model. PTN is significantly different from TiAlV ($p<0.05$) (reprinted from Assad, 2003a, originals generously provided by Biorthex Inc).

9.8.3 Biocompatibility of Nitinol stents and defect closures

The concept of minimally invasive surgery, i.e., entering the body with a minimal profile through small incisions is readily accomplished by using flexible surgical tools and implant devices that take advantage of Nitinol's thermal shape memory effect and superelasticity. The use of self-expandable stents is an excellent example of how superelasticity can benefit implant performance. Stenting is intended to maintain the patency of ducts, vessels, or passageways in transport systems throughout the body, including airway passages, digestive and urinary tracts, and the vascular system. Upon deployment in the body, stents quickly expand and exert a constant radial force against strictures. The flexibility of Nitinol allows stents to adapt to cyclic pulsations in blood vessels as well as to peristaltic motion (e.g., in the esophagus), while also being able to collapse during contractions of the airways as during coughing, or in response to injuries, and then recovering *in situ*.

Two major clinical complications with endovascular stents and stent grafts are subacute stent thrombosis and neointimal proliferation, which lead to restenosis. Restenosis is defined as a repeated narrowing of operated blood vessels with greater than 50% luminal closure. Based on clinical studies, restenosis rates range from 8 to 10% for ideal lesions, and up to 30 to 50% for complex conditions, or associated pathologies (Thierry, 2003). Although the exact mechanisms of thrombosis and restenosis are still being investigated, both of them involve activation of a blood coagulation cascade – that is, activation of platelets and their aggregation through binding to fibrinogen adsorbed to implant surface. Activated platelets release a growth factor (a potential stimulator of smooth muscle cell proliferation), which results in intimal hyperplasia. From the objective of preventing extensive proliferation of SMCs, fast stent endothelialization is beneficial. There are three major approaches to avoiding restenosis: 1) improve stent biocompatibility; 2) cover the stent frame with a graft; or 3) use aggressive anticoagulation drug therapy, or radiotherapy (brachytherapy), to inhibit neointimal proliferation. Although all three methods are in use to combat restenosis, we will consider here only aspects related to the first.

Stent biocompatibility is improved either by minimizing surgical trauma, optimizing the design and mechanical properties of the device, or making the stent compatible with the blood by avoiding metal toxicity and thus reducing the inflammatory response. Based on animal studies using balloon-expandable stents, it was postulated that the absolute amount of neointimal proliferation in an arterial segment is proportional to the amount of injury sustained (Sarembock, 1989, Schwartz, 1992). This approach was further extended to studies of self-expandable coronary stents (Sheth, 1996, Kobayashi, 2001) assuming that Nitinol stents may allow deployment at lower pressure, thereby causing smaller initial trauma and less marked thrombosis – especially early thrombosis that occurs in 7–16% cases

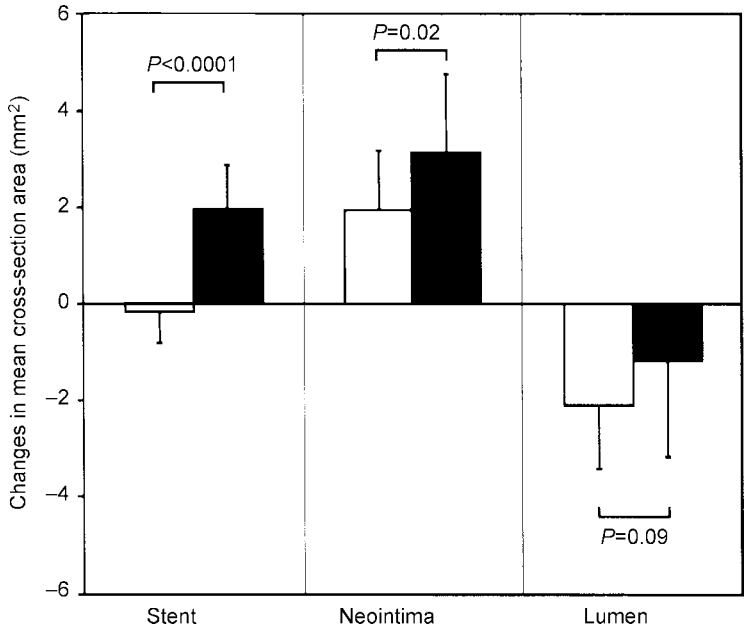

9.16 Mean stent, neointimal and lumen area changes within the stented segment during the follow-up period. Notably that Nitinol stents increased by 1.9 ± 1.0 mm² in mean stent area while stainless-steel stents showed no significant changes. Nitinol stent, however, had a greater amount of neointimal proliferation then SS stents. Values are expressed as mean ± SD. Open box = Palmaz – Schatz SS stent, solid box = Nitinol RADIUS stent (reprinted from Kobayashi, 2001, © The American College of Cardiology, 2001).

after implantation of diseased blood vessels (Sheth, 1996). Data from a porcine stent model of restenosis suggested that early thrombus formation may stimulate neointimal proliferation (Schwartz, 1992). Furthermore, the placement of balloon-expandable SS stents has also been associated with stent recoil, which is a small decrease in stent diameter after the balloon is deflated.

Studies involving coronary self-expanding stents in animal and humans (Roguin, 1999, Kobayashi, 2001) have concluded that Nitinol stents continuously expand after placement. In a six month follow-up period, the increase in Nitinol stent diameter might reach 21–24%. Contrary to expectations, however, Nitinol self-expanding stents caused higher intimal proliferation. The proliferative response was maximal at three–six months, while considerable regression occurred after 12 months (Bayer, 1997).

Owing to the interplay between a follow-up increase in stent diameter and neointimal proliferation, the total late lumen loss was smaller for Nitinol (Fig. 9.16) compared with SS, even though that decrease was not statistically significant (Kobayashi, 2001). It is not clear at the moment whether continuing self-expansion

provokes an excessive SMC proliferation over that of balloon-expandable stents. On the other hand, several studies (Greanadier, 1994, Schurmann, 1996, Hong, 1997) showed no difference between rigid and self-expandable stents with respect to neointimal proliferation. Among the factors that could stimulate neointimal hyperplasia, Kabayashi *et al.* (2001) mentioned hypersensitivity to stent materials. Indeed, the increasing Ni release, with saturation at six-month exposure depicted in Fig. 9.2, could induce a toxic effect, while significantly contributing to intimal proliferation in the studies (Roguin, 1999, Kobayashi, 2001). It should be noted that the success rate of coronary self-expandable stents expressed in the percentage of event-free stenting was 80 and 85% for six- (Bayer, 1997) and 12-month follow-ups (Roguin, 1999), respectively.

Self-expandable Nitinol stents are especially suitable for treatment of torturous femoral or popliteal arteries, situated at flexion points, where stents may be subjected to external compression. In a study involving 110 patients with femoropopliteal obstructive diseases, no stent-related major complications were observed after stenting (Henry, 1996, Janke, 2002). Primary patency (defined as the absence of restenosis) was reported as 97.1 and 86.2% for six and 12 months, respectively. Suggested explanation for the absence of acute thrombosis was very low metal coverage (only 9.5–13.3%) of coil stents inside the treated vessels; coil stents could also be retrieved with minimal tissue damage. A lower thrombosis rate for Nitinol coil stents compared with SS stents, was also reported (Henry, 1995).

In another study (Sabeti, 2004), 175 patients with peripheral artery disease were subjected to femoropopliteal artery implantation with Nitinol or SS stents. During the median follow-up period of nine months, approximately 50% of the operated patients developed restenosis. The group with Nitinol stents had significantly better primary patency rates than those with SS stents (Fig. 9.17). The cumulative patency rates at 24 months were 69% and 39% for Nitinol and SS stents, respectively. This data suggests that Nitinol stents are effective regardless of lesion characteristics. For comparison, the patency rates of traditional Dacron woven aortofemoral grafts are close to 90% at five years and 80% at ten years (Lindenauer, 1984, Seaden, 1986); and a two-year primary patency of ePTEE femopoptiteal grafts is 80% (Veith, 1986).

The use of endovascular stent grafts (ESGs) for the treatment of traumatic arterial injuries and aneurysms was first proposed by Dotter (1964, 1969); the first endovascular aneurysm repair was performed in the United States in 1990 (Parodi, 1995). Over the following 10-year period, an additional 817 patients received ESG treatment (Marin, 2003). In this latter study, the performance of Nitinol was compared with Elgiloy steel and to 316L SS; freedom from thoracic and abdominal aneurysm rupture was 98% at 9 years. Upon implantation of rigid ESGs, which were unable to accommodate to the vessel wall geometry, an abnormal aortic bend was formed that might contribute to early and late type I endoleaks (Cao, 2002). It was concluded that the rigidity of prostheses may increase the risk of late stent failure when deployed in settings such as an angulatedaortic neck. Marin *et al.*

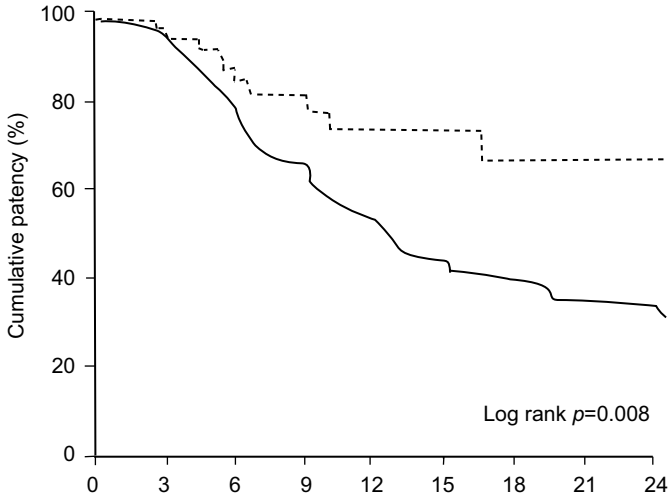

9.17 Kaplan–Meier curves of cumulative patency rates for self-expanding Nitinol and balloon-expandable stainless-steel stents implanted into femoropopliteal arteries. Patients in the Nitinol group (dashed upper curve) had significantly better patency rate as compared with the stainless-steel group (solid lower curve); p=0.008, a standard error was below 10% in both groups (reprinted from Sabeti, 2004 by permission from the Radiological Society of North America, © RSNA, 2004).

(2003) reported that approximately 8% of the mechanical failure of the devices was due to the fracture of longitudinal metal bars.

In contrast to the situation with stent implantation, cell proliferation plays a different role after implantation of an occlusion device. Thus, the initial mechanism of Patent Ductus Arteriosus (PDA; a cardiovascular defect caused by failure of the arterial canal to close after birth) occlusion is formation of thrombus within the implant (Sigler, 2005). Therefore, thrombogenic occlusion is part of the therapeutic concept in occlusion devices, whereas it represents a major complication in stent implantation. Textile fabric is often incorporated into implant design in order to enhance the thrombogenicity of coils or occlusion devices. Using appropriate treatment for Nitinol surface, its thrombogenicity may be enhanced, and a need for fabric could be eliminated. In an animal study of PDA closure devices, thrombus cellular organization was completed in six weeks for Nitinol coil but only after six months for a SS coil (Sigler, 2000), which suggests that Nitinol is the preferred material for this type of device.

One final aspect to be touched upon here is related to the adequacy of implantation results for Nitinol obtained in animal models compared with humans. Follow-up periods in animal studies usually occur from three months to three years, even though the expected performance of long-term implants in children with congenital defects is over the entire course of their lives (i.e., 70–80 years).

Additionally, experimental animals have artificially created defects that could potentially alter healing patterns and immune responses to implantation. In a comparative study (Sigler, 2007), an implantation analysis of occluder devices for the treatment of atrial septal defects (ASD; an opening in the atrial septum, or the wall between the two upper chambers of the heart**)** in animals and humans was presented. It was concluded that tissue reactions in experimental animals adequately reflected the healing response to septal occluder devices in humans with regard to neoendothelialization, cellular organization of initial thrombus, and a chronically persisting inflammatory response to polyester. No reaction directed against Nitinol metal framework was reported.

9.8.4 Stent failures

Much effort goes into the design and fabrication of Nitinol stents to ensure that they have appropriate mechanical properties, durability, functionability, and biocompatibility. Vascular stents should withstand a strain of to 8% in catheters up during the loading stage, and then they should survive at least 400 million cycles in the human body (Food and Drug Administration requirement) while performing in Nitinol's superelastic mode. The factors affecting stent life in the body and cases of stent failures should be scrutinized to improve their performance.

In this section, the results of investigations into Nitinol ESGs used for the treatment of abdominal and infrarenal aorta aneurysms and explanted from the human body, will be discussed. In the first study (Guidoin, 2000), the structural failure of an ESG (Stentor) explanted from abdominal aorta from 13 to 53 months after implantation was attributed to severe compression and dislocation of the metallic frame due to suture breaks. Corrosion marks were observed in all six endoprostheses studied. However, there was no inflammation or sign of bacterial colonization, or calcification in any of the tissue specimens in contact with Nitinol wires. It should be noted, however, that a depth profile presented in Figure 14 of the study (Guidon, 2000) exhibits very high Ni content (~20 at.%) in the external surface layer.

In the other study of explanted Nitinol endografts (46 Stentor, 9 Vangard, 1 Cragg), the mean duration of implantation was approximately 29 months. ESGs that had failed in the body were used for treatment of abdominal (Heintz, 2001) and infrarenal aorta (Riepe, 2002) aneurysms.

Historically, the first generation of commercial ESG prototypes were Stentor grafts, which were taken off the market in 1996 due to ruptures and other complications; later generation Vangard grafts were modified. Common features of all explants were damage to the polyester textile used to cover metal stents, rupture of the ligatures binding stent wire to the polyester cover, excessive corrosion, and metal frame fractures. Three types of metal surface damage were mentioned: 10–25 μm pits, 100–180 μm craters, and 200–500 μm surface deficiencies depleted on Ni (Fig. 9.18a). Complete wire fracture was observed in 32% of explants; occasionally, four to six fractures could be detected on one explanted

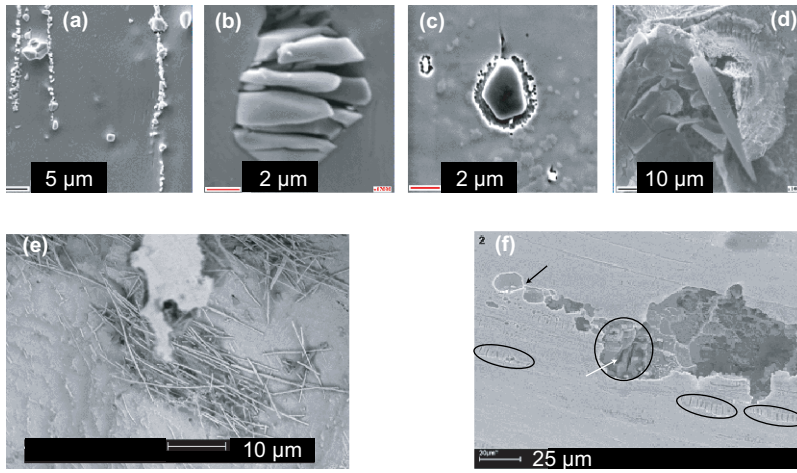

9.18 SEM images of particulates on Nitinol surfaces (Shabalovskaya 2007b): (a) electropolished stent strut illustrates the presence of long particle chains from 50 to 200 µm; (b) a fragment of this chain; (c) electropolished wire after potentiostatic polarization at +800mV (the perforated, corroded area surrounding the particle is where the alloy chemical composition was altered due to formation of the particle); (d) heat treated disk sample after potentiostatic polarization at +800 mV (a 70 µm Ti dioxide particle and thick external surface oxide layer (TiO_2) survived but the matrix alloy dissolved by corrosion); (e) fragment of a wire sample heat treated at 500 °C for 15 min and strained to 2.5% in tension mode during potentiodynamic polarization (the matrix alloy corroded but the needle-shaped particulates survived); (f) SEM image of Nitinol wire segment from an explanted endovascular graft after 16 months in the human body, showing multiple pits of various sizes. The original image can be viewed online (Heintz 2001). Reprinted by permission from *J of Cardiovasc Ther*. Copyright International Society of Endovascular Specialists, 2001. The peculiarities of the figure discussed in this chapter are marked by circles and arrows.

graft. Both research groups mentioned that the colour of stent wires was non-uniform, with variations of grey, blue, pink, and gold observed. Based on these investigations, it was concluded that ligature rupture, wire dislocation, and polyester damage were due to the continuous pulsatile movement of stent wire. While corrosion was considered to be the initiator of metal frame fracture, possible causes of corrosion were attributed to inflammation induced by polyester textile as well as the electrical activity of adherent cells (fibroblasts, white blood cells, and ECs) that could eventually polyester. It was also questioned whether the heterogeneous thickness of surface oxide (≤50 nm for grey to golden and ~1000 nm for black) deduced from wire colours could play any role in implant failure. Significant differences in surface oxide thickness mentioned in both publications (Heintz,

2001, Riepe, 2002) caused heterogeneous distribution of surface stresses; thick oxides (>100 nm) are prone to stress-corrosion cracking.

Importantly, it was also mentioned that 'the ceramic-like nature of the titanium dioxide layer on the surface of Nitinol must resist cracking in the pulsative oscillation and wear on contact points with other materials' (Heintz, 2001, Riepe, 2002). It should be emphasized, however, that the ceramic nature of TiO_2 acts against both Nitinol superelasticity and the cyclic pulsation of blood vessels. Ceramic materials are held together by ionic and covalent bonds, which tend to fracture before any plastic deformation takes place; even small superelastic deformations experienced by Nitinol would be in plastic limits for TiO_2. Indeed, the first cracks of titanium dioxide surface layer of ~125 nm thickness formed during heat treatment Ti–Ni at 540 °C for 30 min in air were observed already at strain levels lower than 0.6% (Undisz, 2008). Thus there are at least two plausible mechanisms that may lead to cracking of TiO_2: (1) stress-corrosion cracking due to very thick and non-uniform oxide layers, and (2) cyclic strain in Nitinol's superelastic regime.

Another factor that should be considered while analysing stent failures is heterogeneity of Nitinol. This heterogeneity is rooted in both the extreme reactivity of Ti, which results in the formation of inclusions during alloy melting (Ti-based oxides and carbides), and binary Ti_xNi_y phases formed through solid state reaction. These latter phases are easily oxidized into $Ti_xNi_yO_z$ phases. All these particulates are hard and rather brittle, and can vary in size from a few nanometres to hundreds of micrometres (Fig. 9.18). While inclusions are usually distributed quite uniformly in Nitinol (Shabalovskaya, 2007), precipitate particles can form clusters or chains of 50–300 μm length as it illustrated in Fig. 9.18a,b on the example of a stent strut. Some of the particles may be conductive and thereby galvanic corrosion can be activated.

More importantly, however, formation of these particulates in Nitinol is associated with the alteration of the composition of the surrounding matrix, which makes the areas adjusting to the particles vulnerable to localized corrosion (Fig. 9.18c) especially under strain (Fig. 9.18d,e). The images d and e represent Nitinol disk and wire samples, respectively, which were heat treated at 500 °C for 15 min before the corrosion test. The wire sample was strained to 2.5% in tension mode during potentiodynamic polarization in 0.9% NaCl solution when localized corrosion occurred. Although there was only one real pit revealed on the surface of the 10 cm long wire sample exposed to corrosive solution, the result is devastating. As one can see, the matrix alloy was completely corroded but the particles survived.

During material processing, brittle particles do not remain intact but break to create voids (Fig. 9.18b). These voids may serve as reservoirs for corrosive body fluids. Penetrating first through the cracks on the surface, the fluids provide the electrolyte for the initiation of corrosion. Most of the particulates we observed in Ti–Ni survived corrosion testing, while matrix material suffered (Shabalovskaya, 2004b, 2007b, Heßing, 2007).

Figure 9.18f, reproduced from the work of Heintz (2001) demonstrates localized corrosion observed on explanted stents. It shows a number of small (~10–20 μm)pits as well as a large lacuna with a typical honeycomb structure of the bottom of the pit. Figure 9.18f also exhibits various surface sublayers. The external surface layer is partially missing, thereby providing a view of another deeper sublayer. The upper surface layer is locally cracked. The particular shape of cracked areas and their uniform size indicate that hidden underneath are broken particles. Interestingly, the lower left corner of lacuna does not have a specific honeycomb structure as would result from corrosion; instead, what is visible are split slices of material intact by corrosion separated by 1 μmgaps. This is a fractured particle, with a size and appearance reminiscent of those particles observed in chains on Nitinol stent struts and identified as Ti_2NiO (Fig. 9.18b). Pits of smaller size, propagating in the longitudinal direction to the left (arrow), most probably reflect the location of a hidden particle chain, of which the fractured particle is just one fragment. The longitudinal cracks observed after application of tension strains to oxidized Ti–Ni surfaces (Undisz, 2008) could also be attributed to the particulates clustered in longitudinal chains emerging from the surface. It was noted that crack initiation of the oxide layers and Ti–Ni coatings occurred primarily at inhomogeneities (Heing, 2007, Undisz, 2008).

As a result of corrosion, particulates of various sizes are released into the area adjacent implants. Particle debris smaller than 5 μm in diameter, would be phagocytized by macrophages; unable to digest metal, these macrophages would probably die, thereby contributing to the increased acidic environment around the implant and aggravating corrosion. Although debris from microphages would be disposed of by the body, metal particles would either remain in the proximity of the implant, or be taken away by the circulatory system and deposited in various organs. Heintz *et al.* (2001) analysed elute from two grafts, which had been washed for 2h, and recovered a granular material of 0.5–2.5 μm (identified with EDAX as 'nickel-free titanium oxide'). Debris around Nitinol stents were also reported by Cragg *et al.* (1993). It is not clear what the total size of that particle identified in Fig. 9.18f was, but the size of uncovered area providing a view of the particle is at least 20 μm in diameter; this is 1/15 of the overall wire diameter. Assuming that there are long chains of large particles (that may be deduced from the corrosion patterns), it is reasonable to conclude that they were implicated with mechanical instability, corrosion, and stent fracture.

Jacobs *et al.* (2003) presented an analysis of ESG failure modes based on 10 years of experience in the treatment of aortic aneurysms. They emphasized that, although fundamental mechanical and technical problems identified in the first-generation stent grafts have been addressed, and individual implants have improved, problems related to device fatigue (e.g., suture disruption, metal fracture, or fabric erosion) have been also discovered in second-generation stent grafts. In a following study of 404 patients who underwent endovascular aneurysm repair, 60 patients with seven different devices had stent graft fatigue. Among these cases, 43 had metallic stent fractures (28 Talent, 7 Gore, etc.), 14 had suture disruption

(Vangard), and 3 had graft holes. Metal stent fracture occurred from one to 48 months following implantation, depending on stent type. Fatigue fracture was visible within several different regions of the stent grafts – either along the longitudinal bar of the graft, or in the serpentine-shaped Nitinol. In contrast to Stentor grafts (Heintz, 2001, Riepe, 2002), there was minimal evidence of corrosion. The variation in corrosion of explants may partially be attributed to the cleaning procedure if bleaching agents were used (Lasley, 2003). It should be noted, however, that the surface oxide layer on the explanted samples presented (Jacob, 2003) was very thick and uniformly cracked, thereby suggesting the possibility of stress-corrosion cracking *in vivo*. In agreement with the previous studies (Guidoin, 2000, Heintz, 2001), it was also concluded (Jacob, 2003) that the tortuousity of implant vessels increased stress across the Nitinol wire, which resulted in stress fatigue and fracture of the longitudinal stent bars.

9.8.5 Biological effect of metal debris

For a long time, it was recognized that particulate debris was not biologically inert (Rae, 1975). Wear debris induces several cells (monocyte/macrophages, lymphocytes, synoviocytes, and fibroblasts) to secrete cellular products mediating inflammation (Kohilas, 1999), which eventually may result in implant loosening and failure. It was shown that particulate debris smaller than 10 μm in diameter (similar to cell dimensions) causes adverse effects to surrounding tissues, disregarding their chemistry (Evans, 1994) either through damage to cell membranes (Galante, 1991) or phagocytosis (Kumazawa, 2002).

Weight-bearing implants may undergo severe fretting corrosion, which results in the formation of corrosion product debris. Use of porous implants implies even higher probability of debris accumulation. It is important to understand that debris may also be caused by release of inclusions and precipitate particles from Nitinol owing to general or galvanic corrosion. Thus, the increase in acidity accelerated corrosion *in vitro* (Rondelli, 1999, Clarke, 2006) and addition of cysteic acid to corrosive solution was accompanied by particle release (Brown, 2000). Particulate aggregation was also observed after corrosion testing (Shabalovskaya, 2003b).

The effect of Ti, V, and Ni particles (1–3 μm and 10 μm sizes) on the function and morphology of human neutrophils was studied *in vivo* and *in vitro* by Kumazawa *et al.* (2002). While Ni particles significantly suppressed neutrophil survival rate, the effect of Ti particles *in vitro* was not very different from that of the control. However, 1–3 μm size Ti particles induced TNF-α release by neutrophils, and their implantation into the abdominal region caused inflammation. These small Ti particles were phagocytized into the cytoplasm by macrophages.

In another study (Chang, 2004) of slightly larger particles (5–15 μm), Ti-wear debris implanted into the retroperitoneal and epidural space in the lumbar spine (L2–L3 area), travelled from deposition sites to all investigated organs (kidneys, spleen, lungs) and tissues (lymph nodes), but elicited almost no biological effects.

At the moment, no corresponding data on the biological effects of small particulates originating from Nitinol are available for comparison.

The effects of large particulates (106–300 μm size), the wear products of porous Nitinol, were compared with 1–25 μm size particles of powdered Ti6V4Al alloy (Rhalmi, 2007). This study showed that no metallic particles were found in the macrophages of the lymph nodes. One week following surgery, both materials showed an acute inflammation limited to the epidural space at the implantation site. Cell infiltration was resorbed at 4–12 weeks; at long term (26–52 weeks), a dense connective tissue embedded the particles, and a mild inflammation consisting mainly of macrophages was observed in the particle/fibrosis interface. Regardless of the observation periods, however, the inflammatory cells did not penetrate dural matter; sub-dural space, nerve roots, and the spinal cord were free of inflammation. Macroscopically, the particles of both materials remained at the lumbar implantation site.

For a comparison of the results obtained for Nitinol by Rhalmi *et al.* (2007), we will cite also the study of Kraft *et al.* (2003), where the effects of similar size SS particles (200 μm) on the microcirculation in the skeletal muscle were evaluated. Implantation of SS bulk and debris led to a distinct activation of leukocytes, disruption of the microvascular endothelial integrity, as well as massive leukocyte extravasation, severe inflammation, and massive edema. Free Ni detected on the surfaces of wear particles was suspected of being implicated in the devastating response to SS debris.

9.9 Conclusions and future trends

Thirty years ago, when the first study on Nitinol implantation was completed, Castleman (1976) had written that, while the development road for Nitinol as a biomaterial may be long, its future looked bright. We are operating now in that future. From its discovery in 1962 at the US Naval Ordnance Laboratory, the Nitinol road has not always been smooth or paved. Being American in origin, Nitinol quickly established roots in other parts of the world, where researchers from both West and East (Fig. 9.19) contributed to the maturation of Nitinol as a biomaterial: new shape memory features were discovered, new multicomponents and porous shape memory alloys were developed, and new operation techniques utilizing Nitinol's potential were elaborated. *In vitro* and *in vivo* studies in animal and human models, as reviewed in the present chapter, unanimously concluded that Nitinol is biocompatible and efficacious as a biomaterial.

Non-appropriately treated Nitinol will always present a problem with Ni release. In order to avoid troubling issues with Ni release and stent metal failures, the surface and bulk of the alloy need to be scrutinized. Nitinol chemical heterogeneity needs to be eventually recognized with regards to medical applications, the specifics of particulate size and distribution need to be better understood aiming at better corrosion resistance and fatigue life. The approach of using a thicker surface

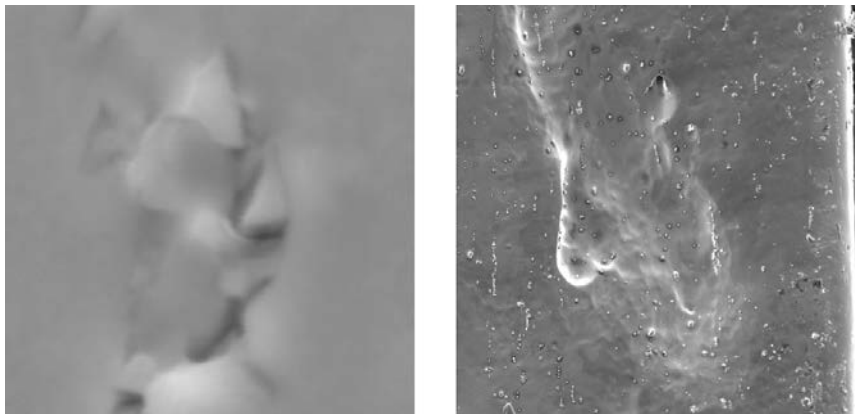

9.19 Electropolished Nitinol surface revealed the faces of the researchers, who contributed extensively to the study of this material, as observed by S. Shabalovskaya and J. Anderegg during long SEM sessions.

oxide layer to give the better protection against corrosion and Ni release is not applicable to superelastic Nitinol. Surface coatings and modifications with various energy sources do not seem to improve Nitinol biocompatibility. The Ti–Ni matrix alloy itself is not a reservoir for Ni release, but Ni-enriched interfaces formed due to heat treatments (and especially Ni in a non-oxidized, elemental state) are such a source.

The immuno-stimulatory effect of Ti–Ni, which may be deduced from *in vitro* and *in vivo* studies, merits further in-depth investigation. A new aspect of bare Nitinol surfaces, related to the possibility of manipulating Nitinol thrombogenicity, is also of great interest for both the applications requiring non-thrombogenic surfaces, like stents, and for high-thrombogenic surfaces required for defect closures and orthopaedic, and osseogenic implants. In order to improve the immediate response to implantation and also long-term implant performance, it is necessary to understand specifics of plasma proteins and platelet interactions with Nitinol surfaces. A deeper insight is needed into Nitinol surfaces:

1 the electronic structure of Nitinol surface oxides, their conductivity and reactivity, nano-structure and defects, surface charge, and oxide stoichiometry;
2 their fracture mechanics, microstructure, compositions;
3 the studies of explants.

To readers interested in obtaining a deeper knowledge into Nitinol as a biomaterial, we recommend the following readings. The biocompatibility aspects of Nitinol are discussed in topical books on shape memory alloys by Funakubo (1984) and also by Otsuka and Wayman, editors (1998), by Gunther, editor (2000), by Yahia, editor (2000), and in reviews on surface and biocompatibility by Shabalovskaya (1996, 2001, 2002 and 2008a), Ryhänen (2000), and Miyazaki (1998).

Biomechanics by Fung (1991) is of interest from the perspective of mechanical properties of living tissues. An excellent publication by Schetky (1997) should not be missed. Original articles concerning implantation analysis over a10-year experience with endovascular stent grafts (Marin, 2003, Jacob, 2003) are similarly valued. From the point of view of humanitarian and ethical aspects of ESG implantation, the discussion following the article of Marin *et al.* (2003) is of interest. A cycle of original papers of Sigler (2000, 2005, 2007) on the biocompatibility screening of cardiovascular implants (especially those related to defect closures) would also be very useful.

The authors are grateful to the Katholieke University Leuven Research Fund for supporting our benevolent effort. We are thankful to J. Willett who contributed his precious time to the editing of the manuscript and the enthusiastic help of the younger generation V. Koysin and A. Sezonenko with preparation of illustrations for this chapter is appreciated.

9.10 References

Al-Waheidi E (1995), 'Allergic reaction to nickel (Nitinol) orthodontic wires: A case report', *Quinte Int*, **26**(6), 385–388.

Armitage D, Parker T, Grant D (2003), 'Biocompatibility and haemocompatibility of surface-modified Ti–Ni alloys', *J Biomed Mater Res*, **66A**, 129–37.

Assad M, Jarzem P, Leroux M, Cillard C, Chernyshov A, Charette S, Rivard C (2003a), 'Porous Titanium–Nickel for intervertebral fusion in a sheep model: Part 1. Histomorphometric and radiological analysis', *J Biomed Mater Res,* **64B**, 107–120.

Assad M, Chernyshov A, Jarzem P, Leroux M, Cillard C, Charette S, Rivard C (2003b), 'Porous Titanium–Nickel for intervertebral fusion in a sheep model: Part 2. Surface analysis and nickel release assessment', *J Biomed Mater Res,* **64B**, 121–129.

Ayers R, Simske S, Bateman T, Petkus A, Sachdeva R, Gyunter V (1999), 'Effect of Nitinol implant porosity on cranial bone ingrowth and apposition after 6 weeks', *J Biomed Mater Res*, **45**, 42–47.

Balakrishnan N, Uvelius B, Zaszczurynski P, Lin D, Damasker M (2005), 'Biocompatibility of Nitinol and stainless steel in the bladder: an experimental study', *J Urol*, **173**, 647–650.

Bayer R, Roguin A (1997), 'Early and late results of self-expandable Nitinol stents: Interim report from multicenter European study', *J Interven Cardiol*, **10**, 207–213.

Berger-Gorbet M, Broxup B, Rivard C, Yahia L (1996), 'Biocompatibility testing of Ti–Ni screws using immunohistochemistry of section containing metallic implants', *J Biomed Mater Res*, **32**, 243–8.

Bogdanski D (2005), '*Untersuchungen zur biocompatibilität and biofunctionalität von implantatmaterialien am beispiel von Nickel-Titan-formgedächtnislegierungen*', Dissertation, Ruhr-Universität Bochum, Germany.

Brown S (2000), 'On methods used for corrosion testing of Ti–Ni', *Int Conf Shape Memory and Superelastic Technologies*, Asilomar, CA, Pacific Grove, 271–279.

Cai K, Bossert J, Jandt K (2006), 'Does the nanometer scale topography of titanium influence protein adsorption and cell proliferation?' *Colloids and Surfaces*, **49**, 136–144.

Cao P, Verzini S, Zannetti S (2002), 'Device migration after endolumenal abdominal aortic aneurysm repair: analysis of 113 cases with minimum follow-up period of two years', *J Vasc Surg*, **35**, 229–235.

Castleman L, Motzkin S, Alicandry E, Bonavit V (1976), 'Biocompatibility of Nitinol alloy as an implant material', *J Biomed Mater Res*, **10**, 695–731.

Chang B-S, Brown P, Sieber A, Valdevit A, Taneto K, Kostuik J (2004), 'Evaluation of biological response to wear debris', *The Spine J*, **4**, S239–S244.

Cheng Y, Zheng Y (2006), 'The corrosion behavior and hemocompatibility of TiNi alloys coated with DLC by plasma based ion implantation', *Surf Coat Technol*, **200**, 4543–4548.

Choi J, Bogdanski D, Köller M, Esenwein S A, Müller D, Muhr G, Epple M (2003), 'Calcium phosphate coating of nickel–titanium shape-memory alloys. Coating procedure and adherence of leukocytes and platelets', *Biomaterials,* **24**, 3689–3696.

Cisse O, Savagodo O, Wu M, Yahia L (2002), 'Effect of surface treatment of Ti–Ni alloy on its corrosion behavior in Hanks' solution', *J Biomed Mater Res*, **61**, 339–345.

Clarke B, Carroll W, Rochev Y, Hynes M, Bradley D, Plumley D (2006), 'Influence of Nitinol wire surface treatment on oxide thickness and composition and its subsequent effect on corrosion resistance and nickel ion release', *J Biomed Mater Res*, **79A**, 61–70.

Clarke B, Kingshott P, Hou X, Rochev Y, Gorelov A, Carroll W (2007), 'Effect of Nitinol wire surface properties on albumin adsorption', *Acta Biomater*, **3**, 103–111.

Cooke F (2000), 'Bulk properties of materials', in Ratner B and Hoffman A, Schoen F, Lemons J, *Biomaterials Science*, Boston, Academic Press, 11–35.

Cragg A, De Jong C, Barnhart W, Landas S, Smith T (1993), 'Nitinol intravascular stent: results of preclinical evaluation', *Radiol*ogy, **189**, 775–778.

Dotter C (1969), 'Transluminally-placed coil-spring endarterial tube grafts', *Invest Radiol*, **4**, 329–332.

Dotter C, Judkins M (1964), 'Transluminal treatment of arteriosclerotic obstruction', *Circulation*, **30**, 654–660.

Evans E (1994), 'Cell damage *in vitro* following direct contact with fine particles of titanium, titanium alloy and cobalt–chrome–molybdenum alloy', *Biomaterials*, **15**, 713–717.

Funakubo H (1984), *Shape memory alloys*, Gordon and Breach Science Publishers.

Fung Y (1991), *Biomechanics. Mechanical properties of living tissues*, New York, Springer–Verlag.

Galante J, Lemons J, Spector M, Wilson P, Wright T (1991), 'The biological effect of implant materials', *J Orthoped Res*, **9**, 760–775.

Goodman S (1999), 'Sheep, pig, and human platelet-material interactions with model cardiovascular devices', *J Biomed Mater Res,* **45**, 240–50.

Grenadier E, Shofti R, Beyer M, Beyer R (1994), 'Self-expandable and highly flexible Nitinol stent: immediate and long-term results in dogs', *Am Heart J*, **128**, 87–878.

Guidon R *et al.* (2000), 'First-generation aortic endiografts: Analysis of explanted Stentor devices from the EUROSTAR registry', *J Endovasc Ther*, **7**, 105–122.

Gunther V *et al.* (2000), *Delay Law in new class of materials and implants in medicine*, Northampton, MA, STT Publishing.

Gunther V, Sisolyatin P, Tomerkhanova P (1995), 'Superelastic and shape memory implants', in: *Maxillofacial surgery, traumatology, orthopaedics, and neurosurgery*, Mirgazizov M, Ziganshin R, eds, Tomsk University Publishing, Tomsk.

Heintz C, Riepe G, Birken L, Kaiser E, Chakfe N, Morlock M, Delling G, Imig H (2001), 'Corroded Nitinol wires in explanted aortic endografts: An important mechanism or failure?' *J Endovasc Ther*, **8**, 248–253.

Henry M, Amor M, Bayer R, Henry I, Park J M, Mentre B, Tricoche O, Ethevenot G (1996), 'Clinical experience with a new Nitinol self-expanding stent in peripheral arteries', *J Endovasc Surg*, **3**, 369–379.

Henry M, Amor M, Ethevenot G, Henry I, Amicabile C, Beron R, Mentre B, Allaoui M,

Touchot N (1995), 'Palmaz stent placement in iliac and femopopliteal arteries: primary and second patency in 310 patients with 2–4 year follow-up', *Radiol*ogy, **197**, 167–174.

Heßing C, Frenzel J, Pohl M, Shabalovskaya S (2007), 'Effect of martensitic transformation on the performance of coated Ti–Ni surfaces', *Mater Sci Eng*, doi:10.1016/j.msea.2007.09.029.

Hong M, Beyer R, Kornowski R, Tio F, Bramwell O, Leon M (1997), 'Acute and chronic effects of self-expanding Nitiniol stents in porcine coronary arteries', *Coron Artery Dis*, **8**, 45–48.

Itin V, Gyunter V, Khodorenko V, Chobanyan M, Mirgazizov M, Korsteleva E, Belyalova M (1996), 'Dynamic of ingrowth of living tissues in porous permeable implant. Mechanical behavior of the Nitinol-living tissue composite', *Letters J Tech Phys*, **22**(6), 37–42.

Itin V, Kotenko V (2006) 'Mechanical behavior of living tissues and the problems of functional materials for implantation', Proc Int Symp S*hape Memory Implants*, UNTPS JPC, Novosibirsk, p. 3–7.

Jacobs T, Won J, Gravereaux C, Faries P, Morryssey N, Teodorescu V, Hollier L, Marin M (2003), 'Mechanical failure of prosthetic human implants: a 10-year experience with aortic stent graft devices', *J Vasc Surg*, **37**, 16–26.

Janke T, Voshage G, Müller-Hülsback S, Grimm J, Heller M, Brossmann J (2002), 'Endovascular placement of self-expending Nitinol coil stents for the treatment of Femoropopliteal obstructive disease', *J Vasc Interv Radiol*, **13**, 257–266.

Kobayashi S, Ohgoe Y, Ozeki K, Sato K, Sumiya T, Hirakuri K (2005), 'Diamond-like carbon coatings on orthodontic archwires', *Diamond Related Mater*, **14**, 1094–1097.

Kobayashi Y *et al.* (2001), 'Long-term vessel response of self-expending coronary stent: A serial volumetric intravascular ultrasound analysis from the ASSURE trial', *J Am College Cardiol*, **37**(5), 1329–1334.

Kohilas K, Lyons M, Lofthouse R, Frondoza CG, Jinnah R, Hungerford DS (1999), 'Effect of prosthetic titanium debris on mitigen-induced monocyte and lymphoide activation', *J Biomed Mater Res*, **47**, 95–103.

Kong X, Grabitz W, Van Oeveren W, Klee D, Van Kooten T, Freudenthal F, Qing M, Von Bernuth G, Seghaye MC (2002), 'Effect of biologically active coating on biocompatibility of Nitinol devices designed for the closure of intra-atrial communications', *Biomaterials*, **23**, 1775–1783.

Koster R, Vieluf D, Kiehn M, Sommerauer M, Kahler J, Baldus S, Meinertz T (2000), 'Nickel and molybdenum contact allergies in patients with coronary in-stent restenosis', *Lancet*, **356**, 1895–1897.

Kraft C, Diedrich O, Burian B, Schmitt O, Wimmer M (2003), 'Microvascular response of striated muscle to metal debris', *J Bone Joint Surg*, **85B**, 133–141.

Kujala S, Ryhänen J, Danilov A, Tuukkanen J (2003), 'Effect of porosity on osteointegration and bone ingrowth of a weight bearing nickel–titanium bone graft substitute', *Biomaterials,* **24**, 4691–4697.

Kumazawa R, Watari F, Takashi N, Tanimura Y, Uo M, Totsuka Y (2002), 'Effect of Ti ions and particles on neutrophil function and morphology', *Biomaterials,* **23**, 3757–3764.

Lacy S, Meritt K, Brown S, Puryear A (1996), 'Distribution of nickel and cobalt following dermal and systematic administration with *in vitro* and *in vivo* studies', *J Biomed Mater Res*, **32**, 279–283.

Lasley C, Mitchell M, Dooley B, Bruchman W, Warner C (2003) 'Corrosion of Nitinol by exposure to decontaminating solutions', *Int Conf Shape Memory and Superelastic Technologies*, Asilomar, 375–384.

Lindenauer S, Stanley J, Zelenock J, Cronewett J, Whitehouse W, Erlandson E (1984), 'Aorto-iliac reconstruction with Dacron double velour', *J Cardiovasc Surg,* **25**, 36–42.

Lu S (1990), 'Medical applications of Ni–Ti alloys in China', in*: Engineering aspects of shape memory alloys*, T. Duerig, K. Melton, D. Stoeckel, C. Wayman, eds, Butterworth–Heinemann, 445–451.

Lucassen M, Sarkar B (1997), 'Nickel-binding constituents of human blood serum', *J Toxic Environ Health*, 5, 897–905.

Maitz M, Shevchenko N (2006), 'Plasma-immersion ion-implanted Nitinol surface with depressed Ni concentration for implants in blood', *J Biomed Mater Res*, **76A**, 356–365.

Marin M, Hollier L, Ellozy S, Spielvogel D, Mitty H, Griepp R, *et al.* (2003), 'Endovascular stent graft repair of abdominal and thoracic aortic aneurysms. A ten-year experience with 817 patients', *Ann Surg*, **238**, 586–595.

Menchaka L, Lam H, Leong I, Li S, Johnson D (2004), 'Endothelial and smooth muscle cell growth on titanium nickel thin film', *Int Conf Shape Memory and Superelastic Technologies, Germany*, Baden-Baden, 381–386.

Michel R (1987), 'Trace metal analysis in biocompatibility testing', CRC *Crit. Rev Biocompat*, **3**, 235–317.

Michiardi A, Aparicio C, Planell J, Gil F (2006a), 'New oxidation treatment of Ti–Ni shape memory alloys to obtain Ni-free surfaces and to improve biocompatibility', *J Biomed Mater Res,* **77B**, 249–256.

Michiardi A, Aparicio C, Ratner B, Planell J, and Gil J (2006b), 'The influence of surface energy on competitive protein adsorption on oxidized Ti–Ni surfaces', *Biomaterials,* **29**, 586–594.

Miyazaki S (1998), 'Medical and dental applications of shape memory alloys', in: *Shape Memory Materials*, K. Otzuka, C.M. Wayman, eds, Cambridge University Press, 267–281.

Morais S, Sousa J, Fernandes M, Carvalho G, J. de Bruijn, Van Blitterswijk C (1998), 'Effect of AISI 316 corrosion products in *in vitro* bone formation', *Biomaterials*, **19**, 999–1007.

Ohgoe Y, Kobayashi S, Kobayashi O, Aoki H, Nakamori H, Hirakuri K (2006), 'Reduction effect of nickel ion release on diamond-like carbon film coated onto an orthodontic archwire', *Thin Solid Films*, **497**, 218–222.

Okazaki Y, Rao S, Ito Y, Tateishi T (1998), 'Corrosion resistance, mechanical properties, corrosion fatigue strength and cytocompatibility of new Ti alloys without Al and V', *Biomaterials*, **19**, 1197–1215.

Otsuka K, Wayman C (1998), *Shape memory materials*, Cambridge, University Press, p. 284.

Palmaz J, Bailey D, Marton D, Sprague E (2002), 'Influence of stent design and material composition on procedure outcome', *Basic Sci Rev*, Article 36, 1031–1040.

Park J, Gemmel H, Davies J (2001), 'Platelet interactions with titanium: modulation of platelet activity by surface topography', *Biomaterials*, **22**, 2671–2682.

Parodi J, Marin M, Veuth F (1995), 'Transfemoral endovascular stent graft repair of an abdominal aortic aneurysm', *Arch Surg*, **130**, 549–552.

Peitsch T, Klocke A, Kahl-Nieke B, Prymak O, Epple M (2007), 'The release of nickel from orthodontic Ti–Ni wires is increased by dynamic mechanical loading but not constrained by surface nitridation', *J Biomed Mater Res*, **82A**, 731–739.

Plant S, Grant D, Leach L (2005), 'Behavior of human endothelial cells on surface modified Ti–Ni alloy', *Biomaterials*, **26**, 5359–5367.

Ponsonnet L, Reybier K, Jaffrezic N, Comte V, Lagneau C, Lissac M, Martelet C (2003), 'Relationship between surface properties (roughness, wettability) of titanium and titanium alloys and cell behaviour', *Mater Sci Eng*, **23C**, 551–560.

Poon R, Yeung K, Liu X, Chu P, Chung C, Lu W, Cheung K M C, Chan D (2005), 'Carbon plasma immersion ion implantation of Ti–Ni shape memory alloys', *Biomaterials,* **26**, 2265–72.

Prymak O, Bogdanski D, Köller M, Esenwein S, Muhr G, Beckmann F, Donath T, Assad M, Epple M (2005), 'Morphological characterization and in vitro biocompatibility of a porous nickel–titanium', *Biomaterials*, **26**, 5801–5807.

Rae T (1975), 'A study of the effect of particulate metals of orthopaedic interest on murine macrophages in vitro', *J Bone Joint Surg* (Br), **5B**, 444–450.

Rhalmi S, Charette S, Assad M, Coillard C, Rivard C (2007), 'The spinal cord dura matter reaction to Nitinol and titanium alloy particles: a 1 year study on rabbits', *Eur Spine*, **16**, 1063–1072.

Riede U, Ruedi T, Rohner Y, Perren S, Guggenheim R (1974), 'Quantitative and morphologisheerfassung der geweberreaction auf metallimplante', *Arch Orthop Unfall Chir*, **78**, 199–214.

Riepe G, Heintz C, Kaiser E, Chakfe N, Morlock M, Delling M, Imig H (2002), 'What can we learn from explanted endovascular devices?', *Eur J Vasc Endovasc Surg*, **24**, 117–122.

Ries M, Kampmann C, Rupprecht H, Hintereder G, Hafner G, Meyer J (2003), 'Ni release after implantation of the Amplatzer occluder', *Am Heart J*, **145**, 737–741.

Roguin A, Granadier E, Linn S, Markiewicz W, Beyer R (1999), 'Continued expansion of Nitinol self-expandable stent angiographic analysis and 1-year clinical follow-up', *Am Heart J*, **138**(2), 326–333.

Rondelli G, Vicentini B, Cigada A (1990), 'The corrosion behavior of nickel titanium shape memory alloys', *Corr Sci,* **30**, 805–812.

Ryhänen J, Kallioinen M, Serlo S, Peramaki P, J. Junila, Sandvik P, Niemelä E, Tuukkanen J (1999), 'Bone healing and mineralization, implant corrosion and trace metals after nickel–titanium shape memory metal intramedullary fixation', *J Biomed Mater Res*, **47**, 472–480.

Ryhänen J, Kallioinen M, Tuukkanen J, Junila J, Niemelä E, Sandvik P, Serlo V (1998), '*In vivo* biocompatibility evaluation of nickel–titanium shape memory alloy. Muscle and peripheral tissue responses and encapsule membrane thickness'*, J Biomed Res*, **41**, 481–488.

Ryhänen J, Niemi E, Serlo S, Niemelä E, Sandvik P, Pernu H, Salo T (1997), 'Biocompatibility of nickel–titanium metal and its corrosion behaviour in human cell cultures'*, J Biomed Mater Res*, **35**, 451–457.

Sabeti S, Schillinger M, Amighi J, Sherif C, Mlekush W, Ahmadi R, Minar E (2004), 'Primary patency of femoropopliteal arteries treated with Nitinol versus stainless steel self-expendindg stents: propensity score-adjusted analysis', *Radiol*ogy, **232**, 516–521.

Saraf H, Ramesh K, Lennon A, Merkle A, Roberts J (2007), 'Mechanical properties of soft human tissues under dynamic loading', *J Biomech*, **40**, 1960–1967.

Sarembock I, LaVeau P, Sigal S, Timms I, Sussman J, Haudenschild C, Ezekowitz M D (1989), 'Influence of inflation pressure and balloon size on the development of intimal hyperplasia after balloon angioplasty; a study in the atherosclerotic rabbit', *Circulation*, **80**, 1029–1040.

Schetky McD (1997), 'Shape Memory Alloys'*, Kirk–Othmer encyclopedia of chemical technology*, V. 21 by John Wiley & Sons, Inc, 962–976.

Schmutz P, Frankel G, Serry F (2005), 'Corrosion studies with AFM, Part 1: Characterization of potential inhomogeneities on passive surfaces by surface potential imaging', *Veeco Instruments Inc*, **5**, AN87–91.

Schürmann K, Vorwerk D, Kulisch A, Ströhmer-Kulisch E, Biesterfelds S, Stopinski T, Günther R W (1996), 'Neointimal hyperplasia in low-profile Nitinol stents, Palmaz stents

and Wall stents: a comparative experimental study', *Cardiovasc Intervent Radiol*, **19**, 248–254.

Schwartz R, Huber K, Murphy J, Edwards W, Camrud A, Vlietstra R, Holmes D (1992), 'Restenosis and the proportional neointimal response to coronary artery injury: results in a porcine model', *J Am Coll Cardiol*, **19**, 267–274.

Shabalovskaya S (1996), 'On the nature of biocompatibility and medical applications of Ti–Ni shape memory alloys', *Bio Med Mater Eng*, **6**, 267–290.

Shabalovskaya S (2001), 'Physicochemical and biological aspects of Nitinol as a biomaterial', *Int Mater Rev*, **4**, 233–250.

Shabalovskaya S (2002), 'Surface, corrosion and biocompatibility aspects of Nitinol as an implant material', *Bio Med Mater Eng*, **12**, 69–109.

Shabalovskaya S, Anderegg J, Laabs F, Thiel P, Rondelli G (2003a), 'Surface conditions of Nitinol wires, tubing, and as-cast alloys: The effect of chemical etching, aging in boiling water, and heat treatment', *J Biomed Mater Res*, **65B**, 193–203.

Shabalovskaya S, Anderegg J, Rondelli G, Vanderlinden W, De Feyter S (2008a), Comparative in vitro performances of bare Nitinol surfaces', *Biomed Mater Eng*, 1**8**(1), 1–14.

Shabalovskaya S, Anderegg J, Rondelli G, Xiong J (2003b), 'The effect of surface particulates on the corrosion resistance of Nitinol wire', *Int Conf Shape Memory and Superelastic Technologies*, Asilomar, 399–408.

Shabalovskaya S, Anderegg J, Van Humbeeck J (2008b), 'Critical overview of Nitinol surfaces and their modifications for medical applications', *Acta Biomater*, **4**(3), 447–467.

Shabalovskaya S, Anderegg J, Van Humbeeck J (2007b), 'Recent observations of particulates in Nitinol', *Mater Sci Eng*, **481–482C**, 431–436.

Shabalovskaya S, Rondelli G, Anderegg J, Xiong J, Wu M (2004b), 'Comparative corrosion performance of black oxide, sandblasted, and fine-drawn Nitinol wires in potentiodynamic and potentiostatic tests: Effects of chemical etching and electropolishing', *J Biomed Mater Res*, **69B**, 223–231.

Shabalovskaya S, Wataha J, Anderegg J, Hauch K, and Cunnick J (2004a), Surface treatments and biocompatibility of Nitinol, *Int Conf Shape Memory and Superelastic Technologies.* Germany, Baden-Baden, 367–373.

Sheth S, Litvack F, Visha D, Fishbein M, Forrester J, Eigler N (1996), 'Subacute thrombosis and vascular injury resulting from slotted-tube Nitinol and stainless-steel stents in rabbit artery model', *Circulation,* **94**, 1733–1740.

Shevchenko N, Pham M, Maitz M (2004), 'Studies of surface modified Ti–Ni alloys', *Appl Surf Sci*, **235**, 126–31.

Shih C, Lin S, Chen Y, Su Y. Lai S, Wu G, Kwok C, Chung K (2000), 'The cytotoxicity of corrosion products of Nitinol stent wires on cultured smooth muscle cells', *J Biomed Mater Res,* **52**, 395–403.

Sigler M, Handt S, Seghaye M C, Van Bernuth G, Grabitz R (2000), 'Evaluation of in vivo biocompatibility of different devices for interventional closure of the patent ductus arteriosus in animal model', *Heart*, **83**, 570–573.

Sigler M, Jux C (2007), 'Biocompatibility of septal defect closure devices', *Heart*, **93**, 444–449.

Sigler M, Paul T, Grabitz R (2005), 'Biocompatibility screening in cardiovascular implants', *Z Kardiol*, **94**, 383–391.

Simske S, Sachdeva R (1995), 'Cranial bone apposition and ingrowth in a porous Ti–Ni implant', *J Biomed Mater Res*, **29**, 527–533.

Sladen J, Gilmour J, Wong R (1986), 'Cumulative patency and actual palliation in patients with claudication after aortofemoral bypass. Prospective long-term follow-up of 100 patients', *Am J Surg*, **152**, 190–195.

Sui J, Cai W (2006), 'Effect of diamond-like carbon (DLC) on the properties of Ti–Ni alloys', *Diamond Relat Mater*, **15**, 1720–1726.

Sunderman F (1984), 'Carcinogenicity of nickel compounds in animals', in: *Nickel in human environment*, International Agency for Research on Cancer, Leon, 127–143.

Sysolyatin P, Gyunter V, Starokha A (1994), 'The use of Ni–Ti implants in maxillofacial surgery', *1st Int Conf Shape Memory and Superelastic Technologies*, Pacific Grove, California, A. Pelton, D. Hodgson, T. Duerig, eds, 461–464.

Takeshita F, Takata H, Ayukawa Y, Suetsugu T (1997), Histomorphometric analysis of the response of rat tibia to shape memory alloy (Nitinol)', *Biomaterials,* **18**, 21–25.

Tepe G, Schmehl J, Wendel H, Schaffner S, Heller S, Gianotti M, Claussen C, Duda S (2006), 'Reduced thrombogenicity of Nitinol stents – in vitro evaluation of different surface modifications and coatings', *Biomaterials*, **27**, 643–650.

Thierry B, Merhi Y, Bilodeau L, Trepanier C, and Tabrizian M (2002), 'Nitinol versus stainless-steel stents: Acute thrombogenicity study in an *ex vivo* porcine mode', *Biomaterials,* **23**, 2997–3005.

Thierry B, Tabrizian M (2003), 'Biocompatibility and biostability of metallic endovascular implants: State of art and perspectives', *J Endovasc Ther*, **10**, 807–824.

Undisz A, Schrempel F, Wesch W, Rettenmayr M (2008), 'In-situ observation of surface oxide layers on medical grade Ni–Ti alloy during straining', *J Biomed Mater Res*, in press.

Uo M, Watari F, Yokoyama A, Matsuno H, Kawasaki T (1999), 'Dissolution of nickel and tissue response observed by X-ray scanning analytical microscopy', *Biomaterials,* **20**, 747–755.

Veith F, Gupta S, Ascer E, White-Flores S, Samson R, Scher L, *et al.* (1986), Six-year prospective multicentral randomized comparison of autologus saphenous vein and expanded grafts in infrainguinal arterial reconstructions', *J Vasc Surg,* **3**, 104–114.

Versaigne S, Wolke J, Naert, Jansen J (1998), 'Histomorphometrical and mechanical evolution of titanium plasma spray-coated implants, placed in the cortical bone of goats', *J Biomed Mater Res,* **41**, 41–48.

Wang J, Mwickland B**,** Gustilo R, Tsukayama D (1996), 'Ti, Cr, and Co ions modulate the release of bone-associated cytokines by human monocytes/mackrophages *in vitro'*, *Biomaterials*, **17**, 2233–2240.

Wataha J, Lewis J, Volkman K, Lockwood P, Messer R, Bouillaguet S (2004), 'Sublethal concentrations of Au(III), Pd(II), and Ni (II) differentially alter inflammatory cytokine secretion from activated monocytes', *J Biomed Mater Res*, **69B**, 11–17.

Wataha J, Lockwood P, Marek M, Ghazi M (1999), 'Ability of Ni-containing biomedical alloys to activate monocytes and endothelial cells *in vitro', J Biomed Mater Re*s, 45, 252–257.

Wataha J, O'Dell N, Singh B, Ghazi M, Whitford G, Lockwood P (2001), 'Relating nickel-induced tissue inflammation to Ni release *in vivo*', *J Biomed Mater Res*, **58**, 537–544.

Wever D, Velderhuizen A, De Vries J, Busscher H, Uges D, and Van Horn J (1998), 'Electrochemical and surface characterization of Ti–Ni alloy', *Biomaterials*, **19**, 761–69.

Williams D F (1987), Definitions in biomaterials, *Proc Consensus Conf Europ Soc Biomaterials*, Chester, England, V. 4, Elsevier, New York.

Yahia L'H, Hernandez R, Rhalmi S, Turenne S, Prudhommeaux F, Tabrizian M (2000), 'A biocompatibility study of porous Ti–Ni', *3rd Int Conf Shape Memory and Superelastic Technologies*, Pacific Grove, CA, 353–359.

Yeung K, Poon R, Liu X, Ho J, Chung C, Chu P, *et al.* (2005), 'Improvement of corrosion resistance, mechanical properties and cyto-compatibility of Ti–Ni shape memory alloys using nitrogen, and oxygen plasma immersion ion implantation', *J Biomed Mater Res*, **75A**, 256–267.

10

Self-expanding Nitinol stents for the treatment of vascular disease

D. STOECKEL, A. PELTON and T. DUERIG
Nitinol Devices & Components, USA

Abstract: Self-expanding Nitinol stents have revolutionized the treatment of peripheral vascular disease. Nitinol stents are manufactured to a size slightly larger than the target vessel size and delivered constrained in a delivery system. After deployment, they position themselves against the vessel wall with a low, 'chronic' outward force. They resist outside forces with a significantly higher radial resistive force. This unique behaviour can be directly attributed to the unusual properties of Nitinol, particularly its stress/strain hysteresis. How these material properties relate to the characteristic performance of self-expanding stents is explained. Biocompatibility and corrosion resistance of Nitinol stents are critically reviewed, as well as durability and fatigue. Commercially available stents are listed and differentiated.

Key words: Nitinol, Ni–Ti, Ti–Ni, self-expanding stents, vascular disease, biocompatibility.

10.1 Introduction

Self-expanding Nitinol stents have found widespread use in the treatment of peripheral vascular disease and the treatment of obstructions in non-vascular vessels. They represent one of the largest volume users of superelastic/shape memory alloys. Stents are scaffolding devices placed in a vessel to maintain patency of the vessel lumen for as long as possible. They are typically classified as either balloon-expandable (BX) or self-expanding (SX) depending on how deployment is effected.[1] BX stents are manufactured in the crimped state and expanded to the vessel diameter by inflating a balloon, thus plastically deforming the stent. SX stents, on the other hand, are manufactured slightly above the vessel diameter. They are crimped and constrained in a delivery catheter. At the treatment site the constraint is removed and the stent expands elastically until it hits the vessel wall, where it continues to exert a gentle outward force. Thus, the function of BX stents is based on the plastic deformation of the stent material (typically stainless steel or cobalt based alloys), while SX stents are made from materials exhibiting high elasticity. The superelastic behavior of Nitinol makes this material particularly suitable for self-expanding stents.

When Charles Dotter experimented with Nitinol wire coils as intra-arterial

scaffolds back in the early 1980s, Nitinol was known only for its unusual shape memory effect.[2] A coil wound to a small diameter and delivered through a catheter into the vessel, would expand to a larger diameter, e.g. the diameter of the vessel lumen, upon warming with 60 °C saline solution. Although the shape memory effect looked ideally suited for the scaffolding of vessels, it took many more years for Nitinol stents to appear in the market. Dotter clearly was ahead of his time. The melting and processing of Nitinol had not been fully developed with consistent quality, nor had the properties of this material been fully understood. Today, 25 years after Dotter's experiments, Nitinol stents are self-expanding without the need for post-deployment heating. All major medical device companies as well as many smaller producers now offer Nitinol stents for (mainly peripheral) vascular and non-vascular indications.

In the following, we will describe the unique material properties of Nitinol and how they relate to the performance characteristics of Nitinol stents.

10.2 Nitinol specific device characteristics

As described earlier in this book, Nitinol is an alloy composed of approximately 55 wt% nickel and balance titanium. It has found widespread acceptance as a material of choice for medical implants and devices.[3] It derives its unique properties from a solid state transformation, which can be triggered thermally or mechanically, and is dependent on the composition and processing history of the material. This adds another level of complexity to material specifications and may explain why ASTM specifications[4,5,6] describing material composition and test methods have only recently been issued. In addition to, or even instead of, the commonly known material characteristics like chemical composition, Young's modulus, yield strength, ultimate tensile strength and elongation to failure, properties like transformation temperature, upper and lower plateau stress, recoverable strain and permanent set have to be taken into account. As mentioned above, these properties are strongly dependent on the processing history and play an important role in the design and manufacturing of self-expanding stents.[7]

The most unusual property of Nitinol alloys is *stress hysteresis*. While in most engineering materials stress increases linearly with strain upon loading and decreases along the same path upon unloading, Nitinol exhibits a distinctly different behavior. After an initial linear increase in stress with strain, large strains can be obtained with only a small further stress increase along the loading plateau. The end of this plateau is reached at about 8% strain. Unloading from the end of the plateau region, causes the stress to decrease rapidly until the unloading plateau is reached. Strain is recovered in this region with only a small decrease in stress. The last portion of the deforming strain is finally recovered in a linear fashion.

The stress hysteresis or path dependence of Nitinol results in a device feature termed *biased stiffness*.[8] This concept is illustrated in Fig. 10.1, which shows a schematic superelastic stress–strain curve for Nitinol, illustrating both non-linear

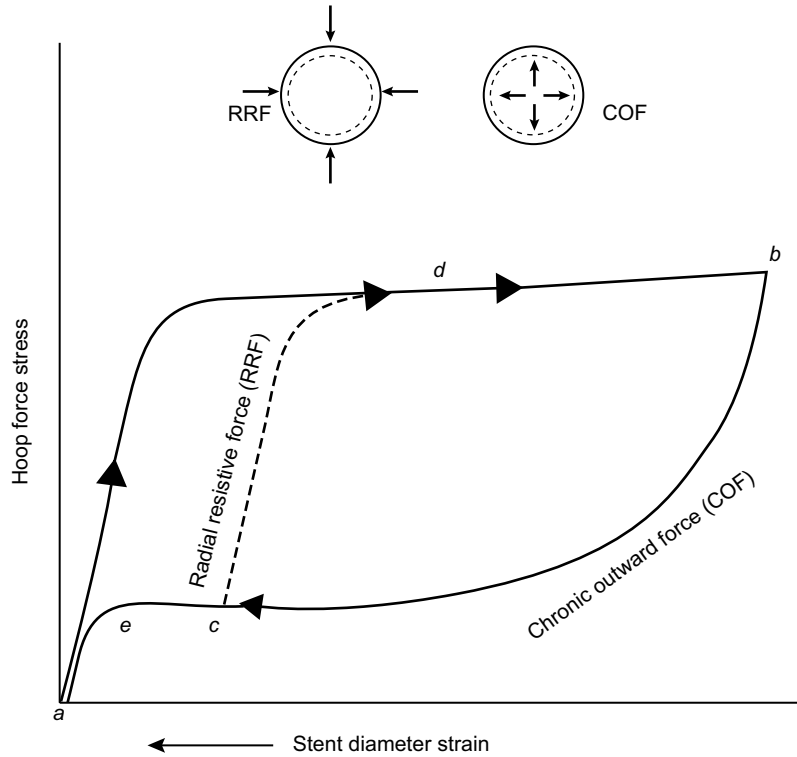

10.1 A typical stress–strain curve transposed onto a hoop force/diameter diagram, illustrating the concept of biased stiffness: *a* stent with a given diameter a is compressed into a delivery system with a diameter *b*, deployed in a vessel and expanding from *b* until movement is stopped by impingement with the vessel at diameter *c*, further deformation forces resisted by radial resistive force along *c* to *d*, while the chronic outward force remains constant and gentle (to *e*). Note that stent diameter is decreasing from left to right along the *x*-axis for this demonstration.

response and hysteresis. Using this graph, we will follow the cycle of crimping a stent into a delivery system, deploying it and have it expand and interact with the vessel. For this purpose, the axes have been changed from stress–strain to hoop force–stent diameter. A stent of a given size larger than the vessel (point 'a') is crimped into a delivery system (point 'b'), then packaged, sterilized and shipped. After insertion to the target site, the stent is released into a vessel, expanding from 'b' until movement is stopped by impingement with the vessel (point 'c'). At this point, further expansion of the stent is prevented. Because the stent did not expand to its pre-set shape, it continues to exert a low outward force, termed *chronic outward force* or COF. However, it will resist recoil pressures or any other external compression forces with forces dictated by the loading curve from point 'c' to 'd',

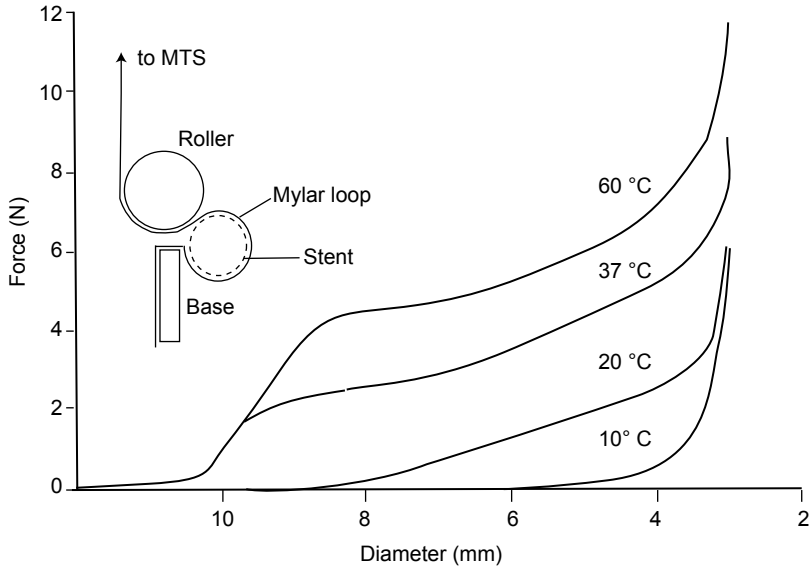

10.2 Unloading curves of Nitinol stents (Cordis SMART stent with a nominal transition temperature A_f of 30 °C) at different deployment temperatures; insert: radial force test set-up, schematic.

which is substantially steeper (stiffer) than the unloading line (towards 'e'). These forces are called *radial resistive forces* or RRF.

The unusual elastic behavior of Nitinol allows the continuing opening force, COF, of the stent acting on the vessel wall to remain very low even through large deflections and oversizing of the stent (it is typically recommended to use a size of a stent that is 1–2 millimeters larger than the inner diameter of the target vessel). Meanwhile the forces generated by the stent to resist compression, RRF, increase rapidly with deflection until the plateau stress is reached. Although most self-expanding stent placements are preceded by a percutaneous transluminal balloon angioplasty, there are indications that the chronic outward force of a Nitinol stent placed without prior percutaneous transluminal angioplasty (PTA) causes the vessel to remodel with less intimal hyperplasia than if PTA is performed before to stenting.[9]

Another unusual feature of Nitinol stents is their *temperature-dependent stiffness*. Stents with a transition temperature of 30 °C feel quite weak when squeezed or crushed at room or lower temperature. In contrast, they feel much stiffer when squeezed at body temperature. Figure 10.2 shows actual unloading curves of a Nitinol stent (Cordis SMART Stent) with a fully expanded diameter of 10 mm at different temperatures. The test set-up (insert) is described in.[10] As can be seen from this graph, the chronic outward force actually doubles when the temperature is increased from 20 to 37 °C. As mentioned before, the transition temperature of the stent can be adjusted to a certain extent during processing. This gives the

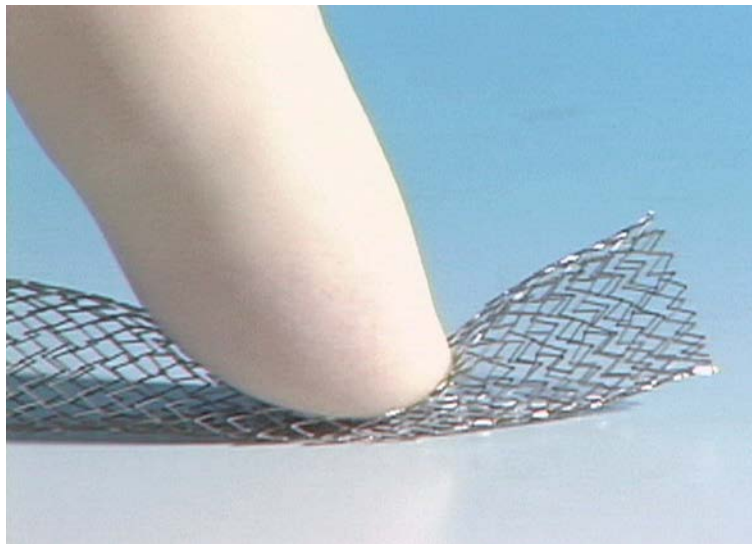

10.3 Extreme deformation of a Nitinol stent (Cordis SMART stent); the stent recovers after the load is removed.

designer another option to increase or decrease the radial forces of the stent without changing the design or physical dimensions, as for each degree that the transition temperature is below body temperature, the loading and unloading forces increase by approximately 4 N mm^{-2}.

Kink resistance is an important feature of Nitinol for stents in superficial vessels that could be deformed through outside forces. The carotid artery is a prime example. There is a perceived risk for balloon-expandable stents in carotid arteries to be permanently deformed through outside pressure resulting in a partially or completely blocked vessel, once the buckling strength of the stent is exceeded. Although Nitinol stents typically do not have the buckling strength of stainless-steel stents, they cannot be permanently deformed through outside forces. Nitinol stents can be completely compressed (crushed) flat and will return to their original diameter when the deforming force is removed (Fig. 10.3). A quantitative analysis of the forces relevant to the performance of superelastic stents was carried out by Wang.[11]

Nitinol is non-ferromagnetic with a lower magnetic susceptibility than stainless steel. The magnetic resonance imaging (*MRI) compatibility* is directly related to the susceptibility properties of a material, relative to human tissue.[12] Therefore, Nitinol produces fewer artifacts than stainless steel, similar to pure titanium. It has to be noted, however, that processing of the material can influence the quality of the MRI image substantially.

10.3 Nitinol stent designs

While the goal of stenting is clearly to maintain patency of the vessel lumen for as

Table 10.1 Approval status of some Nitinol self-expanding stents in the USA

Company	Stent	Indication				
		Biliary	Carotid	Iliac	SFA	Other
Abbott	Xact	X	X			
Abbott	Xceed	X				
Abbott	Xpert	X				
Abbott	JoStent SelfX	X				
Bard	Fluency	X				
Bard	Luminexx	X				
Bard	Conformexx	X				
Bard	Vivexx		Trial			
BSC	Sentinol	X				
BSC	Symphony	X				
BSC	NexStent		X			
Cook	Zilver	X			Trial	
Cordis	SMART	X		X	Trial	
Cordis	Precise	X	X			
Edwards	LifeStent NT	X			Trial	
ev3	Intracoil	X			X	
ev3	Protégé	X	X			
Gore	Viabahn	X			X	
Gore	Viatorr	X				TIPS
Guidant	Absolute	X				
Guidant	Acculink		X			
Guidant	Dynalink	X				
Medtronik	Aurora	X				
Medtronik	Bridge SE Aurora	X				
Medtronik	Exponent		Pending			

long as possible, there is a multitude of design parameters that may affect the clinical performance of the stent. Amongst those are strength and stiffness (radial resistive and chronic outward forces), scaffolding (window size and shape), conformability, flexibility during delivery as well as after deployment, fatigue durability in pusatile and non-pulsatile deformation modes, crush recoverability, delivery profile, expansion ratio, oversizing strategy, foreshortening, radiopacity, and last but not least biocompatibility and corrosion resistance. There is no clear indication that any one of those parameters has a more pronounced impact on clinical performance than the others. In the end, it is the combination of many aspects that influences stent performance. As all design parameters are interrelated, a change in one input results in changes in many outputs, requiring compromises in optimization.

Worldwide, there are probably close to 100 different Nitinol Stent designs being marketed or in evaluation. Table 10.1 shows a list of self-expanding Nitinol stents currently available in the US and their approved indications. Basically all stents are FDA approved for the treatment of biliary blockages or obstructions. While this is a non-vascular application, most stents have been, and are, used off-label to treat

peripheral vascular desease. Only a limited number of Nitinol stents are approved for specific vascular indications, like the carotid, iliac, or superficial femoral arteries.

Most reviews differentiate stents by their clinical use, e.g. vascular or non-vascular, coronary or peripheral, carotid or femoral, etc.[13] As the focus of this book is on Nitinol, we will differentiate stent designs by the form of material used for their production (wire, sheet or tubing), and will mention or describe typical examples. Stents included in this chapter have been shown in conference presentations, company brochures and websites. Like others, this review is not complete and it may describe, besides stents that are being marketed, stents that are not yet or no longer on the market.

10.3.1 Wire-based stent designs

The evolution of Nitinol stent designs is clearly linked to the development of the material itself. Early on, Nitinol was only available in wire form. Consequently, early Nitinol stents were wire coils, similar to Dotter's experimental device. Today, coil stents made from round or flat Nitinol wire are rarely used. They are mainly used for non-vascular applications (e.g. Endocare's Horizon Stent for the relief of bladder outlet obstruction[14]), with the exception of the IntraCoil Stent (eV3), which was approved in 2002 for the treatment of patients with superficial femoral artery and popliteal artery lesions.[15] One advantage of simple wire coils is their retrievability in certain applications. As described earlier, Nitinol loses its stiffness when cooled. The EndoCare Horizon or the D&E Memokath prostatic stents can be retrieved from the prostate by chilling the device with cold solution. The stents become soft and pliable and can be retrieved with a grasping forceps.

Other early wire based stent designs are the Cragg Stent (MinTec),[16] a sinusoidal coil with peak-to-valley suture connections for vascular and non-vascular applications, and the knitted Ultraflex Esophageal Stent (Boston Scientific).[17] The ZA biliary stent (Cook Medical)[18] employs a modified knitted design (Fig. 10.4). The Supera Stent (Idev Technologies),[19] which recently received FDA 510k clearance for use in the biliary tree, is made from braided Nitinol wire. Gore uses a wire scaffold in its ViaBahn stent graft, a device that is approved by the FDA for treating the superficial femoral artery (SFA).[20] The Boston Scientific Symphony Stent is a wire formed design with struts welded to form hexagonal cells (Fig. 10.5).[21] While wire-based stents generally are very flexible, the Symphony Stent is quite rigid.

10.3.2 Sheet-based stent designs

A perceived disadvantage of braided or knitted wire-based stents is the crossing of the filaments. This increases the 'wall thickness' of the stent and the delivery profile. Moreover, there are concerns about fretting corrosion or the wear of the Nitinol at the cross-over points. When Nitinol sheet became available, Angiomed

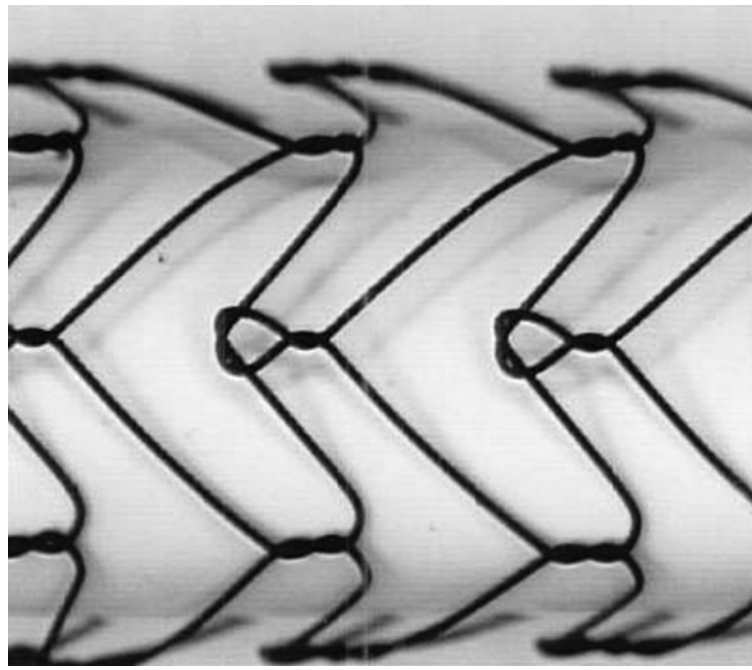

10.4 Knitted wire stent (Cook Medical ZA).

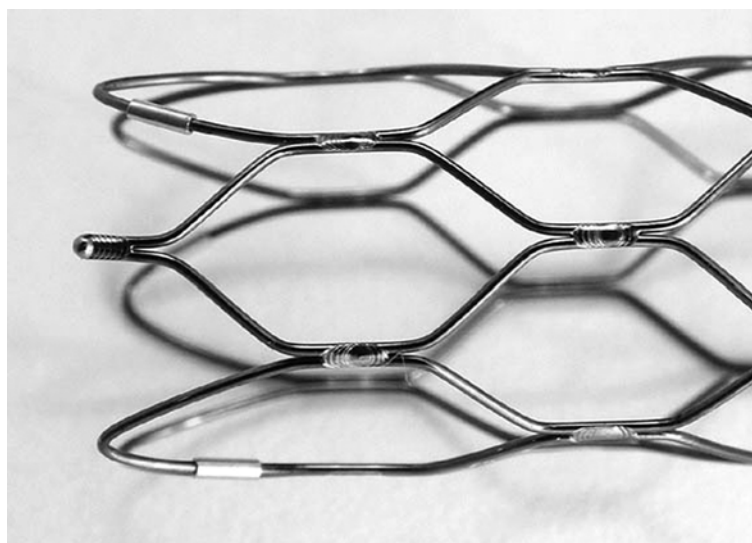

10.5 Formed and welded wire stent (Boston Scientific Symphony).

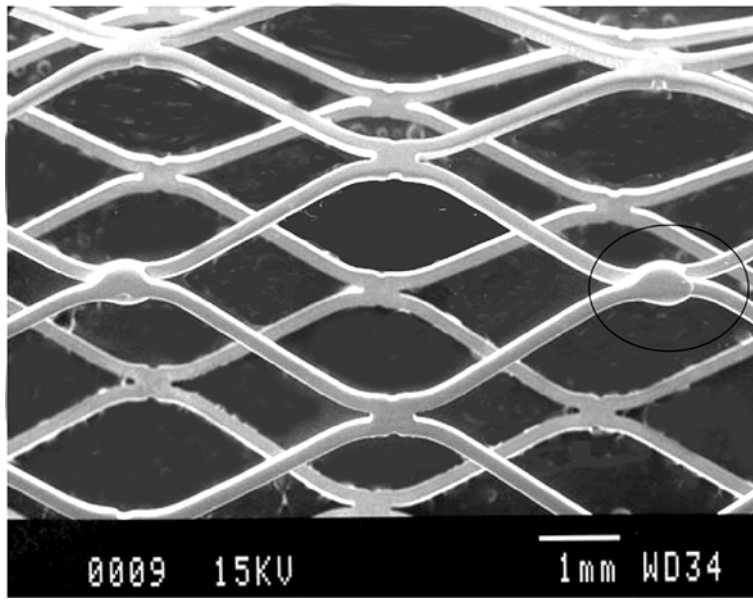

10.6 Early stent laser-cut from sheet and overlap welded (Bard Angiomed Memotherm).

(Bard) developed the Memotherm stent, the first laser-cut Nitinol stent, by cutting a pattern from sheet, rolling it up and welding at specific strut locations (Fig. 10.6).

In 2006, the FDA approved Boston Scientific's NexStent for use in patients with carotid artery disease.[22] The NexStent is made from a laser cut Nitinol sheet that, for delivery in a catheter, is tightly rolled up. After being released from the delivery system, it 'un-coils' and can adapt to multiple diameters in tapered or non-tapered vessel configurations.

Reva Medical is developing a sheet-based Nitinol stent that can be balloon expanded based on a 'slide and lock' design.[23] This idea is similar to the experimental 'ratcheting' EndoTex stent. This stent is photochemically etched from thin Nitinol sheet to produce a series of windows and a locking feature at one edge. It is rolled up to a small diameter roll and placed onto a percutaneous transluminal coronary angioplasty (PTCA) balloon. The assembly is then placed into the vessel and the diameter of the stent is adjusted by inflating the balloon. As the balloon expands, the stent uncoils to the desired diameter to prop open the vessel. The stent is locked into place by unique tabs that slide into the stent 'windows' upon balloon deflation. This design provides a wide range of diameters to custom fit for each treatment. It combines balloon expandability with the superelasticity after deployment. However, it has some of the perceived disadvantages of the knitted wire stents with non-uniform cross-section and potential fretting cross-over points.

Vascular Architect's aSpire stent uses a 'dual-rail ladder type' frame that can

also be photo-etched from Nitinol sheet and covered with ePTFE. It is helically coiled onto a delivery system that allows deployment with a variable pitch to keep vessel sidebranches open.[24]

10.3.3 Tube-based stent designs

In the mid 1990s, Nitinol seamless tubing appeared on the market in production quantities. With it came laser cutting of tubular Nitinol components. Today, most self-expanding Nitinol stents are produced by laser cutting of Nitinol tubing. A pattern is cut into Nitinol tubing with a diameter close to the delivery size. Subsequently, the cut part is expanded to the final stent diameter (slightly larger than the target vessel diameter) in a sequence of forming and heat-treating steps, which also control the transformation temperature. In a final step, the stent is electropolished to create a smooth and biocompatible surface. For delivery, it is crimped back to the original tubing size and constrained in a delivery system. This is typically done at temperatures below the transformation temperature of the stent.

Early examples of tube-based laser-cut stents are the Angiomed (Bard) Memotherm and the Scimed (BSC) Radius stents. The Memotherm was a rigid, closed-cell design with a diamond-shaped pattern similar to the original Palmaz balloon expandable stent. The Radius, on the other hand, is a flexible open-cell design with sequential rings and periodic peak-to-peak non-flex bridges. The advancement in laser cutting techniques and other processing technologies during the last few years made possible the production of Nitinol stents with small feature sizes, and Nitinol tubes with diameters as small as 0.3 mm can be processed. The Cordis SMART (Fig. 10.7) stent was the first self-expanding stent that employed a 'micromesh' design for improved scaffolding and prevention of tissue prolapse. Most of today's Nitinol stents employ variations of these basic design features (Fig. 10.8). However, despite the similarities in design, different stents can yield different clinical outcomes, and it is still hard to tell what exactly makes one stent better than the other in clinical use.

Laser-cut stents from Nitinol tubing are being produced in a wide range of sizes. Neurovascular stents like the WingSpan Stent (Boston Scientific) are indicated for use in improving cerebral artery lumen diameter in patients with intracranial atherosclerotic disease.[25] 'Vascular reconstruction devices' like the Enterprise device (Cordis) are intended for use with embolic coils for the treatment of wide-neck, intracranial, saccular or fusiform aneurisms in vessels of 3 to 4 mm diameter.[26] At the other end of the spectrum are aortic stents or colonic stents with diameters of >30 mm.

10.3.4 Radiopacity enhancements

Theoretical calculations as well as experimental studies show that the radiopacity of Nitinol is similar to that of stainless steel for equivalent dimensions. However,

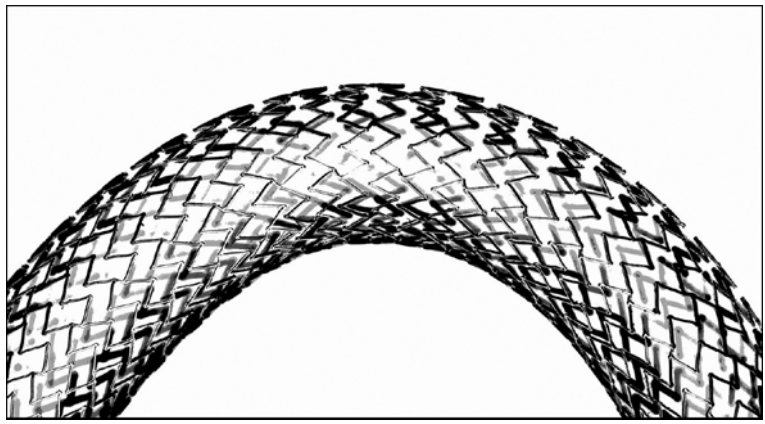

10.7 'Micromesh' design of a stent laser-cut from tube and expanded to a given diameter, demonstrating flexibility in the expanded condition (Cordis SMART stent).

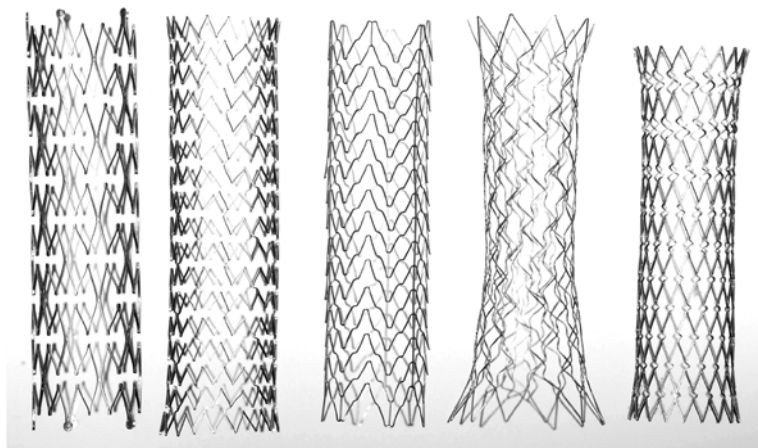

10.8 Different stent designs; stents are laser-cut from tube and expanded (except second stent from right, which is photochemically etched from sheet and rolled up).

as the stent profiles continue to shrink to accommodate smaller delivery systems, the cross section decreases with a concomitant decrease in X-ray visibility. Therefore, to improve the fluoroscopic visibility of the Nitinol stents, radiopaque markers are often attached to or integrated into the design of the stent. Tantalum markers are riveted or coined into eyelet-shaped tabs at the ends of several stent designs (Fig. 10.9). Tantalum and Nitinol are close together in the galvanic series of metals, i.e. galvanic corrosion is not a problem. The Cook Zilver stent is of similar design, but uses gold markers instead of tantalum. It is

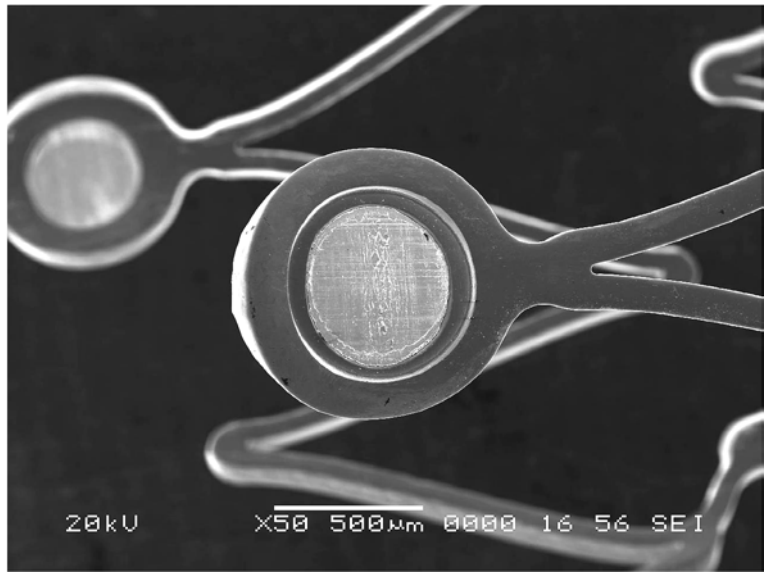

10.9 Tantalum markers riveted and coined into laser-cut eyelets (Cordis SMARTcontrol stent).

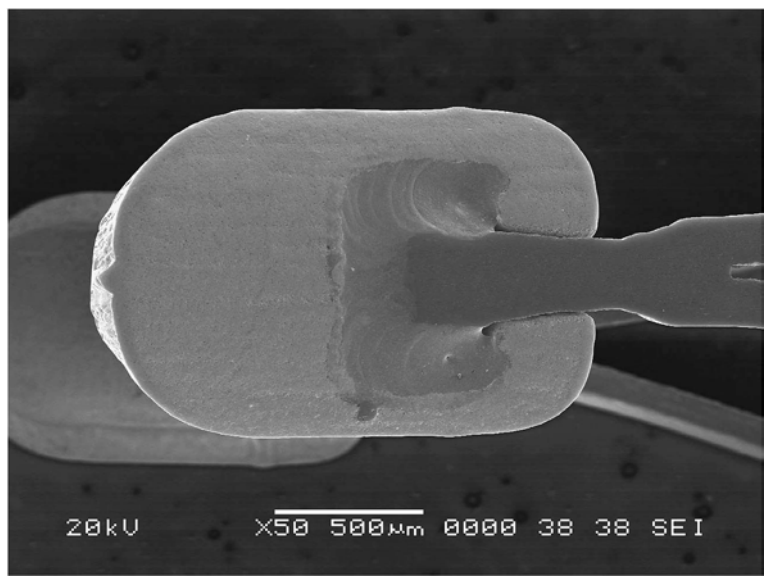

10.10 Tantalum markers laser welded to the ends of struts (Bard Luminexx).

assumed that the entire stent is coated with a thin polymer layer to protect it from galvanic corrosion.

Tantalum tabs are welded to the ends of the Bard Luminexx stents (Fig. 10.10). Because of the large mass of these tabs, the X-ray visibility of this stent is very good. There are concerns, however, that brittle interface layers can be created during welding of Nitinol and tantalum, potentially affecting the weld strength. To alleviate this problem, Guidant uses a weld pad made from a Ti–Ni–Pt alloy with its Acculink stent.

Platinum–iridium sleeves are used as markers for the wire-based BSC Symphony stent while the Cook ZA knitted stent uses gold sleeves. However, as will be shown in the following chapter, compatibility issues have to be considered when using these material combinations.

10.4 Biocompatibility and corrosion

It is well understood that Nitinol self-expanding stents require controlled processing to achieve optimal performance.[7] In the same way, surface processing is required in order to promote optimal corrosion resistance and biocompatibility. The corrosion resistance of properly treated Nitinol rivals that of titanium or other common implant materials.[27] Nitinol, like titanium and stainless steel AO, is a self-passivating material, i.e. it forms a stable surface oxide layer that protects the base material from general corrosion.[28] Considering the high nickel content of the alloy, there are, understandably, concerns that nickel may dissolve from the material owing to corrosion and cause adverse effects. On the other hand, other alloys that contain high levels of nickel, such as MP35N (a Co alloy with 35 wt % Ni), or 300 series stainless steel (approx. 10 wt% Ni) exhibit good biocompatibility, and have long been used as implants in orthodontics, orthopedics and cardiovascular applications.[29]

Several studies have measured nickel release during the exposure of Nitinol implants to body fluids. During an *in vitro* dissolution study of Nitinol dental archwires in saliva,[30] it was found that Nitinol appliances released an average of 13.05 mg/day nickel, which is significantly below the estimated average dietary intake of 200–300 mg/day. In another study,[31] orthodontic patients with Nitinol appliances had the Ni concentration in their blood measured during a period of 5 months. Results showed no significant increase in the nickel blood level throughout the study.

A comparative *in vitro* cell culture study[32] measured nickel release from Nitinol and 316L stainless steel in fibroblast and osteoblast cell culture media. In both media, nickel levels were higher in the Nitinol group on the first day and decreased rapidly with time to achieve similar levels as 316L after 8 days. It is important to highlight that, even though higher levels of nickel were measured in the Nitinol group, nickel did not reach toxic values and cell proliferation or cell growth near the implant surface was not affected. Furthermore, in this study, Nitinol was only

Table 10.2 Ratio of nickel to titanium and chromium in mechanically polished and electropolished surfaces of Nitinol, MP35N and stainless steel

Material	Surface condition	Ni:Ti	Ni:Cr
Nitinol	Mechanically polished	0.18	
Nitinol	Electropolished	0.04	
MP35N	Mechanically polished		0.4
MP35N	passivated		0.08
316L SS	Mechanically polished		0.11
316L SS	Electropolished		0.07

mechanically polished while stainless steel was electropolished. The authors speculated that passivation treatments, such as electropolishing, would decrease the nickel release from Nitinol. To evaluate the effect of different surface treatment methods on the Ni ion release, Trepanier *et al.*[33] immersed mechanically polished and electropolished samples of Nitinol, MP35N and 316L stainless steel in Hank's physiological solution at 37 °C for a period of greater than 1000 h. It was found that samples that were prepared by mechanical polishing released higher amounts of Ni ions than those prepared by electropolishing. Results from surface analysis demonstrate that the electropolishing process removes excess nickel from the surface and forms a layer enriched in Ti (in the form of TiO_2). In contrast, the mechanically polished samples have a relatively high concentration of nickel in the surface (Table 10.2).

Although there is only limited nickel ion release, in cases with known nickel sensitivity an allergic reaction cannot be excluded with certainty. The same precautions should be considered as for other Ni-containing implant materials such as stainless steel or MP35N.

ASTM standard F2129 provides a quantitative method recognized by the FDA for the accelerated assessment of the corrosion resistance of implant materials.[34] The most relevant data derived from this test is the break-down potential E_{bd}, since most biomaterials corrode locally by pit formation. A high breakdown potential indicates that the material is very stable and resists pitting. Although no official limits have been established, materials with an E_{bd} equal to or greater than 500 mV are considered sufficiently corrosion resistant and safe for the use as implants. It corresponds with the corrosion resistance of the stainless-steel Palmaz–Schatz stent as a predicative device, the stent with the longest implantation history.

Anodic polarization tests per ASTM F2129 have been used to evaluate the influence of surface preparation on the corrosion susceptibility of Nitinol stents. Trepanier *et al.*[35] have shown that electropolished Nitinol stents have excellent corrosion resistance with breakdown potentials (E_{bd}) greater than 800 mV, whereas the E_{bd} of non-electropolished stents was on the order of 200 mV. It was further shown that the breakdown potential of electropolished stents was degraded to less than 500 mV after thermal treatments at 400 to 500 °C. This led to the conclusion

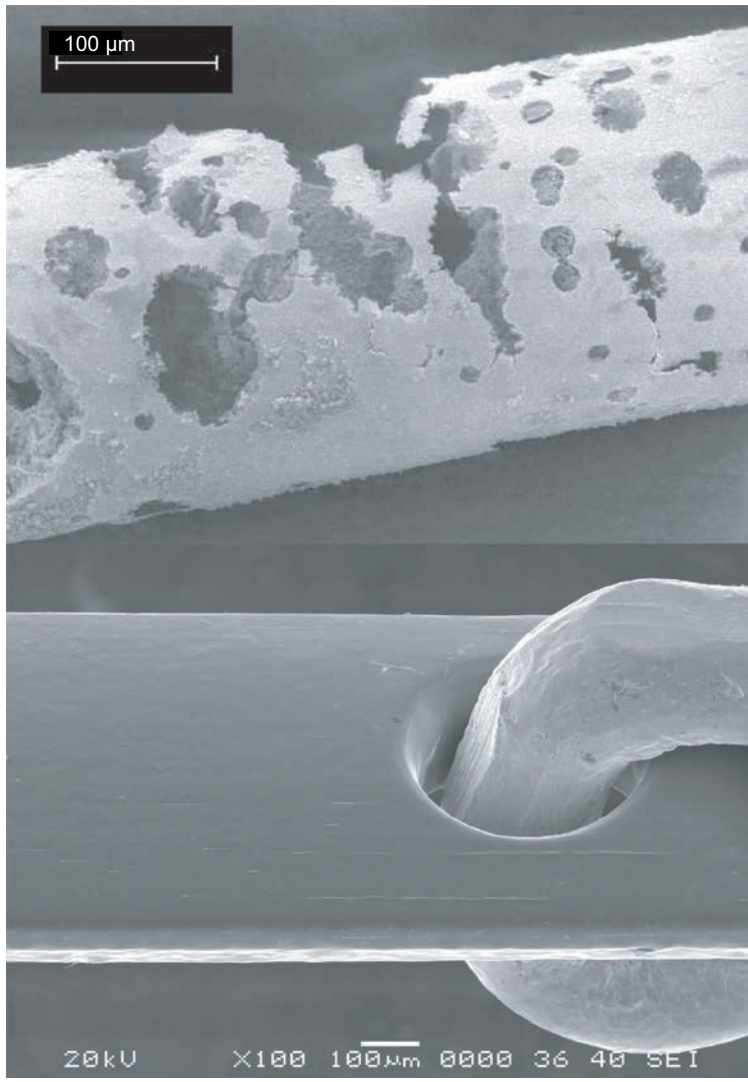

10.11 Top: heavily corroded Nitinol explant (5 months), bottom: 12 months Nitinol explant with electropolished surface (with attached tantalum marker).

that optimal corrosion and biocompatibility results are obtained with a thin, titanium oxide (TiO_2) surface layer formed after electropolishing (passivation) treatments. It further appears that uniformity, rather than thickness, of the oxide is most important to protect the material from corrosion.

In 1999, the medical community as well as the device industry were alerted to the corrosion issue by reports by Riepe *et al.*[36] on the observation of severely

corroded Nitinol graft scaffolds from explanted Stentor aortic stent grafts after 5 months' implantation (Fig. 10.11). It was preliminarily speculated that cell-induced electrochemical corrosion or active cellular destruction of the surfaces (e.g., osteoclasts bone) might have been responsible for the severe corrosion. However, subsequent cell culture testing with Nitinol test samples performed by Riepe's group did not induce any corrosion.[37] Further analysis of the failed components revealed an oxide thickness of 0.2–0.3 μm (determined by Auger analysis) and an E_{bd} of 280 mV (from anodic polarization tests). In contrast, 12-month explants of electropolished graft scaffolds examined by Pelton *et al.* showed no signs of corrosion. The oxide thickness on these devices was approximately 0.01 μm and the $E_{bd} > 900$ mV. This highlights the importance of optimized surface preparation. Most Nitinol stents marketed today have electropolished surfaces. There have been no further reports on corrosion cases.

As shown in a previous chapter, to improve the radiopacity of Nitinol stents, markers are often attached to the stent struts. However, when coupling Nitinol with dissimilar materials, galvanic corrosion effects have to be considered. Markers are typically made from high-density materials such as gold, platinum, or tantalum. Nitinol and tantalum are galvanically similar, and thus, the combination has no significant effect on the corrosion resistance. In contrast, gold and platinum are nobler than Nitinol (or stainless steel) and can cause severe galvanic corrosion of the Nitinol (or stainless-steel) stent. Therefore, the use of the noble metals as markers requires either an insulating layer between the stent and the marker or the assembly has to be coated with a protective coating.

10.5 Fatigue and durability of Nitinol stents

It is probably fair to state that, until recently, stents were designed mostly by engineers with only limited understanding of the anatomical environment and the physiological and biomechanical peculiarities of the vasculature using anecdotal input from physicians. Only after stent fractures had been observed in certain clinical trials,[38] did the medical device industry change its approach to stent design and it now tries to understand the dynamics of the vasculature.[39] The Superficial Femoral Artery (SFA) is a particularly 'dynamic' artery, running from the hip to the knee, through mucle and joints. It undergoes severe changes in geometry associated with leg movement. Duda *et al.* in the Sirocco Trial observed fracture rates of 17% at 6 months and 26% at 18 months in SFAs stented with the Cordis SMART Stent.[38] The clinical results of stenting were still considered excellent, despite the fractures. Scheinert *et al.* subsequently confirmed that the SMART Stent maintained patency even with broken struts. These authors, however, found that other stent designs did not fare as well as the SMART Stent with respect to patency or restenosis rates.[40] Thus, it can be concluded that a fracture does not necessarily equate with device failure. A fracture in some designs leads to a high probability of clinical failure, while

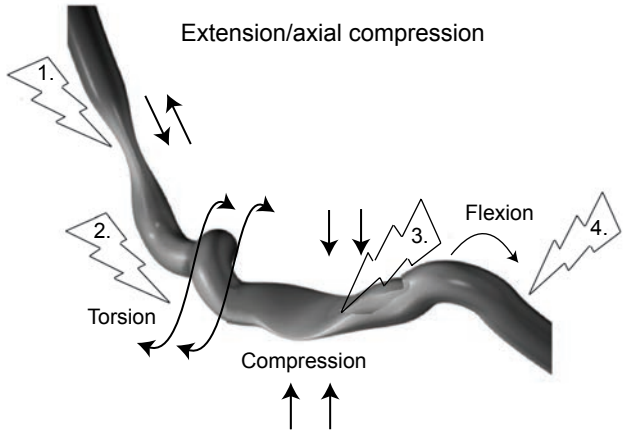

10.12 Schematic representation of different modes of deformation of the superficial femoral artery (SFA).

fractures in others do not. Nevertheless, stent durability and fatigue are major considerations in stent development today.

With the intent of developing a better understanding of the displacements and corresponding strains that stents are subjected to in the body,[39] recent studies have used X-ray computer tomography (X-ray CT) and magnetic resonance angiography (MRA) to measure the *in vivo* displacements of the femoral artery under controlled movements. Their results show, for example, that the total length of a typical SFA undergoes up to ~215° rotation and ~20% contraction as the leg is fully bent from an initially extended position; correspondingly, every time the knee is flexed, a stent deployed in such an SFA location undergoes severe, multiaxial displacements that are superimposed on the omnipresent pulsatile displacements of the cardiac cycle (Fig. 10.12). In terms of a so-called duty cycle per year, the relevant displacements and frequencies include pulsatile motion (~40 million cycles per year) plus bending, torsion, and axial motions at a rate of ~1 million cycles per year[41]). Although there are ~40 times more displacement occurrences due to cardiac cycles, the combined non-pulsatile cyclic motions result in far greater displacements and, therefore, have the possibility of inducing significantly greater cumulative fatigue damage. While in the past the only requirement was to 'test-to-success' up to 400 million pulsatile cycles, to evaluate the cause of fractures in the SFA and to predict the lifetime of stents in this environment, 'tests-to-fracture' also have to be conducted for non-pulsatile musculo-skeletal deformation conditions.[42] The results will help in the design of next-generation stents with optimized fatigue performance.

10.6 Sources of further information and advice

- International Organization on Shape Memory and Superelastic Technology, an affiliate society of ASM International, www.asminternational.org.

- Proceedings of the International Conferences on Shape Memory and Superelastic Technologies, SMST, 1994, 1997, 2000, 2003, 2004, 2007.
- Sigwart U, *Endoluminal stenting*, London, W B Saunders Company Ltd 1996.
- White A R, Fogarty T J, *Peripheral Endovascular Interventions*, St Louis, Mosby 1996.
- Lumsden A B, Lin P H, Bush R L, Chen C, eds., *Endovascular therapy: principles of peripheral intervention*, Oxford, Blackwell Publishing Ltd 2006.

10.7 References

1 Duerig T W, Wholey M (2002), 'A comparison of balloon- and self-expanding stents', *Min Invas Ther and Allied Technol* **11**(4), 173–178.
2 Dotter C T, Buschmann P A C, McKinney M K, Rösch J (1983), 'Transluminal expandable nitinol coil stent grafting: preliminary report', *Radiology* **147**, 259–260
3 Stoeckel D (2000), 'Nitinol medical devices and implants', *Min Invas Ther and Allied Technol* **9**(2), 81–88.
4 ASTM F 2063-00 (2002) Standard Specification for Wrought Nickel–Titanium Shape Memory Alloys for Medical Devices and Surgical Implants.
5 ASTM F 2004-00 (2002) Test Method for Transformation Temperature of Nickel–Titanium Alloys by Thermal Analysis.
6 ASTM F 2082-01 (2002) Method for the Determination of Transformation Temperature of Nickel–Titanium Shape Memory Alloys by Bend and Free Recovery.
7 Pelton A R, DiCello J, Miyazaki S (2000), 'Optimisation of processing and properties of medical grade Nitinol wire', *Min Invas Ther and Allied Technol* **9**(3/4), 107–121.
8 Duerig T W, Tolomeo D E, Wholey M (2000), 'An overview of superelastic stent design', *Min Invas Ther and Allied Technol* **9**(3/4), 235–246.
9 Harnek J, Zoucas E, Stenram U, Cwikiel W (2002), 'Insertion of Self-Expandable Nitinol Stents Without Previous Balloon Angioplasty Reduces Restenosis Compared with PTA Prior to Stenting', *Cardiovasc Intervent Radiol* **5**, 430.
10 Duda S, Wiskirchen J, Tepe G, Bitzer M, Kaulich T W, Stoeckel D, Claussen C (2000), 'Physical Properties of Endovascular Stents: An Experimental Comparison', *JVIR* **11**, 645–654.
11 Duerig T W, Wholey M (2002), 'A comparison of balloon- and self-expanding stents', *Min Invas Ther and Allied Technol* **11**(4), 173–178.
12 Wang Y, Truong T N, Yen C, Bilecen D, Watts R, Trost D W, Prince M R (2003), 'Quantitative evaluation of susceptibility and shielding effects of nitinol, platinum, cobalt alloy, and stainless-steel stents', *Magn Reson Med* **49**(5), 972–976.
13 Leung D A, Spinosa D J, Hagspiel K D, Angle J F, Matsumoto A H (2003), 'Selection of stents for treating iliac arterial occlusive disease', *J Vasc Interv Radiol* **14**, 137–152.
14 Eum J, Wu M H, 'Removable nitinol stent for temporary relief of lower urinary tract obstruction', *Proc. Int Conf SMST*, Pacific Grove 2000, 641–649.
15 Jahnke T, Voshage G, Müller-Hülsbeck S, Grimm J, Heller M, Brossmann J (2002), 'Endovascular placement of self-expanding nitinol coil stents for the treatment of femoropopliteal obstructive disease', *J Vasc Interv Radiol* **13**, 257–266
16 Henry M, Amor M, Ethevenot G, Henry I, Abdelwahed W, Leborgne E, Allaoui M 1994, 'Initial experience with the Cragg Endopro System 1 for intraluminal treatment of peripheral vascular disease', *J Endovasc Surg* **1**, 31–43.

17 Franco G, Enrique C, Flandes A J, Zapatero G J (2005), 'Ultraflex expandable metallic stent for the treatment of a bronchopleurall fistula after pneumonectomy', *Ann Thorac Surg* **79**, 386.
18 Cook Medical company literature.
19 www.idevtechnologies.com.
20 www.fda.gov/cdrh/pdf4/p040037a.pdf.
21 Boston Scientific company literature.
22 www.fda.gov/cdrh/pdf5/p050025a.pdf.
23 www.teamreva.com.
24 www.vascular architects.com.
25 Bose A, Hartmann M, *et al.* (2007), 'A novel self-expanding nitinol stent in medically refractory intercranial atherosclerotic stenoses: The Wingspan Study', *Stroke* **38**, 1531–1537.
26 Higashida R T, Halbach V V, Dowd C F, Jurvsky L, Meagher S (2005), 'Initial clinical experience with a new self-expanding nitinol stent for the treatment of intracranial cerebral aneurysms: The Cordis Enterprise Stent', *Am J Neuroradiol* **26**, 1751–1756.
27 Wever DJ, Veldhuizen, AG, Sanders, MM, Schakenraad, JM (1997), 'Cytotoxic, allergic and genotoxic activity of a nickel–titanium alloy', *Biomaterials* 18, 1115.
28 Wever D J, Veldhuizen, A G, de Vries, J, Busscher, H J, Uges, D R A, van Horn, J R (1998), 'Electrochemical and surface characterization of a nickel–titanium alloy', *Biomaterials* **19**, 761.
29 Brown S A, Hughes P J, Merritt K (1988), 'In vitro studies of fretting corrosion of orthopaedic materials', *J Ortho Res* **6**, 572.
30 Barrett R D, Bishara S E, Quinn J K (1993), 'Biodegradation of orthodontic appliances, part I biodegradation of nickel and chromium in vitro', *Am J Orthod Dentofac Orthop* **103**, 8.
31 Bishara S E, Barrett R D, Selim M I (1993), 'Biodegradation of orthodontic appliances. Part II. Changes in the blood level of nickel', *Am J Orthod Dentofac Orthop* **103**, 115.
32 Ryhanen J, Niemi E, Serlo W, Niemelä E, Sandvik P, Pernu H, Salo T (1997), 'Biocompatibility of nickel–titanium shape memory metal and its corrosion behavior in human cell cultures', *J Biomed Mat Res* **35**, 451.
33 Trepanier C, Venugopolan R, Messer R, Zimmerman J, Pelton A R (2000), 'Effect of passivation treatments on nickel release from Nitinol', *Proc Soc Biomat*, 1043.
34 ASTM F2129-01, 'Standard test method for conducting cyclic potentiodynamic polarization measurements to determine the corrosion susceptibility of small implant devices' 2002.
35 Trepanier C, Tabizian M, Yahia L'H, Bilodeau L, Piron D L (1998), 'Effect of modification of oxide layer on NiTi stent corrosion resistance', *J Biomed Mat Res* **43**, 433.
36 Heintz C, Riepe G, Birken L, Kaiser E, Chafke N, Morlock M, Delling G, Imig H (2001), 'Corroded Nitinol wires in explanted aortic endografts: an important mechanism of failure?', *J Endovasc Ther* **8**, 248.
37 Kaiser E, 'Cell-induced corrosion in vitro', *2nd European Sym Vasc Biomat*. Hamburg (2002).
38 Duda S H, Bosiers M *et al.* (2005), 'Sirolimus-eluting versus bare nitinol stent for obstructive superficial femoral artery disease: the SIROCCO II trial', *J Vasc Interv Rad* **16**, 331–338.
39 Cheng C P, Wilson N M *et al.* (2006), 'In vivo MR angiographic quantification of axial and twisting deformations of the superficial femoral artery resulting from maximum hip and knee flexion', *J Vasc Interv Rad* **17**, 979–987.

40 Scheinert D, Scheinert S *et al.* (2005), 'Prevalence and clinical impact of stent fractures after femoropopliteal stenting', *J Am Coll Card* **45**, 312–315.
41 Silva M (2002), 'Average patient walking activity approaches two million cycles per year', *J Anthroplasty* **17**, 693–697.
42 Schroeder V, Pelton A *et al.* (2007), 'Non-pulsatile fatigue analysis of nitinol stents', in preparation.

11

Orthodontic devices using Ti–Ni shape memory alloys

F. FARZIN-NIA
Ormco Corporation, USA

T. YONEYAMA
Nihon University School of Dentistry, Japan

Abstract: Superelastic Ti–Ni alloy wires have revolutionized orthodontic treatment by improving treatment efficiency, patient comfort, quality of treatment, and patient safety. In this chapter, a brief description of orthodontic treatment and the philosophies behind the use of various commercially available Ti–Ni alloy wires has been presented. Mechanical properties, frictional characteristics, corrosion resistance, and biocompatibility of Ti–Ni alloy orthodontic appliances have been reviewed and discussed. The role of shape memory and superelastic effects in orthodontic treatment techniques using Ti–Ni appliances was examined.

Key words: orthodontic wires, Ti–Ni alloys, superelasticity, mechanical properties, frictional properties, corrosion, biocompatibility, Ni–Ti, Ti–Ni, Nitinol.

11.1 Introduction

Superelastic and shape memory Ti–Ni wires have revolutionized orthodontic treatment by improving treatment efficiency, patient comfort, quality of treatment, and patient safety. In this chapter the application of Ti–Ni based alloy wires in orthodontic treatment is reviewed and discussed.

The use of Ti–Ni wires as the initial wire during orthodontic treatment has steadily increased since its introduction in the early 1980s to the point that it is now considered a standard material for initial wires. Other applications of Ti–Ni alloys as orthodontic appliances include various forms of springs, including extension/compression coil springs.

In this chapter, a brief description of orthodontic treatment, the wire characteristics, and requirements at different stages of treatment, are presented. A snapshot of the history of the development of use of wires in orthodontic treatment is presented and various commercially available alloys, and their characteristics, as well as the philosophy behind the use of each type of material, are discussed.

Various commercially available alloys such as Ti–Ni, Ti–Ni–Cr, Ti–Ni–Cu–Cr, and Ti–Ni–Fe are briefly reviewed and their physical, mechanical, and frictional

properties discussed. Addition of various elements affects the stress/strain curves, residual strain, load hysteresis, and the transformation temperatures of the alloys. These effects provided opportunities in tailoring the properties of these alloys to specific requirements and characteristics that would enhance the clinical performance of superelastic and shape memory wires, and provide opportunities for the evolution of new clinical techniques.

The very harsh environment in the mouth, combined with stresses caused by the orthodontic forces and mastication can cause the fracture and failure of wires as well as other orthodontic appliances during treatment. Ti–Ni wires are not exempt from this trend. A review of the fractures in orthodontic wires during treatment indicates that fatigue characteristics in Ti–Ni alloys can lead to fatigue failure under certain harsh conditions in the oral environment.

As corrosion and biocompatibility of Ti–Ni alloys have been extensively discussed in Chapter 6, a brief review is presented here on specific concerns regarding the corrosion, biocompatibility, and allergic reactions of orthodontic appliances.

11.2 Wire properties in various stages of orthodontic treatment

In an orthodontic system with fixed appliances, brackets (braces) are attached to teeth and used as handles where wires are engaged in the bracket slots for moving teeth to a pre-determined position in the dental arch, based on the clinician's treatment plan. The relationship between the upper and the lower jaws is then corrected to provide an ideal bite.

Generally, orthodontic treatment can be divided into three stages. Each stage of treatment requires wires with specific properties tailored for certain functions, as follows:

- Initial stage – leveling and alignment of teeth in the mandibular (lower) and maxillary (upper) arches. During the initial stage of treatment teeth are generally crowded, particularly in the anterior sections of the jaws. Highly resilient wires having a relatively low modulus of elasticity (low stiffness) are required to weave through the bracket slots without permanent deformation and, at the same time, the wire must provide sufficient force to gently move the teeth to their new positions. Resilience of the wire refers to the elastic deformation (full recovery after deformation) of the wire (area under the stress/strain curve). Wire stiffness in orthodontics refers to the resistance of the wire to bending and is defined as: $W_s = M_s \times I_c$, where W_s *i*s the wire stiffness, M_s is the modulus of elasticity, and I_c is the moment of inertia for a beam.[1] Wires with a high modulus of elasticity can produce excessive force, causing an adverse biological response to an efficient tooth movement, and this can potentially result in tissue morbidity and root resorption. Various alloys of Ti–Ni wires, because of their

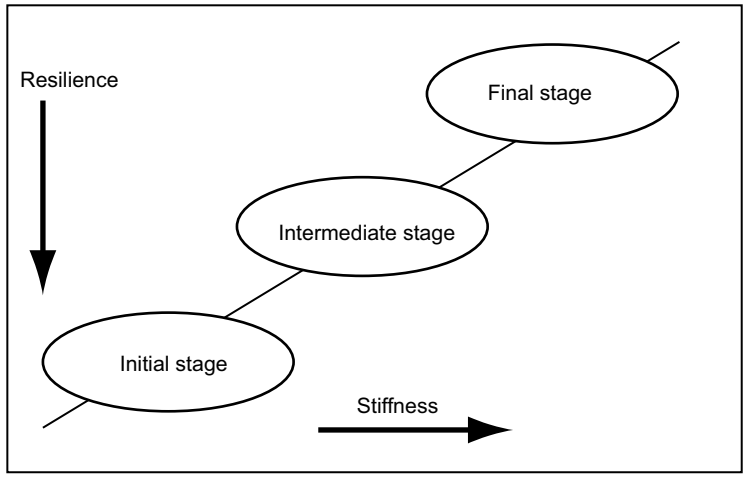

11.1 Schematic representation of the optimum properties of orthodontic wires during each stage of orthodontic treatment.

high resilience and low stiffness, have evolved to become the wire of choice for the initial stage of orthodontic treatment.

- Intermediate stage – root and bite corrections. In this stage of treatment, mandibular and maxillary arches come together for a correct bite. Teeth have been substantially leveled and aligned during the first stage of treatment and the resilience of the wire is less critical. However, the wire is required to have greater force for torque and root corrections as well as the manipulation of the arch shapes. Further, the wire must be bendable by the clinicians to address the needs of specific patients.
- Finishing stage – finishing. The final stage of treatment involves fine adjustments and minor corrections of teeth positions, torques, tips, rotations, etc. After the finishing stage of treatment, the teeth from the upper and the lower jaws interlock during occlusion and the relationship between the teeth within each arch and between the arches is corrected.

In an orthodontic system, wires are the primary members that provide force for moving teeth. Requirements and wire characteristics for each stage of treatment is considerably different. Figure 11.1 presents the general requirements for the wire properties at each stage of treatment. At the initial stage of orthodontic treatment, where there are significant tooth-to-tooth discrepancies, Ti–Ni alloys are most suitable. They provide very high resilience and relatively low stiffness compared with other orthodontic materials such as stainless steel or titanium alloys. Figure 11.2 represents a typical case with anterior crowding where tooth-to-tooth discrepancy relative to their ideal location in an arch form is evident.

At the intermediate stage of treatment where the teeth are mostly leveled and aligned ‘working wires’ have optimum properties. The wires must be bendable by

11.2 A typical orthodontic case where crowding of anterior teeth has resulted in tooth to tooth discrepancies relative to their position in the dental arch.

the clinicians and have greater stiffness than the wires used at the initial stage of treatment, but only limited resilience is necessary.

The ideal finishing wires should generally be highly bendable, accept detailed bends by the clinicians, and have high stiffness. The resilience of wires at the finishing stages of treatment is not very important since the teeth are substantially located in their final positions.

11.3 Evolution of orthodontic wires

Use of wires in orthodontic treatment goes back to the early 1900s. Corrosion resistance and biocompatibility are the primary considerations for use of metallic materials in the oral environment. Few materials, at that time, had sufficient corrosion resistance for use in the mouth. An Au–Ni alloy (white gold) was the material of choice for the early orthodontic wires. These wires had relatively high stiffness and very low resilience, which led to severe limitations in the orthodontic treatment techniques, necessitating frequent patient visits, in some cases on a daily basis.

Early Au–Ni orthodontic wires were round, with a diameter ranging between 0.75 and 1.00 mm. These wires were made into an arch shape, which formed a rigid structure held against the teeth and could expand, moving the teeth facially. The round wire was later evolved into a rectangular shape that was formed into a ribbon arch, where the arch bending is taking place around the larger dimension of the wire cross section, and eventually an edgewise arch form, Fig. 11.3.

Orthodontic treatment philosophy and techniques evolved to accept the extraction of teeth. This procedure demanded increased resilience in the wires that

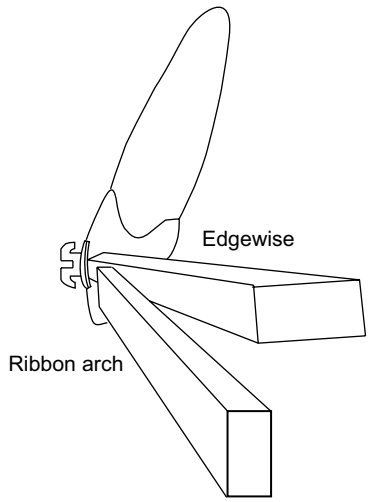

11.3 A schematic representation of ribbon, and edgewise wires where the arch shape is formed around the larger or the smaller dimensions respectively. It can be seen that insertion of an edgewise wire into the bracket slot produces the greatest amount of force for producing and maintaining the archform.

needed to be woven into the bracket slots. In order to gain more resilience from the high stiffness Au–Ni alloys, the wire dimensions were reduced, leading to the use of wire size progressions. Smaller diameter wires with adjustment loops could be engaged into the bracket slot without permanent deformation. Adjustment loops also increase the wire length between the brackets, reducing the apparent stiffness of the wire and improving the treatment efficiency, Fig. 11.4.

In the late 1920s and early 1930s austenitic stainless steels were developed. Stainless steels were the obvious material for replacing the archwires since they had the required corrosion resistance, very high stiffness (about 20% greater than the Au–Ni alloy) and improved resilience. Use of stainless-steel wires paved the way for further wire size reductions and increased resilience leading to appreciable improvements in the treatment efficiency and longer intervals between office visits. Appointment intervals of two to three weeks became standard.

Limitations in materials selection – the need for lower stiffness, and greater resilience, by the clinicians – led to many design innovations which, in turn, produced archwires with improved properties through mechanical designs. These designs included using variable cross-sections in the archwires, twisting very fine diameter wires together forming a rope, and braiding fine wires and rolling the braided wires into various rectangular cross sections that could be engaged in the bracket slot, Fig. 11.5. Braided or twisted stainless-steel wires, as well as very small diameter, approx. 0.25 mm, stainless-steel wires were used as the initial wires before the introduction of superelastic Ti–Ni alloy wires.

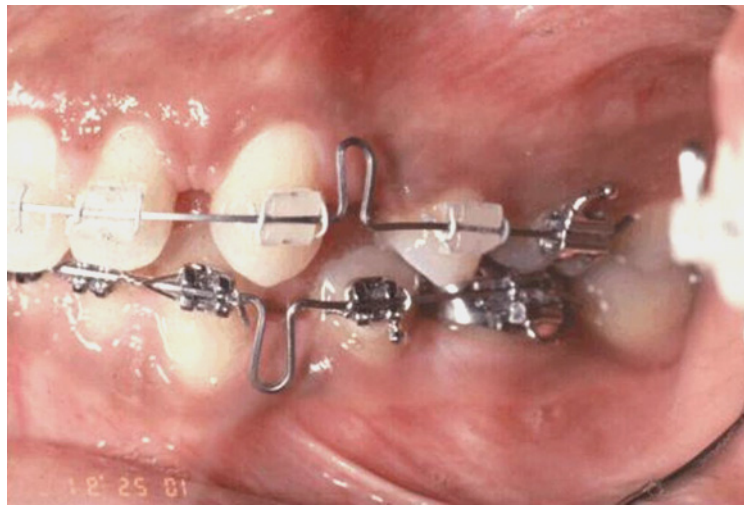

11.4 Increasing the length of the archwires between adjacent teeth is frequently used to reduce the apparent stiffness of archwires made from conventional alloys such as stainless steels. In this case, the loops were used as springs for moving the teeth towards each other as well as stiffness reduction.

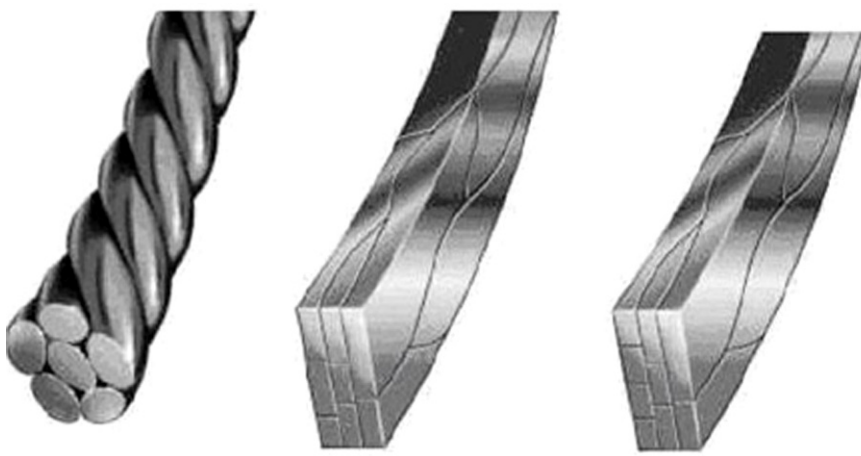

11.5 Twisted or braided stainless steel orthodontic wires provide greater resilience and smaller apparent stiffness. These wires were often used during the initial stage of treatment before the introduction of Ti–Ni alloys.

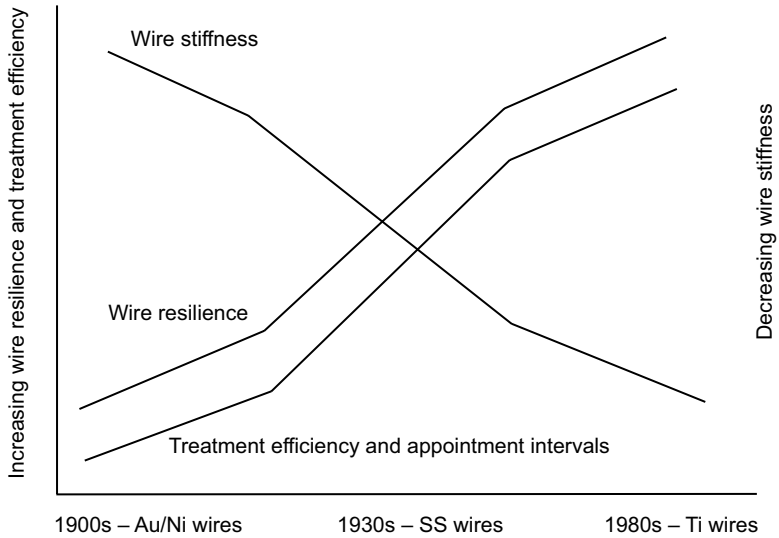

11.6 Over the past century, as the resilience of the wires increased and their stiffness decreased, the efficiency of orthodontic treatment dramatically increased.

More recent developments in materials technology provided the option of using Ti alloys for orthodontic archwires. Many β-Ti alloys have significantly lower stiffness and greater resilience than stainless steels. Burstone *et al.*[1,2] first reported the use of β-III Ti wires in orthodontics. The β-III Ti alloy was processed to produce maximum resilience and relatively low stiffness. This wire was introduced commercially in the early 1980s. In spite of its significantly greater resilience than stainless steel, β-III wires are bendable and have been used as the main working wire during the intermediate and the final stages of treatment by the clinicians over the past three decades. Use of Ti alloy wires provided the opportunity for greater treatment efficiency and further extended the patient appointment intervals. The clinicians further reduced the number of office visits and, at the same time, the total treatment time, by using a combination of Ti alloy and stainless-steel wires during the orthodontic treatment. At the same time, the quality of the treatment improved. Figure 11.6 depicts a reduction in wire stiffness and increased wire resilience during the past century. There seems to be a direct correlation between the wire stiffness and resilience, and the treatment efficiency, which includes shorter treatment time and fewer visits to the doctor's office.

11.4 Ti–Ni orthodontic archwires

11.4.1 History

The potential for the use of Ti–Ni wires in orthodontic treatments was first reported

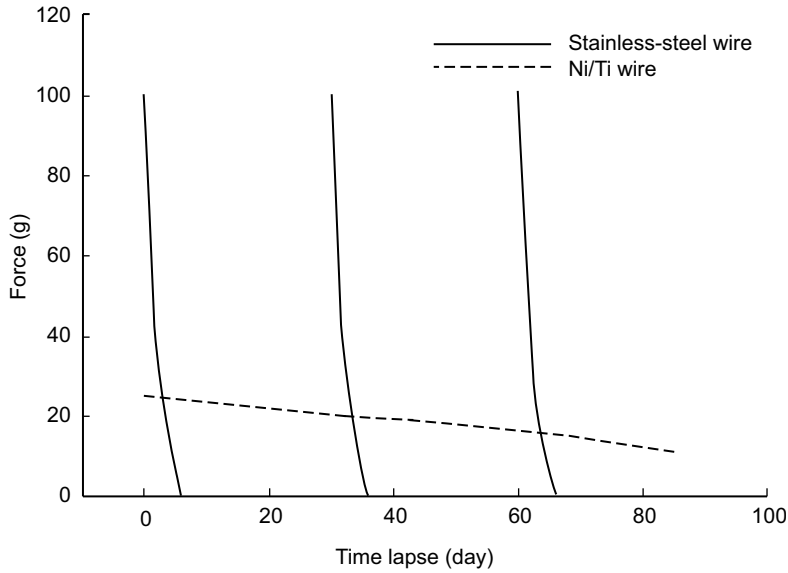

11.7 A schematic representation of the force delivery cycle of a typical stainless steel wire compared with a Ti–Ni wire during the initial stage of orthodontic treatment. As the teeth level and align the force delivery of Ti–Ni wires is decreased slightly while the forces of stainless steel wires drop below the threshold for tooth movement very rapidly owing to the small resilience in stainless-steel wires.

by Andreasen[3] in 1972. The first Ti–Ni wire was commercially introduced in the orthodontic market under the name Nitinol by late 1970s. Nitinol is a cold-worked martensitic wire that has greater resilience and lower stiffness than stainless-steels and β-Ti wires, but it was not treated to exhibit shape memory or superelastic behavior. The unrealized superelastic effect in Nitinol wires limited their use as an initial wire for several years.

Miura *et al*.[4] and Andreasen *et al*.[5–8] were among the first investigators to identify and publish the beneficial effects and the advantages of superelasticity in clinical orthodontics. In the early 1980s, superelastic Ti–Ni wires were introduced in round cross-sections followed by rectangular cross-sections several months later. Shape memory or heat-sensitive wires were introduced a few years later. Superelasticity of Ti–Ni alloys, combined with their relative low stiffness, make these wires ideal for the initial stage of treatment, providing a continuous gentle force for tooth movement combined with seemingly limitless resilience, which has created one of the most significant improvements in orthodontic treatment.

Generally, it has become an accepted principle in orthodontics that light continuous forces are desirable to achieve physiologic and controlled tooth movement, with minimum pathologic repercussions on the teeth and their surrounding tissues. Archwires that can deliver such light forces over long distances

would appear to be most useful to the clinician during the initial alignment phase of fixed appliance treatment. The most desirable physical properties of such wires include good spring back, light and continuous force delivery, attachability, biocompatibility and low cost. [9–16] Figure 11.7 represents a comparison between typical treatment cycles when stainless-steel or Ti–Ni wires were used during the initial stage of orthodontic treatment. It can be seen that stainless-steel wires due to their high stiffness and low resilience would require frequent adjustments by the clinicians to move the teeth to their desired position. Stainless steel wires create very high initial forces that would rapidly diminish within a few days, and would render the wires inactive until the next adjustment by the clinician. Use of stainless-steel wires would necessitate more frequent visits to the doctor's office, more painful treatment, and increased risk to the patient with potential biological side effects, such as root resorption and tissue morbidity. On the contrary, shape memory or superelastic wires can produce low forces and are continuously active, providing force for moving teeth. The introduction of superelastic Ti–Ni alloys into the orthodontic industry made a significant contribution to reducing the treatment time, number of office visits by the patient, patient comfort, patient safety, quality of orthodontic treatment, and reduction of the overall cost of the treatment. The average treatment time before introduction of Ti–Ni wires in orthodontics was in excess of two years. Average treatment time within two decades after the introduction of Ti–Ni wire has reduced to about eighteen months, and most of this improved efficiency can be attributed to the superelastic properties of Ti–Ni wires.

11.4.2 Phase transformation

The use of Ti–Ni type alloys in orthodontics is in the form of archwires or springs. The springs are generally made from binary Ti–Ni alloys exhibiting stress-induced austenite to martensite reversible phase transformation at body temperature, and they are designed to remain continuously active during the orthodontic treatment. The archwires, however, have been designed to have various transformation temperatures A_f, as low as 0 °C and as high as 60 °C.

Techniques often used for identifying the phase transformations in Ti–Ni alloy wires include: differential scanning calorimetry (DSC),[17] X-ray diffraction,[18] and electrical resistivity measurement.[19] Commercially, however, the shape recovery temperature is considered to be an indication of the A_f temperature. Several studies on the transformation of Ti–Ni orthodontic wires have been published, a few of which are cited below. Although these studies confirm the presence of the same austenitic, martensitic, and R phases in Ti–Ni orthodontic wires as in the Ti–Ni alloys used in other applications, there are some discrepancies and disagreements of the results. Thayer *et al.*[20] studied the X-ray diffraction patterns of temperature-induced and stress-induced martensitic transformations in Ti–Ni orthodontic

wires. These wires were processed to have a range of behaviors from complete superelasticity to fully martensitic. They demonstrated that, at 6% strain, the superelastic wires were completely transformed from austenite to martensite. They also determined that increased peak width indicates greater cold work. Transformation to the R phase was not identified for any of the superelastic wires.

McCoy *et al.*[21] studied the phase transformation of Ti–Ni and Ti–Ni–Cu orthodontic wires using DSC and energy-dispersive X-ray spectrometry (EDS). They identified peaks relating to the transformation of martensite to austenite in Ti–Ni–Cu at 27, 35, and 40 °C. However, they also identified a second peak during heating of R phase Ti–Ni–Cu at 35 and 40 °C, in contrast to the earlier reports by Mercier *et al.*[22] and Moberly *et al.*[23] that Ti–Ni–Cu alloys containing 5% or more Cu do not exhibit an R phase. Brantly *et al.*[18] investigated the phase transformations in various Ti–Ni and Ti–Ni–Cu wires by X-ray analysis and compared the results with DSC readings. Although their conclusion was that both X-ray diffraction and DSC provided similar results for the phase transformation of Ti–Ni–Cu orthodontic alloys, the presence of the R phase was not identified either in the X-ray patterns by Brantly's investigation or in the transformation during the cooling cycle from austenite to martensite. Observation of the double peak in the reverse transformation of Ti–Ni–Cu wires, in the heating cycle, could be related to the residual stress induced martensite. DSC tests performed on Ti–Ni–Cu wires, starting with the fully austenitic phase and the cooling cycle, do not exhibit the double peak in the heating cycle. The Cu content in all Ti–Ni–Cu alloys are the same and the wire processing determines the variations in the transformation temperatures of various types of Ti–Ni–Cu alloys.

The phase Transformation Temperature Range (TTR) is one of the primary factors that determine the magnitude of the force delivery of orthodontic wires during the treatment of patients. Design variations in the force delivery of Ti–Ni alloys are primarily accomplished by attempts at controlling the wire TTR. These variations are based on orthodontic treatment philosophies and techniques. The TTR of superelastic wires is near or below the room temperature. These wires are active austenitic, at room temperature and at body temperature, and the force delivery of the wires at body temperature is only slightly greater than at room temperature. Shape memory wires are generally designed to have an A_f temperature above the room temperature, but below body temperature. The archwires in this category are mostly martensitic at room temperature and produce significantly lower forces during the wire engagement into the bracket slots. However, the forces produced at body temperature increase significantly as the wire is fully transformed to austenite during the treatment when the patient's mouth is closed and the temperature of the wire in the patient's mouth rises close to body temperature. Kusy *et al.*[19] studied the transformation temperature of Ti–Ni–Cu and other orthodontic archwires using DSC and dynamic mechanical analysis from –30 to +80 °C. They concluded that, generally, the stiffness of shape memory archwires increased by at least two-fold as the archwires became fully austenitic by increasing the

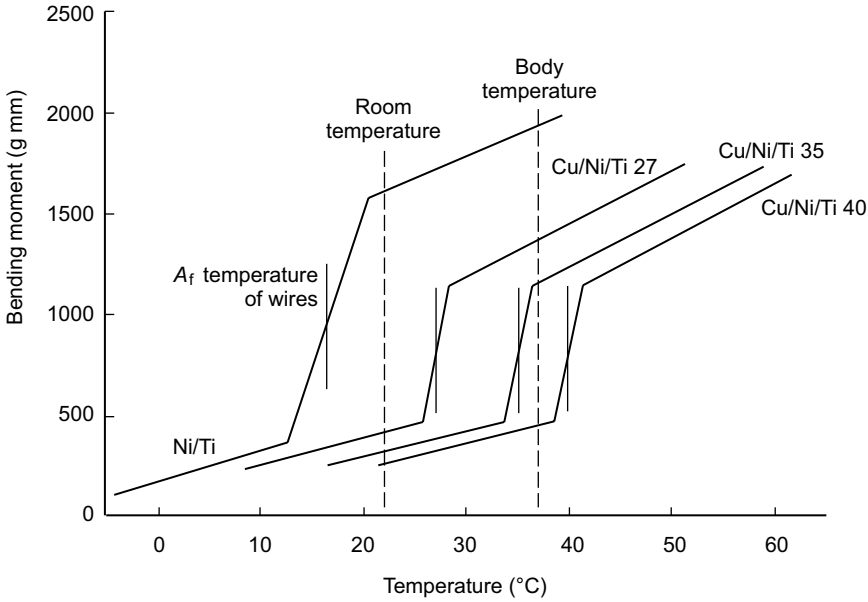

11.8 Representation of the shape memory effect on the force delivery magnitude in orthodontic wires. Transformation of wires into a fully austenitic structure results in a significant jump in the plateau stress levels. This increase in the stress is greater for Ti–Ni than that of Ti–Ni–Cu.

temperature from room temperature (the wire engagement into the bracket slots), to body temperature during the treatment when the patient's mouth is closed.

A third group of alloys are designed with a TTR above the body temperature. These wires remain passive at room temperature and at body temperature, producing relatively low forces. The forces of these wires are similar during the wire engagement into the bracket slots and during the treatment when the patient's mouth is closed. However, when the patients consume hot food, these wires become active for short periods of time. It must be noted that, after these wires have been heated up in the mouth above the body temperature, they retain more of their austenitic structure, imparting more force than when they reach the body temperature from a cold state. This group of wires are designed for patients who are extremely pain sensitive or have periodontal concerns.

Figure 11.8 represents the force delivery of various wires as the temperature rises and they go through austenitic transformation. The relative force magnitude at room and body temperatures are indicated for each type of wire. However, as the temperature approaches the A_f, there is a significant jump in the force level. After the wires are fully austenitic, increases in temperature would result in smaller force increases. Further, as noted by Fletcher *et al.*,[24] deformations occurring at temperatures close to austenitic transformations result in smaller residual strain in the Ti–Ni alloys.

Table 11.1 Typical A_f transformation temperatures and the crystalline structure of Ti–Ni based alloy orthodontic wires at room and body temperatures

Alloy type	Crystal structure		A_f (°C)
	Room temperature	Body temperature	
Superelastic	Austenitic	Austenitic	<20
Shape memory – type 1	Martensitic	Austenitic	25–35
Shape memory – type 2	Martensitic	Mostly martensitic	>37
Nitinol	Martensitic	Martensitic	>45

Finally, the original Nitinol wire has a very high TTR and remains martensitic at all times. This heavily cold worked wire does not exhibit any of the characteristics of typical Ti–Ni alloys. Nitinol wires generally have higher stiffness and lower resilience relative to typical shape memory or superelastic Ti–Ni wires. Approximate A_f temperature ranges and the crystalline structure of various types of commercially available Ti–Ni wires are presented in Table 11.1.

Compositional and processing variations in different batches of products have a major influence on the properties of orthodontic wires. In binary Ti–Ni alloys, variation in the Ni composition of 0.1% can affect the transformation temperature, TTR, by as much as 10 °C. The level of impurities and the interstitial elements C, O, and N, through their presence, size, and distribution in the form of inclusions, can also have a significant influence on the transformation temperature, the mechanical properties, and performance of orthodontic archwires.

Finally, the processing of Ti–Ni alloys into fine orthodontic wires, including the amount of cold work, annealing temperatures, and the final heat treatment conditions can further influence the transformation temperature and the mechanical performance of archwires.

In almost all cases Ti–Ni orthodontic wires exhibit the presence of martensitic, austenitic, and R phases in their transformation during heating or cooling. Figure 11.9 shows a typical phase transformation of Ti–Ni orthodontic wires during heating and cooling. While it is evident that, during cooling, austenite transforms to R phase and subsequently to martensite the interpretation of the reverse transformation may not be straightforward. The reverse transformation involves the presence of martensite, austenite and R phase in varying amounts, at different stages of transformation. As it applies to orthodontic wires, the presence of R phase may have an appreciable influence on the mode of force delivery of the Ti–Ni wires, particularly those with higher TTR, when tested at room or body temperature.

11.4.3 Mechanical properties of orthodontic wires

Mechanical performance of Ti–Ni wires is the only one of all the wire properties by which clinicians can differentiate Ti–Ni wires from other wire materials during the treatment of orthodontic patients. The primary mechanical characteristic of

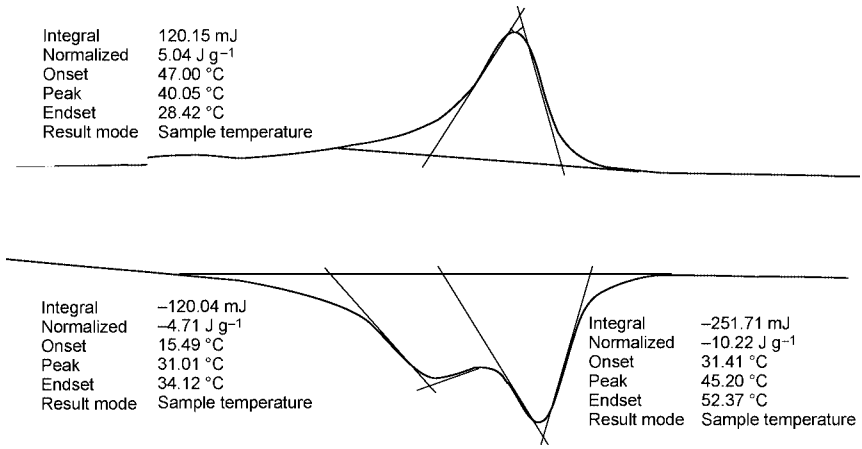

11.9 A typical phase transformation DSC graph during heating and cooling of Ti–Ni wires indicate the presence of R phase during heating and the transformation of austenite to R phase during cooling.

shape memory or superelastic wires are the magnitude and the shape of upper and lower plateau stresses at room and at body temperatures. Large elastic recovery (spring back), relatively low stiffness and producing nearly constant force at relatively large deformations are among the most desirable characteristics of Ti–Ni archwires during the initial stages of treatment. Other desirable mechanical characteristics of Ti–Ni wires are residual strain, fatigue properties and stress hysteresis.

Clinicians' selection of shape memory or superelastic Ti–Ni type wires as the initial wires for their treatment is heavily influenced by their treatment technique and the expectations of the performance of the wires under specific conditions in the oral environment.

Since the introduction of the superelastic Ti–Ni wires in early 1980s, several investigators studied the mechanical behavior of various orthodontic Ti–Ni wires and characterized their mechanical performance in comparison with other types of wires used as initial wires. Andreasen *et al.*[5–8] and Miura[4,25,26] were among the first investigators that evaluated shape memory effect and superelastic behavior of Ti–Ni wires for orthodontic applications. They compared the load/deflection performance of Elgiloy, stainless steel, Nitinol and Ti–Ni wires. The advantages of the use of the superelastic behavior of Ti–Ni wire at the initial stage of orthodontic treatment, where leveling and alignment of crowded teeth is required, was immediately evident when compared with the wires made from the more traditional materials, such as stainless-steels or β-Ti alloys. Although some early studies for quantifying the improved clinical performance of Ti–Ni wires were not conclusive, the overwhelming use of Ti–Ni wires during the initial stage of treatment in virtually all the current orthodontic treatment techniques is a testament to the efficacy and the clinical performance of Ti–Ni wires.[27,28]

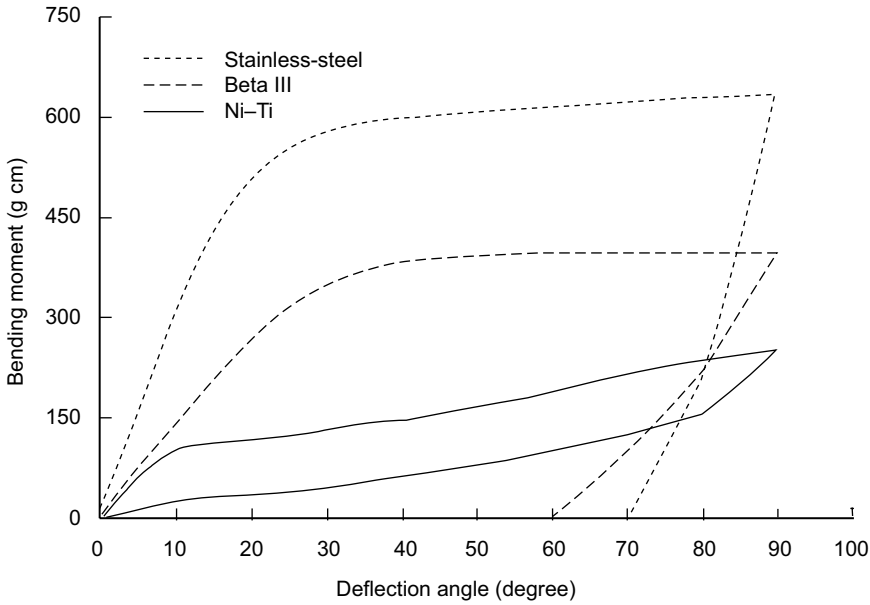

11.10 Representation of relative loading and unloading forces for 17 × 25 orthodontic wires. The graphs were derived from cantilever testing of wires. The bending occurred around the smaller cross-section of wires. The significantly smaller stiffness and greater resilience of the Ti–Ni wire is shown.

Stress/strain behavior of Ti–Ni orthodontic wires

Hudgins *et al.*[29] studied the effect of long-term deflection on permanent deformation of Ti–Ni and other archwires. They determined that long-term deformation increased the permanent deformation of all wires. However, Ti–Ni wires exhibited better spring back compared with stainless steel or TMA.

Figure 11.10 represents the loading and unloading forces of orthodontic wires from various materials of the same cross-section in a cantilever bending test around a 12 mm diameter mandrel. The behavior of stainless-steel and β-III titanium alloy wires is in accord with that expected of conventional alloys, showing a linear elastic strain followed by a plastic deformation. It can be seen that the stiffness of stainless-steel wire is significantly greater than the β-III Ti wires. However, resilience (spring back) of β-III Ti wire is more than twice that of the stainless steel. Ti–Ni wire exhibits linear elasticity at the initial levels of deformation of up to about 1% strain; however, it continues its elastic deformation non-linearly up to 6–8% deformation. Removal of force from Ti–Ni wire (unloading) demonstrates the elasticity of the wire during the entire deformation cycle. However, a loss of energy (hysteresis) due to phase transformation leads to lower forces.

Mechanical performance of commercially available Ti–Ni based orthodontic

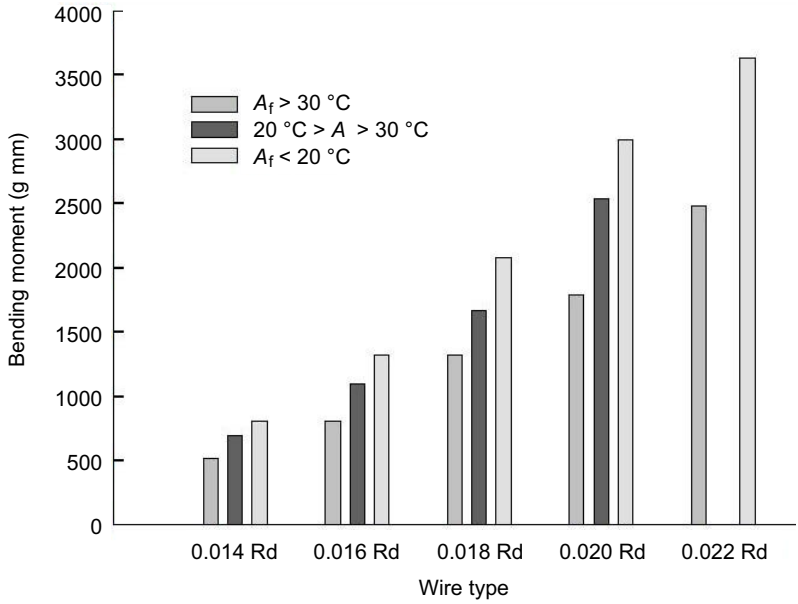

11.11 Relative loading forces for Ti–Ni wires having various diameters and transformation temperatures. The cantilever bending test was performed at 35 °C showing that higher A_f temperatures lead to greater loading forces at body temperature.

wires at the oral environment temperature (approx. 35 °C) is of primary interest. Figure 11.11 represents the loading and unloading forces for many archwires with different transformation temperatures, ranging between 10 and 35 °C, in three-point bend testing at body temperature. The unloading force of these wires, which is the force that is used for moving teeth can vary from a few grams to several tens of grams per tooth. This is partly by design to address the requirements of specific treatment techniques. However, manufacturing variability (batch-to-batch changes) such as the precise control of the compositional elements and production processes can have a significant impact on the mechanical performance of the archwires.

Hurst *et al.*[30] investigated the shape recovery of various orthodontic Ti–Ni wires with different TTRs. They plastically deformed the wires below their TTRs and determined the rate of recovery at a temperature above their TTRs. They concluded that the rate of recovery for various wires ranged between 89 and 94%. However, wires with lower TTRs, closer to room temperature, exhibited significantly less recovery. Many archwires labeled as heat sensitive produce significantly lower forces at room temperature than the body temperature due to their higher A_f temperature. Cyclic bend testing of orthodontic wires indicate that both superelastic and shape memory wires exhibit residual strain after the first bending cycle. This residual strain primarily depends on the processing of the wire as well as its transformation temperature. Figure 11.12 demonstrates the stress/strain behavior

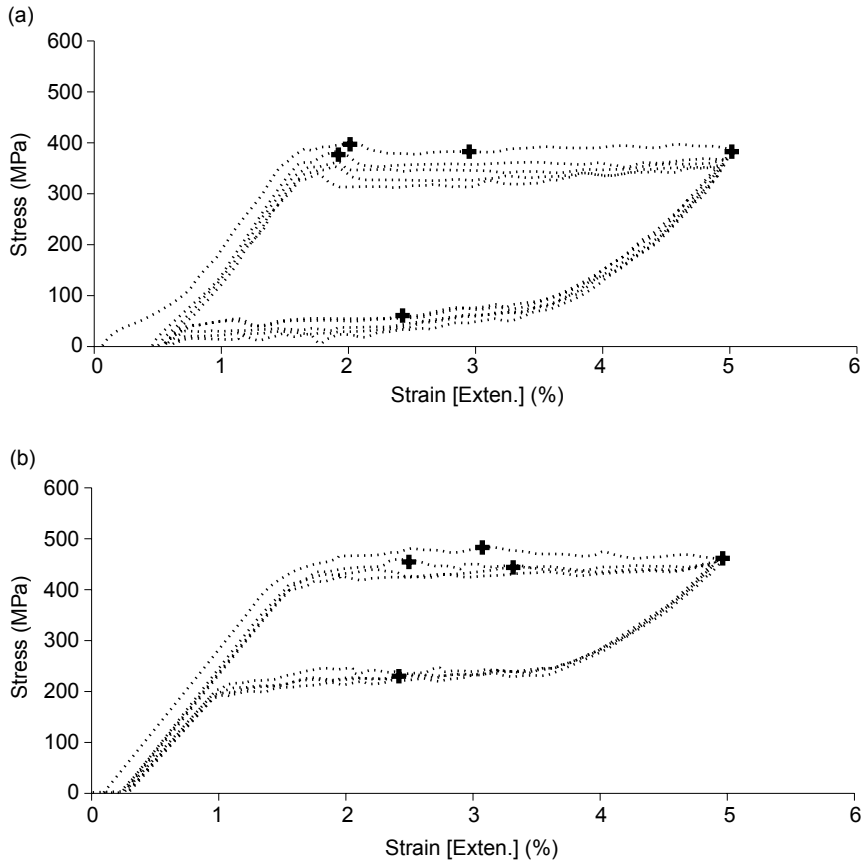

11.12 Loading and unloading forces in a five-cycle tensile testing on (a) shape memory, and (b) superelastic Ti–Ni wires indicate the remnant strains and wide range of forces that are available on commercial orthodontic wires.

of two Ti–Ni wires that have been treated differently after a few cycles in tensile testing. Residual strain after the initial cycle is shown by a shift in the starting point of the subsequent cycles.

Raboud[31] performed an extensive study on the flexural behavior of Ti–Ni archwires and various loops formed in the archwires, using finite element analysis. He identified good agreement between flexural response in the three-point bend testing results and the flexural response in his simulation of superelastic behavior of wires in orthodontic applications. Properties of commercial alloys that are available in the market vary widely. Figure 11.13 presents the typical range of stress/strain properties that are available from commercially available superelastic orthodontic wires. The range of variations in mechanical properties of Ti–Ni wires can be caused by variations between production batches, or by design as required

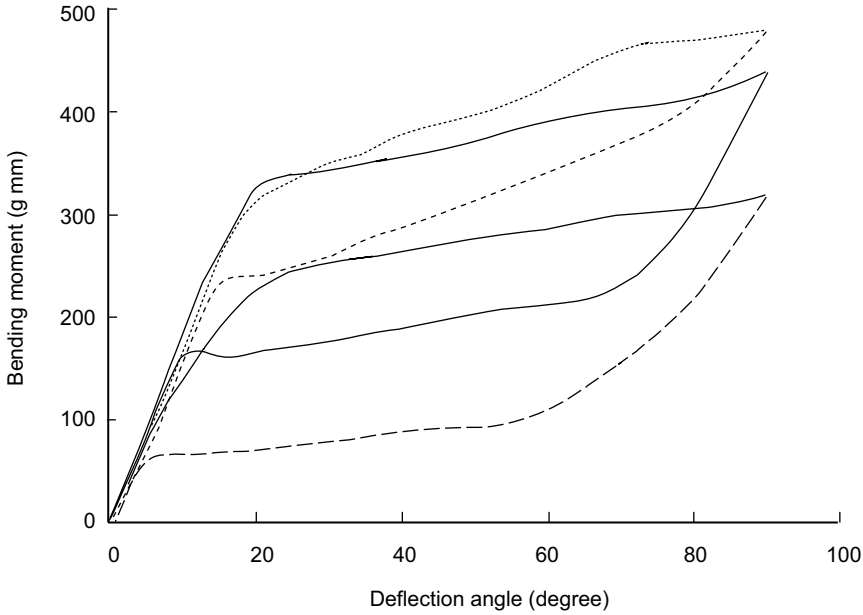

11.13 Loading and unloading forces for various 0.014 diameter superelastic Ti–Ni orthodontic wires show the range of forces that are used by the clinicians in the initial wires for leveling and alignment of teeth.

by treatment philosophies and techniques to provide the clinicians with specific loading and unloading characteristics for tooth movement. Extreme resilience of superelastic Ti–Ni orthodontic wires made it possible to re-use these wires clinically. However, studies on the properties of the recycled wires[32] indicated that the properties of Ti–Ni orthodontic wires generally deteriorate with use. This is particularly true where the wires have experienced significant cyclic strain during their use *in vivo*.

Generally, it is believed that there is a greater propensity for fracture in Ti–Ni orthodontic wires compared with stainless-steel wires.[33–36] Mohlin *et al.*[33] performed *in vitro* and clinical evaluation of Chinese Ti–Ni. They concluded that, in clinical situations, for alignment purposes, Ti–Ni material is much superior to stainless steel and Nitinol. However, they also identified the high rate of Ti–Ni wire fractures in the oral environment as too high and unacceptable. Yokoyama *et al.*[37] studied the degradation and fracture of Ti–Ni superelastic wires in oral environment. Their findings indicated that hydrogen charging increased the critical stress of martensitic transformation and decreased the overall strength, leading to embrittlement. Further, they concluded that the galvanic current in the mouth may lead to hydrogen absorption of Ti–Ni wires resulting in degradation of mechanical properties and fatigue fracture. Zinelis *et al.*[38] performed a fractographic

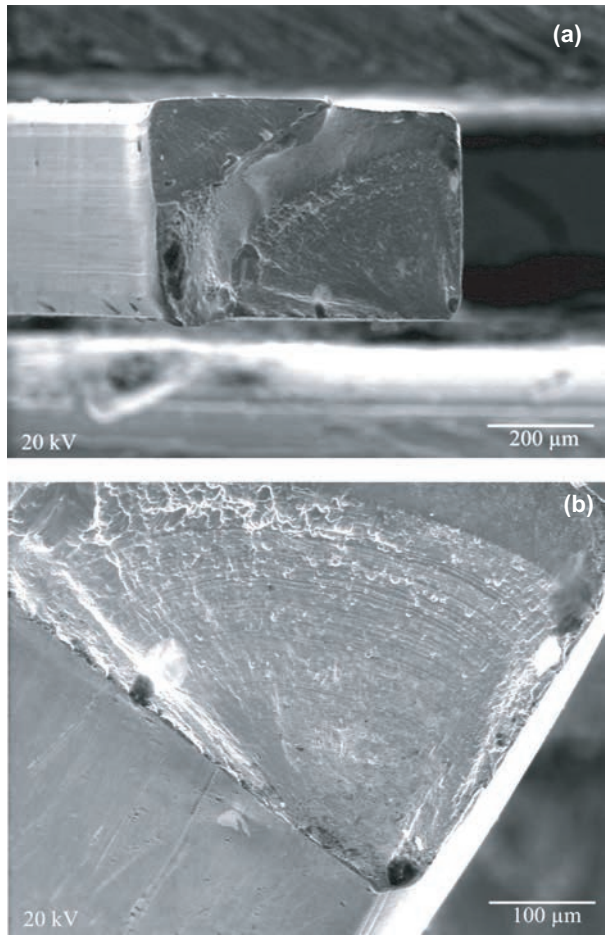

11.14 A cyclic fatigue fracture surface in bending on a rectangular Ti–Ni wire showing (a) two fracture initiation points on opposite surfaces of the wire, (b) striations created by bending cycles during the progression of the fatigue fracture.

analysis of *in vivo* fractured Ti–Ni and Ti–Ni–Cu wires. They concluded that most of the fractures occurred in the posterior section of the archwires and the fractures were brittle without plastic deformation in the areas of fracture or an increase in hardness. They disputed the conclusion that hydrogen embrittlement may be the cause of fracture.

Fracture in orthodontic wires can be attributed to wire fatigue and is partly due to the lower stiffness of Ti–Ni material relative to stainless steel, approximately 10% of the stainless-steel stiffness, which would allow greater cyclic bending of Ti–Ni wires resulting from mastication forces. Figure 11.14 represents an unusual fatigue fracture that occurred in the oral environment during treatment due to

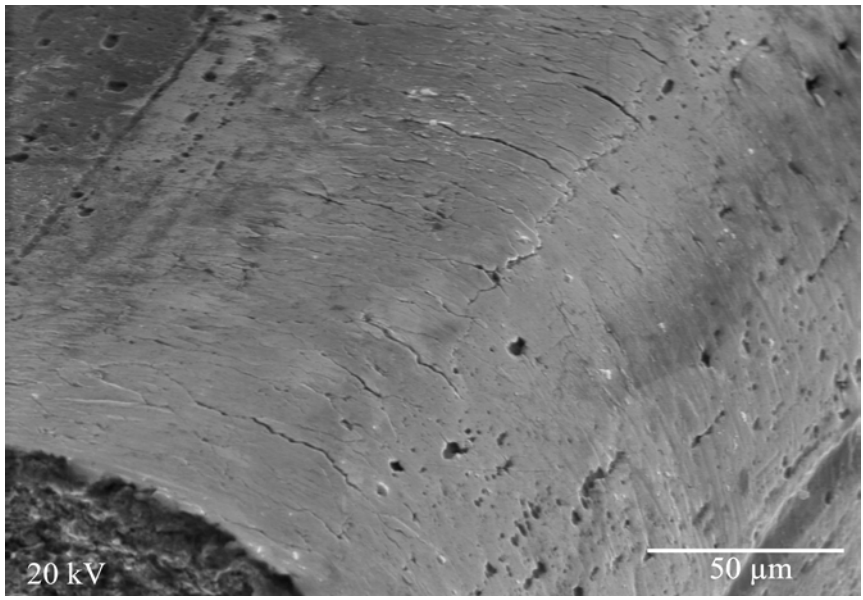

11.15 Radial surface cracks close to a fatigue fracture surface indicate several potential fracture initiation possibilities in the wire cycle bending in the oral environment.

cyclic bending. The crack initiations on this fracture occurred on two points on the opposite sides of the wire. In orthodontic wires fatigue fractures usually have a single initiation point. Figure 11.15 demonstrates the surface of a Ti–Ni orthodontic wire that fractured in the mouth during treatment. Evidence of many radial cracks near the fractured surface can be seen indicating that the wire material has been worked beyond its fatigue limit, and any of these surface cracks could have lead to a fracture. Evaluation of numerous fatigue fractures in Ti–Ni orthodontic wires indicated that a large proportion of fractures occurred at pre-existing flaws on the surface of the wires. Figure 11.16 shows an *in vivo* fractured Ti–Ni wire. The dents on the surface of this wire occurred by improper wire handling, by using hard serrated appliances for handling the wire. These surface flaws lead to the crack initiation and eventually fatigue failure of this wire. To avoid, or minimize, the potential for the fatigue failures of Ti–Ni wires, it is critical to handle the wires in such a way that any damage to the wire surface can be avoided. Pitting corrosion sites, occurring during the processing of the wires or in the oral environment, could also act as crack initiators. Figure 11.17 demonstrates a fatigue fracture in which the crack initiation occurred at a site that is believed to be the site of a pitting corrosion. This particular corrosion site is likely to be caused by the wire processing, or by the *in vivo* corrosive environment. Processing of Ti–Ni wires, particularly the degree of cold work and the transformation temperature can have an appreciable influence on their fatigue performance in cyclic bending. The fatigue

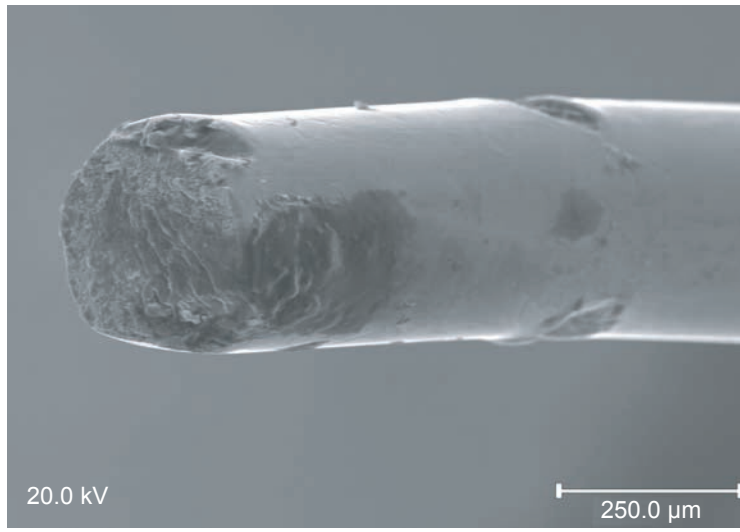

11.16 An example of a fatigue fracture that was initiated at the site of surface damage created by holding the wire with pliers with sharp serrations.

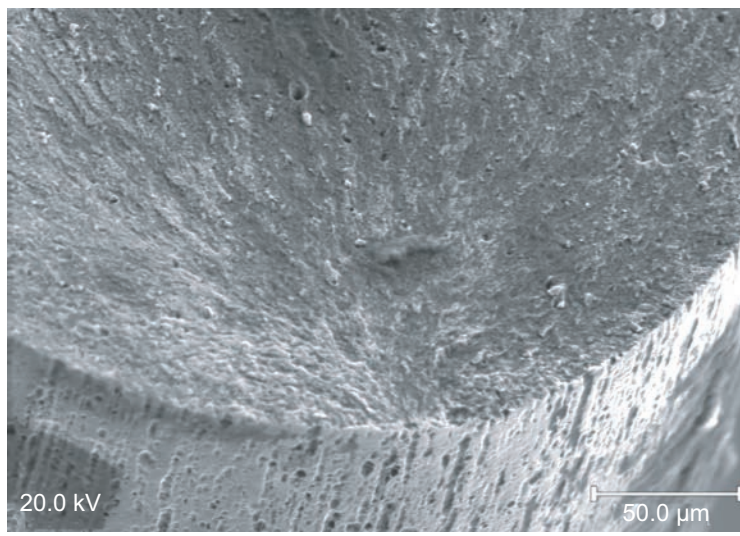

11.17 A typical fatigue fracture that was initiated at the site of a pitting corrosion. Rough wire surfaces appear to enhance fatigue fracture tendencies.

phenomenon in orthodontic archwires has not been extensively studied and understood. Miyazaki *et al.*[39] studied the effect of cyclic deformation on the pseudoelasticity characteristics of Ti–Ni alloys. They concluded that it is possible to stabilize the pseudoelasticity characteristics Ti–Ni alloys in cyclic bending. However, they identified that cyclic bending causes residual strain in Ti–Ni alloys that is accumulative and would increase with increased number of cyclic bending. Plastic deformation can greatly reduce the fatigue life of the wires.[40] Bahia *et al.*[41,42] concluded that fatigue of Ti–Ni alloys in the superelastic regime involves rapid nucleation and slow propagation of fatigue cracks. Further, they stated that in superelastic Ti–Ni alloys stress-induced martensitic transformation of the meta-stable β-phase to R-phase has the highest fatigue resistance.

11.4.4 Frictional properties and treatment techniques

Classical definition of friction, as presented by: $\mu = F_n/F_f$, where F_n is the normal force and F_f is the frictional force, defines only one component of friction in orthodontic systems. In orthodontics, friction is generally referred to as the resistance to sliding of an archwire in a bracket slot during the orthodontic treatment.

Sliding of archwires in the brackets slot is critically important in the movement of teeth and consequently orthodontic treatment. The sliding mechanics become particularly significant during: (a) the initial stage of orthodontic treatment (leveling and alignment) when the teeth are generally crowded and must be unraveled by sliding along a continuous archwire, and (b) when orthodontic space closure is accomplished by using sliding mechanics,[43] with friction, which involves using a continuous archwire. Frictionless space closure is achieved by the use of closing loop retraction archwire, or segmental wires having loops or springs. Most of the research and studies on friction in orthodontics have been focused on the interaction between the wires and the bracket slots and its influence in sliding mechanics with a particular focus on space closures.

The components that contribute to friction in orthodontic systems have been extensively studied over the past few decades, and although qualitatively various components that influence friction have been identified and measured, owing to the significant variations in the orthodontic treatment technique and the individual contributions of the clinicians, it is very difficult to determine the contribution of friction in an orthodontic force system.[44]

Resistance to sliding in a dynamic orthodontic system is a very complicated issue, and investigations on friction of wires in the brackets are focused on certain aspects of the whole system. Factors influencing the sliding mechanics during the orthodontic treatment are dependent on both the bracket system and the wire characteristics. Bracket design elements such as the material, slot dimensions, size, torque, angulations, corner radii, surface finish, and the method of ligation, as well as wire material characteristics, dimensions, surface finish, and the interaction of

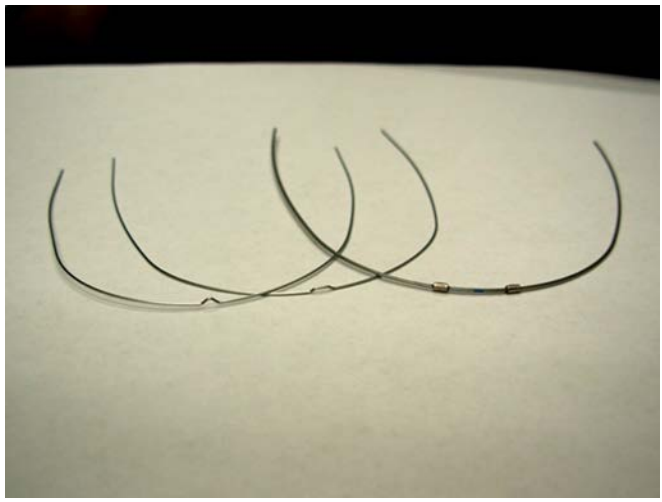

11.18 Examples of dimples and stops placed on orthodontic archwires to prevent the wires from excessive sliding along the dental arch.

the wire and the bracket determine tooth movement, and can dictate the efficiency of the treatment.

Use of sliding mechanics with Ti–Ni type wires as an initial wire is commonplace in today's orthodontics and one of the major practical concerns of the clinicians is controlling the sliding of Ti–Ni type archwires in the bracket slot. Wires with stops or dimples, Fig. 11.18, have been developed by the manufacturers to stop the wires from moving excessively in the bracket slots, along the arch, resulting in poking the patients at the distal end of the archwire. In spite of this clinical fact, many investigators who studied friction on Ti–Ni orthodontic wires reported higher frictional resistance for Ti–Ni wires relative to stainless steel or other materials.

Garner *et al.*[45] designed a study to compare the frictional forces of rectangular Ti–Ni, stainless steels, and beta titanium wires during a simulated canine retraction in artificial saliva. The wires were pulled through a bracket slot at the rate of 2 mm min^{-1}. The results showed that stainless steel had the lowest frictional resistance, followed by Ti–Ni and β-titanium wires. This was attributed to the surface roughness of the wires. Stainless-steel wires had the smoothest surfaces of all the wires tested. The authors recommended the use of stainless-steel wires for retraction over Ti–Ni of β-titanium wires.

Tidy[46] investigated forces caused by two-point contact during bodily movement of tooth along the stainless steel, Ti–Ni, and β-titanium archwires. He concluded that Ti–Ni and β-titanium wires had significantly higher frictional forces than the stainless-steel wires. Kapila *et al.*[47] came to a similar conclusion in their investigation of friction between stainless-steel brackets and various wires. Drescher *et al.*[48]

as well as Tidy concluded that wider brackets had lower frictional resistance than narrow brackets against wires of different materials and sizes, in contrast to Frank and Nikolai[49] who concluded narrow brackets had lower frictional resistance to wires of all materials. Kusy *et al.*[50] measured the surface roughness and the coefficient of friction for various archwire/bracket combinations including Ti–Ni. They concluded that the bracket material and slot size had little influence on the coefficient of friction. However, they found that the average coefficient of friction for stainless-steel archwire/bracket combinations was less than the archwires made from other materials including Ti–Ni. Pratten *et al.*[51] and Angolkar *et al.*[52] also concluded that the frictional resistance for Ti–Ni wires was greater than that of stainless steels. In both cases archwires were allowed to slide in bracket slots under different conditions. The authors attributed the higher frictional resistance of Ti–Ni wires to their greater surface roughness.

Many other studies were conducted for evaluating the frictional behavior of orthodontic wires made from stainless steels, β-titanium, Ti–Ni, and Co–Cr alloys against various stainless steel and ceramic brackets.[53–57] The studies included the use of various wire materials and sizes, various bracket materials and designs, and various tests conditions such as the introduction of torques, angulations, dry, and wet condition, etc. Generally, all studies concluded that frictional resistance of Ti–Ni or Ti–Ni–Cu wires were greater than stainless steels. The results for the β-titanium alloys were mixed, but in all cases stainless-steel wires were identified as producing the least amount of frictional resistance in sliding mechanics. However, Kusy, *et al.*[58,59] reported that the frictional characteristics of stainless-steel and Ti archwires against stainless-steel and PCA brackets were substantially the same in a dry state or in natural saliva.

In contrast to the majority of studies on the frictional resistance of archwires of various alloys, Omana *et al.*[60] and Rose *et al.*[61] concluded that the frictional resistance of Ti–Ni wires was smaller than wires made from stainless steels and other alloys under all conditions used in their evaluation. Rose concluded that the lower friction of Ti–Ni wires could be due to the greater flexibility of Ti–Ni and suggested that wire stiffness is a major determinant of the frictional force in orthodontic systems. The lower frictional resistance of Ti–Ni wires is particularly significant at higher binding angulations.

Smith *et al.*[62] used an apparatus for the friction of various wire and bracket combinations by allowing dynamic and progressive bracket tipping and uprighting, concurrent with linear bracket traction in an experimental canine retraction with sliding mechanics. The authors concluded that passive self-ligating brackets had the lowest frictional resistance to sliding. They further concluded that the level of friction was profoundly influenced by the archwire type, size, and shape as well as bracket types and the archwire/bracket combinations. Ti–Ni wires were identified as having lower frictional resistance at higher second-order angles.

Kusy *et al.*[63,64] investigated the sliding wires of various materials against flats on stainless steel. They concluded that the smoothest wire surfaces resulted in the

lowest coefficient of friction; however, surface roughness did not correlate with the surface roughness. They further concluded that the coefficient of friction was influenced by the speed of sliding for stainless-steel and Ti–Ni wires. They attributed this phenomenon to the removal of oxides from the surface and the recovery of the oxides on the surface during sliding. No conclusions were made on the ramifications of these influences in orthodontic treatment.

Henao *et al.*[65] conducted a study that considered the friction in an orthodontic system using typodonts and wires made from different materials against conventional brackets or self-ligating brackets. They concluded that size of the wires as well as their moduli of elasticity have a significant influence on the frictional characteristics of the system.

Rossouw *et al.*[66] in their review of the variables associated with low velocity frictional dynamics reported that 'frictional dynamics are typically related to systems sustaining substantial load, under conditions of rotational or translational velocities, not applicable to magnitudes or rates common in orthodontics. *In vitro* studies of orthodontic frictional resistance typically report quantification of either static or kinetic frictional resistance as distinctly separate phases'. However, at low velocity, static or kinetic frictional resistances are dynamically related and *in vitro* studies of static or kinetic quantifications could be misleading.

Ho and West[67] concluded that archwire stiffness had the dominant controlling factor for frictional resistance. Conflicting reports on the frictional resistance in the sliding mechanics highlights the fact that friction in orthodontic systems is different and more complicated than the classical definition of coefficient of friction. Kusy, *et al.*[68] developed a theoretical model that identifies friction (FR), binding (Bi), and notching (NO) as factors influencing the resistance of the wire to sliding in an orthodontic system. A relationship offered by the authors is as follows:

$$RS = FR + NO + Bi$$

The friction part of the equation is a material selection issue and although the actual frictional forces between the wires and bracket slot may be a major component of the total resistance to sliding of the wire in the bracket slot, other components such as binding of the wire at the bracket slot corners, bracket design and the roundness of the slot corners, wire stiffness, wire hardness and, finally, the orthodontic treatment techniques often have greater influence in dictating the sliding mechanics during the orthodontic treatment. Their conclusion indicated that there is every indication that classical friction controls sliding mechanics below a certain critical contact angle between the archwire and bracket slot. However, once that angle is exceeded, binding and notching phenomena increasingly restrict sliding mechanics.

Generally, self-ligating brackets with passive ligation systems provide lower forces on the wires than the active self-ligation system counterparts. Conventional brackets that use steel or elastomeric materials for ligation provide the greatest

binding forces between the wire and the bracket slot.[69] Use of Ti–Ni type wires in the self-ligation systems seem to have minimized the binding due to ligation and resulted in minimization of the resistance to movement, hence providing the most efficient sliding mechanics in the current fixed appliance systems.

11.5 Ti–Ni alloy wires – effects of additional elements

Evolution of superelastic and shape memory Ti–Ni orthodontic alloys lead to the refinement of wire properties and their force deliveries through strict control of their compositional elements and processing parameters. New alloying elements added to the Ti–Ni based orthodontic wires include Cu, Cr, and Fe. The effects of these elemental additions will be briefly discussed in this section. Various compositions of Ti–Ni alloys used in orthodontics include:

- Ti–Ni: the Ni concentration in these alloys varies such that their transformation temperatures (A_f) can range from 0 to 35 °C.
- Ti–Ni–Cu–Cr: Cu addition is for the purpose of narrowing the stress plateau stress hysteresis and suppressing the formation of R phase. Cr addition reduces the TTR to that suitable for orthodontic wires.
- Ti–Ni–Cr: Cr addition to the composition of binary Ti–Ni was for the purpose of reducing the transformation temperature and improving the corrosion resistance.
- Ti–Ni–Fe: addition of Fe to Ti–Ni alloys substantially reduces the transformation temperature and is believed to produce greater control over the remnant strain.

These alloys will be discussed further below.

11.5.1 Ti–Ni–Cu

The potential use of Ti–Ni–Cu alloys for orthodontic applications was first suggested by Miyazaki and Sachdeva.[69] Addition of Cu to Ti–Ni alloys reduces the stress hysteresis and the R phase is not observed in this system[10,11] as the martensite and austenite phases are formed. Figure 11.19 represents a typical DSC graph for Ti–Ni–Cu alloys. Ti–Ni–Cu wires with shape memory effect are very soft at room temperature. However, at body temperature, their transformation to austenite creates pronounced recovery forces in the wires. This is due to the sharper peak width and the absence of R-phase in Ti–Ni–Cu wires when compared with the binary Ti–Ni alloys. The composition of Cu-containing orthodontic wires includes approximately 6% Cu and less than 0.5% Cr. The transformation temperature of Ti–Ni–6Cu alloy wires is well above the body temperature. Addition of Cr to Ti–Ni–6Cu alloy was for the purpose of suppressing the A_f temperature. Cr has a positive effect on improving the corrosion resistance of Ti–Ni alloys in oral environments. Three types of Ti–Ni–Cu wires are commercially available having

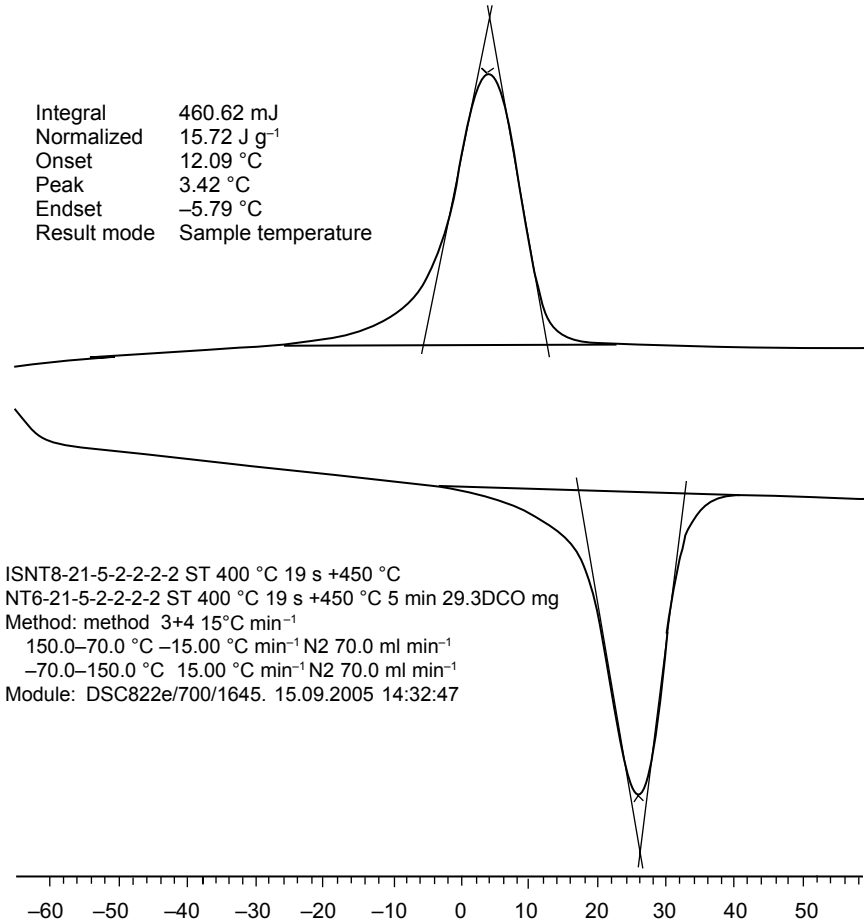

11.19 A typical DSC graph for a Ti–Ni–Cu–Cr alloy orthodontic archwire showing a transformation temperature of about 33 °C. Transformation of this alloy presents a single peak at both cooling and heating cycles.

transformation temperatures of 27, 35, and 40 °C. The average transformation temperatures are selected to give superelastic, shape memory, and mostly martensitic effects in the wires, respectively. Figure 11.20 represents a typical stress/strain graph for Ti–Ni–Cu 35 wire at room and body temperatures compared with a typical Ti–Ni orthodontic wire. Addition of Cu is effective in narrowing the stress hysteresis and stabilizing the superelasticity characteristics against cyclic deformation.[70] The reduced stress hysteresis of Ti–Ni–Cu wires makes the wire engagement into the bracket slot easier for the same unloading forces. It can also be seen that the unloading plateau stress remains consistent and relatively flat providing the necessary force for tooth movement to complete recovery. Figure 11.21 shows the shape memory characteristics of Ti–Ni–Cu 35. At room

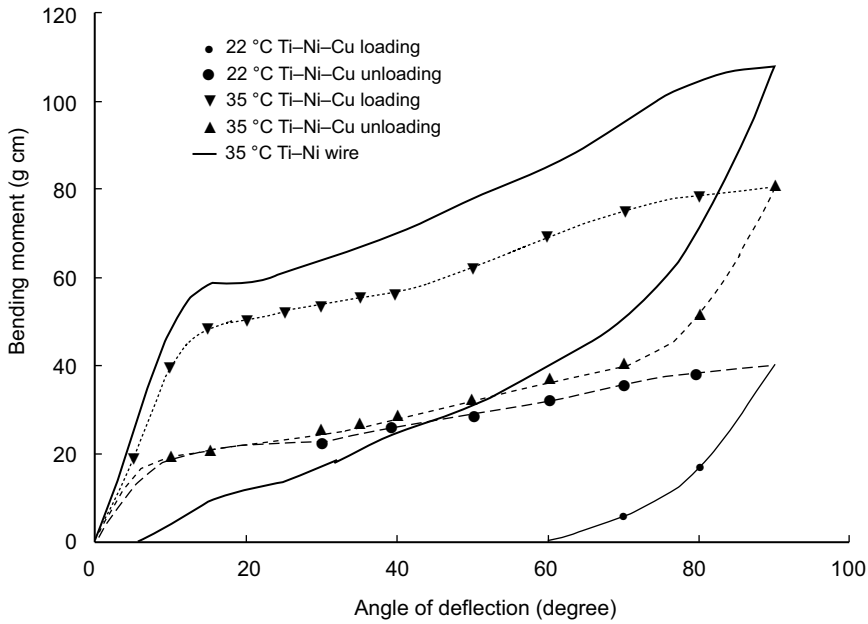

11.20 A typical stress/strain curve in cantilever bending for a Ti–Ni–Cu–Cr 35 wire shows the difference between the loading and unloading forces at room and body temperatures. The stress/strain curves for one type of Ti–Ni wire is also presented for comparison.

temperature, the loading force used for engaging the wire into the bracket slot is relatively small. However, after the wire installation into the bracket slot, when the wire temperature rises to body temperature, the unloading force that is used for tooth movement increases significantly providing an efficient tooth movement. Sakima *et al.*[71] determined that shape memory Ti–Ni–Cu 40 wires produced the lowest and the most consistent forces at mouth temperatures and further concluded that, if low consistent forces are the requirements for orthodontic applications, superelastic wires are not the best choice for orthodontic applications, particularly in self-ligating systems that generally have lower friction.

11.5.2 Ti–Ni–Cr

Addition of Cr to Ti–Ni alloys improves its corrosion resistance in oral environments and suppresses the A_f transformation temperature. The transformation temperature of Ti–Ni alloys with stoichiometric Ni and Ti contents is well above room temperature and orthodontic wire made from this composition is considered heat sensitive, or thermo-active. An alternative method for reducing the A_f transformation temperature in Ti–Ni alloys is by increasing the Ni/Ti ratio of the alloy. The transformation temperature of Ni-rich Ti–Ni orthodontic wires can range

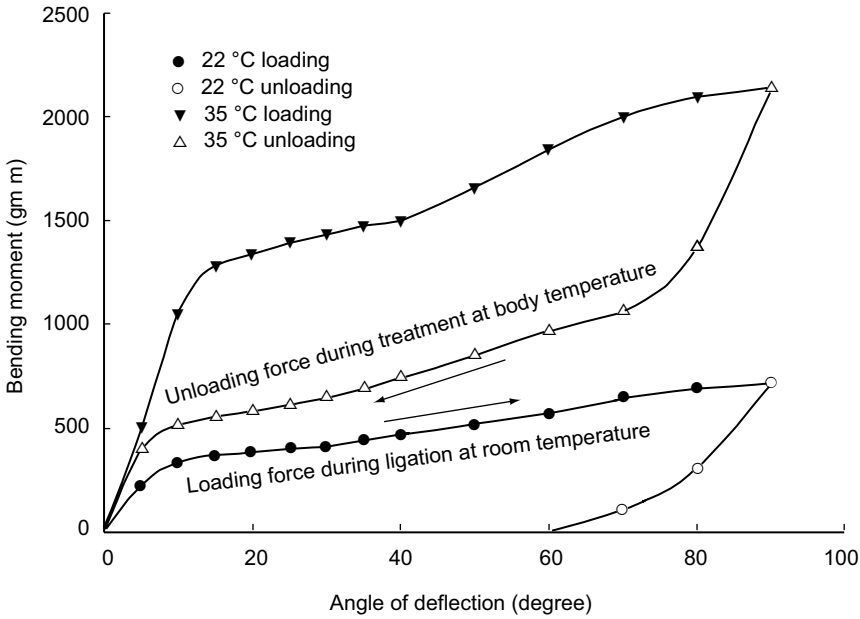

11.21 Representation of the forces used for the wire engagement into the bracket slot, at room temperature, and the unloading forces that would result in tooth movement, at body temperature, in a shape memory (heat-activated) orthodontic alloy wire.

from below the freezing temperature to about room temperature. The A_f transformation temperature of typical Ti–Ni–Cr orthodontic wires ranges from 10 to 20 °C. These alloys exhibit the presence of R phase transformation as they cool down to martensite, or in heating to austenite. The final heat treatment process can lead to a significant shift in the R phase. Figure 11.22 represents a typical phase transformation graph for the Ti–Ni–Cr orthodontic wire, using DSC. In the cooling curve of this graph, the formation of R phase over a broad range of temperatures without clear evidence of a specific peak associated with the R phase is shown. However, the conventional double peak is observable indicating a multiple-phase transformation which involves martensite, R phase, and austenite.

The stress/strain performance of Ti–Ni–Cr orthodontic wires is similar to some of Ni-rich Ti–Ni wires. Figure 11.23 represents the plateau stresses for a typical 0.14 round Ti–Ni–Cr orthodontic wire tested at room and body temperatures. Although there is an appreciable difference between the loading and unloading forces at room and body temperatures, clinically the wire is considered active at all times, including during the bracket engagement.

11.5.3 Ti–Ni–Fe

Fe has the tendency to suppress the TTR and increase the stress hysteresis

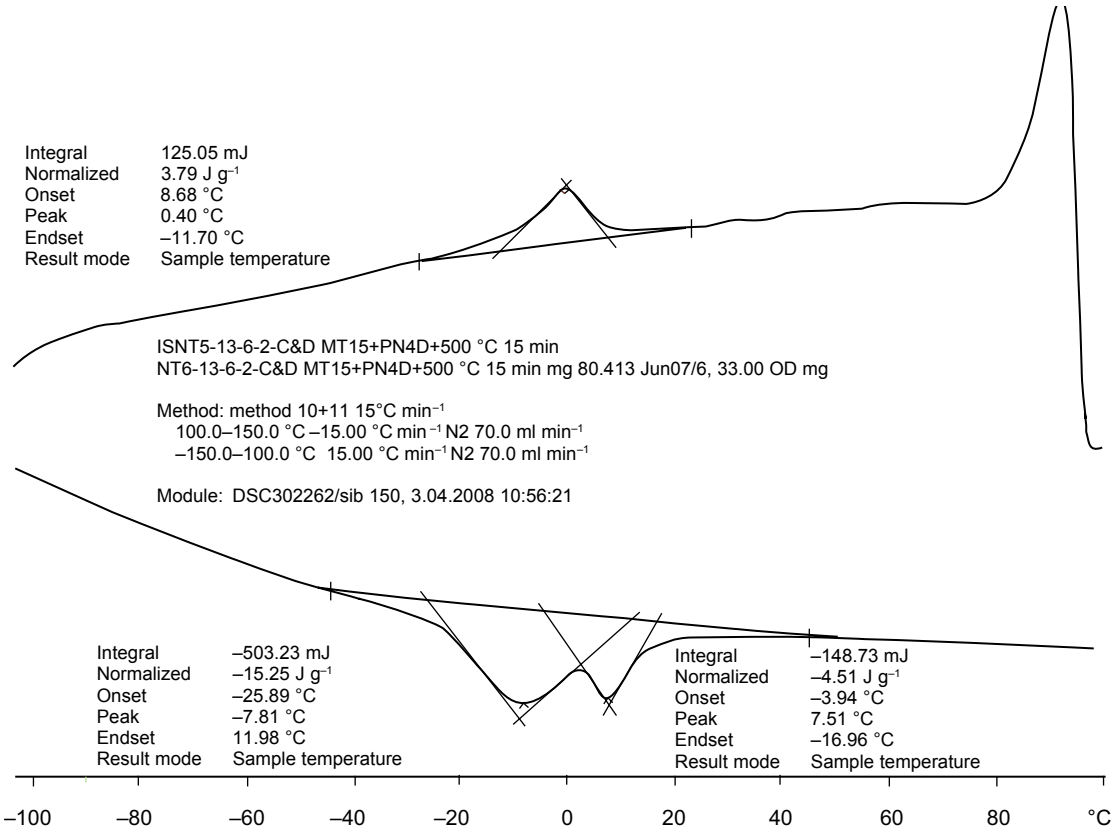

11.22 A typical DSC transformation graph for Ti–Ni–Cr shows that the transformation from martensite to austenite is not a single peak which may be an indication of the presence of R phase. The single peak on the cooling cycle is believed to be the peak for the R phase.

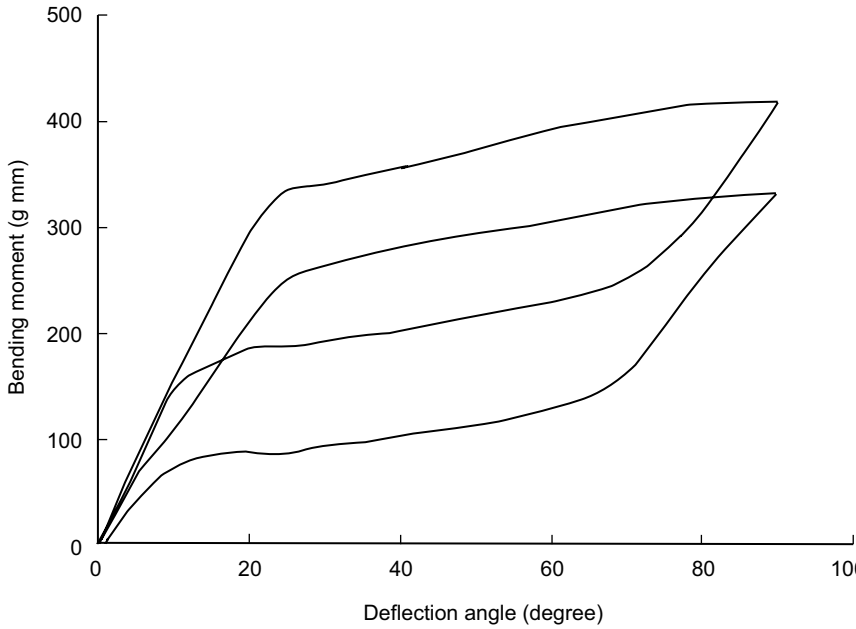

11.23 Stress/strain curves for a typical Ti–Ni–Cr superelastic orthodontic wire tested by cantilever bending at room and body temperatures.

significantly. However, the transformation temperature of Ti–Ni–Fe orthodontic wires is generally greater than room temperature and the wires are fully or mostly austenitic in the oral environment. These orthodontic wires are considered heat sensitive or thermo-active. Chen *et al.*[72] concluded that Chinese Ti–Ni wires reduced the leveling and alignment phase of treatment without discomfort to the patient. Figure 11.24 demonstrates the effect of the final heat treatment temperature on the A_f transformation temperature of Ti–Ni–Fe orthodontic wires. The A_f temperature on this alloy was consistently above the room temperature, ranging between 26 and 31 °C, which shows it is relatively insensitive to variations in the heat treatment temperature. However, the loading and unloading plateau forces for this wire decreased in excess of 50% in cantilever 90° bending around a 12 mm diameter mandrel, as the heat treatment temperature increased, Fig. 11.25, demonstrating the influence of the processing condition on the performance of the wire as well as the transformation temperature. Qing *et al.*[73] concluded that orthodontic wires using shape memory effect, as well as superelasticity, have greater bending, and torsional performance relative to Ti–Ni wires that have lower transformation temperatures.

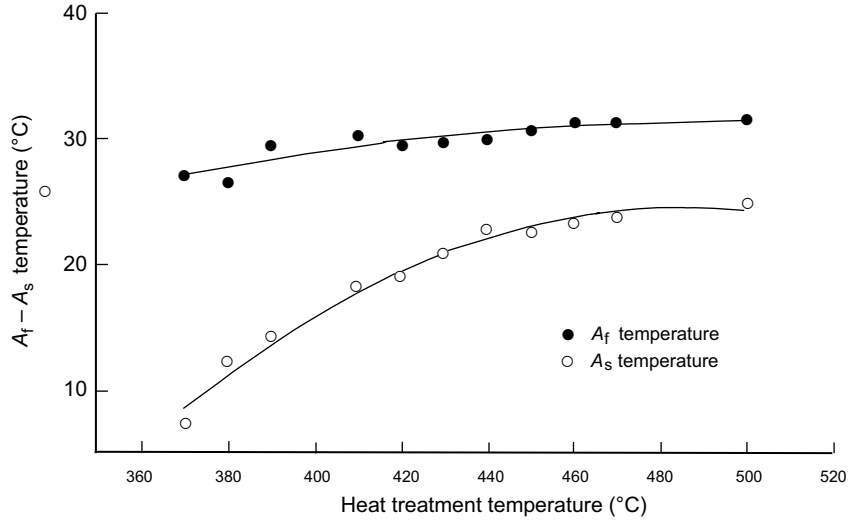

11.24 Effect of the final heat treatment temperatures on the transformation temperatures of 17 × 25 orthodontic wires made from a Ti–Ni–2Fe, having 35% cold work.

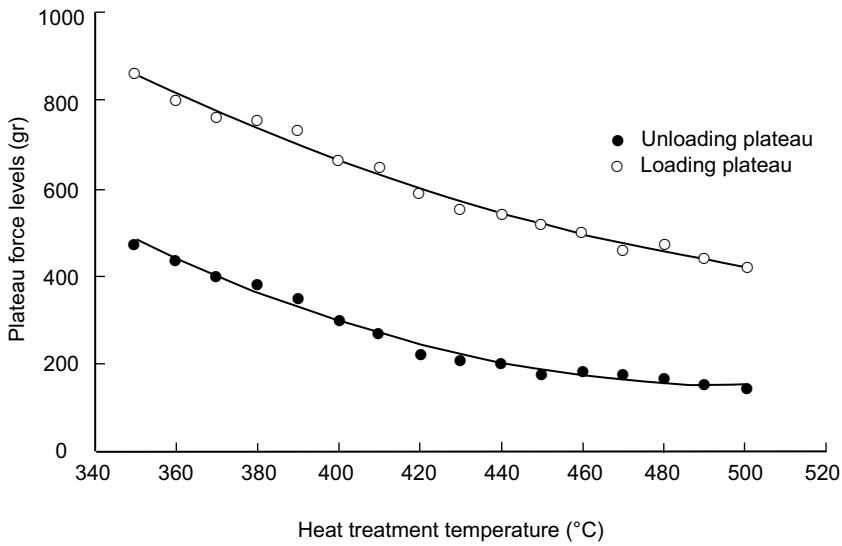

11.25 Typical loading and unloading forces for Ti–Ni–2Fe wires heat treated at different temperatures. Heat-treatment temperatures and conditions as well as the transformation temperatures influence the force delivery of the wires.

11.6 Chemical properties in the oral environment

11.6.1 Corrosion resistance of Ti–Ni alloys

Biocompatibility and corrosion resistance are the primary requirements of the metallic materials that are used in the mouth. The reason for this requirement is that the mouth provides a particularly aggressive environment for corrosion and biodegradation of metals. The oral environment has ionic, thermal and microbiological characteristics, and contains enzymes that attack metal surfaces, all of which cause corrosion and biodegradation. Few studies have been conducted to evaluate the corrosion of orthodontic Ti–Ni wires in the oral environment. Reports on corrosion resistance of Ti–Ni wires have been inconsistent.

Although some investigators[74,75] reported that Ti–Ni wires have similar corrosion resistance to stainless-steel wires, other authors[76,77] found that Ti–Ni wires are more prone to corrosion than stainless-steel wires. Vandenkeckhove *et al*.[78] studied the corrosion of superelastic Ti–Ni orthodontic wires and determined that the wire processing has a significant effect on the corrosion behavior of the wires. Their findings indicated that fully annealed low nickel alloys had a higher corrosion rate compared with Ni-rich alloys; however, aging increases the corrosion rate of the Ni-rich alloys.

Asaoka *et al.*[79] studied hydrogen absorption of Ti–Ni wires in a corrosive biological environment. They found that galvanic currents and fretting corrosion of the Ti–Ni alloys may be significant factors in the material's brittleness and fracture formation.

Schwaninger *et al.*[80] reported that corrosion did not affect the properties of nitinol wires, Lopez *et al.*[81] and Nicholson *et al.*[82] found that the permanent deformation of the wires increased and their elasticity decreased due to the effects of corrosion and cold working. Harris *et al.*[83] investigated the changes in mechanical properties of Ti–Ni orthodontic alloys owing to time elapsed exposure to a simulated oral environment with various levels of acidity. They found that wires that were exposed to a corrosive oral environment under stress showed significant decreases in specific mechanical properties. Long-term use or re-use of nitinol wires may be associated with a significant degradation in the wire's elasticity and performance. In contrast, other investigators[84,85] demonstrated that various forms of disinfection or sterilization did not have any appreciable impact on the mechanical properties of orthodontic wires.

11.6.2 Biocompatibility and allergic reactions

Generally, biocompatibility and corrosion resistance of metallic materials used in the body are closely related. Ni release in the body due to corrosion of Ti–Ni alloys is a major reason that can potentially compromise the biocompatibility of Ti–Ni orthodontic appliances. Ti–Ni is protected by a Ti-based oxide layer that is very

efficient against biocorrosion as described by Trepanier *et al*.[86] They also reported that Ni release from Ti–Ni has shown to be minimal and non-toxic in many studies. Further, *in vitro* and *in vivo* assays show that Ti–Ni exhibits good biocompatibility. Ryhanen *et al.*[87] found that Ni release was higher in Ti–Ni materials than in 316 stainless steels, but it did not reach toxic levels and proliferation of cell growth was not affected near the material. Oshida *et al.*[88] studied the *in vitro* dissolution of Ni in Ti–Ni orthodontic appliances and correlated the Ni dissolution and corrosion of wire. Barrett *et al.*[89] conducted an *in vitro* investigation of orthodontic metallic appliances including Ti–Ni wires. They concluded that Ni release from the surface of Ti–Ni orthodontic wires is substantially similar to that of stainless-steel wires, although Ni content in the Ti–Ni wire composition is approximately five times greater than that of stainless steels. Further, they determined that under their simulated saliva medium the exposure of oral tissues to Ni released from the full orthodontic appliances was significantly smaller (less than 10%) than the daily intake of Ni from food and water, as well as exposure to air. Their data is in agreement with that of other investigators[90–92] indicating that the corrosion of Ti–Ni wires, and the concentration of Ni release declined during the first few days, reached a plateau and did not increase after that.

Eliades *et al.*[93] conducted a detailed analytical evaluation of the retrieved Ti–Ni archwires. They showed that Ti–Ni archwires were coated by intra-orally formed proteinaceous integuments that masked the surface topography, depending on the individual patients oral environmental conditions, and the intra-oral exposure period. The coating consisted of amide, alcohol, and carbonates, whereas the predominant elements in the coating were Na, K, Cl, Ca, and P. They also identified delamination, pitting, and crevice corrosion in the retrieved wires. However, in agreement with Oshida *et al.*[88] they believed that these mineralized regions, specially under low pH conditions, provide a protective effect on the surface of wires. Shabalovskaya[94] published a comprehensive review of the corrosion resistance and biocompatibility of various types of Ti–Ni implant materials.

Although many investigations on the biocompatibility of Ti–Ni wires have indicated various degrees of Ni release, they seem to be all in agreement that Ti–Ni materials are safe and biocompatible for medical applications. Biocompatibility of orthodontic appliances is less stringent than the medical implants and these alloys are considered to have adequate biocompatibility. The author is not aware of any reported allergic reactions to Ti–Ni alloys, but clinicians refrain from using the Ti–Ni wires on patients who have Ni sensitivity or are allergic to stainless steels.

11.7 Other orthodontic appliances

Superelastic and shape memory Ti–Ni alloy archwires have the lion's share of orthodontic appliances. Other appliances include compression and extension

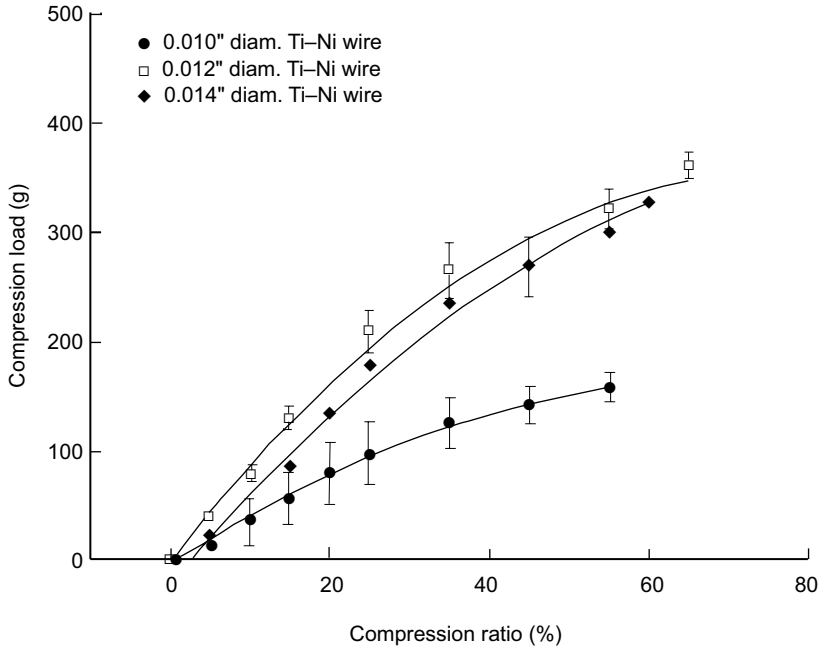

11.26 Force delivery of Ti–Ni orthodontic compression springs of various diameters indicates significant superelasticity. The OD of all the springs are the same.

springs, trans-palatal expanders, and other types of miniature springs with functional applications attached to brackets.

The advantage of Ti–Ni coil springs over elastomeric materials that have traditionally been used during orthodontic treatment is that the springs can elastically deform at similar levels as the elastomeric materials but their force decay over time is negligible.

The extension and compression springs can expand in excess of 500% of their length at rest, while maintaining their complete elastic recovery. However, they do not have plateau stresses similar to solid wires. Figure 11.26 represents a stress/strain relationship for typical Ti–Ni compression springs of various diameters. Low stiffness of Ti–Ni material provides gentle slopes relative to the springs made from other materials such as stainless steels.

Palatal expanders are made from a combination of Ti–Ni wires and connectors for attachments to the lingual sides of molar teeth. The Ti–Ni palatal expanders provide significantly lower forces for arch expansion owing to low stiffness of wires resulting in orthodontic tooth movement compared with traditional expanders, that because of their rigidity, caused breakage of the suture in the mid-palate leading to arch expansion.

Finally, use of miniature springs from Ti–Ni alloys in self-ligating brackets

made the design of these brackets possible by providing the necessary resilience for the extreme design requirements.

11.7.1 Joining technology

Ti–Ni alloys contain two elements that have stable oxides and Ti has a great appetite for reaction and dissolution of interstitial elements. Further, high temperatures and melting of Ti–Ni alloys may lead to formation of brittle phases at the joint. These limitations have, so far, hampered attempts to join Ti–Ni wires in the orthodontic industry. Mechanical means such as swaging, staking, etc. have been employed to attach various parts together.

Laser welding, micro plasma joining and soldering methods have been successfully developed and used for joining the Ti–Ni parts. However, maintaining the superelastic properties of the parent material at the joints still remains a challenge. Further, in many cases the joints become brittle due to microstructural changes. Beyer *et al.*[95] successfully developed a resistance welding process for joining Ti–Ni wires. However, this process has not found any applications in orthodontic industry to date. Yao *et al.*[96] developed a spot welder that is claimed to be usable for joining the Ti–Ni wires in orthodontic clinics. However, this device does not seem to have attracted much attention from the clinicians.

11.8 Future trends

The contribution of Ti–Ni alloys in the advancement of orthodontic treatment and the treatment techniques has made these alloys an integral part of the orthodontic industry demanding performance requirements that pushes the limits of the capabilities of Ti–Ni alloys.

Enhancement of the fatigue performance of these alloys is the most desirable improvement that Ti–Ni materials can offer in the future.

Improvements in the performance of future alloys with superelastic behavior should include greater resilience and smaller stress hysteresis so that clinicians can engage larger size wires into the bracket slot sooner without having to overcome large loading forces of the current superelastic wires, yet the wire would provide sufficient force for efficient tooth movement. This would pave the way for further treatment efficiency improvements and reducions in the treatment time.

Finally, current Ti–Ni materials are limited to wires, strips and other forms produced by drawing and/or rolling processes. Further developments in fabrication technologies, such as forging, metal injection molding, and casting, independently or in combination with esthetic materials would extend the application of Ti–Ni alloys in orthodontic products.

11.9 References

1 Burstone, C J, Goldberg, A J, Beta-titanium: A new orthodontic alloy. *Am J Orthod*, 1980; **77**: 121–132.
2 Burstone, C J, Qin, B, Morton, J Y, Chinese Ni/Ti wire – a new orthodontic alloy. *Am J Orthod*, 1985; **87**: 445–452.
3 Andreasen, G F, Brady, P, A use hypothesis for 55 Nitinol wire in orthodontics. *Angle Orthod*, 1972; **42**: 172–177.
4 Miura F, Mogi M, Ohura Y, Hamanaka H, The super-elastic properties of Japanese Ni–Ti alloy for use in orthodontics, *AJODO*, 1986: **90**, 1–10.
5 Andreason G F, Treatment advantages using nitinol wire instead of 18-8 stainless wire with the edgewise bracket, *Quintessence Int*, 1980; **12**: 319–324.
6 Andreasen G F, Hamilton T B, An evaluation of 55 cobalt substituted nitinol wire for use in orthodontics, *J Am Dent Assoc*, 1971; **82**: 1373–1375.
7 Andreasen G F, Morrow, R E, Laboratory and clinical analyses of nitinol wire, *AJO*, 1978; **73**(2): 142–151.
8 Andreasen G F, A clinical trial of alignment of teeth using a 0.019 inch thermal nitinol wire with a transition temperature range between 31 and 45 degrees C, *AJO*, 1980: **78**, 528–537.
9 West A E, Jones M L, Newcombe R G, Multriflex versus superelastic: A randomized clinical trial of the tooth alignment ability of initial arch wires, *AJODO*, 1995: Nov, 464–471.
10 Sachdeva R, Miyazaki S, Application of shape memory nickel–titanium alloys to orthodontics, *MRS Int Mtg Adv Mater*, 1989; **9**: 605–610.
11 Storey E, Smith B, *Austral J Dent*,1952; **56**: 11.
12 Bustone C J, Baldwin J J, Lawless D T, *Angle Orthod*, 1961; **31**.
13 Mills J R E, *Principles and Practice of Orthodontics*, 1987; 2nd ed.: Edinburgh, Scotland, Churchill Livingstone.
14 Proffit W R, *Contemporary Orthodontics*, 1986; St Louis, CV Mosby Co.
15 Kapila S, Sachdeva R, Mechanical properties and clinical applications of orthodontic wires, *AJODO*, 1989; **96**: 100–109.
16 Sachdeva R C, Miyazaki S, Superelastic Ni/Ti alloys in orthodontics, In: Duerig T W *et al.*, *Engineering Aspects of Shape Memory Alloys*, London: Butterworth–Heinemann, 1990; 452–469.
17 Yoneyama T, Doi H, Hamanaka H, Okamoto Y, Mogi M, Miura F, Super-elasticity and thermal behavior of Ti–Ni ally orthodontic arch wires, *Dent Mat J*, 1992; **11**: 1–10.
18 Brantly W A, Webb C S, Soto U I, Cai Z, McCoy B P, X-ray diffraction analysis of copper Ti–Ni wires, 75th General Session IADR, Orlando, FL, 1997; Abstract No. 3097.
19 Kusy R P, Whitley J Q, Thermal and mechanical characteristics of stgainless steel, titanium–molybdenum, and nickel–titanium archwires, *AJODO*, 2007; **131**: 229–237.
20 Thayer T A, Bagby M D, Moore R N, DeAngelis R J, X-ray diffraction on nitinol orthodontic arch wires, *AJODO*, 1995; **107**: 604–612.
21 McCoy B P, Brantly W A, Culbertson B M, Mitchell J C, DSC and EDS analysis of new Copper Ti–Ni orthodontic wires, 75th General Session IADR, Orlando, FL, 1997; Abstract No. 3096.
22 Mercier O, Melton K N, Gotthardt R, Kulik A, Lattice instability in NiTi and NiTiCu In: Aaronson H L, Laughlin D E, Sekerka R F, Wayman C M, Proceedings – *International Conference on Solid→Solid Phase Transformation*, American Institute of Mining, Metallurgical and Petroleum Engineers, 1981; New York, 1259–1263.

23 Moberly W J, Melton K N, Ti–Ni–Cu Shape Memory Alloys, In: Duerig T W, Melton K N, Stockel D, Wayman C M, *Engineering Aspects of Shape Memory Alloys*, 1990; Butterworth–Heinemann, London, 46–57.
24 Fletcher M L, Miyake S, Brantley W A, Culbertxson B M, DSC and bending studies of a new shape-memory orthodontic wire, *J Dent Res*, 1992; **68**: 169, Abstr. No. 505.
25 Miura F, Mogi M, Ohura Y, Karibe M, The superelastic Japanese Ni/Ti alloy wire for use in orthodontics. Part III. Studies on the Japanese Ni/Ti coil springs, *AJODO*, 1988; **94**: 89–96.
26 Miura F, Discovery and uses of super-elasticity in clinincal orthodontics, *Dentistry in Japan*, 1990; **27**: 187–196.
27 O'Brien K, David Lewis D, William Shaw W, Combe E, A clinical trial of aligning archwires, *Eur J Orthod*, 1990; **12**(4): 380–384.
28 Mandall N A, Lowe C, Worthington H V, Sandler J, Derwent S , Abdi-Oskouei M, Ward S, Which orthodontic archwire sequence? A randomized clinical trial, *Eur J Orthod*, 2006; **28**(6): 561–566.
29 Hudgins J J, Bagby M D, Erickson L C, The effect of long term deflection on permanent deformation of nickel–titanium archwires, *Angle Orthod*, 1990; **60**(4), 283–288.
30 Hurst C L, Duncanson M G, Nanda R S, Angolkar P V, An evaluation of the shape memory phenomenon of nickel–titanium orthodontic wires, *AJO-DO*, 1990; Jul: 72–76.
31 Raboud, D, Simulation of psudoelastic response of SMA orthodontic archwires, Department of Engineering, University of Alberta, Edmonton, Alberta, Canada
32 Kapila S, Reichhold G W, Andreason RS, Watanabe L G, Effect of clinical recycling on mechanical properties of nickel–titanium alloy wires, *AJODO*, 1991; **100**: 428–235.
33 Mohlin, B, Muller, H, Odman, J, Thilander, B, Examination of Chinese Ni/Ti wire by a combined clinical and lab. approach, *Eur J Orthod*, 1991; **13**(5), 386–391
34 Eliades T, Eliades G, Athanasiou A E, Bradley T G, Surface characterization of retrieved Ni/Ti orthodontic archwires, *Eur J Orthod*, 2000; **22**: 317–326.
35 Drescher D, Bourauel C, Sonneborn W, Schmuth G P, The long term fracture resistance of orthodontic nickel–titanium wires, *Schweiz Monatsschr Zahnmed*, 1994; **104**: 578–584.
36 Prymaka O, Klockeb A, Kahl-Niekeb B, Epple M, Fatigue of orthodontic NiTi wires in different fluids under constant mechanical stress, *Mater Sci Eng*, 2004; **378**(1–2): 110–114.
37 Yokoyama K, Hamada K, Moriyama K, Asaoka K, Degradation and fracture of Ti–Ni superelastic wire in an oral cavity, *Biomaterials*, 2001; Aug, **22**(16): 2257–2262.
38 Zinelis S, Eliades T, Pandis N, Eliades G, Bourauel C, Why do nickel titanium archwires fracture intra-orally? Fractographic analysis and failure mechanism of in-vivo fractured wires, *AJODO*, 2007; **132**: 84–89.
39 Miyazaki S, Imai T, Igo Y, Otsuka K, Effect of cyclic deformation on the pseudoelasticity characteristics of Ti–Ni alloys, *Metall Trans A*,1986; **17A**: 115–120.
40 McKelvey A L, Ritchie R O, Fatigue crack propagation in nitinol, a shape-memory and superelastic endovascular stent material, *J Biomed Mater Res*, 1999; **47**(3): 301–308.
41 Bahia M G A, Dias R F, Buono V T L, The effect of cyclic bending strains on the behavior of superelastic nickel–titanium wires and endodontic instruments, Federal University of Minas Gerais, Belo Horizonte, MG, Brazil.
42 Bahia M G A, Dias R F, Buono V T L, The influence of high amplitude cyclic straining on the behaviour of superelastic NiTi, *Int J Fatigue*, 2006; **28**(9): 1087–1091.
43 Staggers, J A, Germane N, Clinical considerations in the use of retraction mechanics, *JCO*, 1991; **25**: 364–369

44 Rossouw P E, Friction: An overview, *Semin Orthod*, 2003; **9**(4): 218–222.
45 Garner, L D, Allai, W W, Moore, B K, A comparison of frictional forces during simulated canine retraction of a continues edgewise archwire, *AJODO*, 1986; **90**: 199–203.
46 Tidy, D C, Frictional forces in fixed appliances, *AJODO*, 1989; **96**: 249–254.
47 Kapila, S, Angolkar P V, Duncanson M G, Nanda R S, Evaluation of friction between edgewise stainless-steel brackets and orthodontic wires of four alloys, *AJODO*, 1990; 117–126.
48 Dreschr D, Bourauel C, Schumacher H A, Frictional forces between bracket and archwire, *AJODO*, 1989; **96**: 397–404.
49 Frank G A, Nikolai R J, A comparative study of frictional resistances between orthodontic bracket and archwire, *AJO*, 1980; **78**: 593–609.
50 Kusy R P, Whitley J Q, Coefficient of friction for archwires in stainless-steel and polycrystalline alumina bracket slots in the dry state, *AJODO*, 1990; **98**: 300–312.
51 Pratten D H, Popli K, Germane N, Gunsolley J C, Frictional resistance of ceramic and stainless-steel orthodontic brackets, *AJODO*, 1990; **98**: 398–403.
52 Angolkar P V, Kapila S, Duncanson M G, Nanda R S, Evaluation of friction between ceramic brackets and orthodontic wires of four alloys, *AJODO*, 1990; **98**: 499–506.
53 Ireland A J, Sherriff M, McDonald F, Effect of bracket and wire composition on frictional forces, *Eur J Orthod*, 1991; **13**: 322–328.
54 Sunders C R, Kusy R P, Surface topography and frictional characteristics of ceramic brackets, *AJODO*, 1994; **106**: 76–87.
55 Bazakidou E, Nanda R S, Duncanson M G, Sinha P. Evaluation of frictional resistance in aesthetic brackets, *AJODO*, 1997; **112**: 138–144.
56 Chaffee M P, Binding friction among various archwire/bracket combinations, Matter's Thesis, The University of Texas – Houston Health Science Center, Dental Branch, 1993.
57 Nelson E M, A comparison of surface roughness and frictional resistance of various archwire/bracket combinations, The University of Texas – Houston Health Science Center, Dental Branch, 1995.
58 Kusy, R P, Schafer, D L, Effect of salivary viscosity on frictional coefficients of orthodontic archwire/bracket couples, *J Mater Sci : Mater Med*, 1995; **6**(7): 390–395.
59 Kusy R P, Whitley B S, Influence of fluid media on the frictional coefficient in orthodontic sliding, *Semin Orthod*, 2003; **9**(4): 281–289.
60 Omana H M, Moore R N, Bagby M D, Frictional properties of metal and ceramic brackets, *JCO*, 1992; **26**: 425–432.
61 Rose C M, Zernik J H, Reduced resistance to sliding in ceramic brackets, *JCO*, 1996; **30**: 78–84.
62 Smith D V, Rossouw P E, Watson P, Quantified simulation of canine retraction: Evaluation of frictional resistance, *Semin Orthod*, 2003; **9**(4): 262–280.
63 Kusy R P, Whitley J Q, Effect of surface roughness on the coefficient of friction in model orthodontic systems, *J Biomech*, 1990; **23**(9): 913–925.
64 Kusy R P, Whitley J Q, Effects of sliding velocity in orthodontics, *Dent Mater*, July 1989; **5**: 235–240.
65 Henao S P *et al.*, Frictional evaluation of dental typodont models using 4 self ligating designs and a conventional design, *Angle Orthod*, 2005; **75**: 75–85.
66 Rossouw P E, Kamelchuck L S, Kusy R P, A fundamental review of variables associated with low velocity frictional dynamics, *Semin Orthod*, 2003; **9**(4): 223–235.
67 Ho K S, West V C, friction resistance between edgewise brackets and archwires, *Aust Orthod J*, 1991; **12**: 95–99
68 Kusy R P, Whitley B S, Influence of archwire and bracket dimensions on sliding

mechanics: derivations and determinations of the criti cal contact angles for binding, *Eur J Orthod*, 1999; **21**: 199–208.
69 Sachdeva, R C L, Miyasaki S, Farzia-Nia F, Orthdontic archwire and method of moving teeth, US patent 5044947, 1991.
70 Gil F J, Planell J A, Effect of copper addition on the superelastic behavior of Ni–Ti shape memory alloys for orthodontic applications, *J Biomed Mater Res*, 1999; **48**: 682–688.
71 Sakima M T, Dalstra M, Melsen B, How does temperature influence the properties of rectangular nickel–titanium wires?, *Eur J Orthod*, 2006; **28**(3): 282–291.
72 Chen R, Zhi Y F, Arvystas M G, Advanced Chinese Ni–Ti alloy wire and clinical observations, *Angle Orthod*, 1992; **62**(1): 59–66.
73 Qing K, Yang F, Liu K, Rong C, Investigation on the properties of Chinese NiTi wire RTF and three other products, *Shape Memory Mater*, 1994; 681–685.
74 Edie J W, Andreason G F, Zaytoun M P, Surface corrosion of nitinol and stainless steel under clinical conditions, *Angle Orthod*, 1981; **51**: 319–324.
75 Clinard K, von Fraunhofer J A, Kuftinec M M, The corrosion susceptibility of modern orthodontic spring wires, *J Dent Res*, 1981; **60**: 628.
76 Sarkar N K, Schwaninger B, The in-vivo corrosion of nitinol wire, *J Dent Res*, 1980; **59**: 528.
77 Sarkar N K, Redmond N, Schwaninger B, Goldberg J, The chloride corrosion behavior of four orthodontic wires, *J Dent Res*, 1979; **58**: 98.
78 Vandenkerckhove R, Chandrasekaran M, Vermaunt P, Portier R, Delaey L, Corrosion behaviour of a superelastic Ti–Ni alloy, *Mater Sci Eng A*, 2004; **378**: 532–536.
79 Asaoka K, Yokoyama K, Nagumo M, Hydrogen embrittlement of nickel–titanium alloy in biological environment, *Metall Mater Trans A*, 2002; **33**(3): 495–501.
80 Schwaninger B, Sarkar N K, Foster B E, Effect of long term immersion corrosion on the flexural properties of nitinol, *Am J Orthod*, 1982; **82**: 45–49.
81 Lopez I, Goldberg J, Burstone C J, Bending characteristics of nitinol wire, *Am J Orthod*, 1979; **75**: 569–575.
82 Nicholson J A, An analysis of nitinol in a simulated oral environment, *Am J Orthod*, 1984; **85**: 453.
83 Harris E F, Newman S M, Nicholson J A, Nitinol archwire in a simulated oral environment: changes in mechanical properties, *AJODO*, 1988; **93**: 508–513.
84 Mayhew M J, Kusy R P, Effects of sterilization on the mechanical properties and surface topography of nickel–titanium arch wires, *AJODO*, 1988; **93**: 232–236.
85 Buckthal J E, Kusy R P, Effects of cold disinfectants on the mechanical properties and the surface topography on nickel–titanium arch wires, *AJODO*, 1988; **94**: 117–1122.
86 Trepanier C, Pelton A, Biocompatibility and corrosion resistance of NiTi, Report, Cordis – NDC, 47533 Westinghouse Dr, Fremont, CA 94539.
87 Ryhanen J, Niemi E, Serlo W, Niemela E, Sandvik P, Pernu H, Salo T, Biocompatibility of nickel–titanium shape memory metal and its corrosion behavior in human cell cultures, *J Biomed Mater Res*, 1997; **35**(4): 451–457.
88 Oshida Y, Sachdeva R C L, Miyazaki S, Microanalytical characterization and surface modification of TiNi orthodontic archwires, *Biomed Mater Eng*, 1992; **2**: 51–69.
89 Barrett R D, Bishara S E, Quinn J K, Biodegradation of orthodontic appliances, Part I. Biodegradation of nickel and chromium in-vitro, *AJODO*, 1993; **103**: 8–14.
90 Park H Y, Shearer T R, In vitro release of nickel and chromium from simulated orthodontic appliances, *AJODO*, 1983; **84**: 156–159.
91 Menne T, Brandryp E, Thestrup-Pedersen K, Veien N K, Andersen J K, Yding F, Valeur G, Patch test reactivity to nickel alloys, *Contact Dermatitis*, 1987; **16**: 255–259.

92 Marek M, Treharne R W, An in vitro study of the release of nickel from two surgical implant alloys, *Clin Orthop*, 1982; **167**: 291–295.
93 Eliades T, Eliades G, Athanasiou A E, Bradley T G, Surface characterization of retrieved NiTi orthodontic archwires, 2000; **22**: 317–326.
94 Shabalovskaya S A, Surface, corrosion and biocompatibility aspects of nitinol as an implant material, 2002; **12**: 69–109.
95 Beyer J, Besselink P A, Lindenhovius J H, Shape memory and microstructure of welded TiNi alloy, Twente University of Technology, Enschede, Netherlands, Internal Report.
96 Yao S, Ying K, Li Z, Shen L, Development and clinical application of dental spot weld & heat-treat tri-uses device, Center of Orthodontics, No 174 Hospital of PLA, 1999; **23**(4): 207-209.

12

Endodontic instruments for root canal treatment using Ti–Ni shape memory alloys

T. YONEYAMA
Nihon University School of Dentistry, Japan
C. KOBAYASHI
Tokyo Medical and Dental University, Japan

Abstract: The special flexibility of superelastic Ti–Ni alloy has been successfully introduced to endodontic treatment by improving treatment quality and efficiency. In this chapter, a brief description of endodontic treatment, conventional stainless-steel instruments, mechanical properties, especially bending and torsional properties, of Ti–Ni alloy instruments, root canal preparation system with Ti–Ni alloy instruments and special engine-driven equipments, and improvement against instrument fracture are reviewed.

Key words: Ti–Ni alloy, endodontic rotary instruments, superelasticity, curved root canal preparation, Ni–Ti, Nitinol.

12.1 Root canal treatment

Soft tissue called dental pulp exists in each tooth and contains nerves and blood vessels. When the pulp is damaged and infected by caries or injury, it is often necessary to remove the infected pulp to save the tooth. The narrow pathways of the pulp through dental roots are called root canals. In the root canal treatment, mechanical shaping of the root canals is performed to remove the infected tissue surrounding the pulp and to shape them for root canal filling.

The instruments for root canal preparation have tapered and spiral blades. These instruments are standardized according to the diameter at the tip. The size number indicates the diameter in hundredths of one millimetre, e.g., a number 30 instrument has a tip of 0.30 mm diameter. There are two types of instruments for root canal preparation: hand instruments and engine-driven instruments.

Hand instruments have been clinically used for many years and are mostly made of stainless steel. They are manually used to enlarge and shape the canal with up-and-down and/or rotational actions. Recently, engine-driven rotary instrumentation has been successfully introduced into endodontic treatment with flexible Ti–Ni alloy rotary instruments. After mechanical preparation and chemical disinfection of the root canals are completed, the canal space is sealed tightly with filling

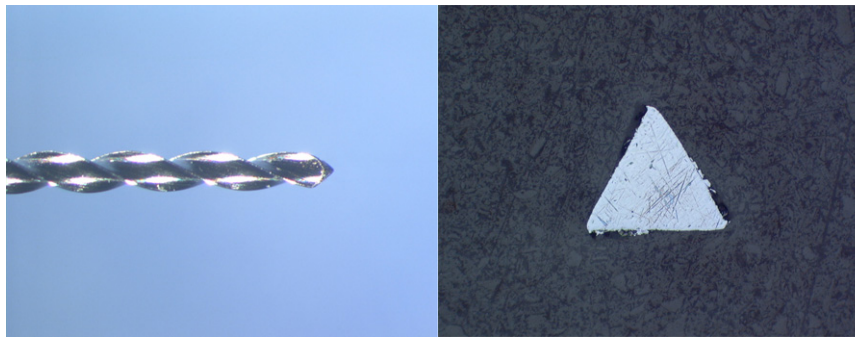

12.1 Tip part and cross-section of a stainless-steel K-file.

materials. Thus, the tooth that had infected pulp becomes ready to be restored after endodontic treatment.

12.2 Stainless-steel instruments

As the endodontic instruments are required to be sterilized, stainless-steel instruments have mainly been used. These hand instruments are called reamers or files. The shapes of the tip part and the cross-section of a typical stainless-steel K-file are shown in Fig. 12.1. The number of the spiral blades is less for reamers than for files. Files are usually more efficient in cutting but less flexible than reamers. Some engine-driven instruments made of stainless steel are used clinically, however, most of them are special instruments for the enlargement of the root canal entrance. Engine-driven reamers or files made of stainless steel should be used with special handpieces of restricted working motion to avoid root perforations and instrument fractures.

12.3 Ti–Ni alloy instruments

12.3.1 Dental application of Ti–Ni alloy

Ti–Ni alloy, consisting of nickel and titanium in nearly equiatomic proportions, is known for its unique mechanical properties of shape memory and superelasticity. These properties occur in association with thermoelastic martensitic transformation. Superelasticity is a phenomenon at a temperature above the reverse transformation temperature range, associated with stress-induced martensitic and reverse transformations. The alloy exhibits high flexibility owing to its wide recoverable strain range, in which the stress is kept low. Since Ti–Ni alloy shows high corrosion resistance and good biocompatibility, it has been applied in the medical and dental fields. This alloy was successfully introduced to orthodontic treatment as explained in the previous chapter.

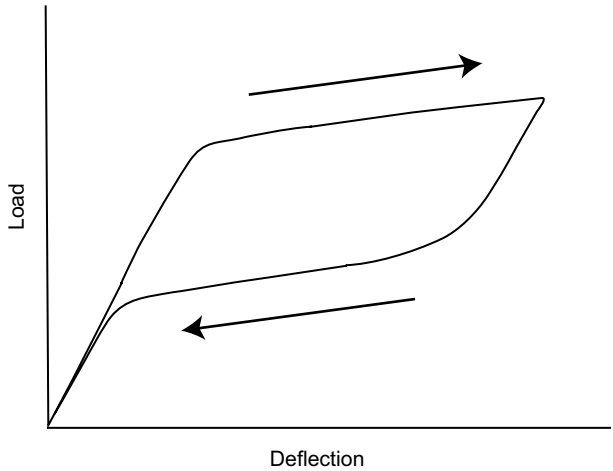

12.2 Schematic diagram of a load–deflection curve of a superelastic Ti–Ni alloy wire in a bending test.

In endodontics, the special flexibility of the Ti–Ni alloy is applied in instruments for root canal preparation. The first study on flexible Ti–Ni alloy for endodontic application was reported in 1988 by Walia *et al.*[1] Since the first Ti–Ni alloy root canal instrument was commercially available in the early 1990s, many manufacturers have developed Ti–Ni alloy root canal instruments with various designs and concepts.

12.3.2 Mechanical properties of Ti–Ni alloy for endodontic treatment

The main advantage of Ti–Ni alloy for root canal treatment is its special flexibility compared with conventional stainless steels. Endodontic instruments made of Ti–Ni showed good preparation performance for curved root canals.[2–8] The flexibility of Ti–Ni is based on the low elastic modulus and superelasticity as shown in Fig. 12.2. When the deformation is within the elastic range, Ti–Ni can be deformed with elastic flexibility. Superelasticity occurs when the stress exceeds the limit for stress-induced martensitic transformation, and the microstructure of Ti–Ni changes from the parent phase to the martensitic one. In this superelastic range, the deformation mode is based on the twin deformation of Ti–Ni alloy martensite, and the flexibility becomes even higher than in the elastic range.

Superelasticity occurs in association with martensitic and reverse transformation, so the transformation temperatures and behaviour of Ti–Ni have a critical influence on the mechanical properties, which can be readily altered by small changes in, e.g., composition, impurities and heat treatment.[9]

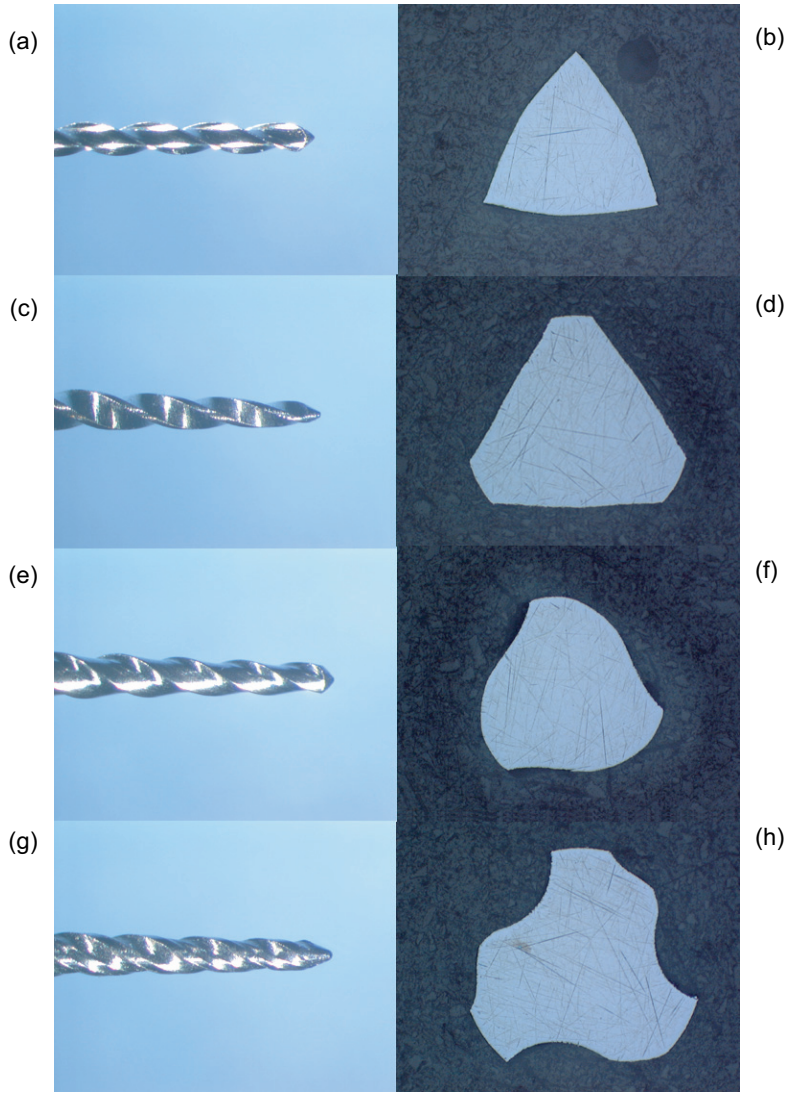

12.3 Tip and cross-section of four Ti–Ni alloy endodontic rotary instruments.

12.3.3 Bending property of Ti–Ni alloy instruments

One of the major factors to decide the flexibility of endodontic instruments is the configuration including the cross-sectional shape and the taper.[10–12] The shapes of the tip part and the cross section of four Ti–Ni alloy endodontic instruments are shown in Fig. 12.3. With respect to the taper of the endodontic instruments, the taper of stainless-steel instruments is usually 0.02 to retain the flexibility, while

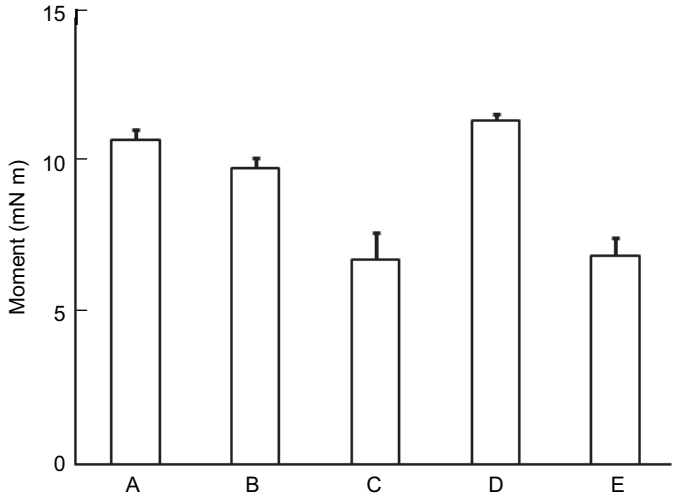

12.4 Moment values of Ti–Ni alloy (A, B, C) and stainless-steel (D, E) endodontic instruments in the bending test according to ISO 3630-1.

that for Ti–Ni alloy instruments is in the range from 0.02 to 0.10 because of the large flexibility. This large taper of Ti–Ni alloy endodontic instruments enables new techniques to be introduced for root canal preparation.

Figure 12.4 shows the bending moment values at 45° of Ti–Ni alloy and stainless-steel endodontic instruments measured according to ISO 3630-1. Instruments A to C are made of Ti–Ni alloy; D and E are made of stainless steel. The instrument size is No. 30 for all the instruments, but the taper is much different: 0.06 for Ti–Ni alloy and 0.02 for stainless steel. Although the Ti–Ni alloy instruments have much thicker configuration because of the taper, their bending moment values are similar to those of stainless-steel instruments.

12.3.4 Torsional property of Ti–Ni alloy instruments

Torsional property is another important mechanical property for rotary endodontic instruments, as the torsional stress closely relates to the fractures of the instruments during treatment.[13–18] Torsional fracture easily occurs if a handpiece continues rotating while the blade at the instrument tip bites the canal wall firmly. Therefore, high torsional resistance of the instrument is required in addition to the use of special low-speed handpieces with a torsional control system.

Figures 12.5 and 12.6 show the torsional moment and angle at fracture of Ti–Ni alloy and stainless-steel endodontic instruments measured according to ISO 3630-1. The codes A to F indicate the same instruments as those in the previous section: Ti–Ni alloy for A to D, and stainless-steel for E and F. Maximum torsional moment values of Ti–Ni alloy instruments are higher than those of stainless-steel instruments, partly because of the thicker configuration. Therefore, Ti–Ni alloy

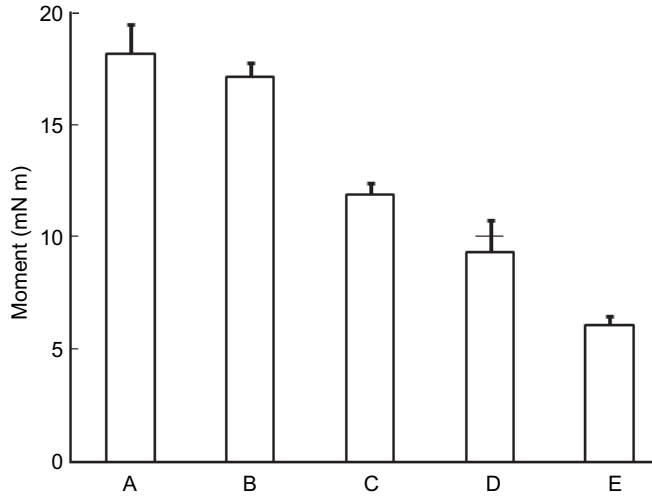

12.5 Maximum moment of Ti–Ni alloy (A, B, C) and stainless-steel (D, E) endodontic instruments in the torsional test according to ISO 3630-1.

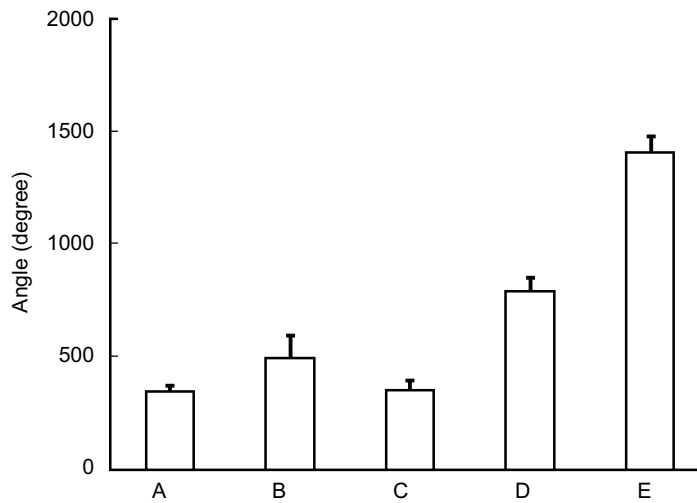

12.6 Angle at fracture of Ti–Ni alloy (A, B, C) and stainless-steel (D, E) endodontic instruments in the torsional test according to ISO 3630-1.

instruments seem to exhibit higher torsional resistance than stainless-steel instruments with similar bending flexibility. However, since they show low torsional angle at fracture, Ti–Ni alloy instruments should be used in low torsional stress to avoid accidental fractures.

12.4 Root canal preparation system with Ti–Ni alloy instruments

The special flexibility of Ti–Ni alloy endodontic instruments enables continuous rotary preparation of root canals. Many manufacturers have developed and designed root canal preparation system with Ti–Ni alloy instruments and special engine-driven equipments including handpieces. Since each Ti–Ni alloy instrument has different features, such as cross-sectional shapes, pitches and tapers, it should be used in the appropriate system and procedure.

One of the most important characteristics for the root canal preparation system is the shaping efficiency of the instruments. The cross-sectional shape and pitch of the instruments relates to the blade angle, which influences the efficiency of shaping root canal walls. The shaping efficiency of Ti–Ni alloy endodontic instruments was low, however, instruments with higher efficiency have been developed recently using torque-controlled engine-driven equipment. In addition, most instruments have tips with low cutting efficiency to avoid biting the root canal walls.

Most engine-driven systems have similar characteristics for safe and effective root canal preparation. One of them is low rotation speed, ranged approximately from 100 to 500 rpm, to avoid the fracture of the instruments or screwing into the canal walls. Another important characteristic is an intelligent torque-control function. When the torsional stress on an instrument exceeds the preset limit value, the motor automatically reverses the rotational direction to escape from further bite on the root canal wall and to reduce the torsional stress on the instrument.

Although each system has its special procedure for root canal preparation, a crown-down technique is commonly used in place of the conventional step-back technique with stainless-steel hand instruments. In the crown-down technique, root canal shaping starts from the coronal (entrance) side and proceeds to the apical (tip) side with use of a series of instruments of various tapers and tip sizes.

12.5 Future development of Ti–Ni alloy instruments

The root canal preparation system with Ti–Ni alloy instruments is still undergoing improvement, but its quality has improved greatly in recent years. One of the major factors to reduce accidental instrument fractures is the torque-controlled motor equipment, and further development is expected on this.

The service life of Ti–Ni alloy rotary instruments is not predictable,[19] because plastic deformation is seldom observed after the use of Ti–Ni alloy instruments unlike stainless-steel ones. This is mainly because of the superelastic shape recovery. It was reported that prolonged use of Ti–Ni alloy instruments increased the fracture rate, particularly for instruments with a small tip size.[20] Therefore, the number of times they can be used is limited to reduce the possibility of instrument fractures. The importance of the root canal curvature on the fracture of Ti–Ni alloy

instruments was also reported.[21] Since the microstructure and transformation behaviour of Ti–Ni alloy material influenced the mechanical property of the instruments,[18,22] the improvement in the alloy quality, machining procedures, and heat treatment conditions is thought to contribute to the reliability of Ti–Ni alloy rotary instruments. Despite these problems that have yet to be solved, root canal preparation with Ti–Ni alloy rotary instruments is likely to become the standard endodontic treatment method because of the quality, effectiveness, and efficiency.

12.6 References

1 Walia H, Brantley W A, Gerstein H (1988), 'An initial investigation of the bending and torsional properties of nitinol root canal files'. *J Endod*, **14**, 346–351.
2 Glosson C R, Haller R H, Dove S B, del Rio C E (1995), 'A comparison of root canal preparation using Ni–Ti hand, Ni–Ti engine-driven and K-flex endodontic instruments'. *J Endod*, **21**, 146–151.
3 Esposito P T, Cunningham CJ (1995), 'A comparison of canal preparation with nickel–titanium and stainless-steel instruments'. *J Endod*, **21**, 173–176.
4 Schäfer E, Tepel J, Hoppe W (1995), 'Properties of endodontic hand instruments used in rotary motion. Part 2. Instrumentation of curved canals'. *J Endod*, **21**, 493–497.
5 Thompson S A, Dummer P M H (1997), 'Shaping ability of ProFile.04 taper series 29 rotary nickel–titanium instruments in simulated root canals. Part 1'. *Int Endod J*, **30**, 1–7.
6 Thompson S A (2000), 'An overview of nickel–titanium alloys used in dentistry'. *Int Endod J*, **33**, 297–310.
7 Schäfer E, Lohmann D (2002), 'Efficiency of rotary nickel–titanium FlexMaster instruments compared with stainless steel hand K-flexofile. Part 1. Shaping ability in simulated curved canals'. *Int Endod J*, **35**, 505–513.
8 Peters O A, Peters C I, Schönenberger K, Barbakow F (2003), 'ProTaper rotary root canal preparation: effects of canal anatomy on final shape analysed by micro CT'. *Int Endod J*, **36**, 86–92.
9 Yoneyama T, Doi H, Hamanaka H, Okamoto Y, Mogi M, Miura F (1992), 'Super-elasticity and thermal behavior of Ni–Ti alloy orthodontic arch wires'. *Dent Mater J*, **11**, 1–10.
10 Turpin Y L, Chagneau F, Vulcain J M (2000), 'Impact of two theoretical cross-sections on torsional and bending stresses of nickel–titanium root canal instrument models'. *J Endod*, **26**, 414–417.
11 Berutti E, Chiandussi G, Gaviglio I, Ibba A (2003), 'Comparative analysis of torsional and bending stresses in two mathematical models of nickel–titanium rotary instruments: ProTaper versus ProFile'. *J Endod*, **29**, 15–19.
12 Schäfer E, Dzepina A, Danesh G (2003), 'Bending properties of rotary nickel–titanium instruments'. *Oral Surg Oral Med Oral Pathol Oral Radiol Endod*, **96**, 757–763. doi: 10.1016/S1079-2104(03)00358-5.
13 Camps J, Pertot W J (1994), 'Torsional and stiffness properties of canal master U stainless-steel and nitinol instruments'. *J Endod*, **20**, 395–398.
14 Sattapan B, Palamara J E A, Messer H H (2000), 'Torque during canal instrumentation using rotary nickel–titanium files'. *J Endod*, **26**, 156–160.
15 Peters O A, Barbakow F (2002), 'Dynamic torque and apical forces of ProFile .04 rotary instruments during preparation of curved canals'. *Int Endod J*, **35**, 379–389.

16 Peters O A, Peters C I, Schönenberger K, Barbakow F (2003), 'ProTaper rotary root canal preparation: assessment of torque and force in relation to canal anatomy'. *Int Endod J*, **36**, 93–99.
17 da Silva F M, Kobayashi C, Suda H (2005), 'Analysis of forces developed during mechanical preparation of extracted teeth using RaCe rotary instruments and ProFiles'. *Int Endod J*, **38**, 17–21.
18 Miyai K, Ebihara A, Hayashi Y, Doi H, Suda H, Yoneyama T (2006), 'Influence of phase transformation on the torsional and bending properties of nickel–titanium rotary endodontic instruments'. *Int Endod J*, **39**, 119–126.
19 Kuhn G, Jordan L (2002), 'Fatigue and mechanical properties of nickel–titanium endodontic instruments'. *J Endod*, **28**, 716–720.
20 Al-Fouzan KS (2003), 'Incidence of rotary profile instruments fracture and the potential for bypassing in vivo'. *Int Endod J*, **36**, 864–867.
21 Pruett J P, Clement D J, Carnes D L Jr (1997), 'Cyclic fatigue testing of nickel–titanium endodontic instruments'. *J Endod*, **23**, 77–85.
22 Kuhn G, Tavernier B, Jordan L (2001), 'Influence of structure on nickel–titanium endodontic instruments failure'. *J Endod*, **27**, 516–520.

13

Regulation, orthopedic, dental, endovascular and other applications of Ti–Ni shape memory alloys

L'H. YAHIA and F. RAYES
École Polytechnique de Montréal, Canada
A. O. WARRAK
University of Montreal, Canada

Abstract: Medical applications of shape memory alloys are widespread and diverse. They have impacted many fields of medicine such as: cardiovascular and endovascular interventions, orthopedics, dentistry and orthodontic and urologic surgery. Some of the most innovative SMA devices include: the self-expanding stents, shape memory staples, vascular filters, orthodontic archwires and porous implants. SMAs are also being used in a variety of surgical instruments for minimally invasive surgery. Large numbers of permanent implantations have been reported in Japan, Germany, China and Russia dating back to the early 1980s. The combination of good biocompatibility, good strength and ductility with the specific functional properties of SMA such as the shape memory effect, damping capacity and superelasticity creates a smart material for medical applications. Since the first application of SMA in medicine over 30 years ago, interest has grown steadily, but not to the extent expected: that is due mainly to biocompatibility and regulation issues.

Key words: Ti–Ni alloys, biocompatibility, medical device, FDA regulation, Ni–Ti, Nitinol.

13.1 Introduction

Since the discovery of the shape memory effect in Ti–Ni alloys in 1962, there has been great interest on the part of physicians, surgeons and orthodontists in applying these interesting alloys for various clinical procedures. The combination of good biocompatibility, good strength and ductility with the specific functional properties of SMA such as the shape memory effect, damping capacity and superelasticity creates a smart material for medical applications. In particular, the damping capacity of Ti–Ni was exploited in many orthopedic and dental implants to solve the mismatching problem leading to loosening. It is known that no hard tissue prosthesis, e.g. total hip prosthesis, lasts a lifetime and there are numerous ideas on how to improve the survival time. Some of the perceived mechanisms of failure have included a lack of good mechanical integration of bone into the metal

interface of uncemented stems. This has led to ideas for changing the interface and has also led to a number of modifications. One of the basic problems is that no conventional material, except SMA, is known to have similar mechanical properties to bone. One of the major differences is that bone displays viscoelastic behavior, whereas metals do not. This mechanical mismatch may lead to direct cellular reactions through mechano-sensors (Jones *et al.*, 1994). The mechanical mismatch will also lead to fretting and several investigations into many aspects of this problem have been carried out (Merritt and Brown, 1995; Lacy *et al.* 1996). Ti–Ni alloy possesses high damping capacity deriving from high internal friction between the martensitic twins or between the martensitic and the parent phases. The superior damping capacity and quasi-static stress absorbability of Ti–Ni alloy have been previously reported: it was found to transmit less impact stress than titanium or stainless steel (Yoneyama, 1988; 1996). The magnitude of damping in Ti–Ni alloys is at least one order of magnitude greater than in conventional alloys such brass, steel or aluminium where damping, measured as specific damping capacity (SDC), is from 0.5 to 1.5%. Grey cast iron, used for machine toolbeds because of its relatively high damping, achieves SDC values of 10 to 12%. By contrast, the SDC of typical SMA is in excess of 40% with values close to those of hard rubber (Yoneyama, 1989). Damping in these alloys increases with stress but, unlike polymers and rubber, is relatively insensitive to frequency. This insensitivity is similar to that found in living tissue where the hysteresis loop is almost independent of the strain rate within several decades of the rate variation (Fung, 1981). Gunter *et al.* (1995) has introduced porous Ti–Ni to further improve the mechanical compatibility (elastic modulus and permeability) of Ti–Ni with spongious bone. The pores of the device are easily filled with growing soft bone tissue, ensuring a compatible assimilation of the implant.

The superelastic effect of SMA results in a unique combination of high strength, high stiffness and high pliability. This concept of a metallic material with a superelasticity and nearly constant stress levels over a large strain area has found many applications in stenting and in orthodontic wires. The following paragraphs summarize the main developments of applications in the biomedical field.

13.2 USA Food and Drug Administration status of Ti–Ni medical devices

Since the first medical application of SMA over 30 years ago (Castleman *et al.* 1976), interest has grown steadily, although not to the extent expected, mainly owing to biocompatibility potential problem and regulation requirements of the USA Food and Drug Administration (FDA).

The FDA does not regulate the materials of medical devices, but regulates the devices themselves. Most of the Ti–Ni devices fall into regulatory class III, which means that human clinical data are required to support full approval to market the device. The problem with most clinical studies is that they rarely satisfy the quality

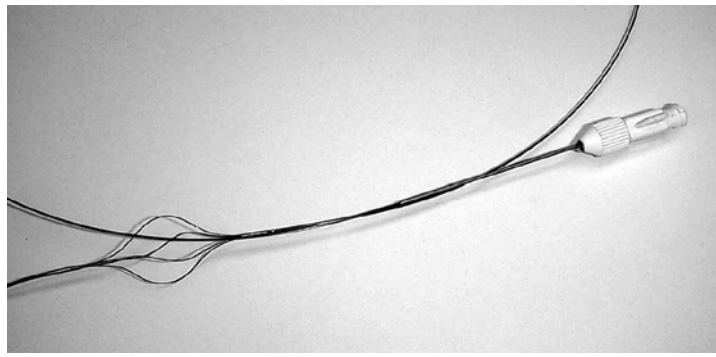

13.1 Shape memory basket for catheter interventions (source: Applications of superelastic nitinol tubing, Philippe P. Poncet, Memry Corporation, 4065 Campbell Avenue, Menlo Park, CA 94025, USA).

criteria of scientific study. It is not enough to say that a certain Ti–Ni implant can be used without harm. To be considered fully successful, it must be proved to be better than the existing competitors. Randomized prospective studies are needed to apply new Ti–Ni implant devices for constant clinical use in humans. Some of the only accepted applications include Simon Nitinol Filter (SNF) and recently (1999), the FDA released on the market a biliary stent. Other devices that have also received pre-market approval from the FDA include:

- (2002) Aplatzer septal occluder for transcatheter closure of an ostium secundum atrial septal defect.
- (2003) S.M.A.R.T.™ Nitinol Stent System for atherosclerotic disease of the iliac arteries.
- (2005) Abbott vascular devices Xact carotid stent system. Currently conducting post-approval studies.
- (2006) The FDA-approved a carotid stent, the Cordis Precise® Nitinol Stent System. Currently conducting post-approval studies.
- (2007) CORDIS ENTERPRISE™ Vascular Reconstruction Device and Delivery System used with Ti–Ni embolic coils for the treatment of intracranial aneurysms. The device was approved under the Humanitarian Device Exemption (HDE) program.

SMAs are used in medical devices in order to take advantage on their highly specific property to provide biofunctionality. With so few alloys displaying the shape memory effect, there is little choice over the composition of the material to be placed in the body and so biocompatibility has to be considered in a different light. The SMAs cannot be selected on the basis of their biocompatibility; they have to be chosen based upon their biofunctionality and then determine whether the biocompatibility characteristics are appropriate. The risk–benefit analysis has to take on a different meaning from that associated with conventional metallic biomaterials.

The FDA requires significant *in vitro* and pre-clinical animal data before approving an investigational device exemption (IDE) to permit device usage on human subjects. In fact, the approbation of the Simon filter and Mitek bone suture anchor means that these companies provided for the FDA enough scientific evidence about safety and effectiveness of Ti–Ni devices and assessment of the risks and benefits of using these Ti–Ni medical devices. However, these data are often kept proprietary and therefore are not available in the public domain. This practice is in contradiction with the Association for the Advancement of Medical Instrumentation (AAMI) recommendations to publish animal studies to reduce animal sacrifices.

13.3 Orthopedic/dental applications of Ti–Ni shape memory alloys

Ti–Ni has also been used as a bone implant material in humans. There are reports that Ti–Ni material has been successfully used in bone-related human applications in Russia and China in a large number of patients (Yang *et al.,* 1987, Kuo *et al.,* 1989, Shabalovskaya, 1996, Dai *et al.,* 1996). Worldwide medical applications have been hindered for a long time because of the lack of knowledge of the biocompatibility of Ti–Ni. Drugacz *et al.* (1995) tested the clinical application of Ti50Ni48.7Co1.3 alloy shape-memory clamps for the fixation of mandibular fractures using transoral access. The clamps were used to treat all types of fractures occurring between the mandibular angles. The clamps were removed after a period of at least 6 weeks, and tissue samples were taken for microscopic examination. Seventy-seven patients with mandibular fractures were treated using the clamps. In 72 patients, the treatment progressed satisfactorily, while in five cases infections occurred. Tissue samples for histologic examination were taken from 58 patients after removal of the clamps. There were no pathologic or atypical tissue reactions or signs of disturbed cell maturation. The authors concluded that the application of shape memory clamps for the surgical treatment of mandibular fractures facilitates treatment while ensuring stable fixation of the bone fragments.

In the studies of Sysolyatin *et al.,* 1994 and Itro *et al.,* 1997, Ti–Ni implants were used in the surgical correction of maxillo-facial fractures. The results showed a good stability and rapid bone healing. Also the time needed for operative procedures and rehabilitation was reduced.

A recent study by Idelsohn *et al.* (2004) utilized superelastic Ti–Ni SMA springs for distraction mandibular osteogenesis. Distraction osteogenesis is a biological process of bone neo-formation between segments subject to tension. A mandibulectomy of 8 mm and corticotomy of 5 mm were done on six 12-month-old female rabbits. All six rabbits successfully completed the distraction. The author concluded that: 'the application of a constant force on distraction osteogenesis, using SMA [Ti–Ni] springs, may be a successful alternative to the conventional gradual distraction' (Idelsohn *et al.*, 2004).

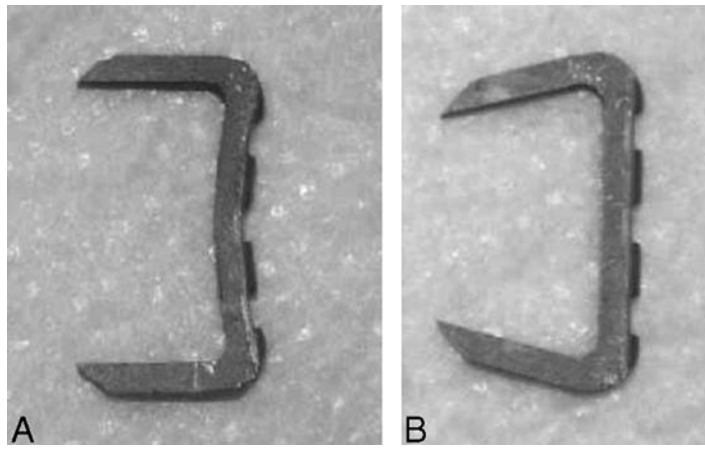

13.2 Shape memory staple for orthopedic applications (source: Braun JT *et al.*, 2006).

The results of ventral intercorporeal lumbar spondylodesis with a Ti–Ni implant were reported by von Salis-Soglio (1989). The primary stabilization of the unstable segment was achieved using an implant that was inserted intercorporeally following ventral removal of the intervertebral disc. The results included 51 cases of bony fusion within an average postoperative period of 9 months, one case of pseudo-arthrosis and 11 cases of delayed bony fusion. The author concluded that, in view of the easier operative technique, the earlier mobilization of the patients and the good fusion rate, the memory spondylodesis seems to have important advantages over the transplantation of bone chips only. The use of a Ti–Ni staple to lock a tri-cortical iliac bone graft in cervical anterior fusion was used by Ricart (1997). Fifty patients with several clinical diagnoses were operated. Good and very good results were reported in 80% of the cases. The average bone fusion rate was fast.

13.3.1 Staples

Amongst the first orthopedic devices used inside the human body were Ti–Ni compression staples. They were first introduced in China in 1981 (Dai, 1983). After that, Ti–Ni staples and clamps have been used in several applications such as comminuted fractures of the short tubular bone (Yang *et al.*, 1992), for fixation of mandibular fractures (Drugacz *et al.*, 1995), for metatarsal osteotomies (Tang *et al.*, 1996), for anterior cervical decompression and fusion (Mei *et al.*, 1997, Ricart, 1997, Silberstein, 1997), for fixation of small bone fragments (Musialek *et al.*, 1998), and for some other cursory applications (Iwabuchi *et al.*, 1975, Kuo *et al.*, 1989, Dai *et al.*, 1996). Several clinical studies and controlled *ex vivo* investigations with human cadaveric specimens comparing the use of staples with conventional 4.5 mm cannulated cancellous demonstrated no significant

biomechanical difference between the techniques. Additionally, bone fusion was obtained with Ti–Ni SMAs in all patients treated (Malal, 2006; Mereau, 2006; Meyer, 1996; Payette, 1998 and Tang, 1996). Good bone apposition and stabilization with compression of bone fragments are crucial to obtain appropriate conditions for bone healing when using Ti–Ni (Mereau *et al.*, 2006).

Shape memory staples were used to manage intra-articular fractures. In a 121 case series of intra-articular fractures, stable fixation, early movement and continuous compression force was obtained in most cases. Early bone union and return to function was achieved in 93.5% of patients (Dai *et al.*, 1993). Combination of SMAs with rods has been used to treat short tubular bone fractures. This combination was particularly useful to treat comminuted fracture difficult to fix by other methods (Yang *et al.*, 1992).

Regions with high tension are amenable to being treated with SMAs. A clinical investigation with 33 cases of patellar fractures showed the benefit of internal fixation with SMAs. After a week, patients recovered the knee range of motion and in 6.8 weeks on average they regained full flexion and extension of this joint. According to this study, complications were non-existent (Zhang, 1989).

Small bones fractures are especially attractive for SMAs treatment due to its versatility, ease of application, small size and mechanical properties. A series of cases of hand and foot fractures treated with only Ti–Ni SMAs showed stable bone union, no suppuration after heating stimulus of the staples and no abnormal tissue reaction. In addition, it was reported that Ti–Ni SMAs bone fixation decreased the length of time necessary for cast use. This is advantageous in terms of early rehabilitation and physical therapy of patients (Musialek *et al.*, 1998). The same observation was made in another retrospective study of 60 cases of scaphoid waist fractures. Pain was absent in 86% of the cases and the patients recovered the pronation and supination wrist range of motion (Rocchi *et al.*, 2005). An *in vivo* humeral fracture animal model that simulated the human humerus anatomical morphology and biomechanical properties was used to investigate the clinical application of SMAs on long bone fracture internal fixation. The results were promising, the bones healed without osteoporosis or exuberant external callus (Kang *et al.*, 2003).

Spinal surgery represents another field in which SMAs have a potential role. A biomechanical assessment of thoracic spine stapling with an *ex vivo* animal model for adolescent scoliosis revealed that staples are able to significantly restrict vertebral motion but not as much as expected in fusion-promoting instrumentation. Also single-prong staples allow more control in placement over the disc space (Puttlitz *et al.*, 2007). A goat model for fusionless scoliosis correction with SMAs showed that an anterior thoracic staple is effective in treating moderately severe scoliosis without vertebral fusion (Braun *et al.*, 2004 and 2005). Another human cadaveric model with cervical spine and clinical study with 30 patients demonstrated that expansion force and pullout strength of SMAs was safe and effective to provide bone fusion in all patients of the study (Mei *et al.*, 1997).

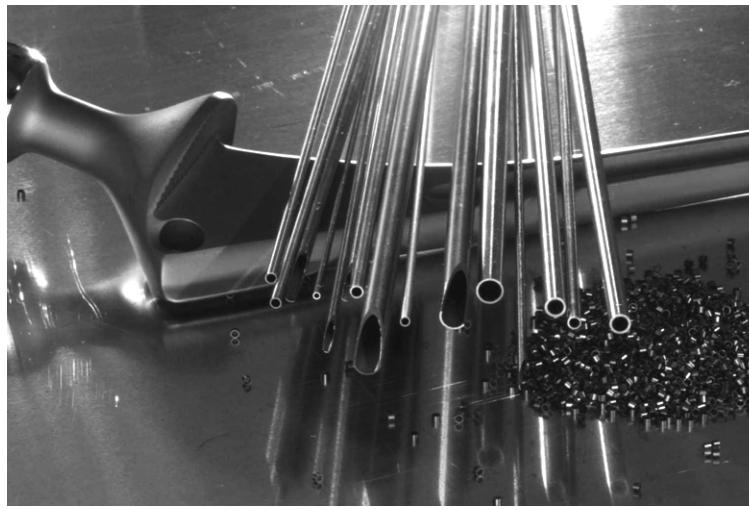

13.3 Superelastic Ti–Ni tubing has many clinical applications such as stents and needles (source: Applications of superelastic nitinol tubing, Philippe P. Poncet, Memry Corporation, 4065 Campbell Avenue, Menlo Park, CA 94025, USA).

Ti–Ni SMAs have the advantages of simple operative procedures, rigid fixation, minimal tissue reaction, fewer postoperative complications and no interference with diagnostic imaging such as computer tomography (CT) and magnetic resonance imaging (MRI) (Wang *et al.*, 1998).

Many other applications in fields such as maxillofacial surgery, physical therapy, gastroenterology surgery, plastic surgery, vascular surgery have also been described or are under investigation owing to the versatility of these devices.

In the late 1960s, the potential of Ti–Ni as an implant material was suggested by Johnson and Alicandri (Castleman *et al.*, 1976). After that, further studies evaluated the ability of the alloy for orthopedic surgery. Some pioneers in this field were Baumgart *et al.* (1978), who examined the Ti–Ni distraction rod in the correction of scoliosis. As early as 1986, Lu *et al.* implanted Ti–Ni rods in patients with scoliosis with good reported results and no complications. Later, Matsumoto *et al.* (1993) and Sanders *et al.* (1993) published more *in vivo* experimental studies.

The Mitek G2 suture anchor is one of the only Ti–Ni orthopedic implants used in the western world. This anchor has superelastic Ti–Ni wings, which prevent the anchor from pulling out of the bone after insertion and secure the tendons or ligaments to the bone (Barber *et al.*, 1996). Another promising application is a Ti–Ni hook used to restore the dislocated acromio-clavicular joint (Ryhänen *et al.*, 1998). In his book, Gunter (1995) has listed over 50 orthopedic and surgical devices using SMA.

There are also a number of implants and tools developed from Ti–Ni alloys for dentistry (Mirgazizov *et al.*, 1997; Shabalovskaya, 1996). Superelastic Ti–Ni

dental implants are constructed so that they allow easy fixation. They have an optimal combination of specific weight, strength, plasticity, damping, high wear characteristics as well as resistance to fatigue. With this unique combination of properties, implants can be fabricated in order to mimics the natural teeth and ligament behavior and function.

13.3.2 Smart intramedullar rod

In order to determine if a smart intramedullary rod made of Ti–Ni SMA is capable of correcting deformed immature long bones, Kujala *et al.* (2002) implanted 12 Ti–Ni rods in the cooled martensitic formed into 12 rat femurs. When returning to their austenitic form, a bending force was generated. Straight Ti–Ni rods were used as control. Radiographs showed bone bowing in the curved nail group while growth retardation and an increase in cortical thickness occurred in both groups. Keikhosrow *et al.* (2004) carried out a similar experiment on eight rabbit tibias. Various radius of curvature were used and the contralateral side served as control. Results showed that a larger radius generated enough force history to create bone remodelling and deformation. From these preliminary studies the technology of the smart intramedullary rod may provide a valuable alternative method to correct paediatric skeletal deformities.

13.3.3 Porous Ti–Ni

Porous equiatomic Ti–Ni SMA has recently been investigated as a material for medical applications (Simske and Sachdeva, 1995; Ayers *et al.*, 1999). In Russia, China and Germany, it has been in clinical use for approximately a decade in maxillofacial surgeries and other orthopedic procedures involving thousands of patients (Shabalovskaya, 1996; Dai, 1996; Airoldi and Riva, 1996). Porous Ti–Ni can be produced by various manufacturing processes, including, but not limited to, sintering of molten Ti–Ni and self-propagating-high-temperature-synthesis (SHS) (Itin *et al.*, 1994; Yi and Moore, 1990). Such methods allow for a controlled range of Ti–Ni porosity, and provide appropriately sized and interconnected (open) pores, creating an implant morphology similar to bone. It has been established that mineralized tissue ingrowth requires pore sizes in the range of 100–400 μm (Klawitter and Hulbert, 1971; Hulbert *et al.*, 1970). A porous implant structure allows ingrowth of mineralized tissue, establishing a biological fixation of the implant. It has been shown that 50% porous Ti–Ni provides greater initial bone ingrowth (as a percentage of the implant cross-section) than 30% porous hydroxyapatite, primarily because of the greater exposed surface area (Simske and Sachdeva, 1995). Moreover, Ti–Ni in this porosity range provides a void space, after bone ingrowth, similar in percentage of cross-section to that of rabbit cranial bone further indicating the ability of Ti–Ni to at least architecturally mimic bone (Simske and Sachdeva, 1995). The shape memory property of Ti–Ni also allows

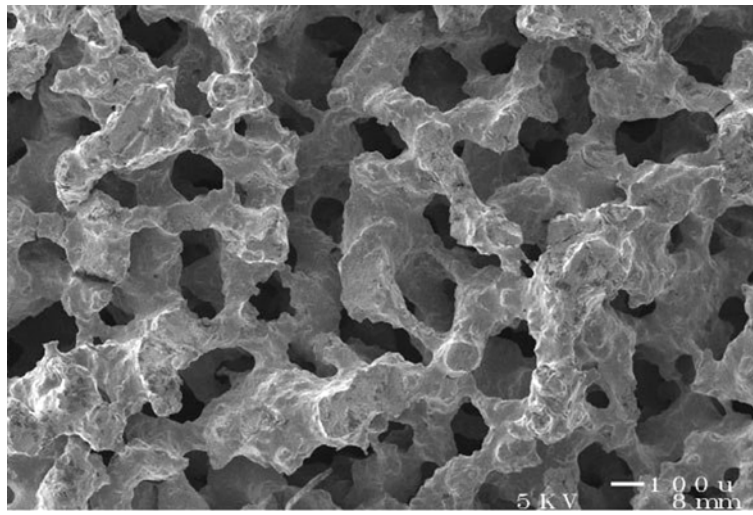

13.4 Scanning electron microscopy of porous Ti–Ni (source: Assad M *et al.*, 2003).

for the possibility of *in situ* implant shape in the case of injury to the implant or surrounding hard tissue.

Itin *et al.* demonstrated further the ability of Ti–Ni to mimic the mechanical properties showing that 40–50% porous Ti–Ni has a recoverable strain of 3.2% near physiological temperatures; this is similar to the recoverable strain of bone at 2% (Itin *et al.*, 1994). This important aspect of Ti–Ni superelasticity suggests that, if the surrounding bone is strained within its elastic region (less than 2%), the implant will deform with the bone and recover its original shape afterwards, preserving the implant/bone bond.

Porous Ti–Ni is an attractive implant material for orthopedics, spine surgery, soft tissue reconstructive surgery, dentistry, and maxillofacial surgery (Shabalovskaya *et al.*, 1995). The results of recent studies on implantation of porous Ti–Ni conducted in the United States, Canada, and Korea (Simske *et al.*, 1995; Ayers *et al.*, 1999; Rhalmi *et al.*, 1999; S-B. Kang *et al.*, 2000) are in agreement with those obtained in earlier studies performed in Russia (Gyunter *et al.*, 1995; Shabalovskaya, 1996). According to these studies, a six-week time-period is sufficient to measure significant ingrowth of immature bone into the pores of implant. After six to twelve weeks of implantation, the porous structure of the implant is filled with the new bone tissue up to 40–80%. Another important parameter, the bone-to-implant surface contact averages 40% for Ti–Ni implants (Ayers *et al.*, 2000) and 14% for untreated pure titanium implanted in tibia of goats (Versaigne *et al.*, 1998).

Silberstein (1997) reported a clinical study where 84 patients with fractures, tumours or intervertebral disc disease of the cervical and lumbal spine were treated

13.5 Self-expanding superelastic Nitinol stents (source: Applications of superelastic nitinol tubing, Philippe P. Poncet, Memry Corporation, 4065 Campbell Avenue, Menlo Park, CA 94025, USA).

with anterior fusion and porous Ti–Ni implant grafts. They concluded that porous Ti–Ni implants can be successfully used and the material itself shows a high degree of biocompatibility.

13.4 Endovascular applications or interventions

Most of the recent commercial Ti–Ni applications are meant for cardiovascular solutions. The idea behind this is to provide minimally invasive treatment instead of major surgery. The Simon Ti–Ninol filter (SNF) was the first clinically successful vascular Ti–Ni device. It has been used to treat pulmonary embolism (Simon *et al.*, 1977).

The general trend in stenting seems to be towards self-expandable Ti–Ni-stents. When a thin stent is placed in the narrowed artery, it expands and dilates the artery. The carotid artery stents and the endoluminal polyester-covered Ti–Ni stent-grafts for infrarenal abdominal aortic aneurysms have been shown to be efficient and technically successful, but a careful long-term evaluation is still necessary (Blum *et al.*, 1997, Wholey *et al.*, 1998). Intracoronary (de Jaegere *et al.*, 1996, Oesterle *et al.*, 1998) and peripheral vascular Ti–Ni stenting (Schwarzenberg *et al.*, 1998) also seems to be increasing. Despite the improvements, restenosis and reocclusion are still a problem and the optimal physical and surface properties of an arterial stent have not been defined yet (Schurmann *et al.*, 1995).

13.4.1 Collapsible heart valve

A defective heart valve fails to fully open or close, letting blood leak back into the heart chamber. This condition most often is treated surgically, and the valve is replaced with a human donor valve, a porcine valve or a mechanical one. All heart

valve replacements have a limited life span and must be replaced eventually, but, for children, there are even greater complications: the valves do not grow as children grow, which could mean as many as three or more open-heart surgeries during childhood and adolescence alone. Open-heart surgery typically requires three to four days in intensive care, at least one or two weeks in the hospital and a lengthy recovery period at home. In contrast, patients who have valves replaced via catheter could go home as early as the following day, with little pain. Although the medical community has used bulk Ti–Ni for the past decade in stents and other implantable biomedical devices, thin-film Ti–Ni has yet to be incorporated into a commercially available biomedical device. Thin film Ti–Ni could allow bioengineers to make a transcatheter heart valve suitable for use even in small children. Recent studies have shown that thin film Ti–Ni can be used to cover stents and to provide a barrier, thus preventing regrowth of tissue into stented arteries and veins. Beyond its use in either percutaneously or surgically placed valves, it is anticipated that thin film Ti–Ni will have a wide variety of applications in the development of future implantable biomedical devices for both adults and children (www.nmtmedical.com).

Using catheters and collapsible valves, heart valves can be replaced without stopping the heart, without cutting the chest open and without long recovery times. The traditional surgery that fixes this anomaly is extremely invasive and dangerous. The thorax of the patient is opened and the atrial hole is sewn. Because of the intrinsic risks of this surgery, several problems might occur. The atrial septal occlusion device is an alternative to this surgery. This device is composed of SMA wires and a waterproof film of polyurethane (Duerig, 1999). As is the case for the Simon filter, the surgery to position this device exploits the shape memory effect, being much less invasive than the traditional one.

The CoreValve ReValving system is currently the subject of a multinational development program. The first case of percutaneous aortic valve replacement (PAVR) using CoreValve was reported by Grube *et al.*, 2005), and Berry *et al.* recently performed the first case in North America (2007) at the Montreal heart institute. Overall, 60 cases have been performed in Europe and in Montreal. Also recently reported is a case of PAVR simultaneously combined percutaneous coronary intervention (Berry *et al.*, 2006).

13.4.2 Endovascular neurointervention

An intracranial aneurysm is a weakness in the wall of a blood vessel in the brain that balloons out, forming a thin-walled bubble or sac. Approximately 30 000 intracranial aneurysms present annually. Some 15 000 patients are treated and up to 4000 of these individuals are likely to need vascular reconstruction. Hemorrhagic stroke occurs when a cerebral aneurysm bursts and bleeds into brain tissue. In the US, stroke is the third leading cause of death, behind heart disease and cancer. Each

year, about 700 000 people suffer a stroke according to the American Heart Association (Sokolowski *et al.*, 2007).

The CORDIS ENTERPRISE™ Vascular Reconstruction Device (CEVRD) is an important advancement in neuro-stent technology. Recently, the FDA has granted Humanitarian Device Exemption (HDE) approval for the CEVRD for use with embolic coils in the treatment of wide-neck intracranial aneurysms. Specifically, the stent is approved to treat wide-neck, intracranial, saccular or fusiform aneurysms arising from a parent vessel with a diameter of greater than or equal to 3 mm and less than or equal to 4 mm. The CEVRD is a new self-expanding, closed-cell design, Ti–Ni stent with good visible proximal and distal markers and an added feature of a horizontal longitudinal marker on the delivery wire to facilitate delivery. Pre-loaded onto a delivery system composed of an introducer and delivery wire for a simple system configuration, the CEVRD enables physicians to recapture the stent, and three radiopaque zones facilitate placement and visibility. However, the effectiveness of the device for this use has not been demonstrated.

A HDE is an application that is similar to a pre-market approval (PMA) application, but exempt from the effectiveness requirements of a PMA. An approved HDE authorizes marketing of a Humanitarian Use Device. A Humanitarian Use Device is a medical device that is intended to benefit patients in the treatment or diagnosis of diseases or conditions that affect, or is manifested in, fewer than 4000 individuals in the United States per year.

13.5 Other applications of Ti–Ni shape memory alloys

13.5.1 Urologic surgery

The use of Ti–Ni prostatic stents has increased since the first reported experiment by Lopatkin *et al.* (1989). For high-risk patients with prostatic carcinoma or benign prostatic hyperplasia, the insertion of a permanent metal stent system offers a useful alternative to transurethral resection (Gottfried *et al.*, 1997). (Gottfried *et al.*, 1995, Gesenberg *et al.*, 1998). The use of urethral stents was found to decrease the number of repeated dilatations and urethrotomies in recurrent urethral strictures (Yachia, 1993). Despite the good biocompatibility of the material in a long-term study on dogs, no complete covering of the stent by epithelialization was found in a study of Latal *et al.* (1994).

An implantable artificial anal sphincter using SMA was developed as a low invasive prosthesis with a simple structure to solve the problem of severe fecal incontinence in patients with hypoplastic sphincters or without anal sphincters (Luo *et al.*, 2004). The artificial anal sphincter consists of SMA plates as the main functional parts to perform two basic functions when the SMA artificial sphincter is fitted around intestines (i.e., an occlusion at body temperature and an opening function on heating). Short-term animal experiments revealed promising properties with the occlusion function of the device, although some complications, such

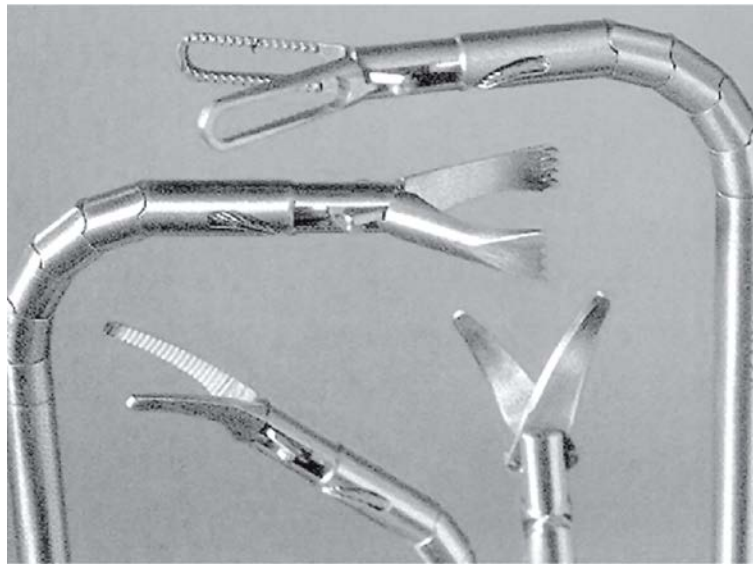

13.6 Laparoscopy tools.The actions of grippers, scissors, tongs and other mechanisms are performed by SMA (source: Duerig TM *et al.,* 1999).

as overpressure-induced ischemia, heat burn, and infections, remained. Results of chronic animal experiments of up to 4 weeks suggested great potential for the improved device (Luo *et al.*, 2004). Functionality and safety of the device have been proved in three-month animal experiments (Luo *et al.*, 2006).

13.5.2 Other medical devices

Ti–Ni SMA is also being used in a variety of surgical instruments for minimally invasive surgery (MIS). The excellent compatibility with magnetic resonance imaging (MRI) has led to the first MRI compatible needles for use in surgical robots (Fischer, 2004). Other applications of Ti–Ni in MIS include graspers, baskets, scissors, and flexible puncture needles, just to name a few.

Orthodontic archwires were the first mass biomedical application (Sachdeva and Miyazaki, 1990; Fukuyo and Sachdeva, 1992). Besides archwires, specific endosseous implants based on the shape memory effect have also been developed (Van Humbeeck *et al.*, 1998).

A Ti–Ni mesh-expanding prosthesis for laparoscopic hernioplasty significantly shortened the operating time in a study by Himpens (1993). The good holding and atraumatic characteristics of the detachable clamp have been confirmed by use in laparoscopic and thoracoscopic surgery on the gastrointestinal tract (Frank *et al.*, 1995).

The use of Ti–Ni stents to prevent major airway occlusion was first reported by

Rauber *et al.* (1990). According to the early tests, they seemed to be very useful and effective in inoperable tracheal or bronchial stenosis due to intraluminal tumour invasion (Yanagihara *et al.*, 1997, Hauck *et al.*, 1997). In addition, a new type of Ti–Ni stapes prosthesis to restore the ossicular fixation after stapedectomy has been reported (Kasano *et al.*, 1997).

13.5.3 Gastroenterologic surgery

The treatment of benign biliary strictures with metallic stents is associated with a low long-term patency rate (Bezzi *et al.*, 1994, Rossi *et al.*, 1994). They are effective in achieving long-term palliation in patients with malignant obstructive jaundice. The use of stents re-establishes bile flow in the occluded biliary tree (Smits *et al.*, 1995).

Esophageal Ti–Ni stents have been found to be easy to implant, provide effective palliation of malignant esophageal obstructions, and have a low risk of severe complications. Ti–Ni stents for esophageal strictures and the palliation of malignomas have been studied by several authors (Cwikiel *et al.*, 1993, May *et al.*, 1995, Acunas *et al.*, 1996). Some problems were related to incomplete initial stent expansion as well as tumour ingrowth/overgrowth. Covering the Ti–Ni-based stent with a thin Gore-Tex sheath give the possibility to avoid ingrowth and to use the stent also in the case of fistulas.

In addition, the insertion of Ti–Ni stents in patients with rectosigmoidal carcinoma provide an alternative to repeated palliative laser therapy or palliative surgery in malignant rectosigmoid obstruction (Tack *et al.*, 1998).

13.6 Conclusions

The medical market is a continuing success story for the application of SMA products. Increasing life expectancy and advances in surgical procedures mean that the medical market will remain an area of great opportunity for commercial applications.

It is shown that Ti–Ni SMAs are generally characterized by good corrosion properties, in most cases superior to those of conventional stainless-steel or Co–Cr–Mo-based biomedical materials. The majority of biocompatibility studies suggest that these alloys have low cytotoxicity (both *in vitro* and *in vivo*) as well as low genotoxicity (Es-Souni *et al.*, 2005).

These smart metallic materials, which are characterized by outstanding mechanical properties, have been gaining increasing importance over the last two decades in many minimal invasive surgical and diagnostic applications.

Even though Ti–Ni represents the best known SMA, its undesirable fatigue properties exemplified by the occurrence of medical-device fracture (Allie *et al.*, 2004), along with large temperature/stress hysteresis and the narrow temperature range of operation translate to a tight margin of error for engineering design of the

devices, and performance has been sacrificed for reliability. Accordingly, further incorporation of SMA into applications has been slow and limited despite its vast potential.

Corrosion of the Ti–Ni wire in endovascular grafts was recently confirmed by Heintz *et al.* (2001). Presumably, the observed pitting and irregularly shaped corrosion defects are the precursors of material failure. They weaken the thin wire, which leads to stress cracks and eventually fracture of the stent wire under circulatory pulsation. Cell-induced electrochemical corrosion and active cellular destruction of surfaces are well-known mechanisms that must be investigated for their possible roles in the corrosion of stent metals.

13.7 Acknowledgement

The authors would like to thank NSERC for their support and funding.

13.8 References

Acunas B, Rozanes I, Akpinar S, Tunaci A, Tunaci M, Acunas G (1996) Palliation of malignant esophageal strictures with self-expanding nitinol stents: drawbacks and complications. *Radiology* **199**: 648–652.

Airoldi G, Riva G (1996) Innovative materials: the NiTi alloys in orthodontics. *Biomed Mater Eng* **6**(4): 299–305.

Allie, D E, Hebert, C J, Walker, C M. Nitinol stent fractures in the SFA. *Endovasc Today* **7**, 22–34 (2004).

Assad M *et al.* (2003) Porous titanium–nickel for intervertebral fusion in a sheep model: Part 1. Histomorphometric and radiological analysis. *J Biomed Mater Res B Appl Biomater* **64**(2): 107–120.

Ayers R A, Simske S J, Bateman T A, Petkus A, Sachdeva R L, Gyunter V E (1999) Effect of nitinol implant porosity on cranial bone ingrowth and apposition after 6 weeks. *J Biomed Mater Res* **45**(1): 42–7.

Barber F A, Herbert M A, Click J N (1996) Suture anchor strength revisited. *Arthroscopy* **12**: 32–38.

Baumgart F, Bensmann G, Haasters J, Nolker A, Schlegel K F (1978) Zur Dwyerschen Skoliosenoperation mittels Drahten aus Memory-Legierungen. Eine experimentelle Studie. *Arch Orthop Trauma Surg* **91**: 67–75.

Berry C, Asgar A, Lamarche Y, Marcheix B, Couture P, Basmadijian A, Ducharme A, Laborde J C, Cartier R, Bonan R (2007) Novel therapeutic aspects of percutaneous aortic valve replacement with the 21F CoreValve Revalving System *Catheter Cardiovasc Interv* **70**(4): 617–618.

Berry C, Lamarche Y, Laborde J C, Laborde J-C, Cartier R, Denault A Y, Basmadjian A, Bonan R (2006) First case of combined percutaneous aortic valve replacement and coronary artery revascularization. *EuroIntervention* **2**: 257–261.

Bezzi M, Orsi F, Salvatori F M, Maccioni F, Rossi P (1994) Self-expandable nitinol stent for the management of biliary obstruction: long-term clinical results. *J Vasc Interv Radiol* **5**: 287–293.

Blum U, Voshage G, Lammer J, Beyersdorf F, Tollner D, Kretschmer G, Spillner G,

Polterauer P, Nagel G, Holzenbein T (1997) Endoluminal stent-grafts for infrarenal abdominal aortic aneurysms. *N Engl J Med* **336**: 13–20.

Braun J T *et al.* (2004) Fusionless scoliosis correction using a shape memory alloy staple in the anterior thoracic spine of the immature goat. *Spine* **29**(18): 1980–1989.

Braun J T *et al.* (2005) The efficacy and integrity of shape memory alloy staples and bone anchors with ligament tethers in the fusionless treatment of experimental scoliosis. *J Bone Joint Surg Am* **87**(9): 2038–2051.

Braun J T *et al.* (2006) Mechanical modulation of vertebral growth in the fusionless treatment of progressive scoliosis in an experimental model. *Spine* **31**(21): 1314–1320.

Castleman L S, Motzkin S M, Alicandri F P, Bonawit V L (1976) Biocompatibility of nitinol alloy as an implant material. *J Biomed Mater Res* **10**: 695–731.

Cwikiel W, Willen R, Stridbeck H, Lillo-Gil R, von HC (1993) Self-expanding stent in the treatment of benign esophageal strictures: experimental study in pigs and presentation of clinical cases. *Radiology* **187**: 667–671.

Dai K, Chu Y (1996) Studies and applications of NiTi shape memory alloys in the medical field in China. *Biomed Mater Eng* **6**: 233–240.

Dai K R (1983) Orthopedic application of a Ti–Ni shape-memory alloy compression staple. *Chung Hua Wai Ko Tsa Chih* **21**: 343–345.

Dai K R, Hou X K, Sun Y H, Tang R G, Qiu S J, Ni C (1993) Treatment of intra-articular fractures with shape memory compression staples. *Injury* **24**(10): 651–655.

De Jaegere P P, Eefting F D, Popma J J, Serruys P W (1996) Clinical trials on intracoronary stenting. *Semin Interv Cardiol* **1**: 233–245.

Drugacz J, Lekston Z, Morawiec H, Januszewski K (1995) Use of TiNiCo shape-memory clamps in the surgical treatment of mandibular fractures. *J Oral Maxillofac Surg* **53**: 665–671.

Duerig T W, Pelton A R, Stockel D (1996) The utility of superelasticity in medicine.*Biomed Mater Eng* **6**: 255–266.

Duerig T W, Pelton A R, Stockel D (1999) An overview of Nitinol medical applications. *Mater Sci Eng A* **273–275**: 149–160.

Es-Souni M, Es-Souni M, Fischer-Brandies H (2005) Assessing the biocompatibility of NiTi shape memory alloys used for medical applications. *Anal Bioanal Chem* **381**(3): 557–567

Fischer H, Vogel B, Welle A (2004) Application of shape memory alloys in medical instruments. *Min Invas Ther Allied Technol* **13**(4): 248–253.

Frank T, Willetts G J, Cuschieri A (1995) Detachable clamps for minimal access surgery. *Proc Inst Mech Eng* **209**: 117–120.

Fung Y C (1981) *Biomechanics, Mechanical Properties of Living Tissues*, Springer-Verlag, New York Inc.

Gesenberg A, Sintermann R (1998) Management of benign prostatic hyperplasia in high risk patients: long-term experience with the Memotherm stent. *J Urol* **160**: 72–76.

Gottfried H W, Gnann R, Brandle E, Bachor R, Gschwend J E, Kleinschmidt K (1997) Treatment of high-risk patients with subvesical obstruction from advanced prostatic carcinoma using a thermosensitive mesh stent. *Br J Urol* **80**: 623–627.

Gottfried H W, Schimers H P, Gschwend J, Brandle E, Hautmann R (1995) Erste erfahrungen mit dem Memotherm-stent in der behandlung der BPH. *Urologe A* **34**: 110–118.

Grube E, Laborde J C, Cartier R, Gerckens U, Serruys P W, Dejaegere P, Schuler G, den Heijer P, Bosmans J, Ruiz C E, Bonan R (2006) Experience with 21 French percutaneous core valve aortic valve replacement in patients unsuitable for surgical aortic valve replacement. *Circulation* **114**(2); 811.

Hauck R W, Lembeck R M, Emslander H P, Schomig A (1997) Implantation of Accuflex and

Strecker stents in malignant bronchial stenoses by flexible bronchoscopy. *Chest* **112**: 134–144.

Heintz C, Riepe G, Birken L, Kaiser E, Chakfé N, Morlock M, Delling G, Imig J (2001) Corroded nitinol wires in explanted aortic endografts: an important mechanism of failure?, *J Endovasc Ther* **8**(3): 248–253.

Himpens J M (1993) Laparoscopic inguinal hernioplasty. Repair with a conventional vs a new self-expandable mesh. *Surg Endosc* **7**: 315–318.

Hulbert S F, Young F A, Mathews R S, Klawitter J J, Talbert C D, Stelling F H. (1970) Potential of ceramic materials as permanently implantable skeletal prostheses. *J Biomed Mater Res* **4**(3): 433–456.

Idelsohn S, Pena J, Lacroix D, Planell J A, Gil F J, Arcas A(2004) Continuous mandibular distraction osteogenesis using superelastic shape memory alloy (SMA). *J Mat Sci: Mat Med* **15**: 541–546.

Itin V I, Gjunter V E, Shabalovskaya S A, Sachdeva R L C (1994), Mechanical properties and shape memory of porous nitinol. *Mater Character*, **32**: 179–187.

Itro A, Garau V, Tartaro G P, Colella G (1997) La nostra esperienza su di una metodica di fissazione rigida in chirurgia maxillo-facciale mediante clips a memoria di forma. *Minerva Stomatol* **46**: 381–389.

Iwabuchi T, Suzuki S, Ebina K, Honma T (1975) Memory clip for intracranial aneurysm surgery. Technical note. *J Neurosurg* **42**: 733–735.

Jones D B, Doty S B, van den Bos R C (1994) Biomechanics and the foreign body response, in *Failure of Joint Replacement, a Biological, Mechanical or Surgical Problem*? (eds S Downes and M Dabestani) Royal National Orthopaedic Hospital.

Kang Q L *et al.* (2003) Swan-shaped bone fixation device made of Ti–Ni shape memory alloy for treating humeral fracture in rabbits. *Di Yi Jun Yi Da Xue Xue Bao* **23**(7): 728–730.

Kang S B, Yoon K S, Lee J H *et al.* (2000) In vivo results of porous Nitinol: surface characterization. *J Biomed Mater Res* **49**: 88–98.

Kasano F, Morimitsu T (1997) Utilization of nickel–titanium shape memory alloy for stapes prosthesis. *Auris Nasus Larynx* **24**: 137–142.

Keikhosrow F, Moheb M (2004) Smart intramedullary rod for correction of pediatric bone deformity: a preliminary study. *Clin Orthop Relat Res* **424**: 194–201.

Klawitter J J, Hulbert S F (1971) Application of porous ceramics for the attachment of load bearing internal orthopedic appliances. *J Biomed Mater Res Symp* **2**, 161–229.

Kujala S, Pajala A, Kallioinen M, Pramila A, Tuukkanen J, Ryhanen J (2004) Biocompatibility and strength properties of nitinol shape memory alloy suture in rabbit tendon. *Biomaterials* **25**(2): 353–358.

Kujala S, Ryhanen J *et al.* (2002) Bone modeling controlled by a nickel–titanium shape memory alloy intramedullary nail. *Biomaterials* **23**(12): 2535–2543.

Kuo P P, Yang P J, Zhang Y F, Yang H B, Yu Y F, Dai K R, Hong W Q, Ke M Z, Cai T D, Tao J C (1989) The use of nickel–titanium alloy in orthopedic surgery in China. *Orthopedics* **12**: 111–116.

Lacy S A, Merrit K, Brown S A, Puryear A (1996) Distribution of nickel and cobalt following dermal and systematic administration with *in vitro* and *in vivo* studies. *J. Biomed. Mater. Res*. **32**: 279–283.

Latal D, Mraz J, Zerhau P, Susani M, Marberger M (1994) Nitinol urethral stents: long-term results in dogs. *Urol Res* **22**: 295–300.

Lopatkin NA , Afanas Z, Zakhmatov I M, Varentsov G I, Chepurov A K (1989) Endourethral drainage of the bladder in patients with prostatic adenoma. *Urol Nefrol (Mosk)* **3**: 5–7.

Lu S B, Wang J F, Guo J F (1986) Treatment of scoliosis with a shape-memory alloy rod. *Chung Hua Wai Ko Tsa Chih* **24**: 129–132, 187.

Luo Y, Takagi T, Yambe T, Matsuki M (2004) Functional evaluation of an artificial anal sphincter using shape memory alloys, *ASAIO J* **50**(4): 338–343.

Luo Y, Higa, Amoe S, Takagi T, Yambe T, Okuyana T, Tanaka H, Kakubari Y, Matsuki M (2004) Preclinical development of SMA artificial anal sphincters. *Minim Invas Ther Allied Technol* **15**(4): 241–245.

Malal, J J, Hegde G, Ferdinand R D (2006) Tarsal joint fusion using memory compression staples – a study of 10 cases. *J Foot Ankle Surg* **45**(2): 113–117.

Matsumoto K, Tajima N, Kuwahara S (1993) Correction of scoliosis with shape-memory alloy. *Nippon Seikeigeka Gakkai Zasshi* **67**: 267–274.

May A, Selmaier M, Hochberger J, Gossner L, Muhldorfer S, Hahn E G, Ell C (1995) Memory metal stents for palliation of malignant obstruction of the oesophagus and cardia. *Gut* **37**: 309–313.

Mei F, Ren X, Wang W (1997) The biomechanical effect and clinical application of a Ti–Ni shape memory expansion clamp. *Spine* **22**: 2083–2088.

Mereau, T M., Ford T G (2006) Nitinol compression staples for bone fixation in foot surgery. *J Am Podiatr Med Assoc* **96**(2): 102–106.

Merrit K, Brown S A (1995) Release of hexavalent chromium from corrosion of stainless-steel and cobalt–chromium alloys *J Biomed Mater Res* **29**: 627–633.

Meyer, M S *et al.* (1996) Triple arthrodesis: a biomechanical evaluation of screw versus staple fixation. *Foot Ankle Int* **17**(12): 764–767.

Mirgazizov M Z, Hafizov R G *et al.* (1997) Dental mechanoactive implants with the effect shape memory, in: *Proceedings of the First International Symposium on Advanced Biomaterials (ISAB)*, Montreal, Canada, p. 182.

Musialek J, Filip P, Nieslanik J (1998) Titanium–nickel shape memory clamps in small bone surgery. *Arch Orthop Trauma Surg* **117**: 341–344.

Oesterle S N, Whitbourn R, Fitzgerald P J, Yeung A C, Stertzer S H, Dake M D, Yock P G, Virmani R (1998) The stent decade: 1987 to 1997. Stanford stent summit faculty. *Am Heart J* **136**: 578–599.

Payette, C R *et al.* (1998) Triple arthrodesis stabilization: a quantitative analysis of screw versus staple fixation in fresh cadaveric matched-pair specimens. *J Foot Ankle Surg* **37**(6): 472–480.

Puttlitz, C M, Masaru F, Barkley A, Diab M, Acaroglu E (2007) A biomechanical assessment of thoracic spine stapling. *Spine* **32**(7): 766–771.

Rauber K, Franke C, Rau W S, Syed A S, Bensmann G (1990) Peroral einfuhrbare endotracheale stutzgeruste aus der memory-legierung NiTi –Tierexperimentelle studie. *Rofo Fortschr Geb Rontgenstr Neuen Bildgeb Verfahr* **152**: 698–701.

Rhalmi S, Odin M, Assad M, Tabrizian M, Rivard C H, Yahia L H (1999) Hard, soft tissue and *in vitro* cell response to porous nickel–titanium: a biocompatibility evaluation. *Biomed Mater Eng* **9**(3): 151–162.

Rhalmi S, Charette S, Assad M, Coillard C, Rivard C H (2007) The spinal cord dura mater reaction to nitinol and titanium alloy particles: a 1-year study in rabbits. *Eur Spine J* **16**(7): 1063–1072.

Ricart O (1997) The use of memory shape staple in cervical anterior fusion. In: Pelton A R, Hodgson D, Russell S M, Duerig T W (eds) *Shape memory and superelastic technologies, Proceedings of SMST -97*, SMST, Pacific Grove, CA, p. 623–626.

Rocchi L, Fanfani F, Paglier A, Catalano F (2005) Treatment of scaphoid waist fractures by shape memory staples. Retrospective evaluation on 60 cases. *Chir Main* **24**(3–4): 153–160.

Rossi P, Bezzi M, Rossi M, Adam A, Chetty N, Roddie M E, Iacari V, Cwikiel W, Zollikofer C L, Antonucci F (1994) Metallic stents in malignant biliary obstruction: results of a multicenter European study of 240 patients. *J Vasc Interv Radiol* **5**: 279–285.

Ryhänen J, Niemi E, Serlo W, Niemelä E, Sandvik P, Pernu H, Salo T (1997) Biocompatibility of nickel–titanium shape memory metal and its corrosion behavior in human cell cultures. *J Biomed Mater Res* **15**: 35(4):451–7.

Ryhänen J, Kallioinen M, Tuukkanen J, Junila J, Niemelä E, Sandvik P, Serlo W (1998) *In vivo* biocompatibility evaluation of nickel–titanium shape memory metal alloy: muscle and perineural tissue responses and encapsule membrane thickness. *J Biomed Mater Res* **41**(3): 481–488.

Ryhänen J, Raatikainen T, Kaarela O (1998) Complete acromioclavicular dislocation repair with a new shape memory AC-hook implant: an operative technique and prospective pilot study. *Proceedings of 7th International Congress on Surgery of the Shoulder*, Sydney, Australia, p. 292.

Ryhänen J, Kallioinen M, Tuukkanen J, Lehenkari P, Junila J, Niemelä E, Sandvik P, Serlo W (1999a) Bone modeling and cell-material interface responses induced by nickel–titanium shape memory alloy after periosteal implantation. *Biomaterials* **20**(14): 1309–1317.

Ryhänen J, Kallioinen M, Serlo W, Perämäki P, Junila J, Sandvik P, Niemelä E, Tuukkanen J (1999b) Bone healing and mineralization, implant corrosion and trace metals after nickel–titanium shape memory metal intramedullary fixation. *J Biomed Mater Res* **47**(4): 472–480.

Sachdeva R, Fukuyo S, Suzuki K, Osida Y, Miyazaki S (1992) Shape memory NiTi alloys: applications in dentistry. *Mater Sci Forum* **56–58**: 693.

Sachdeva R, Sakima T, Miyazaki S, Kapila S (1990) Currently used orthodontic alloys. *Rev Odontol Univ Sao Paulo* **4**(4): 343–348.

Sanders J O, Sanders A E, More R, Ashman R B (1993) A preliminary investigation of shape memory alloys in the surgical correction of scoliosis. *Spine* **18**: 1640–1646.

Schurmann K, Vorwerk D, Bucker A, Neuerburg J, Klosterhalfen B, Muller G, Uppenkamp R, Gunther RW (1997) Perigraft inflammation due to Dacron-covered stent-grafts in sheep iliac arteries: correlation of MR imaging and histopathologic findings. *Radiology* **204**: 757–763.

Schurmann K, Vorwerk D, Kulisch A, Stroehmer-Kulisch E, Biesterfeld S, Stopinski T, Gunther R W (1995) Experimental arterial stent placement. Comparison of a new Nitinol stent and Wallstent. *Invest Radiol* **30**: 412–420.

Schurmann K, Vorwerk D, Uppenkamp R, Klosterhalfen B, Bucker A, Gunther R W (1997) Iliac arteries: plain and heparin-coated Dacron-covered stent – grafts compared with noncovered metal stents –an experimental study. *Radiology* **203**: 55–63.

Schwarzenberg H, Muller-Hulsbeck S , Gluer C C, Wesner F, Heller M (1998) Restenosis of peripheral stents and stent grafts as revealed by intravascular sonography: *in vivo* comparison with angiography. *AJR Am J Roentgenol* **170**: 1181–1185.

Shabalovskaya S A (1996) On the nature of the biocompatibility and on medical applications of NiTi shape memory and superelastic alloys. *Biomed Mater Eng* **6**: 267–289.

Shabalovskaya S A, Itin V I, Gyunter V E (1995) Porous Ti–Ni – a new material for implants and prostheses. In: Pelton A R, Hodgson D E, Duerig D W (eds) *Proceedings of the First International Conference on Shape Memory and Superelastic Technologies, SMST*, Asilomar, CA, 7–12.

Silberstein B (1997) Subtotal and total vertebral body replacement and interbody fusion with porous Ti–Ni implants . In: Pelton A R, Hodgson D, Russell S M, Duerig T W (eds) *Shape memory and superelastic technologies, Proceedings of SMST -97*, SMST, Pacific Grove, CA, p. 617–621.

Simon M, Kaplow R, Salzman E, Freiman D (1977) A vena cava filter using thermal shape memory alloy. Experimental aspects. *Radiology* **125**: 87–94.

Simske S J, Sachdeva R (1995) Cranial bone apposition and ingrowth in a porous nickel–titanium implant. *J Biomed Mater Res* **29**: 527–533.

Smits M, Huibregtse K, Tytgat G (1995) Results of the new nitinol self-expandable stents for distal biliary structures. *Endoscopy* **27**: 505–508.

Sokolowskik W, Metcalfe A, Hayashi S, Yahia L H, Raymond J (2007). Medical applications of shape memory polymers. *Biomed Mater* (2): S23–S27.

Sysolyatin P G, Gyunter V E, Starokha A V, Makarova I A, Sysolyatin S P, Denisov V N, Rahman B Q (1994) The use of Ti–Ni implants in maxillofacial surgery. In: Pelton A R, Hodgson D, Duerig T W (eds) *Shape memory and superelastic technologies, Proceedings of SMST -94*, SMST, Pacific Grove, CA, p. 470–475.

Tack J, Gevers A M, Rutgeerts P (1998) Self-expandable metallic stents in the palliation of rectosigmoidal carcinoma: a follow-up study. *Gastrointest Endosc* **48**: 267–271.

Tang L, Ugarova T P, Plow E F, Eaton J W (1996) Molecular determinants of acute inflammatory responses to biomaterials. *J Clin Invest* **97**: 1329–1334.

Tang R G, Dai K R, Chen Y Q (1996) Application of a NiTi staple in the metatarsal osteotomy. *Biomed Mater Eng* **6**: 307–312.

Thierry B, Tabrizian M, Trepanier C, Savadogo O, Yahia L. (2000) Effect of surface treatment and sterilization processes on the corrosion behavior of NiTi shape memory alloy. *J Biomed Mater Res* **51**(4): 685–693.

Van Humbeeck J, Stalmans R (1998) Characteristics of shape memory alloys. In: Otsuka K, Wayman C M (eds) *Shape memory materials*, Cambridge University Press, Cambridge, p. 149–183.

Versaigne S, Wolke J, Naert I and Jansen J (1998) Histomorphometrical and mechanical evolution of titanium plasma spraycoated implants, placed in the cortical bone of goats, *J Biomed Mater Res* **41:** 41–48.

Von Salis-Soglio G F (1989) Die memory-spondylodese an der lendenwirbelsaule – Ergebnisse nach 76 operationen. *Z Orthop* **127**: 191–196.

Wang Z, Zhou S, Tian F (1998) NiTi shape-memory alloy cramp used in repair of skull defect. *Zhongguo Xiu Fu Chong Jian Wai Ke Za Zhi* **12**(6): p. 347–349.

Wholey M H, Wholey M, Bergeron P, Diethrich E B, Henry M, Laborde J C, Mathias K, Myla S, Yahia L H, Lombardi S, Piron D, Klemberg-Sapieha J E, Wertheimer M R (1996) NiTi shape memory alloys treated by plasma-polymerized tetrafluoroethylene. A physicochemical and electrochemical characterization. *Med Prog Technol* **21**: 187–193.

Yachia D, Beyar M (1993) Self-expanding, self-retaining temporary coil stent for recurrent urethral strictures near the external sphincter. *Br J Urol* **71**(3): 317–321.

Yahia L H, Lombardi S, Piron D, Klemberg-Sapieha J E, Wertheimer M R (1997) NiTi Shape memory alloys treated by plasma-polymerized tetrafluoroethylene. a physicochemical and electrochemical characterization. *Med Pro Technol* **21**(4): 187–193.

Yanagihara K, Mizuno H, Wada H, Hitomi S (1997) Tracheal stenosis treated with self-expanding nitinol stent. *Ann Thorac Surg* **63**: 1786–1789.

Yang P J, Tao J C, Ge M Z, Yang Q M, Yang H B, Sun Q (1992) Ti–Ni memory alloy clamp plate for fracture of short tubular bone. *Chin Med J (Engl)* **105**: 312–315.

Yang P J, Zhang Y F, Ge M Z, Cai T D, Tao J C, Yang H P (1987) Internal fixation with Ti–Ni shape memory alloy compressive staples in orthopedic surgery. A review of 51 cases. *Chin Med J (Engl)* **100**: 712–714.

Yi H C, Moore J J (1990) SHS synthesized Ti–Ni based shape memory alloys for both low- and high-temperature applications. *J Mater Sci Lett* **8**(10): 1182–1184.

Yoneyama T, Tanabe Y, Doi H, Kobayashi E, Hamanaka W, Bonfield W (1996) Stress Reduction by NiTi Alloy in Impact Compression Test. *Proc. Fifth World Biomaterials Congress*, p. 88.

Yoneyama T (1988) Studies on NiTi alloys for dental casting. Part 2: Damping capacity and shock absorptive characteristics. *J Jap Soc Dent Mater Devices* **7**(2): 262–269.

Yoneyama T (1989) Evaluation of super-elasticity characteristics of orthodontic Ti–Ni-alloy wire. *J Stomatol Soc Jap* **56**(1): 93–101.

Zhang, C C (1989) Treatment of patellar fracture using an internal fixator of shape-memory alloy. *Zhonghua Wai Ke Za Zhi* **27**(11): 692–695, 703.

Index